Development of Novel Methacrylic and Supramolecular Comb Polymers of Rylenebisimides for applications in Optoelectronics

Thesis Submitted to

THE UNIVERSITY OF PUNE

For the Degree of

DOCTOR OF PHILOSOPHY

IN CHEMISTRY

By

Ms. REKHA NARAYAN

Under the Guidance of

Dr. S. K. ASHA

POLYMER SCIENCE AND ENGINEERING DIVISION

CSIR-NATIONAL CHEMICAL LABORATORY

PUNE 411 008

INDIA

AUGUST 2013

सीएसआयआर-राष्ट्रीय रासायनिक प्रयोगशाला
(वैज्ञानिक तथा औद्योगिक अनुसंधान परिषद)
डॉ. होमी भाभा मार्ग, पुणे - 411 008. भारत
CSIR-NATIONAL CHEMICAL LABORATORY
(Council of Scientific & Industrial Research)
Dr. Homi Bhabha Road, Pune - 411 008. India.

Dr. S. K. Asha
Senior Scientist
Polymer Science and Engineering Division

CERTIFICATE

Certified that the work incorporated in the thesis entitled **"Development of Novel Methacrylic and Supramolecular Comb Polymers of Rylenebisimides for applications in Optoelectronics"** submitted by **Ms. Rekha Narayan** was carried out by the candidate under my supervision at the Polymer Science and Engineering Division of CSIR-National Chemical Laboratory, Pune. The work presented here or any part of it has not been included in any other thesis submitted previously for the award of any degree or diploma from any other University or Institution.

Place:
Date:

Dr. S. K. Asha
(Research Guide)

DECLARATION

I hereby declare that the matter embodied in the thesis entitled **"Development of Novel Methacrylic and Supramolecular Comb Polymers of Rylenebisimides for applications in Optoelectronics",** submitted for the Degree of Doctor of Philosophy in Chemistry to the University of Pune, is the result of investigations carried out by me at the Polymer Science and Engineering Division of CSIR-National Chemical Laboratory, Pune, India, under the supervision of Dr. S. K. Asha. The work is original and has not been submitted in part or full by me for any other degree or diploma to this or any other University.

In keeping with the general practice of reporting scientific observations, due acknowledgement has been made wherever the work described is based on the findings of other investigators.

Date:

Place: Pune

Rekha Narayan

Dedicated to My Beloved Parents…

Mr. P. K. Narayanan

Mrs. Sujana Narayanan

Acknowledgements

My first and most important acknowledgement goes to my guide Dr. Asha S. K., who is the backbone of this thesis. Holding her hands I ushered the world of research; she is the one who taught me the principles and values of true science. This thesis and myself have grown to maturity, watered by the fantastic ideas, excellent guidance and the intellectual inspiration from my guide. On a personal note, she is a friend as well as mentor, who understands everything without saying a single word; she has always been there for me. I am indebted to you Madam... and I will fondly remember the time spent with you during my Ph.D life.

I am grateful to the present and past directors of NCL, Dr. Sourav Pal and Dr. S. Sivaram, for providing all the facilities for carrying out this research work.

I would like to thank my thank my external and internal examiners; Dr. S. G. Srivatsan, Dr. P. P. Wadgaonkar and Dr. K. Guruswamy for their valuable suggestions and interactive discussions during my upgradation assessments.

I owe my sincere gratitude to Dr. M. Jayakannan for his constant encouragement and timely intervention throughout my Ph.D work.

I thank our collaborators, Prof. K. S. Narayan and Mr. Prashant Kumar, JNCASR, Bangalore for carrying out the device studies of this work.

I would also like to thank Dr. P. A. Joy, Dr. K. Krishnamoorthy and Dr. J. Nithyanandhan from NCL.

This work in its perfection would not have been achieved without the help from many people directly and indirectly. I am thankful to

- *Kamendra Sharma and Guru Sir for teaching me the fundamentals of SAXS.*
- *Archana, Ashok, Arvind and Narasimha from IISER, Pune for the single crystal XRD data analysis.*
- *Shrikant and Snehal for the NMR studies.*

- *Pandi, Pankaj, Anuj and Ketan for TEM and SEM studies.*
- *Mangesh and Manju for in-situ XRD experiments.*

I thank all our former and present group members Deepak, Jancy, Smitha, Amrutha, Deepa, Anil, Jinish, Bala, Mahima, Ghanshyam, Kaushalendra, Nagesh, Chinmay, Nisha, Senthil, Shekhar, Saibal, Prajitha, Swapnil, Sandeep, Smitha, Ananthraj, Pramod, Bapu, Narasimha, Rajendra, Bhagyashree and Moumita. I had a nice time with all of them and they provided me with a friendly and encouraging working atmosphere making every moment in the lab memorable.

My sincere thanks to Jerly Sir and Mahesh Hariharan who showed me the correct path to reach the world of research.

I take this opportunity to thank all my friends Bindu, Reena, Chameshwary, Tanpreet, Reetika, Roopa di, Manaswini didi, Resmi, Bala, Mohan, Ram, Lenin, Pandi, Manju, Mohan Raj, Arul, Ashok, Malli annae and Selva aanae for extending their helping hands at times of need and also to my room partner Priti for bearing me with those late night writings without a single word of complaint. I would also thank my aunty at the Tamil mess who fed me anytime anything like my mother and to Uncle, Prathamesh, Praju, Bhagyam Anni, Bala anne, Sithi, Chinna aaya, Mani and Venky.

Special thanks to Balaji annae, Indira anni, Vinaya and Vignesh for their warm care and help which made me feel less away from home.

Words are not enough to express my gratitude to my best buddy KKM (Kamal Khaja Mohaideen) for standing beside me like a stone pillar till the last moment of completion of this thesis. His selfless friendship is something that I will treasure for a lifetime.

Finally I want to thank my family; without their unconditioned love and supporting, I could have not surpassed these tough years. I thank my father, P. K. Narayanan and my mother, Sujana Narayan for making me what I am today, their prayers and blessings are my strength. My dear sister Meera, my little brother Harikrishnan (Kannan) and my cute (late) Mickey deserves special thanks for their endless affection

and support. Last but not the least, I express my deepest thanksgiving to two persons that I lost during my Ph.D period, my grandparents T.P. Prabhakaran and K. Komalam, who played a key role in moulding the character and personality I am today.

The pride of accomplishing this work is attributed to my complete family.

Rekha Narayan

Science is a way of thinking much more than it is a body of knowledge.

Carl Sagan

Abstract

N-type organic semiconductors have emerged as a subject of intensive research interest due to their inevitable requirement in the field of a variety of organic electronics applications such as photovoltaic cells, n-channel field effect transistors, complementary logic circuits and so on. Significant progress has already been achieved for p-channel organic semiconductors with high performance even before the turn of the millennium, whereas their n-channel counterparts have reached maturity only during the last decade. Amongst the non-fullerene type acceptor materials, the rylenebisimides particularly the perylene and naphthalene bisimides based small molecules as well as polymers have proved to be the most promising n-type semiconductor candidates for a variety of organic electronics applications.

Rylenebisimides are a versatile class of robust fused aromatic electron-deficient materials with strong absorption in the visible region, excellent thermal and photostabilities, high electron affinities and fantastic self-assembling tendencies. This unique combination of desirable properties makes them attractive for various electronic and optical applications. Compared to organic small molecules, polymeric materials readily give rise to solution processable large area and low cost devices. However it has been a difficult challenge to attain design strategies maintaining delicate balance between high crystallinity of small molecules and processability of polymers. Unfortunately little research exists with prime focus on rylenebisimide based polymeric materials with high solubility along with concomitant high crystallinity and device performance. Most of the reports involve cumbersome synthetic procedures and often the resulting polymers exhibit solubility issues with loss of the desired properties such as crystallinity, charge transport efficiency etc. But the field is now under rapid advancement, realizing the alarming need to achieve n-channel materials with high performance, stability and processability that can lead to printable active electronics.

The present thesis entitled as **"Development of Novel Methacrylic and Supramolecular Comb Polymers of Rylenebisimides for applications in Optoelectronics"** describes the results of our attempts to design and develop rylenebisimide based novel polymeric materials that could find potential applications in the field of optoelectronics. The thesis touches all important realms of research in this field starting from synthesis, detailed investigation of structure-property relationships and finally the device performance measurements were also carried out in collaboration with working group of Prof. K.S. Narayan (JNCASR, Bangalore).

The thesis has been divided into six chapters. The **Chapter 1** is a general and broad introduction to the field of organic/plastic electronics. An overview of its variety of applications and review of the materials, structure - mechanism, as well as device fabrication processes are discussed. Particular attention has been paid to focus on the field of n-type semiconductor materials viz., the polymers and small molecules, especially the ones based on the rylenebisimides. The overall aim and outline of the thesis are presented at the end of this chapter.

Chapter 2 describes our initial attempts at developing high molecular weight side-chain perylene bisimide polymers via covalent chemistry approach, by incorporating as pendant groups into a urethane methacrylate comb monomer with sites specific for self-organization via hydrogen bonding and π-π interactions. The approach was initially tried successfully onto two simple phenols with long alkyl chains namely cardanol and 3-pentadecylphenol before attempting the rigid core perylenebisimide. Subsequently different methacrylic comb monomers of unsymmetrical perylenebisimide as pendant groups with and without hydrogen bonding motifs were successfully synthesized by playing around with urethane and

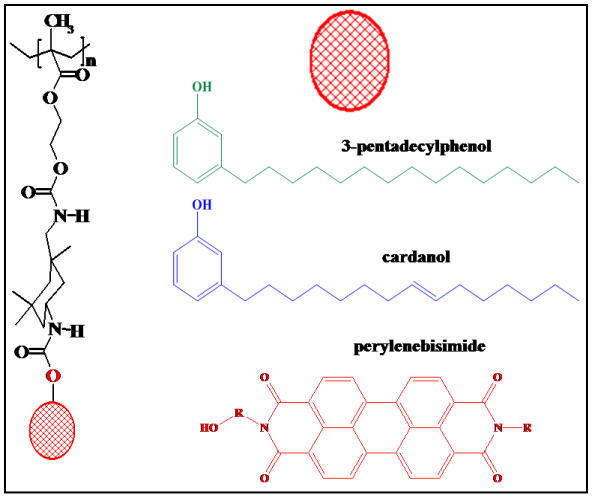

ester chemistry. However the simple and facile free-radical polymerization of the perylenebisimide methacrylate comb monomers failed miserably despite several repeated attempts under varied polymerization conditions. Meanwhile the cardanol and 3-pentadecylphenol based methacrylate comb monomers readily underwent polymerization under similar conditions. Solvent induced self-assembly properties of these cardanol and 3-pentadecylphenol based urethane methacrylate polymers were thoroughly studied using different techniques like scanning electron (SEM), transmission electron (TEM) and atomic force (AFM) microscopy. The polymers exhibited three - dimensional honeycomb morphology in $CHCl_3$ whereas in THF they formed spheres. The cardanol derived polymer PCIH exhibited multiple morphologies like spheres and tubes in THF. However to move forward, the negative results gained from the second chapter led to the search for alternate methods for incorporating rigid perylenebisimide into processable polymer scaffolds.

Chapter 3 explored a different approach by introducing the new use of an old concept: the non-covalent interactions and supramolecular chemistry to overcome the shortcomings of covalent side chain perylenebisimide polymers. We demonstrated for

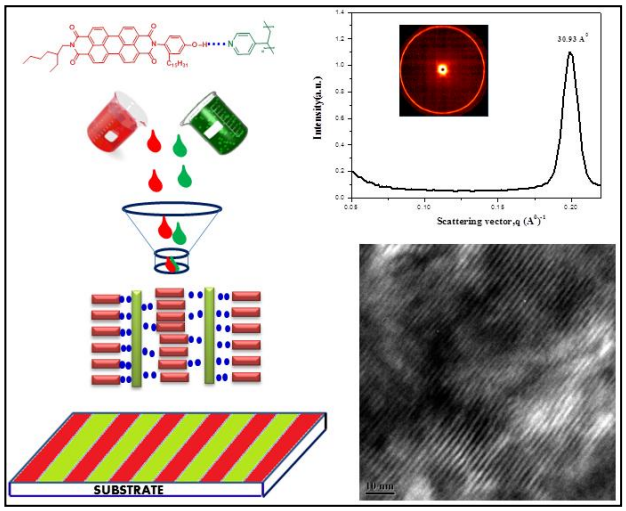

the first time a supramolecular comb polymer of perylenebisimide with unique combination of high crystallinity and solution processability properties that are highly desirable for device applications. A new unsymmetrical perylenebisimide substituted with ethylhexyl chains on one end and 3-pentadecylphenol at the other termini **(PDP-UPBI)** was successfully synthesized and a series of its supramolecular comb polymer complexes with poly(4-vinyl pyridine) (P4VP) of different stoichiometric ratios were prepared by simple solution mixing utilizing the hydrogen

bonding interactions between phenol and pyridine groups. Self-assembly of the supramolecular complex containing 1:1 stoichiometric amount of **PDP-UPBI** formed microphase separated lamellar structures in 5-10 nanometre scale with alternating P4VP and **PDP-UPBI** layers as studied by the small angle and wide angle X-ray scattering (SAXS and WAXS) experiments as well as transmission electron microscopy (TEM) imaging. The outstanding achievement of the work was the ability to preserve the high crystallinity of a small molecule along with the processability of a polymer. The high electron mobility of this supramolecular comb polymer compared to its precursor **PDP-UPBI** molecule, measured by space charge limited current (SCLC) method further proved the existence of highly ordered domains in the former, facilitating efficient charge transport. The chapter thus reinforced the impressive impact of supramolecular polymers, indicating its great prospects in the field of future organic electronics.

In **Chapter 4** the same concept of hydrogen bonded supramolecular comb polymers with P4VP was extended to the lower analogue rylenebisimide namely naphthalenebisimides. The motivation for this chapter was the aim to develop n-type polymeric semiconductor materials with even better performance, because naphthalenebisimides are known to exhibit higher charge carrier mobilities than their perylene counterparts, in addition to their other positive properties such as good electron affinity, better solubility in organic solvents, high crystallinity etc. Similar to the **PDP-UPBI,** unsymmetrical naphthalenebisimide (**PDP-UNBI**) was successfully synthesized and stoichiometrically complexed with P4VP. The uniform lamellar morphology of the naphthalene based supramolecular comb polymer with alternate P4VP and **PDP-UNBI**

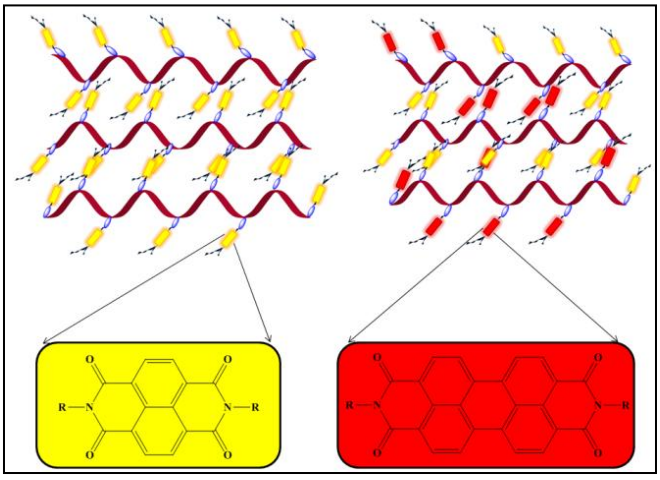

layers was confirmed by X-ray diffraction (XRD) analyses and direct imaging by TEM. Further the packing diagram obtained from the single crystal XRD analysis of the **PDP-UNBI** crystals gave a clear picture of the initial arrangement present in the self-associated **PDP-UNBI** small molecule alone. Correlating this with the XRD data of the hydrogen bonded complex provided insight into the probable packing of the P4VP chains within the crystalline lattice of the small molecule **PDP-UNBI** leading to a highly ordered lamellar packing. In order to combine the high crystallinity and solution processability of naphthalenebisimides with the broader absorption spectra of perylenebisimides, yet another series of stoichiometrically balanced 1:1 random co-comb polymer complexes of P4VP with **PDP-UPBI** and **PDP-UNBI** varying only in the relative compositions of perylene and naphthalene cores were also prepared. These 1:1 random co-comb polymer complexes were also found to exhibit clear lamellar structures but with varying periodicities. The charge carrier SCLC measurements showed that, as anticipated the supramolecular complex of **PDP-UNBI** with P4VP exhibited better electron mobilities than its perylene counterpart. Meanwhile amongst the series of random co-comb polymer complexes, only the sample with equimolar ratios (50/50) of **PDP-UNBI** and **PDP-UPBI** gave reliable electron transport characteristics.

Chapter-5 illustrates the design and development of a novel supramolecular crosslinked polymer network of both perylene and naphthalene bisimides via hydrogen bonding interactions with P4VP. A structural fine tuning of the rylenebisimides (both perylene and naphthalene bisimide) resulted in successful synthesis of two ditopic hydrogen-bond donor dyes viz., **PDP-SNBI** and **PDP-SPBI** that could coordinate to P4VP from both termini using the 3-pentadecylphenol (PDP) groups. An inherent tendency to undergo liquid crystalline columnar self-assembly was found in both these rylenebisimides that was revealed mainly by the combined XRD, polarized optical microscopy (POM) and molecular modeling studies. Upon hydrogen bonded complexation of these ditopic dyes with P4VP via solution mixing, supramolecular semiconductor crosslinked polymer network with preserved mesomorphic properties

were obtained. Bulk packing diagram analysis of the crosslinked polymer networks by XRD experiments revealed a structural transformation from rectangular-columnar to

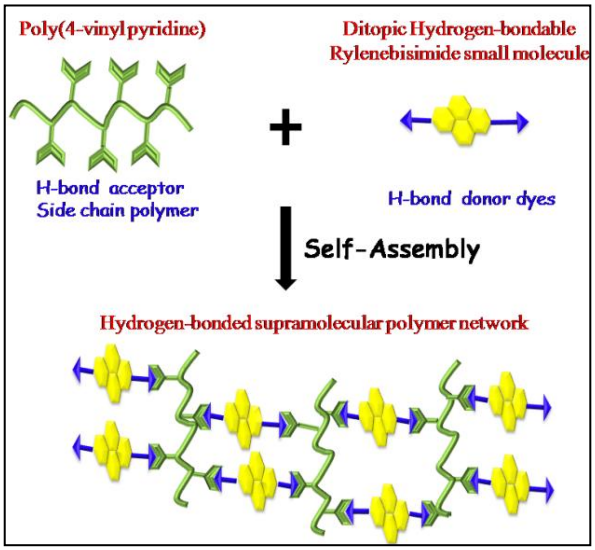

lamello-columnar self-organization on moving from the ditopic small molecules to the polymer network structures. This observation was substantially supported by TEM imaging evidences, that showed uniform lamellar morphology for both perylene and naphthalene based supramolecular crosslinks. Finally the materials were screened for device applications using SCLC measurements which revealed that among the two systems compared, the perylenebisimide based supramolecular polymer network only exhibited better charge transport characteristics.

Chapter 6 presents an overall conclusion and comparison of the work reported in previous chapters with a discussion on the logic behind each chapter and the cumulative outcome of the Ph.D thesis. The scope for further work possibilities in continuation with the present thesis work are also suggested as the probable avenues for future research.

List of Abbreviations

AFM	Atomic Force Microscopy
$CHCl_3$	Chloroform
DMF	N,N'-Dimethylformamide
DSC	Differential Scanning Calorimetry
FL	Fluorescence
FT-IR	Fourier Transform Infrared Spectroscopy
LC	Liquid Crystalline /Liquid Crystal
MCH	Methylcyclohexane
mg	Milligram
mmol	Millimole
NBI	Naphthalenebisimide
NDI	Naphthalenediimide
nm	Nanometer
OFET	Organic Field Effect Transistor
OLED	Organic Light Emitting Diode
OPV	Organic Photovoltaics
P4VP	Poly(4-vinylpyridine)
PBI	Perylenebisimide
PDI	Perylenediimide
PDP	3-pentadecyl phenol
PEDOT:PSS	Poly(3,4-ethylenedioxythiophene): Poly(styrene sulfonate)
POM	Polarized Optical Microscopy
PTCDA	Perylene tetracarboxylic dianhydride
SAXS	Small-angle X-ray scattering
SCLC	Space Charge-Limited Current
SEC	Size Exclusion Chromatography
SEM	Scanning Electron Microscopy
SNBI	Symmetrical Naphthalenebisimide
SPBI	Symmetrical Perylenebisimide
TEM	Transmission Electron Microscopy
TFA	Trifluoroacetic acid
TGA	Thermogravimetric analysis
THF	Tetrahydrofuran
TMS	Tetramethylsilane
UNBI	Unsymmetrical Naphthalenebisimide
UPBI	Unsymmetrical Perylenebisimide
UV/Vis	Ultraviolet–visible spectroscopy
WAXS	Wide-angle X-ray scattering
XRD	X-ray Diffraction

Table of Contents

Chapter- 1

Introduction

1.1. Introduction to Organic/Polymer/Plastic Electronics

1.1.1. History

The history of molecular electronics dates back to 1974 seminal idea of Ari Aviram and Mark Ratner, who proposed for the first time a molecular scale electronic device - a rectifier, in which a single organic molecule contacting two electrodes was used to rectify the current through the molecule.[1] Their proposal was premature in that fabrication of such a single molecule device with organic monolayers of nanometre thickness stacking vertically between metal electrodes was not technically feasible. But the evolution of organic materials based electronics did not stop there. Taking aid of recent advances in synthetic chemistry and techniques of microfabrication, many of the challenges have now been met. Today organic electronics is the latest and the fastest growing branch of electronics, which got its kick start with the 1977 discovery that polyacetylene, a purely hydrocarbon material when chemically doped with iodine leads to materials from insulating to semiconducting to highly conducting π-conjugated systems.[2,3] For this work, three collaborating scientists Alan Heegar, Alan MacDiarmid and Hideki Shirakawa were jointly awarded Nobel Prize for Chemistry in the year 2000. Before that organic compounds were considered as mere hydrocarbons with no electronic properties imaginable and inorganic semiconductors such as silicon, gallium arsenide, silicon dioxide insulators, and metals such as aluminium and copper have been the backbone of the semiconductor industry. However since the discovery of conducting polymers, there emerged an ever-growing interest in organic semiconductor materials as a substitute for the expensive conventional inorganic semiconductor such as silicon, leading to the development of an advanced area of research known as organic/polymer/plastic/printed electronics or sometimes also called organic large area electronics (OLAE).[4-9] The tremendous excitement to research in this field stems from the demand for low cost, large area, flexible and light weight devices. In this regard organic and polymeric semiconducting materials are widely pursued due to their combinational

advantages of versatile structural modifications according to the functionality requirements, processability and compatibility with a range of substrates available. The mid 1980s started off the real steady interest in the devices based on organic semiconductors, with the quasi-simultaneous discovery of the organic photovoltaic cell (OPV),[10] light emitting diode (OLED)[11,12] and field effect transistor (OFET).[13] Ching W. Tang who built the first organic heterojunction solar cell (OSC) and the first organic light emitting diode (OLED) at Kodak in 1980s, is widely considered as the father of organic electronics.[10] At Kodak where Tang was a postdoctoral researcher working on organic solar cells, both OLEDs and OSCs devices were discovered serendipitously from the observation that using the same organic heterojunction - a bilayer device structure consisting of an electron donor and electron acceptor, he could get light emission and charge separation. This first demonstration although could not replace the existing technologies, nevertheless a torrent of activities was generated in this field by Tang's insights, which eventually laid the foundation stone for organic semiconductor industry. Parallel to this, in 1987 Koezuka and co-workers reported the first organic field effect transistor (OFET) based on a conjugated polythiophene material, thus eliminating the use of expensive metal oxide semiconductors.[13] From then onwards, the field of organic electronics has progressed with considerably significant momentum as a result of combinational studies in chemistry, physics and materials science. Despite some key challenges such as poor performance and stability of organic semiconductors still plaguing further advancement, this field is today at the verge of successful commercial applications due to their simplicity in manufacturing and lower costs (Figure-1.1).

Amongst these the most advanced organic electronics technology already in high commercial production are the OLEDs omnipresent in mobile phones, highly colourful and extremely thin displays and lighting markets. With drastic improvements in the advent of new classes of molecular materials in the past three decades, the prospects of organic semiconductor based commercial applications

like low-cost organic solar cell panels integrated onto building roofs, car ceilings, bags, fabric materials etc., inexpensive RFID (radio frequency identification) tags to replace bar codes, light weight ultra thin television panels with crispier displays outweighing even today's LCDs (liquid crystal displays), chemical sensors and other printable single use electronics, have now become greater than ever before.

Figure-1.1. Flexible OLED display technology driven by organic transistors (left) [adapted from *http://www.sony.net/SonyInfo/technology/technology/theme/8ido18000001prgv-img/8ido18000001prpz.jpg*], plastic solar cells (middle) [adapted from *http://www.aps.org/publications/capitolhillquarterly/201302/whatsnewininnov.cfm*] and organic integrated circuits (right). [adapted from *NPG Asia Materials research highlight; doi:10.1038/asiamat.2011.48*]

1.1.2. Organic Versus Inorganic Electronics

Organic semiconductors are primarily hydrocarbon based single molecules, short chain oligomers or polymers, whereas the constituent particles of inorganic semiconductors are atoms. The most relevant characteristics distinguishing the organic/plastic electronics from the traditional inorganic semiconductor technology has been summarized in Table 1.1. Amongst these the key features of organic and polymer semiconductors which make them attractive candidates for electronics industry compared to their inorganic counterparts are their large scale low cost production and ease of fabrication techniques. Because of these superior material properties unique to organics/plastics, ubiquitous cheaper molecular electronics are slowly becoming unavoidable part of modern society.

Table 1.1. Characteristics of inorganic versus organic electronics

Classical Electronics	Organic Electronics
High manufacturing costs	Reduced costs
Complex processing techniques	Simple processing
Small area products	Large area products
Rigid substrates	Flexible substrates
Hard and brittle	Soft and fragile
High performances	Reduced performances

Other major advantages of molecular structures for electronics applications include:

(i) Synthetic tailorability: By choice organics can be chemically functionalized and derivatized via a variety of molecular synthesis tools; thus providing routes for straightforward fine tuning of a molecule's structural, electronic, transport and binding properties. Molecules have size scale in the range 1-100 nm, a scale which allows for incorporation of functional nanostructures by molecular design.

(ii) Processability: Organic materials are highly compatible with plastic substrates commercially used, thereby gaining mechanical flexibility. Moreover these materials can be deposited under ambient conditions utilizing a wide range of simpler conventional processing techniques like spin coating from solutions, thermal evaporation and those conducive to large area products by "roll-to-roll" fabrication processes like inkjet printing, screen printing as well as gravure printing.[14]

(iii) Self-assembly control at nanoscale: Several specific intermolecular interactions can be explored to form desired structures by nanoscale self assembly pre-programmed within the components. Such versatile options can open up new era in the design of novel electronic devices.

Along with a bundle of favourable advantages, molecular electronics are also accompanied by disadvantages such as instability and low performances of organic molecules compared to the inorganics. However, the pros outweigh the cons, rendering the molecules still to be the sought after candidates for the future next generation electronics.

1.1.3. Conduction Mechanisms in Organic Semiconductors

Conduction mechanism in materials refer to the means by which charges move in a material under the influence of an electric field. Band theory distinguishes materials as conductors, semiconductors and insulators on the basis of electron occupancy of the conduction (CB) and valence bands (VB). (Figure 1.2).

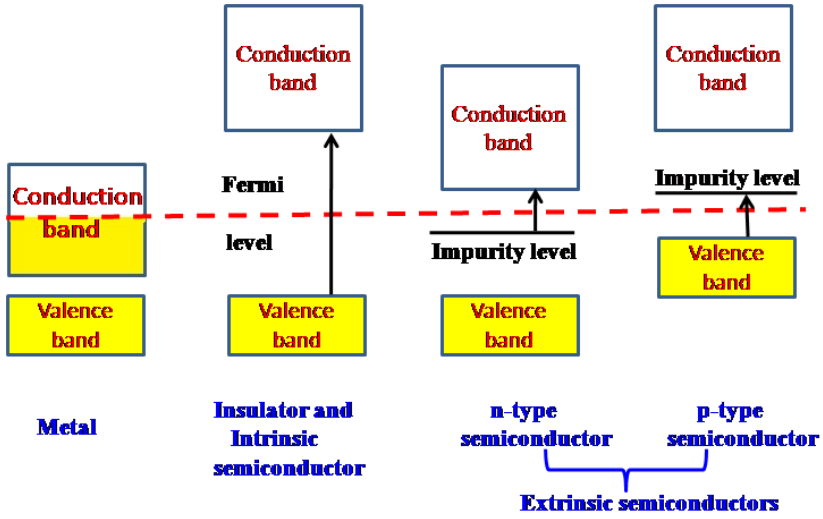

Figure-1.2. Representative energy band diagrams for conductors, semiconductors and insulators.

In theory, the top of valence band of a material would be filled by all the available electrons within an atom of that material at a temperature of 0 Kelvin. In the case of insulators and semiconductors, the valence band is completely filled with electrons while the conduction band is empty. The highest occupied molecular orbital of VB is known as HOMO and lowest unoccupied molecular orbital of CB is known as LUMO. The energy difference between HOMO and LUMO is known as energy band gap (Eg). Thus energy band gap exists in insulators and semiconductors, whereas in metals (conductors) there is no band gap, only a continuous partially filled conduction band exist. This means that in conductors there are plenty of nearby energy levels available for electrons to move in and hence can easily flow from one atom to other when a potential difference is applied across the material (e.g. metals like copper, aluminium etc.). In insulators

the forbidden energy gap is very substantial (> 4eV) that it is not normally practicable to move the electrons from VB to CB (e.g. quartz, wood etc.). On the other hand, semiconductors are further divided into intrinsic and extrinsic. An intrinsic semiconductor, at very low temperatures behave like insulators, but at temperatures > 0 Kelvin the energy of the surroundings (kT, k is the Boltzmann constant and T is the temperature) can become large enough to thermally excite electrons from VB to CB (e.g. undoped Silicon and Germanium). When intrinsic semiconductors are doped with impurities (extra electrons or holes), localized impurity energy levels close to conduction (n-type) or valence (p-type) band edge are induced (see figure.1.2) and this results in narrowing of band gap leading to increase in conductivity. These doped semiconductors now have majority carriers that may be either electrons or holes and are known as extrinsic semiconductors (e.g. doped Si and Ge). Doping with tri-valent elements (Group III) result in p-type extrinsic semiconductor since holes become majority carriers and penta-valent elements (Group V) leads to n-type extrinsic semiconductor since electrons become the majority carriers. Typical band gaps for semiconductors are 1-2 eV. Useful inorganic semiconductors that can be obtained with sufficient purity are less and most organic semiconductors are characterized by intrinsic inhomogeneities as well as chemical impurities (both n- and p-type). These inherent impurities in organic semiconductors causes no significant effect of doping on conductivity and hence they are more similar to insulators. Several models based on many theoretical and experimental studies are described in literature for the charge transport mechanism in organic (including polymeric) semiconductors, but a general unified model is still lacking.[15] However the following discussion will try to introduce the most accepted mechanisms regarding the conduction behaviour of organic semiconductors.

Bulk organic semiconductors are mainly π-conjugated organic molecular crystals, amorphous molecular films or conjugated polymers that are made up of molecular subunits characterized by delocalized π-bonds. Chart-1.1 shows some of the commonly recognized π-conjugated small molecular and polymeric semiconductor materials.

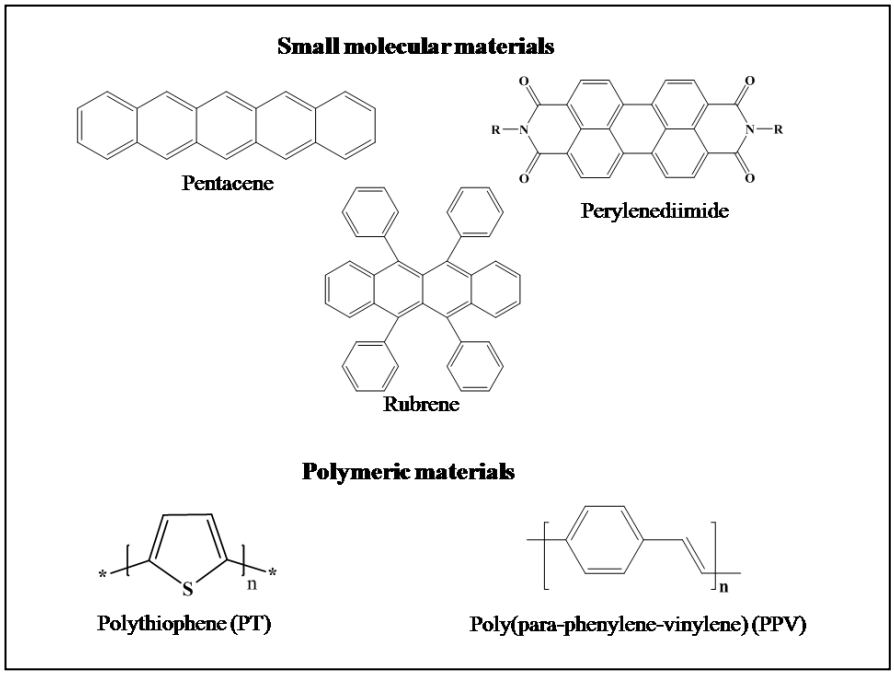

Chart-1.1. Molecular structure of some prototype organic semiconductor small molecules and polymers.

The constituent molecular components in organic semiconductors are held together by weak Van der Waals interactions, with energies typically smaller than 10 kcal mol^{-1} which limits the charge transport mobilities in the range 1-10 $cm^2V^{-1}s^{-1}$. In contrast the constituent atoms in inorganic semiconductors like Si, Ge or GeAs, are held by very strong covalent bonds with energy as high as 76 kcal mol^{-1} for Si and hence they have high mobility of the order of 10^3 $cm^2V^{-1}s^{-1}$ at room temperature. Conjugation, i.e., alternate single and double bonds between carbon atoms is the common structural property of all organic semiconductors (Figure-1.3). Unhybridized p_z orbitals on the sp^2 hybridized carbon atoms of the backbone overlap resulting in extended π-systems. Therefore the HOMO and LUMO of organic semiconductors correspond to the bonding π-MO and antibonding π*-MO respectively. Charge transport in organic solids take place only when there is charge on the molecular unit, which may be an extra electron in the LUMO or one that is removed from HOMO. As a result the molecule no longer remains in the ground state, but goes to charged excited state.

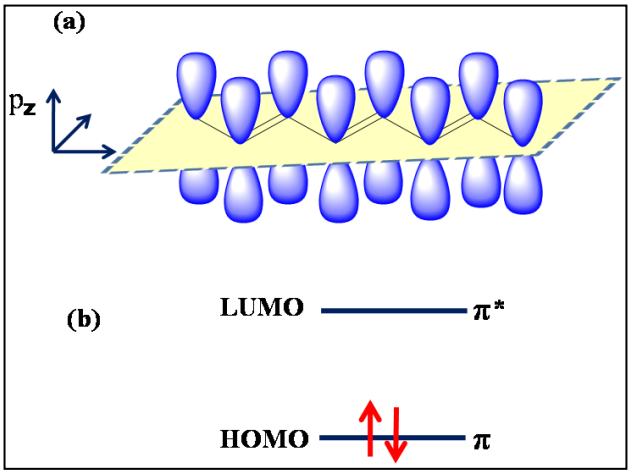

Figure-1.3. (a) A conjugated backbone with p_z orbitals perpendicular to molecular plane (b) HOMO and LUMO orbitals in π-conjugated systems.

Molecules can be made charged in different ways:

(1) Electrons can be injected or extracted at the interface between a metal electrode and the molecule, as in the operation of a LED device.

(2) By reduction or oxidation of the molecule using dopants. High electron affinity atoms or molecules like iodine, antimony pentafluoride ($SbCl_5$) or 2,3,5,6-tetrafluoro-7,7,8,8-tetracyanoquino dimethane (F_4-TCNQ) may oxidize a typical organic semiconductor such as poly(p-phenylene) derivatives leaving them positively charged. Doping with alkali metals result in reduction.

(3) Through exothermic dissociation of a neutral excited state in molecule by electron transfer to a neighbour molecule.

(4) Optical excitation in a molecule, where one electron from HOMO is promoted to LUMO by the absorption of a photon.

Coloumbically bound electron-hole pairs known as excitons are thus generated and these excitons are precursors of free positive and negative charges.[16,17] The energy required to separate electron and hole of an exciton is termed exciton binding energy and organic materials have high exciton binding energies. In contrast, inorganic semiconductors have low exciton binding energies due to which photoexcitation produces free electrons and free holes that

spontaneously travel to the respective electrodes. Since the intermolecular interactions are weak in organic materials the charge carriers and excitons are strongly localized to few molecules or a single conjugated segment. When an electron is taken from a π-orbital or added to a π*-orbital of an organic material, the spatial distribution of electrons in the more strongly bound σ-orbitals is disturbed and consequently bond lengths of the molecule are altered. This change in molecular geometry is associated with geometric reorganization energy and the charge move together with their electronic polarization "cloud". These quasi-free charge carriers are called polarons, [18-21] i.e., an electron or a hole plus a distortion of the charge's surroundings.

Conduction can then occur by the motion of polaron through the material. For example as shown in the case of poly (p-phenylene) in which upon removal of an electron from the π-backbone by chemical oxidation, an unpaired electron (radical) and a positive charge are generated (figure-1.4(a)). Through local bond rearrangement the free radical and the cation couple to form the polaron and the polaronic band appears as localized electronic states located between the gap, where the lower energy state is occupied by single unpaired electron (figure-1.4(b)).

Removal of another electron can occur either from the polaron or from the neutral portion of the chain; the former creates a bipolaron while the latter creates two polarons. The former process is thermodynamically favorable due to large decrease in ionization energy associated with bipolaron formation. Thus charge transport in conducting polymers occurs by movement of carriers between localized states or between polarons or bipolaron states.[22] The physical mechanism of conduction in polymers is dominated by thermally activated hopping mechanism (or tunnelling process) by which charge carriers jump from one monomer to another rather than travelling coherently. Although it is difficult to deny the importance of band transport in the conduction mechanism of especially crystalline small molecule organic counterparts and also for polymeric semiconductors, it is hopping mechanism that contributes more to the carrier

mobility. However for conjugated polymers it is likely that a mix of two occur, since a pure hopping mechanism is also unlikely. Finally it turns out that the charge transport in many organic crystals and highly ordered thin films follows a band-like regime similar to the inorganic counterparts, at low temperature[23] and as temperature increases charge transport operates mainly by hopping mechanism.[24,25]

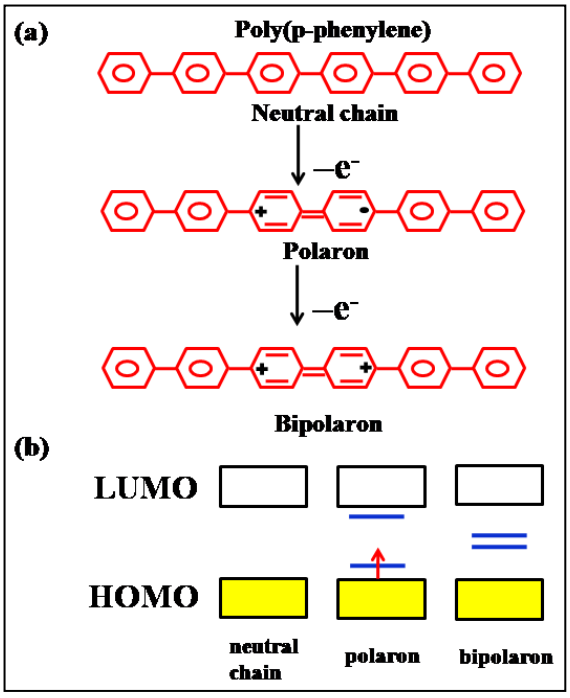

Figure-1.4. Creation of polaron and bipolaron states in poly(p-phenylene).

1.2. Organic Semiconductor Devices

1.2.1. Organic Light Emitting Diodes (OLEDs)

OLED is the latest name of lighting and display technology in market. They are now an indispensable part of digital cameras, mobile phones, television displays etc. OLED display technology has several fold advantages over the LCDs which include high contrast, brilliant colours, unlimited viewing angle, extremely thin and flat displays and so on.[26] Even more revolutionary display and lighting applications using OLEDs are expected in near future.

Basic principles and device architecture

In simple words OLEDs are electroluminescent organic semiconductor based solid state devices which convert electrical energy into light energy. The basic OLED device architecture consists of atleast an undoped organic material sandwiched between two electrodes of different work function, one of which need to be transparent for light to transmit. ITO (Indium Tin Oxide composite) is the most widely used anode in OLEDs due to its high work function (4.5 - 5.1 eV) and high transparency (90 %) to visible light.[27] Since the HOMO energies of organic materials are typically 5-6 eV, a high work function (Φ_0) or Fermi energy (E_f) relative to the organic material is needed for the anode to efficiently inject holes into the organic layers. Low work function materials such as Ca (Φ_0 ~ 3 eV), Mg (Φ_0 ~ 3.7 eV) or Al (Φ_0 ~ 4.3 eV) are usually used as cathode in order to minimize the energy barrier for electron injection from Fermi level of cathode to LUMO level of organic materials. But these metals get easily oxidised or corroded in air, so alloyed electrodes are more preferred. The organic layer sandwiched in between has three main components: a hole transport layer (HTL), an electron transport layer (ETL) and an emissive layer.

A generic OLED device structure and the equilibrium energy levels are shown in figure-1.5.

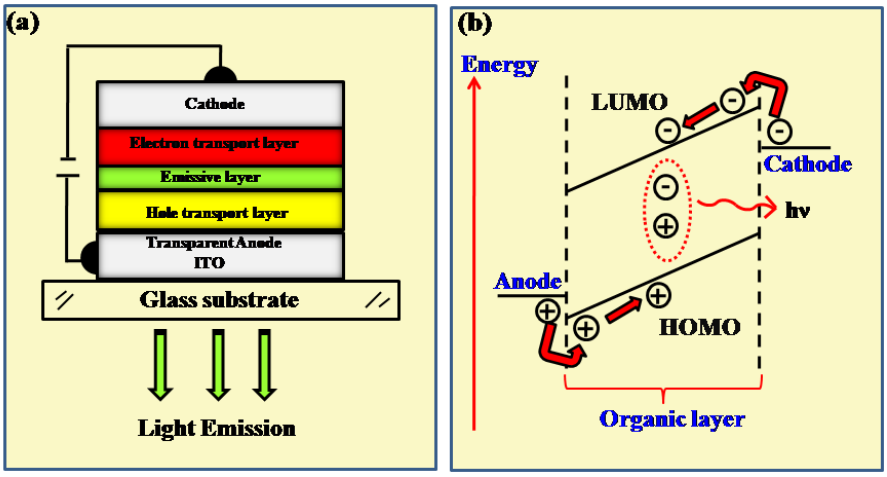

Figure-1.5. OLED (a) device configuration and (b) Energy diagram.

When a forward bias is applied, holes (+) are injected from the anode and electrons (-) are injected from the cathode. These carriers recombine to form excitons (excited state coloumbically coupled electron-hole pair) and their radiative decay results in electroluminescence.[28-30] Therefore the four main processes involved in light generation in OLED devices are :

(1) Charge injection

(2) Charge Transport

(3) Exciton formation

(4) Exciton diffusion and emissive decay generating light.

Efficient charge injection is obtained by selecting proper electrodes in such a way that HOMO and LUMO energy levels of the organic layer are close to the work function of the metal. Additional charge transport layers like p-doped PEDOT:PSS as hole injection layer and LiF as electron transport layer are also used to adapt the different energy levels.[31-34]

1.2.2. Organic Photovoltaic Cells (OPVs)

Organic Photovoltaics in general is the term which refers to the technologies that are used to convert sunlight into electricity utilizing organic semiconductor thin films. Eventhough this field has been the centre of active research for more than 30 years, still OPV based commercial devices have not touched the market with few exceptions, where flexible and thin film plastic solar cells for charging batteries of portable electronics has been launched by Konarka Technologies Inc. [35] They have reported an OPV cell with a record-breaking 8.3 % power conversion efficiency as verified by National Energy Renewable Laboratory (NERL).[36] Very recently only an all polymer Tandem solar cell has been reported with remarkably high efficiency of 10.5 %.[37] Currently solar technologies are dominated by crystalline silicon based wafer-sized single junction solar cells with record lab efficiency of ~ 25 %. Eventhough at present there seems no hope that OPV cells would be able to

replace silicon based cells, advances in interdisciplinary research combining materials chemistry, device physics, micro as well as nanostructural fabrication technology definitely hold promise.

Basic principles and device architecture

The basic device structure of an organic photovoltaic (OPV) cell is same as that of an OLED as discussed in section 1.2(a), only the working principle is opposite. A common OPV cell assembly (see figure-1.6) has a planar layered structure with a PEDOT : PSS layer spin coated onto ITO coated glass substrate, on top of which a blend of donor and acceptor organic materials is deposited and a final LiF/Al layer as the counter electrode completes the device architecture.[38] This kind of OPV cell architecture is typically referred to as a bulk heterojunction (BHJ) solar cell pointing to the donor-acceptor interface within the blend. [39]

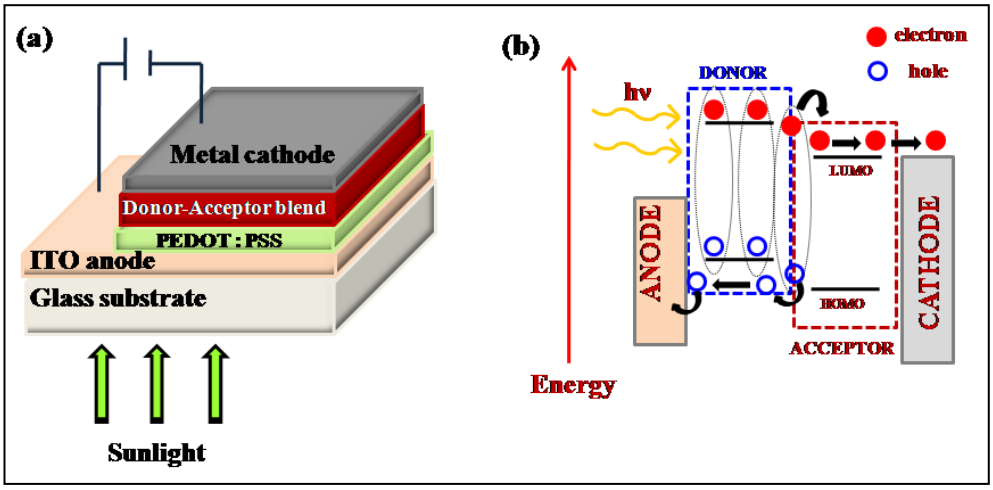

Figure-1.6 (a) OPV cell components (b) Energetics of light absorption and charge collection.

Sunlight is converted into electric power in organic solar cell by a mechanism known as photoinduced electron transfer and the basic steps involved are:

(1) Absorption of photon

(2) Creation of exciton

(3) Exciton diffusion to donor-acceptor interface

(4) Charge transfer from donor to acceptor to form $[D^{\bullet+}A^{\bullet-}]^*$

(5) Charge separation of coloumb bound $[D^{\bullet+}A^{\bullet-}]^*$

(6) Charge transport of holes and electrons through donor and acceptor phase respectively

(7) Charge collection at respective electrodes.

When light is absorbed by the active material, an electron is promoted from the HOMO to the LUMO leaving a hole in former and an electron in the latter. This excited state electron-hole pair called exciton is still held together by columbic forces. The excitons have to diffuse through the material to reach the D-A interface before recombination occurs. When the LUMO of acceptor is minimum 0.3 eV lower than that of donor, efficient charge transfer occurs leading to a radical cation of donor ($D^{\bullet+}$) and radical anion of acceptor ($A^{\bullet-}$). This energy offset is essential to overcome the exciton binding energy (0.3 - 0.5 eV for polymers and upto 1eV for small molecules) and also to slow down back electron transfer.[40-42] Further charge separation occurs at interface giving rise to electrons and holes which can drift and diffuse towards opposite electrodes through acceptor (A) and donor (D) material respectively with efficiency depending on their mobilities. In π-conjugated molecules, since the extent of electron-phonon (lattice vibration) as well as disorder effects are large, each charge is associated with some geometric relaxation and constitute a radical ion or a polaron which hops from molecule to molecule.[43] The average distance travelled by the exciton is called exciton diffusion length which is typically 5-20 nm.[44-46] Thus the donor-acceptor phase separation length should be of the same order of magnitude as the exciton diffusion length or the excitons will decay via radiative or non-radiative pathways and will not contribute to power conversion. Earlier OPV device architectures were of bilayer type where the donor and acceptor layers were stacked on top of each other sequentially. Such devices exhibited very low efficiencies because excitons were produced only within the distance of 10-20 nm from the D-A interface and this lead to loss of photons absorbed away from the interface.[47] To a large extent this problem was

overcome by the bulk heterojunction (BHJ) strategy first offered by Sariciftci *et al.*, where they mixed a fullerene (C_{60}) derivative as the electron acceptor with a donor PPV conjugated polymer.[48,49] In bulk heterojunction a donor-acceptor nanoscale blend network with 10-20 nm scale phase separation is obtained so that each interface is within a distance less than the exciton diffusion length. Eventhough the evolution in OPV structure from bilayer to BHJ improved the solar cell efficiency by several orders of magnitude [50] the morphological instability of blend systems are limiting their use. The ideal desired bulk heterojunction structure is the one in which the donor and acceptor phases are interspaced with an average length scale of 10-20 nm equal to or less than the exciton diffusion length. Interdigitated D-A phases in percolated highways will help ensure high charge carrier mobility with negligible recombination pathways. Block copolymer architectures are good prospects for this purpose, since they undergo a thermodynamically favoured segregation process referred to as microphase separation in nanometre length scale.[51,52,53] Figure-1.7 gives a comparison of the above discussed three types of OPV device structures.

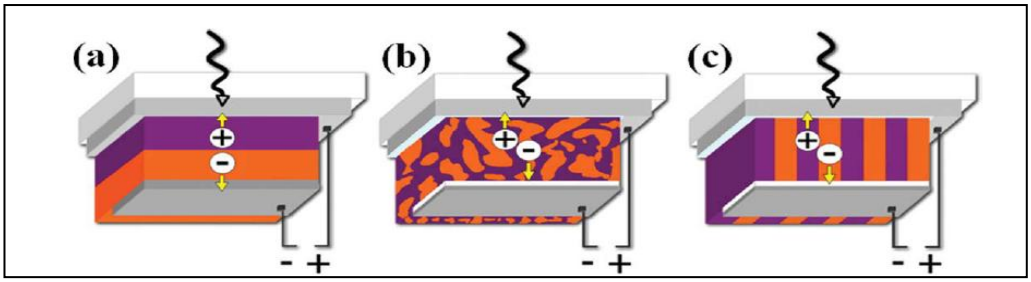

Figure-1.7. A (a) Bilayer (b) Bulk Heterojunction and (c) Ideal interdigitated D-A block copolymer type OPV device architectures.[*Adapted from ref.53*]

Electrical characteristics of a solar cell device

The solar cell in the dark acts as a simple diode and the equivalent circuit is given in figure-1.8 (a). It comprises of (i) a p-n junction diode with saturation current I_0 (current in the dark at reverse bias) (ii) a source to provide current that corresponds

to photocurrent I_L generated during illumination (iii) series resistance R_s that accounts for all the resistances at interface in the layers, the conductivity of semiconductors and electrodes. (iv) shunt resistance R_{sh}, which accounts for the current leakage arising from defects in films. Low value of R_s and high value of R_{sh} gives good device performance.

The characteristic current-voltage (I-V) curve of the cell in dark and light are shown in figures 1.8 (b) & (c) respectively. When the cell is illuminated (i.e., short circuited) the current is maximum through the circuit and is called short circuit current (I_{sc}). Under open circuit conditions (i.e. dark) no current flows and voltage is maximum that can be attained between two electrodes which is referred to as open circuit voltage (V_{oc}). The point in the I-V curve that gives the maximum product of current and voltage is called the maximum power point (MPP).[50]

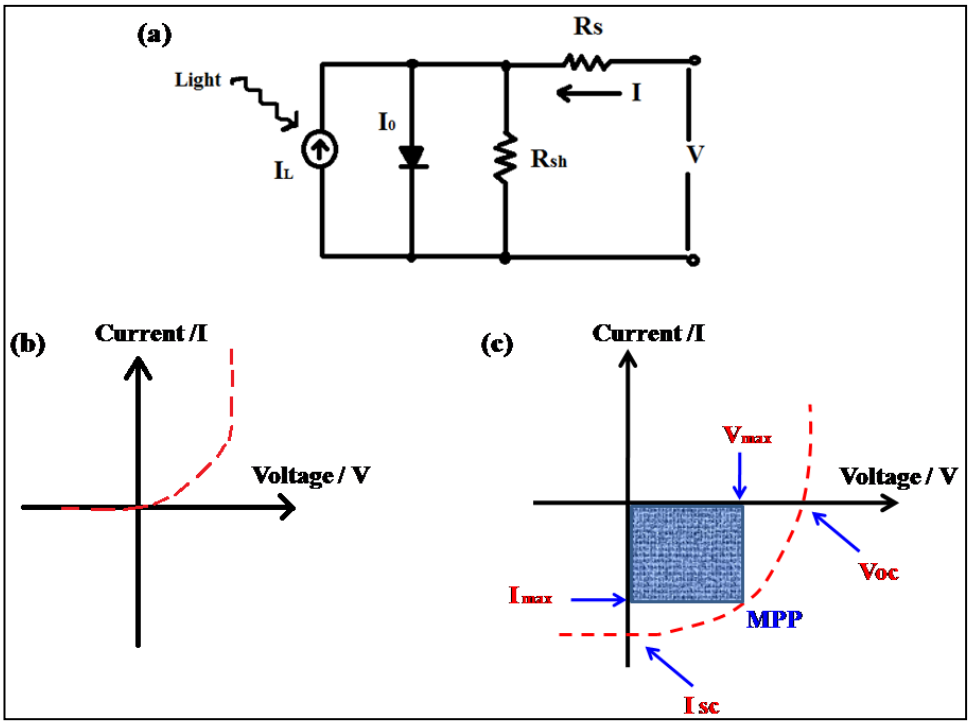

Figure-1.8. (a) Equivalent circuit of solar cell and **I-V curve** under dark (b) & under illuminated (c) conditions. The maximum output is represented by the shaded square in (c) which is the product $I_{max}V_{max}$.

The general expression for current in the circuit is given by equation (1) given below:

$$I = I_0\left[\exp\left[\frac{e(V - IR_s)}{nkT}\right] - 1\right] + \frac{[V - IR_s]}{R_{sh}} - I_L$$

where 'e' is the charge of electron (1.6 x 10^{-19} C), 'k' is the Boltzmann constant (1.38 x 10^{-23} JK^{-1}), T is the absolute temperature of the cell in Kelvin, 'n' is a constant between 1 and 2, V is the terminal voltage.

Some critical parameters determining the solar cell performance are described as

(1) Pmax, which is the maximum power output of a solar cell and is given by

$$Pmax = Imax \times Vmax$$

(2) Fill factor (FF) which shows how much power is produced by the cell with a given Isc and Voc in practice compared to the theoretically possible value. Higher the FF value, better the device.[54,55] Typical FF values for OPVs are in the range 0.4-0.6. It is given by the expression

$$FF = \frac{Imax \times Vmax}{Isc \times Voc}$$

(3) Another term that defines the quality of energy conversion is the quantum efficiency (QE) of the solar cell. It is defined as the number of charge carriers generated at the electrode per number of incident photons. If every incident photon generates one collected charge carrier, QE = 1 (i.e., no recombination losses). For inorganic PVs the value of QE reaches upto 80-90 %, whereas in organic PVs it is only in the order of 1%.

Finally the most important parameter that is used to compare solar cells is their photovoltaic power conversion efficiency (η) - PCE which is the ratio of power output (P_{max}) produced by the cell to the incident light power (P_{input}).

$$\eta = \frac{P_{\max}}{P_{\text{input}}}$$

(or)

$$\eta = \frac{FF \times Isc \times Voc}{P_{\text{input}}}$$

The PCE value of single layered OPV is below 0.1 % compared to crystalline Si cells having nearly 25 % efficiency. The efficiency of solar cells also depend upon the temperature of the cell, quality of illumination (total light intensity) as well as on the spectral distribution of intensity. In order to facilitate comparable testing of solar cells between different laboratories, a standard measurement condition has been developed. Under this standard condition for testing of terrestrial solar cells, the light intensity should be 1000 W/m^2 with a spectral intensity distribution matching that of the sun on earth surface at an incident angle of 48.2°, which is called AM 1.5 global std. solar spectrum (AM - air mass) and temperature should be 25 °C.[56] The output power of solar cell under these conditions is called nominal power of the cell and is reported in Watts peak (Wp).

1.2.3. Organic Field Effect Transistors (OFETs)

Field effect transistors are the basic building blocks of all integrated circuits and their purpose is to amplify and switch electronic signals. OFETs are attractive not only technologically, but also from the scientific point of view they have proven to be a unique tool for investigating charge transport of organic π-conjugated materials. OFET is one among the very important techniques used to determine the charge carrier mobility (μ, the drift velocity of carriers under unit electric field) of organic semiconductors which is the key parameter influencing the device performance of all organic electronics.

Working principles and Device characteristics

The essential components of a general OFET are a substrate, three electrodes (source, drain and gate) and a thin organic semiconducting layer (figure-1.9(a)). An insulating dielectric separates the organic semiconductor from the gate electrode. The source and drain electrodes in contact with the semiconducting layer are

separated by a distance (L) called the channel length and their width is termed channel width (W).[57]

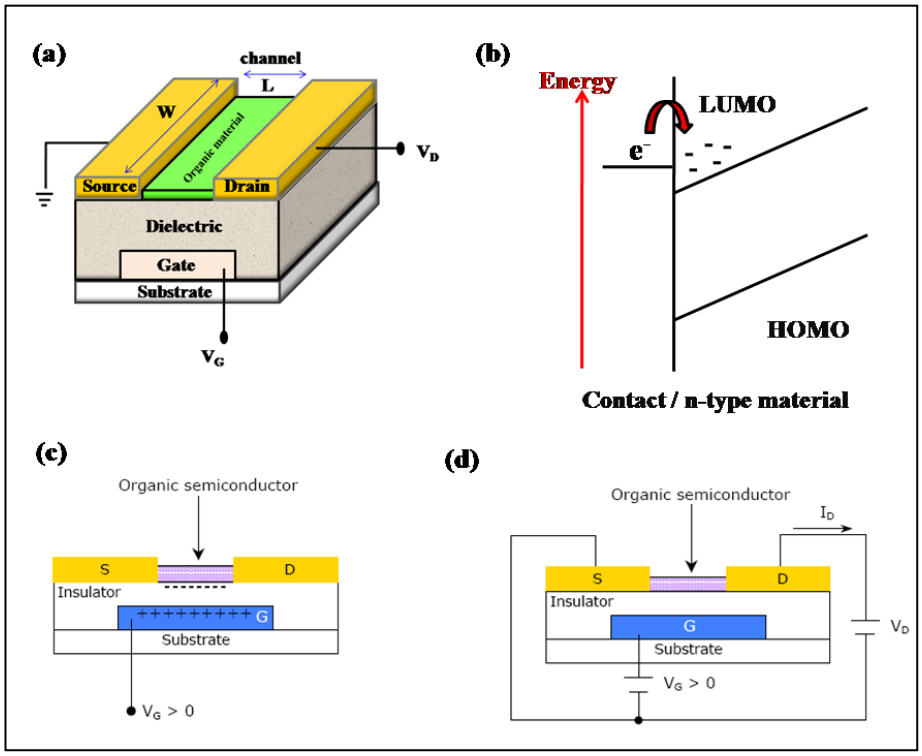

Figure-1.9. (a) Schematic OFET structure (b) Energetics of electron injection from FET source contact into LUMO of n-type semiconductor (c) Accumulation of positive charges when $V_G > 0$ and induced negative charges at the interface (d) Current induced from drain to source when a voltage is applied between source and drain.

The potential difference between the source and the drain is called source-drain voltage (V_D) and that between gate electrode and source is called gate voltage (V_G). When a voltage is applied between gate and source a capacitance (C) is formed and if $V_G > 0$ (i.e., a positive voltage) there will be accumulation of negative charges at the semiconductor- insulator interface within the channel (figure-1.9(c)). At the same time applying a voltage V_D between source and drain makes the induced negative charges to move across the channel resulting in a current flow (I_D) from drain to source (figure-1.9(d)). When V_G is switched off,

induced charges vanish and no current flows. This is called an n-channel OFET. The opposite happens in a p-channel OFET, where the applied voltage $V_G < 0$ (i.e., a negative voltage) with negative charges accumulating in the gate and positive charges induced at interface.

The conductivity (σ) of the semiconductor is proportional to the charge carrier mobility (μ) and concentration (n) of the carriers given by equation (1)

$$\sigma = en\mu \quad (1)$$

where 'e' is the unit electronic charge and 'n' is proportional to the capacitance of the insulator and magnitude of the applied electric field. Thus the conductivity of the semiconductor can be modulated by varying electric field and that is why it is referred to as field effect.

The typical OFET output characteristics (I_D vs V_D at different V_G) is shown in figure 1.10. in which the source-drain current I_D increase with V_D for different values of V_G.

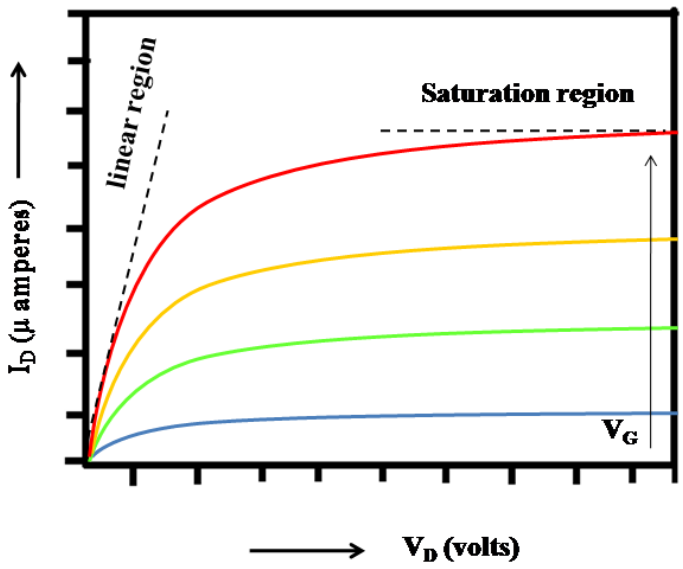

Figure-1.10. (a) Schematic plot of OFET output characteristics.

For low values of $V_D << V_G$, the current I_D increase proportionally to V_D and this region is called 'linear region' where charge carrier mobility (μ) independent of V_G can be described by equation (2). Here μ_{linear} is the mobility in linear regime and V_{Th} is the threshold voltage at which induced carriers start moving, so that a gate voltage V_G greater than threshold voltage has to be applied to make the carriers start moving. A plot of $I_{D,linear}$ versus V_G at constant V_D is referred to as the transfer characteristics plot from which μ_{linear} can be calculated according to equation (3).

$$I_{D,linear} = \frac{W}{L}\mu_{linear} C[(V_G - V_{Th}) - \frac{V_D}{2}] V_D \quad (2)$$

$$\mu_{linear} = \frac{\partial I_{D,linear}}{\partial V_G} \times \frac{L}{WCV_D} \quad (3)$$

When $V_D \geq (V_G - V_{Th})$ the source-drain current I_D becomes saturated and saturation region (flat region shown in the graph) can be described by equation (4) and assuming $\mu_{saturation}$ to be independent of V_G is calculated from the plot of square root of $I_{D,saturation}$ versus V_G in accordance with equation (5). Extrapolation of the linear slope to zero gives the threshold voltage V_{Th}. The V_G dependent saturation mobility can be calculated using equation (6).

$$I_{D,sat} = \frac{W}{2L}\mu_{sat} C (V_G - V_{Th})^2 \quad (4)$$

$$\sqrt{\mu_{saturation}} = (\partial I_D / \partial V_G) \times \sqrt{(2L/WC)} \quad (5)$$

$$\mu_{saturation} = (\partial I_D / \partial V_G) \times \frac{L}{WC(V_G - V_{Th})} \quad (6)$$

Three important parameters defining the OFET device performance are:

(1) threshold voltage (V_{Th}) (2) current on-off ratio (I_{on}/I_{off}) and (3) field effect mobility (μ). The threshold voltage (V_{Th}) determines the value of the gate voltage V_G above which a source-drain current I_D can flow and the effective gate voltage is thus (V_G - V_{Th}). Higher value of (V_{Th}) causes high power consumption and it can be minimized by increasing gate capacitance. The current on-off ratio (I_{on}/I_{off}) defined as the ratio of maximum on-state current to the minimum off-state current,

should be of the order 10^6 - 10^8 in order to obtain a clear distinction between on and off states in electronic circuits.[58] Further the most important factor mobility (μ) should be as high as possible so that power consumption can be reduced maximally.

1.3. Experimental Techniques to Measure Mobility (μ)

Charge carrier mobility (μ) of the active material is the key parameter that affects the efficacy of all the organic electronics mentioned in the above discussion. The different methods that are used to measure the charge mobility in organic materials are divided into two types:

- Steady state methods: Space-charge-limited current (SCLC) characteristics and Field effect transistor (FET) I-V characteristics.
- Transient methods: Time of flight (TOF), dark injection (DI) transient current and time resolved electroluminescence techniques.

Of these, not all the techniques are suitable for a sample and the choice of method depends upon details such as type of material, sample thickness, nature of electrodes as well as energy levels of the materials. The most widely used methods are SCLC, FET and TOF out of which FET technique has already been discussed above. So this section will briefly introduce the SCLC and TOF measurements.

1.3.1. Space-Charge Limited Current-Voltage Characteristics (SCLC)

The experimental set up for this method consists of the organic layer sandwiched between two electrodes and uses a steady state voltage source and after applying a voltage through the sample, the current produced is measured.[15] The current-voltage characteristics are then fitted to particular models based on two assumptions: (i) the charge transport is due to a single type of carrier only and (ii) the contacts are ohmic. From the acquired current-voltage behaviour at high electric fields, the mobility is calculated. However at lower injection levels, the presence of traps due to disordered nature of organic materials causes a reduction

in current. Figure-1.11 shows the predicted crossover from the Ohmic region to the space-charge-limited current at higher electric fields.[59]

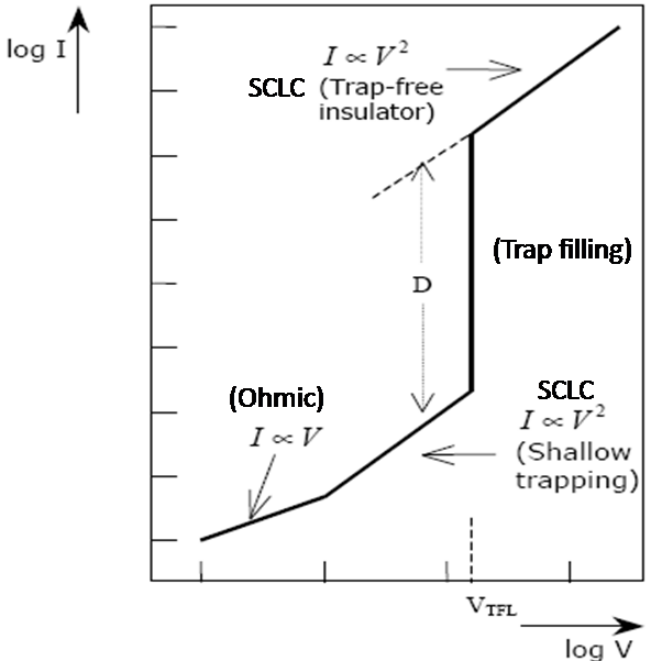

Figure-1.11. (a) Schematic I-V characteristic for one carrier SCLC injection controlled by single set of traps. [*Adapted from ref.59*]

The first part of the graph corresponds to ohmic region (I α V), the second part corresponds to shallow trapping and when electric field is further increased all traps are filled at once. Finally the third part, trap-free SCLC region is reached where I α V^2 and the mobility can be most accurately determined from this region. Even if the trap-free regime is not available by experiments, the lower limits for intrinsic mobilities can be obtained by Child's law (Mott-Gurney equation) [60,61]:

$$J_{SCLC} = \frac{9}{8}\varepsilon_0\varepsilon_r\mu\,\frac{V^2}{L^3}$$

where J_{SCLC} is the current density, V the applied bias voltage, ε_0 the permittivity of free space, ε_0 the relative dielectric constant of the medium and L is the thickness of the device.

1.3.2. Time of Flight Method (TOF)

For TOF measurements an organic layer is embedded between two electrodes and irradiated by a short laser pulse near to one of the electrodes and this generates a thin layer of electron-hole pairs close to the contact.[15,62] Depending on the polarity of the applied electric field the photogenerated charges move across the layer towards the other electrode where the time dependent current is monitored. All the carriers simultaneously reach the electrode in case of highly ordered crystalline materials, whereas for amorphous systems the signal is broadened. Mobility is then calculated according to the equation:

$$\mu = \frac{d}{Ft} = \frac{d^2}{Vt}$$

where d is the distance between the electrodes, F is the electric field, t is the averaged transient time, V is the applied voltage.

1.4. Molecular Packing Dependence of Charge Carrier Mobility

Mobility of charge carriers in conjugated semiconductors is intimately related to the extent of π-overlap between neighbouring molecules which in turn depends upon the conjugation length, degree and packing of the organic molecules.[63-67] Four different types of packing motifs studied in organic molecules [68-72] are (see figure-1.12) (i) herring bone packing (face-to-edge) without π-π overlap between adjacent molecules. This type of molecular arrangement favours 2D transport within the stacked layers but transport between the molecular layers is very much lowered. Pentacene single crystal is an example which exhibits this type of packing in its solid state and its mobility values range from 0.7 -2.3 $cm^2V^{-1}s^{-1}$ when measured in different directions (0 to 360°) due to the anisotropy effect. [71](ii) Herringbone packing with co-facial π-π overlap (face-to-face) between adjacent molecules which is predicted to result in much stronger electronic coupling among molecules and it is also sometimes referred to as slipped π-stacking

arrangement.[73] Rubrene and some derivatized pentacene as well as tetrathiafulvalene molecules have been shown to attain this type of packing.[74-76] However nowhere it has been proved that co-facial packing is superior to herringbone or vice versa. Rest of the two packing types are (iii) lamellar 1D π-stacking and (iv) lamellar 2D π-stacking. Amongst the four packing motifs, lamellar 2D or brickwork π-stacking (e.g. TIPS-PEN which gave mobilities as high as 2.8 $cm^2V^{-1}s^{-1}$)[69] is considered most efficient for transporting charges via shortest route almost a straight line. The best method to track the packing influence of organic semiconductors on mobility is to study the charge transport in highly ordered single crystals which are free of grain boundaries and traps. At the same time device fabrication using crystals has to overcome several shortcomings like small size, fragility etc, which makes it very difficult.[77,78]

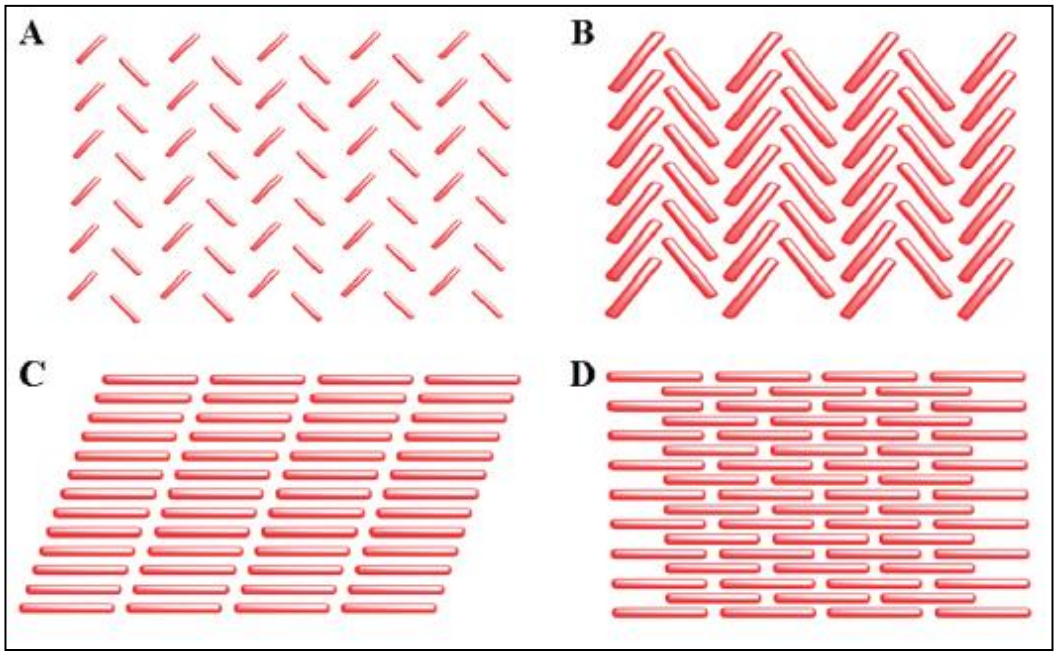

Figure-1.12. Molecular packing motifs (A) Herringbone packing (B) Slipped stack (C) Lamellar 1D stack (D) Lamellar 2D stack or Brickwork packing. [*Adapted from ref.72*]

1.5. Organic Semiconductor Materials

Organic semiconductor materials are classified into two categories: polymers and the small molecules. 'Small molecule' is a phrase widely used to refer to those compounds with a well-defined molecular weight which range from strictly single unit compounds to oligomers of three or four repeat units to low generation dendrimers,[79,80] whereas polymers are long-chain molecules consisting of an indeterminate number of molecular repeat units. Even though differences between the properties of the low molecular-weight organic materials and polymers for organic electronic applications are highlighted more, in fact there are more similarities than differences in terms of both their electronic and optical properties, with the major distinction being in the methods of thin-film deposition and device fabrication.[81,82] There are few strategies for purifying the polymer material based on molecular weight alone, due to the dispersity of molecular weights depending on the length of the polymer chain in solution. On the other hand, small-molecule materials have the possibility of straightforward separation of the host from the impurities because of their well-defined molecular weights. Polymers in general are solution processed, can be uniformly applied across the entire substrate either by spin-on or spray-on techniques. Finally after deposition the solvent is evaporated off resulting in very uniform films of approximately 100 nm thickness, as required in most devices such as OLEDs and OFETs. On the other hand thermal sublimation in vacuum[83] and organic vapour phase deposition (OVPD)[84,85] are the most common means for depositing low-molecular-weight thin films due to their low solubility in common organic solvents. Small molecules have precise dimensions and exact composition, whereas polymers exhibit a higher molecular disorder. Consequently polymers tend to be less efficient charge transporters than small molecules leading to a mobility limit of perhaps two orders of magnitude smaller than that of small molecule. Hence, even though there is least scope for commercial practical application, the fundamental material characteristics of organic semiconductors are best measured in single crystals with highest mobilities obtained due to high molecular order as well as absence of grain boundaries.[74,86]

Depending on the nature of charge carriers organic semiconductor materials are classified into p-type and n-type materials. p-Type semiconductors are materials in which the majority of carriers are holes whereas in n-type semiconductors the majority of carriers are electrons. The device development using the n-type semiconductors are till date far from the performance achieved with p-type materials. This is due to the fact that the transport in n-channel conductors is degraded easily by air, which acts as electron traps together with the dielectric surface trapping sites. Also, most of the known organic materials tend to be better hole conductors than electrons. As a result, there is currently a growing interest in developing new n-type materials in order to meet the desired criteria.[87] Thus it appears imperative to achieve device performances with n-type semiconductors of the same order as the ones already achieved with p-type semiconductors. Further the ultimate challenge lies not only in finding new materials with high electron mobility but also at the same time these materials should be able to surpass the deterioration of the electronic properties over long periods.

1.5.1. p-type Organic Semiconductors

Some of the common and established p-type semiconductors are shown in Chart-1.2. Fused acenes are possibly the most important family of donor organic semiconductors, of which especially pentacene (**p1**) is well known to exhibit extremely high hole mobility upto 3 $cm^2V^{-1}s^{-1}$ in thin films while single crystal mobilities reached upto 35 $cm^2V^{-1}s^{-1}$. [88-91] Modified pentacene derivatives with triisopropylsilylethynyl solubilizing groups (**p2**) named as 'TIPS-PEN' have also been introduced to overcome the disadvantages of "herringbone" packing of pentacene, because it undergoes "bricklayer" crystallization.[72,92-94] Other important class is the dye based donors such as phthalocyanines (Pc) especially Cu-phthalocyanine-CuPc (**p3**), merocyanine-MC (**p4**), squaraine-SQ (**p5**), borondipyrromethene -BODIPY (**p6**), diketopyrrolopyrroles-DPP (**p7**) etc.[95] Oligo- and poly-thiophenes which by themselves form a separate class of p-type

semiconductors have been widely studied due to their high charge carrier mobility and facile synthesis to tune energy levels.[72] For example oligomeric 2,5-linked thiophene rings especially the sexithiophene (hexamer) shows good p-type properties but has solubility issues, whereas regioregular n-hexyl substituted polythiophene-P3HT (**p8**) showed better solubility and self-organization behaviour with improved mobilities upto 0.1 $cm^2V^{-1}s^{-1}$.[96,97] A liquid crystalline thiophene polymer (**p9**) has been reported with mobility of 0.7 $cm^2V^{-1}s^{-1}$.[98] Other solution processable best performing thiophene based donors include benzothieno[3,2-b]benzothiophene (BTBT), dithieno[3,2-d;2',3'-d']benzo[1,2-b;4,5-b']dithiophene (DTBDT) etc.[103-105] Apart from these some discotic liquid crystalline p-type semiconductors such as hexabenzocoronene (**p10**) and triphenylene (**p11**) derivatives are also well studied. [99-102]

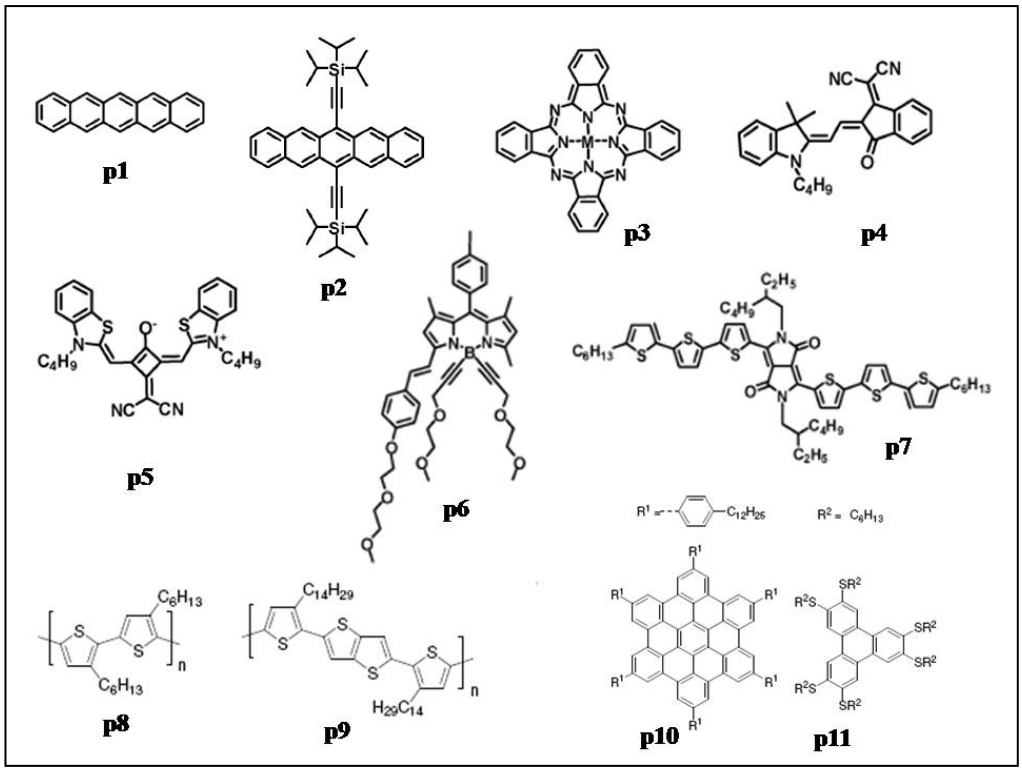

Chart-1.2. A selection of p-type organic semiconductor materials.

1.5.2. n-type Organic Semiconductors

Eventhough n-type semiconductors are of equal importance as p-type semiconductors for the development of high performance organic electronics, much less reports are available in literature for the former compared to latter. One of the possible reasons is that there are only few semiconductors that have high electron affinity and most of the available n-type materials are unstable in air. However past five years have seen tremendous change in the situation and several high performance n-type semiconductors are now being explored. Fullerenes (C_{60}) and their derivatives (especially Phenyl-C61-butyric acid-methyl ester -$PC_{61}BM$) still by far dominates the acceptor class of materials due to their strong tendency to accept upto six electrons per molecule and high electron mobilities (4-6 $cm^2V^{-1}s^{-1}$) even in composite film form.[72] But their insufficiencies such as tedious synthesis procedures, low solubility, limited spectral breadth and bandgap variability have resulted in the search for novel non-fullerene acceptors that combine the favorable electron affinity, high mobiliity as well as broader absorption spectra. Chart-1.3. summarizes the chemical structures of the n-type semiconductors discussed here.

Among the non-fullerene acceptors rylene (perylene and naphthalene) diimides are the most promising candidates due to their attractive package of excellent thermal and photostability, large absorption coefficients, easy modulation of HOMO-LUMO energies through variation of substituents at imide nitrogen atom or rylene core and same time electron affinities and mobility comparable to fullerenes.[72,95,106] These rylene based n-type small molecule and polymeric semiconductors are also the topic of interest for this thesis and therefore will be discussed in detail in the following sections. Other non-fullerene acceptors based on the concept of introducing electron withdrawing groups like fluorine or cyano to the periphery of aromatic groups include examples such as perfluoropentacene,[107] hexadecafluorinated copper phthalocyanine [108,109] with electron mobilities upto $5x10^{-3}$ $cm^2V^{-1}s^{-1}$, oligothiophenes with perfluorinated substituents like DFCO-4T (5,5'''-bis(perfluorophenyl)-2,2':5',2'':5'',2'''-quaterthiophene)[110] with high electron

mobility of 0.5 $cm^2V^{-1}s^{-1}$ from thermally evaporated film, a novel indenofluorenebis(dicyanovinylene) (TIFDMT) core based semiconductor with 0.10-0.16 $cm^2V^{-1}s^{-1}$ electron mobility[111] and so forth. An ideal n-type material requires its LUMO energy level to be close to the work function of metal electrodes. Although lower work function of electrodes like Al, Ca and Mg are matching with the LUMO of n-type materials, they are highly susceptible to oxygen and hence can form charge transfer complexes with semiconductors, which decreases their mobility. Thus it has been reported that n-type materials with ambient stability require desirable electron affinities greater than 4 eV.[112] A best illustration of the current state of knowledge of n-type materials with the highest reported electron mobilities is given by the graph in figure-1.13.[113]

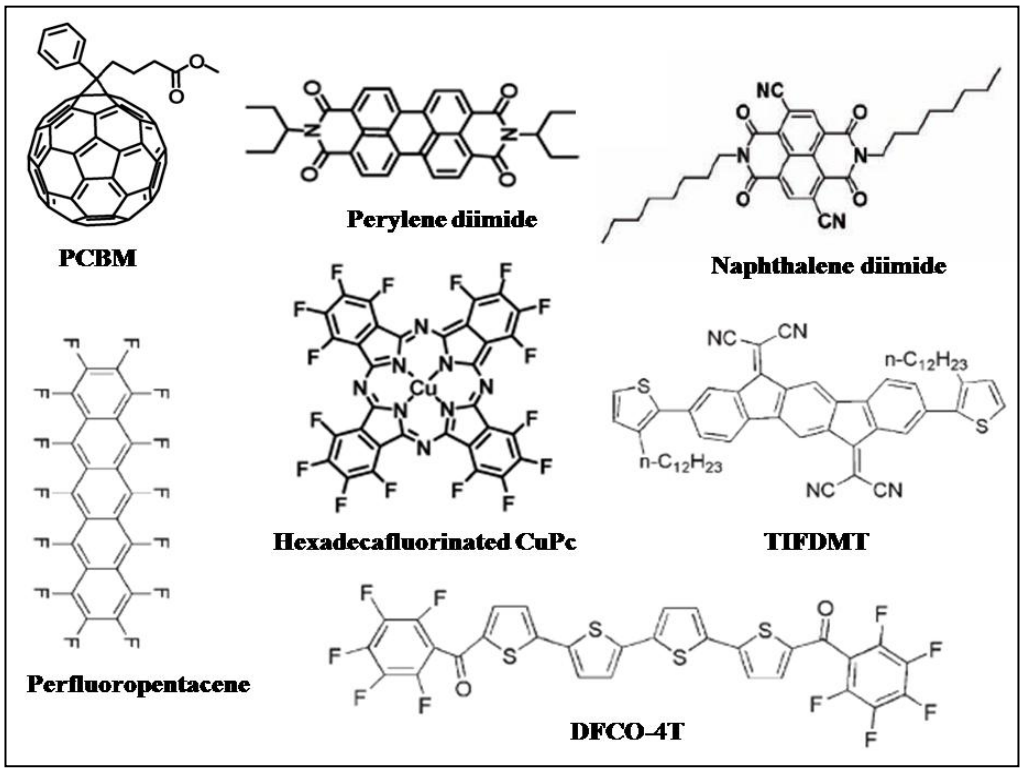

Chart-1.3. A selection of n-type organic semiconductor materials.

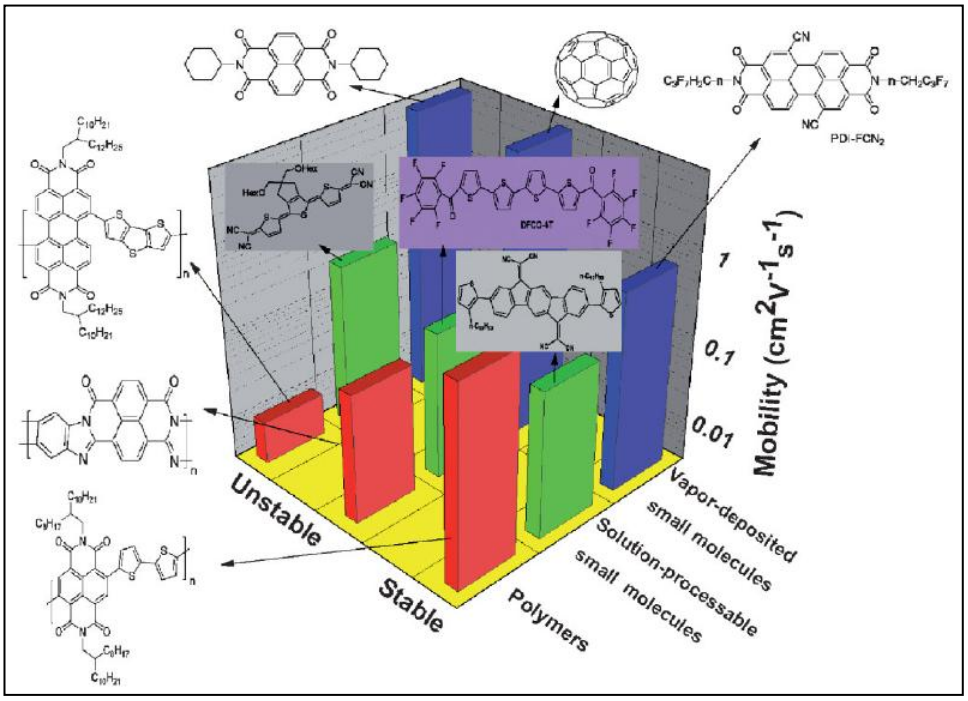

Figure-1.13. Typical n-channel small molecules and polymeric semiconductors with highest reported mobility values. [*Reproduced from ref.113*]

1.6. Rylenebisimides based N-type Semiconductor Materials

Rylenes are a category of organic dyes consisting of basic naphthalene units connected in peri-position; two such units make a perylene, three units a terrylene and so on. With increase in size, the energy gap between the HOMO and LUMO of the dyes decreases and they absorb light at longer wavelengths. Among the rylene dyes the most celebrated member is the perylene dye which is known for nearly 100 years and especially the much more photostable and soluble derivative viz., perylene-3,4,9,10-tetracarboxylic acid diimide first prepared by Kardos in 1913, from the parent compound perylene-3,4,9,10-tetracarboxylic acid dianhydride (PTCDA) (see fig-1.14 for structures).[114,115] Earlier perylene-3,4,9,10-tetracarboxylic acid diimides usually named as perylene diimides or bisimides (PDI or PBI) were extensively used as industrial dyes (soluble) and pigments (insoluble), due to their intrinsic insolubility, light- and weather fastness, high thermal stability, chemical inertness and most importantly due to high tinctorial strength with colors

ranging from red to maroon to violet and even shades of black.[116] The latest application of perylenebisimides are in the field of organic electronics as an established class of n-type semiconductors used in organic field effect transistors and organic photovoltaics including dye-sensitized solar cells.[72,95] This interest in PBIs as acceptor materials originates from their unique combination of properties such as high electron affinity, near unity fluorescence quantum yields, high photochemical stability, large molar absorption coefficients, excellent self-assembling ability via π-π stacking and versatile structural modification by infinitely variable synthetic space.[116-120] Additionally due to their tunable optical and reversible redox properties with easily identifiable excited state, anion and dianion PBIs also play a key role in understanding fundamental research on photoinduced energy and electron transfer processes.[116,121-123]

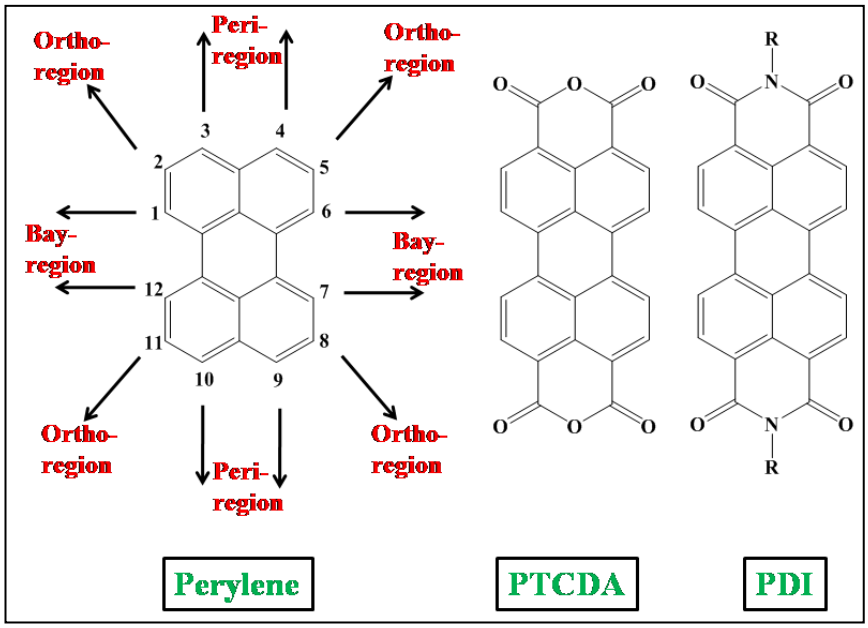

Figure-1.14. Chemical structures of perylene, PTCDA and a generic PDI.

The lower member of the rylene diimide family viz., the naphthalene-1,4,5,8-tetracarboxylic acid diimides (NDI or NBI) have also received significant attention in the recent years as air-stable high mobility n-type semiconductor, for e.g. a recent report from Facchetti *et al.* describing an alternating NDI-bithiophene

polymer exhibiting electron mobilities upto 0.85 $cm^2V^{-1}s^{-1}$ under ambient conditions.[124] NDIs are an attractive class of target materials to be explored as n-type semiconductors due to their robust nature, flexible molecular orbital energetics and excellent charge transport properties tailorable via judicious functionalizations. The naphthalene core possess large electron-affinity and its derivatives are easy to synthesize and purify due to better solubility than PDIs. The NDI derivatives have also been extensively utilized to construct several elegant self-assembled architectures such as organogels, foldamers, synthetic ion channels, rotaxanes and many other supramolecular photosystems.[125-130] However compared to PDI based materials, the smaller fused ring unit NDI derivatives possess a larger bandgap and thus absorb poorly in the visible spectrum (usually onset less than 400 nm). Thus NDIs as acceptors are less successful in OPVs compared to PDIs, but they perform exceedingly well in OFETs. Nevertheless, both these chromophores are most promising candidates for future n-type organic materials.

1.6.1. Synthesis

The perylene core has twelve functionalizable regions at (fig-1.14) - the 3,4,9,10-positions known as the "peri" or imide region; 1,6,7,12- positions known as the "bay"-region and the 2,5,8,11-positions known as the "ortho" regions. Whichever be the type of functionalizations, the starting material for all types of PDI is the commercially available PTCDA, which in turn is obtained industrially through a series of steps beginning with the air oxidation of acenaphthene (A) (fig-1.15) to give naphthalene-1,8-dicarboxanhydride (B) using a vanadium catalyst or nitric acid.[119] This is subsequently treated with ammonia to provide naphthalene-1,8-dicarboxylic acid imide (C) which on oxidative dimerization with molten alkali (KOH) at ~ 200 °C gives perylene-3,4,9,10-tetracarboxylic acid diimide (D). Saponification with hot concentrated sulphuric acid gives the perylene tetracarboxylic acid dianhydride -PTCDA (E). Simple imidization reaction of PTCDA with primary amines gives the insoluble perylene dyes or pigments with high melting points required for industrial applications.[119]

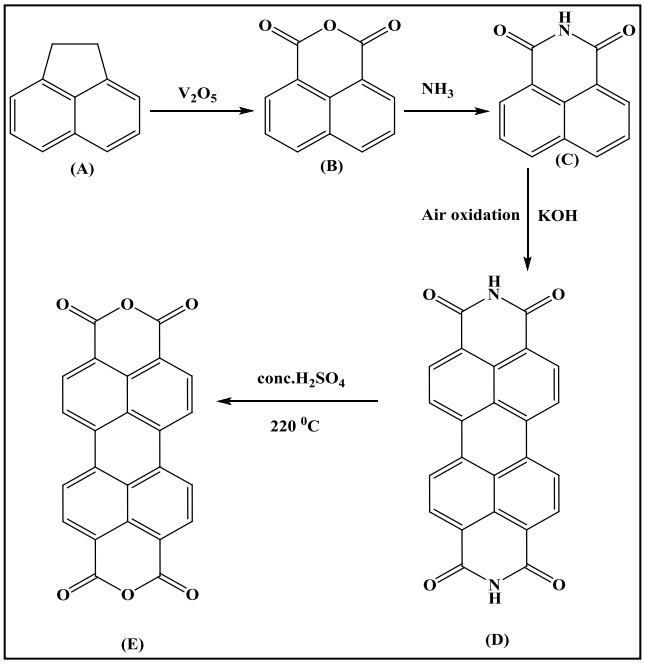

Figure-1.15. Preparation of PTCDA.

Symmetrically substituted derivatives

The synthesis of symmetrically peri-substituted PDIs from the parent PTCDA is straightforward involving the condensation reaction between aliphatic or aromatic primary amines and PTCDA at high temperatures (> 160 °C) leading to different N,N'-dialkyl or N,N'-diaryl PDIs (figure-1.16).[116]

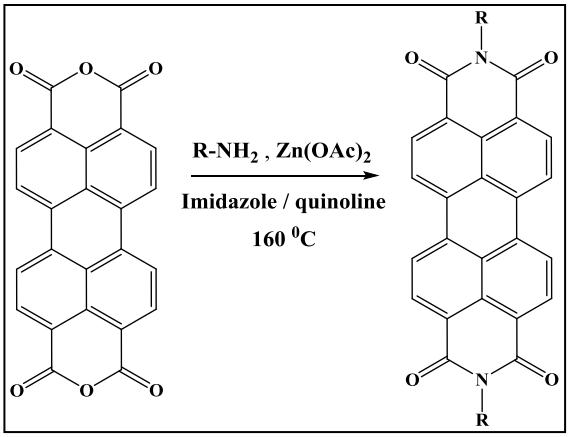

Figure-1.16. Synthesis of symmetric N, N'- dialkyl or diaryl PDIs.

The condensation of PTCDA with reactive aliphatic amines can be carried out without any problems even in water.[119] However for less reactive aliphatic amines and all aromatic amines the use of basic solvents like quinoline or molten imidazole is necessary.[119] Zinc salts like anhydrous zinc acetate or zinc chloride are unavoidable catalysts (10-30 mol %) for the reaction.[119] Other metal salts, for example iron, lead or copper salts are also useful, but less effective. The exact role of zinc salts is not clear - they are denoted as dehydrating reagents. It is proposed that zinc salts might be acting as solubilizers on the basis of complexation with the anhydride.[119] The perylene bisanhydride or the bisimide with no alkyl substitution are insoluble in any organic solvent, hence no coloration or fluorescence. However PDI derivatives for organic electronics applications, photoinduced processes and supramolecular organization requires reasonable solubility in common organic solvents. Langhals and co-workers were the first to employ the solubilizing branched chain alkyl substituents called "swallow tail" to the imide nitrogen atom to produce highly organic-soluble symmetrical PDIs.[119,131] Another approach is to incorporate bulky aryl substituents like diisopropylphenyl group which makes the PDI soluble in most of the organic solvents such as dichloromethane, THF, acetone, toluene etc.[119] By incorporating hydrophilic moieties like oxyethylene groups, Newkome-type carboxylates, phosphate surfactants, polyglycerol dendrons, cyclodextrin etc. water soluble PDIs have been realized.[132-135] Varying the imide substituents does not alter the optical properties and HOMO-LUMO energies of PDIs because the presence of nodes at the imide nitrogen atom prevents the conjugation between perylene core and the imide substituents.[136]

Unsymmetrically substituted derivatives

The synthesis of non-symmetrically substituted PDIs with different substituents on each imide position via stepwise condensation of PTCDA with primary amines is impossible. This is because the minor amounts of each amine reacts with the anhydride to give the corresponding symmetrical PDIs in small amounts plus a large excess of unreacted dianhydride.[119,137] As a result unsymmetrical PDIs are

synthesized using several complex multistep procedures. Earlier attempts from Nagao, Misono and co-workers reported a synthetic route to a mixed mono-imide-mono-anhydride derivative by partial saponification of symmetrically substituted PDIs by conc.H_2SO_4 at 180-200 °C, but rather rough conditions limited this interesting method.[138] Another elegant method developed by Tröster,[139] converted the insoluble PTCDA to the tetrapotassium salt that is readily water soluble (figure-1.17). The monoanhydride monopotassium salt is precipitated by a moderate acidification with orthophosphoric acid or acetic acid since the latter can easily be washed off. [140] The driving force for the formation of monoanhydride monopotassium salt is its extraordinarily high lattice energy - it is absolutely insoluble in any solvent, even at high temperatures which removes it from the protonation equilibria and this salt upon condensation with primary amines in water gives the mono-imide-mono-anhydride derivative in large amounts. The necessity of aqueous medium limits the scope of this method with less water soluble amines and completely hydrophobic amines like the aromatic ones.

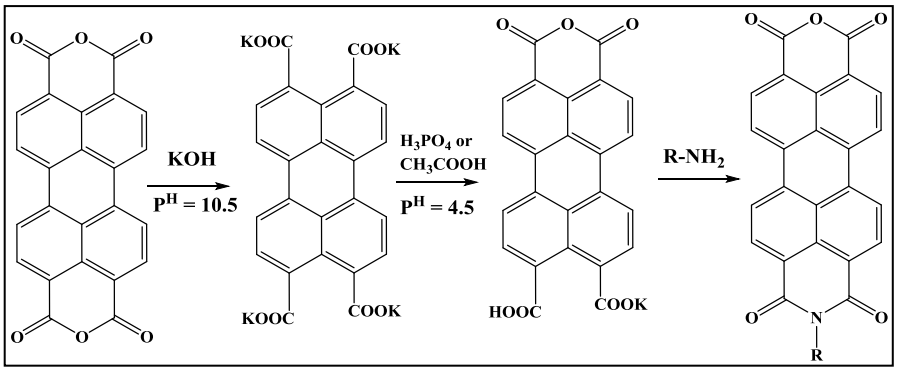

Figure-1.17. Synthesis of unsymmetrical mono-imide-mono-anhydride perylene derivative by Tröster's method.

The most frequently used method for the synthesis of unsymmetrical PDIs was developed by Langhals and co-workers, which involves the partial alkaline saponification of the symmetrically substituted PDIs to perylene mono-imide-mono-anhydride compounds.[119,141-144] The symmetrical bisimides are readily hydrolyzed by a concentrated solution of KOH in *tert*-butyl alcohol or *tert*-amyl

alcohol and this reaction gives yields of ca. 50 % (fig-1.18).[140] Separation of the mono-imide-mono-anhydride from the starting bisimide and the completely saponified product can be easily done because only the PTCDA is soluble in concentrated alkali while the bisimide is insoluble and the mono-imide-mono-anhydride can be isolated by treatment of the residue with hot distilled water followed by acidification with dilute HCl. The anhydride-imides thus obtained can be condensed with another primary amine to give the asymmetrically substituted PDI. The saponification and condensation reactions can be easily monitored by means of FT-IR spectroscopy, since the absorption bands at 1660 and 1701 cm^{-1} indicate the imide group whereas bands at 1733 and 1772 cm^{-1} correspond to the anhydride group.[119] Tam-Chan and co-workers described another similar practical approach to asymmetrical PDI synthesis, involving the partial hydrolysis of PTCDA to mixed anhydride-dicarboxylate salt followed by successive imidization reactions.[145] However the Langhals method still continues to be the most widely utilized method for unsymmetrical PDIs.

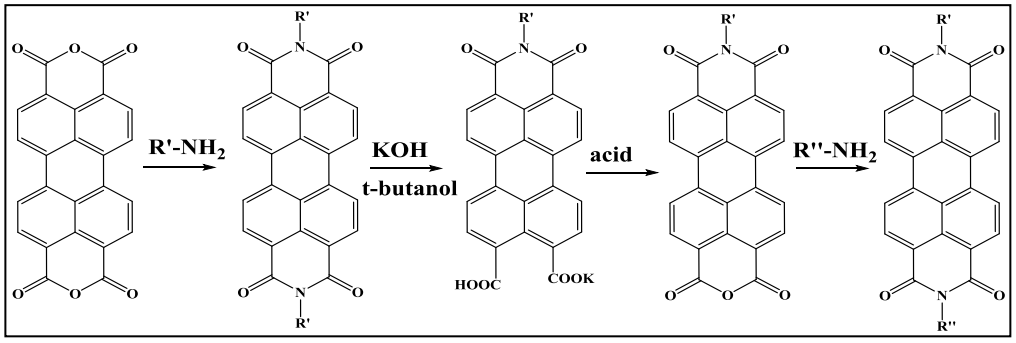

Figure-1.18. Synthesis of unsymmetrical PDI derivatives by Langhals's method.

In some special cases a simultaneous condensation of PTCDA with a mixture of two different primary amines of similar reactivity prove to be useful in the sense, the reaction is complete in one pot synthesis followed by one time separation of the desired unsymmetrical PDI (B) (see fig-1.19) from the mixture by simple column chromatography technique.

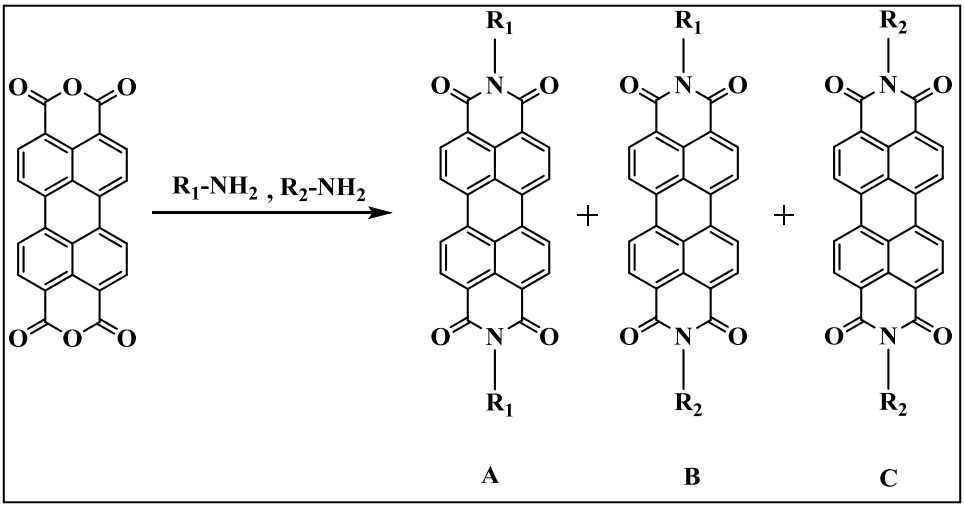

Figure-1.19. Synthesis of unsymmetrical PDI derivatives by simultaneous addition of two different amines.

Bay and ortho- substituted derivatives

Substitution at bay-position of PDIs is the best way to tune the optical and electronic properties, because the substituents are directly connected to the perylene core [146] and also the steric interaction between the substituents leads to twisting of the two naphthalene units in PDIs preventing the aggregation of the chromophores and thereby increasing the solubility remarkably. For e.g., 1,(6)7-dibromo N,N'-dioctly PDI shows good solubility in common organic solvents, whereas its unbrominated derivative is not.[147] The 1,6,7,12-tetrachloro and 1,6(7)-dibromo (which is usually a mixture of 1.6- and 1,7-regioisomers) bay products of PDIs are the key intermediates for a wide range of other bay substituted derivatives obtained by imidization of the halogenated PTCDA derivatives (fig-1.20). Seybold and co-workers were the first to introduce solubilizing tetraphenoxy groups to bay positions of PDIs; 1,6,7,12-tetraphenoxy PDIs were obtained by heating the corresponding tetrachloro species with phenol and potassium carbonate in N-methylpyrrolidone.[148] Similarly the halogen substituted PDIs at bay positions are further functionalized by cyanations via cyano copper (I),[149] fluorinations via potassium fluoride,[150] aminations via piperidine or pyrrolidine.[151]

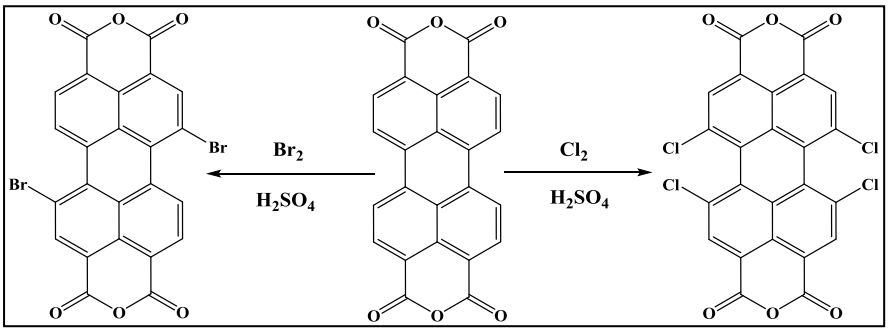

Figure-1.20. Synthesis of core halogenated PTCDA derivatives that are precursors of bay-substituted products.

Apart from the bay-substitution, a recently developed synthetic route to tune the nature of perylene dyes without geometric distortion of the core is the functionalization of the ortho-imide 2,5,8,11-positions via regioselective ruthenium catalyzed direct alkylation or arylation [152,153] as illustrated in figure-1.21. The ortho-substituted PDIs have many unique advantages such as very high solubility without sacrificing planarity of the perylene core, high solid state fluorescence and multiple choice of functionalizations with most organic groups.[153] While bay substitution helps tuning optical and electronic properties but leaves the compounds highly twisted adversely affecting the molecular packing, the ortho-functionalized PDIs which combine a planar core with variable optoelectronic properties are the latest most promising next generation of perylene imides for tomorrow's applications.

Similar to that of PDIs, symmetric NDI compounds are also synthesized by imidization of commercially available 1,4,5,8-naphthalene tetracarboxylic dianhydride with primary amines in high boiling solvents like DMF or DMAc at higher temperatures and sometimes in presence of catalytic amount of K_2CO_3 at lower temperatures when low boiling or heat sensitive amines are used. Using a method developed by Ghadiri *et al.* unsymmetrical NDIs are prepared in a pH controlled reaction similar to that of unsymmetrical PDIs.[154]

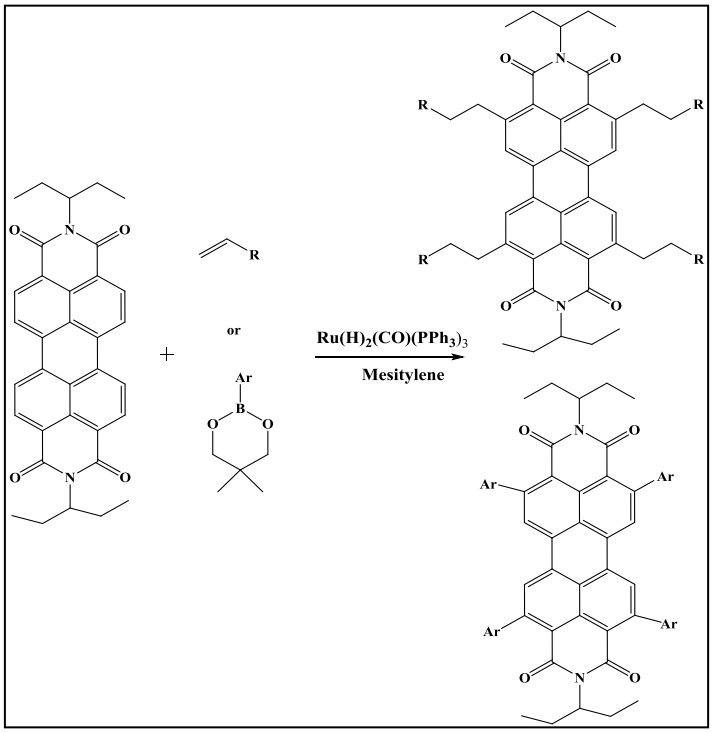

Figure-1.21. Synthesis of aromatic and aliphatic ortho-functionalized PDIs.

1.6.2. Structural and Optoelectronic properties

Structurally the PDI unit constituting the planar aromatic perylene core with two electron withdrawing imide functions on either side is highly symmetric and has been assigned to D_{2h} point group. The PDI core dimensions based on the simplest derivative N, N'-dihydro PBI, shows a length of 11.5 Å for the long N-N' axis and 6.7 Å for the perpendicular axis (from hydrogen to hydrogen), as obtained from the crystal data is shown in figure-1.22(a).[116,155-157] For planar aromatic molecules with D_{2h} symmetry like the PDIs, the electric dipole allowed lowest optical π-π* transition is found to be polarized along the long in-plane N-N' symmetry axis.[158] The DFT (density field theory) calculated HOMO and LUMO of the N, N'-dihydro PBI are shown in figure-1.22 (b) & (c) revealing the nodes at imide nitrogen atoms which results in electronic decoupling of the π-conjugated electron system and its imide substituents.[116]

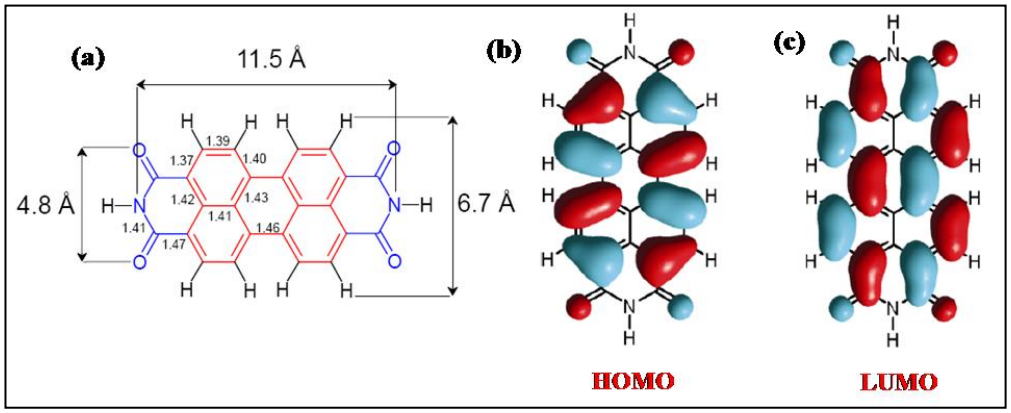

Figure-1.22. (a) Dimensions of perylene core from crystal data of N, N'-dihydro-PBI and its (b) HOMO & (c) LUMO from DFT calculations. [*Adapted from ref.155-157*]

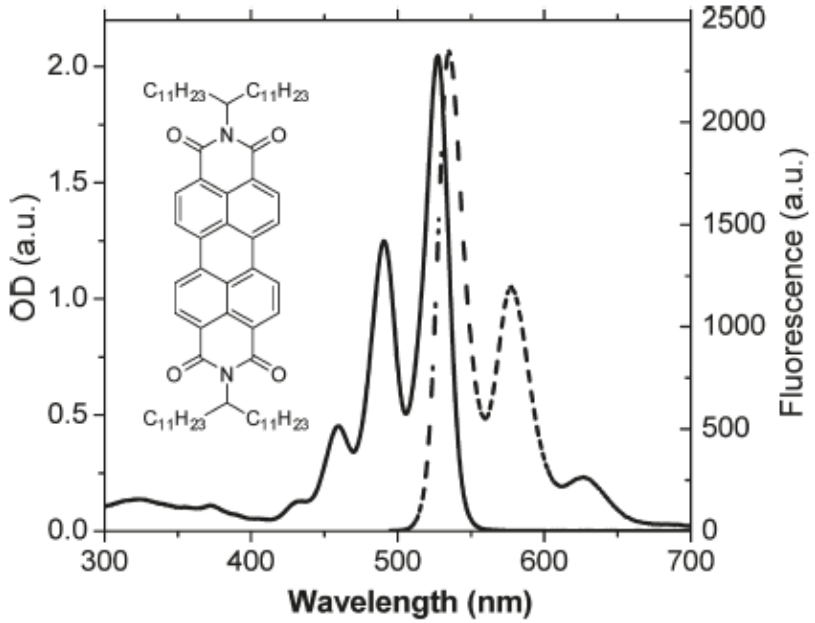

Figure-1.23. Combined absorption (solid line) and emission (dashed line) spectra of a typical PDI in chloroform.

Thus all peri-or imide substituted PDIs exhibit similarly shaped absorption spectra with a characteristic vibronically resolved fine structure of S_0-S_1 transition in the range 450-550 nm corresponding to 0-0, 0-1 and 0-2 transitions respectively. Figure-1.23 shows the combined absorption-emission spectra bearing mirror-image

relation of a typical symmetrical imide-substituted swallow tail PDI in chloroform solvent.[116] The fluorescence quantum yield is nearly unity in most cases and the singlet excited state lifetimes are approximately 4 nanoseconds in common organic solvents.[116] Similarly the absorption and emission properties of N, N'-dialkyl naphthalene bisimides in solvents like dichloromethane shows structured absorptions below 400 nm and usually a weak mirror image emission with ~7 nm stokes shift.[159] In solvents like toluene, excimer-like emissions have been observed suggesting ground state aggregates were formed readily.

In contrast, the bay substitution dramatically alters both the molecular structure and optical properties. Sterically induced twist in the core substituted PBIs causes a potential hypsochromic shift in the absorption maxima and incorporation of extended conjugated groups in the bay region leads to a bathochromically shifted spectra.[123,160] Therefore these twisted dyes are not suitable for generating homogeneous extended π-π stacks.

Crystallochromy

The planar π-conjugated surfaces of rylenebisimides exhibit exceptionally strong secondary π-π stacking interactions which leads to significant aggregation of these chromophores and the properties of such aggregates differ largely from substituent to substituent. One such property is the crystallochromy in PDIs, i.e., color changes resulting from the interaction of π-systems in the crystal lattice. In solution most of the PDIs exhibit an intense fluorescent orange color, but in solid state variety of colors are observed depending on the packing. When the π-π interactions are minimum in the solid state, the PBIs exhibit a brilliant red shade; with small extents of π-π interaction, maroon coloured dyes result and when the electronic interaction between the neighbouring π-systems are strongest the resulting PBI is often black.[116] This class of black PBIs are of special interest when considered for applications like the OFETs and OPVs due to their high exciton or charge carrier mobilities.

Conformation of aggregates - Exciton coupling theory

The electronic interaction between π-conjugated systems leads to formation of aggregates and profound changes are observed in the UV-vis absorption and fluorescence emission spectra depending upon the conformation adopted by the aggregates. Based on the observed spectral shift of the absorption maxima relative to that of the parent monomer, two types of dimer or aggregate geometries arise (i) absorption band at higher energy relative to monomer band, termed 'H-type' aggregates (absorption band shifted hypsochromic) and (ii) absorption band at lower energy relative to monomer band termed 'J-type' (named after their discoverer Jelly) or Scheibe type aggregates (absorption band shifted bathochromic).[161-166] The different packing parameters describing the aggregate geometry are illustrated in figure-1.24, where φ and θ are the rotational and slip angles that define the mutual orientation of the transition dipole moments (i.e., rotational and translational offsets) and 'r' is the centre to centre π-π distance.[167] The observed spectral features of such aggregates with a typical centre to centre distance of 3-4 Å units has been well explained by the exciton coupling theory developed by Kasha *et al.* [162]

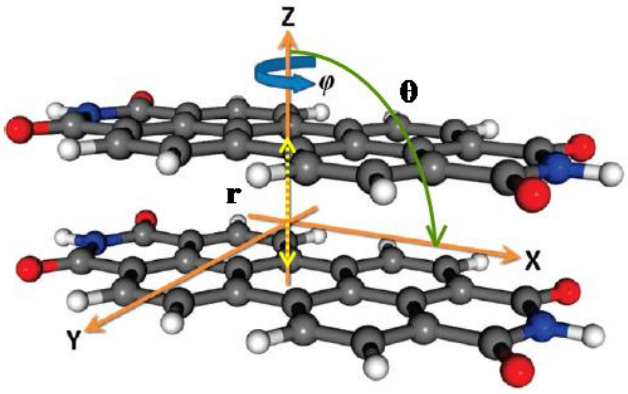

Figure-1.24. Different packing parameters of PBIs describing conformation of aggregates where **φ** is the rotational angle, **θ** is the slip angle and **r** is the centre-to-centre π-π stacking distance ; **θ > 54.7°** H-type and **θ < 54.7°** J-type aggregates. [*Adapted from ref.*167]

According to this exciton coupling theory, [168-170] the excited state is split into two energy levels which are separated by an energy difference of 2ε, where ε is the exciton splitting energy given by the equation:

$$\Delta\varepsilon = 2\varepsilon = \frac{2\mu^2}{4\pi r^3 \epsilon_0} (\cos\phi - 3\cos^2\theta)$$

where μ is the transition dipole moment of the monomer, $\boldsymbol{\epsilon_0}$ is the permittivity of vacuum and r is the centre to centre π-π distance. From the above equation it has been deduced that when the slip angle θ = 54.7° there is no exciton splitting, i.e., Δ ε = 0. Figure-1.25 shows the dependence of exciton splitting energy on slip angle, θ = 0° - 90° at a fixed rotational angle φ = 0° (i.e., there is no rotational displacement).

When θ < 54.7° the allowed transition is to the lower energy exciton band and a red shifted absorption band results characteristic of J-aggregates (head-to-tail arrangement) along with potentially high fluorescence quantum yields and decreased lifetimes compared to parent monomer. When θ > 54.7° the allowed transitions are to the high energy states of the exciton band resulting in a blue shifted absorption maxima with respect to monomer. After exciting at the H-exciton band, a rapid energy relaxation occurs to lower exciton states and their fluorescence is strongly quenched. Thus low fluorescence quantum yield and considerably increased lifetimes are characteristic of face-to-face stacked H-type aggregates (sandwich dimers). [162,171] In the case where the slip angle is constant at θ = 90° with rotational displacement i.e., φ ≠ 0°, for such face-to-face H-aggregates a break in the symmetry causes gradual lifting of the selection rules allowing the transition into the lower excitonic energy band with increasing value of φ. The exciton splitting energy ε decreases with increasing rotational displacement. This category of sandwich H-type aggregates are characterized by a strong blue shifted H-band in the absorption spectra along with a weak bathochromic shifted J-band whose intensity increases with increasing φ. [168-170]

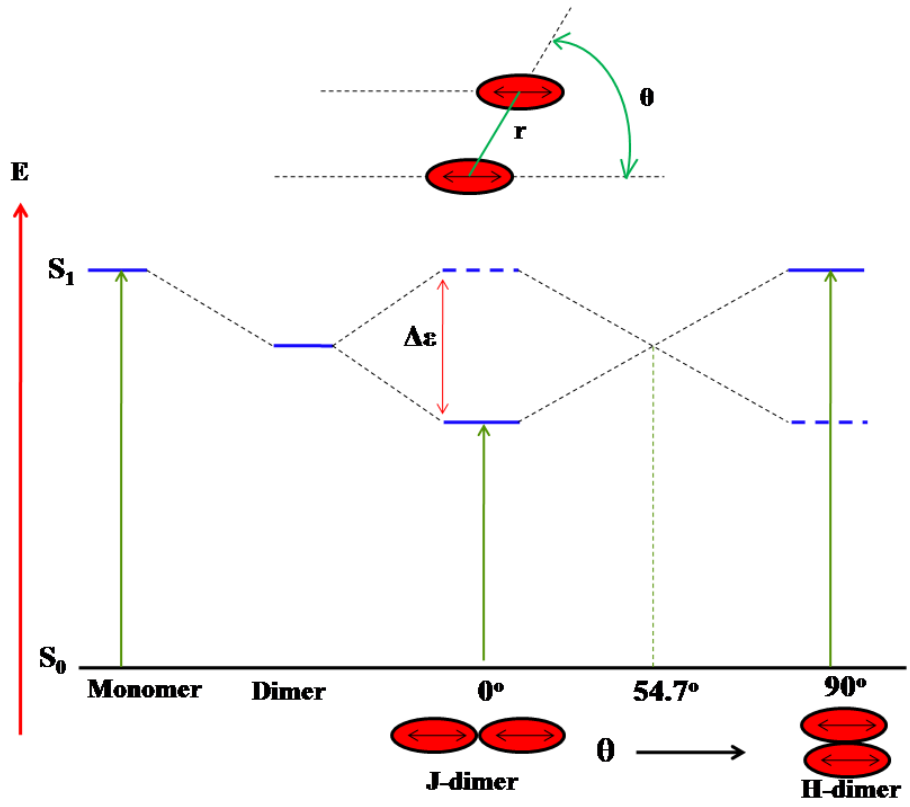

Figure-1.25. Schematic of exciton theory to explain optical properties of H-type and J-type aggregates.

1.6.3. Small Molecule Perylene and Naphthalene bisimide Semiconductors

The early stage utilization of PDI and NDI derivatives as archetype n-type semiconductors from the group of Dodabalapur *et al.* in 1995 demonstrated n-type mobilities of 10^{-3} $cm^2V^{-1}s^{-1}$ for PTCDA [172] and in the same year Horowitz *et al.* already used N,N'- diphenyl PDI derivatives in OFETS with electron mobilities 10^{-5} $cm^2V^{-1}s^{-1}$.[173] Later in 2000 Katz *et al.* demonstrated a breakthrough air stable n-type semiconductor with N,N'-disubstituted H,H-NDI-$CH_2C_7F_{15}$ derivative with electron mobility of 0.1 $cm^2V^{-1}s^{-1}$.[174,175] When fluorine was introduced as the substituent, a favorable packing of NDI core was facilitated and prevented the access of ambient oxidants to the densely packed π-systems. Malenfant *et al.* in 2002 reported a core unsubstituted N,N'-dioctyl PDI with electron mobility as high as 0.6 $cm^2V^{-1}s^{-1}$ under inert conditions.[176] For the same PDI in hydrogen

atmosphere, Chesterfield *et al.* in 2004 reported increased mobility of 1.7 $cm^2V^{-1}s^{-1}$ [177] and another group from Ichikawa *et al.* demonstrated for a similar N,N'-bistridecyl PDI (H,H-PDI-$C_{13}H_{27}$) derivative μ = 2.1 $cm^2V^{-1}s^{-1}$, but only in vacuum.[178] Facchetti, Wasielewski, Marks and co-workers in 2004 put forward the next step towards ambient stable and high carrier mobility via core cyanated PDIs and NDIs.

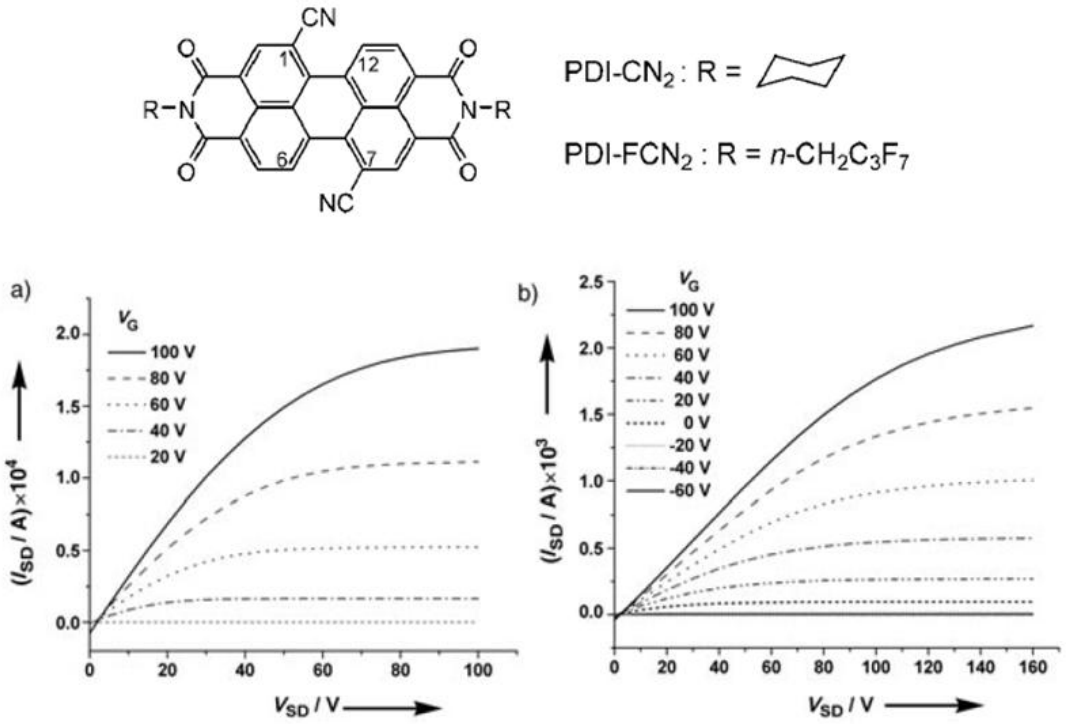

Figure-1.26. Chemical structures and I-V characteristics of PDI-CN_2 and PDI-FCN_2. [*Adapted from ref.179*]

They reported two core cyanated PDIs viz., PDI-CN_2 and PDI-FCN_2 (fig-1.26) which exhibited high air stable n-type mobility of 0.10 $cm^2V^{-1}s^{-1}$ and 0.64 $cm^2V^{-1}s^{-1}$respectively in ambient atmosphere.[179] An optically transparent thin film transistor based on the core cyanated NDI-8CN_2 showed an electron mobility of 0.03 $cm^2V^{-1}s^{-1}$ in air (fig-1.27). [180]

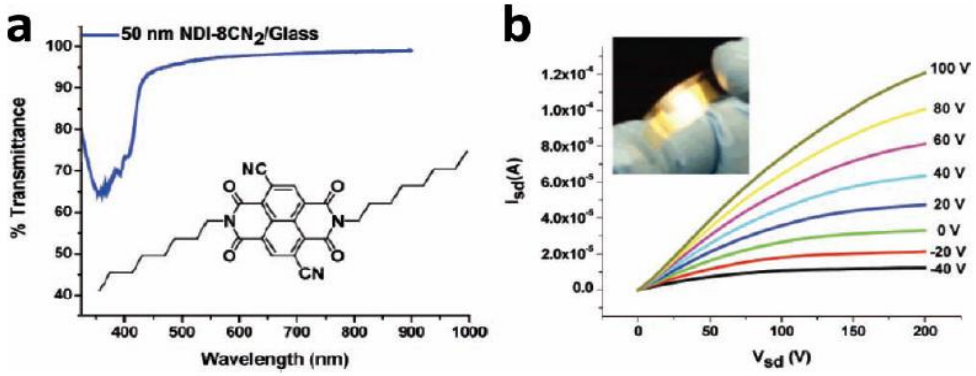

Figure-1.27. Optical absorption and I-V characteristics of thin film transistor based on of NDI-8CN_2. Inset of (b) shows an array of ~100 devices fabricated on transparency film. [*Adapted from ref.180*]

PDI based discotic liquid crystalline small molecules which self assemble into highly ordered one-dimensional stacks are also explored as high charge mobility materials compared to the amorphous counterparts. Marder *et al.* reported a room temperature liquid crystalline N,N'-Di[meth-(3,4,5-tridodecylyoxy)phenyl]-3,4,9,10-perylenediimide (figure-1.28) which showed a space-charge-limited current SCLC mobility as high as 1.3 $cm^2V^{-1}s^{-1}$ in the LC phase under ambient conditions.[181] The flexible -CH_2- linker between the 3,4,5-tridodecyloxy phenyl group and imide nitrogen atom lowered the clearing point of the material significantly thereby rendering it readily processable from the melt.

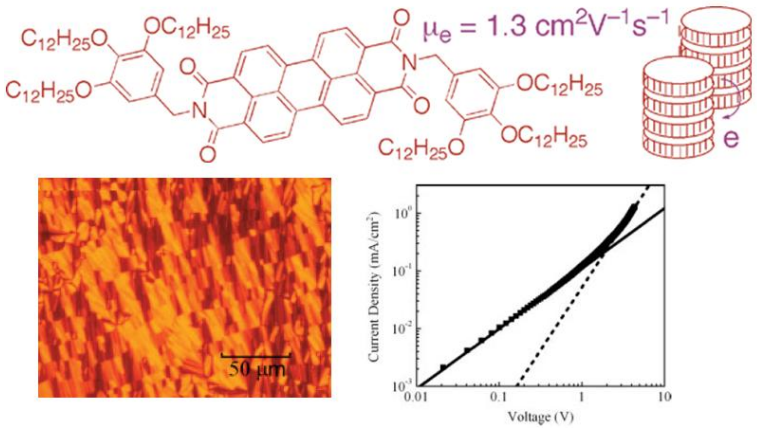

Figure-1.28. Discotic liquid crystalline PDI with high mobility. [*Adapted from ref.181*]

In 2007 Bao, Würthner and co-workers reported for the first time a high mobility core unsubstituted N,N'-bis(2,2,3,3,4,4,4-heptafluorobutyl)-3,4,9,10-PDI with mobility as high as 0.72 $cm^2V^{-1}s^{-1}$ which remained stable for more than 50 days.[182] The stability of this derivative with partial fluorination compared to the N,N'-dialkyl analogue is attributed to the hindrance of O_2 and H_2O diffusion by dense packing of the cores and fluoroalkyl chains. Würthner *et al.* reported a new synthesis method of bay fluorinated PDIs and a difluorinated (F,H-PDI-$CH_2C_3F_7$) derivative with mobility 0.33 $cm^2V^{-1}s^{-1}$.[150,183] More recently, in 2010 the same group of Bao, Würthner *et al.* reported a full core chlorinated PDI (figure-1.29) with H-atom as the imide substituent. This unique molecule with dense molecular packing afforded by hydrogen bonding, π-π stacking as well as halogen-halogen interaction, exhibited ambient stable electron mobility of 0.82 $cm^2V^{-1}s^{-1}$.[184] This exceptionally electron poor molecule crystallized in an ideal brickstone arrangement with close π-π and chlorine-chlorine contacts.

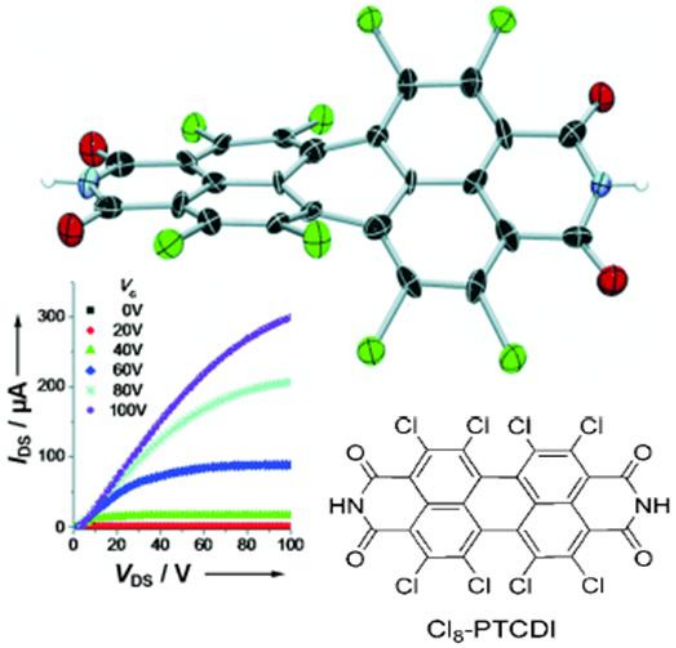

Figure-1.29. Molecular structure from crystal data and I-V characteristics of Cl_8-PTCDI. [*Adapted from ref.184*]

The best mobility reported so far for core-unsubstituted and unfluorinated NDI with cyclohexyl substituents has been by Shukla *et al.* which showed a mobility of 0.41 $cm^2V^{-1}s^{-1}$ on OTS treated substrate in air and upto 6.2 $cm^2V^{-1}s^{-1}$ under inert atmosphere (figure-1.30).[185] The cyclohexyl substituent in the N,N'-bis(cyclohexyl)naphthalene diimide were in the chair conformation with naphthalenediimide at the equatorial positions, providing the optimized bulk phase crystalline packing and thin film morphology essential for efficient charge transport.

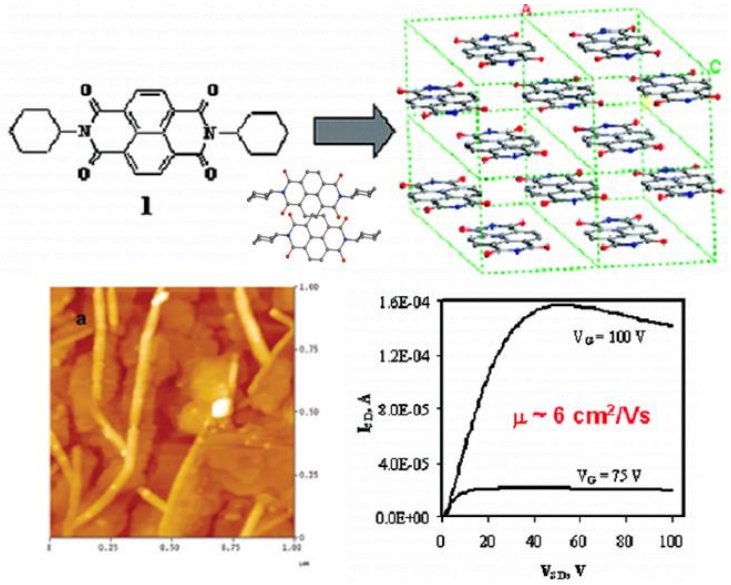

Figure-1.30. Molecular structure, crystal packing (cyclohexyl group omitted for clarity), thin film morphology (AFM) and I-V characteristics of N,N'-bis(cyclohexyl)NDI. [*Adapted from ref.185*]

Recently Marder and co-workers reported a series of triads in which naphthalene diimide (NDI) units were bridged through their 2-positions through different fused ring heterocyclic units (figure-1.31). These bis(NDI) derivatives were fully solution processable and exhibited OFET electron mobility values of upto 1.5 $cm^2V^{-1}s^{-1}$, which is among the highest yet reported for n-channel OFET based on a solution-processed small molecule.[186,187]

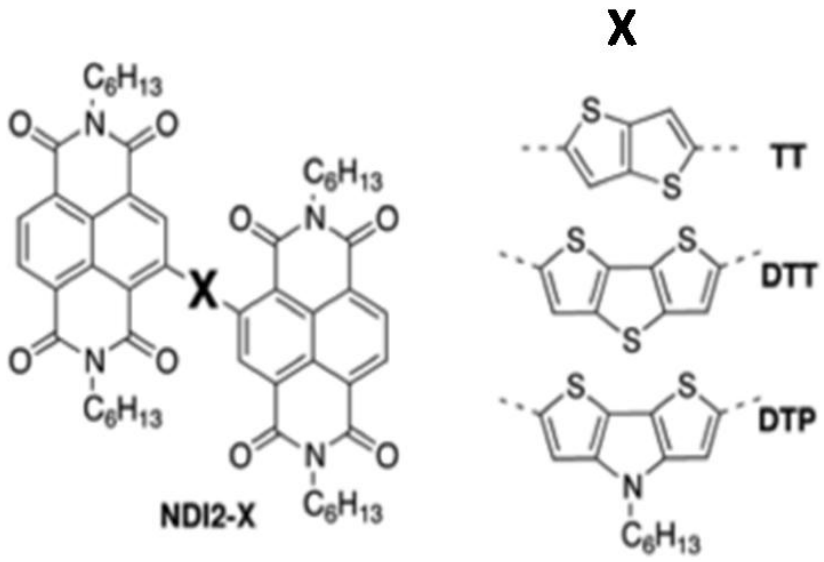

Figure-1.31. Molecular structure of the heterocyclic NDI-bridge-NDI triads. [*Adapted from ref.186*]

1.6.4. Polymeric Perylene and Naphthalene bisimide Semiconductors

Eventhough high device performance is more likely with vacuum deposited small molecules, low cost solution processing techniques such as spin coating, inkjet, gravure or flexographic printing are possible only with polymers since the viscosity ranges required for these methods cannot be achieved with any small molecule. Rylene diimide based polymers for organic electronics applications are still in their infancy compared to small molecule analogues, but development of several main-chain and side-chain PDI and NDI polymers as processable electron transport materials are picking up speed.

Although not strictly a diimide, the ladder polymer BBL ([poly(benzobisimidazo-benzophenanthroline)] (figure-1.32(a)) reported by Babel and Jenekhe in 2003, is the first n-channel TFT-active polymer which is structurally very close to NDIs and spin coated films of this material from methanesulphonic acid afforded OFET electron mobilities upto 0.1 $cm^2V^{-1}s^{-1}$.[188] However the very low solubility of this polymer is a serious limitation. Recently NDI based ladderized polymer (figure-1.32(b)) was also prepared which had

reasonably good solubility in common organic solvents and exhibited electron mobility values of 0.0026 $cm^2V^{-1}s^{-1}$.[189] Zhan, Marder and co-workers in 2007 realized the first soluble fully conjugated rylene polymers in which the rylene cores were bridged by other π-conjugated units. The corresponding PDI based copolymer with dithienothiophene P(PDI-DTT)(figure-1.32 (c)) showed a saturation electron mobility of 1.3 x 10^{-2} $cm^2V^{-1}s^{-1}$ and a low threshold voltage of 4V.[190] But the dithienopyrrole analogue (figure-1.32 (d)) of this copolymer showed only 7.4 x 10^{-4} $cm^2V^{-1}s^{-1}$ mobility which upon thermal annealing increased to 1.2 x 10^{-3} $cm^2V^{-1}s^{-1}$.[191] The PDI-bithiophene copolymer (figure-1.32 (e)) was reported by Facchetti *et al.* with a mobility value of 2 x 10^{-3} $cm^2V^{-1}s^{-1}$. [192]

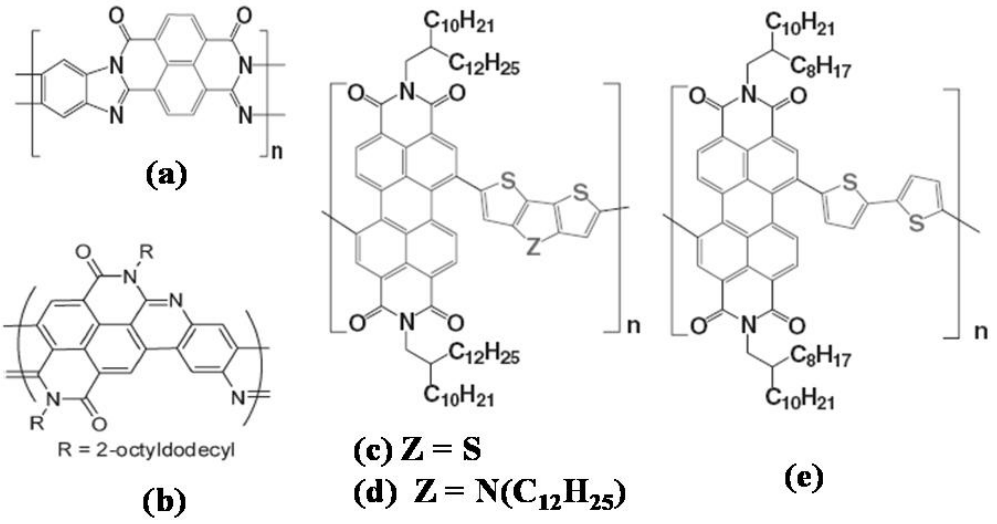

Figure-1.32. Some best performing rylene diimide main chain polymers.

Side-chain polymers containing perylenediimides as pendant groups have been reported by Thelakkat *et al.* where homopolymer poly(perylene acrylate) (PPerAcr) and its diblock co-polymers with polystyrene (PS-*b*-PPerAcr) were synthesized by controlled radical polymerization technique of NMRP (Nitroxide mediated radical polymerization) (figure-1.33).[193] Only after thermal annealing at 210 °C for 60 minutes these side chain polymers showed charge carrier mobilities of 1.2 x 10^{-3} $cm^2V^{-1}s^{-1}$ inside the glove box. [194]

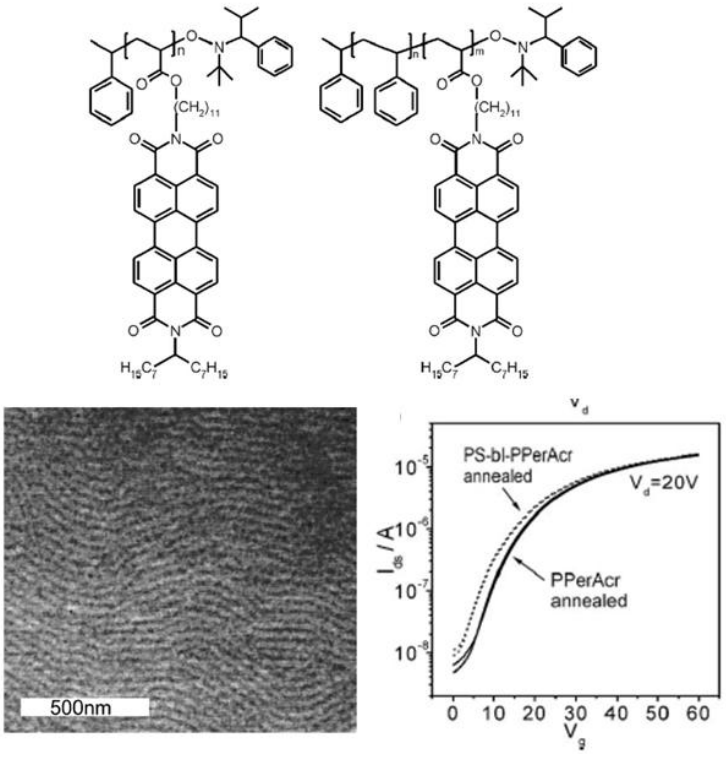

Figure-1.33. Chemical structures of homopolymer (PPerAcr) and block copolymer (PS-*b*-PPerAcr) and its SEM image and I-V characteristics. [*Adapted from ref.194*]

Antonio Facchetti and co-workers have put in tremendous efforts in the field of solution processable n-type polymers to achieve commercial applicability of these polymers. Recently they successfully demonstrated a copolymer of NDI with bithiophene named as P(NDI2OD-T2) exhibiting electron mobility of 0.06 $cm^2V^{-1}s^{-1}$ when measured in vacuum. The device showed good functioning under ambient conditions for at least one month after fabrication.[124] Later, using P(NDI2OD-T2) in combination with various polymer dielectrics, top-gate bottom contact transistors were fabricated by spin coating which exhibited unprecedented OTFT characteristics and electron mobilities of ~ 0.45-0.85 $cm^2V^{-1}s^{-1}$ under ambient conditions (figure-1.34). Moreover, it was also proved that this material could be processed by gravure, flexographic and inkjet printing. Finally they realized in practice the first spin coated and gravure-printed polymeric

semiconductor complementary inverters on PET substrates with large gains (>25-60) operating under normal conditions.[124]

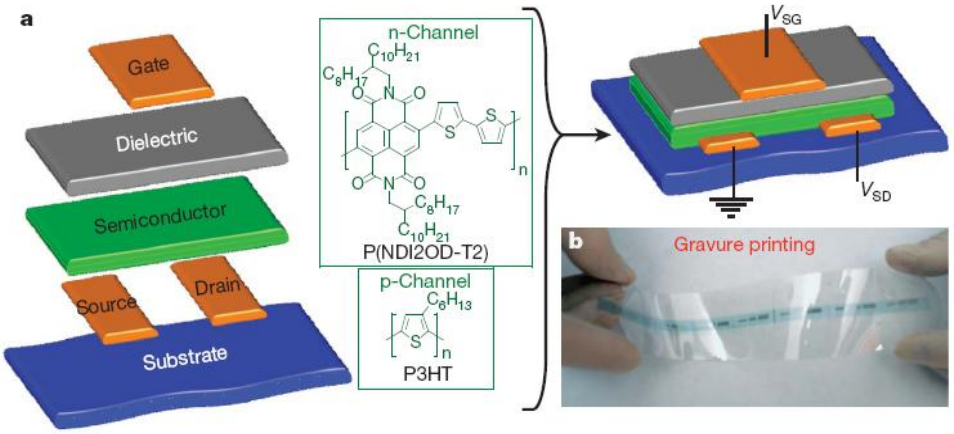

Figure-1.34. (a) Organic thin film transistor (OTFT) based on P(NDI2OD-T2) (b) optical images of gravure-printed OTFT on PET before top-gate contact deposition. [*Adapted from ref.124*]

1.7. Role of programmed Self-Assembly

It is well understood that charge transport properties and in turn, the device performances are strongly influenced by the intermolecular organization or morphology of the π-conjugated materials.[15] Pre-programmed self-assembly using supramolecular design rules is the most satisfying solution to this challenge and has been used by Nature for millennia. The self-assembly of π-conjugated macromolecules forming highly ordered supramolecular architectures through pre-programmed design of functionalities will render the structure control even upto 1-10 nm scale.[195] By combining the concepts of supramolecular chemistry, synthesis methodology and materials processing, molecules could be tailor-made for specific applications. The different types of non-covalent interactions which forms the basis of supramolecular interactions are: (i) Coulombic or electrostatic forces (ii) Hydrogen bond (iii) Ion-dipole interactions (iv) π-π stacking interactions (v) Van der Waals forces and (vi) Metal-ligand co-ordination. The resultant supramolecular entities may be a combination of several such interactions. Amongst these π-π

stacking and hydrogen-bonding are the two important secondary interactions playing a major role in the self-assembly of π-conjugated materials especially for the construction of supramolecular polymers that can combine the high level of ordering characteristic of crystalline small molecules and processability of normal covalent polymers. The term "supramolecular polymer" introduced by Meijer and co-workers is a rather restricted definition confined to supramolecular systems with chain like behaviour.[196] In a broader definition supramolecular polymers can be considered as multiple array of building blocks held together by reversible and highly directional secondary forces resulting in polymeric properties in the dilute as well as bulk phase. All kinds of polymer structures like main chain, side chain or even crosslinked networks can be constructed using tools of supramolecular chemistry with proper design as illustrated in figure-1.35.

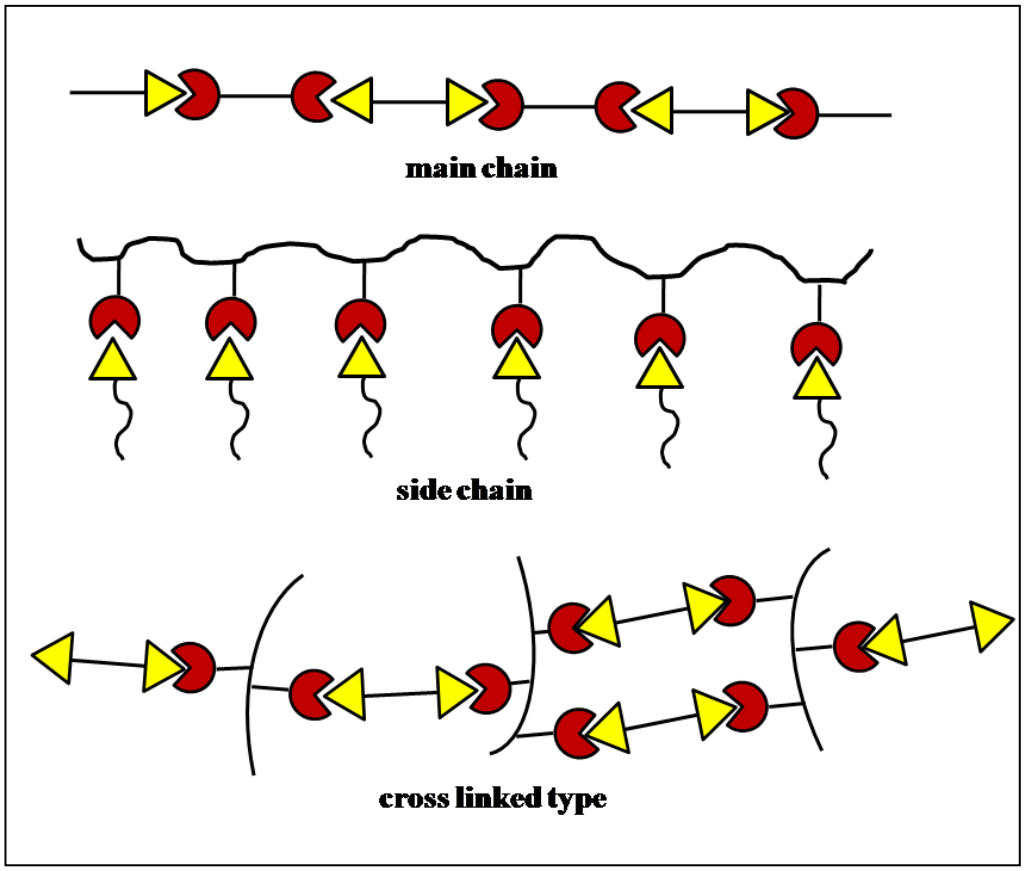

Figure-1.35. Different architectures of supramolecular polymers.

1.8. Objectives and Approach of the thesis

From the detailed discussion presented in this chapter, the relevance of rylenebisimides as potential n-type organic semiconductor materials in different fields of organic electronics has been well understood. Research on rylenebisimide based main chain and side-chain polymeric materials have still not reached a maturity level, although rapid advances are going on. Majority of the high performing examples of rylenebisimides are those based on small molecules and none of the polymeric approaches have been able to cope up to the same level or better. The prevailing situation demands the development of novel advanced strategies to obtain high performance n-type polymeric materials that are inevitable for cost effective printable plastic electronics.

The present thesis work is a systematic investigation for the development of new categories of polymeric materials specifically based on rylenebisimides that could find practical applications in the field of optoelectronics. Different strategies of covalent and non-covalent chemistry were liberally utilized to achieve the target. The work maintains a constant focus revolving around three equally important aspects of the field that are quintessential for successful practical applications: (i) design-synthesis, (ii) structure-morphology and (iii) device properties. (Scheme-1.1)

The main objectives of the present doctoral research were:

1) To design and synthesize novel side-chain rylenebisimide polymers with in-built motifs for self-assembly.
2) To study the self-organized morphologies formed by the resulting polymer architectures.
3) To screen out the best candidates for device applications with better charge carrier mobilities.
4) To gain a deep understanding of the structure-property relationship that may prove useful for the future generation to rationally design the materials for fruitful applications.

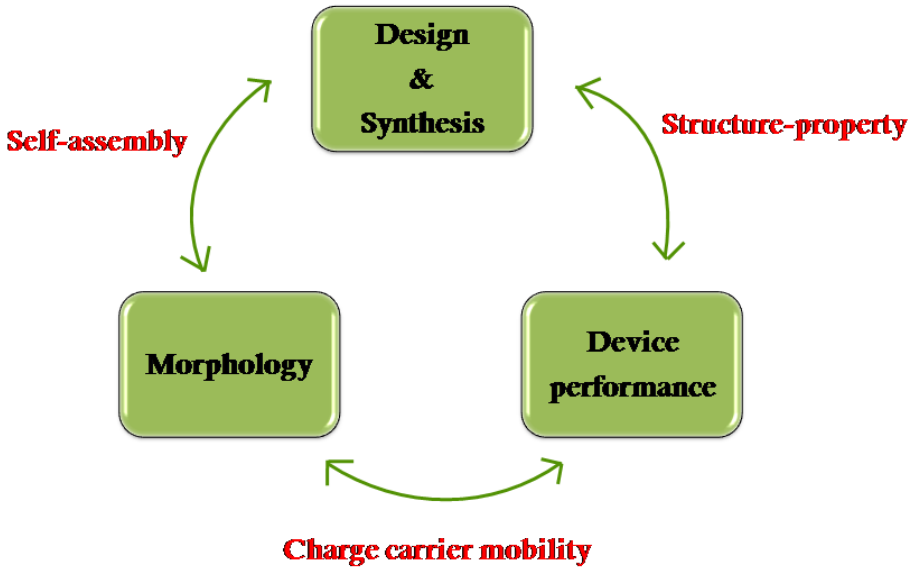

Scheme-1.1. Inter-dependence of structure, morphology and device performance: issues addressed in the thesis.

We have dealt with two main types of approaches in this thesis. The first approach aimed at conventional covalent side-chain polymers whereas the second approach adopts principles of supramolecular chemistry which forms the basis for major part of the thesis work. In the preliminary project discussed in chapter two, covalently connected side-chain perylenebisimide polymers were attempted based on prior studies from our group on a unique urethane methacrylate comb monomer design that had in-built self-assembling motifs for hydrogen bonding and hydrophobic interactions. Two other monomers with similar structural design but with two different pendant groups viz., cardanol and 3-pentadecylphenol were also prepared for model studies. But unfortunately the chapter expands with unsuccessful polymerization of the perylenebisimide based monomers and successful formation of cardanol and 3-pentadecylphenol based urethane methacrylate comb polymers and their solvent dependent self-assembly therein. From this point the thesis took a different turn leading to the third chapter where the concepts of non-covalent interactions were explored judiciously to successfully fabricate supramolecular comb polymers of perylenebisimide possessing high crystallinity and processability. Unsymmetrical perylenebisimide with 3-

pentadecylphenol substitution at one imide position was complexed with poly(4-vinylpyridine) (P4VP) via hydrogen bonding interactions between the phenol and pyridine groups. Packing diagram, thin film morphology and charge transport characteristics of the stoichiometrically balanced supramolecular complex were studied in detail.

The successful application of the supramolecular concepts to form perylenebisimide comb polymers, directed the same in the fourth chapter, to its lower analogue naphthalenebisimides in anticipation to produce n-type polymers with even better electron mobilities retaining the crystallinity of the small molecules. Single crystal X-ray diffraction (XRD) analysis of the unsymmetrical naphthalene bisimide small molecule was used to shed light on its self-aggregation and was correlated to the structural changes brought in by complexation with P4VP. The concept of combining the positive aspects of both perylene and naphthalenebisimides were also explored by preparing randomly mixed supramolecular comb polymer complexes with the two cores in varied ratios. However the best device results were obtained only for the complex with 50/50 composition of the PBI/NBI. In the last working chapter, rylenebisimide based supramolecular crosslinked polymer networks were fabricated via hydrogen bonding interactions with P4VP. For this purpose, ditopic hydrogen bonding modules of both perylene and naphthalene bisimides were synthesized by substituting 3-pentadecylphenol group on both imide positions of the rylene cores. Detailed structural analysis of the ditopic rylenebisimides revealed their inherent tendency to form mesomorphic liquid crystalline phases. The change in the packing diagram occurring upon hydrogen bonded crosslinking with P4VP was also deeply investigated. Finally the materials were subjected to screening test for device applications via space charge limited current (SCLC) mobility measurements. This thesis thus does complete justice to the objectives planned to develop novel rylenebisimide polymeric materials for optoelectronics applications as will be evident from the detailed discussions in the subsequent chapters.

1.9. References

[1] A. Aviram, M. A. Ratner, *Chem. Phys. Lett.* **1974,** *29*, 277.

[2] H. Shirakawa, E. J. Louis, A. G. MacDiarmid, C. K. Chiang, A. J. Heeger, *Chem. Commun.* **1977**, 578.

[3] C. K. Chiang, C. R Fincher, Y. W. Park, A. J. Heeger, H. Shirakawa, E. J. Louis, S. C. Gau, A. G. MacDiarmid, *Phys. Rev. Lett.* **1977,** *39*, 1098.

[4] R. Farchioni, G. Grosso, Eds.; *"Organic electronic materials: conjugated polymers and low molecular weight organic solids."* Berlin, Germany: Springer, **2001.**

[5] G. Malliaras, Ed.; *"Organic semiconductors and devices."* Hoboken, NJ: Wiley, **2003.**

[6] A. Facchetti, M.-H. Yoon, T. J. Marks, *Adv. Mater.* **2005,** *17*, 1705.

[7] M. Muccini, *Nat. Mater.* **2006,** *5*, 605.

[8] C. D. Dimitrakopoulos, P. R. L. Malenfant, *Adv. Mater.* **2002,** *14*, 99.

[9] A. C. Arias, J. D. MacKenzie, I. McCulloch, J. Rivnay, A. Salleo, *Chem. Rev.* **2010,** *110*, 3.

[10] C. W. Tang, *Appl. Phys. Lett.* **1986**, *48*, 183.

[11] N. N. Burroughes, D. D. C. Bradley, A. R. Brown, N. N. Marks, K. Mackay, R. H. Friend, P. L. Burns, A. B. Holmes, *Nature* **1990,** *347*, 539.

[12] P. L. Burns, A. B. Holmes, A. Kraft, D. D. C. Bradley, A. R. Brown, R. H. Friend, R. W. Gymer, *Nature* **1992,** *356*, 47.

[13] H. Koezuka, A. Tsumura, T. Ando, *Synth. Met.***1987,** *18*, 699.

[14] Konarka Technologies Inc., http:// www. konarka. com/ index.php/site/newsdetail.

[15] V. Coropceanu, J. Cornil, D. A. S. Filho, Y. Olivier, R. Silbey, J.-L. Brédas, *Chem. Rev.* **2007,** *107*, 926.

[16] N. Kirova, *Polym. Int.* **2008,** *57*, 678.

[17] A. Dkhissi, **2011,** *161*, 1441.

[18] X. Yang, J. Loos, *Macromolecules* **2007,** *40*, 1353.

[19] N. S. Sariciftci, L. Smilowitz, A. J. Heeger, F. Wudl, *Science* **1992,** *258*, 1474.

[20] T. M. Clarke, J. R. Durrant, *Chem. Rev.* **2010,** *110*, 6736.

[21] A. Kaminski, S. Das Sarma, *Phys. Rev. Lett.* **2002,** *88*, 247202.

[22] M. F. Rubner, In "*Molecular Electronics*" (G. J. Ashwell, Ed.).Wiley, New York, **1992.**

[23] J. H. Schön, C. Kloc, B. Batlogg, *Phys Rev. Lett.* **2001,** *86*, 3843.

[24] J. Y. Kim, A. J. Bard, *Chem. Phys. Lett.* **2004,** *383*, 11.

[25] G. Horowitz, R. Hajlaoui, R. Bourguiga, M. Hajlaoui, *Synth. Met.* **1999,** *101*, 401.

[26] http://www.oled.at/produkte.htm

[27] P. W. Wang, Y. J. Lui, C. Devadoss, P. Bharati, J. S. Moore, *Adv. Mater.* **1996,** *8*, 237.

[28] L. Zou, V. Savvateev, J. Booher, C. H. Kim, J. Shinar, *Appl. Phys. Lett.* **2001,** *79*, 2282.

[29] A. K.-Y. Jen, Y. Liu, Q.-S. Hu, L. Pu, *Appl. Phys. Lett.* **1999,** *75*, 3745.

[30] H. Suzuki, *Appl. Phys. Lett.* **2002,** *80*, 3256.

[31] Y. Fu, M. Sun, Y. Wu, Z. Bo, D. Ma, *J. Polym. Sci. A: Polym. Chem.* **2008,** *46*, 1349.

[32] P. Karastatiris, J. A. Mikroyannidis, I. K. Spiliopoulos, *J. Polym. Sci. A: Polym. Chem.* **2008,** *46*, 2367.

[33] M. Mazzeo, V. Vitale, F. D. Sala, M. Anni, G. Barbarella, L. Favaretto, G. Sotgiu, R. Cingolani, G. Gigli, *Adv. Mater.* **2005,** *17*, 34.

[34] W. R. Salaneck, *et al.*, Eds.; "*Conjugated Polymers and Molecular Interfaces.*" Marcel Dekker: New York, **2002.**

[35] http://www.solarmer.com/

[36] http://www.pv-magazine.com/

[37] J. You, L. Dou, K. Yoshimura, T. Kato, K. Ohya, T. Moriarty, K. Emery, C.-C. Chen, J. Gao, G. Li1, Y. Yang, *Nat. Commun*. **2013,** *4*, 1446.

[38] B. C. Thompson, J. M. J. Frè chet, *Angew. Chem. Int. Ed.* **2008,** *47*, 58.

[39] M. C. Scharber, D. Mühlbacher, M. Koppe, P. Denk, C. Waldauf, A. J. Heeger, C. J. Brabec, *Adv. Mater.* **2006**, *18*, 789.

[40] H. Yokoyama, E. J. Kramer, M. H. Rafailovich, J. Sokolov, S. A. Schwarz, *Macromolecules* **1998,** *31*, 8826.

[41] C. Melzer, E. J. Koop, V. D. Mihailetchi, P. W. M. Blom. *Adv. Funct. Mater.* **2004,** *14*, 865.

[42] M. M. Mandoc, L. J. A. Koster, P. W. M. Blom, *Phys. Rev. B* **2007,** *90*, 133504.

[43] G. Heimel, L. Romaner, E. Zojer, J.-L. Brédas, *Nano Lett.* **2007,** 7, 932.

[44] J. M. Nunzi, *C.R. Phys.* **2002,** *3*, 523.

[45] C. J. Barbec, T. Nann, S. Shaheen, *MRS Bulletin*, **2004,** *19*, 43.

[46] N. S. Sariciftci Ed.; "*Primary photoexcitations in conjugated polymers: molecular Exciton versus Semiconductor Band Model.*" World Scientific Publishers, Singapore, **1998.**

[47] C. Winder, N. S. Sariciftci, *J. Mater. Chem*. **2004**, *14*, 1077.

[48] N. S. Saricitfci, L. Smilowitz, A. J. Heeger, F. Wudl, *Science* **1992,** *258*, 1474.

[49] N. S. Saricitfci, A. J. Heeger, In "*Handbook of Organic conductive molecules and polymers.*" H.S. Nalwa, Ed.; Wiley, NewYork, **1996.**

[50] H. Hoppe, N. S. Saricitfci, *J . Mater. Chem.* **2004,** *19*, 1924.

[51] L. Leibler, *Macromolecules* **1980,** *13*, 1602.

[52] M. W. Matsen, F. S. Bates, *Macromolecules* **1996,** *29*, 1091.

[53] P. D. Topham, A. J. Parnell, R. C. Hiorns, *J. Polym. Sci. Part B: Polym. Phys.* **2011,** *49*, 1131.

[54] C. Deibel, V. Dyakonov, *Rep. Prog. Phys.* **2010,** 73.

[55] C. J. Brabec, *Sol. Energy Mater. Sol. Cells* **2004,** *83*, 273.

[56] J. Rostalski, D. Meissner, *Sol. Energy Mater. Sol. Cells* **2000**, *61*, 87.

[57] J. Zaumseil, H. Sirringaus, *Chem. Rev.* **2007,** *107*, 1296.

[58] S. Allard, M. Forster, B. Souharce, H. Thiem, U. Scherf, *Angew. Chem. Int. Ed.* **2008,** *47*, 4070.

[59] M. Lampert, P. Mark, "*Current injection in solids*" Academic Press, New York, **1970.**

[60] A. Campbell, D. Bradley, H. Antoniadis, *J. Appl. Phys.* **2001,** *89*, 3343.

[61] A. M. Goodman, A. Rose, *J. Appl. Phys.* **1971,** *41*, 2823.

[62] W.-Y. Hung, T.-H. Ke, Y.-T. Lin, C.-C. Wu, T.-H. Hung, T.-C. Chao, K.-T. Wong, C.-I Wu, Appl. Phys. Lett. **2006,** *88*, 64102.

[63] J. L. Brédas, J. P. Calbert, D. A. da Silva, J. Cornil, *Proc. Natl.Acad. Sci. U. S. A.* **2002,** *99*, 5804.

[64] D. A. da Silva, E.-G. Kim, J.-L. Brédas, *Adv. Mater.* **2005,** *17*, 1072.

[65] G. R. Hutchison, M. A. Ratner, T. J. Marks, *J. Am. Chem. Soc.* **2005,** *127*, 2339.

[66] S. T. Bromley, M. M. Torrent, P. Hadley, C. Rovira, *J. Am. Chem. Soc.* **2004,** *126*, 6544.

[67] J. Cornil, J. L. Brédas, J. Zaumseil, H. Sirringhaus, *Adv. Mater.* **2007,** *19*, 1791.

[68] F. Würthner, R. Schmidt, *Chem. Phys. Chem.* **2006,** *7*, 793.

[69] C. Wang, H. Dong, H. Li, H. Zhao, Q. Meng, W. Hu, *Cryst. Growth Des.* **2010,** *10*, 4155.

[70] H. Dong, C. Wang, W. Hu, *Chem. Commun.* **2010,** *46*, 5211.

[71] J. Y. Lee, S. Roth, Y. W. Park, *Appl. Phys. Lett.* **2006**, *88*, 252106.

[72] C. Wang, H. Dong, W. Hu, Y. Liu, D. Zhu, *Chem. Rev.* **2012,** *112*, 2208.

[73] H. Moon, R. Zeis, E. J. Borkent, C. Besnard, A. J. Lovinger, T. Siegrist, C. Kloc, Z. N. Bao, *J. Am. Chem. Soc.* **2004,** *126*, 15322.

[74] V. C. Sundar, J. Zaumseil, V. Podzorov, E. Menard, R. L. Willet, T. Someya, M. E. Gershenson, J. A. Rogers, *Science* **2004**, *303*, 1644.

[75] D. Sheraw, T. N. Jackson, D. L. Eaton, J. E. Anthony, *Adv. Mater.* **2003**, *15*, 2009.

[76] M. M. Torrent, P. Hadley, S. T. Bromley, X. Ribas, J. Tarres, M. Mas, E. Molins, J. Veciana, C. Rovira, *J. Am. Chem. Soc.* **2004,** *126*, 8546.

[77] R. Li, W. Hu, Y. Liu, D. Zhu, *Acc. Chem. Res.* **2010,** *43*, 529.

[78] L. Jiang, H. Dong, W. Hu, *J. Mater. Chem.* **2010,** *20*, 4994.

[79] T. D. Anthopoulos, J. P. J. Markham, E. B. Namdas, I. D. W. Samuel, S.-C. Lo, P. L. Burn, *Appl. Phys. Lett.* **2003,** 82, 4824.

[80] D. G. Ma, Y. F. Hu, Y. G. Zhang, L. X. Wang, X. B. Jing, F. S. Wang, J. M. Lupton, I. D. W. Samuel, S. C. Lo, P. L. Burn, *Synth. Met.* **2003,** *137*, 1125.

[81] E. Greenbaum, I. Lee, J. W. Lee, *Biophys. J. Part 2* **2002,** *82*, 206.

[82] M. Pope, C. E. Swenberg, "*Electronic Processes in Organic Crystals*" Clarendon, Oxford, **1982.**

[83] S. R. Forrest, *Chem. Rev.* **1997,** *97*, 1793.

[84] P. E. Burrows, S. R. Forrest, L. S. Sapochak, J. Schwartz, P. Fenter, T. Buma, V. S. Ban, J. L. Forrest, *J. Cryst. Growth* **1995,** *156*, 91.

[85] M. Shtein, H. F. Gossenberger, J. B. Benziger, S. R. Forrest, *J. Appl. Phys.* **2001,** *89*, 1470.

[86] J. Takeya, M. Yamagishi, Y. Tominari, R. Hirahara, Y. Nakazawa, T. Nishikawa, T. Kawase, T. Shimoda, S. Ogawa, *Appl. Phys. Lett.* **2007,** *90*, 102120.

[87] B. Crone, A. Dodabalapur, Y.-Y. Lin, R. W. Filas, Z. Bao, A. LaDuca, R. Sarpeshkar, H. E. Katz, W. Li, *Nature* **2000,** *403*, 521.

[88] W. P. Wu, Y. Q. Liu, D. B. Zhu, *Chem. Soc. Rev.* **2010,** *39*, 1489.

[89] J. E. Anthony, *Chem. Rev.* **2006,** *106*, 5028.

[90] H. Klauk, M. Halik, U. Zschieschang, G. Schmidt, W. Radlik, W. Weber, *J. Appl. Phys.* **2002**, *92*, 5259.

[91] O. D. Jurchescu, J. Baas, T. T. M. Palstra, *Appl. Phys. Lett.* **2004**, *84*, 3061.

[92] M. T. Lloyd, A. C. Mayer, A. S. Tayi, A. M. Bowen, T. G. Kasen, D. J. Herman, D. A. Mourey, J. E. Anthony, G. G. Malliaras, *Org. Electron.* **2006,** *7*, 243.

[93] S. A. Odem, S. R. Parkin, J. E. Anthony, *Org. Lett.* **2003**, *5*, 4245.

[94] M. M. Payne, S. R. Parkin, J. E. Anthony, C. Kuo, T. N. Jackson, *J. Am. Chem. Soc.* **2005**, *127*, 8028.

[95] Y. Lin, Y. Lia, X. Zhan, *Chem. Soc. Rev.* **2012,** *41*, 4245.

[96] F. Garnier, R. Hjlaoui, A. Yassar, P. Srivastava, *Science* **1994**, *265*, 1684.

[97] H. Sirringhaus, N. Tessler, R. H. Friend, *Science* **1998**, *280*, 1741.

[98] I. McCulloch, M. Heeney, C. Bailey, K. Genevicius, I. MacDonald, M. Shkunov, D. Sparrowe, S. Tierney, R. Wagner, W. Zhang, M. L. Chabinyc, R. J. Kline, M. D. McGehee, M. F. Toney, *Nat. Mater.* **2006**, *5*, 328.

[99] A. M. van de Craats, J. M. Warman, A. Fechtenkötter, J. D. Brand, M. A. Harbison, K. Müllen, *Adv. Mater.* **1999**, *11*, 1469.

[100] D. Adam, P. Schuhmacher, J. Simmerer, L. Häussling, K. Siemensmeyer, K. H. Etzbachi, H. Ringsdorf, D. Haarer, *Nature* **2004**, *371*, 141.

[101] A. M. van de Craats, J. M. Warman, *Synth. Met.* **2001**, *121*, 1287.

[102] I. Parschiv, M. Giesbers, B. van Lagen, F. C. Grozema, R. D. Abellon, L. D. A. Siebbeles, A. T. M. Marcelis, H. Zuilhof, E. J. R. Sudhölter, *Chem. Mater.* **2006**, *18*, 968.

[103] M. M. Payen, S. R. Parkin, J. E. Anthony, C.-C. Kuo, T. N. Jackson, *J. Am. Chem. Soc.* **2005,** *127*, 4986.

[104] H. Ebata, T. Izawa, E. Miyazaki, K. Takimiya, M. lkeda, H. Kuwabara, T. Yui, *J. Am. Chem. Soc.* **2007,** *129*, 15732.

[105] P. Gao, D. Beckmann, H. N. Tsao, X. Feng, V. Enkelmann, M. Baumgarten, W. Pisula, K. Müllen, *Adv. Mater.* **2009,** *21*, 213.

[106] C. Li, H. Wonneberger, *Adv. Mater.* **2012,** *24*, 613.

[107] Y. Sakamoto, T. Suzuki, M. Kobayashi, Y. Gao, Y. Fukai, Y. Inoue, F. Sato, S. Tokito, *J. Am. Chem. Soc.* **2004,** *126*, 8138.

[108] Z. Bao, A. J. Lovinger, J. Brown, *J. Am. Chem. Soc.* **1998,** *120*, 207.

[109] S. P. Singh, A. Sellinger, A. Dodabalapur, *J. Appl. Phys.* **2010,** *107*, 044509.

[110] J. A. Letizia, A. Facchetti, C. L. Stern, M. A. Ratner, T. J. Marks, *J. Am. Chem. Soc.* **2005,** *127*, 13476.

[111] H. Usta, A. Facchetti, T. J. Marks, *J. Am. Chem. Soc.* **2008,** *130*, 8580.

[112] D. M. de Leeuw, M. M. J. Simenon, A. R. Brown, R. E. F. Einerhand, *Synth. Met.* **1997,** *87,* 53.

[113] Y. Wen, Y. Liu, *Adv. Mater.* **2010,** *22,* 1331.

[114] M. Kardos, *Ber.* **1913,** *46*, 2068.

[115] C. Liebermann, M. Kardos, *Ber.* **1914,** *44*, 202.

[116] F. Würthner, *Chem. Commun.* **2004,** 1564.

[117] G. Horowitz, F. Kouki, P. Spearman, D. Fichou, C. Nogues, X. Pan, F. Garnier, *Adv. Mater.* **1996,** *8,* 242.

[118] H. Langhals, *Helv. Chim. Acta.* **2005,** *88,* 1309.

[119] H. Langhals, *Heterocycles* **1995,** *40,* 477.

[120] Y. Avlasevich, C. Li, K. Müllen, *J. Mater. Chem.* **2010,** 20, 3814.

[121] M. P. O'Neil, M. P. Niemczyk, W. A. Svec, D. Gosztola, L. G. Gaines, M. R. Wasielewski, *Science* **1992,** *257,* 63.

[122] S. Prathapan, S. I. Yang, J. Seth, M. A. Miller, D. F. Bocian, D. Holten, J. S. Lindsey, *J. Phys. Chem. B* **2001,** *105,* 8237.

[123] Z. S. An, S. A. Odom, R. F. Kelley, C. Huang, X. Zhang, S. Barlow, L. A. Padilha, J. Fu, S. Webster, D. J. Hagan, E. W. Van Stryland, M. R. Wasielewski, S. R. Marder, *J. Phys.Chem. A* **2009,** *113*, 5585.

[124] H. Yan, Z. H. Chen, Y. Zheng, C. Newman, J. R. Quinn, F. Dotz, M. Kastler, A. Facchetti, *Nature* **2009,** *457,* 679.

[125] P. Mukhopadhyay, Y. Iwashita, M. Shirakawa, S-i. Kawano, N. Fujita, S. Shinkai, *Angew. Chem. Int. Ed.* **2006,** 45**,** 1592.

[126] W. Pisula, M. Kastler, D. Wasserfallen, J. W. F. Robertson, F. Nolde, C. Kohl, K. Müllen, *Angew. Chem. Int. Ed.* **2006,** *45*, 819.

[127] R. S. Lokey, B. L. Iverson, *Nature* **1995,** 375, 303.

[128] H. Y. Au-Yeung, G. D. Pantos, J. K. M. Sanders, *J. Am. Chem. Soc.* **2009,** *131*, 16030.

[129] G. D. Pantos, P. Pengo, J. K. M Sanders, *Angew. Chem. Int. Ed.* **2007,** *46,* 194.

[130] H. Shao, J. Seifert, N. C. Romano, M. Gao, J. J. Helmus, C. P. Jaroniec, D. A. Modarelli, J. R. Parquette, *Angew. Chem. Int. Ed.* **2010,** *49,* 7598.

[131] L. D. Wescott, D. L. Mattern, *J. Org. Chem.* **2003,** *68,* 10058.

[132] Y. Huang, Y. Yan, B. M. Smarsly, Z. Wei, C. F. J. Faul, *J. Mater. Chem.* **2009,** *19,* 2356.

[133] C. Backes, C. Schmidt, F. Hauke, C. Böttcher, A. Hirsch, *J. Am. Chem. Soc.* **2009,** *131*, 2172.

[134] T. Heek, C. Fasting, C. Rest, X. Zhang, F. Würthner, R. Haag, *Chem. Commun.* **2010,** *46*, 1884.

[135] Y. Liu, K.-R. Wang, D.-S. Guo, B.-P. Jiang, *Adv. Funct. Mater.* **2009,** *19*, 2230.

[136] H. Langhals, S. Demming, H. Huber, *Spectrochim. Acta*. **1998**, *44A*, 1189.

[137] Y. Nagao, *Prog. Org. Chem.* **1997,** *31*, 43.

[138] Y. Nagao, T. Misono, *Bull. Chem. Soc. Jpn.***1981,** *54*, 1269.

[139] H. Tröster, *Dyes Pigm.* **1983,** *4*, 171.

[140] H. Kaiser, J. Lindner, H. Langhals, Chem. Ber. **1991,** *124*, 529.

[141] M. Sommer, S. M. Lindner, M. Thelakkat, *Adv. Funct. Mater.* **2007,** *17*, 1493.

[142] M. Sommer, A. S. Lang, M. Thelakkat, *Angew. Chem. Int. Ed.* **2008,** *47*, 7901.

[143] S. M. Lindner, S. Hüttner, A. Chiche, M. Thelakkat, G. Krausch, *Angew. Chem. Int. Ed.* **2006,** *45*, 3364.

[144] S. Hüttner, M. Sommer, M. Thelakkat, *Appl. Phys. Lett.* **2008,** *92*, 093302.

[145] I. K. Iverson, S.-W. Tam-Chang, *J. Am. Chem. Soc.* **1999,** *121*, 5801.

[146] S. Shoaee, T. M. Clarke, C. Huang, S. Barlow, S. R. Marder, M. Heeney, I. McCulloch, J. R. Durrant, *J. Am. Chem. Soc.* **2010**, *132*, 12919.

[147] F. Würthner, A. Sautter, J. Schilling, *J. Org. Chem.* **2002,** *67*, 3037.

[148] G. Seybold, G. Wagenblast, *Dyes Pigm.* **1989,** *11*, 303.

[149] M. J. Ahrens, M. J. Fuller, M. R. Wasielewski, *Chem. Mater.* **2003**, *15*, 2684.

[150] F.Würthner, P. Osswald, R. Schmidt, T. E. Kaiser, H. Mansikkamäeki, M. Köenemann, *Org. Lett.* **2006**, *8*, 3765.

[151] Y. Zhao, M. R. Wasielewski, *Tetrahedron Lett.* **1999**, *40*, 7047.

[152] S. Nakazono, S. Easwaramoorthi, D. Kim, H. Shinokubo, A. Osuka, *Org. Lett.* **2009,** *11*, 5426.

[153] S. Nakazono, Y. Imazaki, H. Yoo, J. Yang, T. Sasamori, N. Tokitoh, T. Cedric, H. Kageyama, D. Kim, H. Shinokubo, A. Osuka, *Chem.-Eur. J.* **2009,** *15*, 7530.

[154] W. S. Horne, N. Ashkenasy, M. R. Ghadiri, *Chem.-Eur. J.* **2005,** *11*, 1137.

[155] F. Graser, E. Hädicke, *Liebigs Ann. Chem.* **1980**, 1994.

[156] F. Graser, E. Hädicke, *Liebigs Ann. Chem.* **1984**, 483.

[157] E. Hädicke, F. Graser, *Acta*. *Crystallogr. Sect. C* **1986**, *42*, 189.

[158] C. W. Struijk, A. B. Sieval, J. E. J. Dakhorst, M. van Dijk, P. Kimkes, R. B. M. Koehorst, H. Donker, T. J. Schaafsma, S. J. Picken, A. M. van de Craats, J. M. Warman, H. Zuilhof, E. J. R. Sudhölter, *J. Am. Chem. Soc.* **2000**, *122*, 11057.

[159] Z. Chen, A. Lohr, C. R. Saha-Möller, F. Würthner *Chem. Soc. Rev.* **2009**, *38*, 564.

[160] S. A. Z. Shoaee, X. Zhang, S. Barlow, S. R. Marder, W. Duffy, M. Heeney, I. McCulloch, J. R. Durrant, *Chem. Commun.* **2009,** 5445.

[161] A.H. Herz, *Adv. Colloid Interface Sci.* **1977,** *8*, 237.

[162] M. Kasha, H. R. Rawls, M. A. El-Bayoumi, *Pure Appl. Chem.* **1965,** *11*, 371.

[163] V. Czikklely, H. D. Försterling, H. Kuhn, *Chem. Phys. Lett.* **1970,** *6*, 207.

[164] G. Scheibe, *Z. Elektrochem.* **1948,** *52*, 283.

[165] D. Möbius, *Adv.Mater.* **1995,** *7*, 437.

[166] E. Rabinowitch, L. Epstein, *J. Am. Chem. Soc.* **1941,** 63, 69.

[167] H.-M. Zhao, J. Pfister, V. Settels, M. Renz, M. Kaupp, V. C. Dehm, F. Würthner, R. F. Fink, B. Engels, *J. Am. Chem. Soc.* **2009,** *131*, 15660.

[168] G. N. Lewis, M. Kasha, *J. Am. Chem. Soc.* **1944**, *66*, 2100.

[169] G. L. Levinson, W. T. Simpson, W. Curtis, *J. Am. Chem. Soc.* **1957**, *79*, 4314.

[170] E. G. McRae, M. Kasha, *J. Chem. Phys.* **1958**, *28*, 721.

[171] U. Rösch, S. Yao, R. Wortmann, F. Würthner, *Angew. Chem. Int. Ed.* **2006,** *45*, 7026.

[172] A. Dodabalapur, H. E. Katz, L. Torsi, R. C. Haddon, *Science* **1995,** *269*, 1560.

[173] G. Horowitz, F. Kouki, P. Spearman, D. Fichou, C. Nogues, X. Pan, F. Garnier, *Adv. Mater.* **1996,** *8*, 242.

[174] H. E. Katz, A. J. Lovinger, J. Johnson, C. Kloc, T. Siegrist, W. Li, Y.-Y. Lin, A. Dodabalapur, *Nature* **2000,** *404*, 478.

[175] H. E. Katz, T. Siegrist, J. H. Schön, C. Kloc, B. Batlogg, A. J. Lovinger, J. Johnson, *Chem. Phys. Chem.* **2001,** *2*, 167.

[176] P. R. L. Malenfant , C. D. Dimitrakopoulos, J. D. Gelorme, L. L. Kosbar, T. O. Graham, A. Curioni, W. Andreoni, *Appl. Phys. Lett.* **2002**, *80*, 2517.

[177] R. J. Chesterfield, J. C. McKeen, C. R. Newman, P. C. Ewbank, D. A. da Silva Filho, J. L. Brédas, L. L. Miller, K. R. Mann, C. D. Frisbie, *J. Phys. Chem. B* **2004**, *108*, 19281.

[178] S. Tatemichi, M. Ichikawa, T. Koyama, Y. Taniguchi, *Appl. Phys. Lett.* **2006**, *89*, 112108.

[179] B. A. Jones, M. J. Ahrens, M.-H. Yoon, A. Facchetti, T. J. Marks, M. R. Wasielewski, *Angew. Chem. Int. Ed.* **2004,** *43*, 6363.

[180] B. A. Jones, A. Facchetti, T. J. Marks, M. R. Wasielewski, *Chem. Mater.* **2007**, *19*, 2703.

[181] Z. An, J. Yu, S. C. Jones, S. Barlow, S. Yoo, B. Domercq, P. Prins, L. D. A. Siebbeles, B. Kippelen, S. R. Marder, *Adv. Mater.* **2005**, *17*, 2580.

[182] J. H. Oh, S. Liu, Z. Bao, R. Schmidt, F. Würthner, *Appl. Phys. Lett.* **2007**, *91*, 212107.

[183] R. Schmidt, M. M. Ling, J. H. Oh, M. Winkler, M. Könemann, Z. Bao, F. Würthner, *Adv. Mater.* **2007,** *19*, 3692.

[184] M. Gsänger, J. H. Oh, M. Könemann, H. W. Höffken, A.-M. Krause, Z. Bao, F. Würthner, *Angew. Chem. Int. Ed.* **2010,** *49*, 740.

[185] D. Shukla, S. F. Nelson, D. C. Freeman, M. Rajeswaran, W. G. Ahearn, D. M. Meyer, J. T. Carey, *Chem. Mater.* **2008,** *20*, 7486.

[186] L. E. Polander, S. P. Tiwari, L. Pandey, B. M. Seifried, Q. Zhang, S. Barlow, C. Risko, J.-L. Brè das, B. Kippelen, S. R. Marder, *Chem. Mater.* **2011,** *23*, 3408.

[187] Y. A. Getmanenkoa, L. E. Polander, D. K. Hwang, S. P. Tiwari, E. Galán, B. M. Seifried, B. Sandhu, S. Barlow, T. Timofeeva, B. Kippelen, S. R. Marder, *J. Org. Semiconduct.* **2013,** *1*, 7.

[188] A. Babel, S. A. Jenekhe, *J. Am. Chem. Soc.* **2003,** *125*, 13656.

[189] S. Kola, J. Sinha, H. E. Katz, *J. Polym. Sci. Part B: Polym. Phys.* **2012,** *50*, 1090.

[190] X. Zhan, Z. Tan, B. Domercq, Z. An, X. Zhang, S. Barlow, Y. Li, D. Zhu, B. Kippelen, S. R. Marder, *J. Am. Chem. Soc.* **2007,** *129*, 7246.

[191] X. Zhan, Z. Tan, E. Zhou, Y. Li, R. Misra, A. Grant, B. Domercq, X. Zhang, Z. An, X. Zhang, S. Barlow, B. Kippelen, S. R. Marder, *J. Mater. Chem.* **2009**, *19*, 5794.

[192] Z. Chen, Y. Zheng, H. Yan, A. Facchetti, *J. Am. Chem. Soc.* **2009**, *131*, 8.

[193] S. M. Lindner, M. Thelakkat, *Macromolecules* **2004,** *37*, 8832.

[194] S. Hüttner, M. Sommer, M. Thelakkat, *Appl. Phys. Lett.* **2008,** *92*, 093302.

[195] F. J. M. Hoeben, P. Jonkheijm, E. W. Meijer, A. P. H. J. Schenning, *Chem. Rev.* **2005,** *105*, 1491.

[196] F. H. Beijer, R. P. Sijbesma, H. Kooijman, A. L. Spek, E. W. Meijer, *J. Amer. Chem. Soc.* **1998**, *120*, 6761.

Chapter-2

Covalent Side-chain Methacrylate Comb Polymer

2.1. Introduction

Extensive research has been done on perylenebisimides (PBI) as stable electron transporting materials as discussed in detail in the previous chapter. Several low molecular weight perylenebisimides with high electron mobilities are reported,[1-13] but these small molecule analogues cannot compete with the polymers in terms of the viscosity range quintessential for the fabrication of flexible large area plastic electronic devices. In this context, polymers containing perylenebisimide groups are attractive because they can be easily processed from solution to give smooth and uniform films, excellent rheological properties for printing techniques as well as good mechanical strength to realize flexible substrates. Polymers owe the interesting properties like film forming ability and processability partly because of their macromolecular size and partly from entanglement behaviour in the bulk. The long polymer chains entangle with each other like strands of cooked spaghetti in a bowl and this gives the polymers resistance to breakage in contrast to small molecules which are like sugar cubes that do not entangle. (see figure-2.1)

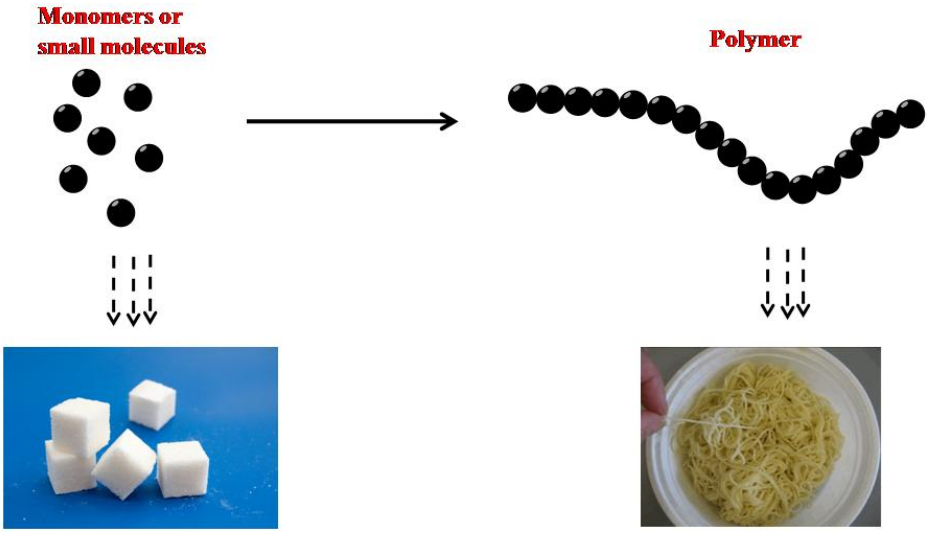

Figure-2.1. Polymers versus small molecules.

Not all polymers are linear chains, several complex polymer geometries like the star polymers, block-copolymers, comb-polymers, branched, crosslinked etc. are explored as illustrated in figure-2.2. When perylenebisimides were incorporated

into polymers exploring the various polymer architectures, the result has been mostly disappointing due to limitations like formation of low molecular weight oligomers with less or no solubility in common organic solvents as evident from several literature reports. For example, a series of homopolyimides of perylene obtained by condensation of PTCDA with different aliphatic amines of varying length as well random copolyimides with commercially available dianhydrides were reported by Wang *et al.* (Figure-2.3(a)-(c)), but unfortunately these polymers were soluble only in concentrated sulphuric acid (H_2SO_4) or very high boiling solvents like ortho-dichlorobenzene (ODCB).[14]

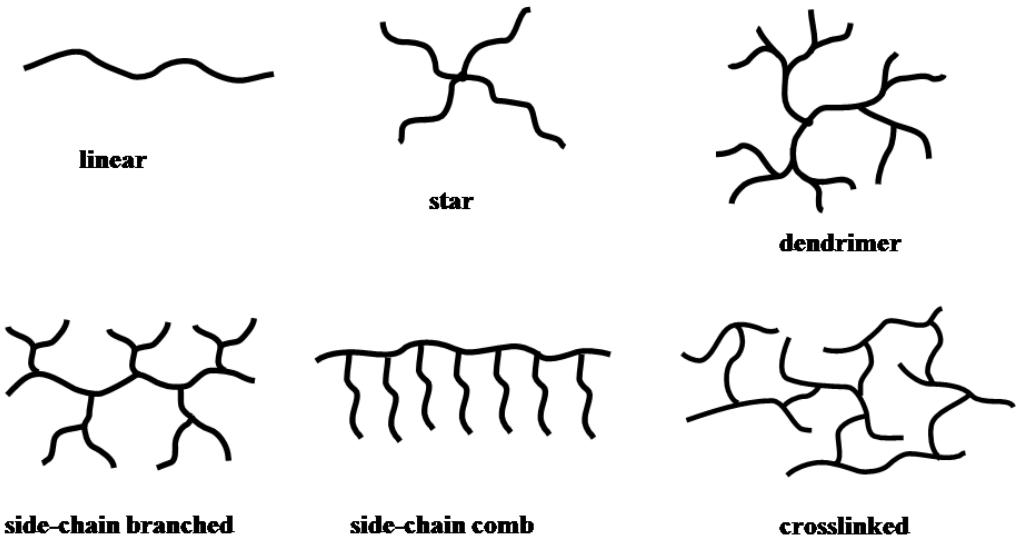

Figure-2.2. Different covalently linked polymer geometries.

Neuteboom *et al.* reported several homopolymers based on perylenebisimide and poly-tetrahydrofuran (poly-THF) (figure-2.3(d)) and studied their self-organization properties.[15] But these polymers were also soluble only in orthodichlorobenzene. Soluble main-chain PBI polymers have been synthesized by introducing highly solubilizing bay substituents. For example Shim *et al.* reported polyesters and polyurethanes based on PBIs with solubilizing p-tert-butylphenoxy groups at the bay position,[16] rendering the polymers soluble in solvents like chloroform ($CHCl_3$), tetrahydrofuran (THF), N,N'-dimethylformamide (DMF) etc.

But bay substitution causes a twist in the perylene core, thus altering the optoelectronic properties.

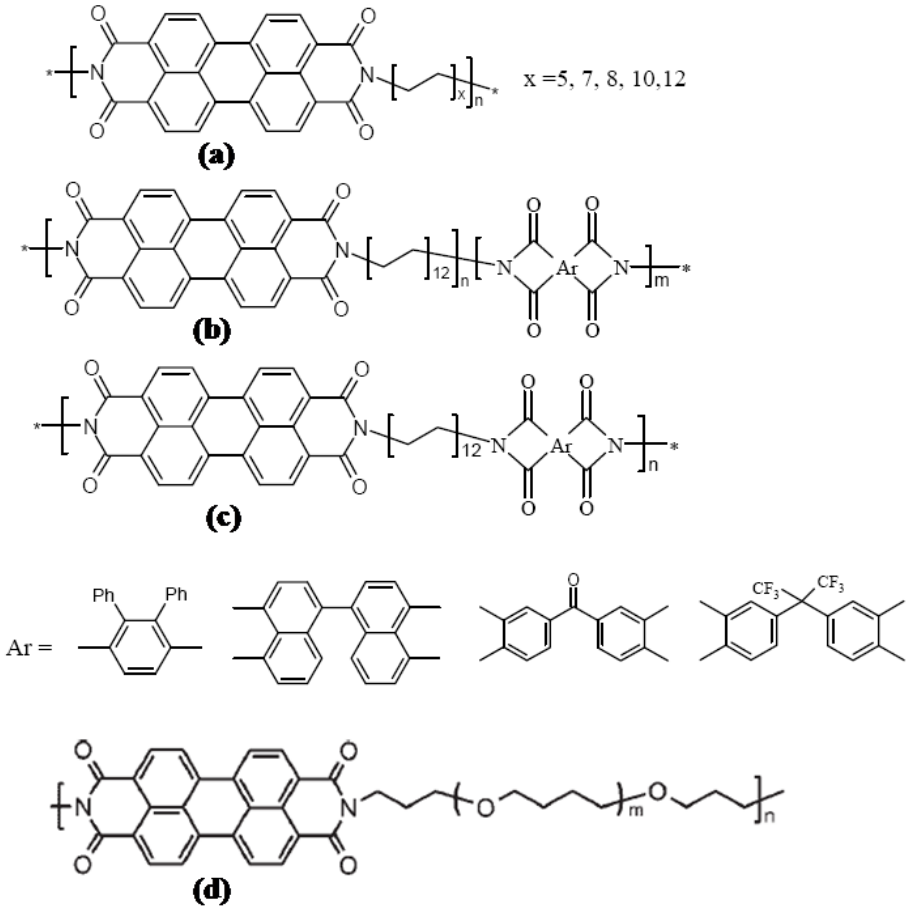

Figure-2.3. Structures of various main chain perylenebisimide polymers reported in literature. [*Adapted from ref.15 and ref.16*]

Copolymerization with other soluble monomers is another approach that has been adopted to improve the solubility of linear PBI polymers. Wang *et al.* has reported poly(aryl ether imide)s incorporating PBI or NBI (naphthalenebisimides) and bisphenol units, but found that soluble high molecular weight polymers could be obtained only with lower feed ratios of rylene diimide units; higher feed ratios resulted in insoluble oligomers.[17] The same inference was observed from our research group where Jancy *et al.* reported a series of soluble random copolyurethanes of PBI and NBI based aliphatic-diols along with

cyclohexyldimethanol and isophorone diisocyanate (figure-2.4).[18] They found that for soluble PBI, the maximum dye loading was only 14% whereas upto 46% dye loading could be achieved for soluble NBI copolymers.

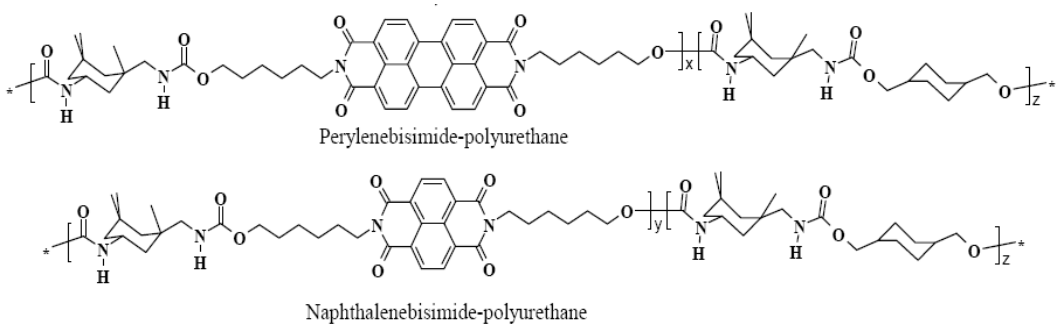

Figure-2.4. Linear copolyurethanes of PBI and NBI with cyclohexyldimethanol and isophorone diisocyanate. [*Adapted from ref.18*]

Yet another report from our group by Nagesh *et al.* studied the synthesis and device characteristics of a novel poly(benzobisoxazole imides) containing perylene and/or naphthalene units in an alternating fashion with the oxazole units (figure-2.5).[19] The polymers showed reasonably good n-type charge transport in FET (field effect transistor) device, but unfortunately could be processed only from protic methanesulphonic acid solvent.

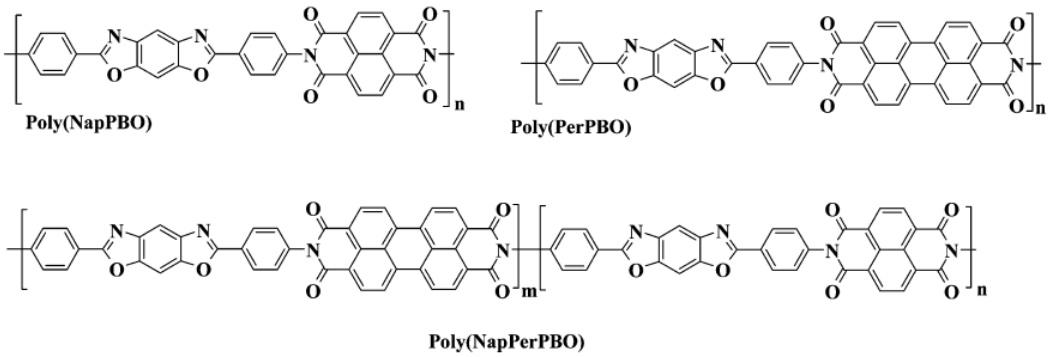

Figure-2.5. Rigid-rod alternating co-poly(benzobisoxazole imides) of PBI and/or NBI. [*Adapted from ref.19*]

But in the last few years several promising solution processable architectures like alternating copolymers PBI or NBI with bithiophene moiety has emerged with the breakthrough discovery from Facchetti *et al.* as discussed in detail in section 1.6(c).[20] Another growing area of polymeric n-type materials is based on the side-chain architecture. Incorporating the rigid PBI cores into a side-chain polymer scaffold has several advantages like a wide range of possibilities to increase the solubility beyond imide and bay functionalizations, more number of PBI units can be accommodated in a single polymer chain and pre-programmed polymer designs with additional self organizing motifs like hydrogen bonding can improve the ordering of PBI units within the chain. Compared to main-chain perylenebisimide polymers very few reports are available on the side chain comb polymers. The major contribution to side-chain perylenebisimide polymers has come from the group of Thelakkat and co-workers.[21-32] They designed a highly soluble and polymerizable PBI derivative referred to as perylenebisimide acrylate (PerAcr) starting from an asymmetrically substituted simple PBI bearing a branched swallow tail at one imide position and a linear acrylate functionalized alkyl spacer at the other imide position without any hydrogen bonding motifs.[21] This acrylate monomer was homo-polymerized by nitroxide mediated radical polymerization (NMRP). It has also been successfully incorporated as the acceptor block into several donor-acceptor block copolymers with different donor blocks such as poly(vinyltriphenylamine) (PvTPA), poly(3-hexylthiophene) (P3HT) etc. to give the corresponding PvTPA-block-PPerAcr,[21] P3HT-block-PPerAcr,[33,34] P3HT-block-poly(BA-stat-PPerAcr)[35] block copolymers which were studied for photovoltaic applications. The homopolymer PPerAcr (figure-2.6 (a)) was demonstrated to exhibit electron mobilities upto 10^{-3} $cm^2V^{-1}s^{-1}$.[36] However, Thelakkat *et al.* also showed that polymerization of perylenebisimide (PBI) acrylate monomers by NMRP was not ideal and was limited to certain specifically substituted monomers, due to which the polymerization worked only in highly concentrated solutions.[29] This put a limitation on the choice of substituents at perylenebisimide pendants and hence on the polymerization conditions due to

solubility issues. They also observed transfer reactions in NMRP of PBI acrylates which lead to broad molecular weight distribution in the homopolymers as well as block co-polymers. To overcome these issues, a combination of NMRP and click chemistry was also demonstrated by the same group.[29] Palermo *et al.* has reported for the first time novel soluble perylenebisimide based poly(isocyanopeptides) (figure-2.6(b)) with precisely organizing chromophoric arrays into functional 2D wires.[37,38] This is the first report on a hydrogen bonded side-chain PBI polymer. Extensive molecular dynamics studies and spectroscopic analyses revealed a well defined 4_1 helix in which the PBI units formed four "helter-skelter-like" (fig-2.6(b) right) overlapping pathways along excitons and electrons could rapidly migrate and a cast film of this polymer fibers showed n-type FET behaviour with an electron mobility of 10^{-3} $cm^2V^{-1}s^{-1}$. [38]

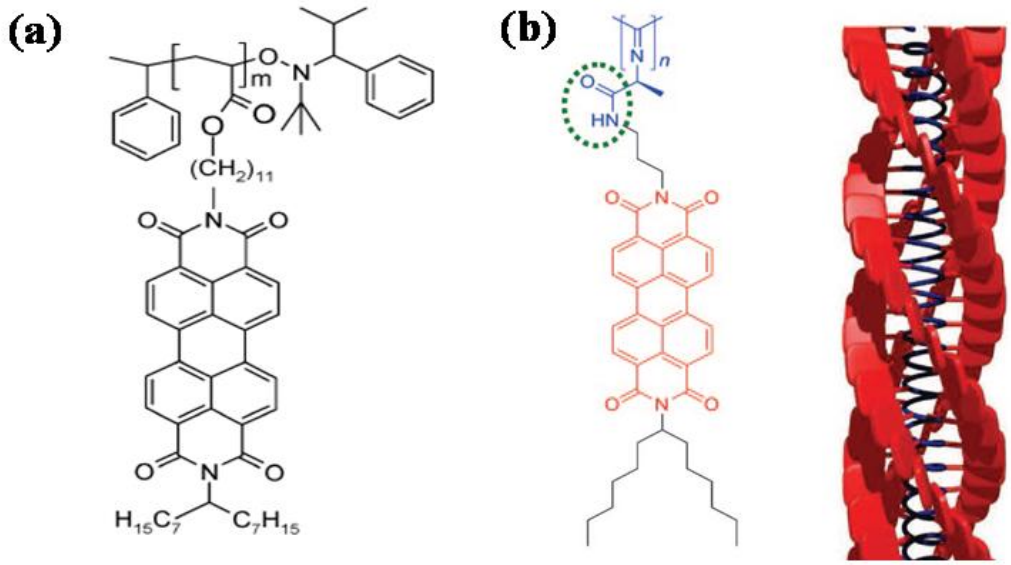

Figure-2.6. **S**tructures of (a) Poly(PerAcr) and (b) PBI based Poly(isocyanopeptide). [*Adapted from ref.21 and ref.37 respectively*]

Orozco and Thelakkat *et al.* recently demonstrated a synthetically novel route to highly soluble PBI based side-chain polymers viz., poly(perylene diester benzimidazole acrylate) (PPDB) and poly(perylene diester imide acrylate) (PPDI) synthesized by nitroxide-mediated radical polymerization (NMRP) (figure-2.7).[39]

The PPDB polymer showed n-type characteristics with electron mobilities of 3.2 $\times 10^{-4}$ $cm^2V^{-1}s^{-1}$ obtained in a diode configuration by fitting the space-charge-limited current (SCLC) according to the Mott–Gurney equation.[39] In contrast, the PPDI polymer preferentially exhibited a p-type behaviour with a hole mobility of 1.5×10^{-4} $cm^2V^{-1}s^{-1}$, which was attributed to the less electron-deficient perylene core of PPDI compared to PPDB.

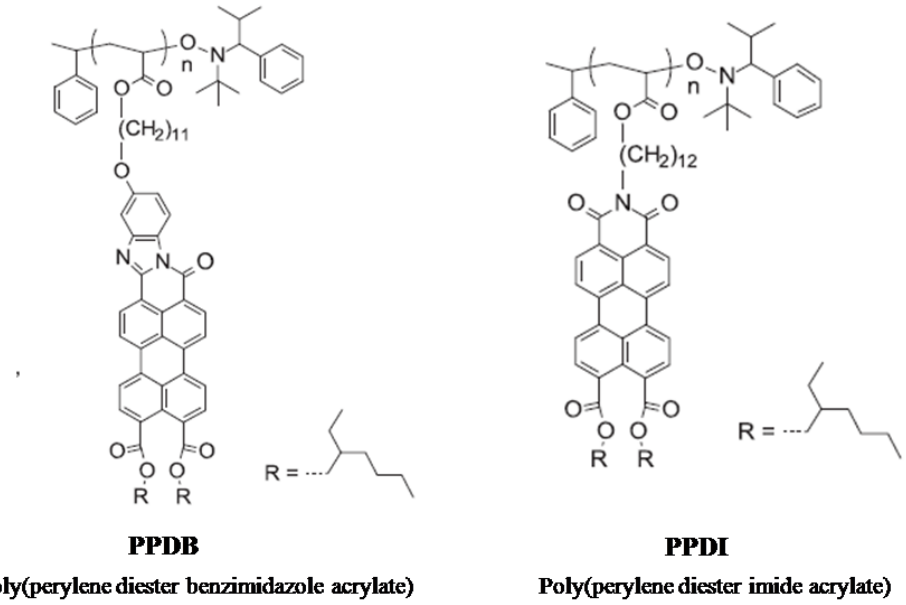

Figure-2.7. Structures of perylene diester acrylates PPDB and PPDI. [*Adapted from ref.39*]

Deepak *et al.* from our group introduced a novel side-chain urethane methacrylate monomer design with a polymerizable methacrylic backbone and side-arm decorated with self-organization driving hydrogen-bondable urethane linkage along with a critical balance of hydrophilic-hydrophobic mass which could be manipulated by varying the bulky pendant groups.[40] They varied the hydrophobicity of the anchoring groups using different linear and cyclo-aliphatic terminal units like ethane, n-decane, tricyclodecane (TCD) and adamantane (Adm) and the corresponding homopolymers (figure-2.8) were obtained by simple free radical polymerization. Solvent assisted self-organization studies of these polymers showed that especially the bulky tricyclodecane and adamantane anchored

methacrylate polymers formed nice 3D-honeycomb patterns when evaporated from THF-water solvent mixture, whereas the linear analogues failed to produce any microstructures. This report provided a platform to investigate the influence of bulky aromatic groups as anchoring groups into this unique polymer design, especially the fused polycyclic perylenebisimide aromatic core which has an intrinsic tendency to self-organize via π-π stacking secondary forces.

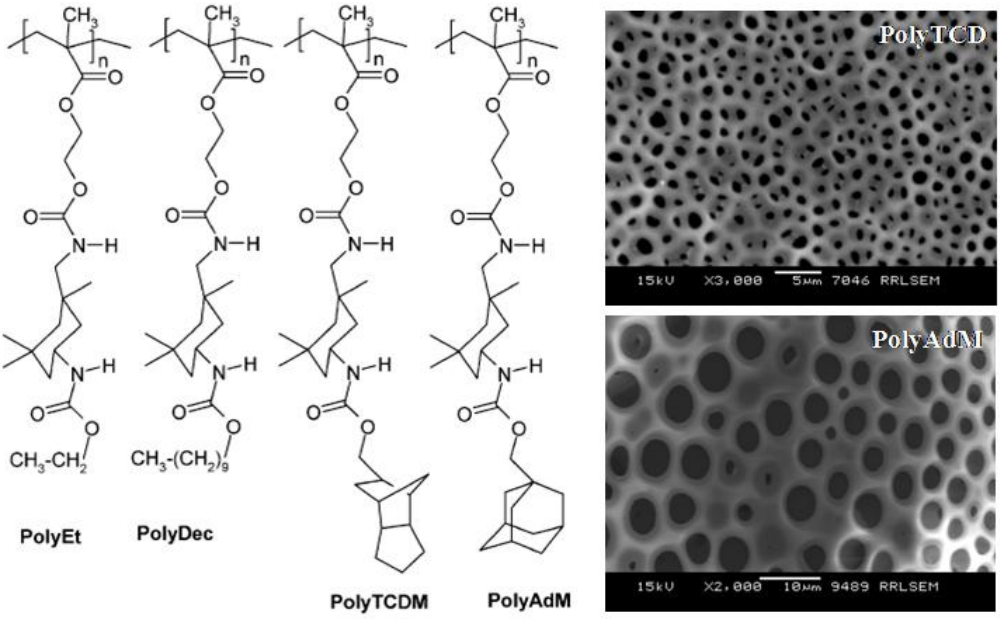

Figure-2.8. Structures of the urethane methacrylate homopolymers with different linear and cyclo-aliphatic pendant groups and SEM images of solvent drop cast PolyTCDM and PolyAdM films. [*Adapted from ref.40*]

So in this chapter the same polymer architecture was extended to incorporate different aromatic moieties and the molecules of choice were a simple renewable resource based phenol - cardanol as well as its saturated analogue 3–pentadecyl phenol[47,48] and an asymmetrically substituted PBI with a branched alkyl chain on one imide position and an alkyl-spacer-OH on the other imide for further functionalization (Scheme-2.1). The monomers were synthesized in one pot by coupling one equivalent of isophorone diisocyanate (IPDI) with one equivalent of cardanol/pentadecylphenol/PBI-OH followed by coupling with one equivalent of

hydroxyl ethyl methacrylate (HEMA). The cardanol and pentadecylphenol based urethane methacrylate macromonomers were highly soluble in almost all common organic solvents, while the PBI based macromonomer showed negligible solubility which prompted the structural redesigning of the monomer for PBI. Thus the rigid cyclo-aliphatic kinked IPDI ring was removed and two new PBI based methacrylic monomers with and without hydrogen bonding motifs were designed and synthesized.

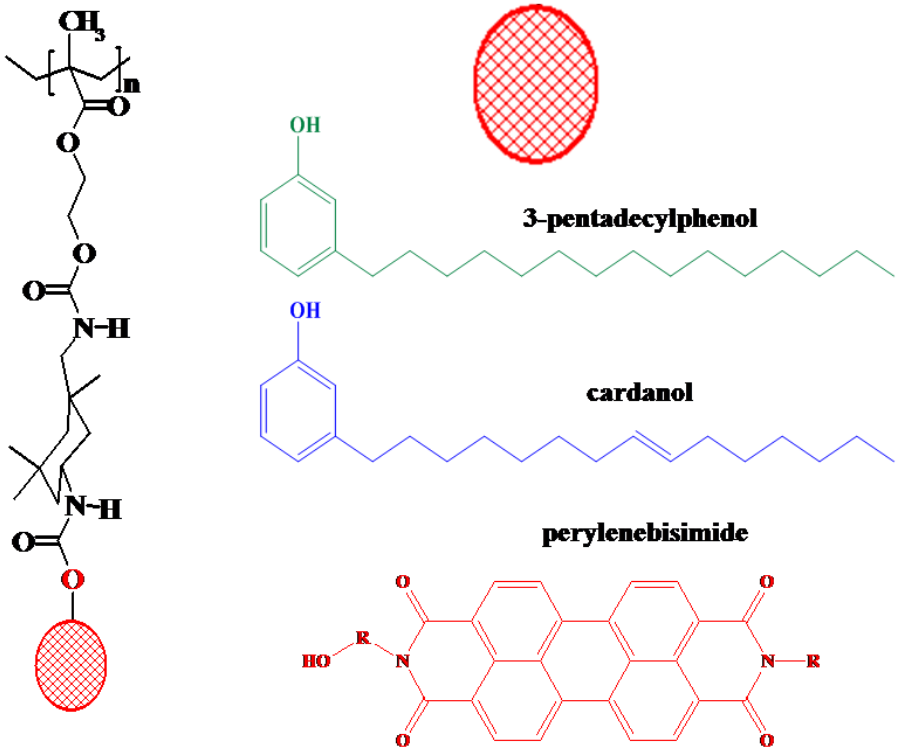

Scheme-2.1

Polymerization of all these monomers were attempted by simple free-radical polymerization in solution. However both the PBI based monomers failed to undergo polymerization even under a condition of varied parameters such as solvent, temperature, initiator etc. On the other hand the simple cardanol and 3-pentadecyl phenol based monomers readily underwent free radical polymerization under identical conditions. Accordingly these two polymers were taken up for further solvent induced self-assembly studies and their morphology analysis from

solvent cast films studied using microscopic techniques like scanning electron microscopy (SEM), transmission electron microscopy (TEM) and atomic force (AFM) microscopy showed the formation of three - dimensional honeycomb morphology in $CHCl_3$ whereas in THF they formed spheres. The cardanol derived polymer PCIH showed a tendency for multiple morphologies like spheres and tubes in THF. These self-assembled structures were proposed to arise from a combination of hydrogen bonding between the urethane groups, aromatic π-π stacking and alkyl chain hydrophobic interactions.

2.2. Experimental Section

2.2.1. Materials: The starting materials perylene tetracarboxylic acid dianhydride (PTCDA), 2-ethylhexyl amine, 6-amino-1-hexanol, isophorone diisocyanate (IPDI), 2-hydroxyethyl methacrylate (HEMA), 2-isocyanatoethyl methacrylate, methacrylic acid, dibutyltindilaurate (DBTDL), 3-pentadecyl phenol (PDP), benzoyl peroxide (BPO), Azobisisobutyrolnitrile (AIBN) and other reagents were purchased from Aldrich and used as received. Cardanol was obtained by double vacuum distillation of CNSL purchased from Vijayalekshmi Cashew Industry, Kollam, India. Solvents used were purchased locally and purified by standard procedures.

2.2.2. Instrumentation Details: ^{1}H NMR spectra were recorded using 300-MHz Bruker NMR spectrophotometer in $CDCl_3$ or ($CDCl_3$ + trifluoroacetic acid (TFA)) deuterated solvents containing small amounts of tetramethylsilane (TMS) as internal standard. The purity of the monomers was determined by JEOL JSM600 fast atom bombardment (FAB) high-resolution mass spectrometry and MALDI-TOF spectral analyses. Infrared spectra were recorded using Perkin Elmer, Spectrum one FT-IR spectrophotometer. The liquid or solid samples were recorded in the range of 4000 to 400 cm^{-1}. The purity of the monomers and the molecular weights of the polymers were determined by SEC (size exclusion chromatography) in THF using polystyrene standards for the calibration. Waters 515 Pump connected through three series of Styragel HR columns (HR-3, HR-4E and HR-5E) and Waters Model 2487 Dual Wavelength UV-Vis Detector and a Waters 2414 Differential Refractometer was used for analyzing the samples. The flow rate of the THF was maintained as 1 mL throughout the experiments and 1 wt % (10 mg in 1 mL) of the polymer solution was filtered and injected for recording of the SEC chromatograms at 30 °C. The GPC (gel permeation chromatography) instrument was calibrated with different polystyrene standards having molecular weights ranging from 2950-177000 g/mol (Polymer Standards Service-USA, Inc.). The thermal stability of the polymers was determined using DTG-60 Shimadzu

thermogravimetric analyzer at a heating rate of 10 °C/min in nitrogen. DSC measurements were performed on a DSC-Perkin-Elmer Pyris 6 DSC instrument at a heating rate of 10 °C/min under nitrogen atmosphere. Typically, 2-3 mg of samples was placed in an aluminium pan, sealed properly and scanned from 10-280 °C. The instrument was calibrated with indium standards before measurements. For SEM (scanning electron microscopy) measurements, polymer samples were provided with a thin gold coating using JEOL JFC-1200 fine coater. The probing side was inserted into JEOL JSM-5600 LV scanning electron microscope for taking photographs. The sample preparation method adopted was as follows. $1x10^{-2}$ M solutions of the polymers in different solvents were prepared. A drop of this clear solution was placed on a clean glass slide and was allowed to evaporate slowly in air. All films were prepared at atmospheric pressure without air flow. Transmission Electron Microscopy (TEM) images were recorded using a JEOL-JEM-1011 instrument at 80 KV. For the measurements, a drop of the polymer solution was deposited directly on Formvar-coated copper grid. No staining treatment was performed for the measurement. AFM (atomic force microscopy) images were taken by a Multimode^{TM} Scanning Probe Microscope equipped with Nanoscope IV^{TM} controller from Veeco Instrument Inc., Santa Barbara in the contact mode using a SiN probe, with maximum scan size 10μm x10μm and with vertical range of 2.5 μm. For the AFM studies, $1x10^{-4}$ M filtered solution in $CHCl_3$ was drop cast on freshly cleaved mica sheet.

2.2.3. Synthesis

Synthesis of Cardanol and 3-Pentadecylphenol based Methacrylic Macromonomers

Synthesis of Cardanol–IPDI-HEMA (CIH). 2-Methyl-acrylic acid 2-(3, 3, 5-trimethyl-5-{[((E)-3-pentadec-8-enyl)-phenoxycarbonylamino]-methyl}-cyclohexyl carbamoyloxy)-ethyl ester: Isophorone diisocyanate (IPDI) (1.71 g, 7.7 mmol) in 6 mL dry DMF was taken in a 100 mL two necked round bottom flask and the contents were cooled with ice. Three drops dibutyltindilaurate (DBTDL) was added as catalyst followed by drop wise addition of cardanol (2.32 g, 7.7 mmol) in 6 mL

dry DMF under nitrogen atmosphere over a period of 0.5 hour. The reaction was allowed to proceed under ice cold conditions for further 2 hours and then left stirring at room temperature overnight. Hydroxyethyl methacrylate (HEMA) (1 g, 7.7 mmol) and 3 mL dry DMF were then added to the reaction mixture under ice cold conditions within 0.5 hours and then slowly heated to 55 °C for 6 hours. The contents were poured into 300 mL water and extracted with dichloromethane (DCM). The extract was washed with plenty of water and 5% NaOH solution and then dried over anhydrous sodium sulphate. The solvent was removed under reduced pressure and dried in vacuum oven at 60 °C for 2 hours. The product was then purified by column chromatography on a 100-200 mesh silica gel column using hexane/ethyl acetate (70:30.v/v) solvent mixture. Yield: 68% (3.42g). ^{1}H NMR (300 MHz, $CDCl_3$) δ ppm: 7.23(t, 1H, Ar-**H**); 7.01-6.91 (m, 3H, Ar-**H**); 6.14, 5.59 (2s, 2H, C**H$_2$**=C, of methacrylic double bond); 5.42-5.32 (m, 2H, C**H**=C**H**, side chain unsaturation of cardanol); 5.02-4.87 (m, -N**H**); 4.34 (b, 4H, -OC**H$_2$**C**H$_2$**O- of HEMA); 3.89 (b, 2H, -C**H$_2$**-NH-COO of IPDI); 2.58 (t, 2H, Ar-C**H$_2$**); 2.05-1.99 (m, 4H, -C**H$_2$**CH=CHC**H$_2$**- of side chain unsaturation); 1.95 (s, 3H, C**H$_3$** of HEMA); 1.59 (b, 2H, Ar-CH_2-C**H$_2$**-); 1.79-0.85 (other aliphatic protons). ^{13}C NMR (75 MHz, $CDCl_3$, δ ppm):167.12, 156.61, 155.33, 154.06, 150.88, 144.28, 135.73, 130.18, 129.92, 129.77, 129.73, 129.64, 129.14, 127.99, 127.84, 127.43, 126.04, 125.15, 121.38, 121.25, 118.65, 118.55, 62.79, 62.47, 34.97, 31.77, 31.13, 29.53, 29.47, 29.23, 29.20, 29.07, 28.82, 27.05, 22.53, 22.49, 13.9. FT-IR (cm^{-1}): 3382, 3010, 2921, 1716, 1638, 1588, 1487, 1306, 1155, 1039, 944, 908, 814, 779, 696. MALDI-TOF MS (MW = 654.99) m/z = 677.23$[M + Na]^+$

The urethane methacrylate monomer of saturated cardanol (3-pentadecyl phenol) was synthesized under similar experimental conditions.

Synthesis of Saturated-Cardanol-IPDI-HEMA (SCIH). 2-Methyl-acrylic acid 2-{3, 3,5-trimethyl-5-[(3-pentadecyl-phenoxycarbonylamino)-methyl]-cyclohexyl carbamoyloxy]-ethyl ester: 2.41 g, 7.9 mmol of saturated cardanol (3-pentadecyl

phenol) was used to obtain the urethane methacrylate monomer. The product was then purified by column chromatography on a 100-200 mesh silica gel column using hexane/ethyl acetate (70:30.v/v) solvent mixture. Yield : 74% (3.85g) ^{1}H NMR (300MHz, $CDCl_3$) δ ppm: 7.22(t, 1H, Ar-**H**); 6.99-6.93 (m, 3H, Ar-**H**); 6.12, 5.58 (2s, 2H, C**H$_2$**=C of HEMA); 5.25-4.94 (m, N**H**); 4.31 (s, 4H, -OC**H$_2$**C**H$_2$**O- of HEMA); 3.93 (b, 2H, -C**H$_2$**-NH-COO of IPDI); 2.57 (t, 2H, Ar-C**H$_2$**); 1.93 (s, 3H, C**H$_3$** of HEMA); 1.58 (b, 2H, Ar-CH_2-C**H$_2$**-); 1.88-0.83(other aliphatic protons). ^{13}C NMR (75 MHz, $CDCl_3$, δ ppm):167.15, 155.65, 150.89, 144.36, 135.77, 128.79, 126.03, 125.17, 121.38, 118.63, 67.79, 62.82, 46.71, 45.93, 36.30, 35.64, 35.01, 31.78, 31.15, 29.55, 29.37, 29.21, 27.55, 25.45, 23.08, 22.55, 18.16, 13.99. FT-IR (cm^{-1}): 3352, 3055, 2924, 2854, 1723, 1633, 1554, 1463, 1386, 1306, 1232, 1155, 1069, 1016, 952, 809, 773, 737, 694. MALDI-TOF MS (MW = 656.9) m/z = 679.61[M+ Na]$^{+}$.

Synthesis of Perylenebisimide based Methacrylic Macromonomers

Synthesis of precursor unsymmetrical Perylenebisimide. N-Ethylhexyl, N'-(6-hydroxyhexyl)-perylene-3,4:9,10-tetracarboxylic bisimide (PBI-2): Perylene-3,4:9,10-tetracarboxylic dianhydride (2.5 g, 6.38 mmol) was heated in 60 mL N,N'-dimethylacetamide (DMAc) for half an hour followed by simultaneous addition of 6-aminohexanol (0.746 g, 6.38 mmol) and 2-ethylhexylamine (0.823 g, 6.38 mmol) under nitrogen atmosphere. The reaction mixture was stirred at 110°C for 4-6 hours in presence of catalytic amount of $Zn(OAc)_2$. The excess DMAc was then removed by vacuum distillation and the slurry was washed with water and then triturated in hexane and finally dried in vacuum oven for 12 hours. This crude mixture which consisted of 3 major components viz., symmetrically substituted ethylhexyl derivative (PBI-1), the desired unsymmetrically substituted perylenebisimide with ethylhexyl group on one imide position and hexanol on other side (PBI-2) and symmetrically hexanol substituted PBI-3 were separated by column chromatography on silica gel using $CHCl_3$/ MeOH mixture. The PBI-1 was eluted

in 100% $CHCl_3$, PBI-2 in $CHCl_3$/ MeOH (97/3 v/v) and PBI-3 in $CHCl_3$/ MeOH (90/10 v/v).

N, N'-Bis-Ethylhexyl-perylene-3,4:9,10-tetracarboxylic bisimide (PBI-1): Yield : 26 % . ^{1}H NMR (300 MHz, $CDCl_3$) δ ppm: 8.64(dd, 8H, perylene); 4.16(m, 4H, imide-C**H**$_2$); 1.99(m, 2H, imide-CH_2-C**H**); 0.98-0.92(2t, 12H, end CH_3 of ethyl hexyl tail); 1.44-1.28(other aliphatic protons). ^{13}C NMR (75 MHz, $CDCl_3$) δ ppm: 159.3, 135.7, 130.9, 129.2, 47.0, 37.0, 31.7, 29.3, 23.0, 14.1 FT-IR (cm^{-1}): 2956, 2931, 2850, 1709, 1649, 1600, 1446, 1336, 1255, 1183, 1086, 1024, 793, 745, 644. MALDI-TOF MS (MW = 614) m/z = 615.05$[M+1]^+$.

N-Ethylhexyl, N'-(6-hydroxyhexyl)-perylene-3,4:9,10-tetracarboxylic bisimide (PBI-2): Yield : 43 % ^{1}H NMR (300 MHz, $CDCl_3$) δ ppm: 8.64(dd, 8H, perylene); 4.18-4.02 (m, 4H, imide-C**H**$_2$); 3.60 (t, 2H, C**H**$_2$-OH); 0.98-0.92 (2t, 12H, end CH_3 group of 2-ethyl hexyl tail). ^{13}C NMR (75 MHz, $CDCl_3$) δ ppm: 163.4, 134.4, 131.3, 129.3, 126.3, 123.2, 100, 72.2, 62.8, 44.4, 40.5, 37.9, 32.6, 29.7, 28.7, 25.3, 23.1, 14.2, 10.7 FT-IR (cm^{-1}) :3436, 2955,2857, 2928, 1694, 1650, 1594, 1577, 1440, 1402, 1380, 1343, 1245, 1177, 1082, 851, 809, 745, 633. MALDI-TOF MS (MW = 603) m/z = 604.16$[M+1]^+$.

N, N'-Bis-(6-hydroxyhexyl)-perylene-3,4:9,10-tetracarboxylic bisimide (PBI-3): Yield : 23 % ^{1}H NMR (300 MHz, $CDCl_3$/TFA) δ ppm: 8.79(dd, 8H, perylene); 4.40(t, 4H, imide C**H**$_2$); 4.26 (t, 4H,C**H**$_2$OH of hexanol chain); 1.80(m, 8H, near to imide group); 1.51(m, 8H, near to OH). ^{13}C NMR (75 MHz, $CDCl_3$/TFA) δ ppm: 165.2, 162.9, 162.1, 161.2, 160.3, 135.6, 132.9, 124.2, 122.7, 122.3, 117.1, 111.4, 105.7, 68.7, 27.8, 26.3, 25.1 FT-IR (cm^{-1}) : 3551, 3518, 2941, 2841, 1682, 1649, 1595, 1437, 1394, 1336, 1250, 1158, 1091, 1024, 971, 797, 755, 625. MALDI-TOF MS (MW = 590) m/z = 590$[M]^+$.

Synthesis of Perylenebisimide-IPDI-HEMA (PBI-IH): Isophorone diisocyanate (IPDI) (0.295 g, 1.32 mmol) in 3mL dry DMAc was taken in a 100 mL two necked round bottom flask and the contents were cooled with ice. Three drops dibutyltindilaurate (DBTDL) was added as catalyst followed by drop wise addition

of unsymmetrical PBI-2 (0.800 g, 1.32 mmol) in 16 mL dry DMAc under nitrogen atmosphere over a period of 0.5 hour. The reaction was allowed to proceed under ice cold conditions for further 2 hours and then left stirring at room temperature overnight. Hydroxyethyl methacrylate (HEMA) (0.173 g, 1.32 mmol) and 3 mL dry DMAc were then added to the reaction mixture under ice cold conditions within 0.5 hour and then slowly heated to 65 °C for 9 hours under inert atmosphere. The contents were poured into 300 mL water, washed thoroughly with 200x3 mL water, filtered and dried in vacuum oven at 60 °C overnight. But this product could not be solubilized in any of the common organic solvents. Accordingly this product was not characterized and further PBI methacrylate monomers without any kinked IPDI units were synthesized as follows.

Synthesis of Perylenebisimide-Methacrylate with hydrogen bonding (PBI-HB).2((((6-(9-(2-ethylhexyl)-1,3,8,10-tetraoxo-3,8,9,10-tetrahydroanthra[2,1,9-*def*:6,5,10*d'e'f'*] di isoquinolin-2(1H)-yl)hexyl)oxy)carbonyl)amino)ethylmethacrylate: Unsymmetrical PBI-2 (0.139 g, 0.23 mmol) dissolved in 15 mL dry DMAc was taken in a 100 mL two-neck round bottom flask. Two drops of DBTDL catalyst were added followed by slow addition of 2-isocyanatoethyl methacrylate (0.042 g, 0.27 mmol) under ice-cold conditions within a period of 30 minutes. The reaction mixture was then left stirring at room temperature for 12 hours under nitrogen atmosphere. The excess solvent DMAc was removed by vacuum distillation and the left over residue was washed sequentially with water, methanol and hexane. Finally dried in vacuum oven at 65 °C overnight. The crude product was purified by column chromatography using solvent mixture of $CHCl_3$/MeOH (97/3 v/v). Yield : 83 % ^{1}H NMR (300 MHz, $CDCl_3$) δ ppm: 8.65 (m, 8H, perylene); 6.14, 5.60 (2s, 2H, C**H$_2$**=C of methacrylate group); 4.27-4.06 (m, combined 8H corresponding to 4H from two imide-C**H**$_2$, 2H from -C**H$_2$**- urethane carbonyl CO and 2H from -C**H$_2$**-O-CO-NH); 3.50 (m, 2H, from -C**H$_2$**- near urethane NH); 1.95 (s, 3H, C**H$_3$** of methacrylate group); 1.88-0.94(other aliphatic protons). ^{13}C NMR (75 MHz, $CDCl_3$) δ ppm: 167.2,167.8, 159.3, 138.2, 135.7, 130.9, 129.2, 125.2,67.4, 47.0, 37.0, 34.97, 31.77, 31.13, 29.53, 29.47, 29.23, 29.20, 23.0, 14.1 FT-IR (cm^{-1}):

3352, 3055, 2956, 2931, 2850, 1709, 1649, 1600, 1446, 1336, 1255, 1183, 1086, 1024, 952, 809, 793, 773, 745, 737, 694, 644. MALDI-TOF MS (MW = 757.34) m/z = 780.40 $[M+Na]^+$.

Synthesis of Perylenebisimide-Methacrylate without hydrogen bonding (PBI-NHB). 6-{9-(2-ethylhexyl)-1,3,8,10-tetraoxo-3,8,9,10-tetrahydroanthra[2,1,9-*def*:6,5,10-*d'e'f'*]diiso quinolin-2(1H)-yl)hexyl methacrylate: The unsymmetrical PBI-2 (0.300 g, 0.51 mmol) in 15 mL toluene was taken in a 100 mL two-neck round bottom flask to which p-toluene sulfonic acid (0.0002 g, 0.0012 mmol), methacrylic acid (0.056 g, 0.65 mmol) and a catalytic amount of hydroquinone was added. The flask was then connected to the Dean Stark apparatus and a water reflux condenser. The reaction mixture was subsequently heated to 135 °C for 24 hours. The contents were then poured to 150 mL water which gave a pasty mass and upon washing with MeOH (methanol) the product was precipitated as fine powder which was filtered, dried and purified by column chromatography using solvent mixture of $CHCl_3$/MeOH (98/2 v/v). Yield : 92 % ^{1}H NMR (300 MHz, $CDCl_3$) δ ppm: 8.70 (m, 8H, perylene); 6.10, 5.55 (2s, 2H, C**H$_2$**=C of methacrylate group); 4.26 - 4.13 (m, 6H, from two imide-C**H**$_2$ groups and C**H$_2$**-O-CO-NH); 1.94 (s, 3H, C**H$_3$** of methacrylate group); 1.88-0.88 (other aliphatic protons). ^{13}C NMR (75 MHz, $CDCl_3$) δ ppm: 167.2, 136.2, 130.9, 129.2, 125.2, 67.4, 47.0, 40.4, 37.0, 34.97, 31.77, 31.13, 29.53, 29.47, 29.23, 29.20, 25.6, 23.0, 14.1 FT-IR (cm^{-1}): 3423, 2931, 2850, 1709, 1649, 1600, 1446, 1336, 1255, 1183, 1086, 1024, 954, 893, 854, 816, 793, 773, 745, 732, 658. MALDI-TOF MS (MW = 670.30) m/z = 671.29 $[M+1]^+$.

Polymerization

Free Radical Polymerization of CIH: CIH (0.879 g, 1.34 mmol) and benzoyl peroxide (BPO) (0.09 g, 0.004 mmol) were taken in THF (3 mL) in a 10 mL round-bottomed flask provided with a water condenser. The reaction mixture was purged with nitrogen for 10 min. The polymerization was carried out by stirring the contents at 65 °C for 24 hours. The viscous liquid was cooled and precipitated into water. Yield : 75.8% ^{1}H NMR (300 MHz, $CDCl_3$) δ ppm: 7.23 (b, 1H, Ar-**H**);

7.01-6.93 (b, 3H, Ar-**H**); 5.41-5.34 (m, 2H, C**H**=C**H**, side chain unsaturation of cardanol); 4.23-3.74 (b, 4H, -OC**H**$_2$C**H**$_2$O- of HEMA); 2.58 (b, 2H, Ar-C**H**$_2$); 2.01-0.85 (aliphatic protons). ^{13}C NMR (75MHz, $CDCl_3$, δ ppm): 177.25, 158.75, 155.51, 150.93, 144.41, 129.90, 129.77, 129.11, 128.02, 125.41, 121.51, 118.82, 44.69, 41.99, 36.45, 35.73, 35.09, 34.31, 31.82, 31.25, 29.65, 29.31, 28.93, 27.16, 25.59, 23.27, 22.622, 14.91, 14.01, 13.35. FT-IR (cm^{-1}): 3380, 3010, 2926, 2852, 1729, 1648, 1560, 1482, 1457, 1383, 1364, 1306, 1229, 1154, 1056, 1012, 996, 905, 798, 693.

A similar procedure was adopted for polymerization of other monomer also.

Free-Radical Polymerization of SCIH: SCIH (0.453 g, 0.69 mmol), BPO (0.005 g, 0.02 mmol) THF (3 mL) Yield: 80 % ^{1}H NMR (300 MHz, $CDCl_3$) δ ppm: 7.19(b,1H, Ar-**H**); 7.01-6.93 (b, 3H, Ar-**H**); 4.34-4.15 (b, 4H, -OC**H**$_2$C**H**$_2$O- of HEMA); 2.56-0.84 (aliphatic protons). ^{13}C NMR (75 MHz, $CDCl_3$, δ ppm): 178.08, 158.96, 156.19, 143.23, 114.71, 128.32, 125.41, 120.79, 119.62, 118.73, 116.79, 115.53, 114.92, 113.21, 112.05, 111.46, 110.86, 109.43, 44.97, 44.47, 36.42, 35.89, 35.74, 35.04, 32.38, 31.88, 31.36, 30.92, 29.66, 29.52, 29.32, 23.11, 22.65, 14.84, 13.29. FT-IR (cm^{-1}): 3378, 2925, 2854, 1730, 1641, 1561, 1481, 1460, 1385, 1364, 1308, 1261, 1229, 1154, 1101, 1018, 867, 801, 694.

Free Radical Polymerization PBI methacrylates (PBI-HB & PBI-NHB): The same generic procedure for free radical polymerization was adopted for both PBI-HB and PBI-NHB in different solvent-initiator combinations. An example recipe is given : PBI-NHB (0.05 g, 0.07 mmol) and benzoyl peroxide (BPO) (0.5 mg, 0.002 mmol) were taken in THF (3 mL) in a 10 mL round-bottomed flask provided with a water condenser. The reaction mixture was purged with nitrogen for 30 min. The polymerization was carried out by stirring the contents at 65 °C for 24 hours. But even after 24 hours or more, there was no viscosity build up and upon precipitation into methanol or water gave only fine powdery material similar to the monomer with no rubbery or elastic characteristics typical of polymers.

2.3. Results and Discussion

2.3.1. Synthesis and Characterization of Monomers

The synthesis of urethane methacrylate homopolymers with bulky aromatic anchoring groups from the simple phenols cardanol as well as its saturated analogue 3-pentadecyl phenol were rather straight forward due to the readymade phenolic-OH group available for further functionalization. But that was not the same in the case of perylenebisimide based monomers. Any side-chain functionalized PBI polymer requires first synthesizing unsymmetrical perylenebisimides provided with functional groups that are capable of further coupling on one end and solubilizing long alkyl chains at the other end. Perylene tetracarboxylic dianhydrides are difunctional molecules which generally undergo identical substitution at either end even if two type of amines are used. Formation of non-symmetrically substituted perylenebisimides by performing the reaction with two different amines usually does not take place because of differences in reactivity of the two amines. Unsymmetrically substituted perylene bisimides are generally obtained in a multistep procedure and the product at each step requires purification by column chromatography.[41] Hence the synthesis of the non-symmetrically substituted perylenebisimide is a challenging task in terms of yield and tedious procedures. But when the two amines are of similar reactivity the easiest and one pot reaction is the simultaneous addition of two amines giving a mixture of the three statistical products from which the desired one could be recovered by single column chromatography. Accordingly the unsymmetrical PBI precursor molecule designed with a branched alkyl chain at one imide position and a 6-spacer aliphatic alcohol group on other was synthesized as shown in scheme-2.2.

The perylenebisimides PBI-1, PBI-2 and PBI-3 were obtained by reacting equimolar ratio of the two different amines viz., 2-ethylhexylamine and 6-amino hexanol with PTCDA and the imidization was carried out using $Zn(OAc)_2$ catalyst

in DMAc. The crude product mixture upon column chromatography yielded the required unsymmetrical PBI-2 in reasonably good yield and the structures of the three PBIs were confirmed by various spectroscopic techniques such as ^{1}H- & ^{13}C-NMR, FT-IR and MALDI-TOF mass spectrometry.

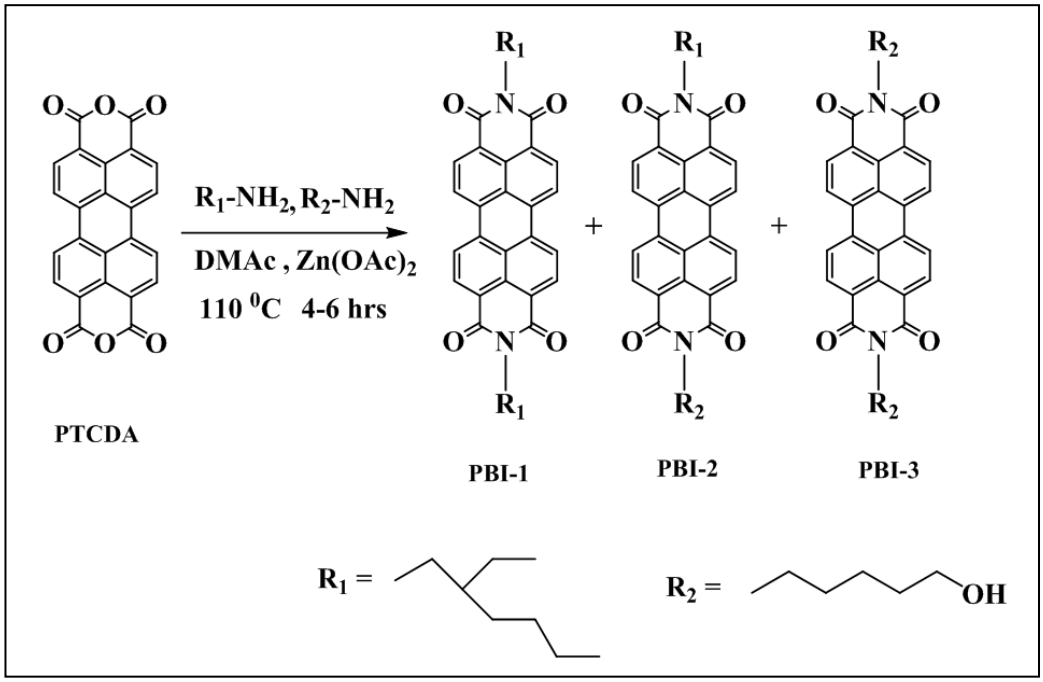

Scheme-2.2

Figure-2.9. shows the ^{1}H-NMR spectra of ethylhexyl-hexanol based perylenebisimides with respective protons labelled. The various types of protons are labeled by alphabets. The intensity of all peaks exactly matched with the number of protons, which confirmed the formation of the expected molecules. The peaks corresponding to the protons of perylene core appeared at highest δ value as a doublet of doublet in each of the three perylenebisimides. The peaks appeared as a doublet of doublet because there are two types of protons in the perylene core- the inner protons and the outer protons. In case of symmetrical ethylhexyl PBI-1 figure 2.9(a), the (imide-C**H**$_2$) protons appeared as a multiplet at δ value 4.16 ppm. The (imide-CH$_2$-C**H)** protons at the asymmetric carbon of the ethylhexyl chain also appeared as a multiplet around 1.99 ppm. The protons labeled as ‘c’ and ‘d’ (end

CH_3 of ethyl hexyl tail) appeared as two triplets in the range 0.98-0.92 ppm. Figure-2.9(b) corresponds to that of the unsymmetrical PBI-2. The protons corresponding to imide-C**H**$_2$ of ethylhexyl group and hydroxy-hexyl group respectively are labeled as 'a' and 'e' which appeared as a multiplet around 4.18-4.02 ppm. The triplet at δ value 3.60 ppm corresponds to protons (C**H**$_2$-OH) labeled as 'f'. The end CH_3 of ethyl hexyl tail protons labeled as 'c' and 'd' appeared as two triplets at δ = 0.98-0.92 ppm.

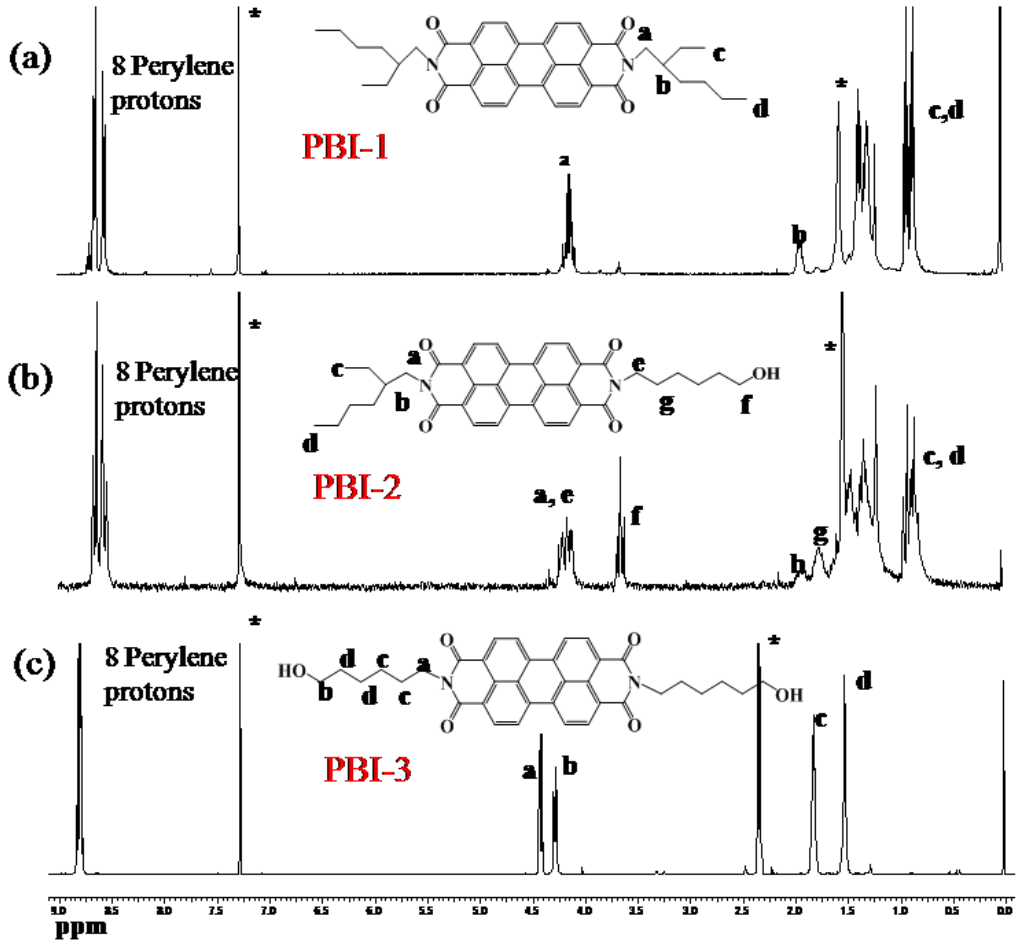

Figure-2.9. ^{1}H-NMR spectra of (a) PBI-1 (b) PBI-2 and (c) PBI-3.

The ^{1}H NMR spectra of the symmetrical hexanol substituted PBI-3 is shown in figure-2.9(c). Here the (imide-C**H**$_2$) protons labeled as 'a' and (C**H**$_2$OH of hexanol) protons labeled as 'b' appeared as clear triplets at δ = 4.40 ppm and δ = 4.26 ppm

respectively. The four protons labeled as 'c' (near to imide group) appeared as a multiplet at δ = 1.80 ppm and the four protons labeled as 'd' (near to OH group) appeared as a multiplet at δ = 1.51 ppm.

The hydrogen-bondable urethane methacrylic macromonomers based on the above discussed unsymmetrical PBI-2, cardanol and 3-pentadecylphenol were synthesized by coupling one equivalent of isophorone diisocyanate (IPDI) with one equivalent of the respective PBI-2/cardanol/saturated cardanol followed by reacting with one equivalent of hydroxyethyl methacrylate (HEMA) as shown in scheme-2.3. These were abbreviated as CIH (for cardanol), SCIH (for saturated cardanol) and PBI-IH respectively. The reaction was followed by means of FT-IR which showed the disappearance of the broad OH peak at 3415 cm^{-1} and appearance of a sharp NH peak at 3338 cm^{-1} indicating the completion of the reaction.[42]

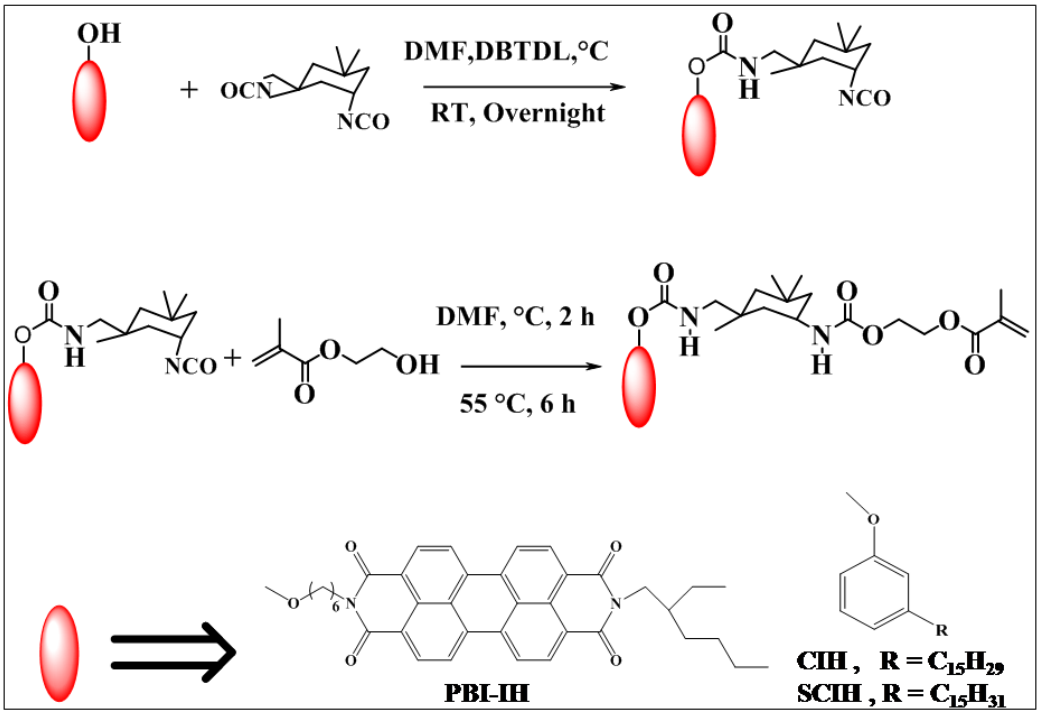

Scheme-2.3

However, unfortunately the perylenebisimide based urethane methacrylate PBI-IH showed very poor or negligible solubility in almost all the common organic

polar or non-polar solvents such as hexane, $CHCl_3$, THF, DMF, DMAc, (dimethylsulphoxide) DMSO, methanol, toluene, anisole etc. As a result the work up of this monomer was impossible and therefore no structural characterization could be done for this monomer. Whereas the cardanol and pentadecylphenol based monomers CIH and SCIH were freely soluble in most of the solvents and their structures were thus fully characterized by means of ^{1}H NMR, ^{13}C NMR, FT-IR and MALDI-TOF-MS spectroscopic techniques. The insolubility of PBI-IH monomer lead to re-designing of PBI methacrylate monomers with sufficient solubility by avoiding the kinked cyclo-aliphatic IPDI unit and incorporating linear structural motifs with and without hydrogen bonding units. Starting from the same unsymmetrical PBI-2, hydrogen bondable and non-hydrogen bondable monomers viz., PBI-HB and PBI-NHB respectively were successfully synthesized accordingly as shown in scheme-2.4 and were completely characterized.

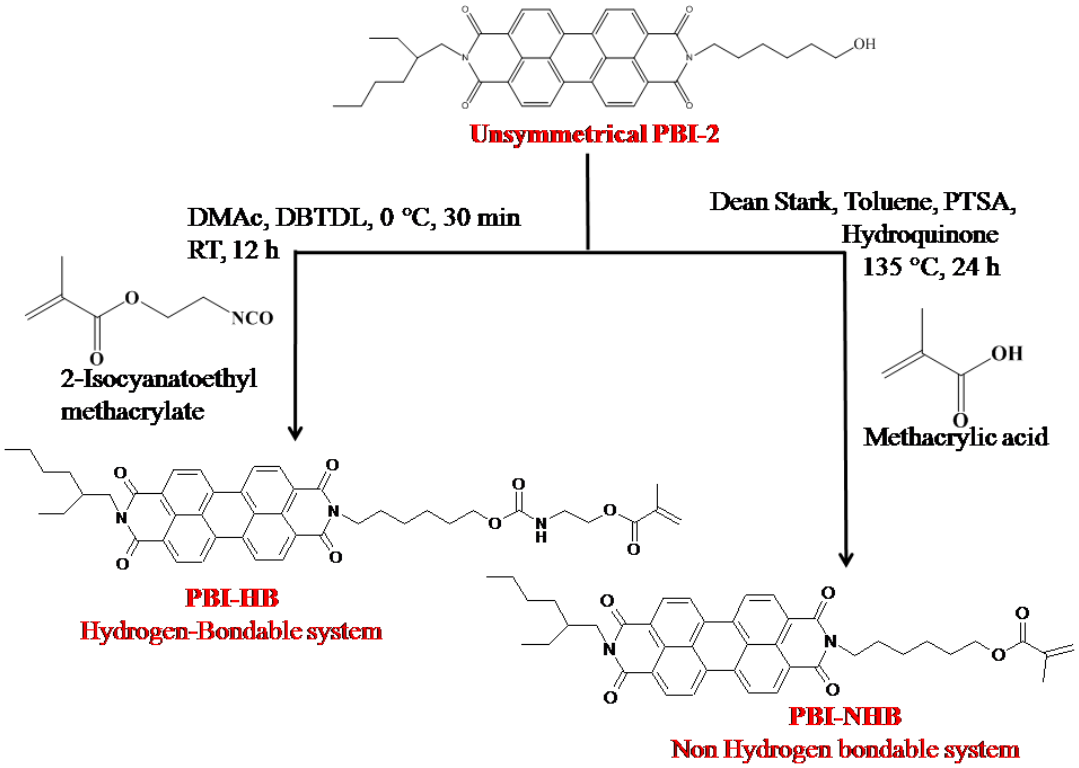

Scheme-2.4

The PBI-HB was obtained by reacting the unsymmetrical PBI-2 with isocyanatoethyl methacrylate in presence of DBTDL catalyst to give the hydrogen-bondable urethane linkage, whereas the non-hydrogen bondable PBI-NHB was prepared by simple esterification reaction between PBI-2 and methacrylic acid in a Dean Stark apparatus. These monomers also were completely characterized with details given in the experimental section and ^{1}H-NMR as shown in figure-2.10. In the ^{1}H-NMR of the PBI-HB (fig-2.10 (a)) peaks at 6.14 and 5.60 ppm labelled 'a' corresponding to the methacrylate double bonds were perfectly matching in integration with the 8 aromatic perylene core protons at 8.65 ppm. The 3H singlet at 1.95 ppm corresponding to -C**H**$_3$ unit of methacrylate group further confirmed the product. The other monomer PBI-NHB which did not have the hydrogen bonding urethane linkage was also designed and synthesized. Here also, the peaks labelled 'a' corresponding to the methacrylate double bonds were perfectly matching in integration with the perylene core protons at 8.70 ppm.

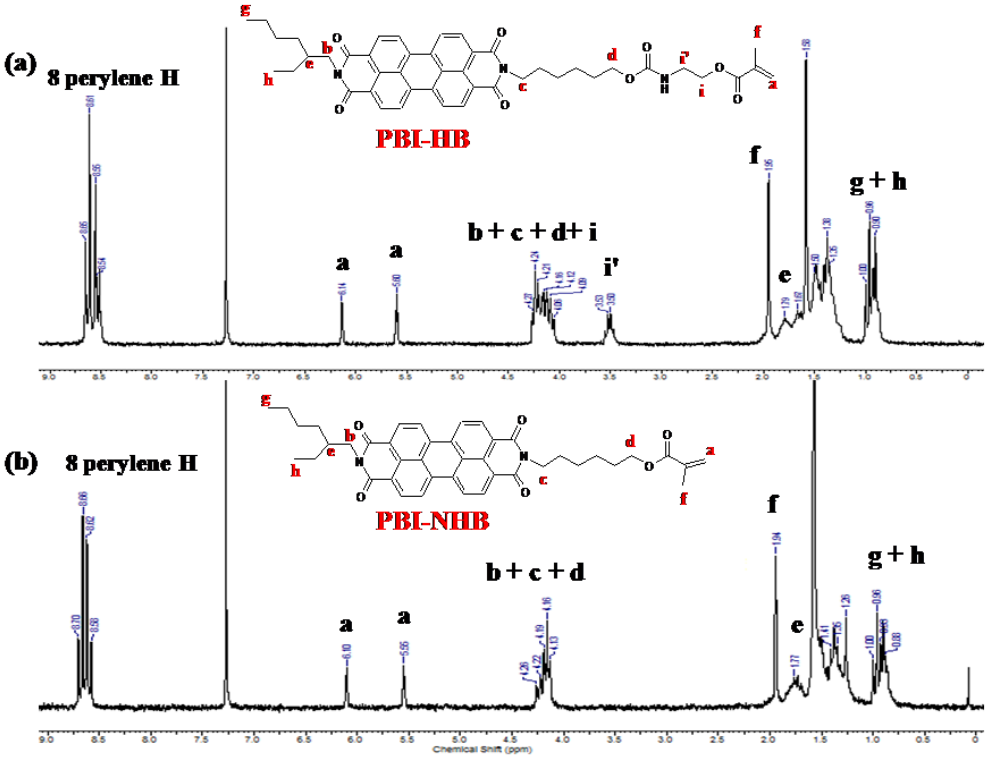

Figure-2.10. ^{1}H-NMR spectra of (a) PBI-HB and (b) PBI-NHB.

2.3.2. Polymerization and Characterization

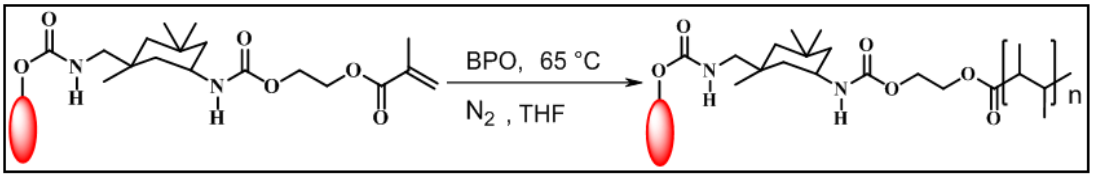

Scheme-2.5

The monomers PBI-HB, PBI-NHB, CIH and SCIH were subjected to normal free radical polymerization using 3 mol% benzoyl peroxide (BPO) as the thermal initiator in tetrahydrofuran (THF) as solvent, at 65 °C. As shown in the polymerization scheme-2.5, after 12 hours the monomers CIH as well as SCIH gave a viscous solution which was concentrated, cooled and then precipitated into water to give the corresponding polymers polyCIH and polySCIH which were abbreviated as PCIH and PSCIH respectively.

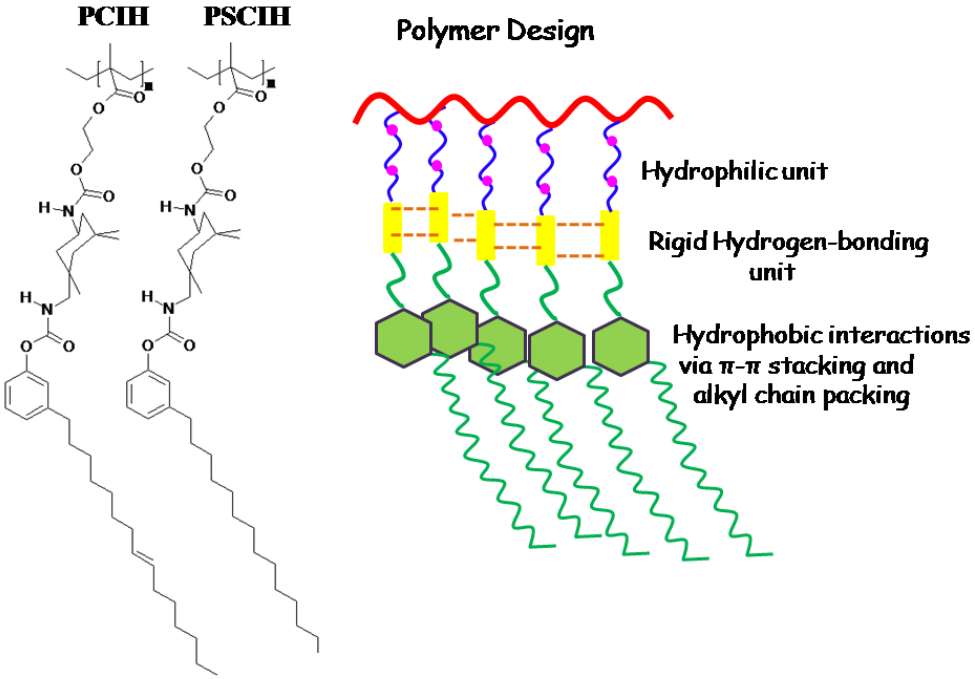

Scheme-2.6

In contrast the perylenebisimide based monomers PBI-HB and PBI-NHB did not show any signs of polymerization as there was no viscosity build up even after 24 hours or more. So the polymerization conditions were varied including the solvent, temperature and initiator. Different solvents typically used for polymerization of methacrylate monomers like THF, dioxane, anisole, DMAc etc. were tried in combination with either BPO or AIBN free radical initiators. But all the attempts resulted in either very low molecular weight oligomers or the monomer was recovered back. Consequently the investigation was confined to the two polymers PCIH and PSCIH and their structures are given in Scheme-2.6 along with a pictorial representation illustrating the crucial balance between flexible hydrophilic unit and rigid hydrogen bonding unit.

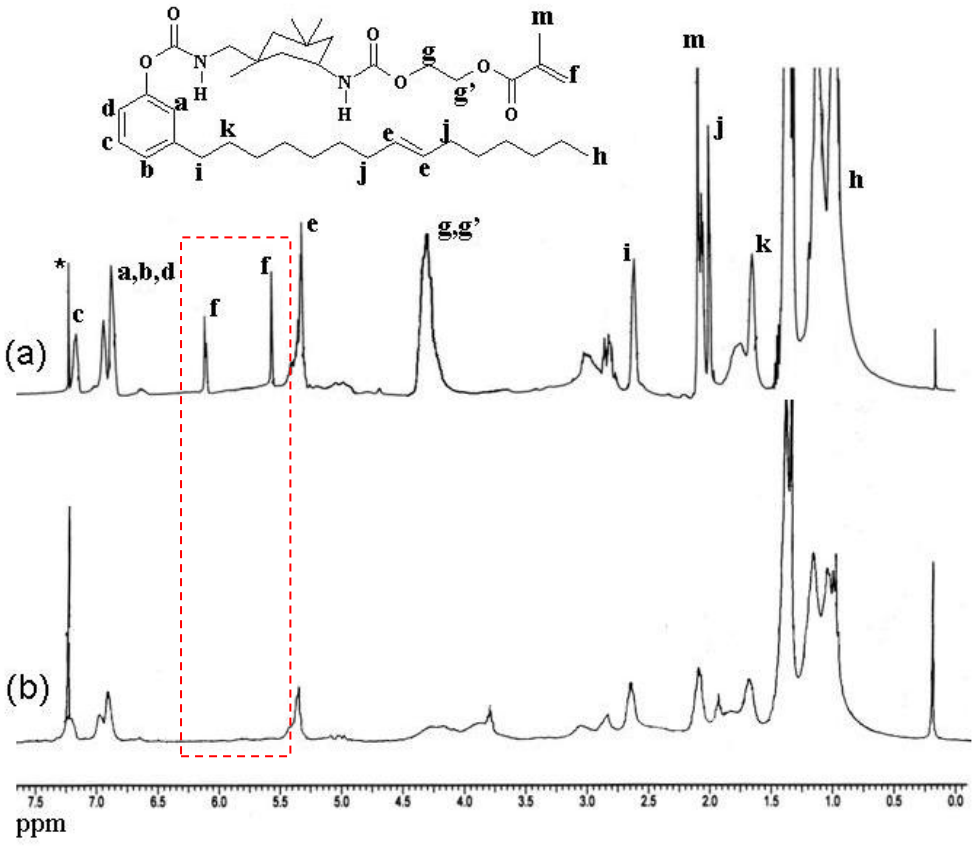

Figure-2.11. ^{1}H NMR spectra of (a) Cardanol-IPDI-HEMA monomer (**CIH**) and (b) polymer **PCIH.**

The polymer structure was analyzed by ^{1}H NMR; Figure-2.11(a) & (b) gives a comparison of the ^{1}H NMR spectra of cardanol based urethane acrylate monomer (CIH) and its polymer (PCIH).The disappearance of the peaks at 6.13 and 5.57 ppm corresponding to methacrylate double bonds clearly indicates the complete polymerization of the monomer.[40,42] The peaks also became broader upon polymerization as seen from figure 2.11(b). The characteristic peak around δ 5.4 ppm due to the unsaturated group in the side chain remained unchanged indicating that under the free radical polymerization conditions it has remained unreacted. The ^{1}H NMR spectra of the saturated analogue based monomer and its polymer had similar features (details given in synthesis section).

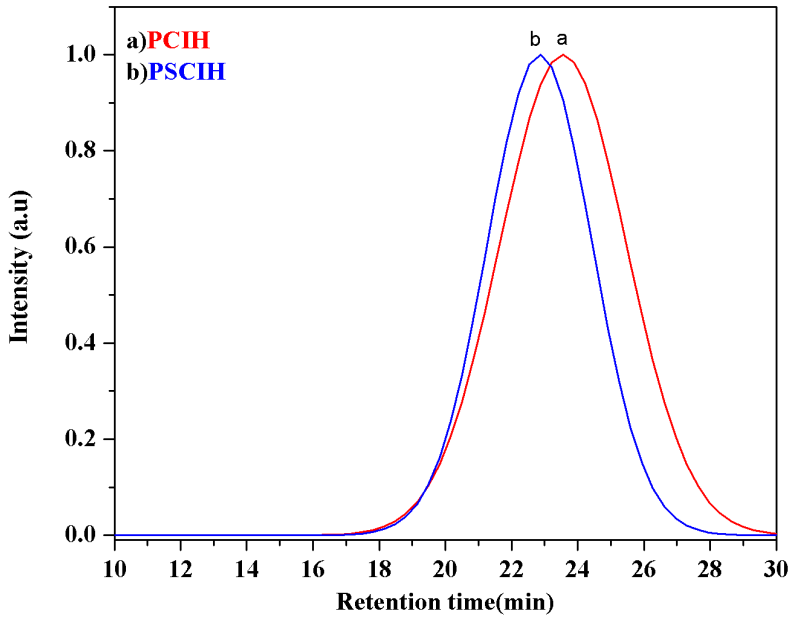

Figure-2.12. GPC chromatogram of polymers PCIH and PSCIH.

The molecular weights of the polymers were determined by gel permeation chromatography (GPC) using THF as eluent. Polymerization results are summarized in Table-2.1 and the GPC chromatograms of the polymers given in Figure-2.12. The molecular weight data indicated that the polydispersity (PDI) was not very high and the number of repeating units ranged from 15-20 for the polymers.

Table-2.1 Yield, Molecular weights and thermal data of the polymers

Polymer	[a]Yield (%)	[b]M_n	[b]M_w	[b]PDI	[c]T_D (°C)	[d]T_g (°C)
PolyCIH	76	9700	16100	1.65	266	78.8
PolySCIH	80	13200	22600	1.71	241	82.5

(a) Calculated for isolated products (b) Determined by Gel Permeation Chromatography in THF at 30 °C using polystyrene standards for calibration. (c) Temperature represents 10 % weight loss in TGA measurements at heating rate of 10 °C/min under nitrogen. (d) Determined by DSC analysis.

2.3.3. Thermal Analysis of Polymers

Thermal stability of the polymers were studied using TGA from ambient temperature to 600 °C, which confirmed that the polymers were stable upto 240 - 265 °C. The TGA as well as the DSC thermograms for the polymers are given in figure-2.13. The 10 % weight loss temperature (T_D) from TGA and T_g values from DSC analyses for the polymers are also given in Table-2.1.

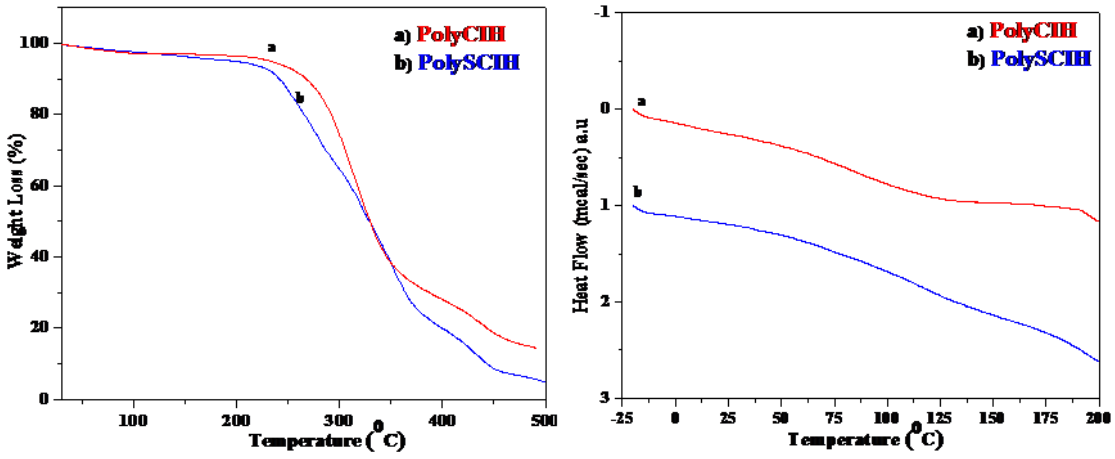

Figure-2.13. TGA and DSC thermogram of polymers PCIH and PSCIH.

2.3.4. Self-Assembly of Polymers in Solution

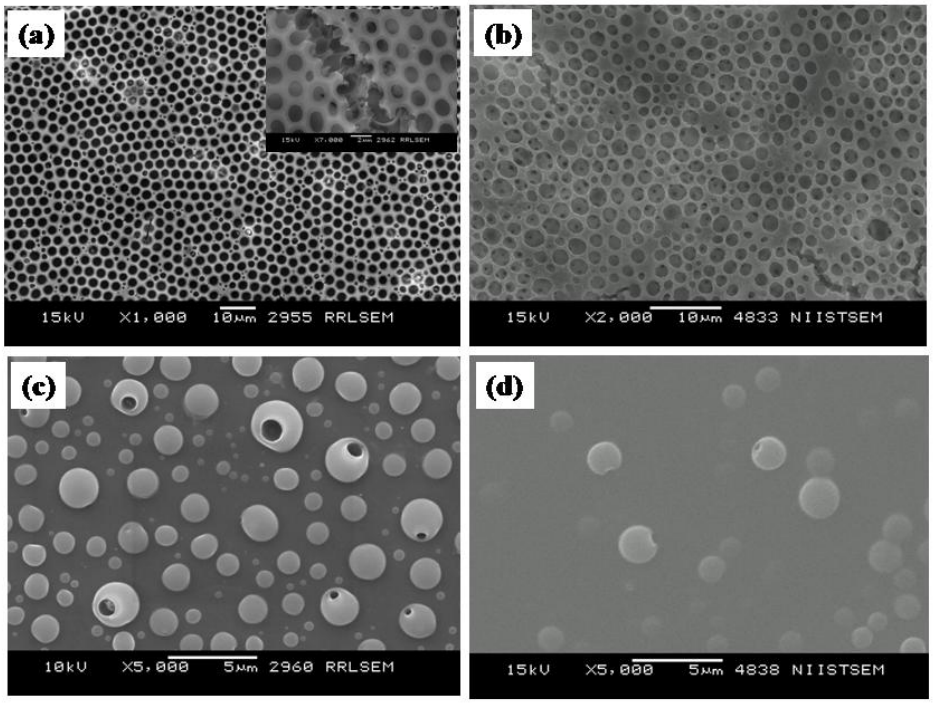

Figure-2.14. SEM images of **PCIH** (a) & (c) as well as **PSCIH** (b) & (d) drop cast from $CHCl_3$ and THF respectively at a concentration of $1x10^{-2}$ M.

Figure-2.14 (a) & (b) shows the SEM images of typical three dimensional honeycomb morphology exhibited by $1x10^{-2}$ M solution of the polymers **PCIH** (a), **PSCIH** (b) from chloroform. 20 µL of the solution was drop cast on a microscopic glass slide and the solvent was allowed to evaporate off slowly under atmospheric conditions. The two polymers formed honeycomb porous structures with pore dimensions in the range of 1.6 – 1.9 µm average diameter. The regularity in shape, size and number of micropores were found to be lower for **PSCIH** compared to **PCIH**. Similar studies were carried out for $1x10^{-2}$ M solutions of the polymers in THF and figure-2.14 (c) & (d) gives the SEM image of **PCIH** (a) and **PSCIH** (b) respectively. Surprisingly, the morphology was totally different from that observed for the same polymers in chloroform. Both polymers formed microspheres with similar dimensions – 1.51±0.22 µm (0.84 for the smallest to 2.52 µm for the

largest) for **PCIH** and 1.76±0.20 μm (1.1 for the smallest to 2.3 μm for the largest) average diameter in the case of **PSCIH**. Many of the spheres in both polymers exhibited open holes on their surfaces.

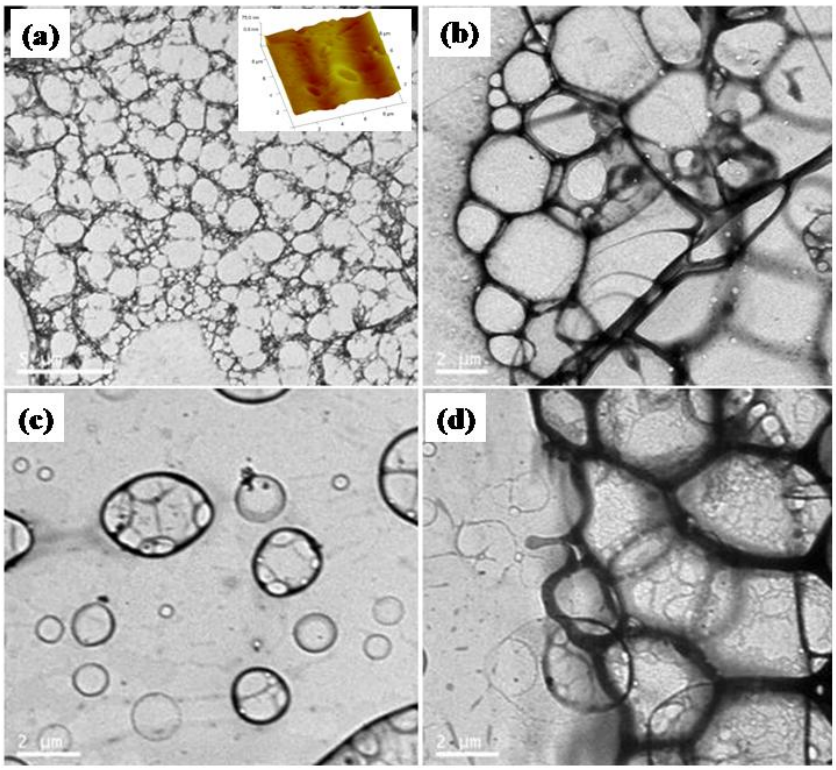

Figure-2.15. TEM images of $1x10^{-3}$ M solutions of **PCIH (**a and b) and **PSCIH** (c and d) drop cast from $CHCl_3$. Inset in (a) shows the AFM image of **PCIH** dropcast on glass slides from $CHCl_3$ at a concentration of $1x10^{-4}$ M.

The morphological features at lower concentrations were probed using transmission electron microscopic (TEM) analysis. Figure-2.15 shows the TEM images of **PCIH** (a and b) and **PSCIH** (c and d) dropcast from $CHCl_3$ at a concentration of $1x\ 10^{-3}$ M onto Formvar coated copper grids, dried in air overnight without any special staining applied. The TEM images revealed the presence of network like structures which could be identified as giant vesicles due to the obvious contrast between the contour and the centre of the features.[43,44] Figure-2.15(c) displays a clear distribution in the sizes of these vesicles with the size

ranging from 1 to 10 μm. The wall thickness ranged from 50-100 nm for the smaller vesicles to 200 nm for the larger ones. The larger ones, growing upto 7 μm in length were formed by the fusion of the smaller ones. The vesicular structures clearly show easily definable hexagonal geometries resembling honeycomb patterns (figures 2.15(b) and (d)) which were coexisting with independent vesicles. The hexagonal vesicles in figure-2.15(d) had wall thickness ranging from 360-630 nm (average: 527 ± 78 nm) which was comparable to the wall thickness of 570 ± 30 nm for the honeycomb pores obtained from SEM. The vesicular nature of the features was further confirmed by the AFM image shown inset of fig-2.15 (a) from $1x10^{-4}$ M **PCIH** in $CHCl_3$ drop cast on to glass slides. The size of the vesicle was in the range of 0.6-0.8μm and the wall thickness ~200 nm.

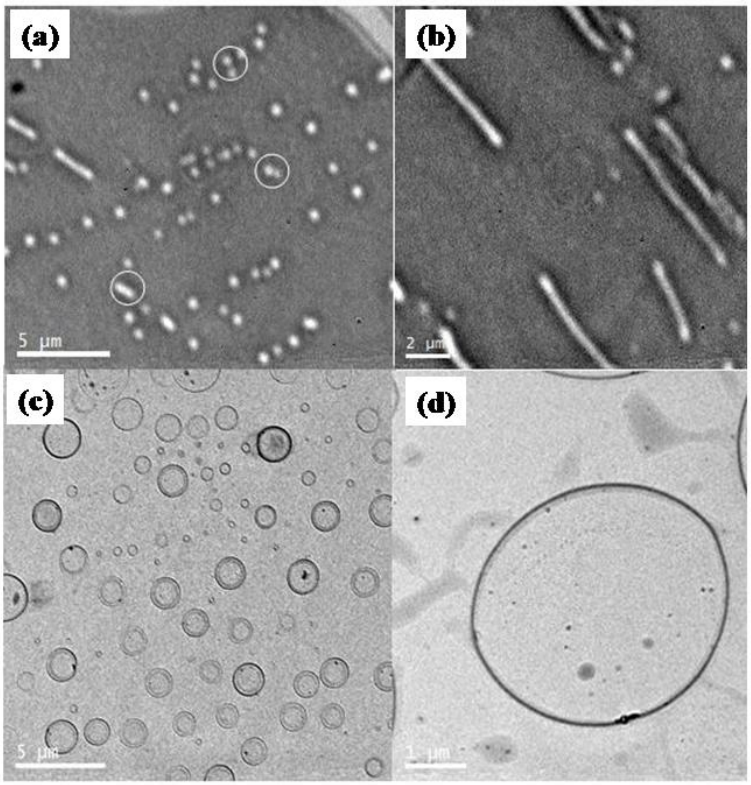

Figure-2.16. TEM images of **PCIH** (a) & (b) ($1x10^{-4}$ M) and **PSCIH** (c) and (d) ($1x10^{-3}$ M) drop cast from THF.

Figure-2.16 shows the TEM images of **PCIH** [(a) & (b) 10^{-4} M)] and **PSCIH** [(c) & (d) 10^{-3} M) drop cast from THF. Similar to the observation in SEM, in TEM also, the morphologies were different in THF compared to that in $CHCl_3$. Fig-2.16 (a) and (b) clearly showed the coexistence of spheres and tubes. The spheres had outer diameter ranging from 0.98 to 1.30 μm with wall thickness ~ 250 nm. The tubes had length ranging upto 7 μm with wall thickness ~ 250 nm similar to that of the spheres. The TEM images also clearly showed some of the adjacent spheres fusing with one another with their edges cohered and membranes shared (encircled in figure-2.16(a)). It could also be seen that the spheres were arranged one-by-one in a linear way thereby facilitating their fusion to form tubular structures. Both the spheres and tubes had similar inner diameter of ~ 400 nm and wall thickness of ~ 250 nm. The TEM images of **PSCIH** (figure 2.16 (c) and (d)) showed vesicles in the size range of 1.32-2.2μm with wall thickness ~ 50 nm. **PSCIH** did not show a tendency to form tubes at 10^{-4} or 10^{-3} M as was observed in the case of **PCIH**; instead, it formed only vesicles in both chloroform and THF. The observation of three dimensional honeycomb patterns for both polymers upon casting from chloroform was explained based on the moisture induced "breathe-figure" mechanism.[46] Chloroform being a denser solvent which is immiscible with water, is more favoured for this type of honeycomb pattern formation compared to a solvent like THF which is miscible with water. The TEM images of the films drop cast from $CHCl_3$ showed vesicles (see figure-2.15(c)) which fused to form bigger vesicles. Figure-2.17 shows the schematic representation of the proposed mechanism of morphology formation occurring in $CHCl_3$ and THF. Figure-2.17(a) shows the process of 3D honeycomb pore formation from vesicles in $CHCl_3$. The vesicles fuse and grow larger and during the process of drying, moisture in the air settles down as water droplets and since chloroform and water are immiscible they do not coalesce; instead they come together as hexagonal close packed arrangement as suggested in the literature.[45,46] Figure-2.17(b) shows the schematic representation of the processes involved in the formation of the particular morphologies observed in THF for **PCIH**.

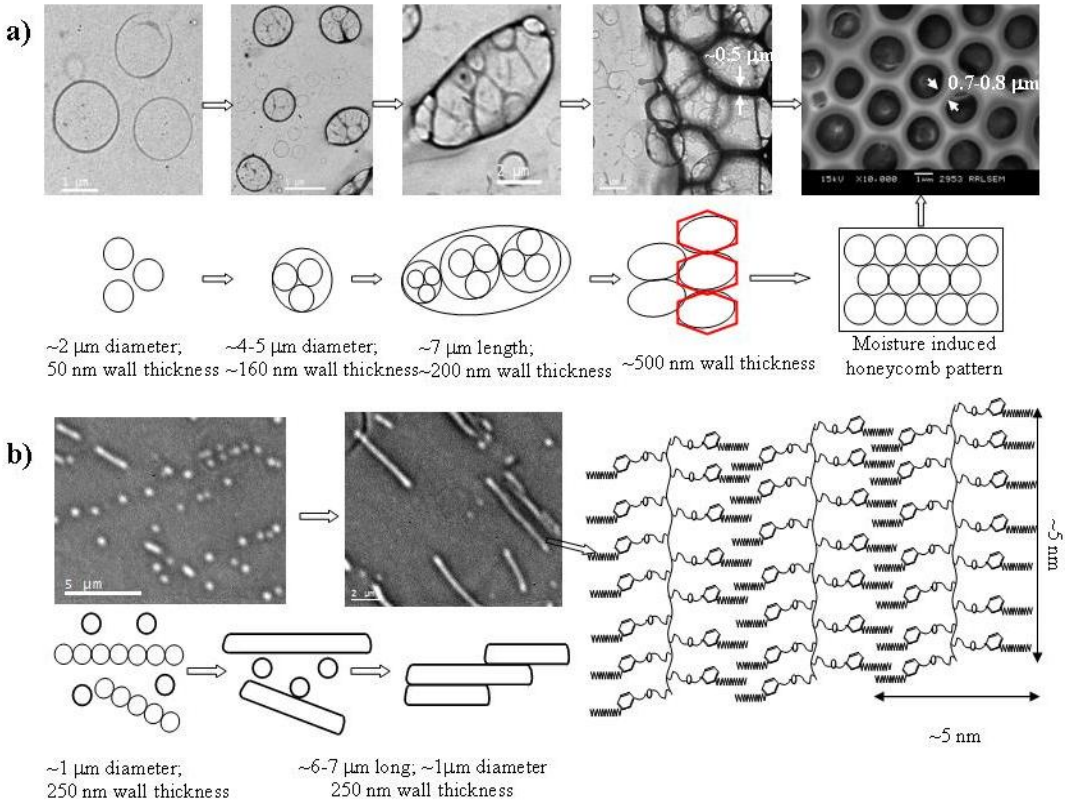

Figure-2.17. Schematic representation of the mechanism of 3D honeycomb pore formation in (a) $CHCl_3$ and morphology in (b) THF.

THF is a polar aprotic solvent which can interfere with the polymer intermolecular hydrogen bonding and thus the polymers are molecularly dissolved in THF, adopting an extended conformation. The repeating units of the polymers (calculated from the GPC molecular weight and monomer mass) is around 15-16 units. The length of the all extended C-C backbone distance is ~ 4-5 nm for a poly(methyl methacrylate) (PMMA) back bone with ~ 15-16 units. The end to end distance from the tip of one C15 terminal alkyl chain to that of another C15 alkyl chain in **PCIH** with two repeat units is ~ 5 nm (50 Å, see figure-2.18). This gives a comb structure to the polymer. However, the presence of the 1,3- IPDI linkage gave a kinked nature to the side chain preventing close packing of the units within the same polymer chain. The C15 terminal alkyl chains of one polymer chain can, however occupy the volume around another polymer chain by way of

interdigitation. This type of an interchain packing of several polymer chains in THF leads to the observed morphology. The pre-organization in THF is maintained upon solvent evaporation as evidenced by TEM, and SEM measurements.

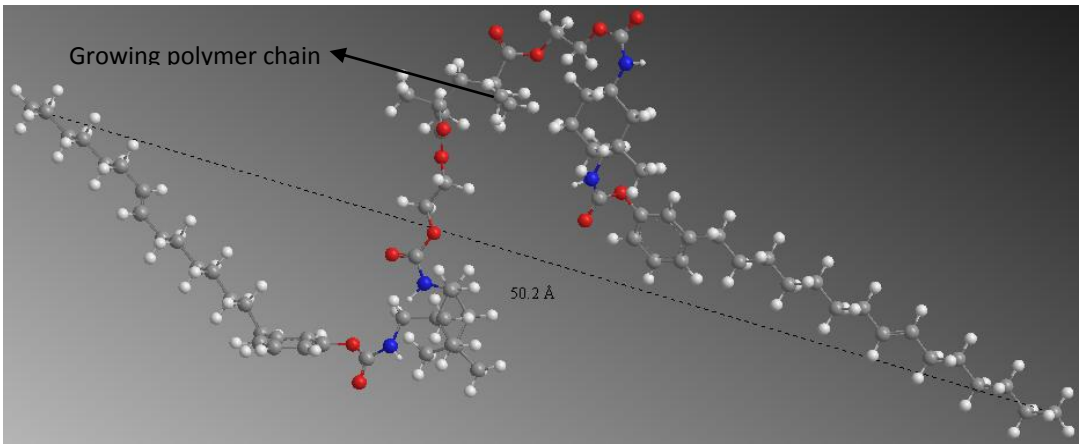

Figure-2.18. Energy minimized structure of PCIH (2 units) done using ChemBio3D Ultra 11.0 showing the end to end distance. (~ 5 nm)

2.4. Conclusions

In conclusion this chapter described a systematic investigation taken up to study the influence of bulky aromatic units as pendants of a unique urethane methacrylate comb polymer. The aromatic units selected were based on (i) an n-type semiconductor material viz., the perylenebisimide (PBI) core (ii) a simple and unique renewable resource based phenol viz., cardanol and (iii) its saturated analogue, 3-pentadecylphenol. The primary target was to incorporate the perylenebisimide core into a soluble side-chain polymer scaffold pre-programmed with different tools for self-assembly. For this a new unsymmetrical PBI-2 with a solubilizing alkyl chain on one end and functionalizable hexyl-spacer-OH group on the other end was also synthesized. The monomer synthesis involved one pot coupling of one equivalent of a kinked isophorone diisocyanate (IPDI) with one equivalent of cardanol/pentadecylphenol/PBI-OH followed by coupling with one equivalent of hydroxyl ethyl methacrylate (HEMA). However due to the intrinsic insolubility problem, the PBI based urethane methacrylate monomer, PBI-IH could not even be structurally characterized, whereas the other two monomers CIH and SCIH were successfully synthesized and characterized. Consequently re-designing of the PBI-methacrylate monomer was done by removing the kinked cyclo-aliphatic IPDI unit and two novel methacrylate monomers with and without H-bonding motifs named as PBI-HB and PBI-NHB were successfully synthesized and well characterized. Facile and easy free radical polymerization was attempted for these monomers. The monomers CIH and SCIH were readily polymerized to give the two urethane methacrylate polymers PCIH and PSCIH, while unfortunately the two perylene monomers PBI-HB and PBI-NHB failed miserably in spite of several varied trials. Further the soluble polymers PCIH and PSCIH were investigated for solvent induced self assembly. The thermal properties of the polymers were studied using thermogravimetric analysis (TGA) and differential scanning calorimetry (DSC) and the polymers were found to have high thermal stability. The morphologies of solvent cast polymer films were studied using microscopic

techniques like scanning electron (SEM), transmission electron (TEM) and atomic force (AFM) microscopy. The polymers exhibited three - dimensional honeycomb morphology in $CHCl_3$ whereas in THF they formed spheres. The direct cardanol derived polymer PCIH showed a tendency for multiple morphologies like spheres and tubes in THF. Among the various self-organization tools present in the polymer design, the self assembly directed by the aromatic/flexible alkyl chain balance in the presence of solvent seemed to have an upper hand in driving the morphology. This work proved that the unique design of the urethane methacrylate comb polymer described in this chapter has vast potentials to produce a variety of self-organized polymeric nanostructures endowed with different properties like fluorescence, liquid crystallinity etc. if properly manipulated. In a nut shell the overall inference gained from this chapter was that the n-type rigid core perylenebisimide could very difficultly be covalently incorporated into a homopolymer design and if at all incorporated the chances of final polymer processability is very low. These unsuccessful attempts at polymerizing the perylene based monomers finally lead to the search for alternate methods of incorporating perylenebisimides into processable polymer scaffolds as will be discussed in the forthcoming chapters.

2.5. References

[1] G. Horowitz, F. Kouki, P. Spearman, D. Fichou, C. Nogues, X. Pan, F. Garnier, *Adv. Mater.* **1996,** *8*, 242.

[2] P. R. L. Malenfant, C. D. Dimitrakopoulos, J. D. Gelorme, L. L. Kosbar , T. O. Graham, A. Curioni, W. Andreoni, *Appl. Phys. Lett.* **2002,** *80*, 2517.

[3] R. J. Chesterfield, J. C. McKeen, C. R. Newman, P. C. Ewbank, D. A. da Silva Filho, J. L. Brédas, L. L. Miller, K. R. Mann, C. D. Frisbie, *J. Phys. Chem. B* **2004,** *108*, 19281.

[4] S. Tatemichi, M. Ichikawa, T. Koyama, Y. Taniguchi, *Appl. Phys. Lett.* **2006,** *89*, 112108.

[5] C. W. Struijk, A. B. Sieval, J. E. J. Dakhorst, M. van Dijk, P. Kimkes, R. B. M. Koehorst, H. Donker, T. J. Schaafsma, S. J. Picken, A. M. van de Craats, J. M. Warman, H. Zuilhof, E. J. R. Sudhölter, *J. Am. Chem. Soc.* **2000,** *122*, 11057.

[6] J. H. Oh, S. Liu, Z. Bao, R. Schmidt, F. Würthner, *Appl. Phys. Lett.* **2007,** *91*, 212107.

[7] B. A. Jones, M. J. Ahrens, M. H. Yoon, A. Facchetti, T. J. Marks, M. R. Wasielewski, *Angew. Chem. Int. Ed.* **2004,** *43*, 6363.

[8] B. A. Jones, A. Facchetti, M. R. Wasielewski, T. J. Marks, *Adv. Funct. Mater.* **2008,** *18*, 1329.

[9] A. S. Molinari, H. Alves, Z. Chen, A. Facchetti, A. F. Morpurgo, *J. Am. Chem. Soc.* **2009**, *131*, 2462.

[10] R. Schmidt, J. H. Oh, Y. S. Sun, M. Deppisch, A.-M. Krause, K. Radacki, H. Braunschweig, M. Könemann, P. Erk, Z. Bao, F. Würthner, *J. Am. Chem. Soc.* **2009**, *131*, 6215.

[11] M. Gsänger, J. H. Oh, M. Könemann, H. W. Höffken, A.-M. Krause, Z. Bao, F. Würthner, *Angew. Chem. Int. Ed.* **2010**, *49*, 740.

[12] F. Nolde, W. Pisula, S. Mueller, C. Kohl, K. Müllen, *Chem. Mater.* **2006**, *18*, 3715.

[13] M. Petit, R. Hayakawa, Y. Shirai, Y. Wakayama, J. P. Hill, K. Ariga, T. Chikyow, *Appl. Phys. Lett.* **2008**, *92*, 163301.

[14] Z. Y. Wang, Y. Qi, J. P. Gao, G. G. Sacripante, P. R. Sundararajan, J. D. Duff, *Macromolecules* **1998**, *31*, 2075.

[15] E. E. Neuteboom, S. C. J. Meskers, E. W. Meijer, R. A. J. Janssen, *Macromol.Chem. Phys.* **2004**, *205*, 217.

[16] J. –J. Shim, C. -W. Lee, M. -S. Gong, *Synth. Met.* **2001**, 435.

[17] S. M. Mackinnon, Z. Y. Wang, *J. Polym. Sci. Part A Polym. Chem.* **2000**, *38*, 3467.

[18] B. Jancy, S. K. Asha, *J. Polym. Sci. Part A Polym. Chem.* **2009**, *47*, 1224.

[19] N. B. Kolhe, S. K. Asha, S. P. Senanayak, K. S. Narayan, *J. Phys. Chem. B* **2010,** *114*, 16694.

[20] H. Yan, Z. Chen, Y. Zheng, C. Newman, J. R. Quinn, F. Dötz, M. Kastler, A. Facchetti, *Nature*, **2009,** *457*, 679.

[21] S. M. Lindner, M. Thelakkat, *Macromolecules* **2004,** *37*, 8832.

[22] M. Sommer, M. Thelakkat, *Eur. Phys. J. Appl. Phys.* **2006,** *36*, 245.

[23] S. M. Lindner, S. Hüttner, A. Chiche, M. Thelakkat, G. Krausch, *Angew. Chem. Int. Ed.* **2006,** *45*, 3364.

[24] M. Sommer, S. M. Lindner, M. Thelakkat, *Adv. Funct. Mater.* **2007,** *17*, 1493.

[25] A. S. Lang, F. R. Kogler, M. Sommer, U. Wiesner, M. Thelakkat, *Macromol. Rapid Commun.* **2009,** *14*, 1243.

[26] S. Hüttner, M. Sommer, A. Chiche, G. Krausch, U. Steiner, M. Thelakkat, *Soft Matter* **2009,** *5*, 4206.

[27] M. Sommer, S. Hüttner, S. Wunder, M. Thelakkat, *Adv. Mater.* **2008,** *20*, 2523.

[28] S. Huettner, J. Hodgkiss, M. Sommer, R. H. Friend, U. Steiner, M. Thelakkat, *J. Phys. Chem. B* **2012,** *116*, 10070.

[29] A. S. Lang, A. Neubig, M. Sommer, M. Thelakkat, *Macromolecules* **2010,** *43*, 7001.

[30] P. Kohn, L. Ghazaryan, G. Gupta, M. Sommer, A. Wicklein, M. Thelakkat, T. Thurn-Albrecht, *Macromolecules* **2012,** *45*, 5676.

[31] A. S. Lang, M. Thelakkat, *Polym. Chem.* **2011,** *2*, 2213.

[32] F. Spreitler, M. Sommer, M. Thelakkat, J. Köhler, *Phys. Chem. Chem. Phys.* **2012,** *14*, 7971.

[33] S. Rajaram, P. B. Armstrong, B. J. Kim, J. M. J. Fréchet, *Chem. Mater.* **2009,** *21*, 1775.

[34] Q. Zhang, A. Cirpan, T. P. Russell, T. Emrick, *Macromolecules* **2009**, *42*, 1079.

[35] Y. Tao, B. McCulloch, S. Kimc, R. A. Segalman, *Soft Matter* **2009,** *5*, 4219.

[36] S. Hüttner, M. Sommer, M. Thelakkat, *Appl. Phys. Lett.* **2008,** *92*, 093302.

[37] E. Schwartz, V. Palermo, C. E. Finlayson, Y.-S. Huang, M. B. J. Otten, A. Liscio, S. Trapani, I. G. Valls, P. Brocorens, J. J. L. M. Cornelissen, K. Peneva, K. Müllen, F. C. Spano, A. Yartsev, S. Westenhoff, R. H. Friend, D. Beljonne, R. J. M. Nolte, P. Samorì, A. E. Rowan, *Chem. -Eur. J.* **2009,** *15*, 2536.

[38] V. Palermo, M. B. J. Otten, A. Liscio, E. Schwartz, P. A. J. de Witte, M. A. Castriciano, M. M. Wienk, F. Nolde, G. De Luca, J. J. L. M. Cornelissen, R. A. J. Janssen, K. Müllen, A. E. Rowan, R. J. M. Nolte, P. Samorì, *J. Am. Chem. Soc.* **2008,** *130*, 14605.

[39] M. -A. Muth, M. C. Orozco, M. Thelakkat, *Adv. Funct. Mater.* **2011,** *21*, 4510.

[40] V. D. Deepak, S. K. Asha, *J. Phys. Chem. B* **2006,** *110*, 21450.

[41] Y. Nagao, *Prog. Org. Chem.* **1997,** *31*, 43.

[42] N. Rekha, S. K. Asha, *J. Polym. Sci. Part A Polym. Chem.* **2009,** *47*, 2996.

[43] P. Deepa, M. Jayakannan, *J. Polym. Sci. Part A Polym. Chem.* **2008,** *46*, 5897.

[44] M. Mu, F. Ning, M. Jiang, D. Chen, *Langmuir* **2003,** *19*, 9994.

[45] G. Widawski, M. Rawiso, B. Francois, *Nature* **1994,** *369*, 387.

[46] M. Srinivasarao, D. Collings, A. Philips, S. Patel, *Science* **2001,** *292*, 79.

[47] G. John, C. K. S. Pillai, *Macromol. Chem. Rapid Commun.* **1992,** *13*, 255.

[48] G. John, M. Masuda, Y. Okada, K. Yase, T. Shimizu, *Adv. Mater.* **2001,** *13*, 715.

Chapter-3

Crystalline Comb Polymer of Perylenebisimide by Hydrogen-bond mediated Self-Assembly with Poly(4-vinylpyridine)

3.1. Introduction

Amongst the rylene based n-type (acceptor) semiconductors perylenebisimides are most widely studied for optoelectronics applications owing to their unique combination of high electron mobility, large molar absorption coefficients, excellent self-assembling ability, versatile structural modification as well as good thermal and photochemical stabilities.[1-5] But their use in applications requires considerable effort to overcome their intrinsically low solubility and therefore the preparation of thin layers is carried out by the vapour deposition method. The alternative method of blending low molecular weight perylene imides with other polymers to prepare smooth films has the inherent problem of macrophase separation. In this context polymer based perylenebisimides had generated a lot of research interest. However, perylenebisimides when covalently tethered to a polymer backbone either in main chain or as side groups of block copolymers, gains in terms of solution processability and microphase separation, but looses out in terms of the intrinsic crystallinity of the small molecule.[6-8]

Whether it is a small molecule or a polymer based organic semiconductor, intermolecular interactions are of chief importance in controlling charge carrier mobility and higher mobilities can be achieved when the electronic coupling between the adjacent molecules is maximized. Therefore it is highly desirable to assemble the semiconductor molecules at the nanometre scale. Thin film morphology is yet another equally important parameter that is in demand for uninterrupted charge transport pathways. Ideally a defect free morphology can be provided by extremely pure organic single crystals grown from small molecules giving rise to a perfect charge transport system.[9,10] For example Wang *et al.* very recently reported a new n-type semiconductor, C12-4CldiPBI a tetrachlorinated diperylenebsimide derivative, the single crystals of which were grown by facile solvent vapor diffusion strategy (Figure-3.1).[11] The OFET devices based on the individual single crystal ribbons were fabricated by a new technique termed "Au stripe mask" method and exhibited excellent n-type transistor behaviour with

negligible hysteresis. Out of 50 devices examined almost all of them gave an electron mobility over 1.0 $cm^2V^{-1}s^{-1}$ with the highest mobility of 4.65 $cm^2V^{-1}s^{-1}$ along with excellent air stability.

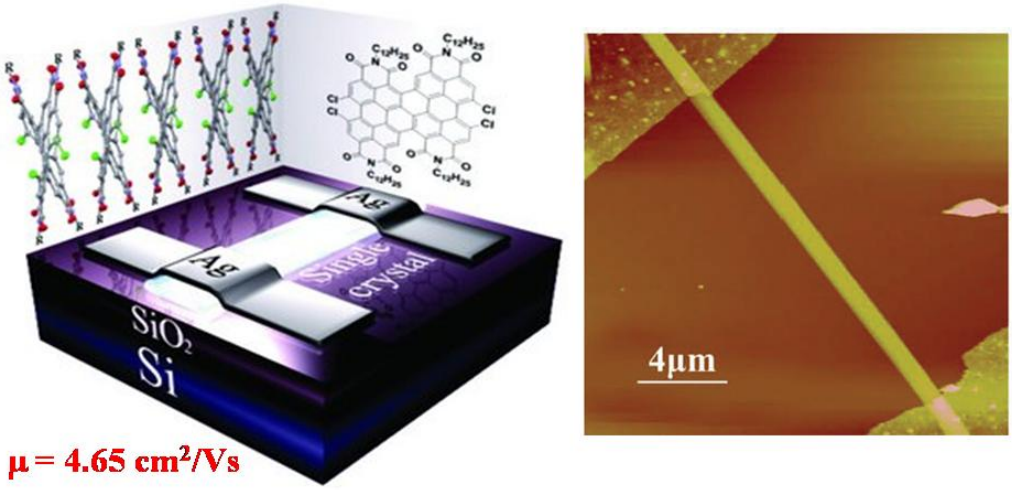

Figure-3.1. High mobility and air stable single crystal ribbon transistor from C12-4CldiPBI. [*Adapted from ref. 11*]

But the single crystal semiconductor materials have the disadvantage that it is very difficult to grow crystals for all types of organic molecules and they lack processability properties to be integrated into industrial processes. For cost effective large area industrial applications, approaches based on solution processing of semiconductor materials are more important.

If it were possible to combine the ready processability of polymers with defect-free crystalline morphology of small molecules, a breakthrough can be expected in this area of research. The ultimate goal in the research on soft nanomaterials is to develop inexpensive, easy to fabricate solution processable crystalline materials with high charge carrier capacity.

Molecular engineering by self assembly of building blocks leading to larger periodic supramolecular architectures has emerged as a potential tool for fabrication of functional nanomaterials and resulted in the field of supramolecular

polymer science. A fundamental precept of supramolecular chemistry is that the information for molecular recognition is manifested through the geometrical and interactional features embodied in the molecular components. In supramolecular polymers, the role played by covalent bonds in conventional polymers is performed by non-covalent interactions such as hydrogen bonding, electrostatic interactions, metal-ion coordination, hydrophobic interactions etc. Out of these, hydrogen bonding is arguably the most widely employed secondary interaction to create pre-programmed sites which dictates the specific self-organization of the precursors.

Molecular recognition and self-assembly through hydrogen bonding interactions are preferred because of its stability, dynamics, directionality and reversibility. Owing to their weak bond strength, single hydrogen bond are easy to break but once aggregated in multiples gives rise to robust assemblies with self-healing capacity. However, even if the synergistic action of numerous H-bonds are brought into play, the overall stability of a superstructure remains nominal. A persistent supramolecular programming requires collective synchronization of all the prominent interactions like H-bonding, van der Waals, steric, π-π stacking as well as solid state packing present within the assembly.

Several design principles have been developed to create different functional materials based on supramolecular polymeric architectures. In this regard, a novel strategy for side-chain hydrogen bonded supramolecular polymers pioneered by Ikkala and ten Brinke *et al.* is very inspiring, where they have studied the bulk state properties of comb-shaped supramolecules obtained by hydrogen bonding of short, flexible, non-mesogenic amphiphiles with a readymade polymer poly(4-vinylpyridine) (P4VP).[12-19] In their work, complexation of P4VP via hydrogen bonding to alkyl phenols, notably pentadecylphenol (PDP) and nonadecylphenol (NDP) explored in detail, showed that for a stoichiometric composition denoted as $P4VP(PDP)_{1.0}$ (figure-3.2) the system orders into a lamellar morphology as corroborated by transmission electron microscopy (TEM) and small angle X-ray scattering (SAXS) data.

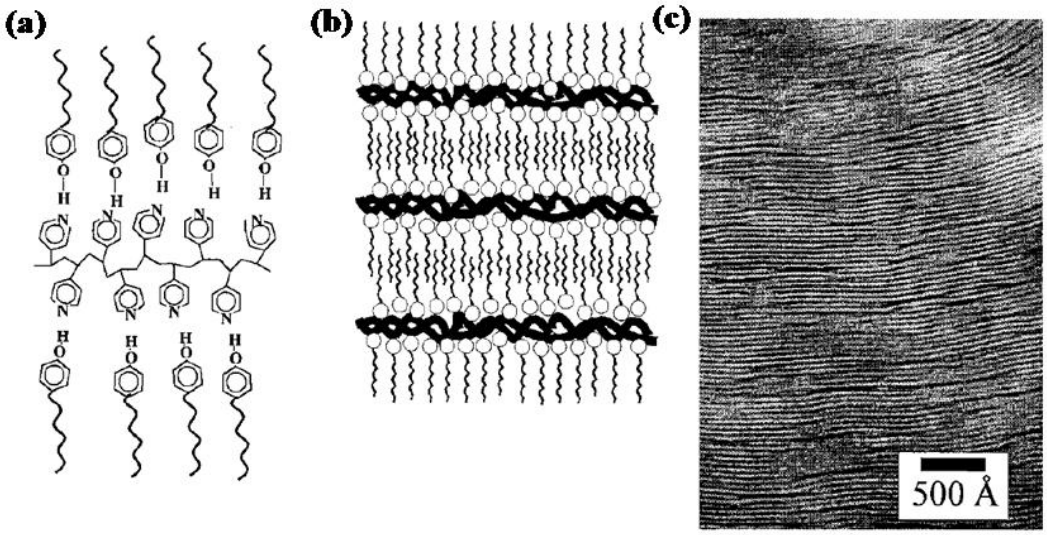

Figure-3.2. (a) Stoichiometric comb-shaped supramolecule P4VP(PDP)$_{1.0}$ (b) & (c) Cartoon and TEM picture of self-organized lamellar structure respectively. [*Adapted from ref.19*]

The same group further extended this concept to the formation of comb-coil supramolecular diblock copolymers where the comb was formed by hydrogen bonded P4VP-PDP block whereas the coil was formed by polystyrene (PS) resulting in block copolymer supramolecule P4VP(PDP)$_{1.0}$-*b*-PS.[13] The resultant overall self-assembly lead to hierarchical structures like lamellar-within-lamellar characterized by two length scales : the microphase separation between the comb-shaped supramolecular block P4VP(PDP)$_{1.0}$ and the linear coil PS block gave rise to a large length scale structure while a small length scale structure was formed by microphase separation within P4VP(PDP)$_{1.0}$ domains. By varying the relative block lengths of the P4VP-*b*-PS selectively all the classical morphologies could be obtained with a series of structure-within-structure morphologies.[13] Figure-3.3 shows the cartoon and TEM images of the different length scale structure-within-structure morphologies for supramolecular comb-coil diblock copolymer P4VP(NDP)$_{1.0}$-*b*-PS with slightly larger nonadecylphenol (NDP) side arms.

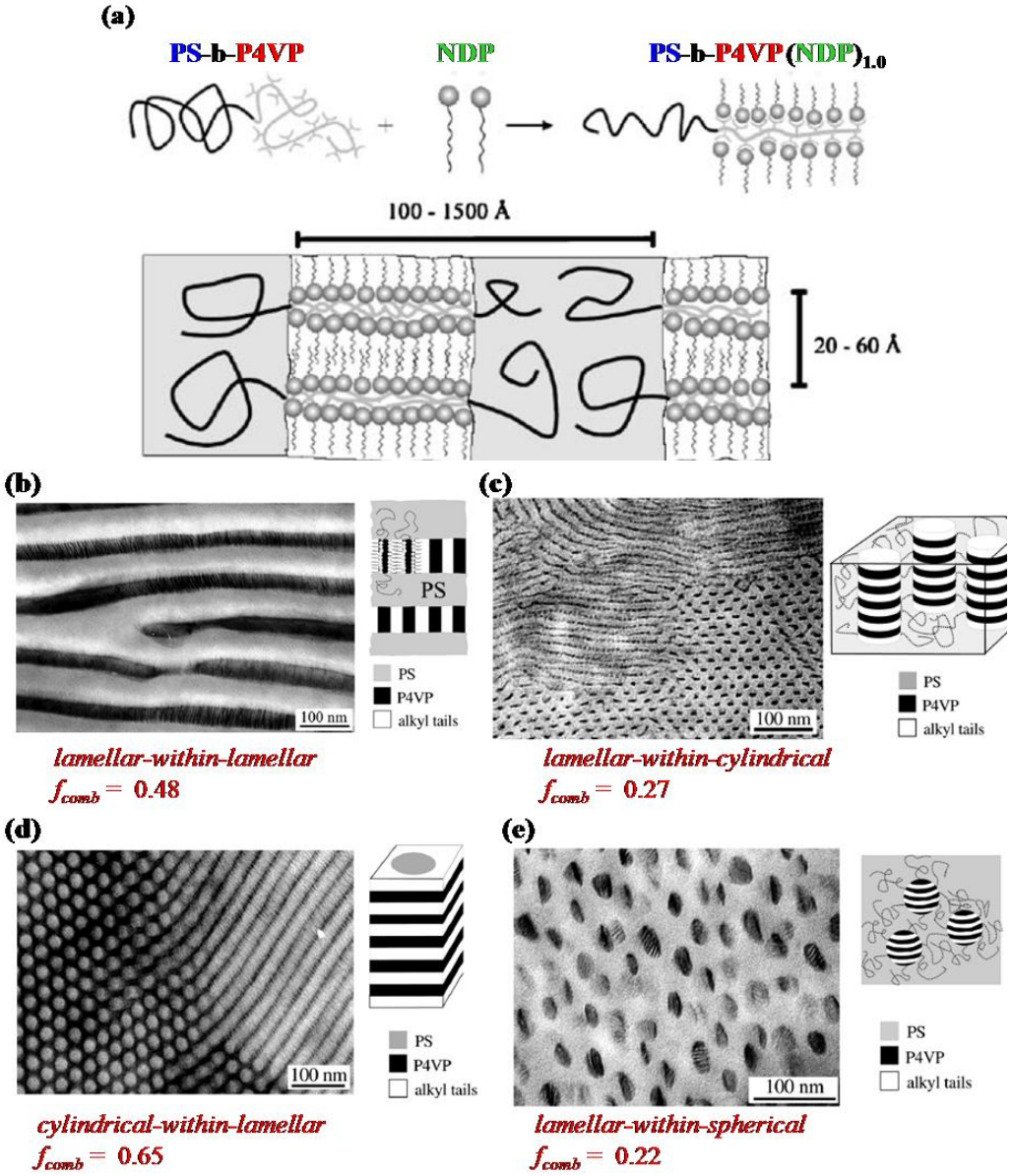

Figure-3.3. (a) Schematic of the PS-*b*-P4VP(NDP)$_{1.0}$ supramolecule showing the two length scale structures and (b) to (e) shows the TEM images of different structure-within-structure morphologies obtained by varying the comb fraction of PS-*b*-P4VP(NDP)$_{1.0.}$ [*Adapted from ref.13*]

This concept of attaching small molecules to block copolymer based supramolecules was applied by the group of Ting Xu and Frè chet *et al.* to a p-type organic semiconductor like quaterthiophene named '4T' which was hydrogen

bonded to PS-*b*-P4VP (figure-3.4) resulting in solution processable nanostructured semiconductor composites with charge carrier mobilities of order 10^{-4} $cm^2V^{-1}s^{-1}$ comparable to the existing semiconductors already used in OPV devices.[20]

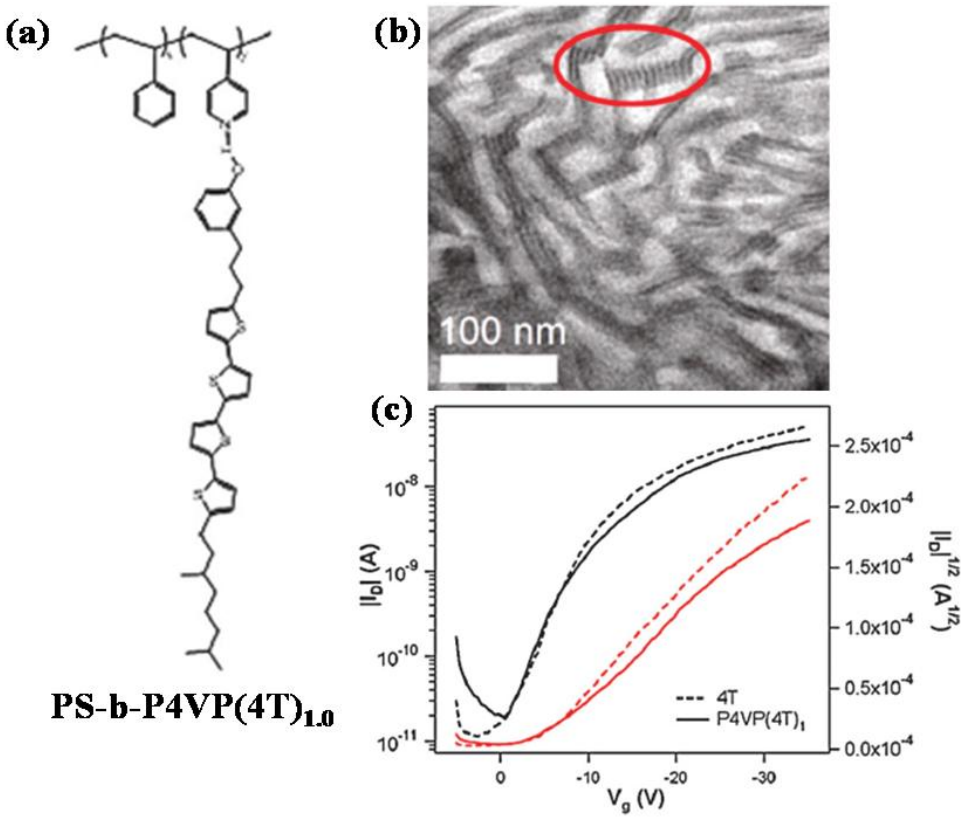

Figure-3.4. (a) Chemical structure of PS-*b*-P4VP(4T)$_{1.0}$ and its TEM image showing lamellar-within-lamellar morphology. (c) I-V curves of OFET devices from '4T' and P4VP(4T)$_{1.0}$ active layers. [*Adapted from ref.20*]

Chen *et al.* developed a series of rod-coil diblock copolymers poly[2,7-(9,9-dihexylfluorene)]-*b*-poly(4-vinylpyridine) abbreviated as (PF-*b*-P4VP) and their P4VP coil blocks were hydrogen bonded with PDP which enabled different morphology transitions from lamellar to cylindrical or from cylindrical to spherical due to the increase of volume fraction of P4VP(PDP) comb blocks.[21] Stamm *et al.* further established that block copolymer and small molecule supramolecular assembly ensured patterning of functional materials into periodic structures in the

nanoscopic length scale.[22,23] In a recent report Mezzenga *et al.* studied blends of regioregular P3HT-*b*-P4VP rod-coil block copolymers with the fullerene derivative PCBM.[24] The design constituted a bicontinuous electron-donor/electron-acceptor network based on supramolecular weak interactions between homogeneous P4VP block with PCBM acting as electron acceptor and the microphase separated P3HT rod segments as the electron donating species. TEM imaging and spectroscopic results showed thermally stable nanostructured thin films self-assembled from ordered P3HT domains and PCBM-enriched P4VP domains. They also studied the device properties of this supramolecular donor-acceptor diblock copolymer as active layer in photovoltaic cells which showed energy conversion efficiencies higher than those containing conventional block copolymers. (Figure-3.5).

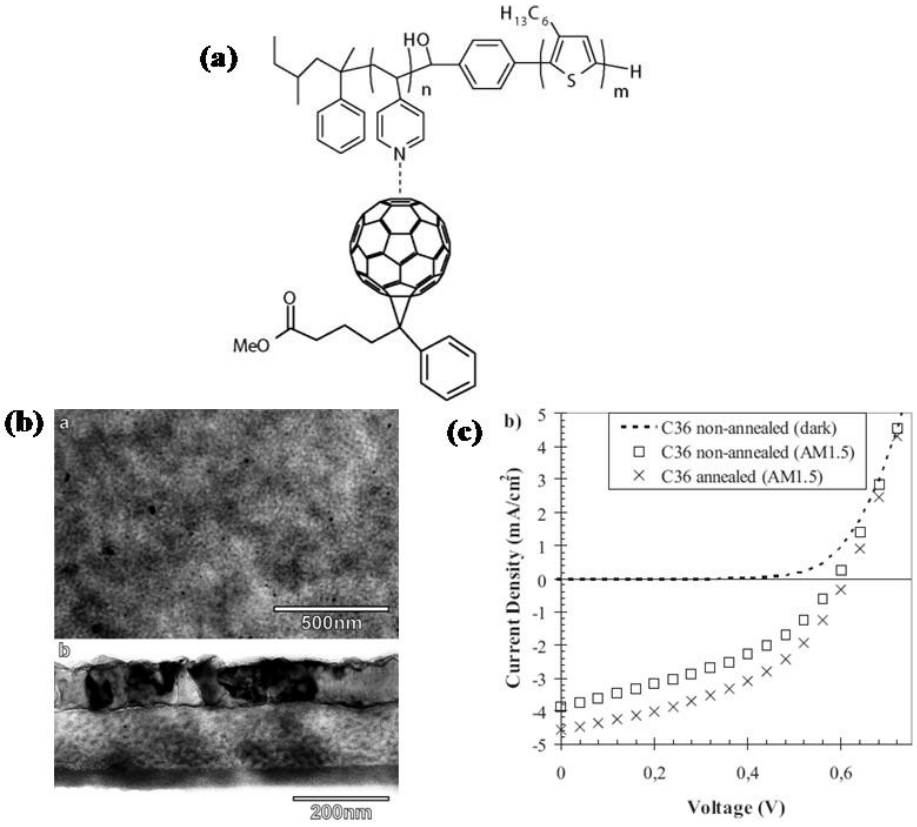

Figure-3.5. (a) P3HT-*b*-P4VP(PCBM) (b) TEM image of the active layer from top view(above) and cross-sectional view showing the percolating structure (c) I-V curve of the solar cell using this supramolecular active layer. [*Adapted from ref.24*]

Motivated by the plethora of successful accomplishments in the field of supramolecular assemblies (SMA), we have initiated a different step incorporating an n-type organic semiconductor molecule, perylenebisimide into polymer scaffold using secondary interactions. The present work describes our attempt at addressing the prevailing situation by combining solution processability with crystallinity in PBI derivatives by supramolecular complexation of a 3-pentadecylphenol based unsymmetrical perylenebisimide (**PDP-UPBI**) to poly(4-vinyl pyridine) (P4VP) polymer via hydrogen bonding (Scheme-3.1). Various stoichiometric complexes of **P4VP(PDP-UPBI)$_n$** where *n* was varied from 0.25 to 1.00 were prepared by simple solution mixing and thoroughly characterized.

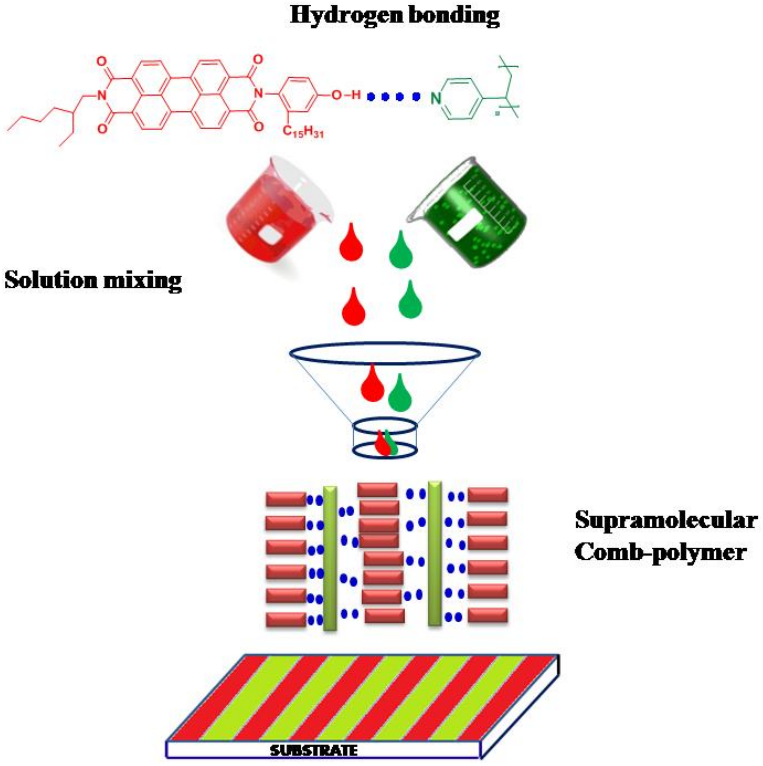

Scheme-3.1

Complexation with P4VP was anticipated to induce solution processability as well as film forming property to the **PDP-UPBI** which were probed by the FT-IR, ^{1}H NMR and UV-Vis/Fluorescence spectroscopic studies. Bulk structure

analyses by XRD experiments indicated that the polymeric complexes retained high crystallinity, which is very difficult to achieve in the case of polymer based systems. We also investigated the morphology of the polymer composites using TEM imaging which showed the presence of microphase separated nanostructures. The charge carrier mobility of these materials were studied using space charge limited current (SCLC) measurements. The study presented here provides a viable route towards low cost semiconducting materials with long range crystalline order favoring electronic coupling between molecular building blocks, processability as well as high electron mobility.

3.2. Experimental Section

3.2.1. Materials: Poly(4-vinylpyridine) (P4VP) (Mw =60,000) was purchased from Aldrich. It was dried in vacuum oven at 60 °C for 3 days prior to use. The other starting materials perylene tetracarboxylic acid dianhydride (PTCDA), 2-ethyl-1-hexyl amine, 3-pentadecylphenol were also purchased from Aldrich and used without any further purification. All solvents used were of analytical grade and carefully dried before use according to standard procedures.

3.2.2. Instrumentation techniques: Infrared spectra were obtained using Bruker α-T spectrophotometer in the range of 4000-400 cm^{-1}. **P4VP(PDP-UPBI)$_n$** complexes dissolved in DMF were directly drop cast onto KBr pellets, solvent evaporated off slowly at 60-70 °C, followed by drying in vacuum oven overnight. ^{1}H and ^{13}C-NMR spectra were recorded in $CDCl_3$ using Bruker AVENS 200 MHz spectrophotometer. Chemical shifts (δ) are reported in ppm at 298 K, with trace amount of tetramethylsilane (TMS) as internal standard. Bruker AVENS 400 MHz spectrometer was used for variable concentration as well as variable temperature measurements in [D_2]-TCE (1,1,2,2-tetrachloroethane) solvent. MALDI-TOF analysis was carried out on a Voyager-De-STRMALDI-TOF (Applied Biosystems, Framingham, MA, USA) instrument equipped with 337 nm pulsed nitrogen laser used for desorption and ionization. The operation was in a reflector mode with an accelerating voltage of 25 kV. Micromolar solutions of the compounds in THF were mixed with Dithranol matrix and spotted on stainless steel MALDI plate and dried well. Size exclusion chromatography (SEC) in THF was done using polystyrene standards for calibration. Waters 515 Pump connected through two series of Styragel HR columns (HR-3 and HR-4E) and Waters 2414 differential refractometer was used for analyzing the samples. The flow rate of the THF was maintained as 1 mL throughout the experiments, and 2-3 mg in 1mL of the samples were filtered and injected for recording the chromatograms at 30 °C. UV-Vis spectra were recorded using a Perkin Elmer Lambda-35 UV-Vis spectrometer with peltier setup in the range of 0 - 100 °C for variable temperature measurement. Steady state fluorescence emission were performed using a HORIBA JOBIN

VYON Fluorolog 3 fluorescence spectrophotometer. The emission as well as excitation slit width was maintained at 1 nm throughout the experiments and the data was obtained in 'S_{1c}/R_1' mode (to account for the variations in lamp intensity). Measurements were made at 90° positions for solutions and 22.5° in front face films. The fluorescence quantum yields of the perylene derivatives were determined in $CHCl_3$ using Rhodamine 6G in ethanol (Φ=0.95) as the standard. Thermogravimetric analysis (TGA) was performed using a PerkinElmer STA 6000 thermogravimetric analyser. Samples were run from 40 to 800 °C with a heating rate of 10 °C/min under nitrogen. DSC (differential scanning colorimeter) measurements were performed on TA Q10 differential scanning calorimeter at a heating rate of 10 °C/min under nitrogen atmosphere. Typically, 3-4 mg of samples was placed in an aluminium pan, sealed properly and scanned from -30 to 380 °C. The instrument was calibrated with indium standards before measurements. The first heating cycles were avoided to get rid of thermal history of the samples. Wide Angle X-ray Diffractogram (WXRD) were obtained using a Philips analytical diffractometer with CuKα emission. All the samples were recorded in the (2θ) range of 3–50 degrees using a PANalytical X'pert Pro dual goniometer diffractometer and analyzed using X'pert software. An X'celerator solid-state detector was employed in wide-angle experiments. The radiation used was CuKα (1.54 Å) with a Ni filter, and the data collection was carried out using a flat holder in Bragg–Brentano geometry. In situ XRD experiments were carried out using an Anton–Paar XRK900 reactor for high temperature measurements. Small angle X-ray scattering (SAXS) was employed to investigate the phase behaviour of the complexes. The scattering experiments were conducted on a three pinhole collimated Bruker Nanostar machine equipped with rotating copper anode, operating at 45 kV and 100 mA providing characteristic Kα radiation of 1.54 Å. The measurements were carried out in the normal resolution mode having a q range of 0.011 – 0.2 $Å^{-1}$. The bulk sample was sandwiched between two kapton films inside the sample holder. The scattered data was collected using a 2-D Histar detector and later converted from 2D to 1D by azimuthal averaging using Bruker software. 1D data presented after background subtraction is plotted as I v/s q,

where q = $(4\pi/\lambda)$ Sinθ, λ is the wavelength of the incident X-rays and 2θ is the scattering angle. Transmission Electron microscopy (TEM) was done using an FEI-Tecnai^{TM}-F20 electron microscope operating at 200 kV. Sandwich structures on ITO coated glass and Au substrates were fabricated for the SCLC studies. Thin films of the samples were drop-cast and spin coated on the substrates. The thickness was determined using Dektak surface profiler. The top Al electrode defining the area of the film (0.1 cm^2) was coated using thermal deposition method in high vacuum. All measurements were carried out under inert atmosphere.

3.2.3. Synthesis

Synthesis of Unsymmetrical perylenebisimide (PDP-UPBI)

(i) 4-amino-3-pentadecyl phenol: 3-pentadecylphenol (30.4 g, 100 mmol), potassium hydroxide (28 g, 500 mmol) and 95% ethyl alcohol (200 mL) were added into a 500 mL, three-necked, round-bottom flask equipped with a reflux condenser. The mixture was stirred and cooled to 25 °C to which diazonium chloride prepared from sulphanilic acid dihydrate (21.0 g, 100 mmol) was added dropwise. The resulting red dye solution was stirred for 2 hours and then heated to 75 °C on a water bath. At this temperature a saturated solution of sodium dithionite (53.0 g, 0.0003 mmol) was added to the dye solution in 10 minutes and was stirred for 30 minutes (color changed from dark red to orange). Acetic acid (18 g, 0.0003 mmol) in water (20 mL) was added to this and refluxed for 1 hour (color changed to pale tan). The reduced solution was then poured into water (2 L) and the product was filtered, dried under vacuum at 50 °C for 2 hours. The crude product obtained was purified by recrystallization using toluene. Yield : 79%. ^{1}H NMR (200 MHz, $CDCl_3$, δ ppm): 7.20 (d, 1H, Ar-H), 6.53-6.47 (m, 2H, Ar-H), 2.63 (t, 2H, Ar-C**H$_2$**-), 1.60 (t, 2H, Ar-CH_2-C**H$_2$**), 1.36–1.23 (b, other aliphatic 24H), 0.86(t, 3H, Ar-$(CH_2)_{14}$-CH_3). ^{13}C NMR (50 MHz, $CDCl_3$,δ ppm): 146.8, 138.7, 126.2, 117.5, 113.4, 30.9, 29.5, 22.7, 14.3. FT-IR (KBr, cm^{-1}): 3432, 3350, 3296, 1647, 1585, 1416, 1334, 914, 675. MALDI-TOF MS (Dihydroxybenzoic acid matrix): m/z calculated for $C_{21}H_{37}NO$: 319.29; found 320.31$[M+1]^+$.

(ii) N, N'-Bis-Ethylhexyl- perylene–3,4:9,10–tetracarboxylic bisimide (1): In a 500 mL round bottom flask (4 g,10 mmol) PTCDA, (2.9 g, 22 mmol) 2-ethyl-1-hexylamine and 0.5 g $Zn(OAc)_2$ in 150 mL N,N'-Dimethylacetamide (DMAc) were stirred at 110 °C for 4 hours under nitrogen atmosphere. The solvent DMAc was removed by vacuum distillation and the reaction mixture was stirred with 400 mL 2N HCl overnight. The dark red precipitate was filtered and rinsed thoroughly with water and methanol. Finally dried at 120 °C to give a red solid. Yield : 93 %. ^{1}H NMR (200 MHz, $CDCl_3$, δ ppm): 8.64(dd, 8H, perylene), 4.16(m, 4H, imide-C**H**$_2$), 1.99(m, 2H, imide-CH_2-C**H**), 0.98-0.88(2t, 12H, end C**H**$_3$ of ethyl hexyl tail), 1.44-1.28(other aliphatic protons).^{13}C NMR (50 MHz, $CDCl_3$,δ ppm): 159.3, 135.7, 130.9, 129.2, 47.0, 37.0, 31.7, 29.3, 23.0, 14.1 FT-IR (KBr, cm^{-1}): 2956, 2931, 2850, 1709, 1659, 1600, 1578, 1512, 1446, 1336, 1255, 1183, 1086, 1024, 793, 745, 644. MALDI-TOF MS (Dithranol matrix): m/z calculated for $C_{40}H_{42}N_2O_4$: 614.31; found 615.21$[M+1]^+$.

(iii) N-(2-Ethylhexyl) perylene– 3,4:9,10 –tetracarboxyl-3,4-anhydride-9,10-imide (2): (4.5 g, 7.3 mmol) symmetrical ethylhexyl perylenebisimide **1** was suspended in 125 mL t-BuOH (tertiary butanol) and refluxed to 90 °C with (2.1 g, 3.6 mmol) solid 85% KOH, until the solution turned dark violet. The mixture was then brought to room temperature and stirred with 62.5 mL acetic acid and 250 mL 2N HCl overnight. The dark red precipitate was filtered, washed with water until washings were neutral and dried at 130 °C. The crude mixture containing the bisimide, monoimide and PTCDA was then purified by column chromatography, first eluted with $CHCl_3$ to get rid of the bisimide, followed by a violet band and then eluted with $CHCl_3$/ Acetic acid 10:1 v/v to get the monoimide 2 as a pure bright red solid. Yield : 62.4 %. ^{1}H NMR (200 MHz, $CDCl_3$ + TFA, 298K) δ ppm: 8.76(dd, 8H, perylene), 4.18(m, 2H, imide-C**H**$_2$), 1.94(m, 1H, imide-CH_2-C**H**), 0.98-0.88(2t, 6H, end CH_3 of ethyl hexyl tail), 1.44-1.28(other 8 aliphatic protons).^{13}C NMR (50 MHz, $CDCl_3$+ TFA) δ ppm: 159.0, 149.7, 130.9, 129.2, 128.4, 123.8, 55.6, 31.9, 29.3, 26.7, 24.9, 22.7, 14.1 FT-IR (KBr, cm^{-1}): 2956, 2931, 2850, 1771, 1734, 1709, 1659, 1595, 1580, 1510, 1446, 1336, 1255, 1183, 1086, 1024, 793, 745, 644. MALDI-TOF MS (Dithranol matrix) : m/z calculated for $C_{32}H_{25}NO_5$: 503.17 ; found 526.11 $[M+Na]^+$.

(iv) N-(2-ethylhexyl) -N'- (4-hydroxy-2-pentadecylphenyl) perylene -3,4,9,10-tetracarboxylic acid bisimide (PDP-UPBI) (3): In a 250 mL single neck round bottom flask (1 g, 1.98 mmol) of compound **2** and (0.761 g, 2.38 mmol) 4-amino-3-pentadecylphenol along with 0.1g $Zn(OAc)_2$ were dissolved in 8g molten imidazole and stirred at 160 °C for 4 hours under N_2 atmosphere. The reaction mixture was then cooled to room temperature and stirred overnight with 250 mL 2N HCl. The precipitate was filtered, washed with water followed by methanol and dried at 120 °C. The crude product was further purified by column chromatography twice with $CHCl_3$ to get the desired **PDP-UPBI**. Yield : 78%. M.P.: 320 °C.^{1}H NMR (200 MHz, $CDCl_3$, δ ppm) : 8.71(m, 8H, perylene), 6.86–7.09 (m, 3H;Ar**H**-PDP), 4.16 (m, 2H, imide-N-C**H**$_2$), 2.41 (t, 4H; Ar-C**H**$_2$), 2.00 (m, 1H, imide-N-CH_2-C**H**), 0.98-0.86 (m, 9H, end CH_3 of ethyl hexyl group + terminal C**H**$_3$ of C-15 alkyl chain), 1.07-1.63(other aliphatic protons). ^{13}C NMR (50 MHz, $CDCl_3$, δ ppm) : 166.3, 163.6, 161.9, 158.9, 155.8, 143.1, 136.7, 130.3, 129.8, 126.2, 124.9, 123.1, 122.6, 113.3, 106.2, 55.6, 32.7, 31.9, 29.9, 26.9, 22.8, 14.3.FT-IR (KBr, cm^{-1}): 3367, 2957, 2921, 2854, 1698, 1655, 1591, 1505, 1463, 1441, 1402, 1348, 1299, 1249, 1177, 1092, 967, 856, 806, 749, 632. MALDI-TOF MS (Dithranol matrix): m/z calculated for $C_{53}H_{60}N_2O_5$: 804.45 ; found 805.41$[M+1]^+$, 827.37 $[M+Na]^+$. Elemental analysis calculated (%): C 79.07, H 7.51, N 3.48; found: C 79.09, H 7.32, N 3.81.

Sample preparation: Poly(4-vinylpyridine) (P4VP) as well as the amphiphilic perylenebisimide (**PDP-UPBI**) was dried in vacuum oven at 60 °C for 3 days. **P4VP(PDP-UPBI)$_n$** complexes were prepared from dry DMF solutions, where 'n' denotes the number of PBI molecules per vinyl pyridine (VP) repeat unit (n= **PDP-UPBI** /VP). In a typical procedure P4VP was first dissolved in DMF to which desired amount of **PDP-UPBI** was added depending on the value of 'n' and the solution was stirred for 24 hours. Concentration of the solutions were kept 1wt%. Subsequently the solvent was evaporated slowly on a hot plate at 60 °C and further dried in vacuum oven at 65 °C for 3 days, slowly cooled to room temperature and stored in dessiccator thereafter.

3.3. Results and Discussion

3.3.1. Synthesis and Characterization of Amphiphilic Perylenebisimide

The supramolecular assembly of n-type organic semiconductor perylenebisimide (PBI) with poly(4-vinylpyridine) (P4VP), involving different non-covalent secondary interactions such as hydrogen-bonding, π- π stacking and hydrophobic interactions were investigated. An unsymmetrical, perylenebisimide amphiphile (**PDP-UPBI**) having a 3-pentadecylphenol moiety which could involve in hydrogen bonding interaction with the pyridine units of P4VP, was synthesized and characterized for this study. Following the reported literature [4] procedure as shown in Scheme-3.2, the synthesis of **PDP-UPBI** was started from the symmetrical ethylhexyl PBI derivative (1) obtained by condensation of the dianhydride PTCDA with excess 2-ethylhexyl amine along with a catalytic amount of Lewis acid $Zn(OAc)_2$.

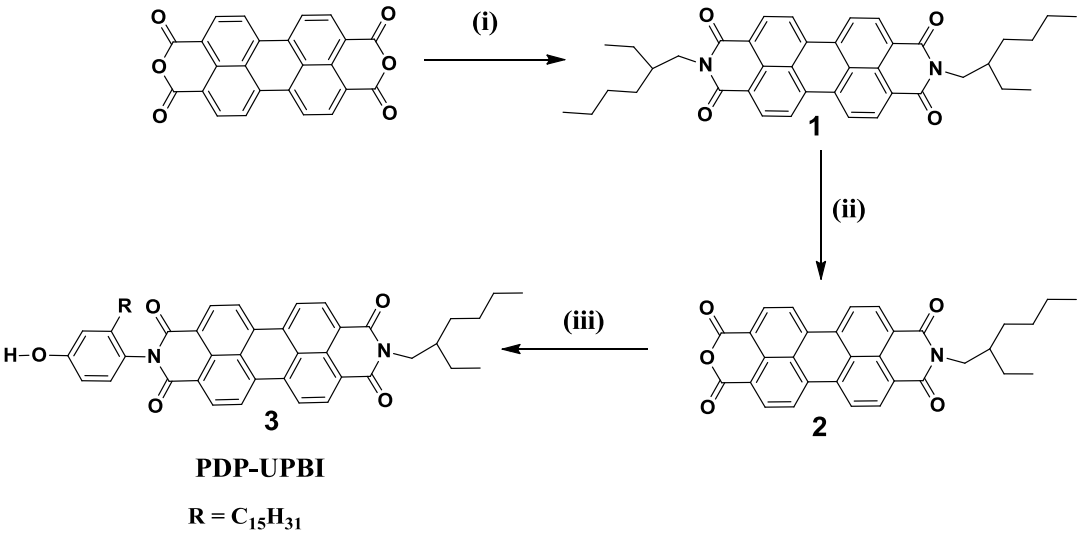

Scheme-3.2. Synthesis of unsymmetrical (**PDP-UPBI**) Perylenebisimide. Reagents (i) 2-Ethylhexylamine, N,N-Dimethylacetamide(DMAc), $Zn(OAc)_2$, 110 °C, 4 hours; (ii) KOH, *t*-BuOH, 90 °C 1-1.5 hours ; (iii) 4-amino-3-pentadecyl phenol, imidazole, $Zn(OAc)_2$, 2-4 hours, 160 °C.

A partial saponification of this symmetric derivative (**1**) under strong basic conditions with KOH in *tert*-BuOH as the reaction medium was done according to Langhals method,[4] which gave the mono-imide-mono-anhydride derivative (**2**). Subsequent condensation of this one side ethylhexyl mono-imide-mono-anhydride derivative (2) with the second amine viz., 4-amino-3-pentadecyl phenol gave the desired unsymmetrical **PDP-UPBI** (**3**) in reasonably good yield. The structures of **PDP-UPBI** along with the intermediate products were fully characterized by ^{1}H-NMR,^{13}C-NMR, FT-IR and MALDI-TOF spectroscopies with details given in experimental section. Figure-3.6. gives a comparison of the ^{1}H-NMR spectra of **PDP-UPBI** with the intermediates.

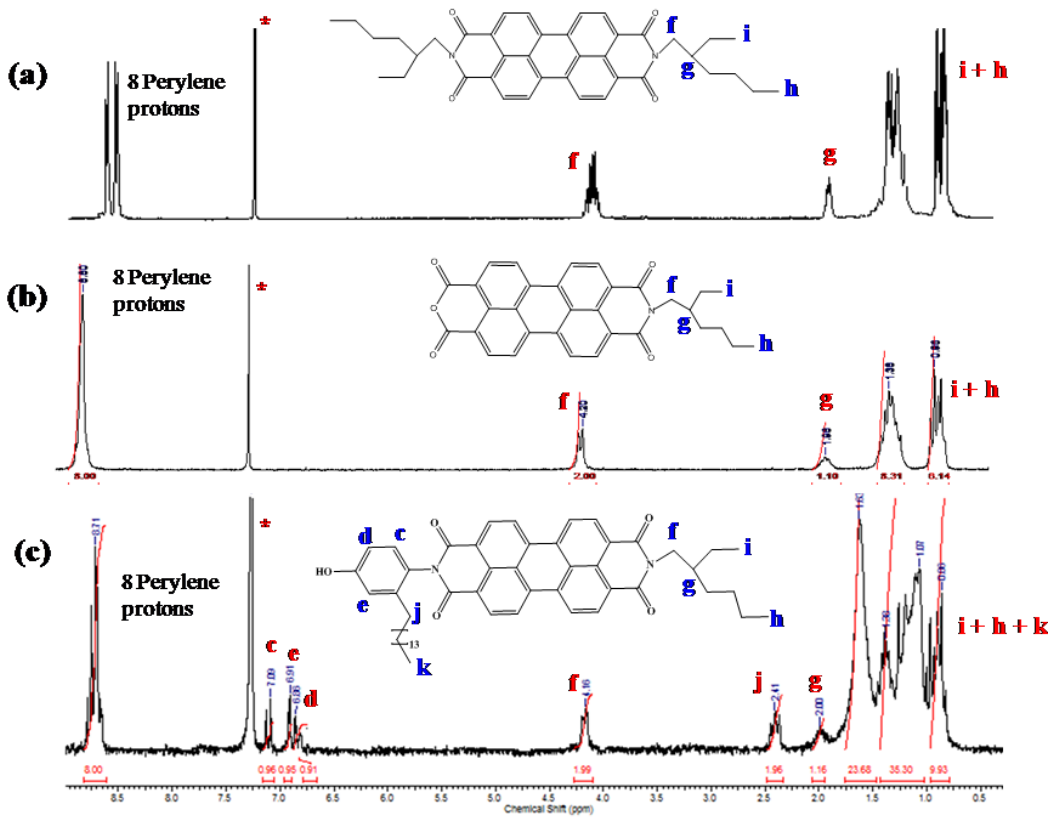

Figure-3.6. ^{1}H-NMR spectra of (a) symmetrical ethylhexyl PBI and (b) ethylhexyl perylene mono-imide-mono-anhydride derivative compared with that of (c) unsymmetrical **PDP-UPBI.**

The **PDP-UPBI** was obtained in extremely pure form by repeated column chromatography purification procedures. The high level of purity was confirmed by the single peak in the size exclusion chromatography (SEC) together with mass data and elemental analysis. Figure-3.7. (a) and (b) shows the SEC chromatogram and MALDI-TOF spectra respectively of PDP-UPBI. Thermal properties of this new unsymmetrical perylenebisimide was studied by thermogravimetric (TGA) and differential scanning calorimetric (DSC) analysis. The PDP-UPBI was found to exhibit high thermal stability upto temperatures of 350-400 °C with no signs of decomposition as observed from the TGA curves (fig-3.7-(c)). From the DSC profile (fig-3.7-(d)) it could be seen that the PDP-UPBI showed a single melting transition (T_m = 324 °C) in the heating cycle and a single crystallization transition ($T_{cryst.}$ = 308 °C) in the cooling cycle as in the case of a typical crystalline molecule.

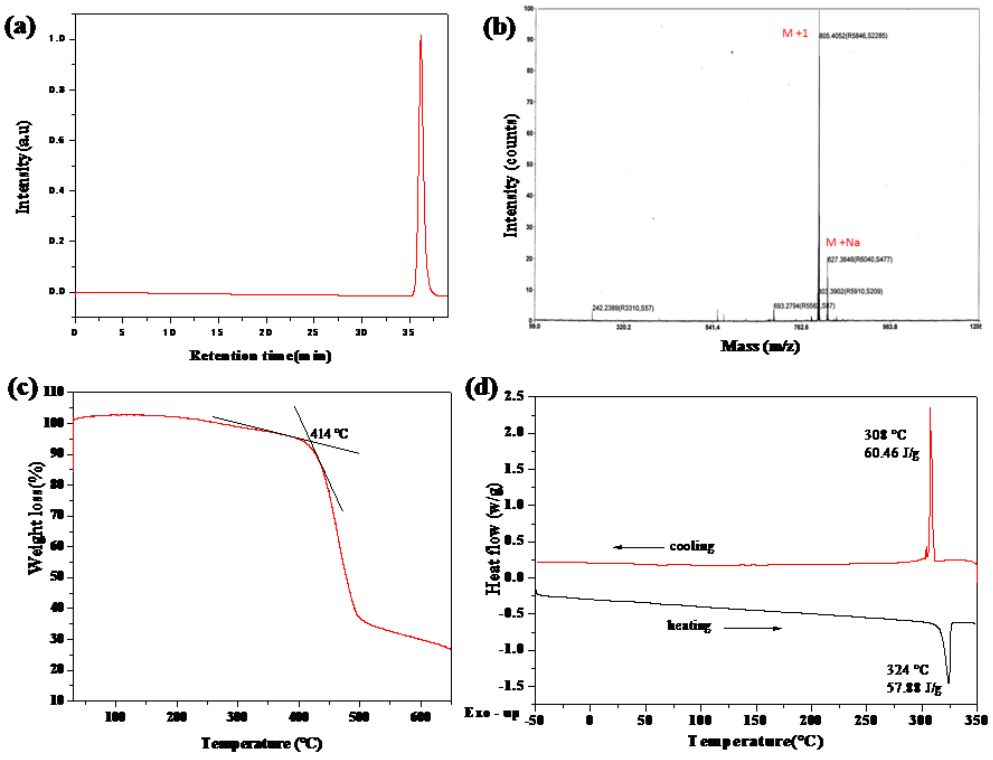

Figure-3.7. (a) SEC chromatogram (b) MALDI-TOF (c) TGA and (d) DSC thermogram of **PDP-UPBI.**

3.3.2. Supramolecular Comb-polymer complexation with P4VP

The hydrogen-bonded complexes were prepared by dissolving different weight ratios of **PDP-UPBI** with fixed amounts of P4VP in DMF as solvent, stirring at ambient conditions for 24 hours, followed by removal of solvent by heating. The complex was named **P4VP(PDP-UPBI)$_n$**, where 'n' denoted the theoretical ratio of **PDP-UPBI** versus 4-vinylpyridine repeat units, which was varied from 0.25 to 1.00 in the present study. The schematic drawing along with the chemical structure of the hydrogen bonded polymeric **P4VP(PDP-UPBI)$_{1.0}$** stoichiometric 1:1 complex is depicted in Scheme-3.2., where each pyridine unit of poly(4-vinyl pyridine) **P4VP** is nominally coordinated to single **PDP-UPBI** perylenebisimide small molecule (denoted by the subscript 1.0 in **P4VP(PDP-UPBI)$_{1.0}$**).

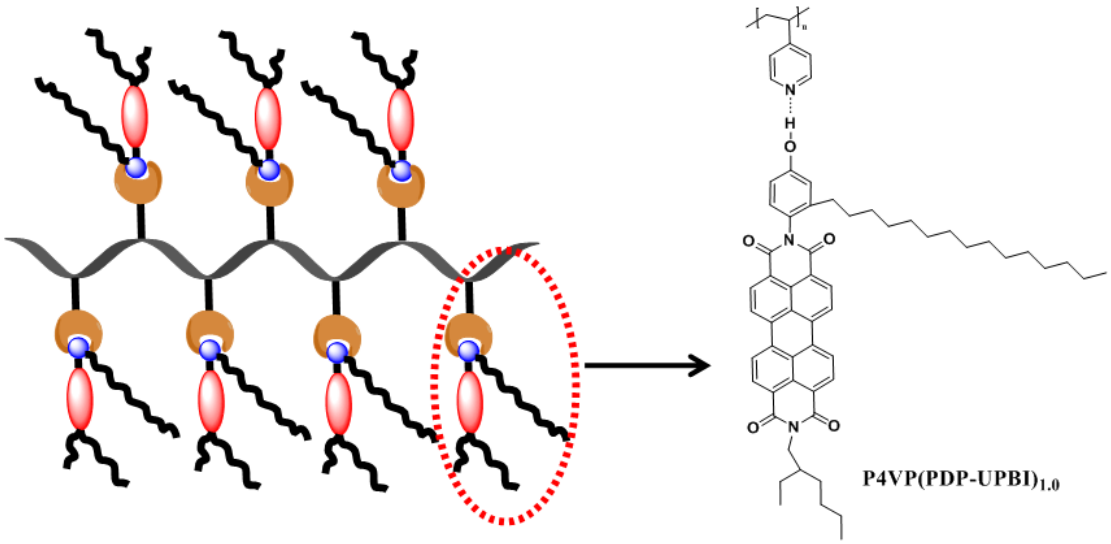

Scheme-3.3. Schematic diagram of the **P4VP(PDP-UPBI)$_{1.0}$** polymeric supramolecular complex formed by 1:1 stoichiometric interaction of the unsymmetrical **PDP-UPBI** with P4VP polymer.

3.3.3. Confirmation of hydrogen-bonded complexation - FT-IR and ^{1}H-NMR studies

The first hint of successful complexation was obtained from the increased solubility of the complex compared to the respective pure components. The formation of the complex was traced by FT-IR spectroscopy as illustrated in literature for the complexes of P4VP with PDP.[18] P4VP shows a symmetric ring stretching mode at 993 cm^{-1} and a strong carbon-nitrogen stretching band at 1597 cm^{-1} for free pyridine groups, which gets shifted to higher wavenumbers upon hydrogen bonding interaction with the phenol unit of PDP.[18] The shift corresponding to the 1597 cm^{-1} peak was difficult to trace in the **P4VP(PDP-UPBI)$_n$** complexes since pentadecylphenol unit attached to the perylene core also had absorption band in the same region. Another characteristic absorption band of pure P4VP around 1413 cm^{-1} was devoid of any overlapping absorptions from pure **PDP-UPBI**. Ikkala *et al.* had shown that for the nominally fully complexed P4VP(PDP)$_{1.0}$, the 1413 cm^{-1} band got shifted to 1421 cm^{-1}.[18] Figure-3.8 shows the FT-IR spectra comparing the 993 cm^{-1} and 1413 cm^{-1} region of the 1:1 complex (equal number of pyridine and phenol groups) **P4VP(PDP-UPBI)$_{1.0}$** along with that of P4VP and **PDP-UPBI**. It could be seen from the figure that the hydrogen bonding of the pyridine ring of P4VP with the phenol of **PDP-UPBI** was almost complete in the 1:1 complex which was indicated by the complete vanishing of 993 cm^{-1} band, with the simultaneous appearance of two new bands at 1003 and 1023 cm^{-1} corresponding to hydrogen bonded pyridine. Similarly, in the 1413 cm^{-1} region, a new peak appeared at 1421 cm^{-1} in **P4VP(PDP-UPBI)$_{1.0}$** which also confirmed the complexation. In fact, the shift of the pristine pyridine bands at 993 cm^{-1} and 1413 cm^{-1} in the complex to higher wavenumbers was not an abrupt phenomenon. A gradual shift in the peak position was observed as the degree of complexation increased from n= 0.25 to 1.00. This could be clearly understood from the FT-IR plots of **P4VP(PDP-UPBI)$_n$** complexes with n = 0.25, 0.50, 0.75 and 1.00 (figure-3.9.). When the degree of complexation was 0.25 the peak shift was relatively small and on going from 0.25 to 0.75, it increased further and

achieved a maximum shift of +10 for 993 cm^{-1} and +8 for 1413 cm^{-1} in the 1:1 complex. The band shift is usually small when the pyridine ring is hydrogen bonded to phenolic moieties. For protonation or coordination type of bonding, relatively larger +20 to +40 shifts have been reported.[25,26]

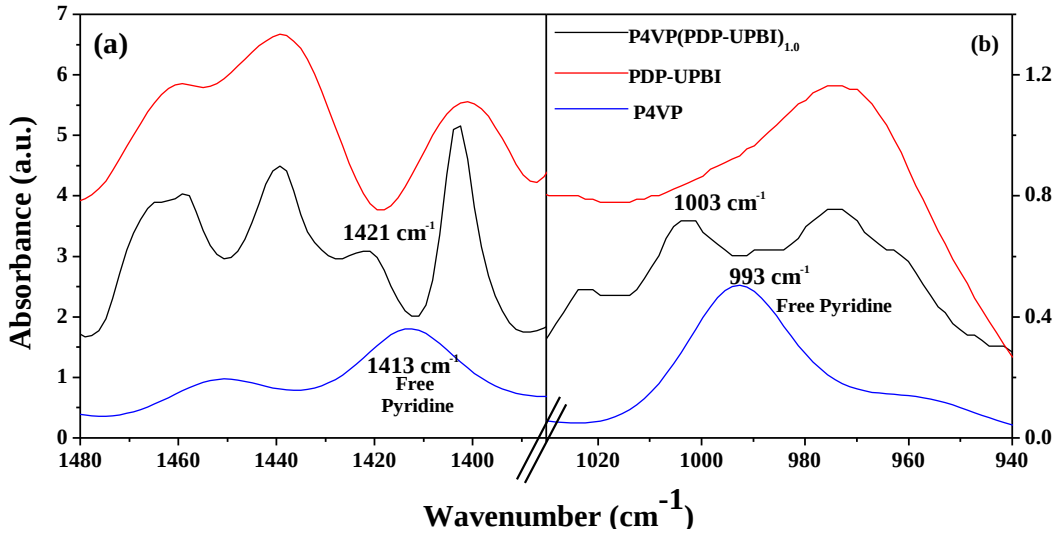

Figure-3.8. FTIR plots comparing the (a) 1413 cm^{-1} and (b) 993 cm^{-1} region of **P4VP(PDP-UPBI)$_{1.0}$** complex with that of pure P4VP and **PDP-UPBI.**

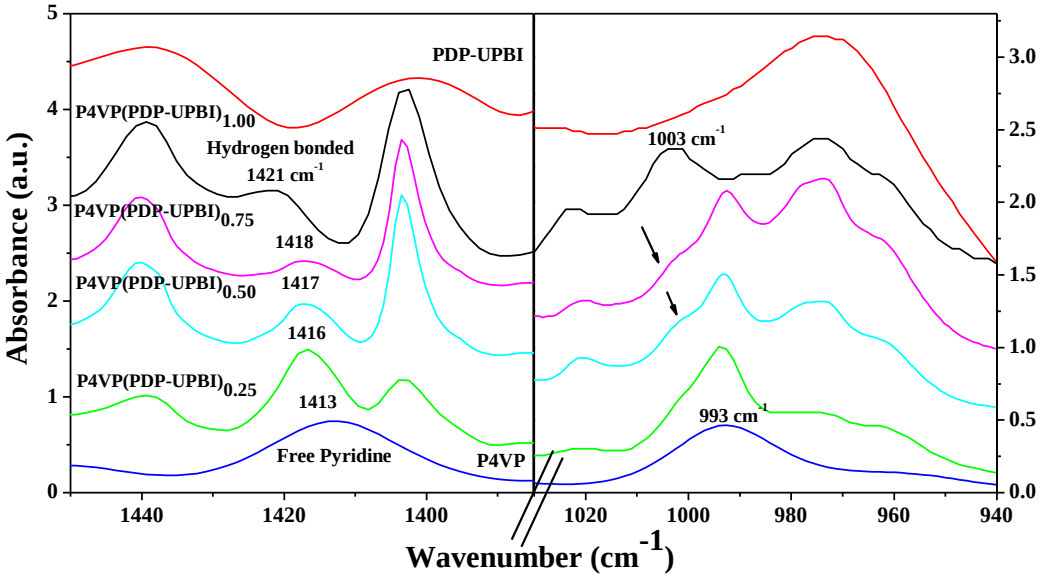

Figure-3.9. FTIR plots comparing the (a) 1413 cm^{-1} and (b) 993 cm^{-1} region of **P4VP(PDP-UPBI)$_n$** with pure P4VP and **PDP-UPBI.** (n = 0.25, 0.50, 0.75, 1.00)

A detailed structural characterization of the complexes was carried out using proton NMR spectroscopy in deuterated chloroform ($CDCl_3$) or deuterated 1,1,2,2-tetrachloroethane ([D_2]-TCE). Figure-3.10. compares the ^{1}H NMR spectra of P4VP, and **PDP-UPBI** along with the 1:1 complex – **P4VP(PDP-UPBI)$_{1.0}$** recorded in $CDCl_3$ at room temperature (25°C).

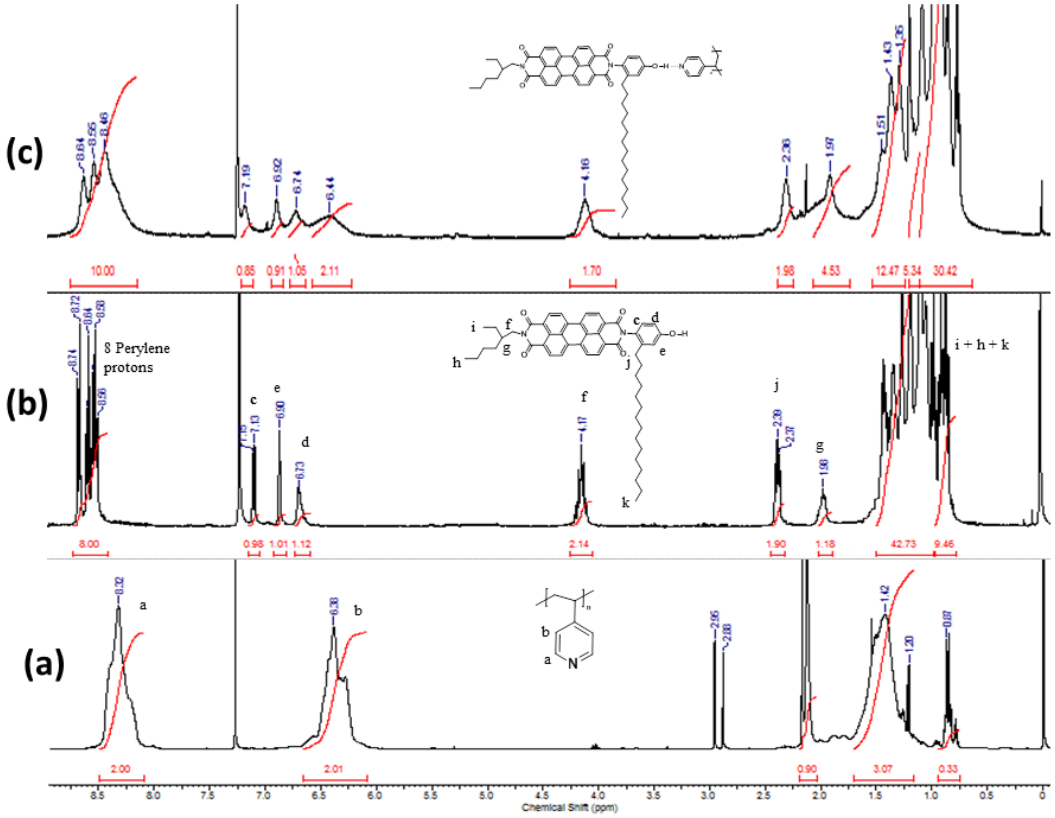

Figure-3.10. Comparison of ^{1}H-NMR spectra of (a) P4VP (b) **PDP-UPBI** and (c) **P4VP(PDP-UPBI)$_{1.0}$** recorded at 25 °C in $CDCl_3$ (15 mg/ml).

The **PDP-UPBI** molecule had sharp signals corresponding to the 8 aromatic protons in the region 8.74-8.56 ppm, and signals corresponding to the 3 aromatic protons of pentadecyl phenol (PDP) unit (labelled as c, e and d) at 7.1 (d, 1H), 6.88 (s, 1H) and 6.72 (d, 1H) ppm respectively. On the other hand, P4VP had two sets of broad signals corresponding to four aromatic pyridine protons with intensity distribution corresponding to two protons each at 8.32 (d, 2H, labeled ‘a’) and 6.36

ppm (d, 2H, labeled 'b') respectively. Detailed labelling of the other protons is also indicated in the figure. Upon comparison, it could be clearly seen that in the 1:1 complex all signals became broadened indicating an overall polymeric nature for the perylene protons also. The PBI core protons also showed an upfield chemical shift of 8.64 – 8.45 ppm. Signal broadening and upfield chemical shifts observed for the perylene core protons are due to the increase in π-stacking ring current shielding the neighboring protons.[27-32] Corresponding chemical shifts were observed for the P4VP protons also. The proton labeled 'a' at 8.32 ppm underwent a downfield shift to 8.46 ppm (0.14 ppm difference) and merged with the broad perylene core protons with just a hump visible. This peak position could be confirmed from the proton integration value of 10 under the peaks in the range 8.64 – 8.46 ppm corresponding to 8 perylene + 2 pyridine protons which matched well in intensity with the two aliphatic protons labeled 'f' at 4.16 ppm. The downfield shift of the two aromatic pyridine protons near to nitrogen occurs because the hydrogen bonding between the phenolic OH of **PDP-UPBI** and lone pair of electrons on nitrogen atom of pyridine decreases the electron density around the pyridine nitrogen atom, thereby deshielding the 'a' protons of the pyridine ring. The 'b' protons are affected less by this deshielding due to its increased distance away from the hydrogen bonding site and hence does not show any significant chemical shift from 6.38 to 6.44 ppm (0.06 ppm difference) upon complexation.

Figure-3.11. compares the expanded aromatic region (6-9 ppm) in the ^{1}H NMR spectra of the **P4VP(PDP-UPBI)$_n$** complexes for n = 0.25, 0.50, 0.75 and 1.0 with **PDP-UPBI**, which were recorded in deuterated tetrachloroethane ([D_2]-TCE). The relative ratio of the intensity of the 8 aromatic perylene ring protons (8.63 ppm) and the two aromatic pyridine protons ('a') of P4VP at 8.31 ppm, increased on going from n = 0.25 to n = 1.0 in the **P4VP(PDP-UPBI)$_n$** complexes. At n = 1.0, both perylene and P4VP showed 1:1 ratio for their respective aromatic proton intensities giving strong support for the stoichiometric 1:1 complex formation. Only in the 1:1 complex, i.e., **P4VP(PDP-UPBI)$_{1.0}$** the integration value of 8 for eight PBI core protons corresponded to 2 each for the two sets of pyridine ring

protons 'a' and 'b' of P4VP at 8.31 and 6.40 ppm respectively. The integration values for the other complexes with n < 1 suggested incomplete complexation with more uncomplexed nitrogen on P4VP. Hydrogen bonding is a concentration as well as temperature dependent phenomenon. Therefore, the structural changes in the 1:1 complex were probed using variable concentration as well as variable temperature ^{1}H NMR experiments.

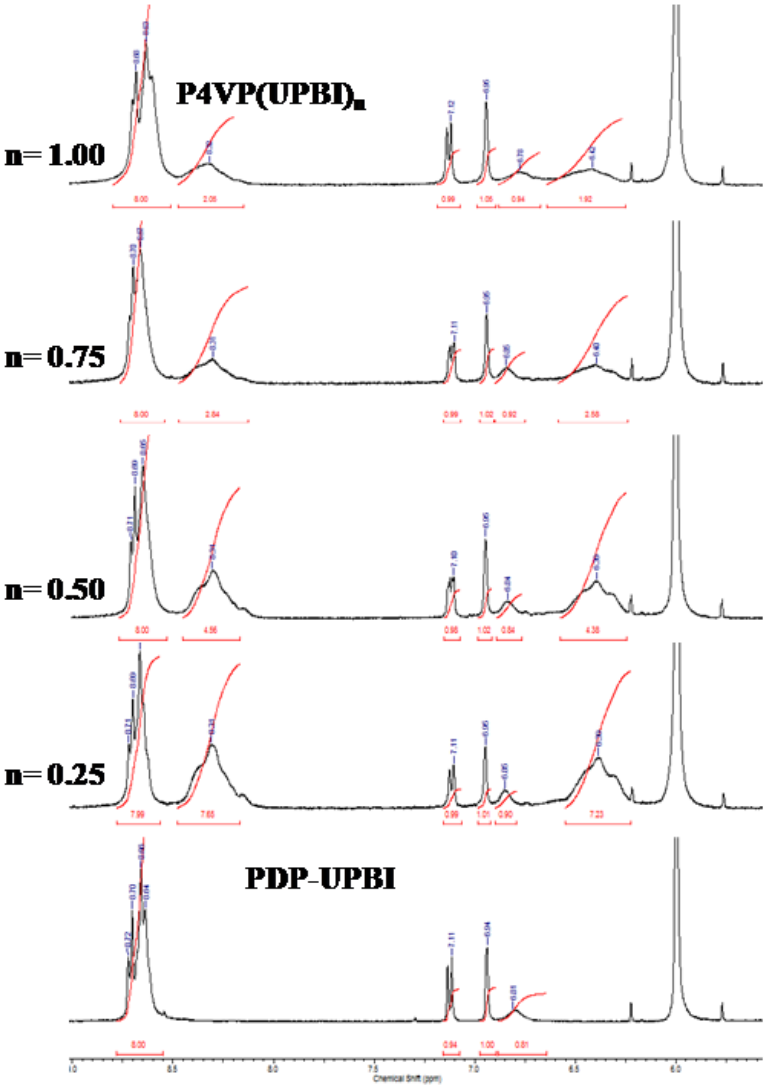

Figure-3.11. Expanded ^{1}H NMR aromatic region from 6-9 ppm of **P4VP(PDP-UPBI)$_n$** complexes compared with **PDP-UPBI**, each 5mg/mL in [D_2]-TCE.

Figure-3.12 compares the ^{1}H NMR spectra of **P4VP(PDP-UPBI)$_{1.0}$** at three different concentrations – 2, 6 and 15 mg respectively recorded at 25°C in 1.1 mL of $CDCl_3$. Since the complexes were bound by intermolecular hydrogen bonding, upon dilution from a highly concentrated solution, the signals showed a dramatic change from a broad overlapped pattern to sharp peaks similar to **PDP-UPBI** alone with no trace of P4VP observable. At dilute conditions of the 1:1 complex, even though P4VP was present, the weight ratio of **PDP-UBPI** was comparatively more, resulting in the lack of observation of P4VP signals.

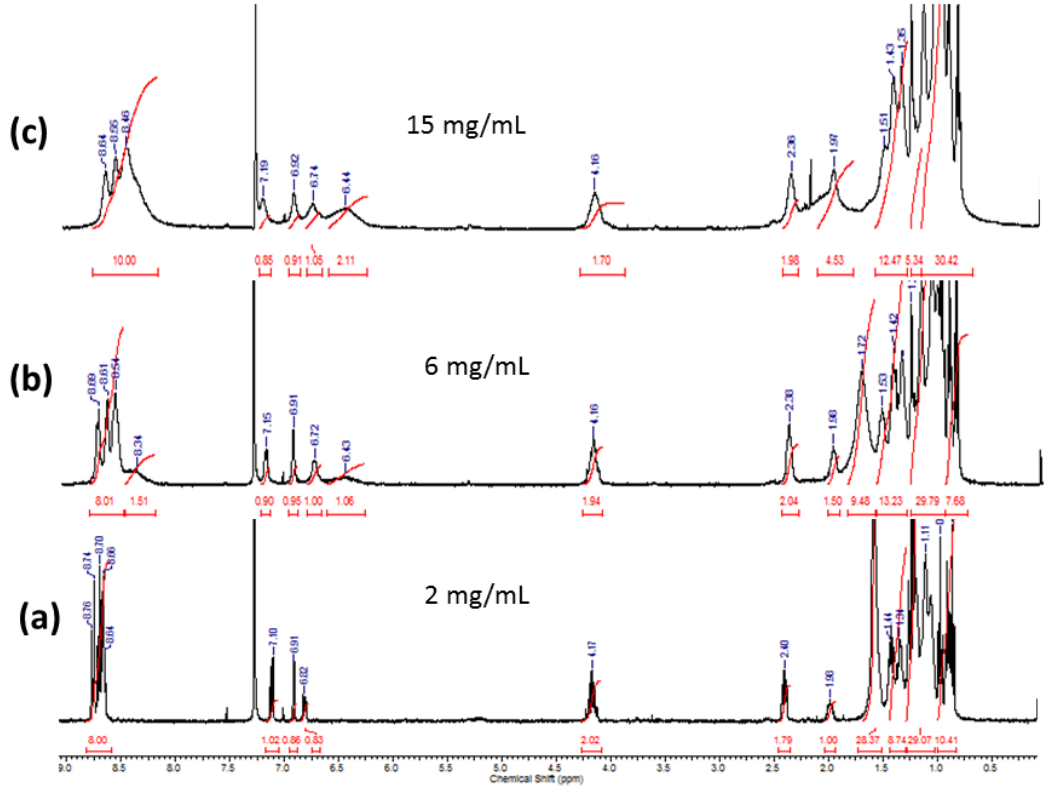

Figure-3.12. Variable concentration ^{1}H-NMR spectra of **P4VP(PDP-UPBI)$_{1.0}$** recorded at 25 °C in $CDCl_3$, (a) 2 mg/mL (b) 6 mg/mL (c) 15 mg/mL.

The possibility of the **PDP-UPBI** molecules self-assembling by themselves aided by the hydrogen bonding interaction among the hydroxyl groups and π stacking interactions of the aromatic core was also taken into consideration. The figure-3.13 compares the expanded aromatic region from 6-9 ppm in the ^{1}H NMR spectra of

PDP-UPBI and **P4VP(PDP-UPBI)$_{1.0}$** at low and high concentrations. Except for an upfield shift in the proton NMR signal, the perylene aromatic protons did not exhibit any broadening in **PDP-UPBI** alone. Therefore, the broadening observed in the complex was confirmed to be due to the hydrogen bonding assisted comb-polymer formation.

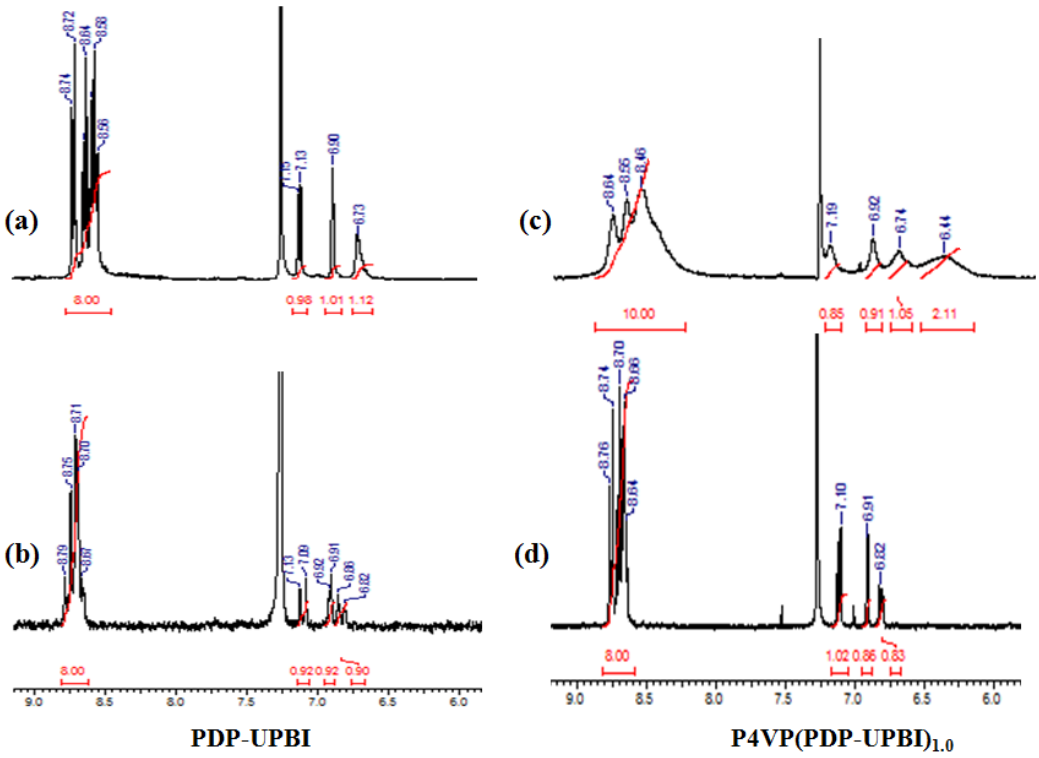

Figure-3.13. Expanded ^{1}HNMR aromatic region from 6-9 ppm at a high concentration (15mg/mL) and a low concentration (2mg/mL) for both **PDP-UPBI** (a) & (b) and **P4VP(PDP-UPBI)$_{1.0}$** (c) & (d) respectively.

However in both cases i.e., **PDP-UPBI** and **P4VP(PDP-UPBI)$_{1.0}$** the PDP aromatic protons labeled 'd' showed a change in splitting pattern and chemical shift upon varying the concentration. This was indicative of an intermolecular kind of association existing in both **PDP-UPBI** and **P4VP(PDP-UPBI)$_{1.0}$** although the extent of association were different. Figure-3.14. shows the NOESY spectra recorded for **PDP-UPBI** showing the absence of any cross coupling peaks for the perylene or the PDP region. This ruled out any intramolecular interaction as the

cause of aggregation in **PDP-UPBI**. Similar effects were observed as a function of temperature which was carried out in deuterated 1,1,2,2-tetrachloroethane ([D_2]-TCE, boiling point: 147 °C) for both **PDP-UPBI** and **P4VP(PDP-UPBI)$_{1.0}$**. Figure-3.15(a) compares the ^{1}H NMR spectra of **P4VP(PDP-UPBI)$_{1.0}$** recorded in ([D_2]-TCE at various temperatures from 25 °C to 90 °C. Figure-3.15(b) shows the similar spectra for **PDP-UPBI**. Drastic changes were observed in the chemical shift as well as splitting pattern of the aromatic perylene proton signals and the aromatic proton labeled 'd' on the PDP ring in both the **PDP-UPBI** and the 1:1 complex as a function of temperature. The PDP ring protons labeled 'd' was observed as a broad peak at 6.80 and 6.76 ppm in **PDP-UPBI** and its 1:1 complex respectively, which split into two doublets with downfield shift, upon increasing the temperature. In general, the perylene bisimides show two aromatic peaks corresponding to two sets of inner and two sets of outer ring protons.[33] The peak pattern changes into four doublets when the outer ring protons become non-equivalent as in unsymmetrical perylenebisimides.[34]

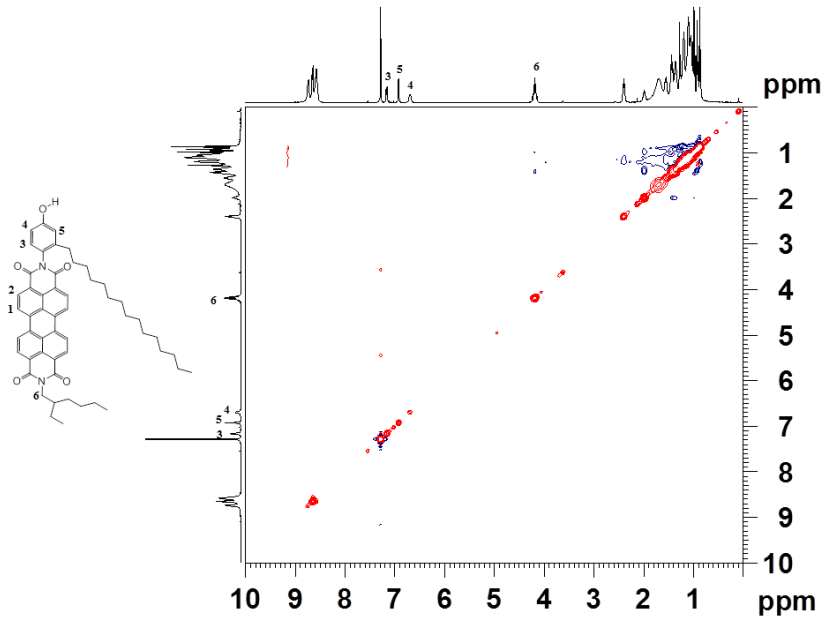

Figure-3.14. NOESY spectra of **PDP-UPBI** (400MHz, $CDCl_3$, 298K).

(a)

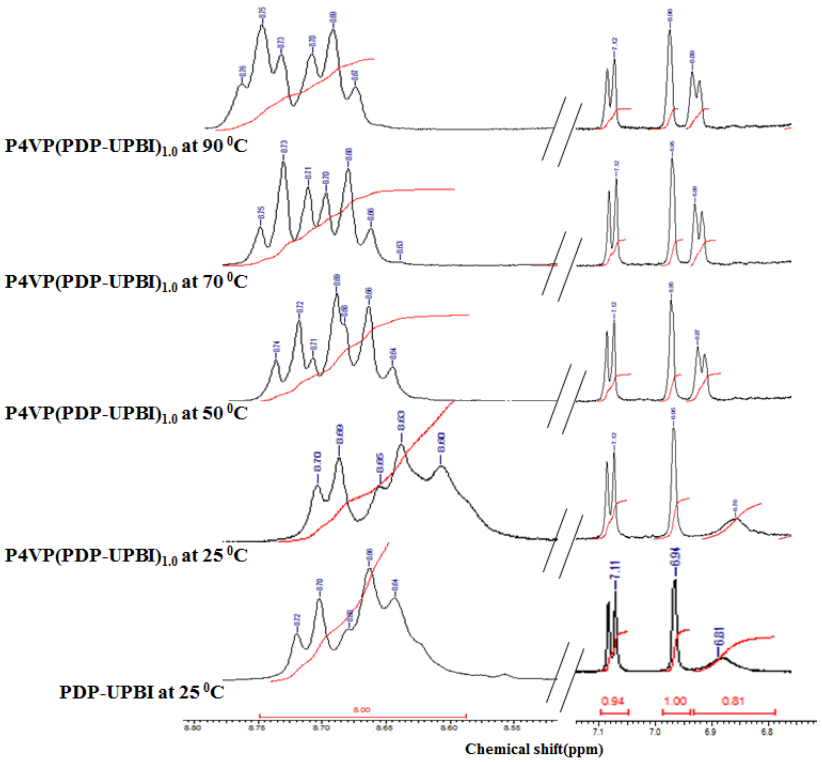

(b)

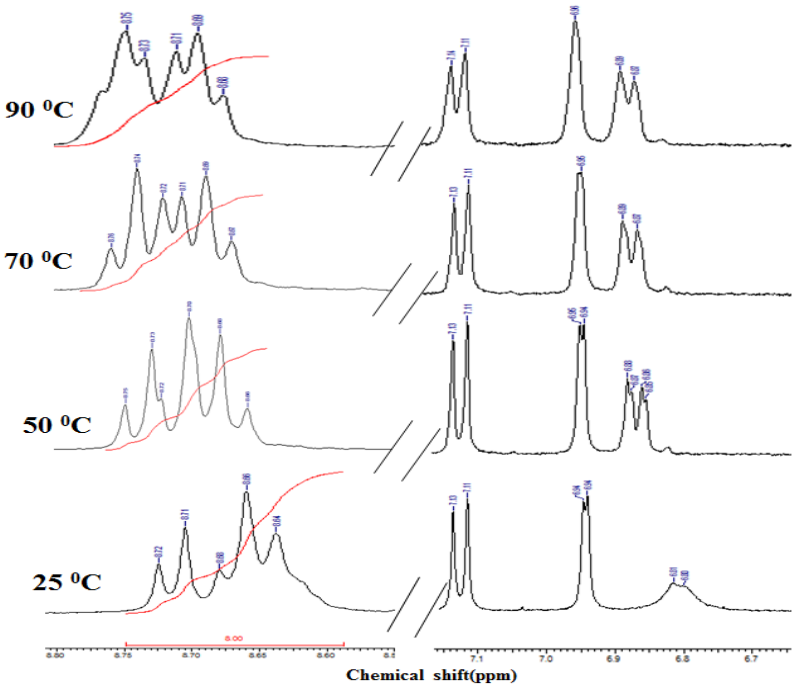

Figure-3.15. Expanded aromatic regions ^{1}H NMR spectra of (a) **P4VP(PDP-UPBI)$_{1.0}$** and (b) **PDP-UPBI** recorded in [D_2]-TCE as a function of temperature.

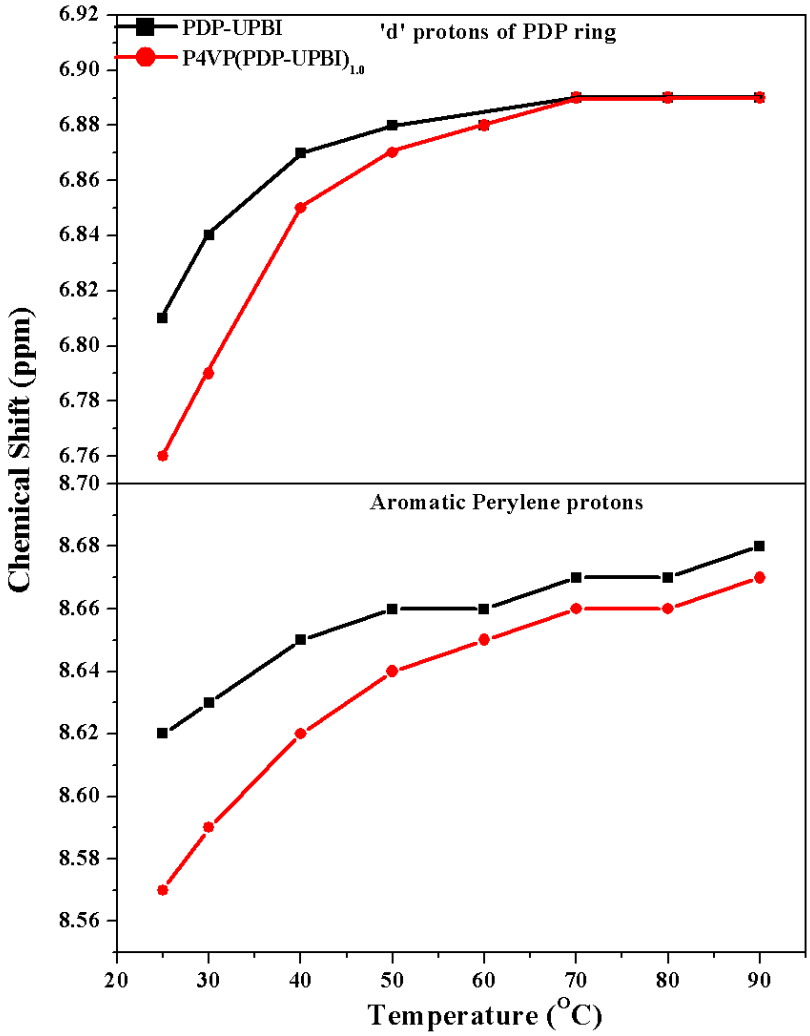

Figure-3.16. Chemical shift from the ^{1}H NMR spectra for the aromatic protons of **P4VP(PDP-UPBI)$_{1.0}$** and **PDP-UPBI** recorded in ([D_2]-TCE as a function of temperature.

The perylene aromatic ring proton pattern was complex with several peaks ranging from 8.61 to 8.72 ppm at 25°C in both **PDP-UPBI** and **P4VP(PDP-UPBI)$_{1.0}$**. The significant upfield shift in the inner perylene core protons of **P4VP(PDP-UPBI)$_{1.0}$** complex at 25°C compared to that of **PDP-UPBI** at the same temperature indicated that the perylene ring experienced much stronger intermolecular forces in the former compared to the latter. Consequently the inner hydrogen nuclei in **P4VP(PDP-UPBI)$_{1.0}$** experienced much higher shielding by

induced ring currents within an adjacent molecule, which indirectly suggested an intensified co-facial π-π stacking of PBI units in the 1:1 complex than in **PDP-UPBI** alone. Upon increasing the temperature from 25 °C to 90 °C the line width became much narrower and deshielded from 8.57 – 8.70 to 8.67 – 8.76 ppm, due to the decrease in the extent of dynamic self-assembly caused by breaking of the hydrogen bonds at higher temperature. Figure-3.16 gives the overall comparison of the changes in the chemical shift of the aromatic protons of the perylene and PDP ring in both **PDP-UPBI** and **P4VP(PDP-UPBI)$_{1.0}$** with respect to temperature. Two facts were clearly observed from this comparison. Firstly, the aromatic protons (perylene and PDP ring) of the 1:1 complex were upfield shifted compared to that of **PDP-UPBI** alone at all temperatures. This gave direct evidence for the higher extent of association present in the complex compared to the **PDP-UPBI** alone. Secondly, at higher temperature (above 70 °C) the difference in chemical shift between the 1:1 complex and **PDP-UPBI** gradually reduced. Above this temperature, **PDP-UPBI** as well as **P4VP(PDP-UPBI)$_{1.0}$** remained molecularly dissolved in tetrachloroethane.

3.3.4. Photophysical Properties - UV-Vis / Fluorescence Studies

It has been well studied that π-π stacking of extended aromatic π-systems like perylenebisimide are strongly solvent dependent.[35-39] Therefore, the UV-vis absorption studies were carried out for the **P4VP(PDP-UPBI)$_{1.0}$** in chloroform ($CHCl_3$) which is a polar 'good' solvent for the π-core and also in a non-polar 'bad' solvent like methylcyclohexane (MCH).[81] Figure-3.17(a) shows the normalized absorption spectra of **P4VP(PDP-UPBI)$_{1.0}$** recorded in these two solvents of opposite polarity. In chloroform, the complex exhibited the characteristic absorption of isolated perylene bisimide chromophore with peaks in the range of 400-530 nm, corresponding to the S_0–S_1 transition with well resolved vibronic structure from 0–0, 0–1, 0–2, and 0–3 transitions respectively.[40,41] But in MCH, the absorption was broad, peak maxima blue shifted; two new red-shifted peaks appeared at 547 and 579 nm respectively.

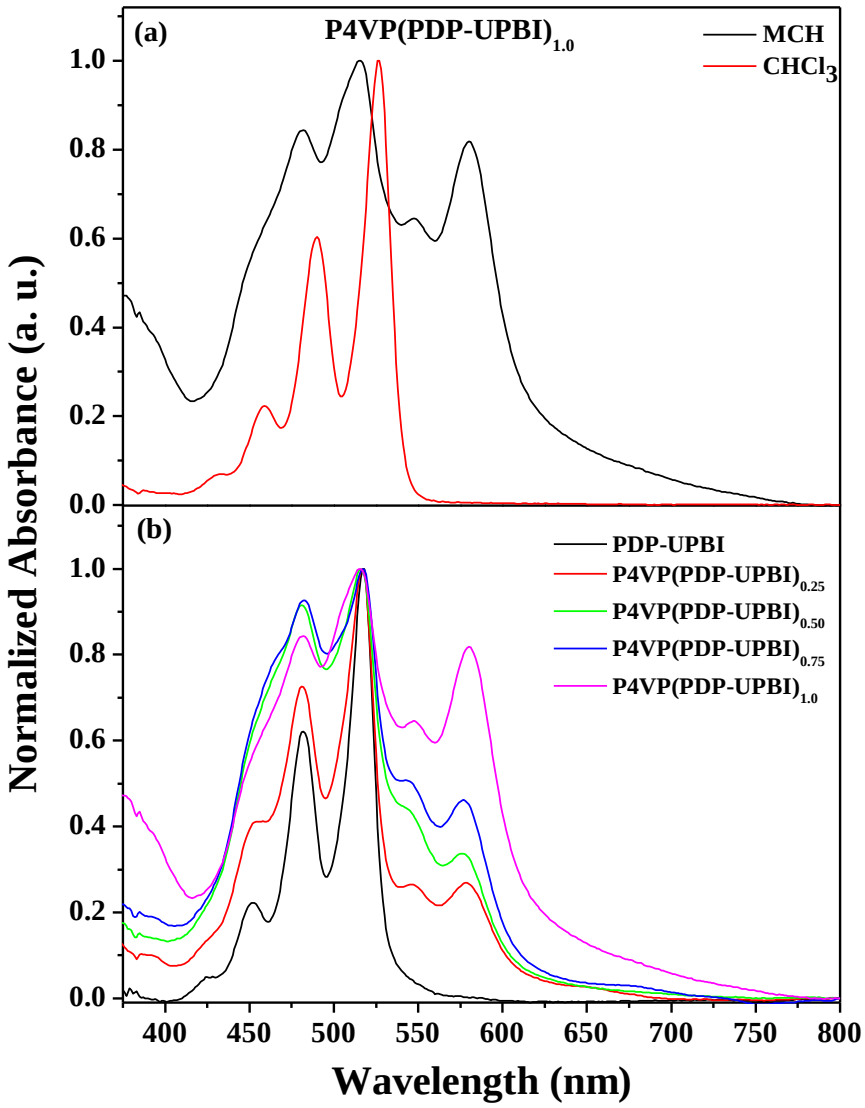

Figure-3.17. Normalized absorption spectra of (a) **P4VP(PDP-UPBI)$_{1.0}$** in MCH and $CHCl_3$. (b) **PDP-UPBI** and **P4VP(PDP-UPBI)$_n$** in MCH at 25 °C.

The absorption spectra of non-aggregated perylenebisimides are known to show the ratio of absorbance $A^{0\rightarrow0}$ / $A^{0\rightarrow1}$ value greater than 1.6 whereas lower values pointed towards aggregation.[42-44] The $A^{0\rightarrow0}$ / $A^{0\rightarrow1}$ ratio from the absorption spectra of **P4VP(PDP-UPBI)$_{1.0}$** in MCH was found to be 1.18, while in chloroform it was 1.65. This observation along with the bathochromically shifted band at 580 nm clearly indicated aggregation in MCH. Chloroform being a good solvent for the

π-conjugated systems, the complex remained molecularly dissolved with small aggregation constants at the concentrations used for the absorption studies.[45] Aggregation of fluorophores in solution state can lead to different extents of electronic interaction between the π-electron systems, which is reflected in their absorption spectral pattern. On the basis of observed spectral shifts, according to Kasha's rule, dye aggregates are classified into (1) face-to-face stacked sandwich-like geometries termed as H-aggregates, characterized by blue shifted absorption band and (2) J-aggregates with a head-to-tail geometry of the chromophores along with bathochromically shifted absorption band.[46] The absorption spectra of **P4VP(PDP-UPBI)$_{1.0}$** in MCH exhibited both a strongly blue shifted 0–0 absorption band as well as two bathochromically shifted shoulder bands around 547 nm and 580 nm questioning the assignment of exact nature of chromophore packing as to H-type or J-type.

To further understand the nature of self assembly in MCH, the absorption spectra were recorded for **PDP-UPBI** monomer alone as well as its various complexes **P4VP(PDP-UPBI)$_n$** in MCH, where n = 0.25, 0.50, 0.75 and 1.0. The solubility of **PDP-UPBI** alone in MCH was rather low – less than 1 mg/mL ; whereas upon complexation the solubility increased considerably. Figure-3.17(b) compares the normalized (at the λ_{max} 517 nm) absorption spectra of the **PDP-UPBI** along with that of its complexes with P4VP in MCH. **PDP-UPBI** remained molecularly dissolved in MCH at 25°C with the spectra resembling that of the 1:1 complex in chloroform. Upon 25 percent complexation with P4VP itself, the shape of the absorption spectra changed in MCH. The ratio of the intensity I_{579}/I_{516} increased from 0.27 for **P4VP(PDP-UPBI)$_{0.25}$** to 0.8 for **P4VP(PDP-UPBI)$_{1.0}$** indicating increased extent of aggregation with increase in extent of complexation. A variable concentration absorption measurement (figure-3.18(a)) of the complexes showed some interesting observation. The spectra of **P4VP(PDP-UPBI)$_{1.0}$** remained very broad at all concentrations; the ratio of the intensity I_{579}/I_{516} did not vary much upon dilution (inset in figure compares the normalized spectra).

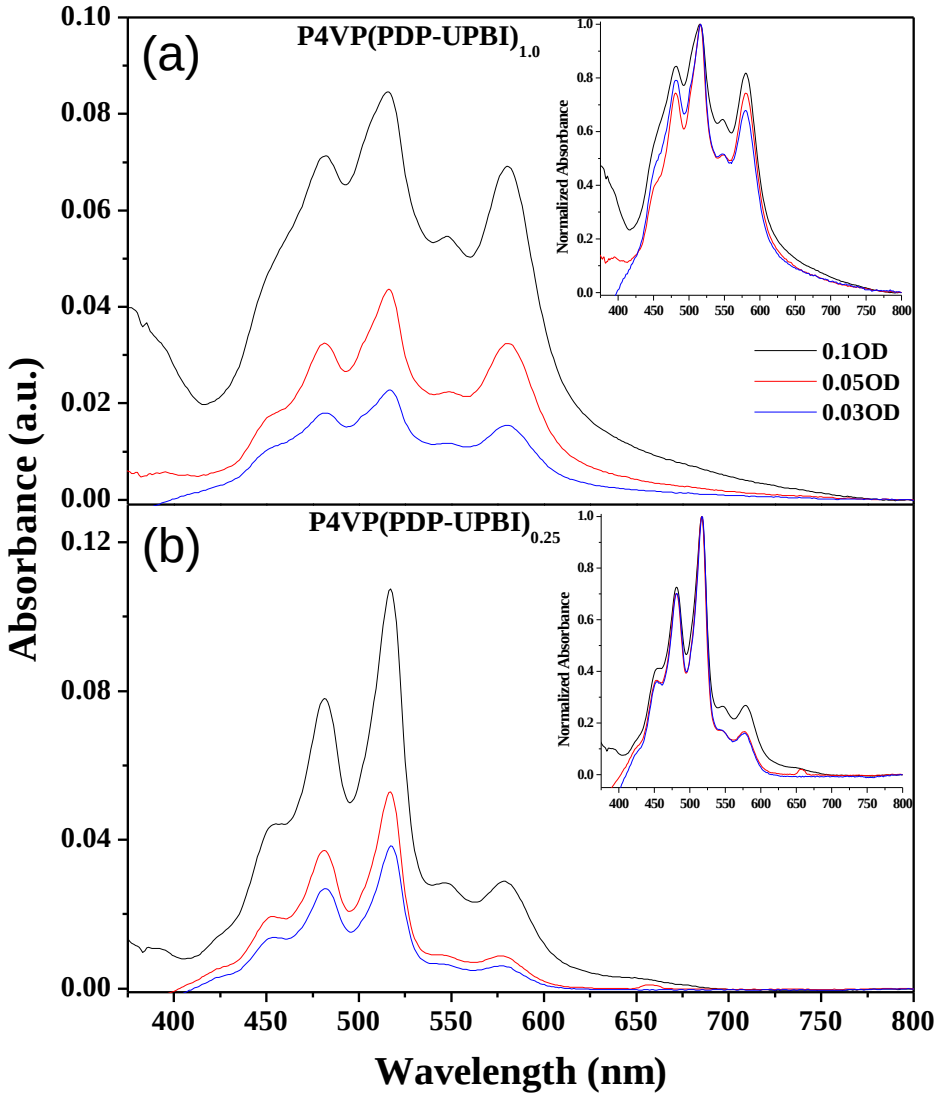

Figure-3.18. Variable concentration absorption spectra of (a) **P4VP(PDP-UPBI)$_{1.0}$** and (b) **P4VP(PDP-UPBI)$_{0.25}$** in MCH.

Similarly, for the **P4VP(PDP-UPBI)$_{0.25}$** complex (figure-3.18(b)) also this ratio did not vary upon dilution, which gave evidence for both the strength of the hydrogen bonded complexation as well as stoichiometric interaction between the **PDP-UPBI** molecules and pyridine units of P4VP. The absorption spectra of the various **P4VP(PDP-UPBI)$_n$** complexes in MCH showed that upon dilution, the complex behaved as a single entity rather than as a mixture of two components.

Thermal stability of the self-assembled aggregates of **P4VP(PDP-UPBI)$_{1.0}$** in MCH was studied by variable temperature UV-Vis experiments. Figure-3.19 shows the absorption spectra for a 0.1 OD solution of **P4VP(PDP-UPBI)$_{1.0}$** as a function of temperature in MCH. Isosbestic points were observed at 534 nm during this transition from the aggregated species to molecularly dissolved species at higher temperature. The bottom half of the figure shows the same spectra after normalization at the absorption wavelength maxima. Even at the highest temperature of 90 °C, the aggregate peak remained clearly observable with significant reduction in intensity. The extent of aggregation can be quantified by calculating the degree of aggregation α using the equation (1):

$$\alpha(T) = A(T) - A(M) / A(A_{agg}) - A(M) \quad (1)$$

where A(T) is the intensity of absorption at temperature T, A(M) and A(A_{agg}) are those for the molecularly dissolved species and fully aggregated species respectively.[47]

The inset in figure shows the degree of aggregation as a function of temperature for a 0.1 OD and 0.03 OD solution of the 1:1 complex. It could be seen from the figure that the $\alpha_{0.5}$(T) (the temperature at which α=0.5) was the same (~75 -80°C) for both solutions irrespective of their concentration. Similar variable temperature measurements carried out for the different **P4VP(PDP-UPBI)$_n$** showed that the $\alpha_{0.5}$(T) was around 75 to 80 °C for the four complexes indicating the high thermal stability of the aggregates. These spectral features indicated the formation of face-to-face stacked H-type aggregates.[47-51] The fluorescence emission spectra of 0.1 OD solutions of **P4VP(PDP-UPBI)$_{1.0}$** was also studied by exciting at 490 and 517 nm respectively in $CHCl_3$ and MCH as given in figure-3.20. The spectral pattern was similar in both solvents, with approximately 10 nm shift in the emission wavelength maxima between two solvents. In chloroform, typical emission of perylene bisimides was observed with line shape bearing mirror-image relationship with the absorption spectrum and gave peak maxima at 534, 576, 626 nm. However, in MCH the emission was very much quenched and

had peak maxima at 524, 562 and 608 nm respectively. Excitation at the red shifted absorption band at 580 nm due to the aggregates in MCH did not give rise to any emission peaks, indicating the occurrence of symmetry forbidden transition between the ground state and lower energy excited state.[52,53]

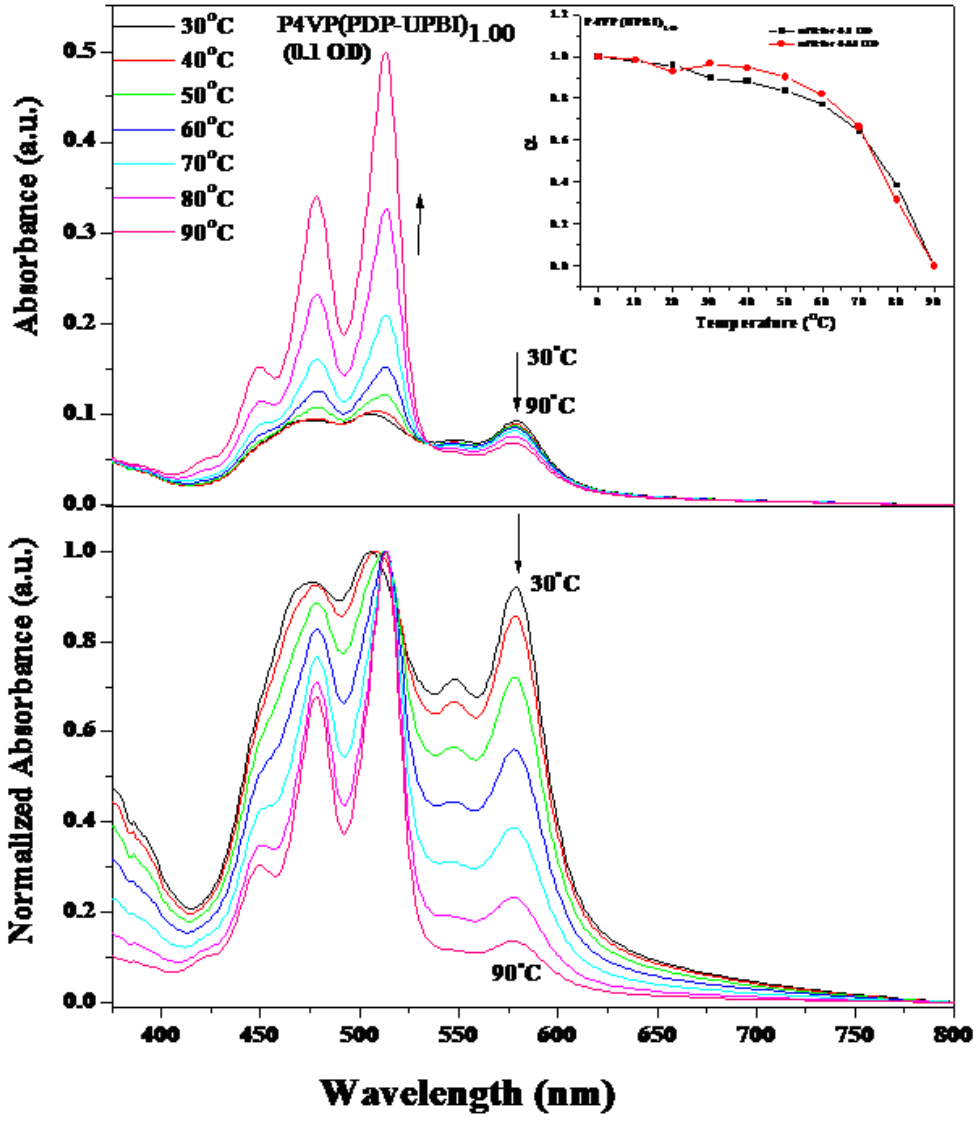

Figure-3.19. Variable temperature absorption spectra of **P4VP(PDP-UPBI)$_{1.0}$** in MCH. Inset shows the degree of aggregation (α) as a function of temperature for a 0.1 OD and 0.03 OD solution. Normalized (at the absorption wavelength maxima ~ 507-512 nm) variable temperature absorption spectra shown in the bottom.

The fluorescence quantum yield of **P4VP(PDP-UPBI)$_{1.0}$** in both chloroform and MCH were calculated using Rhodamine 6G as the standard. The quantum yield values were 0.14 and 0.06 in $CHCl_3$ and MCH respectively, whereas quantum yield for **PDP-UPBI** alone in $CHCl_3$ was 0.66. The reduction in fluorescence quantum yield values for the complex compared to that of the **PDP-UPBI** molecule alone pointed towards quenching due to presence of aggregates.

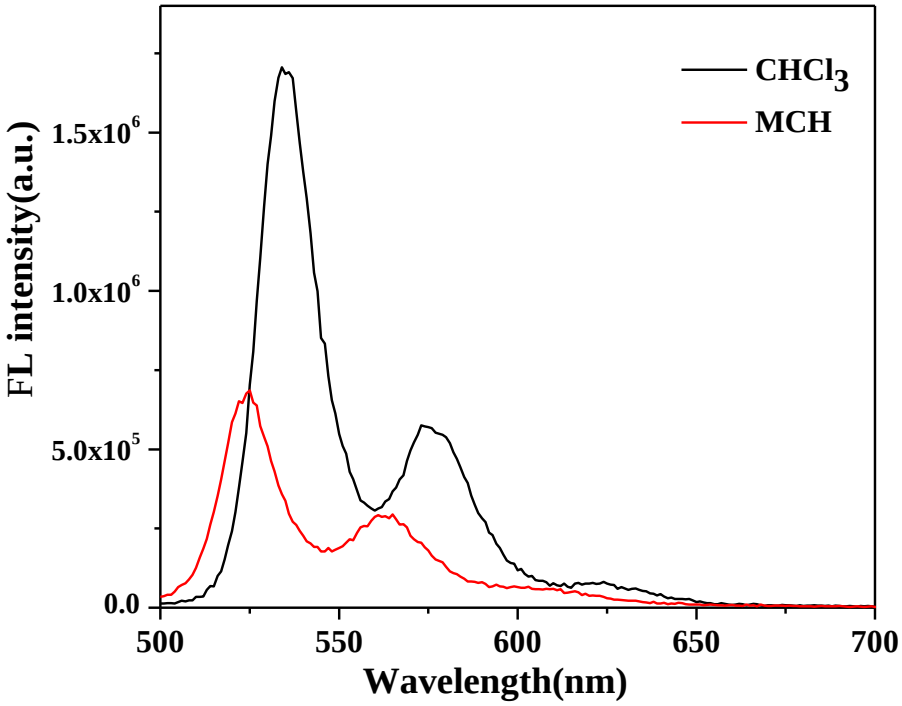

Figure-3.20. Emission spectra of 0.1OD solutions of **P4VP(PDP-UPBI)$_{1.0}$** in MCH and $CHCl_3$.

Although the absorption spectra did not indicate any signs of aggregation in chloroform, the NMR spectra had pointed towards aggregation at much higher concentrations in the same solvent. The higher extent of quenching of fluorescence of **P4VP(PDP-UPBI)$_{1.0}$** complex in MCH indicated the existence of strong face-to-face π-stacked H-type aggregates in that solvent. The stacking of chromophores one on top of the other as in an H-type sandwich aggregate results in strong

interaction between the chromophores. This in turn, leads to a rather strong coupling of the electronic energy to the lattice vibrations, which enhances the excited state energy transfer to lattice vibrations leading to quenching of fluorescence.

The solid state UV-Vis absorption and emission spectra of **P4VP(PDP-UPBI)$_{1.0}$** spin coated from $CHCl_3$ and MCH is given in figure-3.21. Compared with the solution state absorption-spectra of **P4VP(PDP-UPBI)$_{1.0}$** in MCH, in the solid state the aggregation band at 580 nm became pronounced in intensity with an overall broadening of the vibronic features. On the other hand in chloroform, the solid state UV-Vis spectra presented a loss of fine structure along with blue shift of absorption maximum from 526 nm in solution to 497 nm in thin film along with the appearance of a weak band at a longer wavelength of 540 nm.

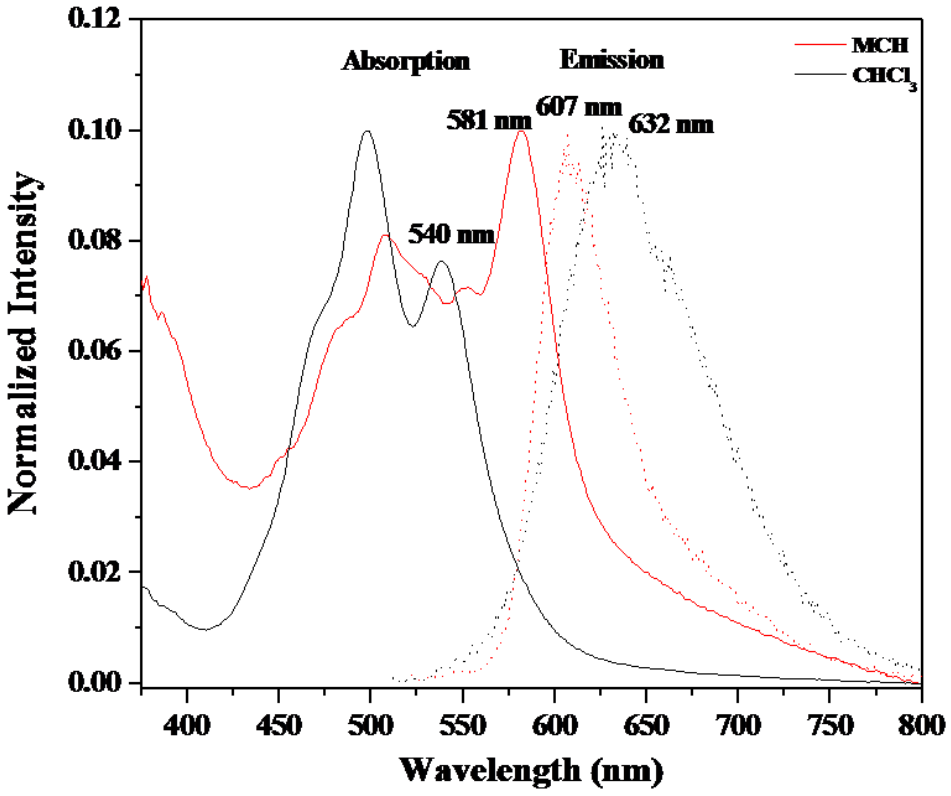

Figure-3.21. Combined solid state absorption and emission spectra of P**4VP(PDP-UPBI)$_{1.0}$** spin coated from 1 wt% solutions in MCH and $CHCl_3$.

Thus the solid state absorption features of **P4VP(PDP-UPBI)$_{1.0}$** in $CHCl_3$ indicated a typical face-to-face stacked rotationally displaced H-type aggregates.[49,54,55] In the case of rotationally displaced H-type aggregates, the symmetry of stacking is broken because the rotational angle between the chromophores $\phi \neq 0$ and therefore excimer-like transitions occur from lower excitonic states characterized by strong H-transitions shifted to higher energy along with a bathochromic shifted J-band absorption, whose intensity increases with increase in ϕ.

Figure-3.21 also compares the emission from the two films spin coated from chloroform and MCH solutions. The emission spectra were characterized by the total absence of monomeric (molecularly dissolved species) emission with only a broad emission beyond 600 nm for both the films. Compared to their respective emission in the solution state the emission wavelength maxima were red shifted by 97 nm in the case of $CHCl_3$ and 82 nm in MCH. Excitation at different wavelength ranging from 490 to 580 nm resulted in emission centered at the same wavelength beyond 600 nm indicating its origin from the lowest excimer-like state.[56-60] Although in the solution state, excitation at the aggregation band of 580 nm did not produce any emission, in the solid state weak emission from the symmetry forbidden transition was observed.[52,53] Based on the experimental observation and in agreement with the literature reports the self assembly of **P4VP(PDP-UPBI)$_{1.0}$** in MCH in the solution state could be attributed to strong π-π stacked H-type aggregates. In thin films spin coated from MCH, the same molecular packing is retained but with increased extent of π-π interaction leading to weak emission from the symmetry forbidden low energy excitonic transition.[61,62] In a 'good' solvent like chloroform, the extent of self assembly was low under dilute conditions but at higher concentrations (similar to those used in proton NMR studies) or upon spin coating to form thin solid films, rotationally displaced H-type aggregates were observed.

3.3.5. Bulk Structure Analysis - XRD and DFT Studies

The supramolecular organization in the complexes in the solid state was investigated using both wide angle and small angle X-ray analyses. SAXS recorded in the very low angular range, usually θ = 0.1 – 1.5° provides information regarding the morphology at the level of microphase separated structure of repeat distances upto 150 nm. On the other hand, WAXS is used to probe structure at the length scale of the crystal unit cell. Several mesomorphic structures like spheres, rods, cylinders, lamellae are known for surfactant induced self-assembly in block co-polymeric systems.[63-66] The hydrogen bonded systems formed by P4VP and PDP were shown to form lamellar structures.[67] Other morphologies like planar bilayers, perforated or undulating bilayers, cubic and hexagonal phases have also been reported for similar systems.[68-70] The perylene chromophore has a planar nature when the substituents are at the imide position. So it could be expected that the **P4VP(PDP-UPBI)**$_n$ complexes in the 1:1 case would ideally form planar bilayers or lamellae with alternating polymer layer and perylene layer, within which the perylenebisimide molecules would be self organized by π- π stacking as well as the hydrophobic interactions such as interdigitation of the long C-15 alkyl chains. Figure-3.22 shows the SAXS intensity curves obtained for **P4VP(PDP-UPBI)$_n$** complexes at room temperature. The diffractogram of P4VP alone and **PDP-UPBI** are also included for comparison.

Amorphous P4VP does not exhibit any peak in SAXS. The **PDP-UPBI** showed a distinct first order peak at q* = 0.196 Å^{-1} corresponding to a Bragg spacing (d) ~ 32 Å, calculated using the formula d = 2π/q, where q is the scattering vector. With increase in the degree of complexation from *n* = 0.25 to 1.0, the q maxima also shifted to higher angle region (although the shift was small) leveling off to an interplanar spacing of d ~ 31 Å for the **P4VP(PDP-UPBI)$_{1.0}$** complex. The inset in figure-3.22 shows the complete 2D scattering pattern for the **P4VP(PDP-UPBI)$_{1.0}$**, from which the 1D data was obtained by azimuthal averaging.

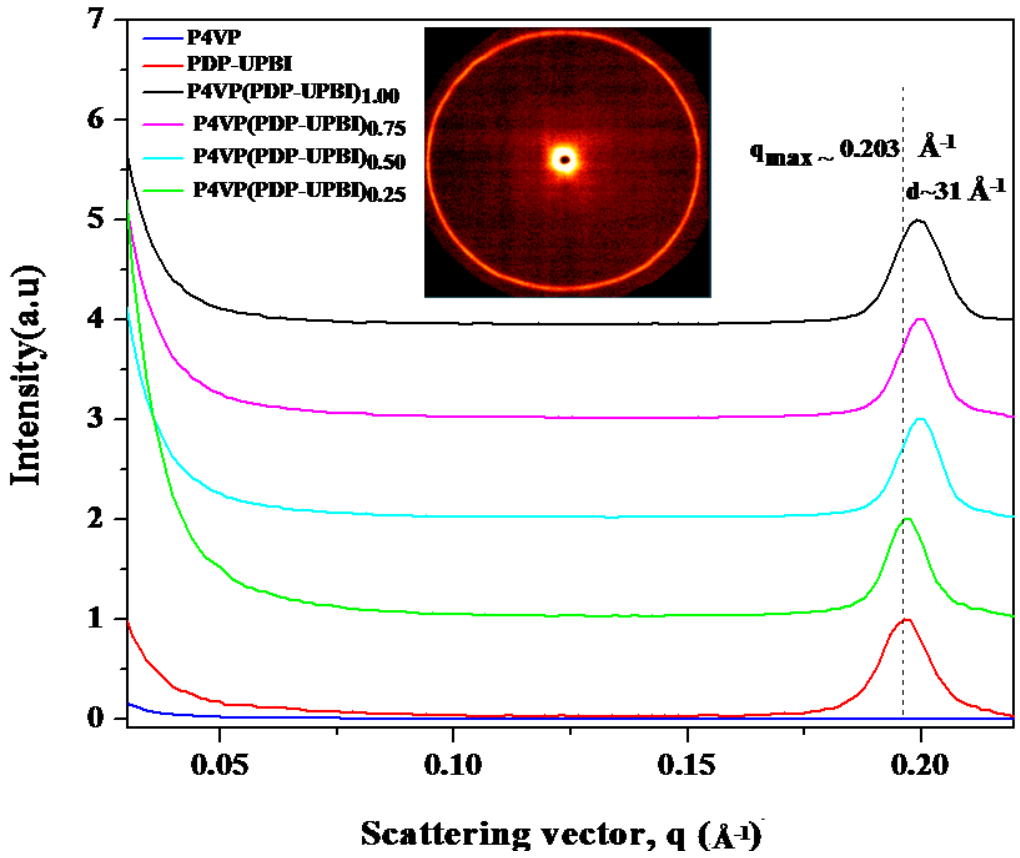

Figure-3.22. SAXS data for **P4VP(PDP-UPBI)$_n$** complexes at room temperature. Inset shows the complete 2D pattern for **P4VP(PDP-UPBI)$_{1.0}$**.

Unlike the SAXS data which had only very small shift (~ 1 Å) in the primary reflection and no new structural features, the WAXS pattern showed dramatic changes. Figure-3.23 shows the WAXS data for the same set of complexes measured at room temperature (25°C) in the range 2θ = 0.5-10°. The expanded 2θ region from 4-10° is provided inset for clarification. Careful observation revealed the presence of faint higher order wave vectors indicating lamellar organization of this P4VP-PBI complex system for various compositions. Table-3.1 shows the interlayer distances (Å) related to the reflections obtained from the WAXS pattern for the complexes as well as **PDP-UPBI**. It could be noted that **PDP-UPBI** itself showed distinct d-spacings estimated from Bragg reflections in the ratio 1: 1/2: 1/3

etc. typical of a layered structure, at 2.75° (32.04 Å), 5.49° (16.07 Å) and 8.21° (10.76 Å) respectively.

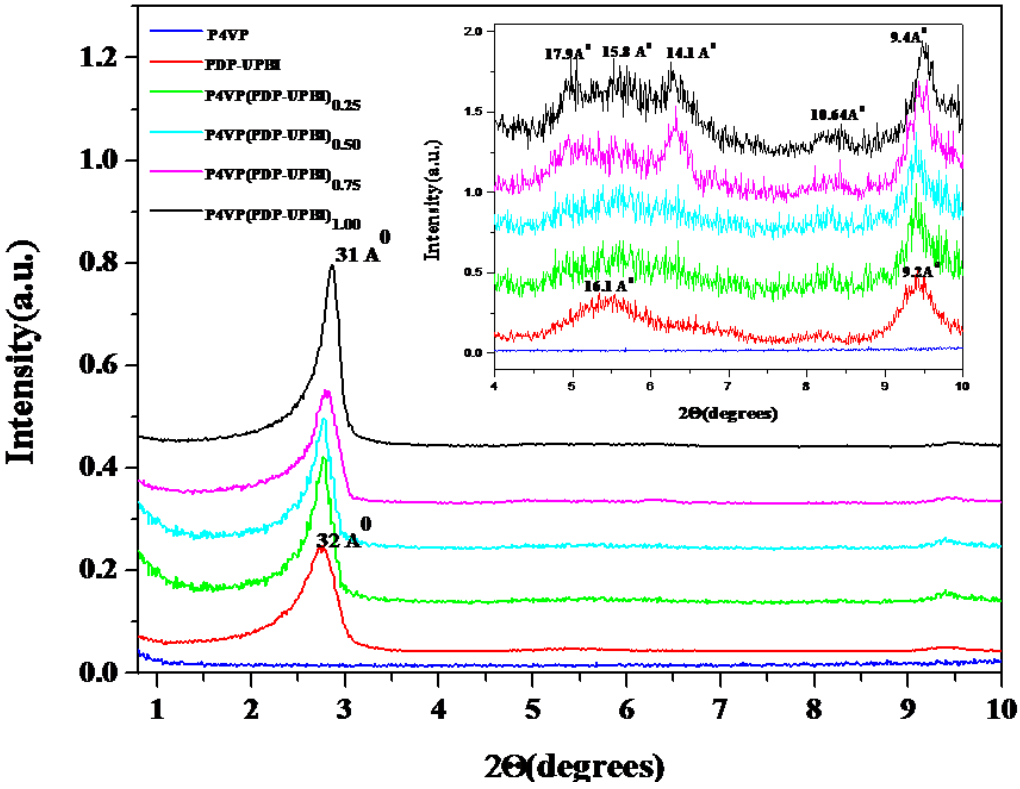

Figure-3.23. WAXS data (2θ = 0.5 – 10°) for **P4VP(PDP-UPBI)$_n$** complexes at room temperature. Inset shows the expanded region from 2θ = 4 – 10°.

In the **P4VP(PDP-UPBI)$_n$** complexes, when the extent of complexation was small the interlayer separations were similar to that in **PDP-UPBI**, with the smallest interlayer separation observed for the 1:1 complex. At lower extents of complexation, for example when n=0.25, the P4VP polymer is expected to form a thick layer between the PBI layers without causing much disturbance to it. As the extent of complexation was increased to 1:1 as in **P4VP(PDP-UPBI)$_{1.0}$**, the **PDP-UPBI** molecules are uniformly distributed along the P4VP backbone resulting in a thin polymer layer and maximum stretching and interpenetration of the alkyl chains of **PDP-UPBI** molecules. Additionally, some unexpected new structural changes were also observed in the 2θ range 4.5-7° on moving from the pure **PDP-UPBI** to

P4VP(PDP-UPBI)$_{1.0}$ complex. The second order reflection at 5.49° (16.07 Å) in **PDP-UPBI**, got transformed into 3 distinguishable peaks at 4.93° (17.91 Å), 5.57° (15.85 Å) and 6.27° (14.08 Å) upon complexation. This is discussed later on when the WXRD studies measured from 2θ range 2-35° are analyzed. Generally, increased number of sharp reflections in the lower angle region is indicative of long range ordering at the nanometer scale.

Table-3.1. Interlayer distances of the lamellar phase for **P4VP(PDP-UPBI)$_n$** complexes and **PDP-UPBI** from the WAXS data recorded at room temperature (25 °C).

Sample	Peak 1		Peak 2						Peak 3		Peak 4	
	2Θ [^{0}]	d [Å]	Peak 2(a)		Peak 2(b)		Peak 2(c)		2Θ [^{0}]	d [Å]	2Θ [^{0}]	d [Å]
			2Θ[^{0}]	d [Å]	2Θ[^{0}]	d [Å]	2Θ[^{0}]	d [Å]				
PDPUPBI	2.75	32.04	5.49	16.07	-	-	-	-	8.21	10.76	9.43	9.37
P4VP(PDPUPBI)$_{0.25}$	2.76	31.99	5.54	15.94	-	-	-	-	8.23	10.73	9.42	9.39
P4VP(PDPUPBI)$_{0.50}$	2.78	31.82	5.47	16.10	-	-	-	-	8.27	10.68	9.39	9.41
P4VP(PDPUPBI)$_{0.75}$	2.79	31.56	5.03	17.56	5.54	15.76	6.31	14.10	8.29	10.65	9.46	9.34
P4VP(PDPUPBI)$_{1.00}$	2.86	30.93	4.93	17.91	5.57	15.85	6.27	14.08	8.31	10.64	9.50	9.31

Understanding the mode of assembly in **PDP-UPBI** would enable better insight into the bulk ordering of the complexes. Unfortunately, in spite of all attempts, we were unable to grow single crystals of the **PDP-UPBI** molecule. Therefore, we carried out energy minimization – DFT calculations using turbomole suit of programs for the **PDP-UPBI** molecule.[71,72] The resultant energy minimized structure of **PDP-UPBI** molecule viewed from different angles, with the different theoretically calculated length scales are shown in figure-3.24 (a) to (c). The

perylene core adopted a planar geometry with the phenyl ring out of plane by 90°. The fully extended molecular length of **PDP-UPBI** from the phenolic oxygen at one end to the tip of the ethylhexyl substitution at the other end was 24.05 Å. Taking into account the non-planarity of the phenyl ring and the ethylhexyl chains, the distance from the phenolic oxygen through the perylene to the first **CH_2** carbon of ethylhexyl substituent was 18.503 Å, i.e. the molecular axis along which the perylene core and phenyl ring lie in one line but perpendicular to each other (the ethylhexyl or pentadecyl C_{15} chain does not lie in this line). From the energy minimized structure of **PDP-UPBI** it could be seen that the molecule had an approximate 'V' shape with both the arms nearly equal in length.

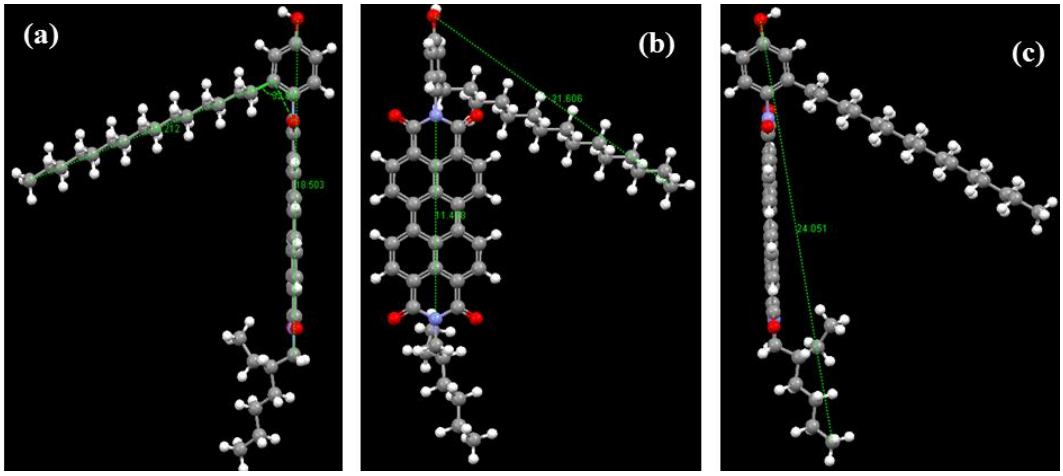

Figure-3.24. Energy minimized DFT structures of **PDP-UPBI** viewed from a plane (a) & (c) parallel and (b) perpendicular to the perylene core.

The WAXS pattern showed a primary reflection at 31.86 Å corresponding to the interplanar spacing which could have originated by the interdigitation of the molecules either along the alkyl chain arm (21.6 Å x 2 = 42 Å) or the along the rigid perylene core (18.5 Å x 2 = 37 Å). The alkyl chains are known to undergo interdigitation in the all-trans conformation. In general, peaks for all trans extended chains are observed in the IR in the narrow range of 2846 – 2850 and 2915 – 2920 cm^{-1} respectively, whereas bands in the range 2854 – 2856 and 2924 – 2928 cm^{-1}

indicate significant presence of gauche conformers.[73] However in **PDP-UPBI** as well as the **P4VP(PDP-UPBI)$_n$** complexes the alkyl chain bands were observed around 2924 and 2853 cm^{-1} (figure-3.25) which indicated considerable gauche conformers. These gauche conformers could be expected to hinder interdigitation of the long alkyl chains. Besides this, other observations based on WAXS data of the complex also suggested that packing along the rigid perylene core was more appropriate.

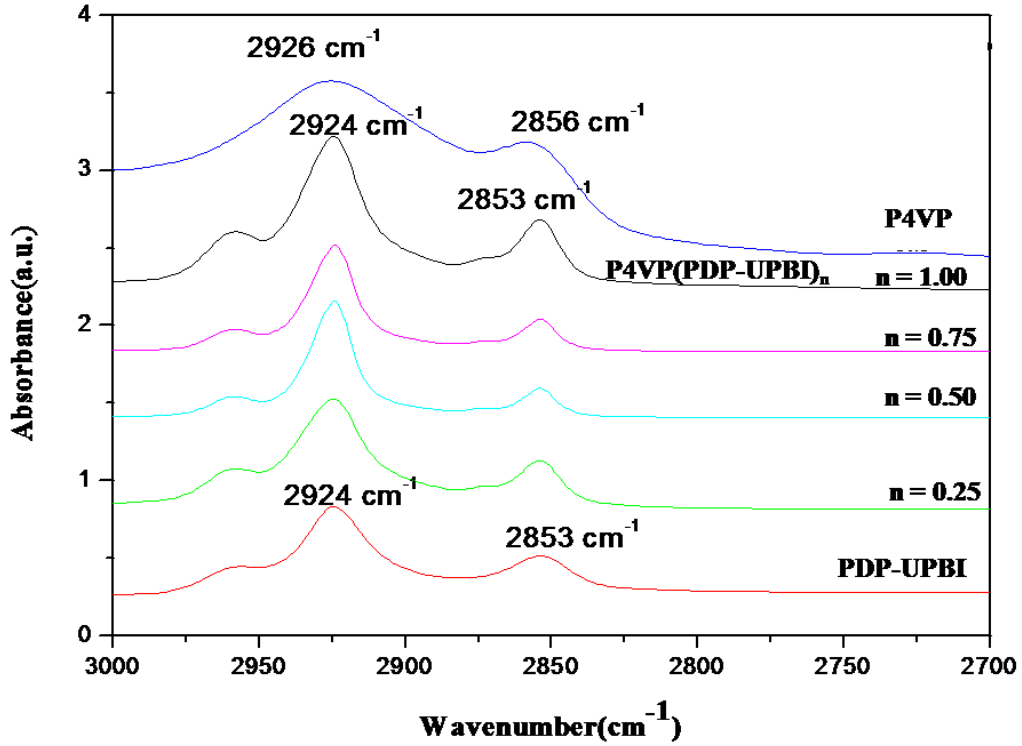

Figure-3.25. FTIR plots comparing the alkyl chain packing region of **P4VP(PDP-UPBI)$_n$** with pure P4VP and **PDP-UPBI.**

Based on these observations, a plausible mode of self-association among the **PDP-UPBI** molecules is given in figure-3.26. The different handles of self-assembly present within the single **PDP-UPBI** molecule - the hydrogen bonding with phenol head groups, π-π stacking of conjugated perylene cores as well as the hydrophobic interaction between alkyl chains is also shown in figure-3.26(a). A co-operative interplay of these non-covalent interactions is expected to give rise to a

three dimensional packing and crystallographic orientation as shown schematically in figure-3.26(b). The corresponding 2D view of two alternating planes using the DFT-energy minimized structures is also given in figure-3.26(c).

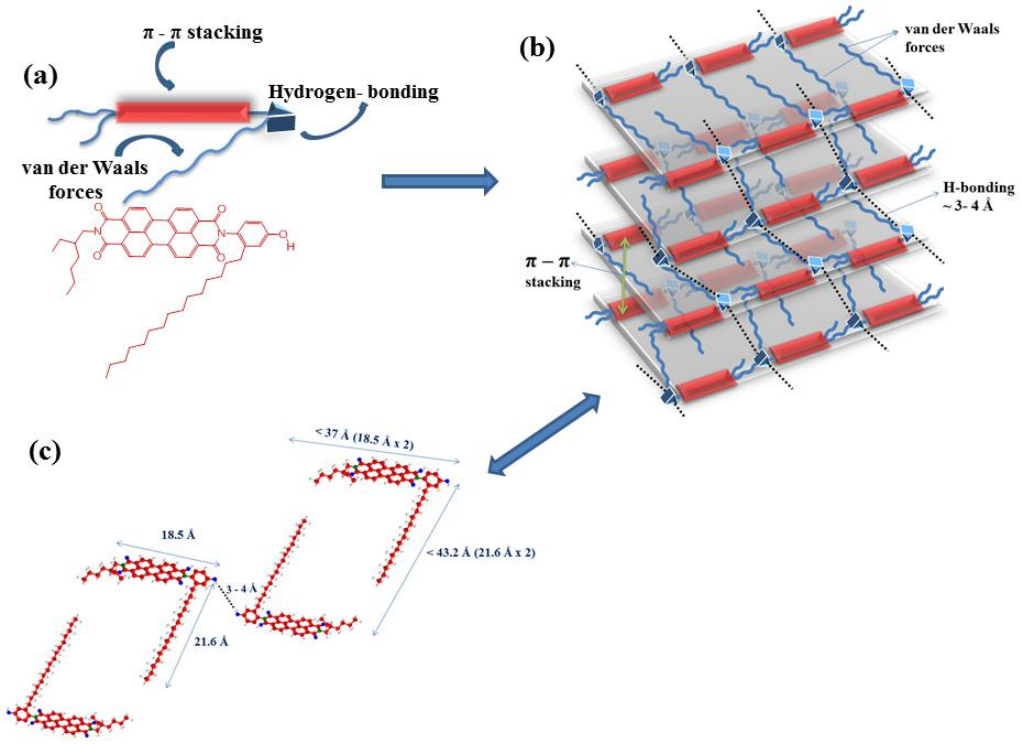

Figure-3.26. (a) Schematic representation of **PDP-UPBI** molecule highlighting the various modes of self-assembly **(b)** Schematic diagram showing 3D-mode of association of **PDP-UPBI** molecules and **(c)** 2D projection of alternate double layer involved in self-association.

The π-π stacking of perylene cores between the adjacent layers occurs in conjunction with hydrogen bonding between phenolic –OH group on one **PDP-UPBI** molecule in one layer to that of another **PDP-UPBI** molecule lying diagonally opposite in the neighboring plane. In the solid state, molecules that can form hydrogen bonds tend to arrange themselves so as to maximize the formation of linear hydrogen bonds. Usually the distance of separation in a H-bond involving a proton donor (C-H, O-H, N-H) and a basic acceptor atom (O, N) is ~ 3- 4 Å, with strong directionality. But the strength of π-π stacking is not as strong or as

directional as the H-bonding. Therefore in the **PDP-UPBI** molecule H-bonding could be expected to in figure-3.26(b) where the H-bond and π-π stack direction were the same, within 3-4 Å scale. This packing model for the **PDP-UPBI** molecule was found to be in good correlation with the observed WXRD pattern. The **PDP-UPBI** molecule being highly crystalline, showed several sharp peaks in the entire 2θ region in its room temperature powder WXRD pattern measured from 2θ = 2-35° (figure-3.27).

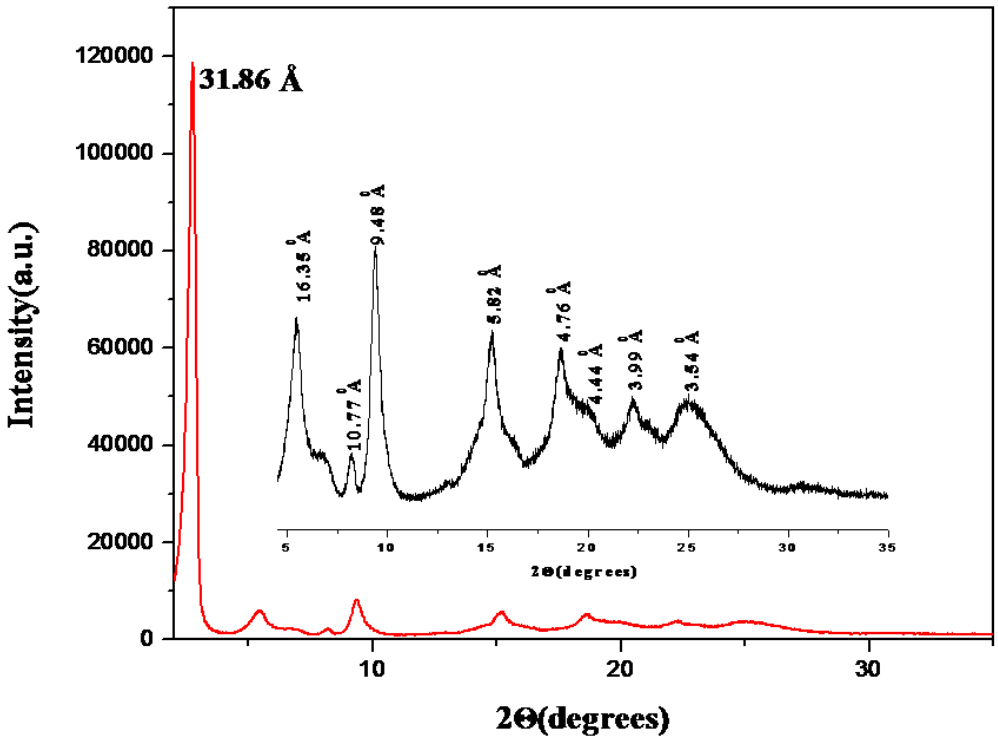

Figure-3.27. Powder WXRD of **PDP-UPBI** from 2θ = 2-50°, the expanded region from 5-35° is also given.

The first and most intense sharp peak at 31.86 Å in the low angle region, which was noticeably larger than the individual molecule size, was assigned to the inter planar periodicity of **PDP-UPBI** layers, as explained earlier. The second peak observed at 16.11 Å closely matched the single molecule length of 18.5 Å between two ends of perylene core as demonstrated in figure-3.26(c). The peak at 10.76 Å corresponded to the length of perylene core alone obtained as 11.43 Å from DFT

calculations. A comparatively broad reflection at 2θ = 25.071° corresponding to a short range repeat distance of 3.55 Å could be attributed to π-π stacking distance of adjacent perylene cores. Generally, only a diffused halo is observed in the 2θ region beyond 15° when the alkyl chains have a liquid like conformation.[74] But in case of **PDP-UPBI** molecule several sharp peaks in the 2θ =15 – 22° range indicated highly ordered aliphatic components.

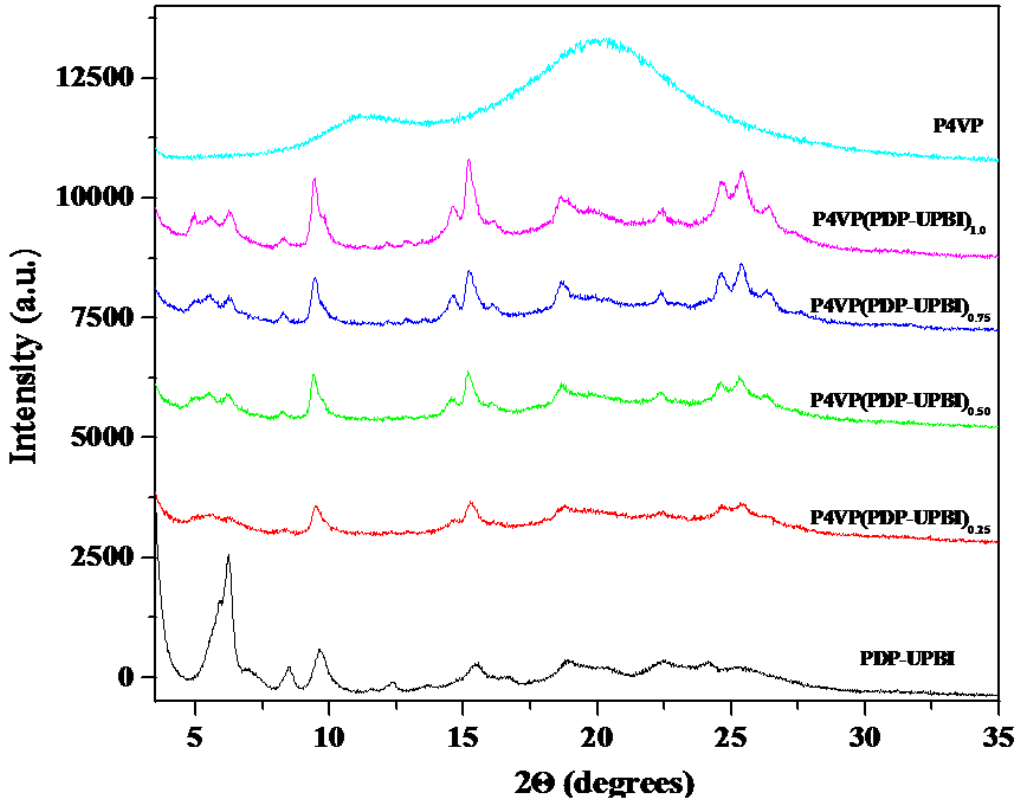

Figure-3.28. WXRD pattern of **P4VP(PDP-UPBI)$_n$** complexes from 2θ = 3-35° recorded at 25 °C compared with that of **PDP-UPBI** and P4VP.

Figure-3.28 compares the WXRD of the complexes **P4VP(PDP-UPBI)$_n$** with that of **PDP-UPBI** and P4VP in the range 2θ = 3-35°. It could be observed that the complexes remained highly crystalline with multiple sharp reflections in the entire 2θ range from 3 to 27°, whereas pure P4VP showed only two broad halos - one around 2θ = 11° and another at ~ 20°.[75] The same observation of splitting of the peak at 2θ = 5.47° upon complexation observed previously from the WAXS,

was visible here also with more clarity. These three new spacings at 17.91 Å (4.93°), 15.85 Å (5.57°) and 14.08 Å (6.27°) in the **P4VP(PDP-UPBI)$_{1.0}$** complex could be attributed to the internal structure of aromatic sublayers correlating with length scales derived from the energy minimized structure. The relative sharpness of all the reflections increased on going from **P4VP(PDP-UPBI)$_{0.25}$** to **P4VP(PDP-UPBI)$_{1.0}$** complexes. This could be considered as an indication of the increased ordering of the domains with increase in the extent of complexation.

In the region 2θ = 21 – 27°, the peak at 2θ ~ 25° corresponding to π-π stacking distance (3.56 Å) was relatively broad in **PDP-UPBI** alone; a gradual increase was observed in this peak intensity with increase in the extent of complexation from n = 0.25 to 1.00. The 1:1 complex exhibited the highest intensity peak at 2θ ~ 25.44° corresponding to d = 3.50 Å indicating an increase in the extent of π-π stacking upon complexation. Additionally, a new peak around 2θ ~ 26° (3.37Å) which was absent in **PDP-UPBI** was observed in the complex **P4VP(PDP-UPBI)$_{0.25}$**, and the intensity of this peak was highest in the **P4VP(PDP-UPBI)$_{1.0}$** complex. This further proved the well-defined ordering of domains even less than 3Å in the 1:1 P4VP-PBI complex, with the crystalline arrangement of complexes significantly differing from that of pure **PDP-UPBI**. In contrast, almost all of the reports on perylenebisimide polymers (main chain or side chain), in literature are conspicuous by the absence of peaks corresponding to crystallinity in the wide angle region.[76-78] In fact, the wide angle region of most polymers were characterized by featureless broad reflection where even the peak corresponding to $d_{\pi-\pi}$ becomes visible only after significant magnification, indicating the loss of PBI crystallinity upon polymerization.[76-78] Retaining the high crystallinity of PBI derivative in a processable polymer format is the major highlight of the present approach.

The aggregation behavior of the complexes in the bulk state was further investigated by temperature dependent WXRD studies, since hydrogen bonding is known to break at higher temperatures. Figure-3.29 shows the variable temperature

WXRD data for the **P4VP(PDP-UPBI)$_{1.0}$** complex heated to 125 °C. The room temperature diffractogram of **PDP-UPBI** is also included for comparison. The three distinct spacings at 17.91 Å (4.93°), 15.85 Å (5.57°) and 14.08 Å (6.27°) in the **P4VP(PDP-UPBI)$_{1.0}$** complex at room temperature showed significant changes upon increasing the temperature to 75 °C. Beyond 100 °C, the π-π stacking region from 2θ = 24 – 27° became featureless and the peaks around 15.85 Å and 14.08 Å almost vanished. The reflection at 17.91 Å which corresponded to the single molecule length also increased in intensity with increase in temperature. The changes in the peak pattern of the 1:1 complex with increase in temperature indicated a decrease in the degree or ordering which was originally present at room temperature. All these observations substantiated that complexation with P4VP through hydrogen bonding had enhanced the nano level organization within the crystalline **PDP-UPBI** domains with strengthened directionality.

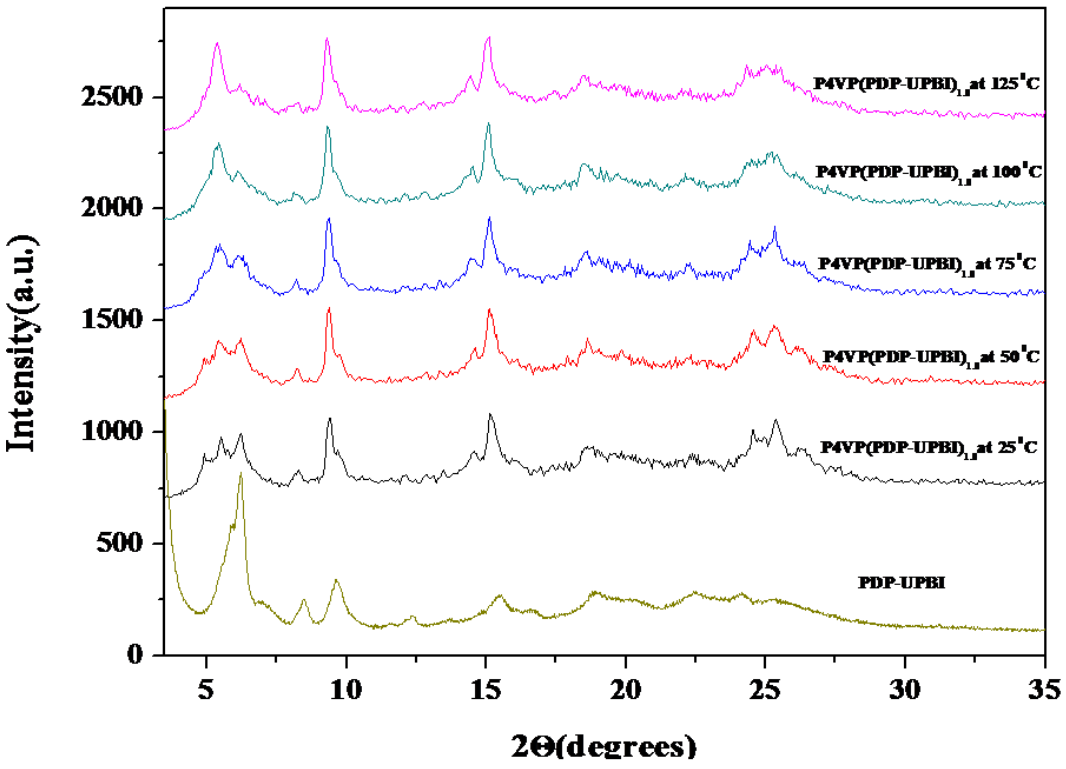

Figure-3.29. Variable temperature WXRD pattern of **P4VP(PDP-UPBI)$_{1.0}$** complexes from 2θ = 3-35°.

3.3.6. Morphology Analysis - TEM imaging studies

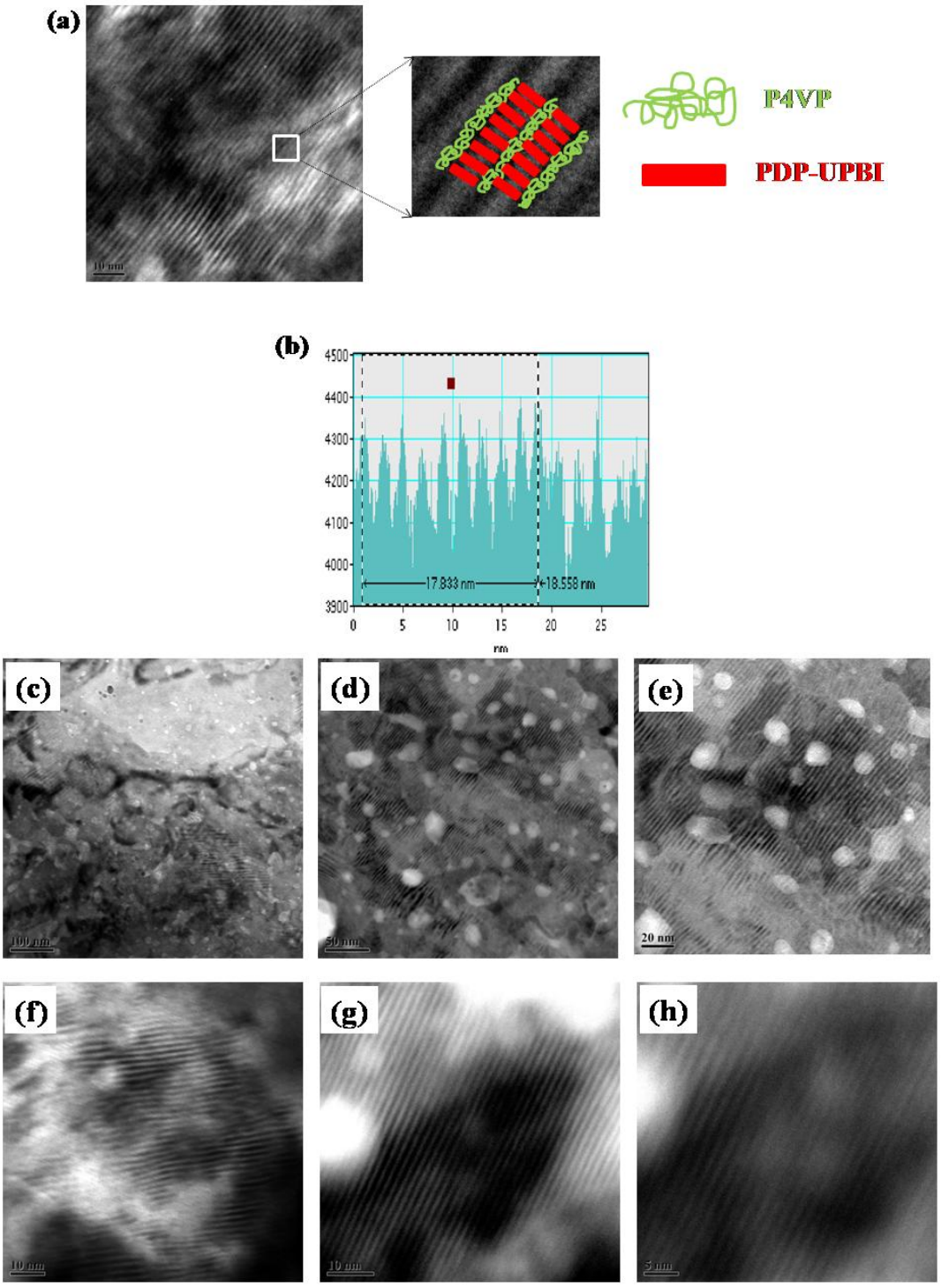

Figure-3.30. TEM images of **P4VP(PDP-UPBI)$_{1.0}$** from DMF drop cast samples at different magnifications**.**

Thin film morphology of the complex was analyzed using transmission electron microscopy (TEM). A representative TEM image of a very thin film of the **P4VP(PDP-UPBI)$_{1.0}$** complex is shown in figure-3.30 (a). The histogram for the same nanostructure image automatically generated using Gatan Digital Micrograph software is also given (figure-3.30 (b)).

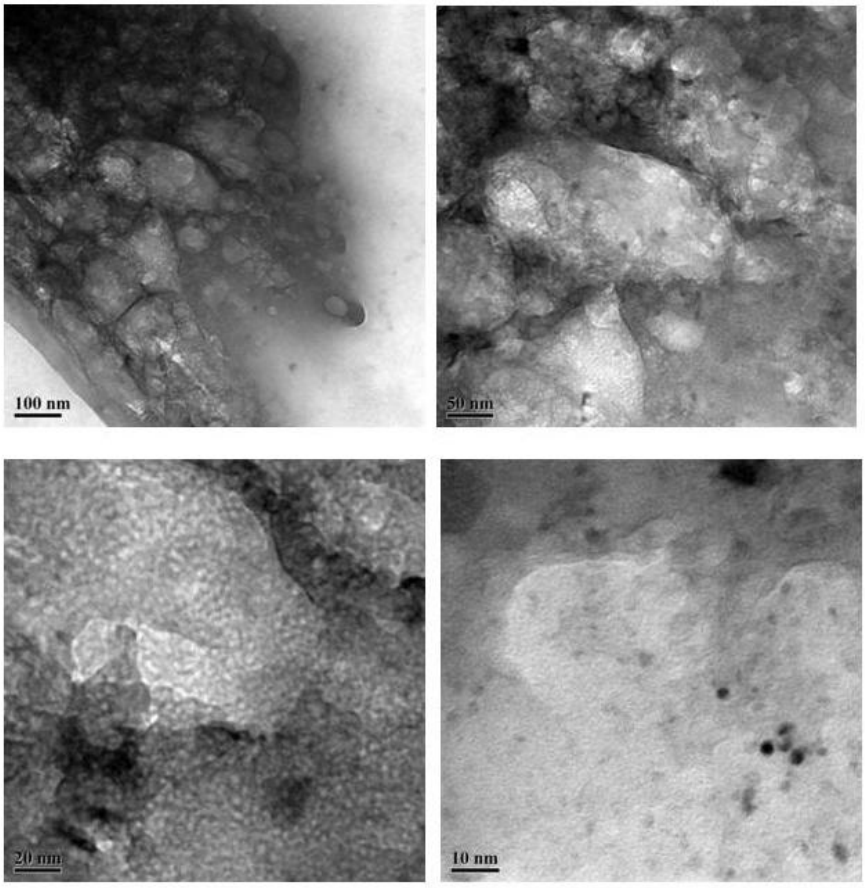

Figure-3.31. TEM images of **PDP-UPBI** from DMF drop cast samples at different magnifications.

Attempts to get thin sections of the complex by microtoming failed since sections thinner than 110 nm could not be obtained. But good TEM images of the thin film morphology was obtained directly from drop cast samples. The thin film was drop cast from 2mg/mL DMF solution of the 1:1 complex onto the copper grid and stained with I_2 vapors to improve the contrast.[67] **PDP-UPBI** by itself did not show

any specific pattern in TEM imaging under identical conditions (figure-3.31). On the other hand clear striated nanostructure formed by **P4VP(PDP-UPBI)$_{1.0}$** lamellae could clearly be observed over a wide area (> 100 nm) (figure-3.30 (c) to (h)). The dark lines corresponded to the polar P4VP layers selectively stained by I_2, while the bright lines were the crystalline perylene blocks. The statistically averaged thickness of the bright line measured from the TEM image using the instrument software was ~ 18.5 Å, which matched very well with the rigid **PDP-UPBI** core length calculated from DFT. This lamellar structure could be described as a set of parallel planes formed by alternating P4VP and perylene layers.

3.3.7. Self-organization Model for the Nanostructure Formation

A rationalized self-organization model was also proposed based on the insights gathered from FT-IR, NMR, XRD and TEM studies, for the evolution of the solution processable polymeric perylenebisimide nanostructured lamellae that is illustrated through the cartoon given in figure-3.32. The length scales shown are based on the XRD data which were well correlated with that obtained from energy minimized structures. The **PDP-UPBI** molecule alone formed a loosely packed layered structure with a periodicity in between a completely non-interpenetrated end-to-end dimer (37Å (18.5Å x2) and a monomer length (18.5 Å). Meanwhile in **P4VP(PDP-UPBI)$_{1.0}$** , complexation resulted in a highly ordered lamellae with the **PDP-UPBI** monomers tightly packed with significant interpenetration leading to single layer structure. In **P4VP(PDP)$_{1.0}$** the alkyl chains were shown to crystallize perpendicular to the plane formed by P4VP backbone.[79] But here in the **P4VP(PDP-UPBI)$_{1.0}$** complex the steric demand by the rigid perylene core with phenol unit hydrogen bonding to the P4VP chain, confined the alkyl chain orientation in a plane almost parallel to that of P4VP backbone. The alternate parallel layers of P4VP and **PDP-UPBI** as viewed from the top is also shown. (see figure-3.32(c)).

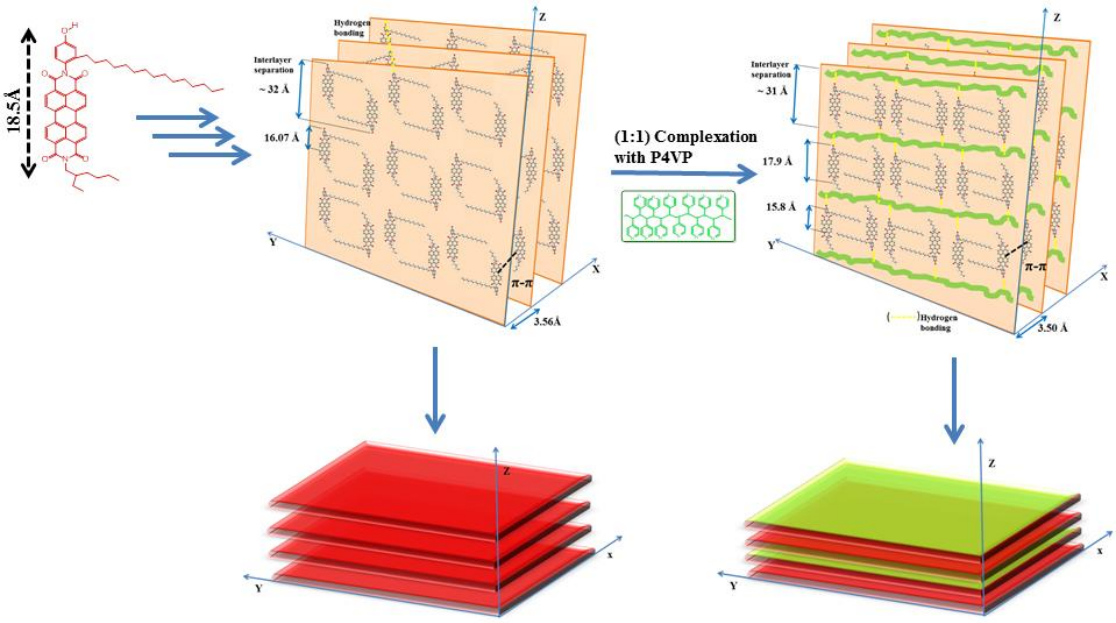

(a) Loosely packed **PDP-UPBI** layers.

(b) Tight packed **P4VP(PDP-UPBI)$_{1.0}$** lamellae.

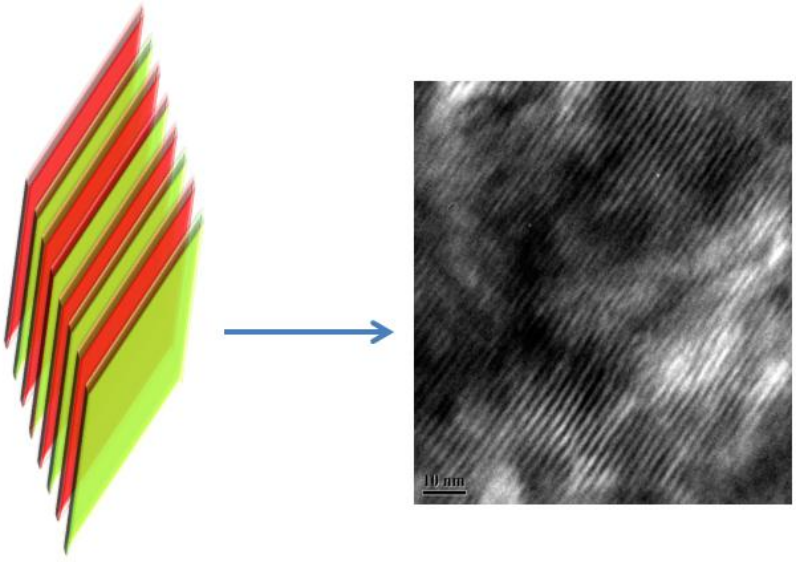

(c) Top view of **P4VP(PDP-UPBI)$_{1.0}$** lamellar structure.

Figure-3.32. Proposed model for the nanostructure formation in **P4VP(PDP-UPBI)$_{1.0}$** complex.

3.3.8. Charge Carrier Mobility Measurements - SCLC Studies

The charge carrier mobility in the small molecule **PDP-UPBI** as well as the polymeric **P4VP(PDP-UPBI)$_{1.0}$** complex was evaluated using space-charge-limited-current (SCLC) measurements.[82] A simplified schematic diagram of the device architecture used is given in figure-3.33. Clear space charge regime in I(V) was observed in both the systems for most of the devices tested.

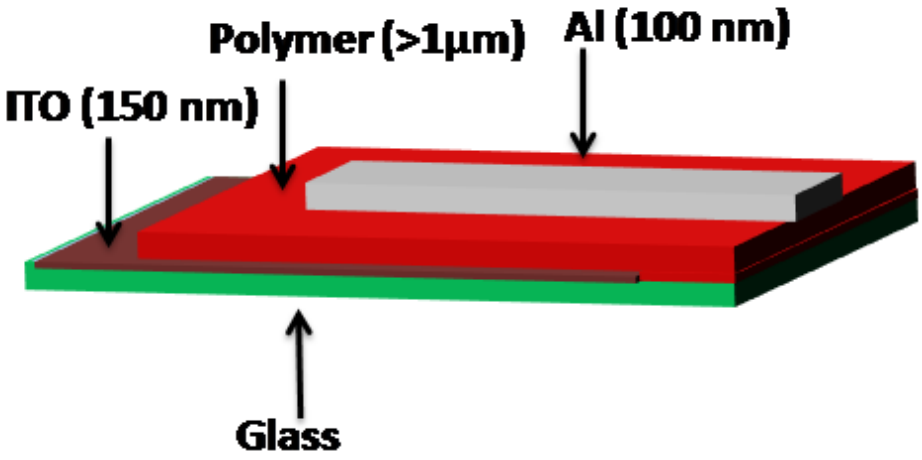

Figure-3.33. Device architecture used in SCLC mobility measurements.

The pristine **PDP-UPBI** as shown in figure-3.34(a) exhibited the classical SCLC $I = (9/8)\ \varepsilon\varepsilon_0\mu V^2/L^3$ regime,[80] with a bulk mobility estimate of $\approx 10^{-6}$ $cm^2V^{-1}s^{-1}$. In case of the 1:1 complex, the trap modified behaviour in the I(V) response was present, and a clear trend of higher conductance was observed for **P4VP(PDP-UPBI)$_{1.0}$** compared to pristine **PDP-UPBI** devices as indicated by the magnitude of the current density for relatively thicker sample of the composite (Figure-3.34(b)). The transport mechanism in **P4VP(PDP-UPBI)$_{1.0}$** consisting of aggregate of ordered units is expected to be complicated. The ordered segments distinctly enhanced the transport parameters. The choice of a trap-free regime in I(V) was apparently critical in the analysis. Both the Au and ITO coated devices yielded similar profiles. An analysis of a representative I(V) obtained from

studying several samples in the trap-free regime indicated mobility estimate of ≈ 10^{-3} $cm^2V^{-1}s^{-1}$ (Figure-3.34(b)).

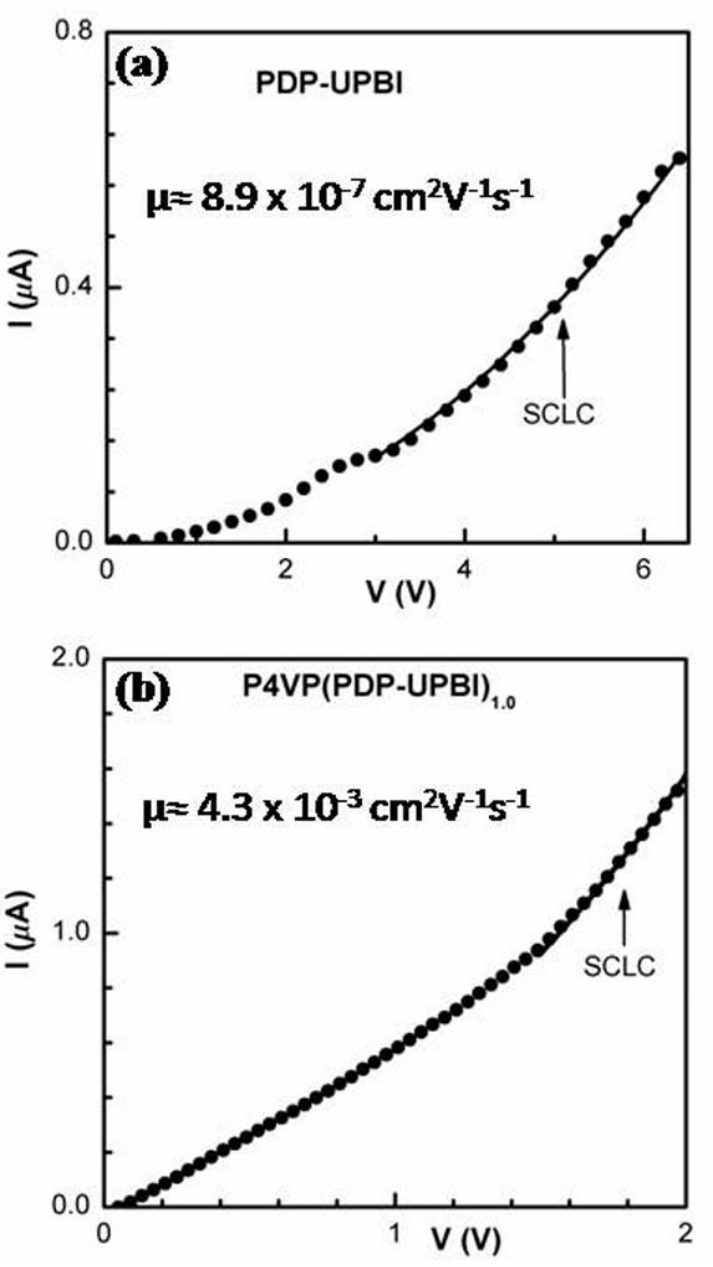

Figure-3.34. (a) I(V) of **PDP-UPBI** with ITO and Al electrodes (thickness ~ 1.2 μm)and (b) I(V) of **P4VP(PDP-UPBI)$_{1.0}$** with ITO and Al electrodes (thickness ~ 7.3 μm). Dashed-line is a fit to the SCLC response.

3.4. Conclusions

As a solution to the issues raised in chapter-2, this chapter adopted a new approach by introducing the new use of an old concept : the non-covalent interactions and supramolecular chemistry to overcome the shortcomings of a covalently connected side chain perylenebisimide polymer. This study reinforced the impressive impact of supramolecular polymers, the most recent branch in the tree of 'chemistry beyond covalent bond' as supramolecular chemistry is often called. Here we elaborated the synthesis and characterization of an unsymmetrical perylene bisimide **PDP-UPBI**, suitably functionalized for hydrogen bonding interactions and their self-organization into lamellar structures in the domain range 5 to 10 nm using the concept of supramolecular comb polymer assembly with poly(4-vinyl pyridine) (P4VP). Thus a series of supramolecular comb-polymer complexes viz., **P4VP(PDP-UPBI)$_n$** with n = 0.25, 0.50, 0.75 and 1.00 were prepared and thoroughly characterized. Complexation improved the solubility and hence solution processability by several folds. Solution state studies including variable temperature UV-Vis and proton NMR spectroscopies and solid state measurements like FTIR, SAXS, WAXS and thin film morphology using TEM were undertaken to understand the self-organization in depth. Solution studies of the **P4VP(PDP-UPBI)$_n$** complexes using ^{1}H NMR gave conclusive proof for stoichiometric complexation in each case. UV-Vis absorption studies showed that in a non-polar solvent like methylcyclohexane (MCH) which is well known to self organize the rigid perylene cores, the hydrogen bonded complex showed characteristics of highly packed face-to-face H-type aggregates with strong intermolecular interactions. Whether in a concentrated form (^{1}H NMR) or dilute (UV-Vis absorption), the complex behaved as a single entity rather than as a blend of two substances. Further these studies clearly demonstrated that although the **PDP-UPBI** alone also was capable of self-assembly, the association was much stronger in the complex compared to the small molecule. The solid state studies using X-ray diffraction showed that both **PDP-UPBI** and its complexes with P4VP exhibited

layered assembly. But the packing order was drastically improved in the complex compared to the small molecule itself. Although both showed layered structure, only the complex could exhibit a phase separated nanostructure with ordering in the 5-10 nm range as visualized using transmission microscopy (TEM) imaging. Additional structural hierarchies could be obtained by extending this concept to block copolymer based supramolecules like PS-*b*-P4VP. The most important highlight of this approach was the ability to retain the crystallinity of the perylene bisimide in the supramolecular polymer complex, thereby combining the advantage of the small molecule with the processability afforded by the polymer. A clear trend of improved electrical parameters in **P4VP(PDP-UPBI)** system compared to pristine **(PDP-UPBI)** was observed from space charge limited current (SCLC) measurements. Thus a simple and facile method to obtain spatially defined organization of n-type semiconductor perylenebisimide molecules using hydrogen bonding interactions with P4VP giving rise to long range crystalline order favoring electronic coupling between molecular building blocks, processability as well as high electron mobility, has been successfully developed.

3.5. References

[1] F. Würthner, *Chem. Commun.* **2004,** *14*, 1564.

[2] G. Horowitz, F. Kouki, P. Spearman, D. Fichou, C. Nogues, X. Pan, F. Garnier, *Adv. Mater.* **1996,** *8*, 242.

[3] H. Langhals, *Helv. Chim. Acta.* **2005,** *88*, 1309.

[4] H. Langhals, *Heterocycles* **1995,** *40*, 477.

[5] Y. Avlasevich, C. Li, K. Müllen, *J. Mater. Chem.* **2010,** *20*, 3814.

[6] Nalwa, H. S. *Handbook of Organic Conductive Molecules and Polymers*, Vol.4, Ed., John Wiley & Sons, N.Y., **1997,** Chapter 1.

[7] K. V. Rao, R. Haldar, C. Kulkarni, K. T. Maji, S. J. George, *Chem. Mater.* **2012,** *24*, 969.

[8] A. S. Lang, M. Thelakkat, *Polym. Chem.* **2011,** *2*, 2213.

[9] K. Xiao, J. Tao, Z. Pan, A. A. Puretzky, I.N. Ivanov, S. J. Pennycook, D. B. Geohegan, *Angew. Chem. Int. Ed.* **2007,** *46*, 2650.

[10] J. H. Schön, Ch. Kloc, A. Dodabalapur, B. Batlogg, *Science* **2000,** *289*, 599.

[11] A. Lv, S. R. Puniredd, J. Zhang , Z. Li, H. Zhu, W. Jiang , H. Dong, Y. He, L. Jiang, Y. Li, W. Pisula, Q. Meng, W. Hu, Z. Wang, *Adv. Mater.* **2012,** *24*, 2626.

[12] J. Ruokolainen, R. Mäkinen, M. Torkkeli, R. Serimaa, T. Mäkelä, G. Ten Brinke, O. Ikkala, *Science* **1998,** *280*, 557.

[13] J. Ruokolainen, G. Ten Brinke, O. Ikkala, *Adv. Mater.* **1999,** *11*, 777.

[14] K. de Moel, A. G. O.R. van Ekenstein, H. Nijland, E. Polushkin, G. Ten Brinke, *Chem. Mater.* **2001,** *13*, 4580.

[15] O. Ikkala, G. Ten Brinke, *Science* **2002,** *295*, 2407.

[16] O. Ikkala, G. Ten Brinke, *Chem. Commun.* **2004,** 2131.

[17] W. Van Zoelen, T. Asumaa, J. Ruokolainen, O. Ikkala, G. Ten Brinke, *Macromolecules* **2008,** *41*, 3199.

[18] J. Ruokolainen, G. Ten Brinke, O. Ikkala, *Macromolecules* **1996,** *29*, 3409.

[19] G. Ten Brinke, O. Ikkala, *Macromol. Symp.* **2003,** *203*, 103.

[21] H.-S. Sun, C.-H. Lee, C.-S. Lai, H.-L. Chen, S.-H. Tung, W.-C. Chen, *Soft Matter* **2011,** *7*, 4198.

[22] B. Nandan, B. K. Kuila, M. Stamm, *Eur. Polym. J.* **2011,** *47*, 584.

[23] B. Nandan, M. K. Vyas, M. Böhme, M. Stamm, *Macromolecules* **2010,** *43*, 2463.

[24] N. Sary, F. Richard, C. Brochon, N. Leclerc, P. Lévêque, J.-N. Audinot, S. Berson, T. Heiser, G. Hadziioannou, R. Mezzenga, *Adv. Mater*. **2010,** *22*, 763.

[25] O. Ikkala, J. Ruokolainen, G. Ten Brinke, M. Torkkeli, R. Serimaa, *Macromolecules* **1995,** *28*, 7088.

[26] J. Ruokolainen, O. Ikkala, J. Tanner, G. Ten Brinke, M. Torkkeli, R. Serimaa, *Macromolecules* **1995,** *28*, 7779.

[27] J. Wang, A. Kulago, W, R. Browne, B. L. Feringa, *J. Am. Chem. Soc*. **2010,** *132*, 4191.

[28] W. Wang, L.-S. Li, G.Helms, H.-H. Zhou, A. D. Q. Li, *J. Am. Chem. Soc.* **2003,** *125*, 1120.

[29] J. S. Waugh, R. W. Fessenden, *J. Am. Chem. Soc.* **1957,** *79*, 846.

[30] D. J. Edwards, J.W. Jones, O. Lozman, A. P. Ormerod, M. Sintyureva, G. J. T. Tiddy, *J. Phys. Chem. B.* **2008,** *112*, 14628.

[31] R. B. Martin, *Chem. Rev.* **1996,** *96*, 3043.

[32] J.C. Nelson, J.G. Saven, J.S. Moore, P. G. Wolynes, *Science* **1997,** *277*, 1793.

[33] F. Würthner, C. Thalacker, S. Diele, C. Tschierske, *Chem. -Eur. J.* **2001,** *7*, 2245.

[34] A. Syamakumari, A. P, H, J. Schenning, E. W. Meijer, *Chem. -Eur. J.* **2002,** *8*, 3353.

[35] R. F. Fink, J. Seibt, V. Engel, M. Renz, M. Kaupp, S. Lochbrunner, H.-M. Zhao, J. Pfister, F. Würthner, *J. Am. Chem. Soc.*, **2008,** *130*, 12858.

[36] H. Adams, J.-L. J. Blanco, G. Chessari, C. A. Hunter, C. M. R. Low, J. M. Sanderson, J.G. Vinter, *Chem. -Eur. J.* **2001,** *7*, 3494.

[37] F. J. Carver, C. A. Hunter, P. S. Jones, D. J. Livingstone, J. F. McCabe, E. M. Seward, P. Tiger, S. E. Spey, *Chem. -Eur. J.* **2001,** *7*, 4854.

[38] L. Zang, Y. Che, J. S. Moore, *Acc. Chem. Res.*, **2008,** *41*, 1596.

[39] F. Würthner, S. Yao, *Angew. Chem. Int. Ed.*, **2000,** *39*, 1978.

[40] J. Wang, A. Kulago, W. R. Browne, B. L. Feringa, *J. Am. Chem. Soc.*, **2010,** *132*, 4191.

[41] B. Rybtchinski, L. E. Sinks , M. R. Wasielewski, *J. Am. Chem. Soc.*, **2004,** *126*, 12268.

[42] R. Gómez, D. Veldman, R. Blanco, C. Seoane, J. L. Segura, R. A. J. Janssen, *Macromolecules* **2007,** *40*, 2760.

[43] C.D. Schmidt, C. Böttcher, A. Hirsch, *Eur. J. Org. Chem.* **2009,** *31*, 5337.

[44] C. Shao, M. Grüne, M. Stolte, F. Würthner, *Chem. -Eur. J.* **2012,** *18*, 13665.

[45] Z. Chen, A. Lohr, C. R. Saha-Möller, F. Würthner, *Chem. Soc. Rev.*, **2009,** *38*, 564.

[46] M. Kasha, H. R. Rawls, M. A. El-Bayoumi, *Pure Appl. Chem.*, **1965,** *11*, 371.

[47] G. A. Bhavsar, S. K. Asha, *Chem. -Eur. J.* **2011,** *17*, 12646.

[48] Z. Chen, U. Baumeister, C. Tschierske, F. Würthner, *Chem. -Eur. J.* **2007,** *13*, 450.

[49] S. Ghosh, X.-Q. Li, V. Stepanenko, F. Würthner, *Chem. -Eur. J.* **2008,** *14*, 11343.

[50] B. Jancy, S. K. Asha, *Chem. Mater.* **2008,** *20*, 169.

[51] E. H. Beckers, Z. Chen, S. C. J. Meskers, P. Jonkheijm, A. P. H. J. Schenning, X.-Q. Li, P. Osswald, F. Würthner, R. A. J. Janssen, *J. Phys. Chem. B.* **2006,** *110*, 16967.

[52] K. Balakrishnan, A. Datar, R. Oitker, H. Chen, J. Zuo, L. Zang, *J. Am. Chem. Soc.*, **2005,** *127*, 10496.

[53] K. Balakrishnan, A. Datar, T. Naddo, J. Huang, R. Oitker, M. Yen, J. Zhao, L. Zang, *J. Am. Chem. Soc.*, **2006,** *128*, 7390.

[54] Z. Chen, V. Stepanenko, V. Dehm, P. Prins, L. D. A. Siebbeles, J. Seibt, P. Marquetand, V. Engel, F. Würthner, *Chem. -Eur. J.* **2007,** *13*, 436.

[55] F. Würthner, Z. Chen, V. Dehm, V. Stepanenko, *Chem. Commun.* **2006,** *11*, 1188.

[56] H. Langhals, R. Ismael, *Eur. J. Org. Chem.* **1998,** *9*, 1915.

[57] S.Yagai, Y. Monma, N. Kawauchi, T. Karatsu, A. Kitamura, *Org. Lett.* **2007,** *9*, 1137.

[58] V. Dehm, Z. Chen, U. Baumeister, P. Prins, L. D. A. Siebbeles, F. Würthner, *Org. Lett.* **2007,** *9*, 1085.

[59] G. D. Luca, A. Liscio, P. Maccagnani, F. Nolde, V. Palermo, K. Müllen, P. Samori, *Adv. Funct. Mater.* **2007,** *17*, 3791.

[60] M. J. Ahrens, L. E. Sinks, B. Rybtchinski, W. Liu, B. A. Jones, J. M. Giaimo, A. V. Gusev, A. J. Goshe, D. M. Tiede, M. R. Wasielewski, *J. Am. Chem. Soc.* **2004,** *126*, 8284.

[61] Y.Luo, J. Lin, H. X. Duan, J. Zhang, C. K. Lin, *Chem. Mater.* **2005,** *17*, 2234.

[62] Y. Huang, B. Quan, Z. Wei, G. Liu, L. Sun, *J. Phys. Chem. C* **2009,** *113*, 3929.

[63] W. Van Zoelen, T. Asumaa, J. Ruokolainen, O. Ikkala, G. Ten Brinke, *Macromolecules* **2008,** *41*, 3199.

[64] J. Wang, W. H. de Jeu, P. Müller, M. Möller, A. Mourran, *Macromolecules* **2012,** *45*, 974.

[65] W -T. Chuang, H -W. Shen, U -S. Jeng, H -H. Wu, P -D. Hong, J -J. Lee, *Chem. Mater.* **2009,** *21*, 975.

[66] S. Valkama, T. Ruotsalainen, A. Nykänen, A. Lahio, H. Kosonen, G. Ten Brinke, O. Ikkala, J. Ruokolainen, *Macromolecules* **2006,** *39*, 9327.

[67] J. Ruokolainen, J. Tanner, O. Ikkala, *Macromolecules* **1998,** *31*, 3532.

[68] M. Antonietti, C.Burger, J. Eiffing, *Adv. Mater.* **1995,** *7*, 751.

[69] S. Zhou, F.Yeh, C. Burger, B. Chu, *J. Phys. Chem. B.* **1999,** *103*, 2107.

[70] M. Antonietti, J. Conrad, *Angew. Chem. Int. Ed. Engl.* **1994,** *33*, 1869.

[71] R. Ahlrichs, M. Br, H. P. Baron, R. Bauernschmitt, S. Bçcker, M.Ehrig, K. Eichkorn, S. Elliott, F. Furche, F. Haase, M. Hser, H.Horn, C. Huber, U. Huniar, M. Kattannek, C. Kçlmel, M. Kollwitz,K. May, C. Ochsenfeld, H. _hm, A. Schfer, U. Schneider, O. Treutler,M. von Arnim, F. Weigend, P. Weis, H. Weiss, TURBOMOLE(Version 5.3); Universitt Karlsruhe, Karlruhe, Germany, **2000**.

[72] A. D. Becke, *Phys. Rev. A.* **1988,** *38*, 3098.

[73] S-H. Park, C. E. Lee, *Chem. Mater.* **2006,** *18*, 981.

[74] Y. Huang, Y. Yan, B. M. Smarsly, Z. Wei, C. F. J. Faul, *J. Mater. Chem.* **2009,** *19*, 2356.

[75] S. Valkama, O. Lehtonen, K. Lappalainen, H. Kosonen, P. Castro, T. Repo, M. Torkkeli, R. Serimaa, G. Ten Brinke, M. Leskelä, O. Ikkala, *Macromol. Rapid Commun.* **2003,** *24*, 556.

[76] Z. Zhou, J. L. Brusso, S. Holdcroft, *Chem. Mater.* **2010,** *22*, 2287.

[77] A. S. Lang, A. Neubig, M. Sommer, M. Thelakkat, *Macromolecules* **2010,** *43*, 7001.

[78] A. S. Lang, M. Thelakkat, *Polym. Chem.* **2011,** *2*, 2213.

[79] M. C. Luyten, G. O. R. A. Van Ekenstein, G. Ten Brinke, *Macromolecules* **1999,** *32*, 4404.

[80] A. M. Goodman, A. Rose, *J. Appl. Phys.* **1971,** *41*, 2823.

[81] R. Narayan, S. K. Asha, *J. Mater. Chem. C,* **2013,** DOI:10.1039/C3TC31015A.

[82] R. Narayan, P. Kumar, K. S. Narayan, S. K. Asha, *Adv. Funct. Mater.* **2013**, *23*, 2033.

Chapter-4

Naphthalenebisimide-Poly(4-vinylpyridine) Supramolecular Comb-polymer and its Random Copolymers with Perylenebisimides

4.1. Introduction

Materials research in the past few years has witnessed a tremendous growth in the search for new n-type organic semiconductor materials that can compete with the device performances exhibited by already well established p-type semiconductors. For example, organic p-type semiconductors based on a series of benzothiophene derivatives exhibiting high hole mobility values even upto 31.3 $cm^2V^{-1}s^{-1}$ has been reported by Hasegawa *et al.*[1,2] whereas organic n-type semiconductors with electron mobilities higher than 1.0 $cm^2V^{-1}s^{-1}$ still remain limited. Currently the most extensive studies on non-fullerene category of n-channel organic materials are based on the rylene diimide cores viz., perylene and naphthalene diimides. Eventhough outstanding results are obtained with vacuum deposited thin films of the rylene molecules, fully solution processable polymeric derivatives are scarce. From the rylene family of electroactive compounds, compared to the larger core analogues like perylenebisimides the simplest diimide member naphthalenebisimide derivatives have attracted a great deal of attention because they show better solution processability and sensitivity of electronic as well as spectroscopic properties towards core or imide nitrogen substitution.

The 1,4,5,8-Naphthalenebisimides (NBI) are neutral, planar and compact electron deficient molecules usually with high melting points. They are chemically robust and redox-active compounds that can undergo single reversible one-electron reduction, both chemically as well as electrochemically at modest potentials and so make excellent models for photoinduced electron transfer or photosynthetic mimicry studies.[3] The absorption pattern of NBIs are significantly shifted hypsochromically well below 400 nm and usually very weak emission properties are known.[3] Nevertheless the absorption and emission properties of NBI derivatives can be tuned by functionalization at the naphthalene core or the imide nitrogen positions. However the naphthalene ring being small in size, substitution at the bay region usually leads to significant distortion in the overall planarity of the NBI molecule which adversely affects the self-organization via π-π stacking

which in turn reduces the intermolecular electronic communication. But for applications requiring highly fluorescent NBI derivatives core substitution can generate brilliant hues from blue to red depending on the substituents. In the case of core unsubstituted NBIs, aromatic substituents at the imide nitrogens produce typically non-fluorescent or weakly fluorescent derivatives while simple alkyl groups at these same positions gives rise to white-blue fluorescence for this class of molecules. Due to their unique combination of properties naphthalenebisimides have been extensively used as supramolecular building blocks of functional materials such as organogels,[4,5] liquid crystals,[6,7] foldamers, [8,9] catenanes, [10,11] nanotubes [12,13] etc. Recently Ghosh *et al.* reported a carboxylic acid appended naphthalenediimide (NDI) derivative with pure white-light emission (fluorescence quantum yield=0.70) from hydrogen bonding induced self-assembly in non-polar methylcyclohexane (MCH) (Figure-4.1).[14]

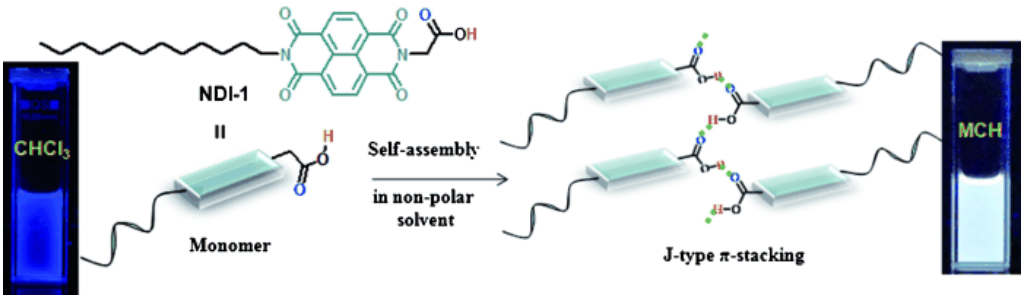

Figure-4.1. Carboxylic acid appended Naphthalenediimide with monomeric blue emission and bright white light emission from hydrogen bonded aggregates in MCH. [*Adapted from ref.14*]

Aggregation-induced modulation of photophysical properties from this remarkably simple single-component was attributed to J-type π stacking among the NDI chromophores. The same group also explored a two- component gelation and morphology dependent conductivity of an n-type naphthalenediimide utilizing an external structure directing agent to induce orthogonal hydrogen bonded self-assembly (Figure-4.2).[15] In another very recent study, Bhosale and co-workers demonstrated the self-assembly of naphthalenediimide motif bearing phosphonic

acid functionalities with L- and D-arginine leading to the formation of micrometer long nanobelts and spherical aggregates respectively in water at pH 9 (Figure-4.3).[16] The tunable nanostructures were formed through chirality induced molecular recognition with arginine in water and such studies extend the application of NBIs to nano- and biomaterial research.

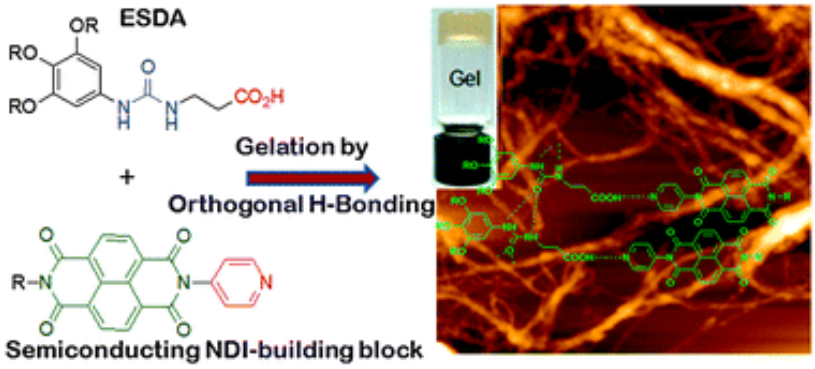

Figure-4.2. Two-component Naphthalenediimide gels by orthogonal hydrogen-bonding. [*Adapted from ref.15*]

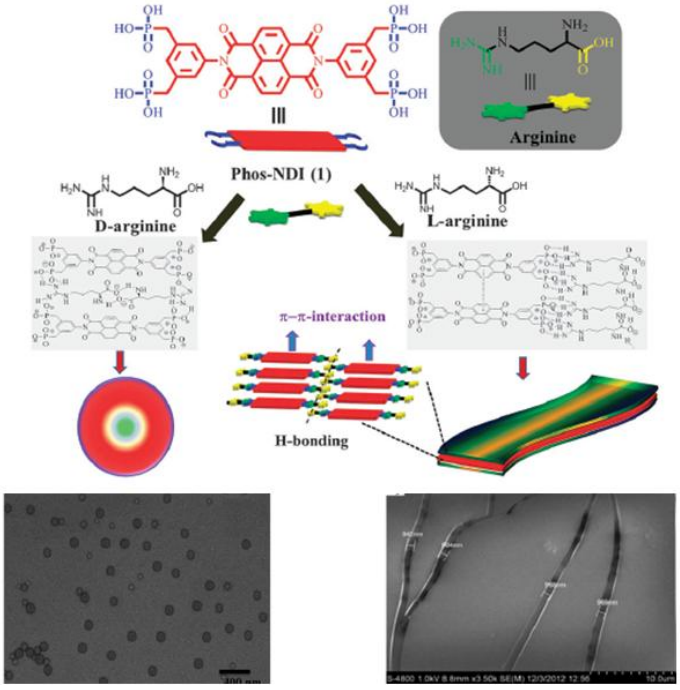

Figure-4.3. Self-assembly of a NBI-phosphonic acid derivative forming tunable nano-aggregates. [*Adapted from ref.16*]

Apart from these the NBIs are also excellent n-type semiconductor materials suitable for applications in organic electronics and more particularly in the fabrication of n-channel field effect transistors.[17-21] The key features of the naphthalenebisimides rendering them attractive for low cost optoelectronic applications are better fabrication properties, low lying LUMO (lowest unoccupied molecular orbital) levels, high crystallinity, good self assembling characteristics, high electron affinity and field effect mobilities.[22-28] Small molecule based NBI derivatives have proved to be among the best performing n-type organic semiconductors known so far. For instance, the core substituted NBI small molecule NDI-8CN with electron withdrawing -CN groups showed an average electron mobility value only about 4.7 x 10^{-3} $cm^2V^{-1}s^{-1}$ while the disubstituted $NDI\text{-}8CN_2$ exhibited a drastic improvement to 0.15 $cm^2V^{-1}s^{-1}$.[29] A symmetrically substituted cyclohexyl NBI derivative based thin film transistor reported by Shukla *et al.* exhibited n-type performances with high electron mobilities up to 6.2 $cm^2V^{-1}s^{-1}$ (figure-4.4), which is one of the highest values reported so far.[30]

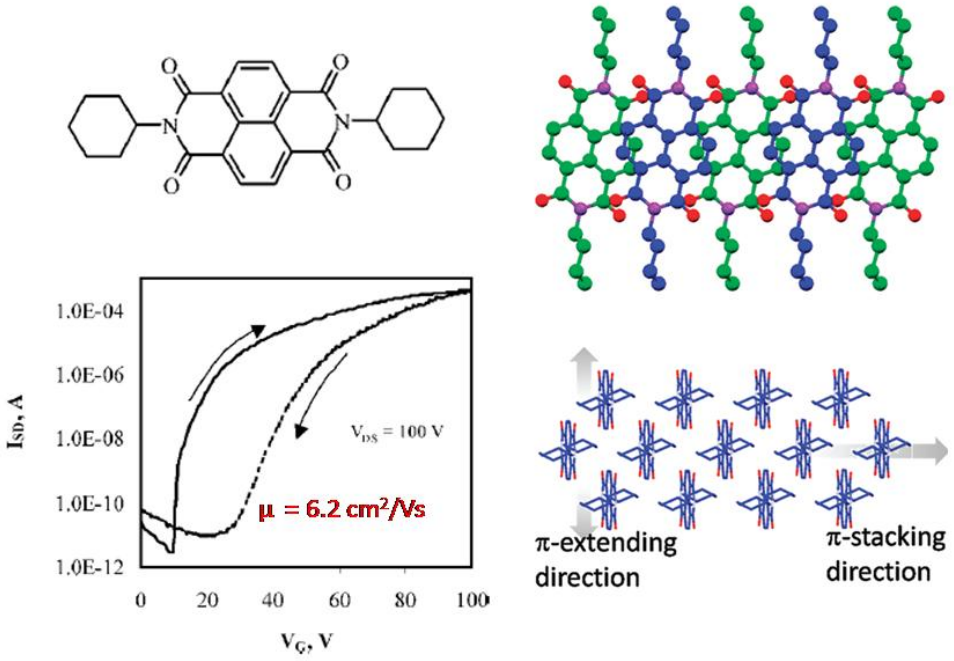

Figure-4.4. Cyclohexyl-NBI small molecule with excellent n-type mobility. [*Adapted from ref.30*]

Through single crystal analysis they showed that each cyclohexyl-NBI molecule was in close contact with four other neighboring molecules via π-π stacking interactions resulting in 2D lamellar packing such that reticular electron charge transport pathway and hence high device performance was achieved.

Katz *et al.* reported fluoroalkylated benzyl NBI derivatives exhibiting good air stability and high electron mobilities in the range 0.1 - 0.57 $cm^2V^{-1}s^{-1}$.[31] In addition to these simple small molecules several core extended NBI derivatives are also reported that have been designed to obtain n-type semiconductors with enhanced performance. The naphthalene framework has been subjected to various chemical modifications including (i) fusion of additional rings to NBI core positions,[32-36] head positions of imide groups [37-40] as well as transformation of imide groups into additional rings at shoulder positions.[41,42] Examples include electron-withdrawing 2-(1,3-dithiol-2-ylidene) malononitrile groups containing core expanded NBI reported by Gao *et al.* resulting in n-type OFETs with electron mobility of 1.2 $cm^2V^{-1}s^{-1}$ in air. [32-34] A very recent systematic investigation by Zhu *et al.* demonstrated the influence of varied length branched alkyl substituents on the microstructure and charge transport properties of naphthalene diimides fused with 2-(1,3-dithiol-2-ylidene) malononitrile groups (NDI-DTYM2).[43] (Figure-4.5)

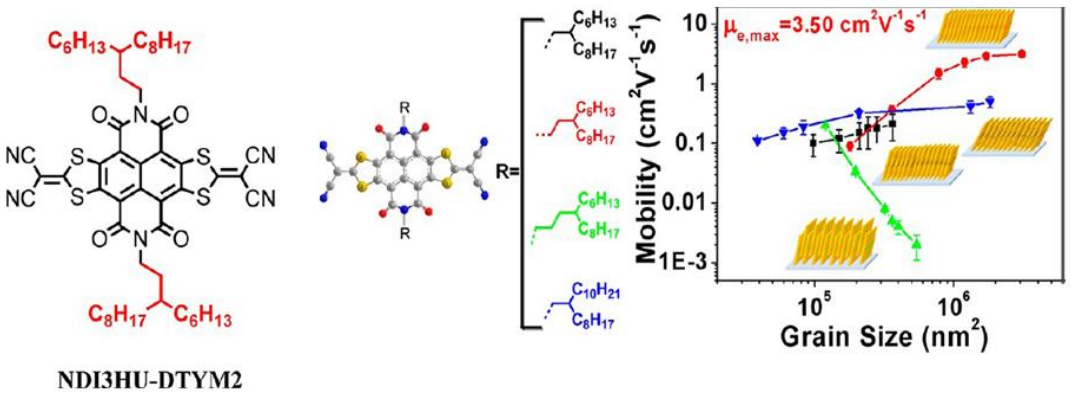

Figure-4.5. NBI derivatives fused to 2-(1,3-dithiol-2-ylidene)malononitrile groups with varying alkyl chain length and high mobility. [*Adapted from ref.43*]

They found that incorporating three-branched N-alkyl substituents of $C_{11,6}$ to NDI-DTYM2 core resulted in a dense, in-plane molecular packing with an unit cell area of 127 $Å^2$, larger domain sizes of up to 1000 × 3000 nm^2, and high electron mobility of up to 3.50 $cm^2V^{-1}s^{-1}$, which is an unprecedented value for ambient stable n-channel solution-processed OTFTs reported to date.

Würthner *et al.* disclosed for the first time ambipolar characteristics of a core extended NDI with electron rich carbazole groups that showed a hole mobility of 0.56 $cm^2V^{-1}s^{-1}$.[35] NBI derivatives with n-type or p-type or ambipolar behaviour have been explored by Liu *et al.* by entailing electron-donating tetrathiafulvalene or 1,3-dithole-2-thione(-one) moieties to the core.[36,44] Some representative examples of core extended NBI small molecule derivatives are given in figure-4.6.

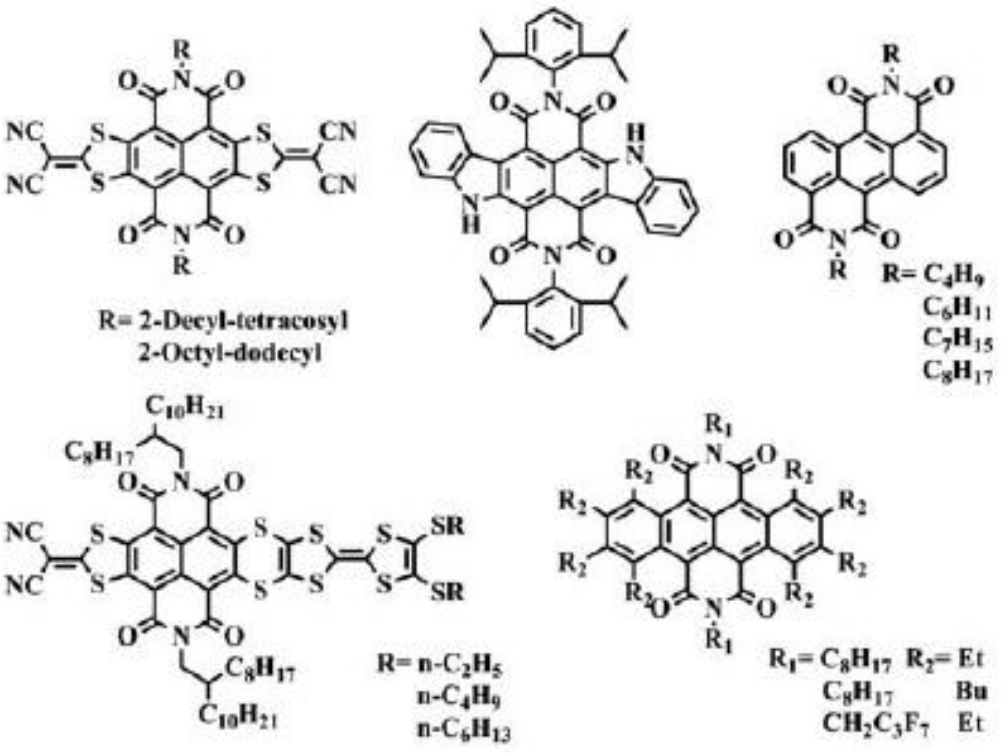

Figure-4.6. Representative examples for core-expanded NBI small molecules. [*Adapted from ref.47*]

Marder *et al.* reported NBI derivatives with rings fused to shoulder positions of imide groups namely the 2,6-diacylnaphthalene-1,8:4,5-bis(dicarboximides) which were synthesized by transformation of NBI into 2,6-diacyl derivative and further reaction with hydrazine.[41] This moiety was incorporated by Luscombe *et al.* into ladder n-type polymers with mobility upto 0.0026 $cm^2V^{-1}s^{-1}$.[42] A detailed study by Marks *et al.* revealed a family of naphthaleneamidinemonoimide-fused oligothiophenes that exhibited ambipolar or n-type semiconducting characteristics.[45] Another set of π-extended NBI molecules at shoulder positions have been very recently reported by Zhang *et al.* utilizing intramolecular cyclization with ethynyl and imidecarbonyl groups.[46] In an attempt to extend the π-system along the equatorial axis of rylenes, Wang *et al.* have prepared hybrid rylene arrays via combination of Stille coupling and C-H transformation (figure-4.7).[48] The advantage of this approach was that it not only leads to broadened light absorption but also increases the electron affinity facilitating electron injection and transport with ambient stability.

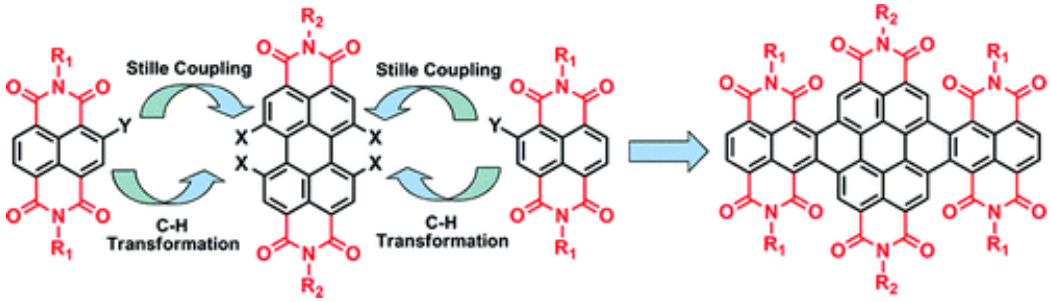

Figure-4.7. Representative hybrid rylene arrays combining naphthalene and perylene bisimides via core expansion. [*Adapted from ref.48*]

Literature is surplus with reports on naphthalenebisimide based polymeric materials, but a vast majority of them are donor-acceptor type main-chain copolymers with different donor monomers and NBI as the acceptor monomer in a conjugated fashion designed to alter the electronic properties suitably for optoelectronic applications. The different donor groups explored includes thiophene,[20,24,25,49,50] thiazole,[51] fluorene,[52] 1,5-dihydroxynaphthalene (DAN)[53] and so on. In fact the first n-channel polymer OFET reported by Jenekhe *et al.* was

also based on a naphthalene ladder polymer named BBL with an imide like structure showing an electron mobility of 0.1 $cm^2V^{-1}s^{-1}$.[39] Independently Watson *et al.* and Facchetti *et al.* have pioneered the studies of NBI based main chain polymers for OFET applications.[24-27,54] A novel n-type co-polymer developed by Facchetti and co-workers based on naphthalenebisimide and bithiophene named as P(NDI2OD-T2) (also commercialized as Polyera ActivInk N2200) demonstrated an unprecedented OFET characteristics with high electron mobility up to 0.85 $cm^2V^{-1}s^{-1}$ in top gate/bottom contact device architecture (figure-4.8(a)).[25,55-62] Till date a plethora of NBI based copolymer semiconductors are reported. Some of them worth mentioning are the series of conjugated polymers reported by Jenekhe and Watson *et al.* prepared through Stille coupling of regioisomerically pure dibromo-naphthalenediimide with various stannylated thiophene monomers.[24,54] They kept the acceptor NBI moiety constant and varied the donor thiophene moieties with different electron donating strength and these copolymers were used in n-channel as well as ambipolar OFETs (figure-4.8(b)).

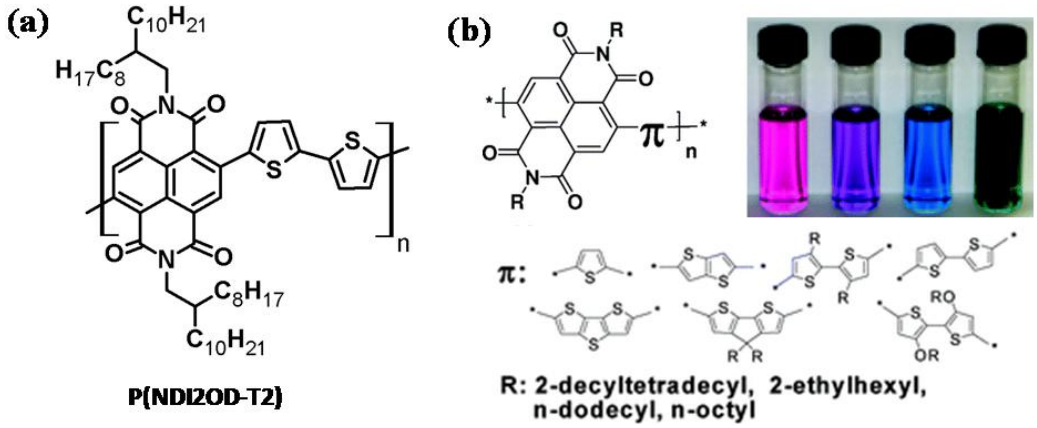

Figure-4.8. Structures of NDI thiophene co-polymers. [(a) and (b) *adapted from ref.25 and ref.24 respectively*]

Jenekhe *et al.* in another independent study demonstrated a new crystalline copolymer viz., poly(naphthalene-diimide-*alt*-biselenophene) (PNDIBS) with a high field effect electron mobility of 0.07 $cm^2V^{-1}s^{-1}$.[63] This polymer also exhibited broad visible-near-IR absorption band with an optical band gap of 1.4 eV and the

bulk heterojunction solar cell comprised of PNDIBS and P3HT (poly(3-hexylthiophene) showed a photovoltaic power conversion efficiency of 0.9 % (figure-4.9(a)).

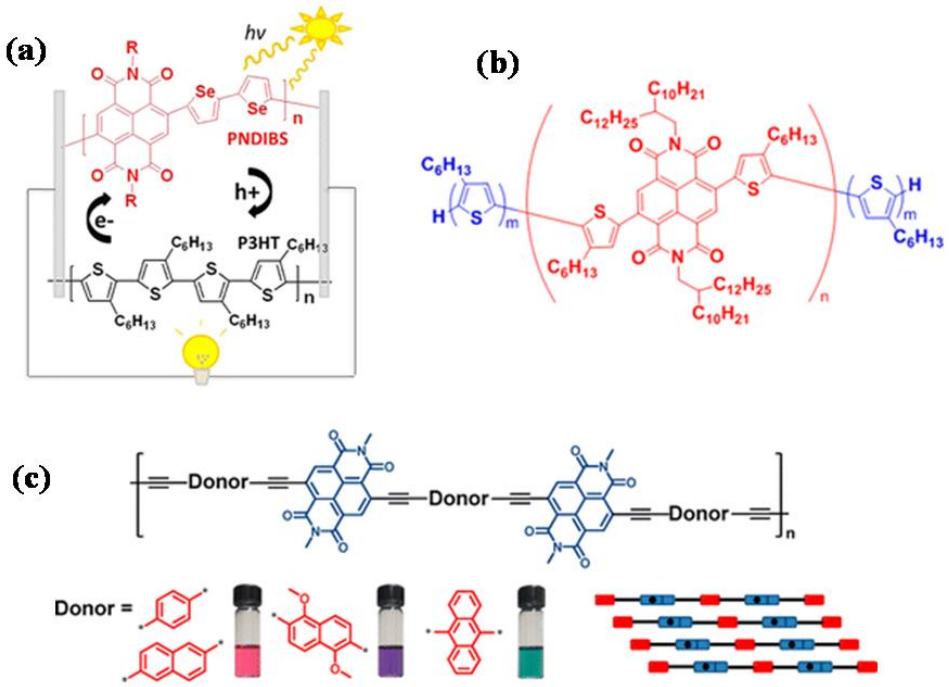

Figure-4.9. Donor-acceptor copolymers with NDI acceptor and different donors. [(a), (b) & (c) a*dapted from ref.63, ref.64 and ref.53 respectively*]

Nakabayashi *et al.* reported a fully conjugated donor-acceptor (D-A) block copolymer P3HT-PNBI-P3HT synthesized using quasi living Grignard metathesis polymerization and Yamamoto coupling.[64] They fabricated all polymer solar cells using this copolymer blended with P3HT namely P3HT:(P3HT-PNBI-P3HT) (figure-4.9(b)) which exhibited a power conversion efficiency of 1.28 %. Along a similar line Iverson *et al.* prepared conjugated D-A copolymers with electron-deficient NBI linked via ethynyl spacers to electron rich aromatics (figure-4.9(c)) especially 1,5-dialkoxynaphthalene (DAN) units and it was found that irrespective of the donor co-monomers used the NBI units in the polymer stacked in an offset face-to-face manner unlike typical D-A alternating stacks.[53]

Chen, Higashihara and co-workers investigated a series of NBI based all conjugated graft copolymers comprising of n-type or p-type backbone with P3HT side-chains (figure-4.10(a)) by Stille coupling and Kumada catalyst transfer polycondensation.[65] Although the graft polymers were anticipated to show ambipolar nature due to the presence of both n-type as well as p-type blocks, unfortunately only p-type charge transfer characteristics with moderate hole mobility value of 10^{-4} $cm^2V^{-1}s^{-1}$ was obtained.

Similarly in a very recent study Yao and Fu *et al.* demonstrated naphthalenediimide-benzothiadiazole based copolymer semiconductors connected through thiophene linkers named as PNDI-*m*T(BZ)*m*T (m = 1, 2) (figure-4.10(b)).[66] OFETs based on these copolymers showed good air stability and ambipolar charge transport especially with the PNDI-T(BZ)T exhibiting average electron and hole mobility values of 0.05±0.02 and 0.1±0.03 $cm^2V^{-1}s^{-1}$ respectively.

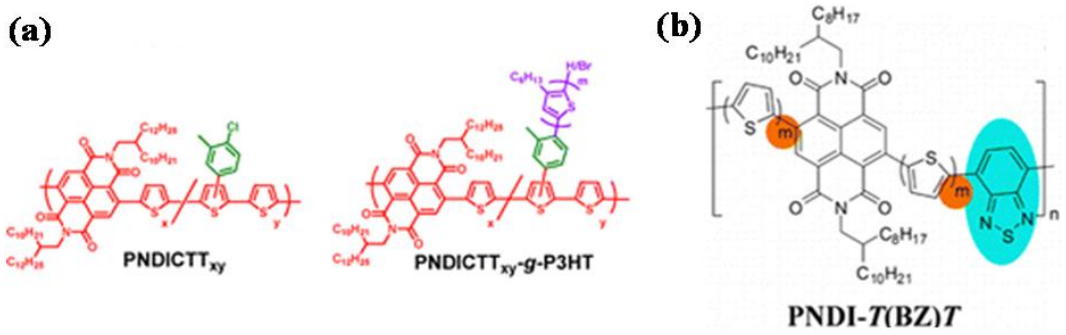

Figure-4.10. Thiophene graft and benzothiadiazole based NBI co-polymers. [(a) and (b) *adapted from ref.65 and ref.66 respectively*]

Compared to main-chain polymers, naphthalenebisimide based side-chain polymer reports are very less or rare. Recently Ghosh *et al.* reported on a NBI-end functionalized amphiphilic polymer (figure-4.11) with thermodynamically stable π-stacking induced blue emitting vesicle and reverse vesicle via self-assembly in water and benzene respectively.[67]

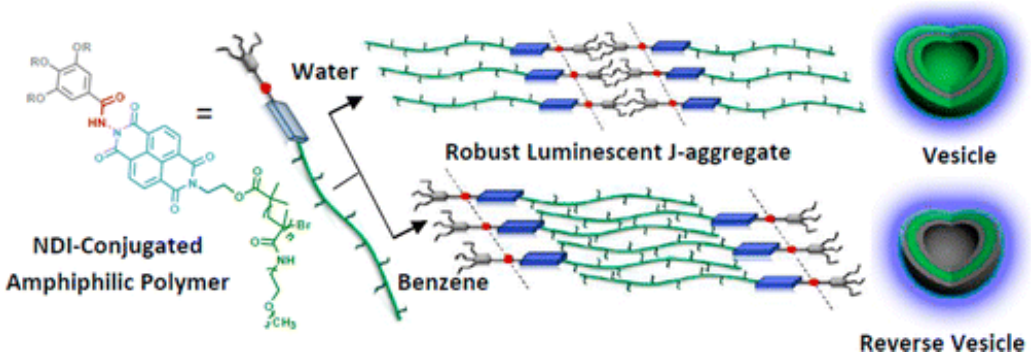

Figure-4.11. End functionalized NBI amphiphilic polymer. [*Adapted from ref.67*]

A key issue regarding the development of polymeric semiconductor materials for organic electronics applications is the innovation of rational design and control of easily accessible novel polymer architectures by simple, smart strategies and same time capable of performing crucial functions. Strategies that can build ordered structures with tailor-made optical, electronic and mechanical properties are in high demand for material science. Functional comb polymer architecture via a modular approach based on supramolecular hydrogen bonding interactions were explored in the previous chapter involving the larger core perylenebisimide n-type organic semiconductor material. Self assembly of such kind of comb shaped supramolecules created by attaching short chain molecules (amphiphiles or surfactants) through physical interactions to either a homopolymer [68] or to one of the blocks of a di-block copolymer, are well known to form mesomorphic structures, as reported in the extensively studied P4VP-PDP based non-covalent surfactant-polymer system by Ikkala and ten-Brinke group and later on by others.[69-71] The simplest morphology is usually lamellar structure with alternating polymer-surfactant lamellae accompanied by the crystallization of the aliphatic components. Irrespective of the surfactants used, all such self-assembled structures are dependent on the side-chain/polymer backbone interactions with the periodicity length scale controlled by two opposing effects, i.e., minimization of interfacial area and chain stretching. Researchers are now exploring the significant potentials of this concept in many possible permutations and combinations

possible. Recently the group of Loos and ten Brinke *et al.* reported supramolecular double-comb diblock copolymer complexes using poly(4-vinylpyridine)-*b*-poly-(N,N-dimethylacrylamide) (P4VP-*b*-PDMA) by hydrogen bonding of 3-pentadecylphenol (PDP) to both blocks resulting in self-assembled lamellar-in-lamellar morphology (Figure-4.12).[72]

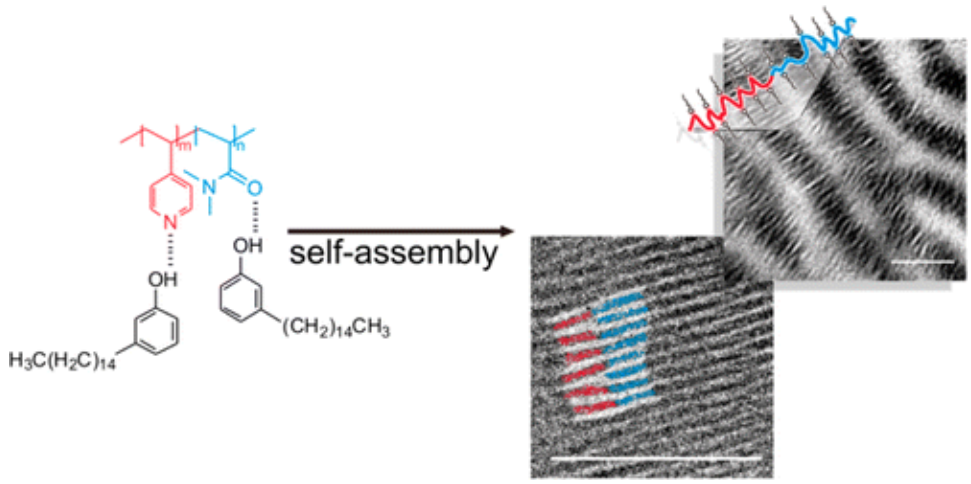

Figure-4.12. Supramolecular double comb diblock copolymers. [*Adapted from ref.72*]

Fresh results from Osuji and Campos *et al.* revealed highly ordered supramolecular assemblies of perylenebisimide mesogen with an imidazole head group hydrogen-bonded to acrylic acid units of poly(styrene-*b*-acrylic acid) utilizing external magnetic field alignment, thus created organic monoliths with single orientation of the microstructure throughout the sample (Figure-4.13).[73]

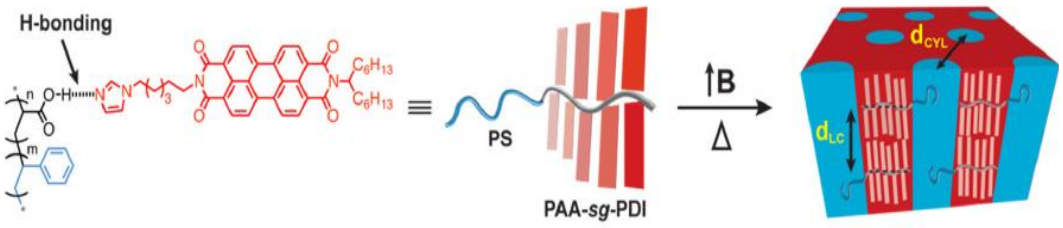

Figure-4.13. Magnetic alignment of supramolecularly grafted perylenebisimide mesogen into an organic monolith. [*Adapted from ref.73*]

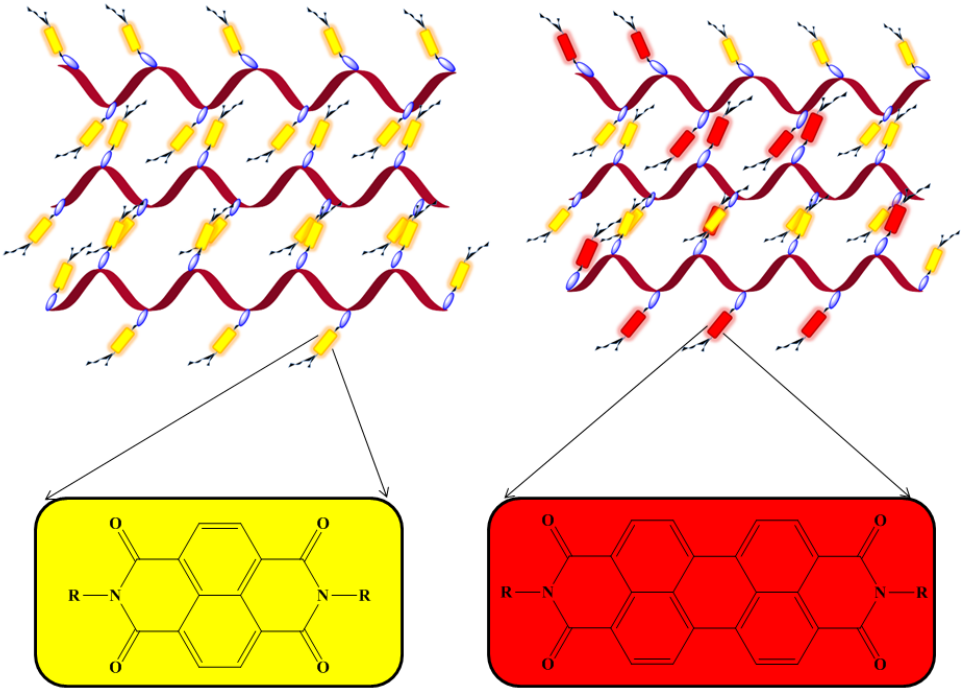

Scheme-4.1

Considering the importance and performance of the lower member of the rylenebisimides family namely the naphthalenebisimides (NBI) in the field of n-type organic semiconductors, this chapter extends the study to material properties of the supramolecular comb polymer based on pentadecyl phenol functionalized naphthalenebisimide (**PDP-UNBI**) with poly(4-vinyl pyridine) P4VP mediated by hydrogen bonding interactions. It was envisaged that using the same concept when PBIs are replaced by NBIs, high electron mobility polymeric n-type semiconductor material could be obtained. Also another series of stoichiometrically balanced 1:1 random co-comb polymer supramolecules of P4VP with **PDP-UPBI** and **PDP-UNBI** varying only in the relative compositions of perylene and naphthalene cores were also studied. The discussion format on the self-assembly of these systems will be similar to that used for the **PDP-UPBI/P4VP** based system. The overall theme of the present chapter is represented in scheme 4.1. Non-covalent attachment of surfactants in the case of homo and co-comb polymer complexation via hydrogen

bonding was monitored and confirmed by means of FT-IR and ^{1}H-NMR spectroscopic methods. The solid state packing of the mesogens in the bulk structure was analysed in detail using different X-ray diffraction techniques (low angle and wide angle). Additionally more light was shed on the packing nature of the complexes utilizing the single crystal analysis of the **PDP-UNBI** as a model study.

Transmission microscopy (TEM) imaging was used for probing the visual evidence for the mesomorphic morphologies. Finally the charge transport properties of the complexes investigated by SCLC method are also discussed. The set of fundamental studies presented here pave pathways toward simple and smart polymeric functional materials that can serve as precursors of well organized hybrid nanocomposites for optoelectronic applications.

4.2. Experimental Section

4.2.1. Materials: Poly(4-vinylpyridine) (P4VP) (Mw =60,000) was purchased from Aldrich. It was dried in vaccum oven at 60 °C for 3 days prior to use. The other starting materials naphthalenetetracarboxylic acid dianhydride (NTCDA), perylenetetracarboxylic acid dianhydride (PTCDA), 2-ethyl-1-hexyl amine, 3-pentadecylphenol and other reagents were also purchased from Aldrich and used without any further purification. All solvents used were of analytical grade and carefully dried before use according to standard procedures.

4.2.2. Instrumentation Details: ^{1}H and ^{13}C-NMR spectra were recorded in $CDCl_3$ using Bruker AVENS 200 MHz spectrophotometer. Chemical shifts (δ) are reported in ppm at 298 K, with trace amount of tetramethylsilane (TMS) as internal standard. MALDI-TOF analysis was carried out on a Voyager-De-STRMALDI-TOF (Applied Biosystems, Framingham, MA, USA) instrument equipped with 337 nm pulsed nitrogen laser used for desorption and ionization. The operation was in a reflector mode with an accelerating voltage of 25 kV. Micromolar solutions of the compounds in THF were mixed with Dithranol matrix and spotted on stainless steel MALDI plate and dried well. Size exclusion chromatography (SEC) in THF was done using polystyrene standards for calibration. Waters 515 Pump connected through two series of Styragel HR columns (HR-3 and HR-4E) and Waters 2414 differential refractometer was used for analyzing the samples. The flow rate of the THF was maintained as 1 mL throughout the experiments, and 2-3 mg in 1 mL of the samples were filtered and injected for recording the chromatograms at 30 °C. Infrared spectra were obtained using Bruker α-T spectrophotometer in the range of 4000-400 cm^{-1}. All the complexes were directly solution drop cast onto KBr pellets and solvent evaporated off slowly at 60-70 °C, followed by drying in vacuum oven overnight. UV-Vis spectra were recorded using a Perkin Elmer Lambda-35 UV-Vis spectrometer. Steady state fluorescence emission were performed using a HORIBA JOBIN VYON Fluorolog 3 fluorescence spectrophotometer. The emission as well as excitation slit width was maintained at 1 nm throughout the experiments and the

data was obtained in 'S_{1c}/R_1' mode (to account for the variations in lamp intensity). Measurements were made at 90° positions for solutions and 22.5° in front face films. Thermogravimetric analysis (TGA) was performed using a PerkinElmer STA 6000 thermogravimetric analyser. Samples were run from 40 to 800 °C with a heating rate of 10 °C/min under nitrogen. DSC (differential scanning calorimetry) measurements were performed on TA Q10 differential scanning calorimeter at a heating rate of 10 °C/min under nitrogen atmosphere. Typically, 3-4 mg of samples was placed in an aluminum pan, sealed properly and scanned from -50°C to 250 °C. The instrument was calibrated with indium standards before measurements. The first heating cycles were avoided to get rid of thermal history of the samples. Wide Angle X-ray Diffractograms (WXRD) were obtained using a Philips analytical diffractometer with CuKα emission. All the samples were recorded in the (2θ) range of 3–50 degrees using a PANalytical X'pert Pro dual goniometer diffractometer and analyzed using X'pert software. An X'celerator solid-state detector was employed in wide-angle experiments. The radiation used was CuKα (1.54 Å) with a Ni filter, and the data collection was carried out using a flat holder in Bragg–Brentano geometry. Single crystals were subjected to data collection at 100 K on a Bruker APEX duo CCD-X-ray diffractometer equipped with graphite monochromated Mo Ka radiation (λ = 0.71073 Å). The frames were integrated with a Bruker APEX software package. The structures were solved by direct methods and refined with a full matrix least-squares technique using SHELX S v97 programs. The optical microscope images of the single crystals were taken on a LEICA DM2500 polarized light microscope, attached with a digital camera. Transmission Electron microscopy (TEM) was done using an FEI-Tecnai^{TM}-F20 electron microscope operating at 200 kV. Sandwich structures on ITO coated glass and Au substrates were fabricated for the SCLC studies. Thin films of the samples were drop-cast and spin coated on the substrates. The thickness was determined using Dektak surface profiler. The top Al electrode defining the area of the film (0.1 cm^2) was coated using thermal deposition method in high vacuum. All measurements were carried out under inert atmosphere.

4.2.3. Synthesis

(i) 4-amino-3-pentadecyl phenol. The synthesis procedure followed was the same as described in section 3.2.3(i). Yield : 81%. ^{1}H NMR (200 MHz, $CDCl_3$, δ ppm): 7.20 (d, 1H, Ar-H), 6.53-6.47 (m, 2H, Ar-H), 2.63 (t, 2H, Ar-C**H$_2$**-), 1.60 (t, 2H, Ar-CH_2-C**H$_2$**), 1.36–1.23 (b, other aliphatic 24H), 0.86(t, 3H, Ar-$(CH_2)_{14}$-CH_3). ^{13}C NMR (50 MHz, $CDCl_3$, δ ppm): 146.8, 138.7, 126.2, 117.5, 113.4, 30.9, 29.5, 22.7, 14.3. FT-IR (KBr, cm^{-1}): 3432, 3350, 3296, 1647, 1585, 1416, 1334, 914, 675 cm^{-1}. MALDI-TOF MS (Dihydroxybenzoic acid matrix): m/z calculated for $C_{21}H_{37}NO$: 319.29; found 320.31$[M+1]^+$.

Synthesis of Unsymmetrical naphthalenebisimide (PDP-UNBI)

Naphthalene-1,4,5,8-tetracarboxylic dianhydride (2.0 g, 7.54 mmol) was heated in 25g molten imidazole reagent for half an hour followed by simultaneous addition of 4-amino-3-pentadecylphenol (2.37 g, 7.54 mmol) and 2-ethylhexylamine (0.962 g, 7.54 mmol) under nitrogen atmosphere. It was stirred at 160 °C for 12 hours in presence of catalytic amount of $Zn(OAc)_2$. The reaction mixture was then cooled to room temperature and stirred overnight with 250 mL 2N HCl. The precipitate was filtered, washed with water followed by methanol and dried at 120 °C. This crude product comprised of a mixture of 3 major components viz., symmetrically substituted ethylhexyl derivative (NBI-1), the unsymmetrically substituted naphthalenebisimide with ethylhexyl group on one imide position and 3-pentadecyl phenol (PDP) group on other side (NBI-2) named as PDP-UNBI and symmetrical PDP substituted NBI-3. The unsymmetrical PDP-UNBI was separated from this mixture by column chromatography on silica gel using $CHCl_3$/ MeOH mixture. The NBI-1 was eluted in 100% $CHCl_3$, PDP-UNBI in $CHCl_3$/ MeOH (99/1 v/v) and NBI-3 in $CHCl_3$/ MeOH (97/3 v/v).

(ii) N, N'-Bis-Ethylhexyl-naphthalene–1,4:5,8–tetracarboxylic bisimide (NBI-1): Yield : 35 %. ^{1}H NMR (200 MHz, $CDCl_3$, δ ppm): 8.77(m, 4H, naphthalene ring), 4.14(m, 4H, imide-C**H$_2$**), 1.94(m, 2H, imide-CH_2-C**H**), 1.36 (broad multiplet,

corresponding to other aliphatic protons), 0.96(2t, 12H, end C**H**$_3$ groups of ethyl hexyl tail).^{13}C NMR (50 MHz, $CDCl_3$,δ ppm): 163.3, 162.7, 153.5, 131.1, 129.2, 126.9,72.3, 70.8, 67.5, 59.1, 47.0, 37.0, 31.7, 29.3, 23.0, 14.1 FT-IR (KBr, cm^{-1}): 2939, 2850, 1709, 1659, 1600, 1578, 1512, 1446, 1336, 1255, 1183, 1086, 1024, 793, 745, 772, 708, 644. MALDI-TOF MS (Dithranol matrix): m/z calculated for $C_{30}H_{38}N_2O_4$: 490.28; found 491.31[M+1]$^+$.

(iii) N- (2-ethylhexyl) -N'- (4-hydroxy-2-pentadecylphenyl) naphthalene -1,4,5,8-tetracarboxylic acid bisimide -PDP-UNBI (NBI-2): Yield : 24 %. M.P.: 106 ^{0}C.^{1}H NMR (200 MHz, $CDCl_3$, δ ppm) : 8.82(m, 4H, naphthalene ring), 7.03–6.74 (3t, 3H, Ar**H**-PDP), 4.18 (m, 2H, imide-N-C**H**$_2$), 2.35 (t, 4H; Ar-C**H**$_2$), 1.96 (m, 1H, imide-N-CH_2-C**H**), 0.90-0.86 (m, 9H, end CH_3 of ethyl hexyl group + terminal C**H**$_3$ of C-15 alkyl chain), 1.51-1.0(other aliphatic protons). ^{13}C NMR (50 MHz, $CDCl_3$, δ ppm) : 163.3, 159.9, 158.3, 143.1, 139.6, 136.7, 135.2, 130.3, 129.8, 126.2, 124.9, 123.1, 122.6, 113.3, 106.2, 55.6, 32.7, 31.9, 29.9, 26.9, 22.8, 14.3. FT-IR (KBr, cm^{-1}): 3408, 3190, 3075, 2923, 2853, 1705, 1661, 1581, 1495, 1454, 1373, 1343, 1297, 1245, 1191, 1154, 1092, 1056, 982, 958, 874, 810, 771, 731, 702, 638. MALDI-TOF MS (Dithranol matrix): m/z calculated for $C_{43}H_{56}N_2O_5$: 680.42 ; found 681.38[M+1]$^+$. Elemental analysis calculated (%): C 75.85, H 8.29, N 4.11; found: C 75.74, H 8.36, N 3.67.

(iv) N,N'-Bis-(3-pentadecylphenyl)-naphthalene-1,4:5,8-tetracarboxylic bisimide (NBI-3) : Yield : 19 %. ^{1}H NMR (200 MHz, $CDCl_3$) δ ppm: 8.87(dd, 4H, naphthalene), 7.07-6.79(3t, 6H, PDP-Ar**H**), 2.39 (t, 4H; PDP-Ar-C**H**$_2$), 1.54(t, 4H; PDP-Ar-CH_2-C**H**$_2$), 0.87 (m, 6H, terminal C**H**$_3$ groups of C-15 alkyl chain), 1.24-1.13(other aliphatic protons). ^{13}C NMR (50 MHz, $CDCl_3$, δ ppm) : 162.4, 159.2, 158.6, 142.9, 139.8, 135.7, 135.2, 131.3, 129.7, 127.2, 125.1, 123.3, 122.8, 113.3, 106.2, 55.6, 32.7, 31.9, 29.9, 26.9, 22.8, 14.3.FT-IR (KBr, cm^{-1}): 3365, 2928, 2854, 1711, 1664, 1582, 1499, 1452, 1345, 1298, 1250, 1180, 1094, 979, 876, 839, 768, 643. MALDI-TOF MS (Dithranol matrix): m/z calculated for $C_{56}H_{74}N_2O_6$: 871.22 ; found 872.13[M+1]$^+$.

Sample preparation: The unsymmetrical amphiphilic naphthalenebisimide (**PDP-UNBI**) and Poly (4-vinylpyridine) (P4VP) were dried in vacuum oven at 60 °C for 3 days. **P4VP(PDP-UNBI)$_n$** complexes were prepared from dry $CHCl_3$ solutions, where 'n' denotes the number of PBI molecules per vinyl pyridine (VP) repeat unit (n= **PDP-UNBI** /VP). In a typical procedure P4VP was first dissolved in $CHCl_3$ to which desired amount of **PDP-UNBI** was added depending on the value of 'n' and the solution was stirred for 24 hours under nitrogen atmosphere. Concentration of the solutions were kept as low as 1wt%. Subsequently the solvent was evaporated slowly on a hot plate at 45 °C and the complexes were further dried in vacuum oven at 40 °C for 3 days, slowly cooled to room temperature and stored in dessiccator thereafter. In the case of mixed complexes of **PDP-UNBI** and **PDP-UPBI** with P4VP were prepared using N,N'-dimethylformamide (DMF) solvent in a similar manner but at slightly higher temperatures around 60 °C for the solvent removal. The **PDP-UPBI** was synthesized exactly same as described in previous chapter (section-3.2.3).

4.3. Results and Discussion

4.3.1. Synthesis and Characterization of Amphiphilic Naphthalenebisimide (PDP-UNBI)

The amphiphilic unsymmetrical naphthalenebisimide derivative was designed in the same way as the perylenebisimide derivative PDP-UPBI described in the previous chapter with the hydrogen bondable pentadecylphenol (PDP) group on one side and a branched alkyl unit, the ethylhexyl chain on the other side. The synthesis strategy that was adopted is outlined in Scheme-4.2 along with the corresponding reagents and reaction conditions.

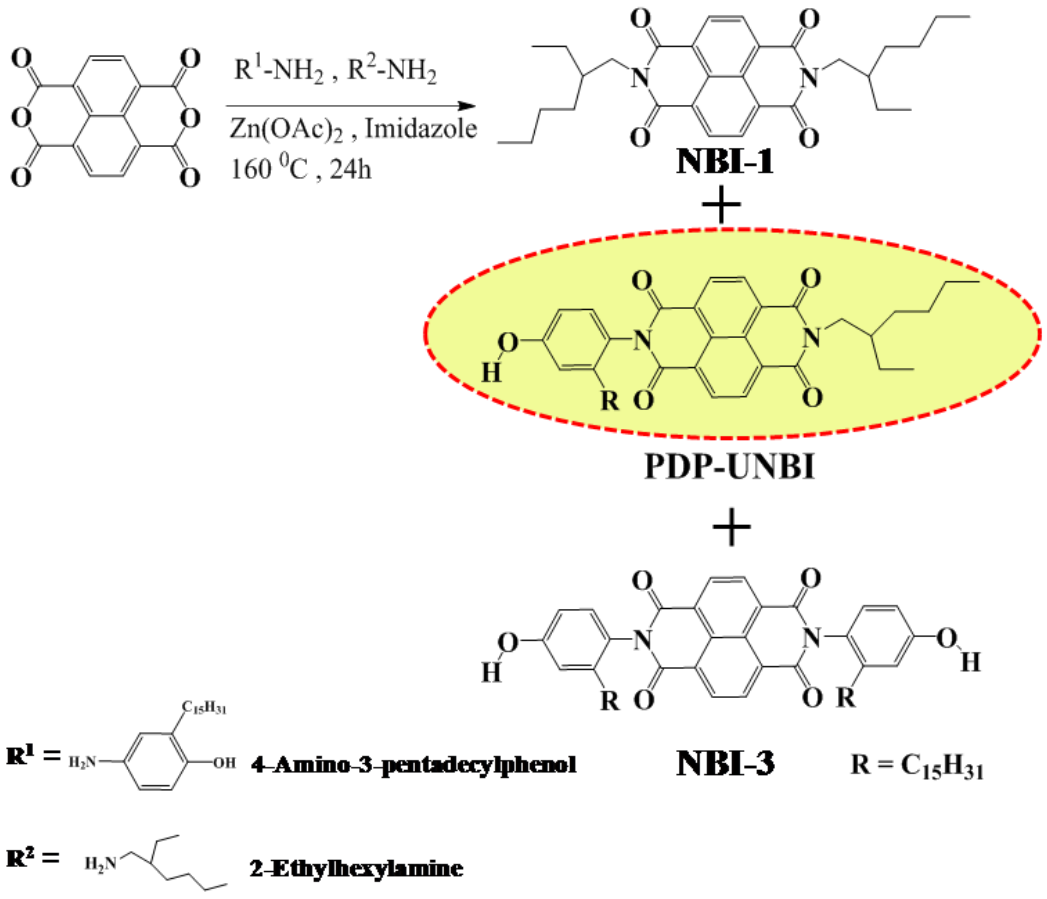

Scheme-4.2. Synthesis of unsymmetrical naphthalenebisimide **PDP-UNBI** by statistical condensation with equivalent ratios of two amines.

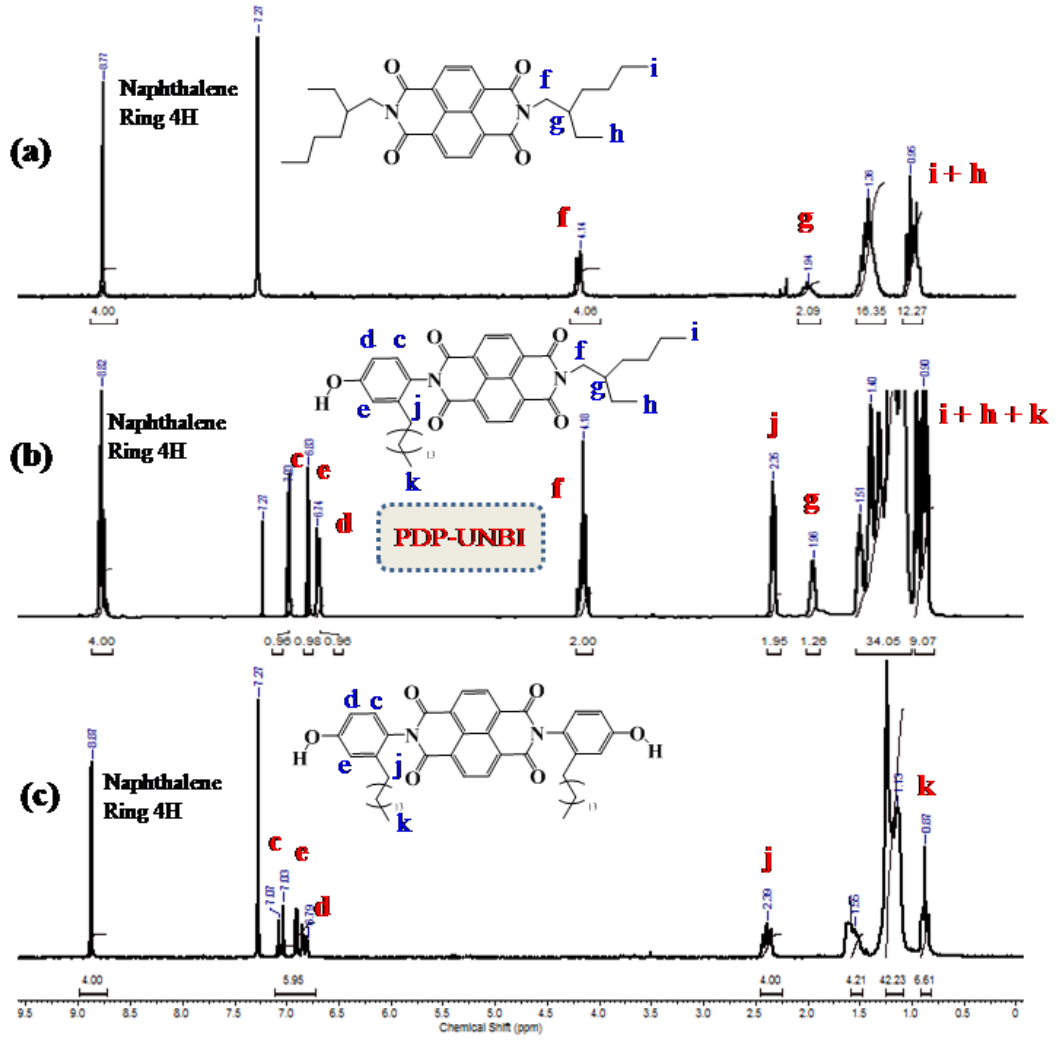

Figure-4.14. ^{1}H-NMR spectra of the naphthalenebisimide derivatives NBI-1, **PDP-UNBI** and NBI-3 recorded in $CDCl_3$ at room temperature.

A statistical condensation reaction of 1,4,5,8-naphthalenetetracarboxylic dianhydride (NTCDA) with equimolar ratios of the two amines viz., 4-amino-3-pentadecylphenol and 2-ethyl hexyl amine using molten imidazole as the solvent, gave the unsymmetrical naphthalenebisimide molecule which was named as **PDP-UNBI**, similar to the perylene analogue. This reaction in fact yielded the unsymmetrical **PDP-UNBI** in moderate yields but along with a mixture of other two statistical symmetric derivatives (NBI-1 and NBI-3). The molecule of interest **PDP-UNBI** was isolated from the mixture by column chromatography techniques

using $CHCl_3$/methanol eluent system. Structure confirmation was done for all three above mentioned products through ^{1}H-NMR, ^{13}C-NMR, FT-IR and MALDI-TOF spectroscopic methods with details given in the experimental section. Owing to the smaller size of the NBI aromatic core, these products were freely soluble in most common organic solvents like chloroform ($CHCl_3$), dichloromethane (DCM), tetrahydrofuran (THF) etc. A comparison of their ^{1}H-NMR spectra recorded in $CDCl_3$ is given in figure-4.14 and the respective protons are labelled by alphabets.

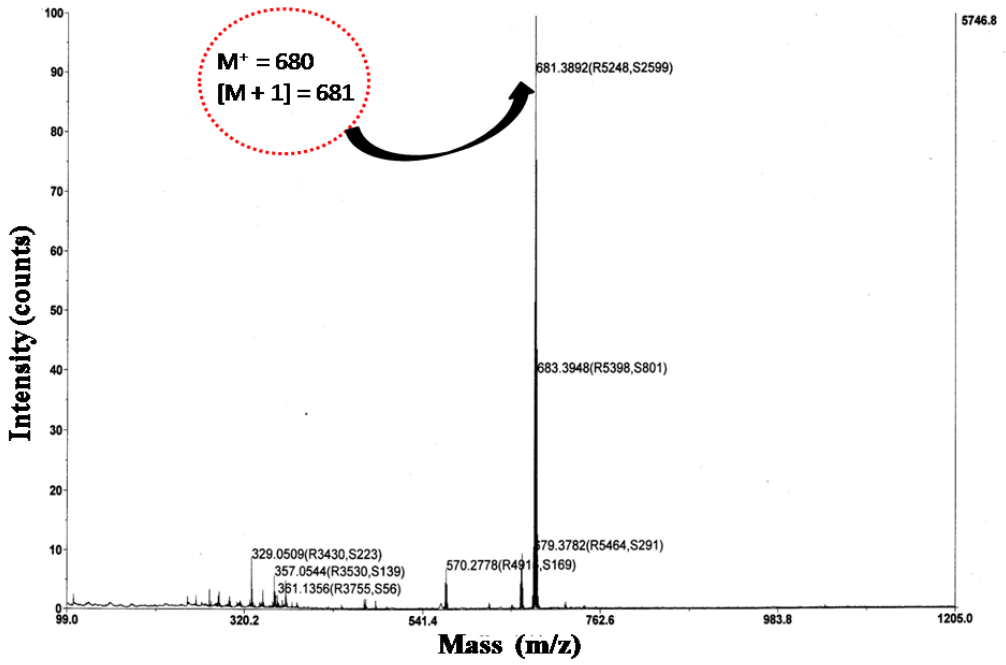

Figure-4.15. MALDI-TOF spectra of the unsymmetrical naphthalenebisimide **PDP-UNBI.**

The **PDP-UNBI** molecule had well resolved ^{1}H-NMR peaks in the region from 6.5 - 9.5 ppm corresponding to two set of aromatic protons (i) from the 4 protons of naphthalene ring core appearing around 8.82 ppm and (ii) from the set of 3H of the pentadecylphenol (PDP) ring labelled as 'c', 'e' and 'd' at 7.03, 6.83 and 6.74 ppm respectively both matching in integration values indicating the attachment of PDP unit on one end of the NBI. The peak at 4.18 ppm labelled 'f'

corresponding to the -C**H**$_2$- group immediate to the imide nitrogen confirmed the attachment of ethylhexyl chain at other end of the NBI core.

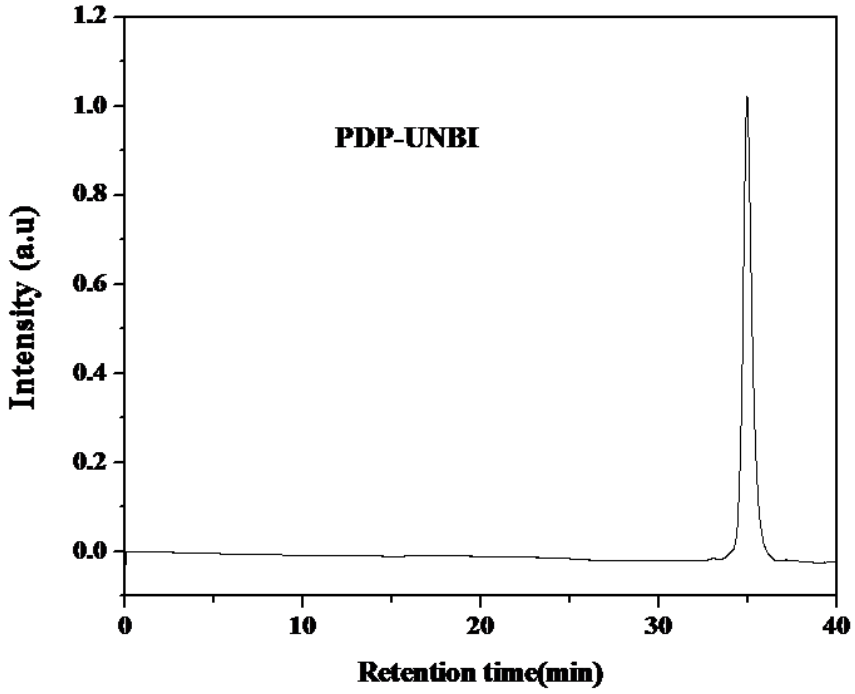

Figure-4.16. Size exclusion chromatogram of **PDP-UNBI** run using THF solvent.

Apart from the ^{1}H-NMR data, further evidences for the structure confirmation was obtained from ^{13}C-NMR, FT-IR and especially the MALDI-TOF (figure-4.15) spectra that showed a single m/z (100%) peak at 681.38 which happens to be the [M+1] peak of **PDP-UNBI** and no peaks beyond at higher mass. The purity confirmation for **PDP-UNBI** was obtained from single peak in the size exclusion chromatogram (SEC) carried out in THF solvent (figure-4.16) and matching elemental analysis data (given in experimental section).

The thermal stability of the **PDP-UNBI** was studied by thermogravimetric analysis (TGA) under nitrogen atmosphere from 30 - 800 °C. The molecule exhibited high thermal stability upto 400 °C and the 10 % weight loss temperature was found to be 392 °C as shown in the TGA thermogram shown in figure-4.17.

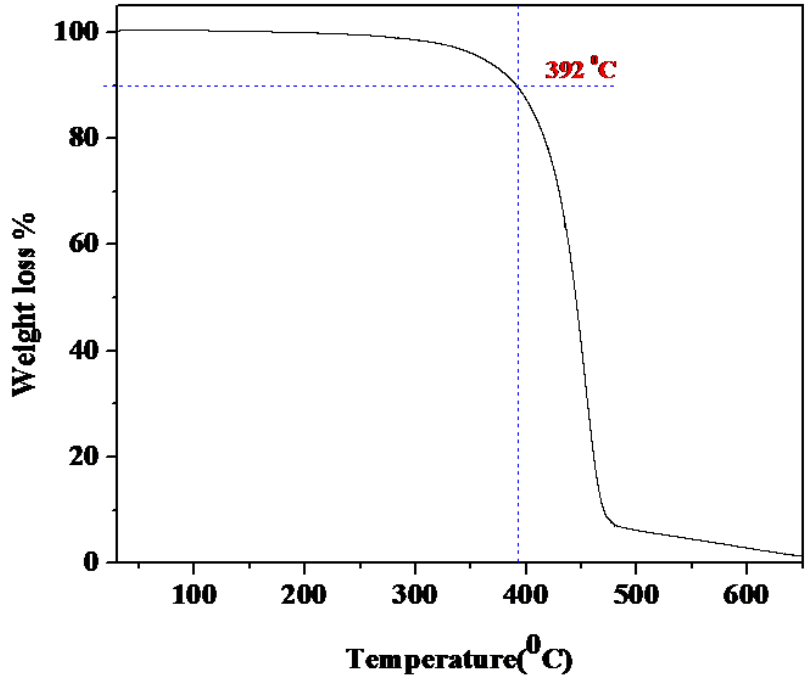

Figure-4.17. TGA thermogram of **PDP-UNBI** with the 10 % weight loss temperature.

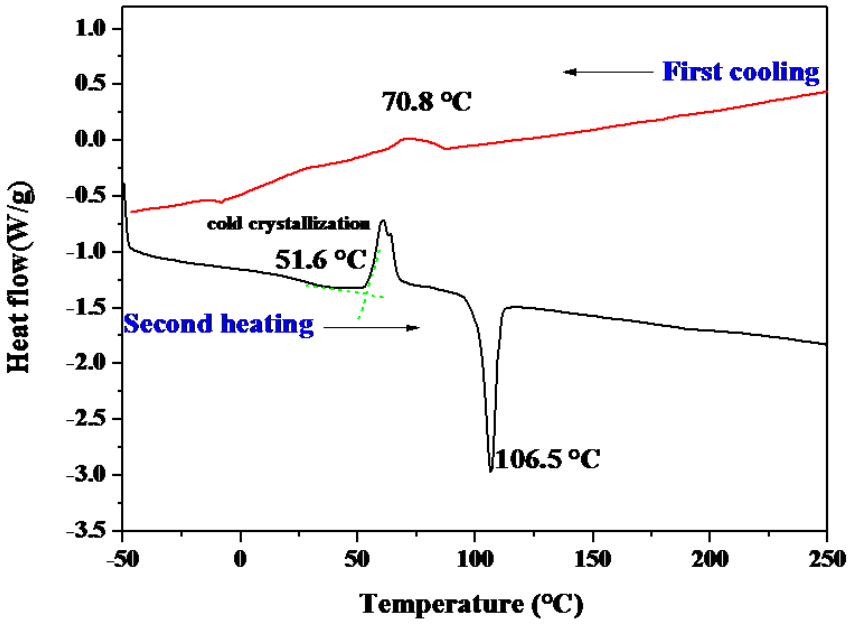

Figure-4.18. DSC profile of **PDP-UNBI** showing the second heating and first cooling cycles.

The thermotropic phase behaviour of **PDP-UNBI** was investigated by means of differential scanning calorimetric (DSC) analysis. Approximately 2-3 mg of the sample was heated and subsequently cooled in the temperature range -50 °C to 250 °C at the rate of 10 °C/min. The DSC thermogram showing the different phase transitions is given in figure-4.18. Thermal history of the sample was erased in the first heating cycle and the second heating cycle of **PDP-UNBI** showed two endotherms. The low temperature endotherm corresponds to the cold crystallization onset at 51.6 °C and the higher temperature endotherm is the result of complete melting of the crystals around 106.5 °C. The first cooling cycle accordingly exhibited a very small and broad exotherm near 70.8 °C.

4.3.2. Supramolecular PDP-UNBI/P4VP Homo-Comb polymers and its random co-comb polymer with PDP-UPBI

Two sets of n-type semiconductor supramolecular comb polymers were prepared by complexation with P4VP : one set comprising of the homo-comb polymers of amphiphilic naphthalenebisimide **PDP-UNBI** and another set involving random co-comb polymers of **PDP-UNBI** and **PDP-UPBI,** hydrogen-bond between the pyridine and phenol groups being the mode of non-covalent attachment in both sets. The **PDP-UNBI** based homo-comb polymers were named as **P4VP(PDP-UNBI)$_n$** where 'n' denotes the number of surfactant molecules per vinyl pyridine repeat unit and this ratio was varied from 0.25 to 1.00. Under normal conditions, chemically similar but different molecules like **PDP-UNBI** and **PDP-UPBI** do not mix because of the unfavourable intermolecular interactions. Free miscibility of these cores can occur, provided they are bound by some specific interactions like hydrogen bonding. One effective method to create miscible polymeric ensemble of PBI and NBI together is to incorporate them as components of a random copolymer as part of supramolecular random co-comb polymer complexation with P4VP. The perylene and naphthalene bisimide cores were combined into such a single macromolecular ensemble in anticipation that the resulting material may provide broadened light absorption from 300-600 nm as well as a better tight packed

structural ordering that could arise from alternating NBI/PBI cores and thus result in better performing high charge carrier mobility materials. Therefore the co-assembly of such supramolecules were systematically investigated as a function of relative loading of **PDP-UNBI** and **PDP-UPBI** in a set of stoichiometrically balanced 1:1 random co-comb complexation with P4VP which were short named as **P4VP(UNBI$_m$/UPBI$_n$)$_{1.0}$**. Here each pyridine unit gets one rylene surfactant either **PDP-UNBI** or **PDP-UPBI** as denoted by the subscript 1.0 and the relative ratios of **PDP-UNBI** to **PDP-UPBI** indicated by subscripts 'm' and 'n' was varied as m:n = 0.5:0.5, 0.25:0.75 and 0.75:0.25 respectively. Figure-4.19 depicts the chemical structure of the **P4VP(PDP-UNBI)$_{1.0}$** homopolymer and the **P4VP(UNBI$_m$/UPBI$_n$)$_{1.0}$** random co-comb polymers.

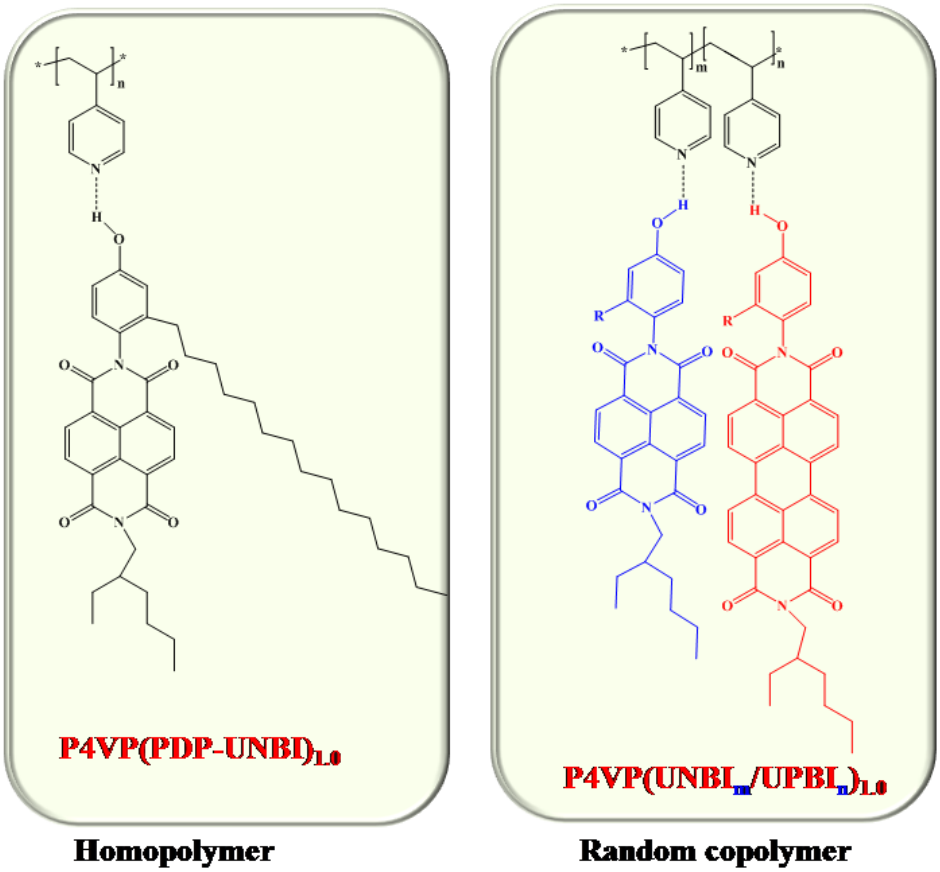

Figure-4.19. Chemical structures of **P4VP(PDP-UNBI)$_{1.0}$** homopolymer and the **P4VP(UNBI$_m$/UPBI$_n$)$_{1.0}$** random co-comb polymers.

All the supramolecular comb polymers discussed in this study were prepared by solution mixing and evaporation technique, in which the hydrogen bond donor **PDP-UNBI** and/or **PDP-UPBI** were dissolved in suitable solvents to which desired amounts of P4VP in the same solvent were added and the mixture was stirred under inert atmosphere for one day to ensure homogenised hydrogen bond formation nominally. Finally slow evaporation of the solvents yielded the microphase separated supramolecular comb-polymer complexes. Due to the high solubility limit of smaller **PDP-UNBI** molecule, chloroform was the solvent of choice for preparation of **P4VP(PDP-UNBI)$_n$** homopolymers, whereas due to the lower solubility of **PDP-UPBI** more polar N,N'-dimethylformamide (DMF) was used for the **P4VP(UNBI$_m$/UPBI$_n$)$_{1.0}$** random co-comb polymers.

4.3.3. Evidence for Hydrogen-bonding in the Complexes - FT-IR and ^{1}H-NMR Characterizations

FT-IR spectroscopy has been successfully employed in tracing the intermolecular interaction through hydrogen bonding in numerous supramolecular polymer systems including blends.[68,74] The most commonly studied polymer for supramolecular comb-like structures is the poly(4-vinyl pyridine) (P4VP) because its pyridine groups can easily form hydrogen bonds or ionic bonds with small molecules.[75,76] Upon hydrogen bond formation with amphiphiles several bands of free pyridine ring of P4VP undergoes shift to higher wavenumbers, as a result of the change in electronic distributions. As extensively studied in numerous literature examples, the bands of particular interest are 1597 (+6), 1413 (+6) and 993 (+15), where the values in brackets denotes the typical shifts observed for hydrogen bonding interaction.[68-71] The complete FT-IR spectra recorded from 4500 to 600 cm^{-1} for the pure constituents namely P4VP, **PDP-UNBI** and **PDP-UPBI** is given in figure-4.20.It could be seen that the peaks around 992 and 1413 cm^{-1} present in pure P4VP were absent in both pure **PDP-UNBI** and **PDP-UPBI**, all the three constituents had strong bands around 1598 cm^{-1}.

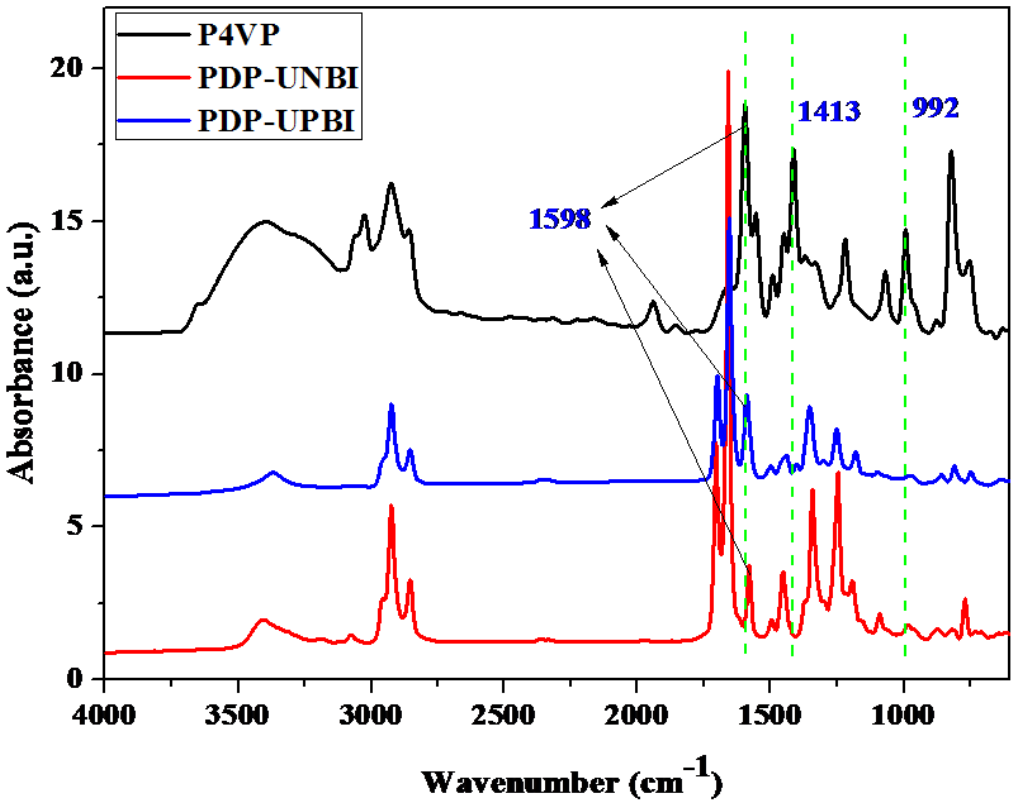

Figure-4.20. FT-IR spectra of P4VP, **PDP-UNBI** and **PDP-UPBI** from 4000 to 600 cm^{-1}.

Consequently the peaks at 992 and 1413 cm^{-1} were used for tracing the hydrogen bonding interaction in all the complexes. In the case of **P4VP(PDP-UNBI)$_{1.0}$** homopolymer these peaks showed a shift to 1007 and 1421 cm^{-1} respectively as visible from the scale enlarged FT-IR spectra given in figure-4.21(a) & (b). This gave evidence for the successful hydrogen bonding of phenol group of **PDP-UNBI** to pyridine unit of P4VP and thus the formation of **P4VP(PDP-UNBI)$_{1.0}$** supramolecule was confirmed. It was also noted that the relative intensities of the hydrogen bonded pyridine band at 1007 cm^{-1} increased systematically as the chromophore content was increased from 25 % to 100 % with concomitant steady vanishing of free pyridine band at 993 cm^{-1}. Similarly there was a gradual shift in the 1413 cm^{-1} band on moving from **P4VP(PDP-UNBI)$_{0.25}$** to **P4VP(PDP-UNBI)$_{1.0}$** (figure-4.22 (a) & (b)).

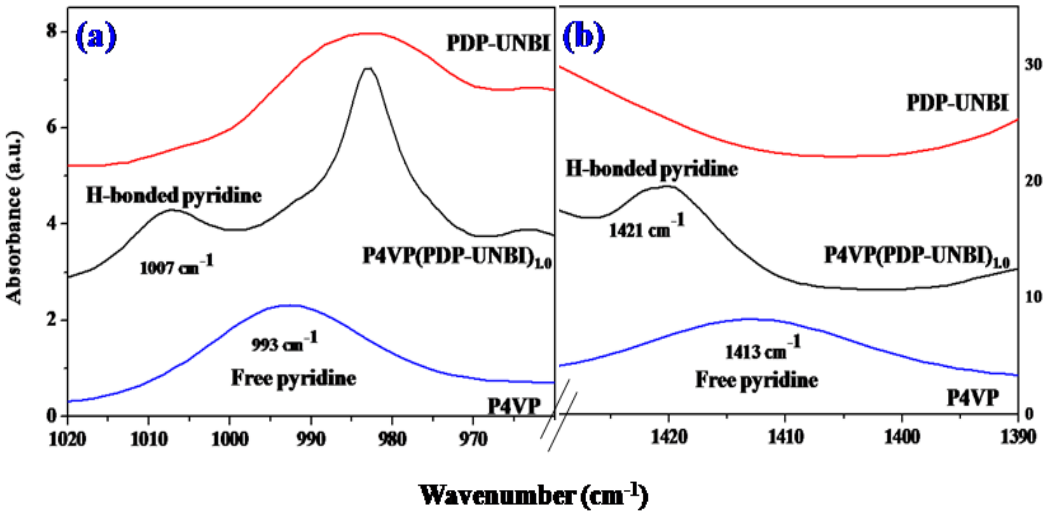

Figure-4.21. FT-IR spectra of P4VP, **PDP-UNBI** and **P4VP(PDP-UNBI)$_{1.0}$** in the regions (a) 1020 to 990 cm^{-1} and (b) 1430 to 1390 cm^{-1}.

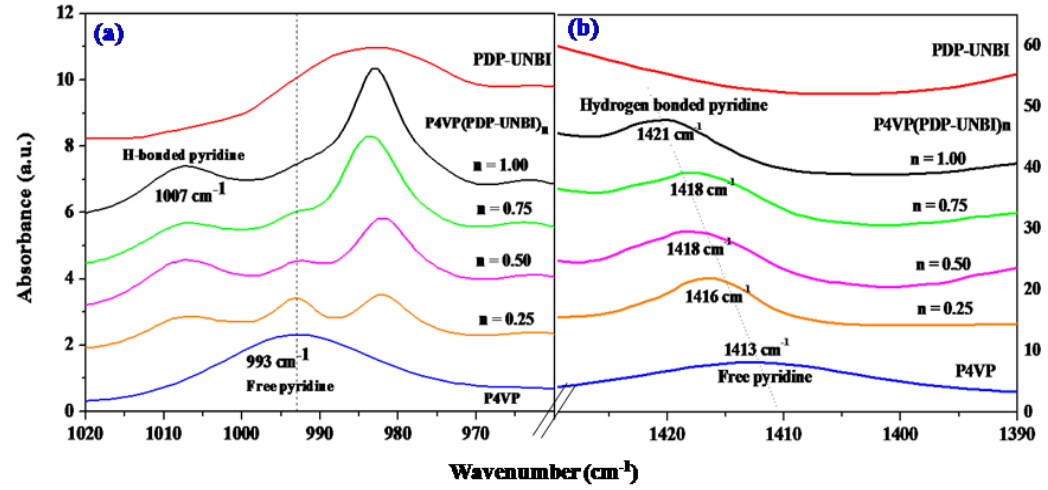

Figure-4.22. FT-IR spectra of P4VP, **PDP-UNBI** and **P4VP(PDP-UNBI)$_n$** (n = 0.25,0.50, 0.75 and 1.00) in the regions (a) 1020 to 990 cm^{-1} and (b) 1430 to 1390 cm^{-1}.

Hydrogen bonding in the random co-comb polymers **P4VP(UNBI$_m$/UPBI$_n$)$_{1.0}$** were also confirmed through a similar infrared studies. Figure-4.23(a) & (b) shows the magnified regions of FT-IR absorption spectra for the set of random co-polymers **P4VP(UNBI$_m$/UPBI$_n$)$_{1.0}$**, where the ratio m/n was

varied with values 0.50/0.50, 0.25/0.75 and 0.75/0.25. In these set of complexes, the free pyridine bands at 993 cm^{-1} and 1413 cm^{-1} got vanished completely and shifted new peaks around 1007-1004 cm^{-1} and 1420-1419 cm^{-1} respectively appeared. This verified the formation of **P4VP(UNBI$_m$/UPBI$_n$)$_{1.0}$** random co-comb polymers via hydrogen bonding between phenol and pyridyl functional groups.

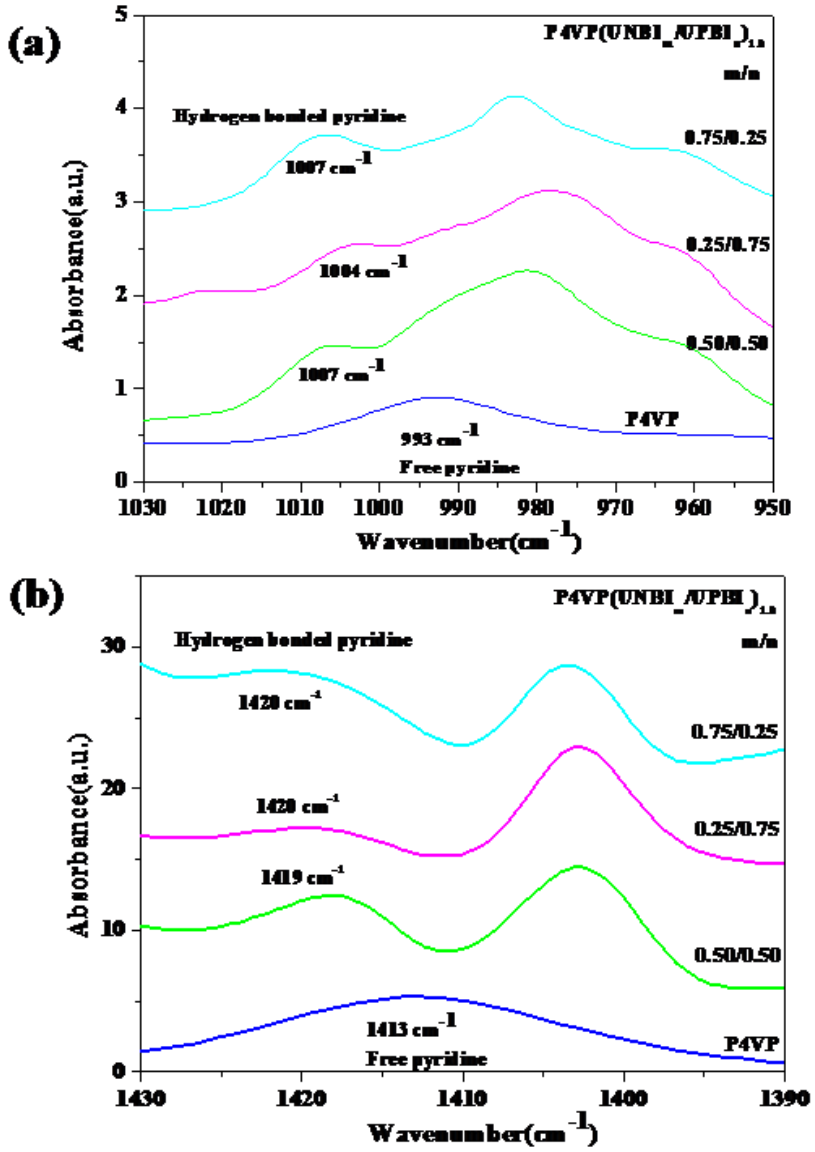

Figure-4.23. FT-IR spectra of **P4VP(UNBI$_m$/UPBI$_n$)$_{1.0}$**, with m/n = 0.50/0.50, 0.25/0.75 and 0.75/0.25 recorded in the regions (a) 1020 to 990 cm^{-1} and (b) 1430 to 1390 cm^{-1}.

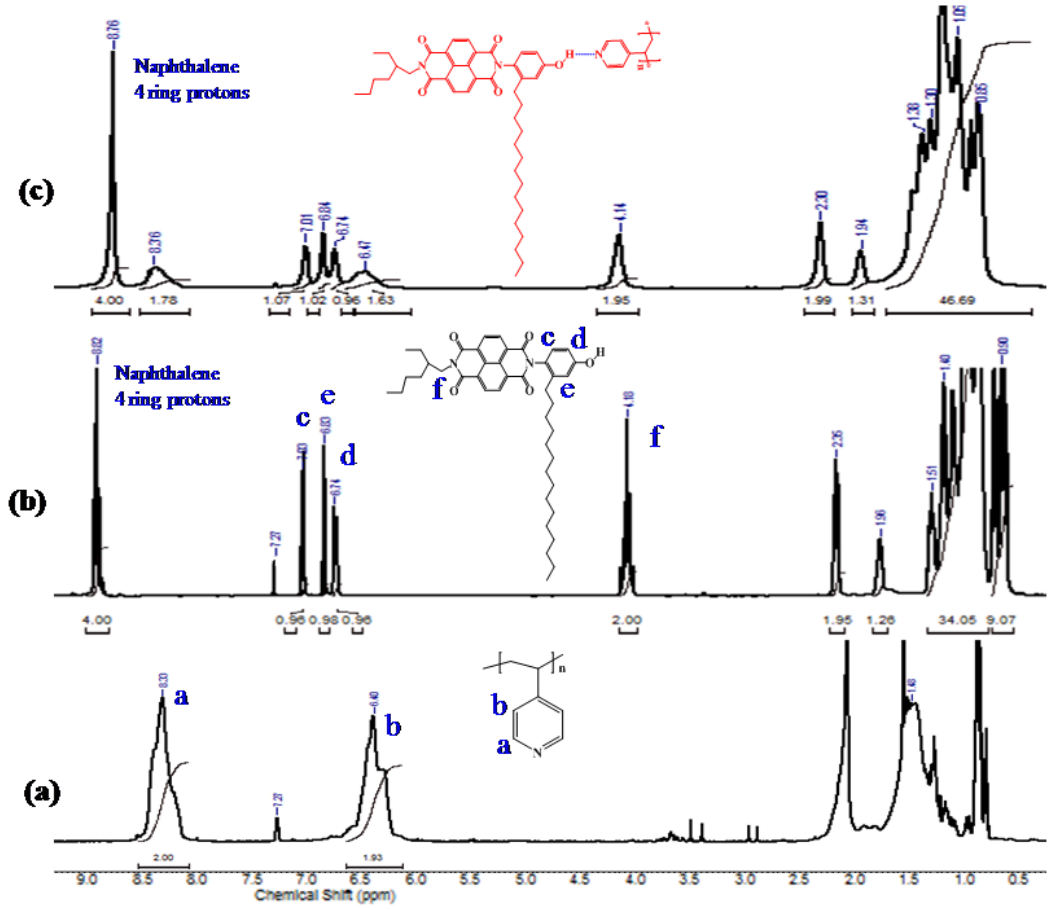

Figure-4.24. ^{1}H-NMR spectra of (a) P4VP (b) **PDP-UNBI** and (c) **P4VP(PDP-UNBI)$_{1.0}$** recorded in $CDCl_3$ at room temperature.

The supramolecular interaction between the **PDP-UNBI** and P4VP in the **P4VP(PDP-UNBI)$_n$** complexes were further probed by ^{1}H-NMR spectroscopy. Figure-4.24 illustrates a comparison of the ^{1}H-NMR spectra of **P4VP(PDP-UNBI)$_{1.0}$** with that of neat constituents P4VP and **PDP-UNBI**, all recorded at a concentration of 20 mg/mL in deuterated chloroform ($CDCl_3$) solution at ambient temperature. In comparison to the proton NMR spectra of **PDP-UNBI,** first striking observation was the peak broadening found for all the protons in the 1:1 **P4VP(PDP-UNBI)$_{1.0}$** complex including the aliphatic protons, which is typically found for high molecular weight polymeric materials. The protons that are directly influenced by the hydrogen bonding between phenol group of PDP unit and the

ring protons of pyridine unit in P4VP alone are labelled (rest of the aliphatic protons of **PDP-UNBI** were labelled and fully explained in section 4.3.1). Of these the pyridine ring protons labelled 'a' and 'b' underwent a deshielded shift from 8.33 to 8.66 ppm and 6.42 to 6.47 ppm respectively which is caused by the involvement of nitrogen atom lone pair of electrons in hydrogen bonding with phenol-OH of **PDP-UNBI**. Another important observation was that the four naphthalene ring protons located around 8.82 ppm in the small molecule moved upfield to 8.76 ppm in the 1:1 complex, which gave indirect evidence for the increased extent of association of the naphthalene core, because upfield chemical shift of fused aromatic ring protons occurs as a result of the "ring current" effect generated by neighboring rings in close proximity as in a self-assembled π-stack.[77-79]

The extent of association in **P4VP(PDP-UNBI)$_n$** as a function of 'n' was also studied by proton NMR spectroscopy, where n = 0.25, 0.50, 0.75 and 1.00. Figure-4.25 shows the expanded aromatic region of the ^{1}H-NMR spectra of **P4VP(PDP-UNBI)$_n$** complexes from 6.00 to 9.00 ppm where the effect of self assembly is reflected the most when recorded in $CDCl_3$ at room temperature. As observed in the case of perylenebisimide based **P4VP(PDP-UPBI)$_n$** complexes described in the previous chapter, here also it was confirmed that when the stoichiometry of hydrogen-bondable surfactant to the pyridine unit is below 1.00, unarguably there exists more domains of un-complexed or free pyridine units and it is only in the stoichiometrically balanced 1:1 complex that each pyridine ring could be considered to be associated nominally with one surfactant molecule. This is evident from the figure-4.25, where it could be seen that only in the **P4VP(PDP-UNBI)$_{1.0}$** 1:1 complex, the integration value of 4 corresponding to four naphthalene core protons matched in intensity to 2 each for the two sets of pyridine ring protons ‘a’ and ‘b’ of P4VP at 8.33 and 6.42 ppm respectively. For all other values of 'n' corresponding to integration value 4 for NBI core protons, the pyridine proton integrations came more than 2, which indicated that for systems **P4VP(PDP-UNBI)$_n$** with n = 0.25, 0.50 or 0.75, at any given instant all the pyridine units of P4VP chain are not involved in hydrogen bonding. Furthermore, the naphthalene

core protons in the δ region from 8.78 - 8.87 ppm, were split into multiplets for the complexes **P4VP(PDP-UNBI)$_n$** with imbalanced pyridine to **PDP-UNBI** stoichiometry (n<1), whereas an overall broadened peak was observed for the 1:1 complex pointing towards strong aggregation of the naphthalene cores when each pyridine unit of the polymer chain is associated with one **PDP-UNBI** molecule.

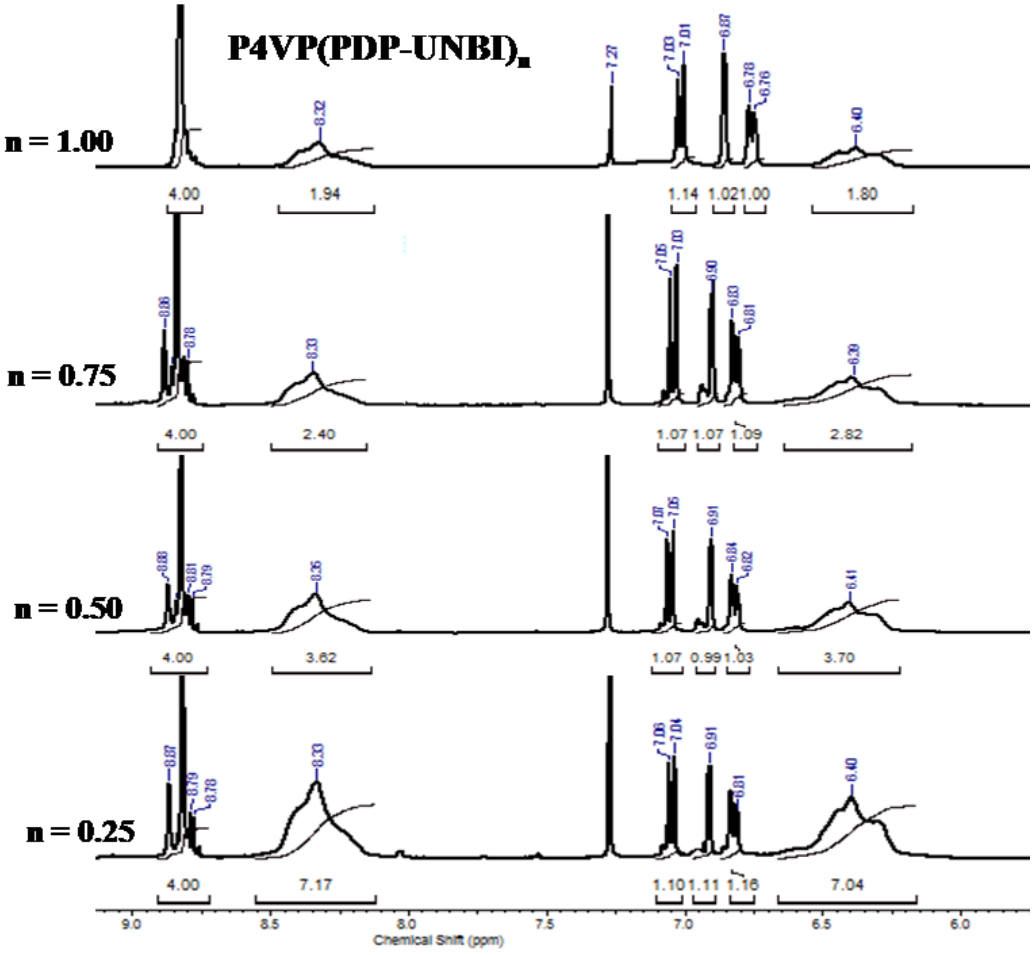

Figure-4.25. Expanded aromatic region of ^{1}H-NMR spectra of **P4VP(PDP-UNBI)$_n$** recorded in $CDCl_3$ at room temperature as a function of n = 0.25, 0.50, 0.75, 1.00.

4.3.4. Photophysical Properties of the Complexes

The molecular interactions in the **PDP-UNBI** appended supramolecular comb-polymeric systems were investigated by UV-vis absorption and fluorescence emission spectroscopic studies. The **PDP-UNBI** small molecule as well as its 1:1 complex with P4VP showed very high solubility in most organic solvents like $CHCl_3$, DCM, Toluene, THF, MCH (methylcyclohexane) etc. In the present study the two common solvents of opposite polarity viz., $CHCl_3$ and MCH were chosen for the investigation of optical properties as a tool to probe the molecular organization of NBI chromophore within the comb-polymer supramolecular assembly. Both **PDP-UNBI** and **P4VP(PDP-UNBI)$_{1.0}$** showed sharp well resolved absorption bands at 380, 360, 342 nm corresponding to the 0-0, 0-1 and 0-2 vibronic transitions respectively, characteristic of molecularly dissolved monomeric type NBI chromophores in an extremely dilute 0.1OD (optical density) solutions in $CHCl_3$ with absorption maxima at 380 nm.[3] However in non-polar MCH solution, the absorption maxima showed a gradual blue shift of the λ_{max} (5 nm shift, 380 to 375 nm) for both **PDP-UNBI** and **P4VP(PDP-UNBI)$_{1.0}$** with three characteristic peaks at 375, 355, 337 nm. Figure-4.26 shows the normalized absorption spectra of 0.1 OD solutions of **PDP-UNBI** in $CHCl_3$ and MCH. (**P4VP(PDP-UNBI)$_{1.0}$** exhibited exactly same spectra and therefore not shown here).

Comparing the corresponding fluorescence emission spectra, the MCH solution of both **PDP-UNBI** and **P4VP(PDP-UNBI)$_{1.0}$** exhibited complete quenching of fluorescence, while the $CHCl_3$ solutions showed emission peaks at 404, 432 and 460 nm respectively, keeping mirror image relationship with the absorption spectra and stokes shift value about 24 nm. However, notably the emission in **PDP-UNBI** was highly quenched in comparison to the **P4VP(PDP-UNBI)$_{1.0}$** (Figure-4.27). The blue shifted absorption spectra and quenched fluorescence indicated the presence of H-type aggregates in MCH solution. Hydrogen bonding induced self-organization in these systems would be more

reflected in the solid state than in solution. Therefore the solid state absorption and emission spectra of the samples were analysed from solid thin films obtained by spin coating from corresponding $CHCl_3$ and MCH solutions.

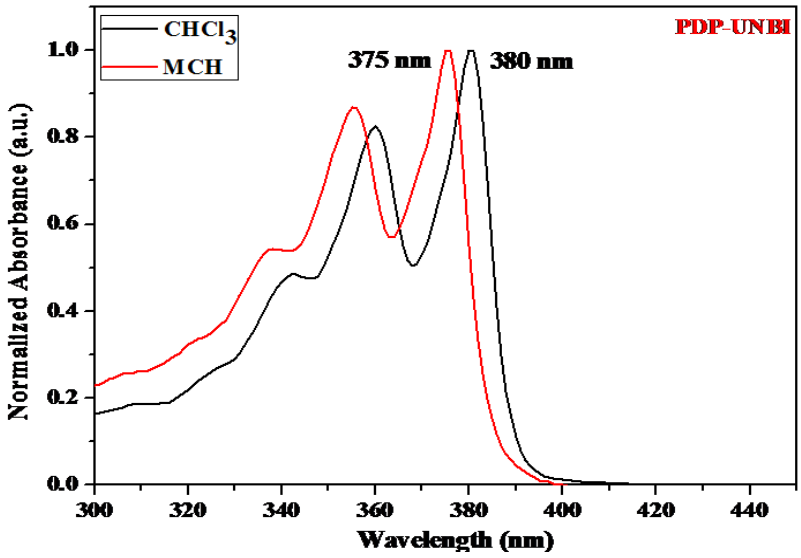

Figure-4.26. Normalized absorption spectra of **PDP-UNBI** recorded in MCH and $CHCl_3$.

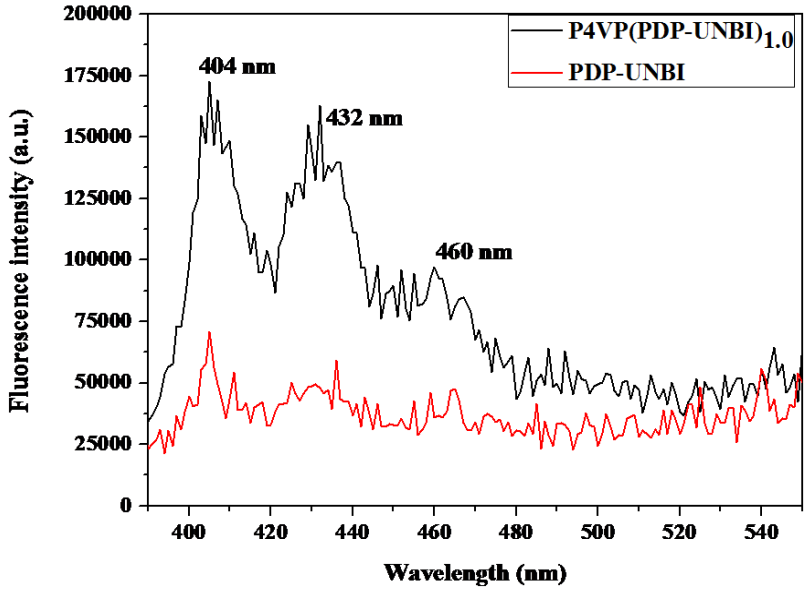

Figure-4.27. Fluorescence emission spectra of **PDP-UNBI** and **P4VP(PDP-UNBI)$_{1.0}$** in $CHCl_3$.

Figure-4.28(a) & (b) shows the combined solid state absorption and emission spectra for **PDP-UNBI** and its 1:1 complex **P4VP(PDP-UNBI)$_{1.0}$** from $CHCl_3$ and MCH solutions. In the solid state both **PDP-UNBI** and **P4VP(PDP-UNBI)$_{1.0}$** showed very similar absorption and emission pattern from $CHCl_3$ as well as MCH. On moving from solution to solid state in MCH, the absorption maxima underwent a red shift from 375 nm to 383 nm, meanwhile the emission spectra was weak and unstructured typical of aggregated species.

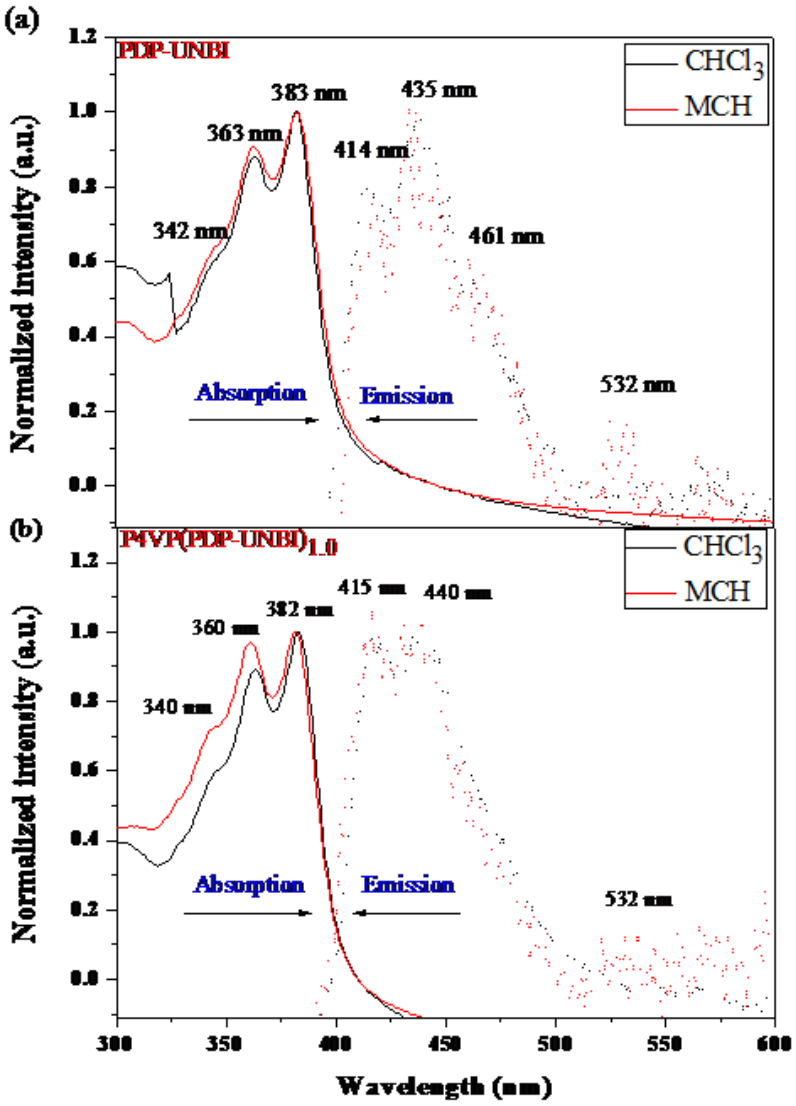

Figure-4.28. Combined solid state Absorption and Fluorescence emission spectra of **PDP-UNBI** and **P4VP(PDP-UNBI)$_{1.0}$** spin coated from $CHCl_3$ and MCH.

The photophysical properties of the random co-comb polymers **P4VP(UNBI$_m$/UPBI$_n$)$_{1.0}$**, with m/n = 0.50/0.50, 0.25/0.75 and 0.75/0.25 were also studied similarly in $CHCl_3$ and MCH solutions. The complete absorption and emission spectra of these co-polymers both in solution and solid state from $CHCl_3$ is given in figure-4.29 and figure-4.30 respectively. The absorption spectra was completely covered from 300-600 nm with NBI core absorbing in the 300-400 nm region and PBI core in the 400-600 nm range. In $CHCl_3$ solution both **PDP-UNBI** and **PDP-UPBI** chromophores exhibited their typical monomeric type of absorption spectra with maxima around 526, 490, 458, 380, 360 and 342 nm irrespective of the m/n ratio of **P4VP(UNBI$_m$/UPBI$_n$)$_{1.0}$** complexes.

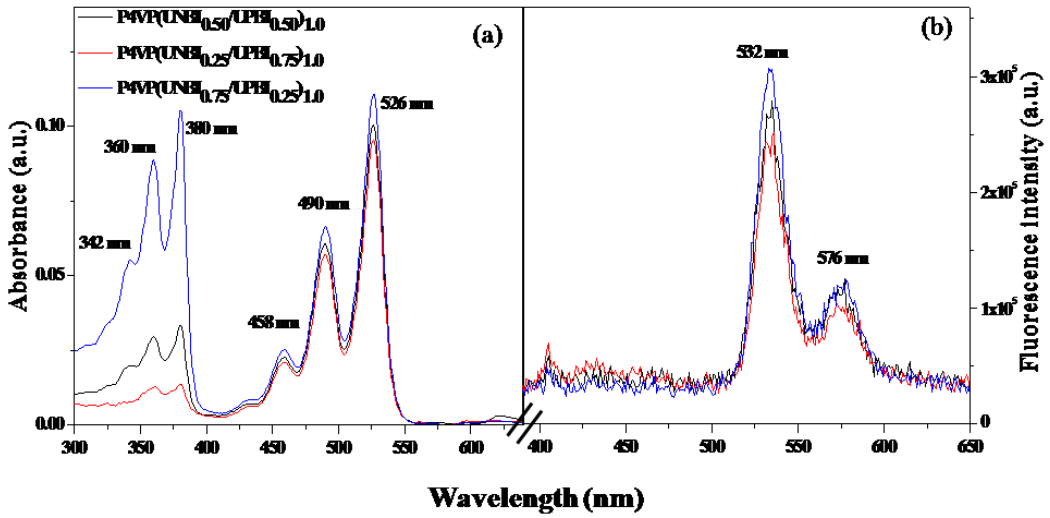

Figure-4.29. Combined solution state (a) absorption and (b) emission spectra of P4VP(UNBI$_m$/UPBI$_n$)$_{1.0}$ random complexes in chloroform.

However in **P4VP(UNBI$_{0.5}$/UPBI$_{0.5}$)$_{1.0}$** where the **PDP-UNBI** and **PDP-UPBI** chromophore content were equal and **P4VP(UNBI$_{0.25}$/UPBI$_{0.75}$)$_{1.0}$** where **PDP-UNBI** content was less than **PDP-UPBI,** the perylene absorption peaks completely dominated that of the naphthalene core. In the **P4VP(UNBI$_{0.75}$/UPBI$_{0.25}$)$_{1.0}$**, where the naphthalene content was more, the absorption spectra demonstrated equal intensities for **PDP-UNBI** and **PDP-UPBI** absorptions. The solid state UV-spectra of these complexes spin coated from

$CHCl_3$ solutions showed some differences (figure-4.30(a)). One common observation was an overall broadening of the vibronic structures corresponding to **PDP-UPBI** absorption, with the λ_{max} blue shifted to 500 nm compared to solution state and concomitant appearance of a red shifted shoulder band at 540 nm which were characteristics of face-to-face stacked rotationally displaced H-type aggregates.[80,81] It is worth mentioning here that the same observation was found for **P4VP(PDP-UPBI)$_{1.0}$** homo-complexes solid films spin coated from $CHCl_3$ solutions (Chapter 3, section 3.2.4).

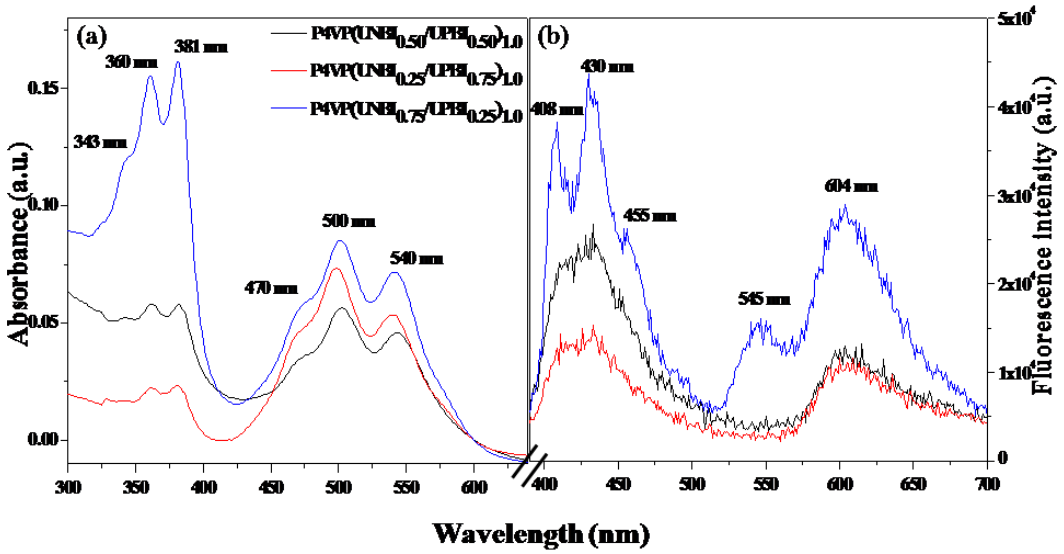

Figure-4.30. Combined solid state (a) absorption and (b) emission spectra of P4VP($UNBI_m$/$UPBI_n$)$_{1.0}$ random complexes spin coated from chloroform ($CHCl_3$).

The emission spectra in solution was marked by the complete absence of emission from naphthalene core. Only monomeric emission from the perylene bisimide was observed. On the other hand, the emission in the solid state exhibited contribution from both naphthalene and perylene chromophores. The co-polymers **P4VP(UNBI$_{0.50}$/UPBI$_{0.50}$)$_{1.0}$** and **P4VP(UNBI$_{0.25}$/UPBI$_{0.75}$)$_{1.0}$**, exhibited broad featureless emission from naphthalene in the range 400 to 480 nm and a reduced characteristic aggregate emission from perylene around 600 nm. The sample **P4VP(UNBI$_{0.75}$/UPBI$_{0.25}$)$_{1.0}$**, was slightly different from the other two copolymers in that it exhibited typical monomeric emission from naphthalene with vibrational

fine structures in the region 408 to 455 nm and both monomeric as well as excimeric emission from perylene in the region 545 and 600 nm respectively. These differences in behavior among the random co-comb polymers would be a reflection of their varied organization within the P4VP template with regions of homo chromophores and regions of mixed chromophores.

Figure-4.31 and figure-4.32 shows the complete absorption-emission spectra of the **P4VP(UNBI$_m$/UPBI$_n$)$_{1.0}$** random complexes in solution and solid state respectively from MCH solvent. In the non-polar MCH solution, the random co-polymers exhibited **PDP-UNBI** core absorptions (figure-4.31(a)) that were blue shifted by ~5 nm, whereas the **PDP-UPBI** absorption pattern became completely unstructured with blue shifted maxima around 503 and 467 nm along with two highly red shifted aggregation bands at 540 and 580 nm respectively. This observation provided evidence for the highly aggregated perylene chromophores existing even in solution state. On moving to the solid state (figure-4.32(a)) the intensity of the aggregation peak at 580 nm increased and rest of the absorption pattern was retained as that in the solution state confirming the complete aggregation.

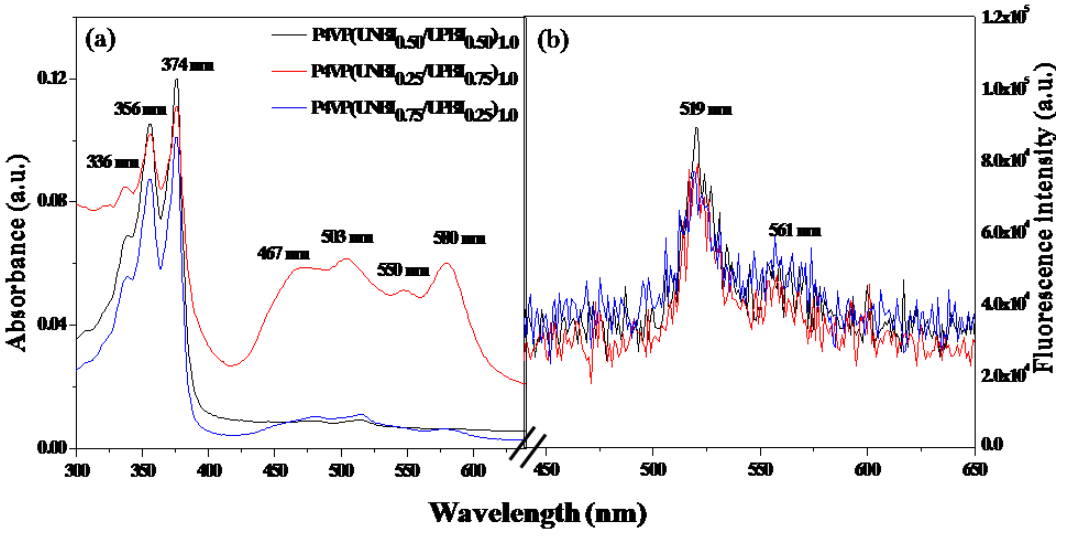

Figure-4.31. Combined solution state absorption and emission spectra of P4VP(UNBI$_m$/UPBI$_n$)$_{1.0}$ random complexes in methylcyclohexane (MCH).

The emission characteristics of all the three random co-polymers from MCH solution (figure-4.31(b)) was similar in features to that from chloroform solution with very weak monomeric emission observed form perylene chromophores with complete absence of emission corresponding to naphthalene. Despite the evidence of aggregated perylene chromophores as indicated by the absorption spectra, the emission spectra did not indicate any signs of aggregation other than an overall quenching. No aggregated emission beyond 600 nm typical of ground state aggregated perylene was observed in the emission spectra recorded in MCH solution. On the other hand the emission in the solid state (figure-4.32(b)) exhibited broad featureless peaks in the range 417 to 438 nm corresponding to naphthalene chromophore emission and ~604 nm corresponding to PBI aggregate emission.

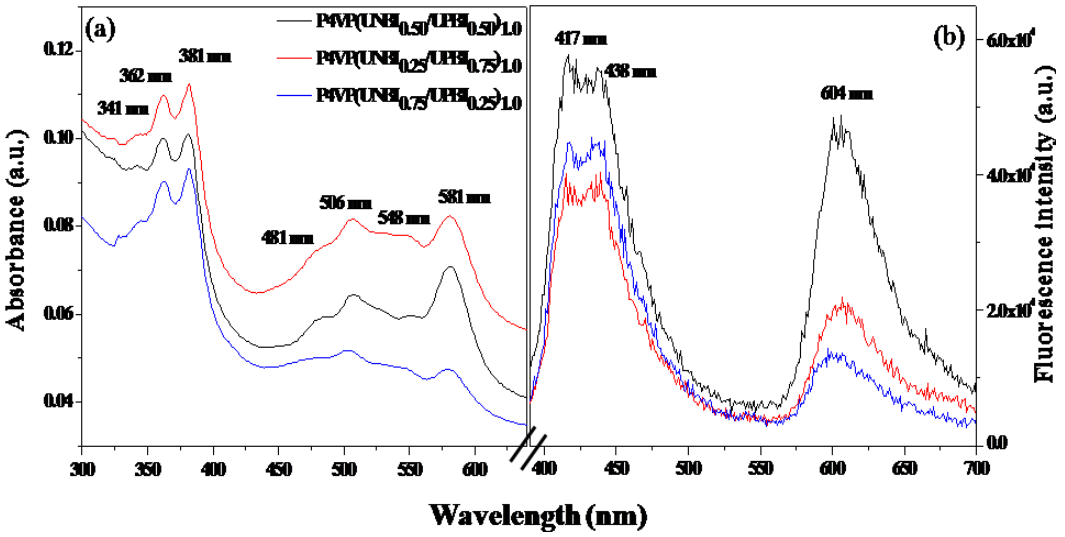

Figure-4.32. Combined solid state absorption and emission spectra of P4VP(UNBI$_m$/UPBI$_n$)$_{1.0}$ random complexes in methylcyclohexane (MCH).

The absence of emission from naphthalene in the solution state both in chloroform as well as MCH, indicated energy transfer occurring from naphthalene to perylene upon exciting at the naphthalene absorption wavelength maxima in solution. On the other hand, regions of homo aggregated domains would hinder or reduce such energy transfer in the solid state. From the combined solid state

absorption and emission spectra it was concluded that in the **P4VP(UNBI$_m$/UPBI$_n$)$_{1.0}$** random co-comb polymers the **PDP-UPBI** molecules undergo very strong π-π stacked H-type aggregation leading to weakly emitting crystal phase from MCH solutions, while the **PDP-UNBI** molecules in these aggregates appeared to be arranged in a J-type fashion as evident from the aggregation induced emission in the solid state. Also in this set of complexes there may be isolated domains of **PDP-UNBI** or **PDP-UPBI** homo-aggregates as well as their hetero-aggregated domains which are difficult to distinguish.

4.3.5. Structural Analysis of the Self-assembled Comb-polymer Complexes

(a) Small Angle and Wide Angle X-ray diffraction studies

Polymeric comb-architectured supramolecules are found to exhibit different self-assembled structures which could be typical lamellar type organization as in the case of homopolymeric comb-complex of P4VP with pentadecylphenol (PDP) or nonadecylphenol (NDP)[68,82] or cylindrical structures formed by semirigid polyaniline simultaneously complexed electrostatically with camphor-sulphonic acid as well as via hydrogen bonding to hexylresorcinol[83] or even ordered hexagonal self-organization obtained as in the case of multi-comb polymer complex of P4VP with $Zn(DBS)_2$ (Zinc-dodecylbenzene sulphonate) and 2,6-bis(octylaminomethyl pyridine) via coordination and electrostatic interactions and so on.[84] A combination of block copolymers with such comb-shaped supramolecules potentially gives rise to hierarchically structured materials.[82] The self-organized phases of the supramolecular comb-complexes can be tuned, in principle by varying the size of the side-chain surfactants and a control of the steric crowding could also be achieved. But such a fine tuning indirectly also affects different aspects of the complexes such as the packing of the surfactant molecules amidst the polymer domains, the overall repeat distances etc. However the perylenebisimide appended **P4VP(PDP-UPBI)$_{1.0}$** complex, studied in the previous chapter, was found to form self-organized lamellar phases in the 5-10 nm size range. Consequently, the **P4VP(PDP-UNBI)$_{1.0}$** with the structurally similar smaller

analogue naphthalenebisimide was also expected to undergo microphase separation with same kind of morphology. Both small angle and wide angle X-ray diffraction measurements were conducted to analyze the self-assembled structures formed by the **PDP-UNBI** based supramolecular comb-polymers. Figure-4.33 shows the small angle XRD trace of the **P4VP(PDP-UNBI)$_{1.0}$** from 2θ = 2-5° and it is compared with that of **P4VP(PDP-UNBI)$_{0.25}$** which had lowest loading of **PDP-UNBI** such that only 25% of the pyridine rings were engaged in hydrogen-bonding at any given instant. The neat constituents P4VP and **PDP-UNBI** are also considered for comparison as a reference. As already known, due to its amorphous nature, neat P4VP does not show any peak in the low angle region. Notably for all the other samples there were no peaks found lower than angle 2θ = 2°. Generally in the bulk materials the small molecule surfactants undergo ordering at relatively small length scale of approximately 2-5 nm range.

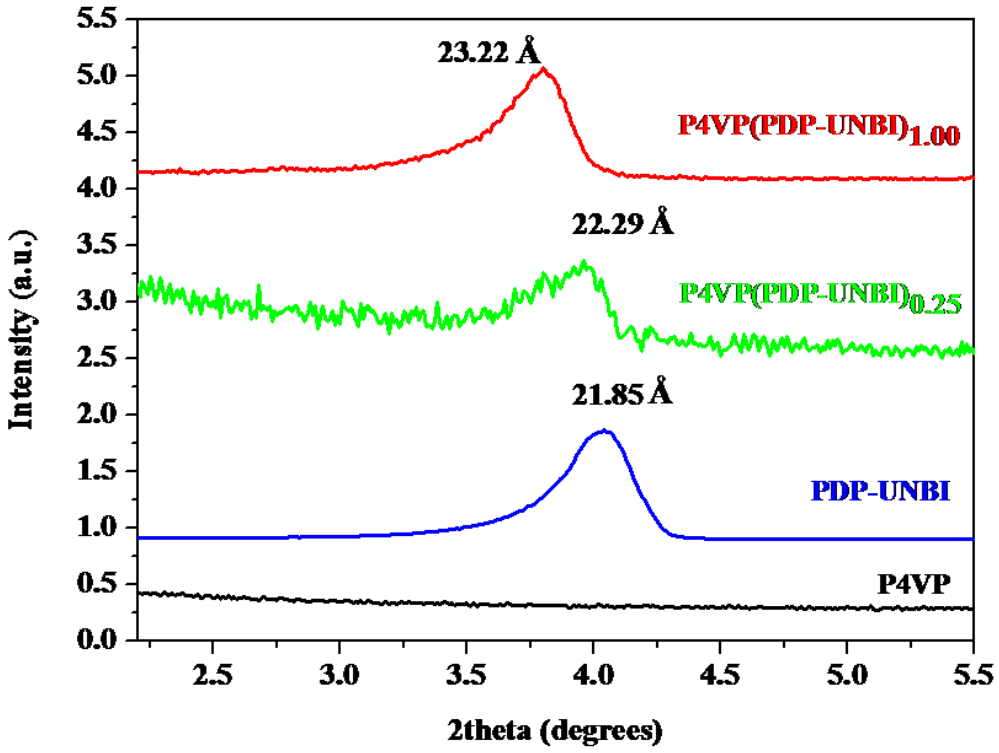

Figure-4.33. Small angle XRD trace of **P4VP(PDP-UNBI)$_{1.0}$** compared with that of pure P4VP, **PDP-UNBI** and **P4VP(PDP-UNBI)$_{0.25}$** recorded at room temperature, with d-spacing values given nearby the peaks.

The intensity curve of pure **PDP-UNBI** shows a diffraction maximum around 2θ = 4.04° corresponding to the fundamental packing distance of 21.85 Å, calculated using Bragg's equation, nλ = 2dSinθ where λ is the wavelength of X-ray i.e., 1.54 Å, d is the spacing between the reflecting planes and 2θ is the diffracting angle. For the **P4VP(PDP-UNBI)$_{0.25}$** sample, where only 25 % of the pyridine rings are complexed with **PDP-UNBI**, the packing distance slightly increased to 22.29 Å, whereas the fully complexed **P4VP(PDP-UNBI)$_{1.0}$** sample had a periodicity length around 23.22 Å which was ~1 Å larger than that of the neat **PDP-UNBI**. The layering distance of these supramolecular structures depend upon a delicate balance between the surfactant-polymer interaction and entropic penalty associated with the polymer chain conformational restrictions imposed upon incorporation of the surfactant molecules to the polymer chains otherwise adopting a coiled conformation. Upon attachment of the surfactants by attractive hydrogen-bonding interactions, the polymer chains are proposed to suffer a stiffening of the chains induced by the additional ordering or crystallization of these surfactant molecules which determines the repeat distance of the layers. The WAXS data recorded from 2θ = 2 -15° for the same set described above is given in figure-4.34.

From the WAXS data it could be seen that **P4VP(PDP-UNBI)$_{1.0}$** showed almost equally spaced peak patterns typical of microphase separated lamellar phase with Bragg reflections following the ratio 1: 1/2 : 1/3 : 1/4 : 1/5 at 3.80° (23.22Å), 7.76° (11.37Å), 10.25° (8.61Å), 11.89° (7.42Å), 14.42° (6.12Å) respectively. Notably the **PDP-UNBI** small molecule also exhibited similar layered structure and the difference between the two being the different layer spacing values. The magnified region from 2θ = 6 -15° in figure-4.34 clarifies the reflections at higher multiples. The detailed calculated and observed interlayer spacing distances (in Å) with the corresponding 2θ values tabulated from the WAXS results are given in table-4.1.

When analysed carefully it was found that the stoichiometric 1:1 complex **P4VP(PDP-UNBI)$_{1.0}$** had the observed d-spacing values more closer to the

perfectly layered structure upto the fifth order diffraction peak confirming lamellar phase with long range orientation and order. Interestingly in the lowest chromophore loaded sample namely **P4VP(PDP-UNBI)$_{0.25}$** the peak corresponding to the second order reflection was found to be completely absent. This provided the hint regarding the existence of some extent of disorder in the system when the un-complexed P4VP domains were more. In particular it proved that in these hydrogen bonded complexes the P4VP and **PDP-UNBI** domains were not macrophase separated. Thus it could be concluded that the **P4VP(PDP-UNBI)$_{1.0}$** complex forms a microphase separated lamellar structure with alternating P4VP and **PDP-UNBI** layers with the overall conformation of each layer being affected by one another in a synergistic manner.

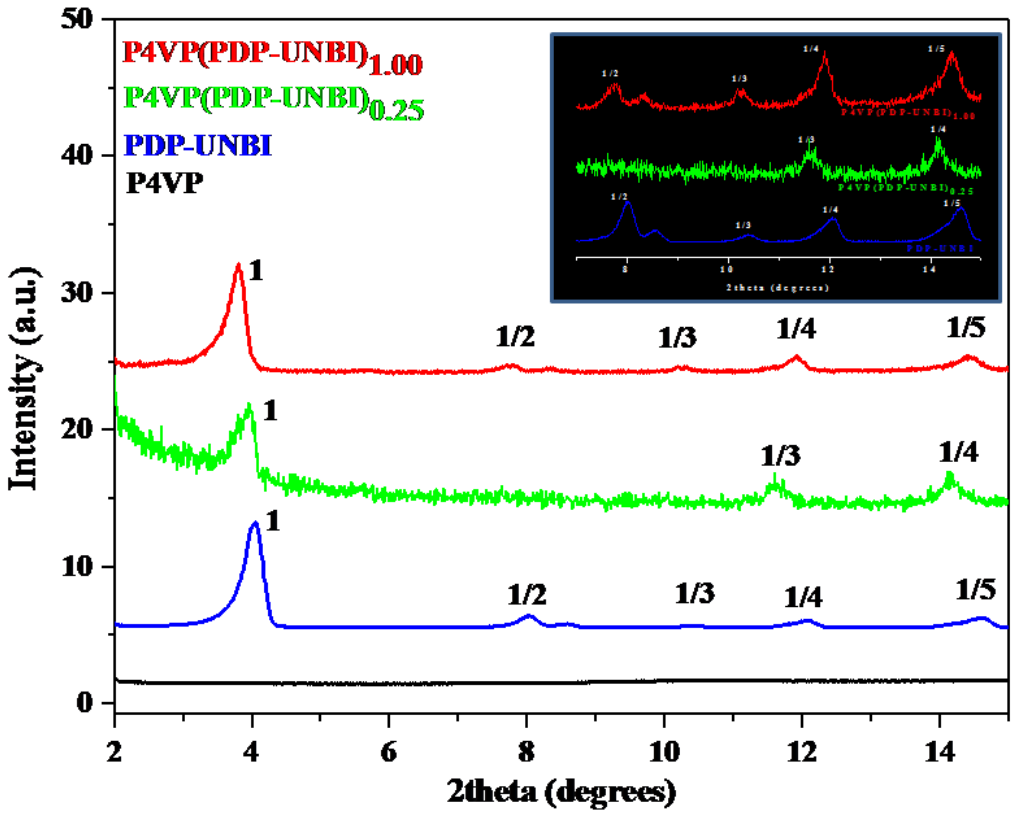

Figure-4.34. WAXS data showing the layered structure of **P4VP(PDP-UNBI)$_{1.0}$** and compared with that of pure P4VP, **PDP-UNBI** and **P4VP(PDP-UNBI)$_{0.25}$**. (Inset shows the magnified region from 2θ = 6 -15°).

Table-4.1. Interplanar **d**-spacing and **2θ** values of the layered structures for **P4VP(PDP-UNBI)$_n$** (n = 0.25 & 1.00) complexes and **PDP-UNBI** from the WAXS data recorded at room temperature (25 °C).

Sample	Peak 1		Peak 2		Peak 3		Peak 4		Peak 5	
	2Θ [^{0}]	d [Å]	2Θ [^{0}]	d [Å]	2Θ [^{0}]	d [Å]	2Θ [^{0}]	d [Å]	2Θ [^{0}]	d [Å]
PDP-UNBI	4.02	21.85	8.01	11.02 (10.93)*	10.04	8.49 (7.28)*	12.08	7.31 (5.46)*	14.60	6.04 (4.37)*
P4VP(PDP-UNBI)$_{0.25}$	3.95	22.29	-	-	11.59	7.60 (7.43)*	14.15	6.24 (5.57)*	17.27	5.11 (4.46)*
P4VP(PDP-UNBI)$_{1.00}$	3.80	23.22	7.76	11.37 (11.61)*	10.25	8.61 (7.74)*	11.89	7.42 (5.81)*	14.42	6.12 (4.65)*

* The values in the bracket correspond to the calculated d-spacing at ratios 1/2, 1/3, 1/4..etc with respect to the fundamental reflection in the case of each sample.

Further the mesomorphic structures of these complexes at much lower length scales were examined from the complete WXRD pattern from 2θ = 5 -30° given in figure-4.35. In the wide angle range 2θ = 5 -30° the **PDP-UNBI** had large number of reflections consistent with the highly crystalline nature of this small molecule, whereas the amorphous nature of P4VP was evident from two broad halos around 2θ values 10° and 20°. But the amazing result was that when this crystalline small molecule was incorporated into side chains of amorphous P4VP via attractive hydrogen bonding interactions, the resulting 1:1 complex became all the more crystalline or in other words the overall ordering was drastically improved as evident from the multitude of sharp reflections that emerged in the region 2θ = 16 -28°, many of which were absent in the neat **PDP-UNBI**. Several new peaks that appeared included packing distances around 5.07Å (17.39°), 4.75Å (18.57°), 4.34Å (20.32°), 4.16Å (21.21°), 3.82Å (23.09°), 3.61Å (24.48°), 3.43Å (25.67°) and 3.26Å (27.11°). When the mole fraction of **PDP-UNBI** versus P4VP repeat unit was reduced from 1.00 to 0.25, the wide angle region exhibited several faint

crystalline reflections in addition to amorphous character possibly due to the dominating P4VP domains in the **P4VP(PDP-UNBI)$_{0.25}$** sample. This again proved that **PDP-UNBI** and P4VP domains were not independent of each other. The packing behaviour of the random co-complexes **P4VP(UNBI$_m$/UPBI$_n$)$_{1.0}$** (m/n = 0.5/0.5, 0.25/0.75, 0.75/0.25) were also analysed in a similar manner.

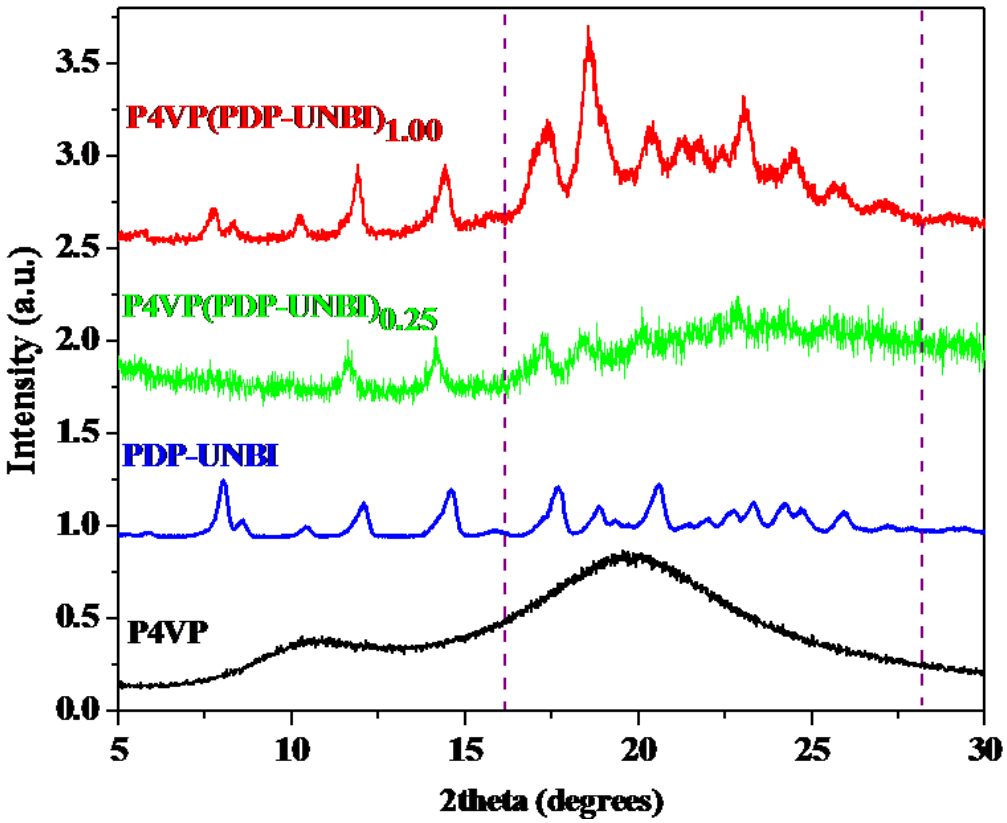

Figure-4.35. Wide angle XRD trace from 2θ = 5 -30° of **P4VP(PDP-UNBI)$_{1.0}$** compared with that of pure P4VP, **PDP-UNBI** and **P4VP(PDP-UNBI)$_{0.25}$** recorded at room temperature.

Figure-4.36 depicts the low angle XRD trace of the random co-complexes of **PDP-UNBI/ PDP-UPBI** and compared with that of their corresponding homo-complexes viz., **P4VP(PDP-UNBI)$_{1.0}$** and **P4VP(PDP-UPBI)$_{1.0}$** respectively. All of the random co-comb polymers irrespective of the relative **PDP-UNBI/PDP-UPBI** ratio showed fundamental periodicity length greater than that of the homo-comb polymer **P4VP(PDP-UPBI)$_{1.0}$**. This seemed to be quite reasonable because

in a random mixture of bigger sized **PDP-UPBI** and smaller sized **PDP-UNBI** with all combinations of random arrangements possible, the final average packing distance would predominantly be determined by the bigger sized chromophore. In accordance with the same logic it was also found that amongst the three random co-polymers, the one with relatively highest loading of **PDP-UPBI** molecule namely the **P4VP(UNBI$_{0.25}$/UPBI$_{0.75}$)$_{1.0}$** complex exhibited the largest periodicity of 34.33Å, while the other two co-polymers had more or less the same periodicity.

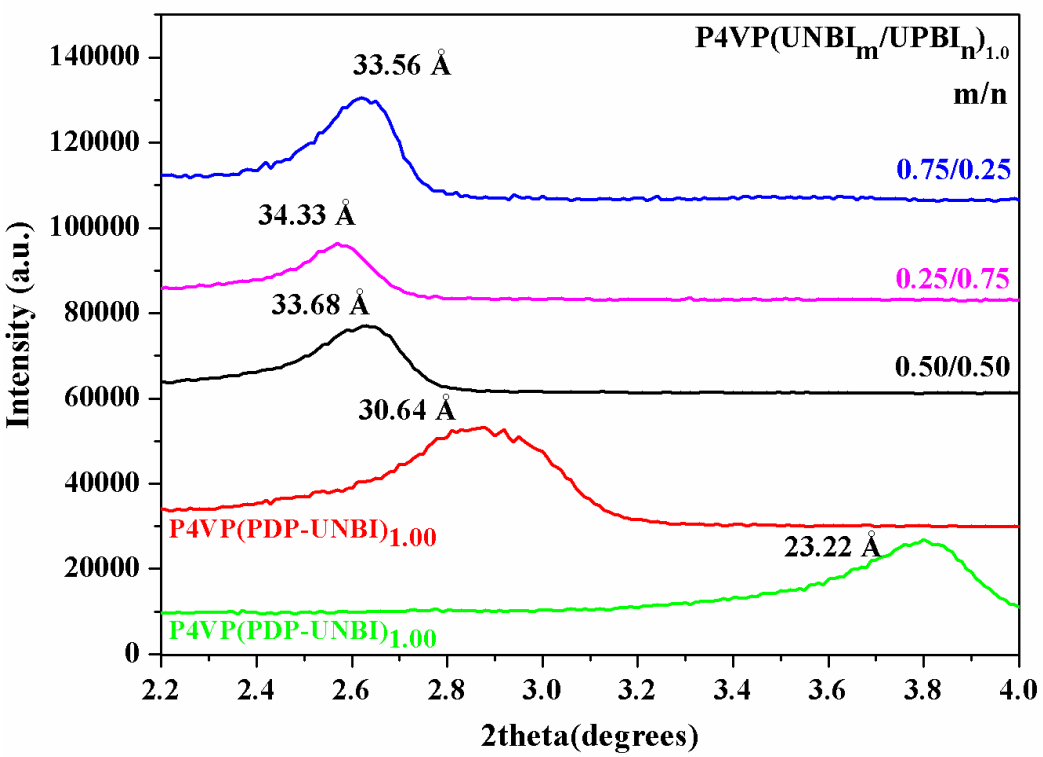

Figure-4.36. Low angle XRD trace of **P4VP(UNBI$_m$/UPBI$_n$)$_{1.0}$** (m/n = 0.5/0.5, 0.25/0.75, 0.75/0.25) and compared with that of **P4VP(PDP-UNBI)$_{1.0}$** and **P4VP(PDP-UPBI)$_{1.0}$.**

The WXRD data for the same set of random co-polymers as above mentioned is given in figure-4.37. Good extent of crystallinity was observed in all the samples, with lowest extent visible in the **P4VP(UNBI$_{0.75}$/UPBI$_{0.25}$)$_{1.0}$** complex which contained more amount of **PDP-UNBI** than **PDP-UPBI**. But surprisingly the wide angle region of all the three **P4VP(UNBI$_m$/UPBI$_n$)$_{1.0}$** samples showed

very close resemblance to that of the **P4VP(PDP-UPBI)$_{1.0}$** homo-comb polymer only, with no reflections related to homo stacks of **P4VP(PDP-UNBI)$_{1.0}$** observed. One possible explanation might be that due to the smaller size of **PDP-UNBI** molecule and its structural similarity to **PDP-UPBI**, the naphthalene chromophore could have efficiently been intercalated into strongly aggregating perylene stacks via inter-chromophore π-π stacking interactions.

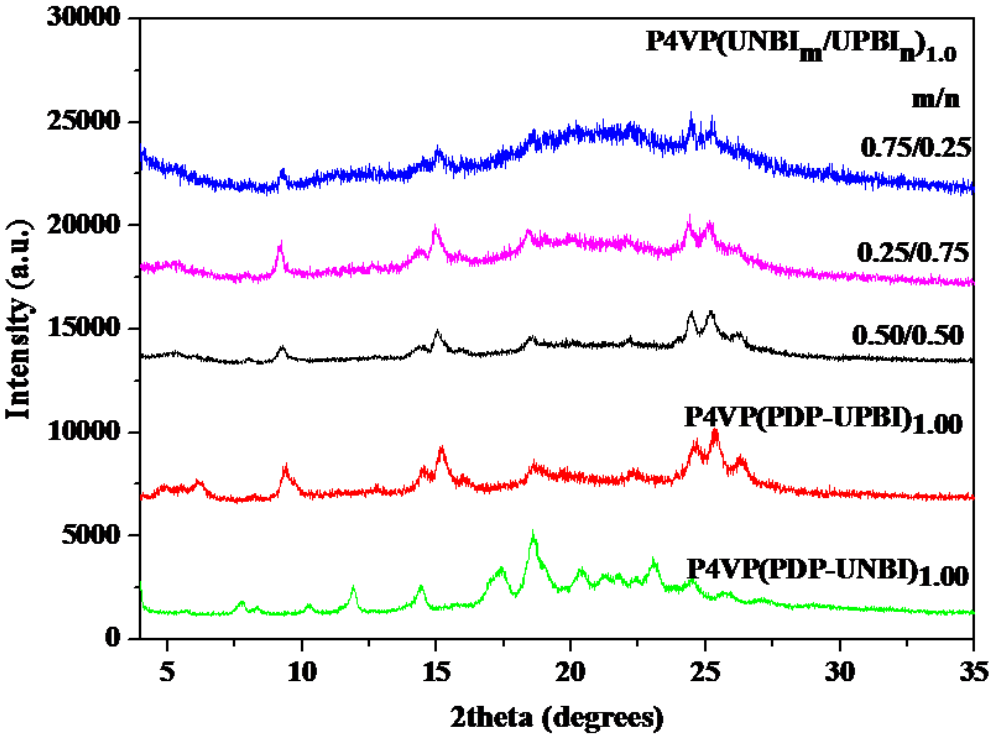

Figure-4.37. WXRD data of **P4VP(UNBI$_m$/UPBI$_n$)$_{1.0}$** (m/n = 0.5/0.5, 0.25/0.75, 0.75/0.25) and compared with that of **P4VP(PDP-UNBI)$_{1.0}$** and **P4VP(PDP-UPBI)$_{1.0}$**.

(b) Single Crystal XRD studies

The molecular conformation of a single surfactant unit is very important, since it determines the further overall packing in the bulk structure and the variations thereafter bestowed by hydrogen bonding with P4VP chains. Compared to the perylenebisimide small molecules the naphthalenebisimides are easy to crystallize taking advantage of their smaller cores. Thus in order to shed more light on the

packing motifs in the hydrogen bonded supramolecular polymer complexes, single crystals of **PDP-UNBI** small molecule were grown. This was taken as a model or control study, because it is well known that relative orientation of the substituents at the imide nitrogen of NBIs greatly affect the molecular packing, morphology and hence the charge transport property.[85]

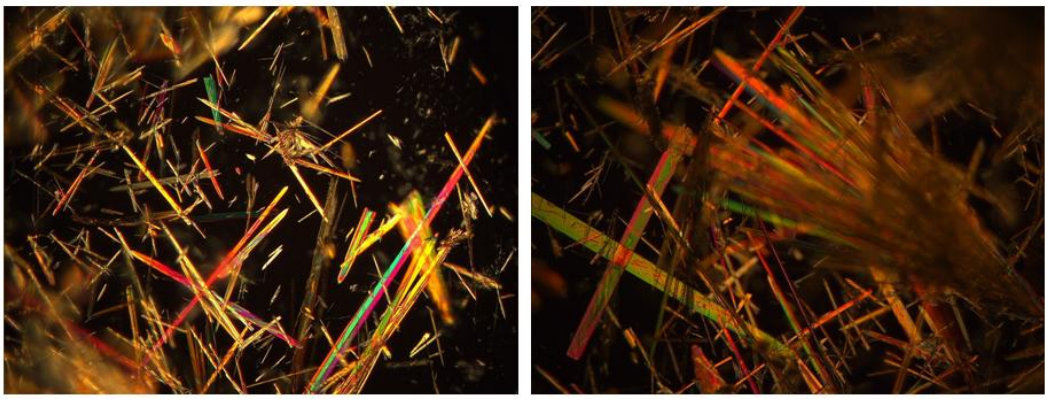

Figure-4.38. Optical microscopy images of thin and needle-like **PDP-UNBI** single crystals grown from DMF solution.

Single crystals of **PDP-UNBI** were in fact readily obtained from saturated solutions in organic solvents $CHCl_3$, DMF and THF with a growth period of 1-2 weeks. However irrespective of the solvent used, the crystals formed were extremely thin needle-like and often grew in bunches, such that single crystals for XRD analysis were taken by cutting. Optical microscope images of the yellow needle like **PDP-UNBI** crystals grown from saturated DMF solution that were used for single crystal XRD analysis are shown in figure-4.38. The poor diffraction from the thin crystals was very well reflected in the structure refinement data also. The rigid aromatic cores could easily be solved with good precision, but the long $C_{15}H_{31}$ alkyl chain of the PDP group showed high degrees of flexibility such that it was difficult to fix the electron densities beyond 6^{th} carbon atom of the chain, even when the measurements were conducted at low temperature. However since the present study required more focus on the packing of rigid aromatic core involved in hydrogen bonding, the obtained crystallographic data was analysed to get an

approximate packing picture existing in the small molecule alone. According to the single crystal XRD pattern the crystallization of **PDP-UNBI** was best indexed on an orthorhombic unit cell with dimensions a = 20.076 Å; b = 49.223 Å; c = 8.695 Å and a molecular length of 14.104 Å along the rigid aromatic cores. The complete crystallographic data for the **PDP-UNBI** molecule is listed in table-4.2.

Table-4.2. Crystallographic data and Structure refinement summary.

Compound	**PDP-UNBI** (phenol)
Empirical formula	$C_{43}H_{56}N_2O_5$
Crystal color, habit	Yellow thin needles
Preparation	Recrystallization from DMF
Temperature	100 K
Crystal system	Orthorhombic
Space group	Iba2
Unit cell dimensions	a = 20.076(8) Å b = 49.223(19) Å c = 8.695(3) Å α = β = γ = 90°
Volume	8592(6) $Å^3$
Density (calculated)	1.096 Mg/m^3
Z	8
Theta range for data collection	0.83 to 22.14°
Reflections collected	44362
Independent reflections	5240 [R(int) = 0.1967]
Refinement method	Full-matrix least-squares on F^2
Goodness-of-fit on F^2	1.526
R-factor	12 %

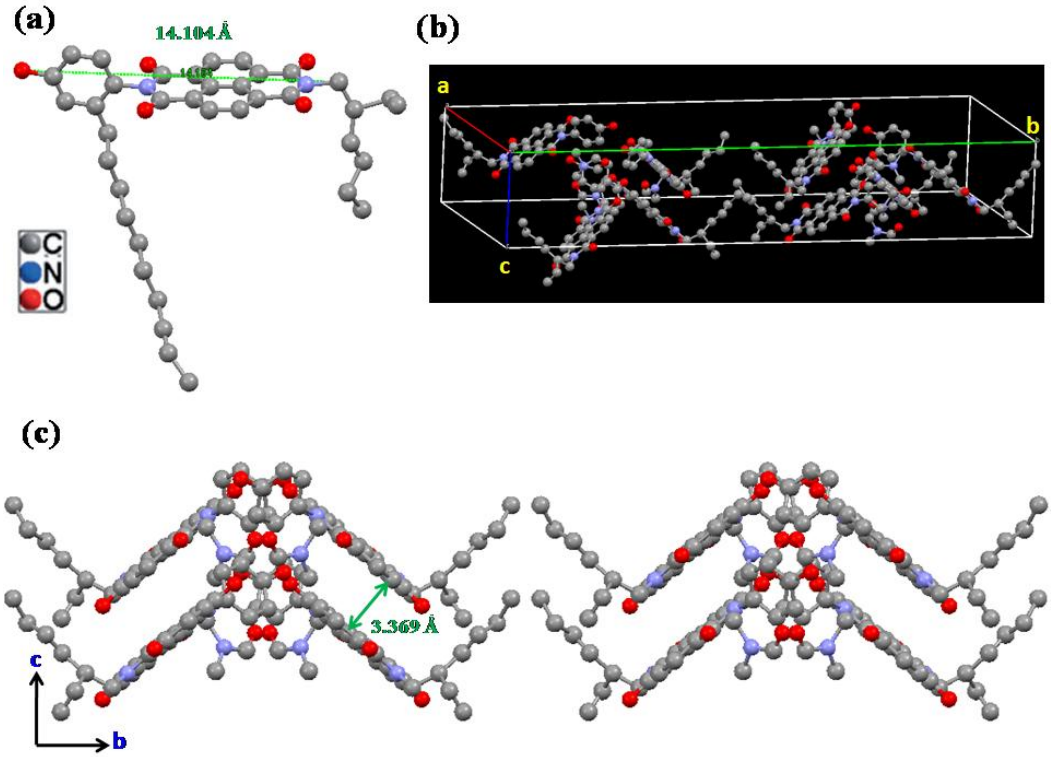

Figure-4.39. (a) Crystal structure of **PDP-UNBI** (only upto ten carbon atoms of the $C_{15}H_{31}$ chain are shown) with molecular length 14.104 Å along the rigid core. (b) Orthorhombic unit cell structure with 8 molecules per cell. (c) Herringbone stacking of NBI cores with interplanar π-π distance of 3.369 Å viewed along crystallographic a-axis (hydrogen atoms and $C_{15}H_{31}$ alkyl chain omitted for clarity).

The crystal structure is shown in figure-4.39(a), where the polycyclic NBI ring adopted a planar geometry with both the imide substituents i.e. the ethyl hexyl chain and PDP phenyl ring perpendicular to the naphthalene core. The hydrogen atoms and the co-crystallized DMF solvent molecules were omitted for clarity. There were eight independent units per cell as visible in figure-4.39(b). When one looks along the a-axis (i.e., in the c-b plane), the aromatic NBI cores could be found stacked in a typical herringbone like fashion with two nearby independent core planes more or less orthogonal to each other giving rise to a face-to-edge contact pattern (see figure-4.39(c)). This type of stacking is preferentially induced by the perpendicular orientations of the imide end substituents which determines

the bulk packing. The closest interplanar spacing between neighboring **PDP-UNBI** molecules featured a short vertical distance of 3.369 Å, which correspond to the π-π stacking interactions. Furthermore the single crystal XRD analysis revealed that, in the crystal lattice each **PDP-UNBI** molecule was associated with one DMF (N,N'-dimethylformamide) solvent molecule via hydrogen bonding between the phenolic-OH group of the PDP unit and oxygen atom of carbonyl (CO) group of DMF, as found in the H-bond contacts developed from the crystal packing (figure-4.40). So in the original crystal lattice of **PDP-UNBI** where no solvent molecules would be present, it appeared from this packing diagram that the next closest contact for H-bonding was with the imide carbonyl (CO) group of the neighboring naphthalene ring (indicated in red dotted circles in the fig-4.40). Therefore it was concluded that the crystalline assembly of **PDP-UNBI** molecules were held together by two major driving forces namely, π-π stacking interactions between the naphthalene rings in a herringbone manner and intermolecular hydrogen bonding between imide carbonyl group and phenolic-OH of neighboring stacks.

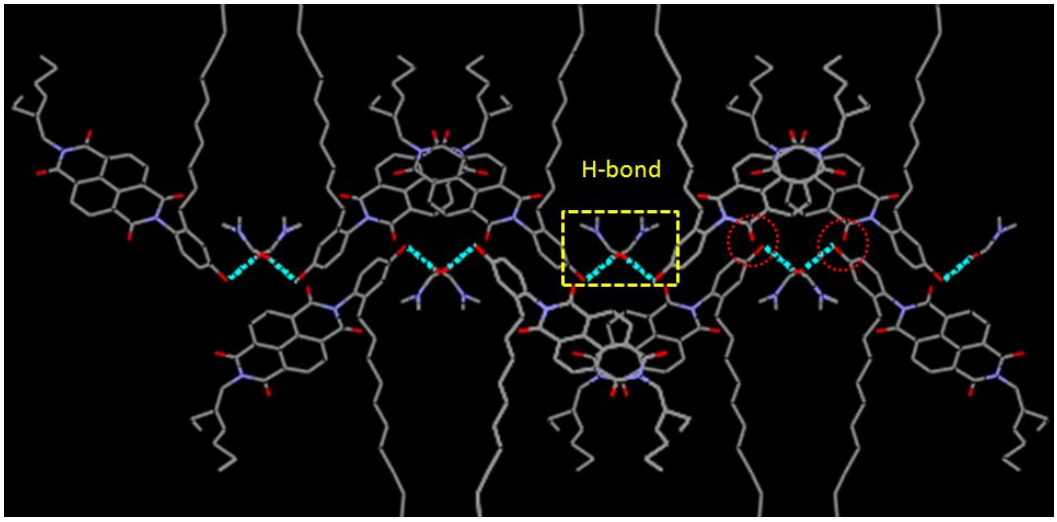

Figure-4.40. Packing structure of **PDP-UNBI** viewed through c-axis showing the hydrogen bonding with one DMF molecule co-crystallized per PDP unit (yellow dotted box) and the next closest contact for H-bonding possible between PDP-phenol and imide carbonyl of nearest naphthalene ring (red dotted circles).

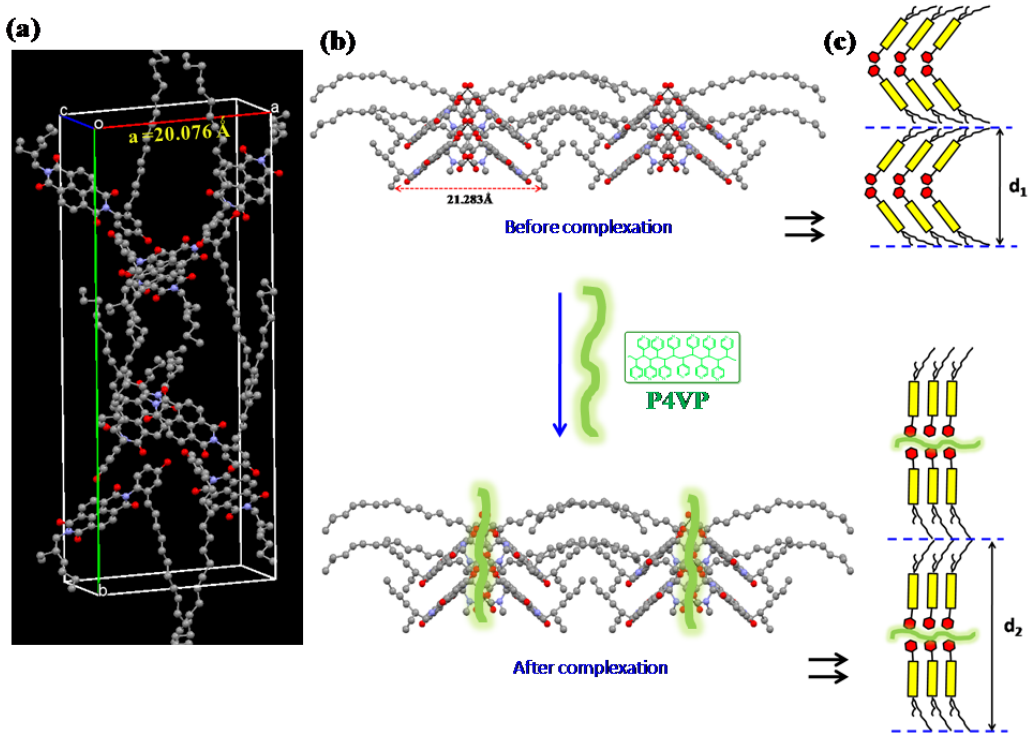

Figure-4.41. (a) Molecular arrangement of tilted **PDP-UNBI** along a = 20.076 Å. (b) schematic picture showing the P4VP chains attacking the hydrogen bonded sites of **PDP-UNBI** and (c) the resulting change in molecular orientation from tilted to extended rods causing the increase in layer periodicity ($d_2 > d_1$).

Based on the packing information from the **PDP-UNBI** small molecule alone, some inference could be made regarding the changes in the packing upon complex formation with P4VP. Upon complete stoichiometric complexation with P4VP, the fundamental periodicity length got increased to 23.22 Å as seen from the low angle XRD data (figure-4.33). From this the main layering distance that got altered by interference by P4VP would be the a-axis along which the **PDP-UNBI** molecules adopted a tilted orientation (figure-4.41(a)). Therefore the overall packing picture before and after complexation has been envisioned as given in figure-4.41(b) & (c). The hydrogen bonding of pyridine rings of P4VP chains to the PDP phenol groups of **PDP-UNBI** breaks the previously present phenol-carbonyl (O-H$^{\cdots}$CO) H-bonding and hence the homo-stack assembly of **PDP-UNBI** gets

disrupted. As a result the slight increment in layer spacing observed from the low angle XRD data could be rationalized by the change in orientation of the **PDP-UNBI** from tilted to extended rods due to invasion of stretched P4VP chains as illustrated in figure-4.41(c). However it has to be remembered that the increased layer thickness shown in schematic fig-4.41(c) is the idealised extreme stretching possible, whereas in reality the difference between d_1 and d_2 was only ~1 Å, with more probability towards a face-to-face packed slipped π-stacking arrangement which is known to exhibit better electronic communication between the active cores compared to typical face-to-edge herringbone packing.[86] Thus, based on the model study on single crystal analysis of **PDP-UNBI** molecule, it was confirmed that supramolecular complexation with P4VP ensured an ordered lamellar state with enhanced intermolecular interactions that are strongly desirable for achieving high degree of crystallinity, better molecular orbital coupling and efficient charge transport pathways.

4.3.6. Oriented Lamellar Nanostructures - TEM Analysis

The direct imaging of the microphase separated morphologies formed by the hydrogen bonded supramolecular complexes was investigated by transmission electron microscopic technique (TEM). Very thin films of the bulk samples were first prepared by solution drop casting directly onto copper grids for analysis. The samples were stained with iodine vapors to get images with enhanced contrast.[71, 87-88] Figure-4.42 shows the TEM images of the **P4VP(PDP-UNBI)$_{1.0}$** homo-comb polymer cast from 2mg/mL $CHCl_3$ solution, at two different magnifications and the corresponding histogram profile is also given. The bright regions are the **PDP-UNBI** and the dark regions corresponded to the P4VP which was preferentially stained by iodine. Similarly the TEM images of the other three random co-comb polymers **P4VP(UNBI$_m$/UPBI$_n$)$_{1.0}$** with m/n = 0.5/0.5, 0.25/0.75 and 0.75/0.25 are also given in figure-4.43(a), (b) & (c) respectively. As anticipated lamellar nanostructures could be observed in the case of all these stoichiometrically balanced 1:1 complexes, where the microdomains of P4VP phase correspond to the

dark lines of the lamellae and the microdomains of **PDP-UNBI**/**PDP-UPBI** correspond to the bright lines.

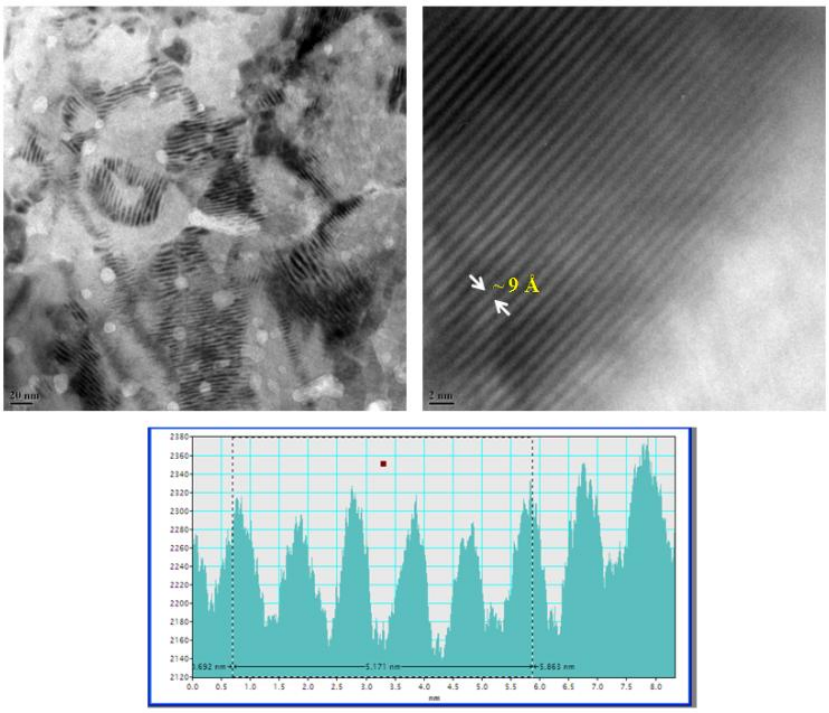

Figure-4.42. TEM images of **P4VP(PDP-UNBI)$_{1.0}$** homo-comb polymer showing the microphase separated lamellar nanostructures and its histogram given at bottom.

The domain spacing of the **PDP-UNBI** layer obtained from the histogram profile was around 9Å which was found to be close to the molecular length along the rigid part (~ 14 Å). In the case of mixed complexes this spacing varied from approximately 18 Å to 38 Å. Figure-4.43(a) shows the images corresponding to **P4VP(UNBI$_{0.50}$/UPBI$_{0.50}$)$_{1.0}$** complex, where the bright lines appeared reasonably swelled with an average periodicity length of 37 Å. This is quite possible because the comb architecture of the complexes demands more space for the equal ratios of **PDP-UNBI** and **PDP-UPBI** amphiphiles to stretch and their non-interdigitated combined rigid molecular length happens to be around 32 Å (14 Å + 18 Å).

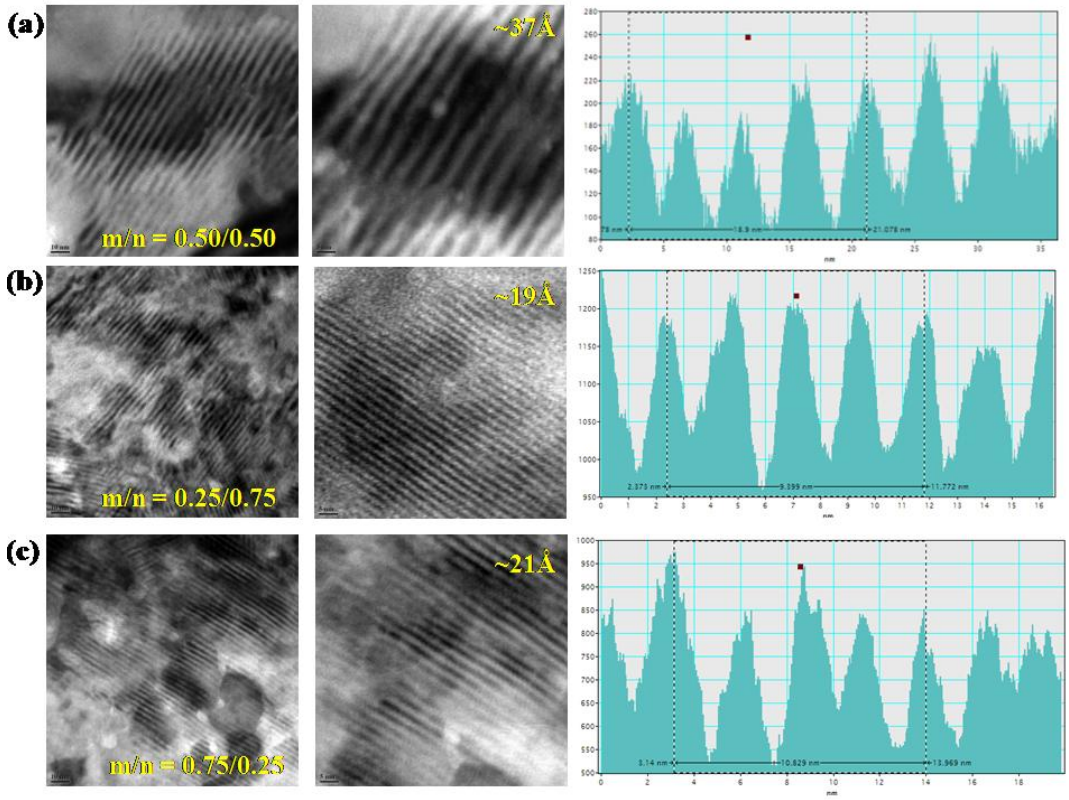

Figure-4.43. TEM images and histogram of the self-assembled morphologies from **P4VP(UNBI$_m$/UPBI$_n$)$_{1.0}$** random co-comb polymers (m/n = 0.5/0.5, 0.25/0.75, 0.75/0.25).

The other two random co-comb polymers **P4VP(UNBI$_{0.25}$/UPBI$_{0.75}$)$_{1.0}$** as well as **P4VP(UNBI$_{0.25}$/UPBI$_{0.75}$)$_{1.0}$** (figure-4.43(b) & (c) respectively) showed more or less the same domain spacing in the range 19 - 21 Å more closer towards the theoretical molecular length value of bigger sized PDP-UPBI molecule which was approximately 18.5 Å as determined from the DFT calculations (discussed in previous chapter). The domain spacings from the TEM images are obtained by averaging over a number of planes and since the TEM pictures are not calibrated the deviation in the periodicities from XRD measurements are always subject to certain error margin.

4.3.7. Charge Transport Properties of the Complexes - SCLC Measurements

The electron transport characteristics of the hydrogen bonded homo as well as random co-comb supramolecular polymers were investigated by space-charge-limited current (SCLC) method.[89,90] The basic device configuration used was ITO/H-bonded supramolecular complex/Au. For the sake of comparison devices with pristine **PDP-UNBI** molecule were also fabricated in a similar manner. The electron mobilities were extracted from the I-V curve by fitting with the Mott-Gurney equation[90]:

$$J_{SCLC} = \left(\frac{9}{8}\right) \varepsilon\varepsilon_0 \mu \left(\frac{V^2}{L^3}\right)$$

where J_{SCLC} is the current density in SCLC region, V is the applied voltage, ε and ε_0 are the relative dielectric constant of the organic layer and permittivity of the free space respectively, μ is the charge carrier mobility, and L is the thickness of the organic layer.

Figure-4.44 (a) & (b) depicts the SCLC I(V) responses corresponding to the 1:1 homo-complex **P4VP(PDP-UNBI)$_{1.0}$** and the precursor molecule **PDP-UNBI** respectively. The bulk estimate of electron mobility for **PDP-UNBI** was found to be about 8 x 10^{-3} cm^2/Vs and this value is quite in agreement with the face-to-edge herringbone type of molecular packing as observed from the single crystal analysis, which is certainly not the most suitable arrangement for long range diffusion of injected charge carriers. On the other hand the hydrogen bonded polymeric complex **P4VP(PDP-UNBI)$_{1.0}$** exhibited a one order enhanced electron mobility estimate around 1 x 10^{-2} cm^2/Vs, which very well corroborated with the packing model estimation from X-ray analyses that upon complexing with P4VP the packing motif of the active **PDP-UNBI** molecules have inclined more towards face-to-face stacked arrangement facilitating better charge carrier mobility. Eventhough reports are available demonstrating the conducting properties of P4VP, almost all of them were doped samples and the conductivity values obtained were

well below 10^{-6} S cm^{-1}.[91] Therefore the electron conductivity behaviour found in the hydrogen bonded complexes in the present study definitely owes to that of the electronically active rylenebisimide cores.

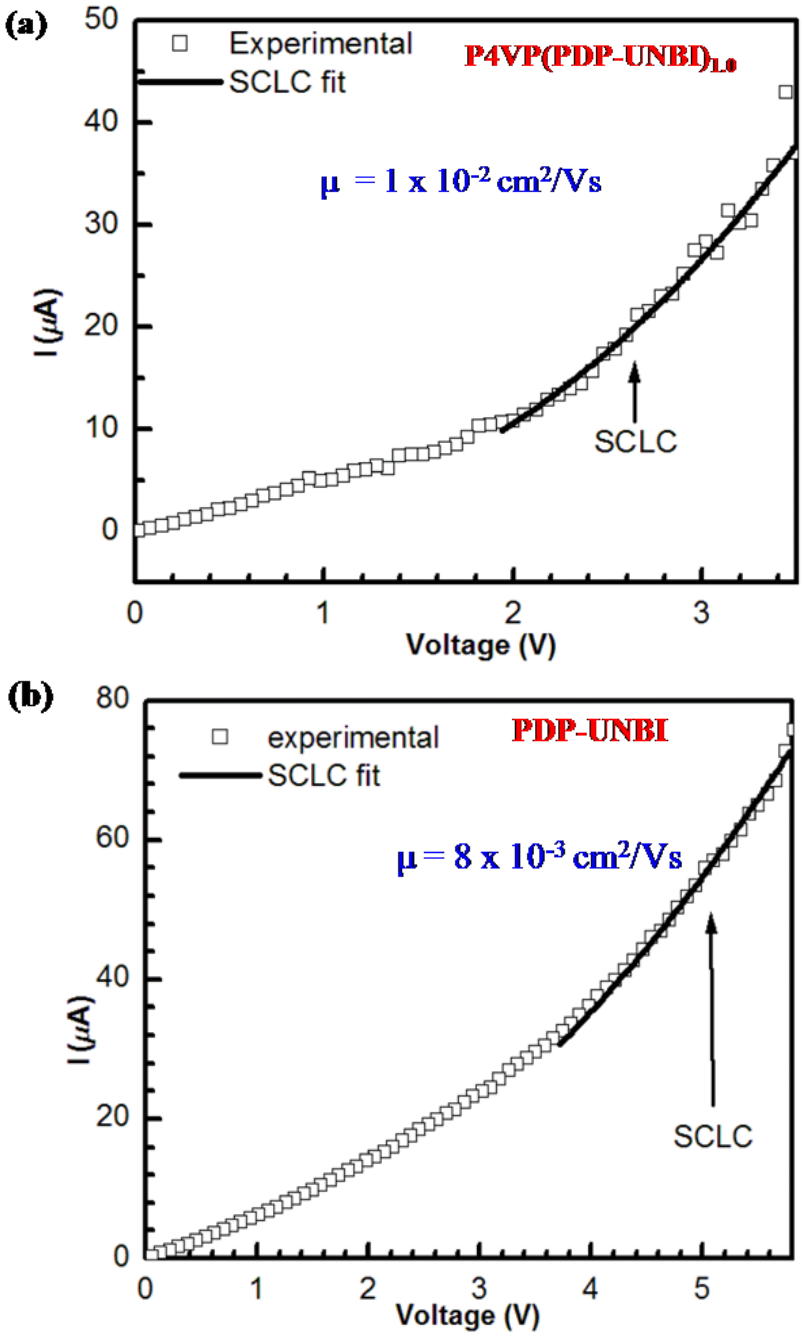

Figure-4.44. I(V) characteristics of (a) **P4VP(PDP-UNBI)$_{1.0}$** and (b) **PDP-UNBI** with the dashed line indicating the SCLC fit.

Further from the set of three random co-comb polymers **P4VP(UNBI$_m$/UPBI$_n$)$_{1.0}$** only the m/n = 0.5/0.5 sample with equimolar ratios of **PDP-UNBI** and **PDP-UPBI** gave reliable electron transport characteristics. The other two samples (m/n = 0.25/0.75 & 0.75/0.25) exhibited a strange observation of burning of the electrodes, the reason for which is not clear at present. The **P4VP(UNBI$_{0.50}$/UPBI$_{0.50}$)$_{1.0}$** displayed a high SCLC electron mobility value of 1.01 cm^2/Vs and its corresponding I(V) response is given in figure-4.45. Although the exact reason for this unexpectedly high mobility value is presently not understood, the most probable deciding factors appeared to be the broadened absorption profile and better conduction pathways that could have been afforded by alternating tight packed perylene and naphthalene layers.

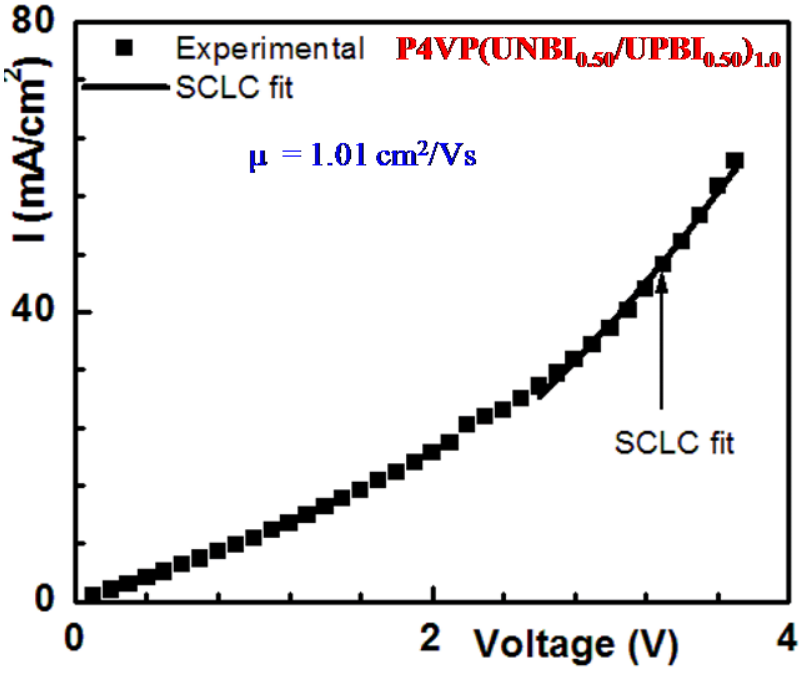

Figure-4.45. I(V) characteristics of **P4VP(UNBI$_{0.50}$/UPBI$_{0.50}$)$_{1.0}$** with the dashed line indicating the SCLC fit.

4.4. Conclusions

To summarize, this chapter re-confirmed the reliable and controllable self-assembly route for preparation of functional polymeric materials for application of optoelectronics specifically n-type semiconducting materials endowed with highly desirable properties such as crystallinity, processability and hence high charge transport mobilities. The study presented here started with a complete description of the synthesis and thorough characterization of an amphiphilic 3-pentadecylphenol substituted unsymmetrical naphthalene bisimide **PDP-UNBI**. Similar to the **PDP-UPBI** case, the **PDP-UNBI** molecule with phenol head group on one imide position lead to successful complexation with poly(4-vinyl pyridine) P4VP via hydrogen bonding with the nitrogen lone pair of pyridine ring of the polybase P4VP. A series of homopolymer complexes of **P4VP(PDP-UNBI)$_n$** with n = 0.25, 0.50, 0.75 and 1.00 were prepared. Another series of stoichiometrically balanced 1:1 random co-polymer complexes of P4VP with **PDP-UPBI** and **PDP-UNBI** varying only in the relative compositions of perylene and naphthalene cores were also prepared. The confirmation of complexation via hydrogen bonding was done using FT-IR and ^{1}H-NMR spectroscopic methods. Bulk structure analysis using different X-ray diffraction techniques (low angle and wide angle) demonstrated that complexation with P4VP lead to highly ordered layered assembly with essentially improved nanoscale packing of the semiconductor moieties in combination with sufficient solution processability. The packing diagram obtained from the single crystal analysis of the **PDP-UNBI** as a control study gave a clear picture of the initial herringbone type arrangement originating from the hydrogen bonding interactions among the self-associated **PDP-UNBI** small molecule alone. Correlating this with the X-ray diffraction analyses of the **P4VP(PDP-UNBI)$_{1.0}$** complex provided insight into the probable face-to-face packing of extended crystalline lattice of the small molecule **PDP-UNBI** leading to highly ordered lamellar stacks with alternate stretched P4VP layers. The visual evidence for the same was obtained from transmission microscopy (TEM) imaging

which confirmed the microphase separated lamellar morphologies for all the stoichiometrically balanced homo as well as random co-comb polymers. The charge transport properties studied using SCLC technique showed improved electron mobilities of the complexes in comparison to the pristine molecules. Thus the overall message to be carried forward was that the concept of supramolecular chemistry applied here with tunable functionalities and self-organized morphologies opens a platform that allows facile generalization for a variety of applications.

4.5. References

[1] H. Minemawari, T. Yamada, H. Matsui, J. Tsutsumi, S. Haas, R. Chiba, R. Kumai, T. Hasegawa, *Nature* **2011,** *475*, 364.

[2] K. Takimiya, S. Shinamura, I. Osaka, E. Miyazaki, *Adv. Mater.* **2011,** *23*, 4347.

[3] S. V. Bhosale, C. H. Janiab, S. J. Langford, *Chem. Soc. Rev.* **2008,** 37, 331.

[4] P. Mukhopadhyay, Y. Iwashita, M. Shirakawa, S-i. Kawano, N. Fujita, S. Shinkai, *Angew. Chem. Int. Ed.* **2006,** 45**,** 1592.

[5] R. K. Das, S. Banerjee, G. Raffy, A. D. Guerzo, J-P. Desvergne, U. Maitra, *J. Mater. Chem.* **2010,** *20*, 7227.

[6] W. Pisula, M. Kastler, D. Wasserfallen, J. W. F. Robertson, F. Nolde, C. Kohl, K. Müllen, *Angew. Chem. Int. Ed.* **2006,** *45*, 819.

[7] L. Y. Park, D. G. Hamilton, E. A. McGehee, K. A. McMenimen, *J. Am. Chem. Soc.* **2003,** *125*, 10586.

[8] R. S. Lokey, B. L. Iverson, *Nature* **1995,** 375, 303.

[9] V. J. Bradford, B. L. Iverson, *J. Am. Chem. Soc.* **2008,** *130*, 1517.

[10] H. Y. Au-Yeung, G. D. Pantos, J. K. M. Sanders, *J. Am. Chem. Soc.* **2009,** *131*, 16030.

[11] S. A. Vignon, T. Jarrosson, T. Iijima, H-R. Tseng, J. K. M. Sanders, J. F. Stoddart, *J. Am. Chem. Soc.* **2004,** *126*, 9884.

[12] G. D. Pantos¸, P. Pengo, J. K. M Sanders, *Angew. Chem. Int. Ed.* **2007,** *46*, 194.

[13] H. Shao, J. Seifert, N. C. Romano, M. Gao, J. J. Helmus, C. P. Jaroniec, D. A. Modarelli, J. R. Parquette, *Angew. Chem. Int. Ed.* **2010,** *49*, 7598.

[14] M. R. Molla, S. Ghosh, *Chem. -Eur. J.* **2012,** *18*, 1290.

[15] H. Kar, M. R. Molla, S. Ghosh, *Chem. Commun.* **2013,** *49*, 4220.

[16] P. N. Kamalakar, S. V. Bhosale, K. V. S. Rama Krishna, A. Gupta, S. V. Bhosale, *Chem. Commun.* **2013,** *49*, 5444.

[17] L. L. Miller, K. R. Man, *Acc. Chem. Res.* **1996,** *29*, 417.

[18] H. E. Katz, A. J. Lovinger, J. Johnson, C. Kloc, T. Siegrist, W. Li, Y. Y. Lin, A. Dodabalapur, *Nature* **2000,** *404*, 478.

[19] J. M. Warman, M. P. de-Haas, G. Dicker, F. C. Grozema, J. Piris, M. G. Debije, *Chem. Mater.* **2004,** *16*, 4600.

[20] B. A. Jones, A. Facchetti, M. R. Wasielewski, T. J. Marks, *J. Am. Chem. Soc.* **2007,** *129*, 15259.

[21] J. H. Oh, S. –L. Suraru, W. -Y. Lee, M. Könemann, H. W. Höffken, C. Röger, R. Schmidt, Y. Chung, W. -C. Chen, F. Würthner, Z. Bao, *Adv. Funct. Mater.* **2010,** *20*, 2148.

[22] I. Tszydel, M. Kucinska, T. Marszalek, R. Rybakiewicz, A. Nosal, J. Jung, M. Gazicki-Lipman, C. Pitsalidis, C. Gravalidis, S. Logothetidis, M. Zagorska, J. Ulanski, *Adv. Funct. Mater.* **2012**, *22*, 3840.

[23] Y. Geng, S. -X. Wu, H. -B. Li, X. -D. Tang, Y. Wu, Z.-M. Su, Y. Liao, *J. Mater. Chem.* **2011,** *21*, 15558.

[24] X. G. Guo, M. D. Watson, Org. Lett. **2008,** *10*, 5333.

[25] H. Yan, Z. H. Chen, Y. Zheng, C. Newman, J. R. Quinn, F. Dotz, M. Kastler, A. Facchetti, *Nature* **2009,** *457*, 679.

[26] M. M. Durban, P. D. Kazarinoff, C. K. Luscombe, *Macromolecules* **2010,** *43*, 6348.

[27] F. S. Kim, X. Guo, M. D. Watson, S. A. Jenekhe, *Adv. Mater.* **2010,** *22*, 478.

[28] K. Szendrei, D. Jarzab, Z. Chen, A. Facchetti, M. A. Loi, *J. Mater. Chem.* **2010,** *20*, 1317.

[29] B. A. Jones, A. Facchetti, T. J. Marks, M. R. Wasielewski, *Chem. Mater.* **2007,** *19*, 2703.

[30] D. Shukla, S. F. Nelson, D. C. Freeman, M. Rajeswaran, W. G. Ahearn, D. M. Meyer, J. T. Carey, *Chem. Mater.* **2008,** *20*, 7486.

[31] K. C. See, C. Landis, A. Sarjeant, H. E. Katz, *Chem. Mater.* **2008**, *20*, 3609.

[32] X. Gao, C. Di, Y. Hu, X. Yang, H. Fan, F. Zhang, Y. Liu, H. Li, D. Zhu, *J. Am. Chem. Soc.* **2010,** *132*, 3697.

[33] Y. Zhao, C. Di, X. Gao, Y. Hu, L. Zhang, Y. Liu, J. Wang, W. Hu, D. Zhu, *Adv. Mater.* **2011,** *23*, 2448.

[34] Y. Hu, X. Gao, C. Di, X. Yang, F. Zhang, Y. Liu, H. Li, D. Zhu, *Chem. Mater.* **2011,** *23*, 1204.

[35] S. L. Suraru, U. Zschieschang, H. Klauk, F. Wu□rthner, *Chem. Commun.* **2011,** *47*, 11504.

[36] L. Tan, Y. Guo, G. Zhang, Y. Yang, D. Zhang, G. Yu, W. Xu, Y. Liu, *J. Mater. Chem.* **2011,** *21*, 18042.

[37] M. Herbst, K. Hunger, *Industrial Organic Pigments*; VCH: New York, 1993.

[38] M. Quinto, S. A. Jenekhe, A. J. Bard, *Chem. Mater.* **2001,** *13*, 2825.

[39] A. Babel, S. A. Jenekhe, *J. Am. Chem. Soc.* **2003,** *125*, 13656.

[40] H. Langhals, H. Jaschke, *Chem.-Eur. J.* **2006,** *12*, 2815.

[41] L. E. Polander, L. Pandey, A. Romanov, A. Fonari, S. Barlow, B. M. Seifried, T. V. Timofeeva, J. Brédas, S. R. Marder, *J. Org. Chem.* **2012,** *77*, 5544.

[42] M. M. Durban, P. D. Kazarinoff, Y. Segawa, C. K. Luscombe, *Macromolecules* **2011,** *44*, 4721.

[43] F. Zhang, Y. Hu, T. Schuettfort, C. Di, X. Gao, C. R. McNeill, L. Thomsen, S. C. B. Mannsfeld, W. Yuan, H. Sirringhaus, D. Zhu, *J. Am. Chem. Soc*. **2013,** *135*, 2338.

[44] L. Tan, Y. Guo, Y. Yang, G. Zhang, D. Zhang, G. Yu, W. Xu, Y. Liu, *Chem. Sci.* **2012,** *3*, 2530.

[45] R. P. Ortiz, H. Herrera, C. Seoane, J. L. Segura, A. Facchetti, T. J. Marks, *Chem.-Eur. J.* **2012,** *18*, 532.

[46] Y. Li, G. Zhang, G. Yang, Y. Guo, C. Di, X. Chen, Z. Liu, H. Liu, Z. Xu, W. Xu, H. Fu, D. Zhang, *J. Org. Chem.* **2013,** *78*, 2926.

[47] H. Luo, Z. Cai, L. Tan, Y. Guo, G. Yang, Zi. Liu, G. Zhang, D. Zhang, W. Xu, Y. Liu, *J. Mater. Chem. C* **2013,** *1*, 2688.

[48] W. Yue, A. Lv, J. Gao, W. Jiang, L. Hao, C. Li, Y. Li, L. E. Polander, S. Barlow, W. Hu, S. D. Motta, F. Negri, S. R. Marder, Z. Wang, *J. Am. Chem. Soc.* **2012,** *134*, 5770.

[49] Z. Chen, Y. Zheng, H. Yan, A. Facchetti, *J. Am. Chem. Soc.* **2008,** *131*, 8.

[50] J. Chen, M.-M. Shi, X.-L. Hu, M. Wang, H.-Z. Chen, *Polymer* **2010,** *51*, 2897.

[51] C. J. Kudla, D. Dolfen, K. J. Schottler, J.-M. Koenen, D. Breusov, S. Allard, U. Scherf, *Macromolecules* **2010,** *43*, 7864.

[52] P. Piyakulawat, A. Keawprajak, J. Wlosnewski, M. Forster, U. Asawapirom, *Synth. Met.* **2011,** *161*, 1238.

[53] P. M. Alvey, R. J. Ono, C. W. Bielawski, B. L. Iverson, *Macromolecules* **2013,** *46*, 718.

[54] X. Guo, F. S. Kim, M. J. Seger, S. A. Jenekhe, M. D. Watson, *Chem. Mater.* **2012,** *24*, 1434.

[55] R. Steyrleuthner, M. Schubert, F. Jaiser, J. C. Blakesley, Z. Chen, A. Facchetti, D. Neher, *Adv. Mater.* **2010,** *22*, 2799.

[56] M. Caironi, C. Newman, J. R. Moore, D. Natali, H. Yan, A. Facchetti, H. Sirringhaus, *Appl. Phys. Lett.* **2010,** *96*, 3.

[57] M. Rao, R. P. Ortiz, A. Facchetti, T. J. Marks, K. S. Narayan, *J. Phys. Chem. C* **2010,** *114*, 20609.

[58] J. C. Blakesley, M. Schubert, R. Steyrleuthner, Z. H. Chen, A. Facchetti, D. Neher, *Appl. Phys. Lett.* **2011,** *99*, 3.

[59] J. H. Li, J. Du, J. B. Xu, H. L. W. Chan, F. Yan, *Appl. Phys. Lett.* **2012,** *100*, 4.

[60] I. Lange, J. C. Blakesley, J. Frisch, A. Vollmer, N. Koch, D. Neher, *Phys. Rev. Lett.* **2011,** *106*, 4.

[61] M. Caironi, M. Bird, D. Fazzi, Z.; Chen, R. Di Pietro, C. Newman, A. Facchetti, H. Sirringhaus, *Adv. Funct. Mater.* **2011,** *21*, 3371.

[62] D. Fazzi, M. Caironi, C. Castiglioni, *J. Am. Chem. Soc.* **2011,** *133*, 19056.

[63] Y. -J. Hwang, G. Ren, N. M. Murari, S. A. Jenekhe, *Macromolecules* **2012,** *45*, 9056.

[64] K. Nakabayashi, H. Mori, *Macromolecules* **2012,** *45*, 9618.

[65] J. Wang, C. Lu, T. Mizobe, M. Ueda, W.-C. Chen, T. Higashihara, *Macromolecules* **2013,** *46*, 1783.

[66] C. Gu, W. Hu, J. Yao, H. Fu, *Chem. Mater.* **2013,** *25*, 2178.

[67] A. Das, S. Ghosh, *Macromolecules* **2013,** *46*, 3939.

[68] J. Ruokolainen, G. Ten Brinke, O. Ikkala, *Macromolecules* **1996,** *29*, 3409.

[69] B. J. Rancatore, C. E. Mauldin, S.-H.Tung, C. Wang, A. Hexemer, J. Strzalka, J. M. J. Frè chet, T. Xu, *ACS Nano* **2010,** *4*, 2721.

[70] B. Nandan, M. K. Vyas, M. Böhme, M. Stamm, *Macromolecules* **2010,** *43*, 2463.

[71] C. -H. Lee,S.-H. Tung, *Soft Matter* **2011,** *7*, 5660.

[72] M. Faber, A. H. Hofman, E. Polushkin, G. A. van Ekenstein, J. Seitsonen, J, Ruokolainen, K. Loos, G. ten Brinke, *Macromolecules* **2013,** *46*, 500.

[73] H. Tran, M. Gopinadhan, P. W. Majewski, R. Shade, V. Steffes, C. O. Osuji, L. M. Campos, *ACS Nano* **2013,** *7*, 5514.

[74] S. -W. Kuo, *J. Polym. Res.* **2008,** *15*, 459.

[75] O. Ikkala, J. Ruokolainen, G. Ten Brinke, M. Torkkeli, R. Serimaa, *Macromolecules* **1995,** *28*, 7088.

[76] J. Ruokolainen, O. Ikkala, J. Tanner, G. Ten Brinke, M. Torkkeli, R. Serimaa, *Macromolecules* **1995,** *28*, 7779.

[77] J. Wang, A. Kulago, W, R. Browne, B. L. Feringa, *J. Am. Chem. Soc***. 2010**, *132*, 4191.

[78] W. Wang, L.-S. Li, G.Helms, H.-H. Zhou, A. D. Q. Li, *J. Am. Chem. Soc.* **2003,** *125*, 1120.

[79] J. S. Waugh, R. W. Fessenden, *J. Am. Chem. Soc.* **1957,** *79*, 846.

[80] Z. Chen, V. Stepanenko, V. Dehm, P. Prins, L. D. A. Siebbeles, J. Seibt, P. Marquetand, V. Engel, F. Würthner, *Chem. -Eur. J.* **2007,** *13*, 436.

[81] F. Würthner, Z. Chen, V. Dehm, V. Stepanenko, *Chem. Commun.* **2006,** *11*, 1188.

[82] J. Ruokolainen, G. Ten Brinke, O. Ikkala, *Adv. Mater.* **1999,** *11*, 777.

[83] H. Koskonen, J. Ruokolainen, M. Knaapila, M. Torkkeli, R. Serimaa, G. ten Brinke, W. Bras, A. Monkman, O. Ikkala, *Macromolecules* **2000,** *33*, 8671.

[84] S. Valkama, O. Lehtonen, K. Lappalainen, H. Kosonen, P. Castro, T. Repo, M. Torkkeli, R. Serimaa, G. ten Brinke, M. Leskelä, O. Ikkala, *Macromol. Rapid Commun.* **2003,** *24*, 556.

[85] Y. Wen, Y. Liu, *Adv. Mater.* **2010,** *22*, 1331.

[86] C. Wang, H. Dong, W. Hu, Y. Liu, D. Zhu, *Chem. Rev.* **2012,** *112*, 2208.

[87] B. Nandan, M. K. Vyas, M. Böhme, M. Stamm, *Macromolecules* **2010,** *43*, 2463.

[88] M. C. Luyten, G. O. R. A. Van Ekenstein, G. Ten Brinke, *Macromolecules* **1999,** *32*, 4404.

[89] M. -A. Muth, M. C. -Orozco, M. Thelakkat, *Adv. Funct. Mater.* **2011**, *21*, 4510.

[90] A. M. Goodman, A. Rose, *J. Appl. Phys.* **1971,** *41*, 2823.

[91] J. R. Chetia, M. Moulick, A. Dutta, *Indian J. Chem. Technol.* **2004,** *11*, 80.

Chapter-5

Liquid Crystalline Supramolecular Crosslinked Polymer Network : Ditopic Hydrogen-Bonded Rylenebisimides with Poly(4-vinylpyridine)

5.1. Introduction

Ordering of macromolecules is one of the most essential factor that determines the final material properties by influencing the crystallization behaviour, phase separation etc. and thus in turn affects the final performance. The significance of mutual alignment of electronically active cores for enhanced performance in the case of organic polymer based semiconductor devices has widely been recognized.[1-4] In the case of conventional long covalent polymeric semiconductors, the probability of charge conduction is more within the isolated polymer chain mainly of intramolecular type. But a three dimensionally oriented polymer architecture have the advantages of carrier transport not only along individual chains, but also among the neighbouring chains in all directions. In such a three dimensional crystalline lattice the intermolecular type of charge transport would always be favoured with well defined percolation pathways. Furthermore the intermolecular charge transport occurring via hopping or tunnelling mechanism strongly depends upon the packing of active cores with minimal separation distances in the polymer matrix.[5] A densely packed and highly oriented three dimensional network can facilitate elimination of grain boundary defects and can thereby enhance interchain charge transfer rates.[6,7] Hence designs and methodologies needs to be developed that can bring about the intrinsic structural ordering within organic polymer semiconductors for low cost high efficiency devices.

In this context, supramolecular engineering of functional assemblies taking aid of reversible as well as directional non-covalent interactions appears to be most suitable and efficient methodology to attain predictable, well defined nano-architectures desirable for high performance optoelectronic devices such as photovoltaic cells, organic field effect transistors etc.[8-19] In comparison to other supramolecular interactions such as metal complexes, the hydrogen bonding systems have the unique advantage that the association strength can be tuned over a wide range depending on the number of hydrogen bonds. As a thumb rule more

number of hydrogen bonds imply much stronger binding interaction or in other words the strength goes on increasing from one hydrogen bond to two-centred to three to four and so on.[20,21] Moreover the hydrogen bonded systems often display host-guest complementarity which helps excluding self-association phenomena, facilitating highly controllable level of intermolecular ordering. Self-assembly effects endowed by other concurrent secondary electronic interactions such as π-π stacking, hydrophobic forces etc. together with multiple hydrogen bonding modules fix the internal pre-organization within the supramolecular systems.

The field of hydrogen bonded supramolecular polymer networks have made an impressive progress since the first pioneering work from group of Sijbesma and Meijer *et al.* where they showed 2-ureido-4[1*H*]-pyrimidinone (UPy) units to assemble into long chains through quadruple cooperative hydrogen bonds in an array, yielding products with mechanical properties that until then were exclusively associated with covalent polymers (figure-5.1).[21-24]

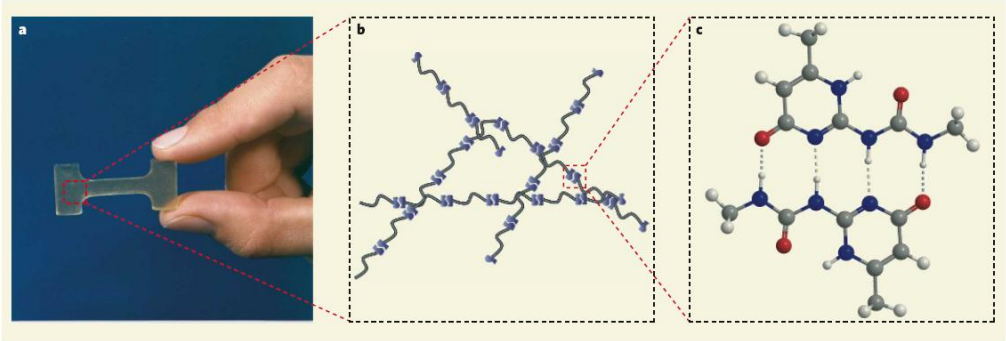

Figure-5.1. (a) A plastic component made from the hydrogen bonded supramolecular polymer network of UPy. (b) Network of monomers connected by hydrogen bonds. (c) Quadrupolar hydrogen bonds between UPy units. (Carbon atoms are shown in grey; nitrogen in blue; oxygen in red; and hydrogen in white) [*Adapted from ref.24*]

The UPy units form quadrupolar hydrogen bonds with each other that makes the monomers undergo spontaneous self-assembly to form the polymer network. This well defined dimerization of UPy moiety resulting in a network does not require

any additional stabilization such as crystallization or phase separation and the resulting material exhibited well defined viscoelastic transition.

Another well studied hydrogen bonded system as an alternative to ureidopyrimidones is the sextuple hydrogen bonding moiety DAD-DAD (D = donor; A = acceptor), named by Hamilton *et al.*[25-27] with complementary barbituric acid or N-alkyl cyanurates. Lehn *et al.* utilized this multivariant receptor to form supramolecular polymeric fibers, gels and crosslinked networks (figure-5.2) mediated by the hydrogen bonded self assembly of both bivalent and trivalent building blocks. [28]

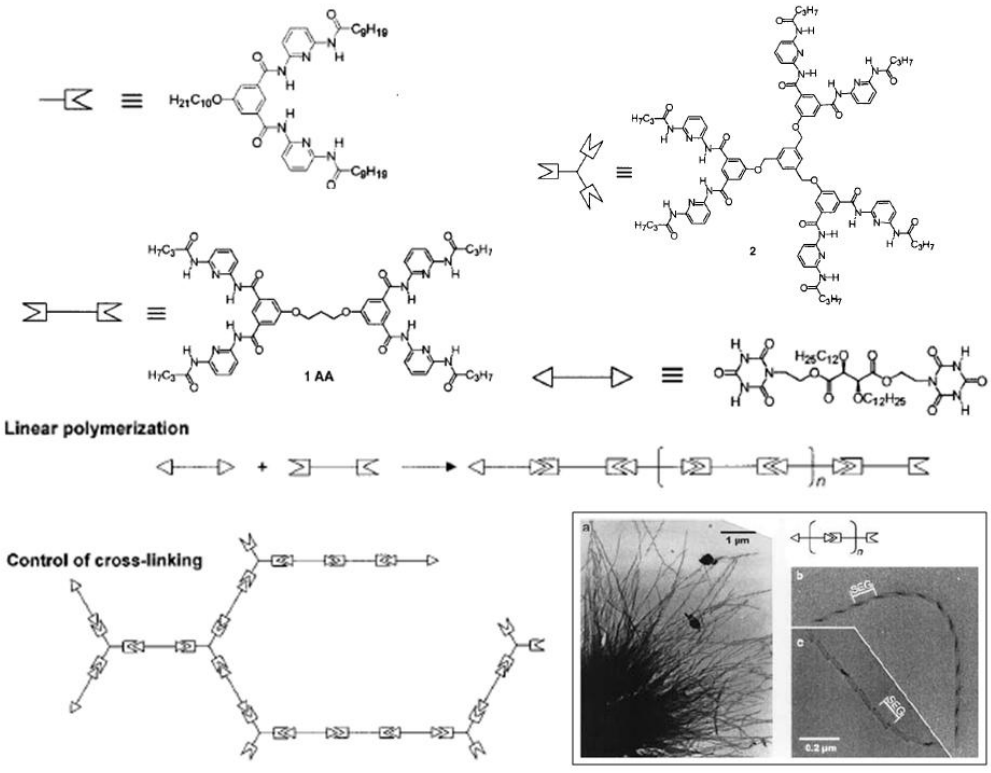

Figure-5.2. Supramolecular linear and crosslinked polymers generated from Hamilton receptor/cyanurate multiple hydrogen-bonding interaction and the formation of corresponding fibers. [*Adapted from ref.28*]

It has been well recognized that multiple hydrogen bonded systems offer the possibility to form network structures that can give rise to supramolecular

strands, sheets, rosettes etc.[29] The effects of such multivalent network assemblies are usually less prominent in solution, but more pronounced in the solid state.

Recently the group of Yagai *et al.* disclosed hydrogen bonded self-aggregation and co-aggregation of ditopic melamines bearing one or two perylenebisimides with complementary dodecyl cyanurate (dCA) or barbiturate which led to formation of optically transparent organogels in non-polar solvents.[30,31] These multiple hydrogen bonded supramolecular assemblies exhibited highly ordered lamellar architectures and showed typical electron transport behaviour in organic field effect transistors (OFET) but with low mobility values of the order of 10^{-5} $cm^2V^{-1}s^{-1}$ (Figure-5.3). However atomic force microscopy observation of these OFET devices showed typical "terraced" multilayer morphologies with no noticeable grain boundaries.

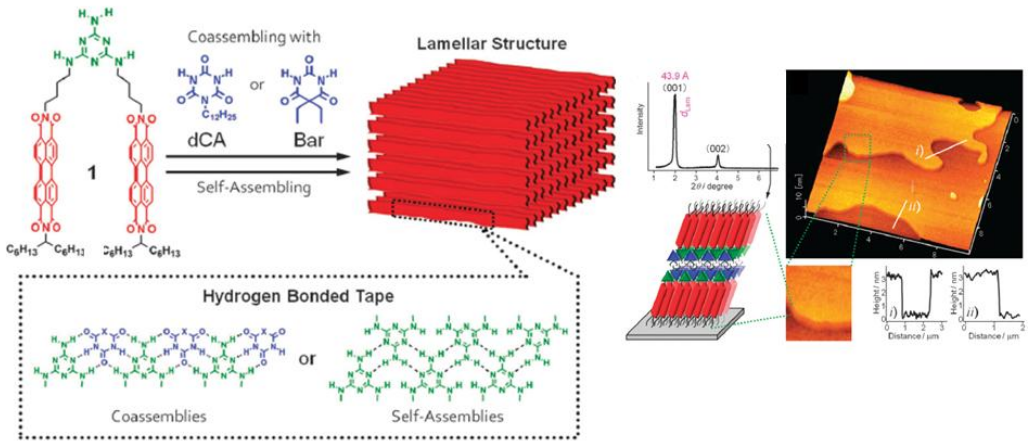

Figure-5.3. Supramolecular lamellar architectures formed by hydrogen bonded assemblies of ditopic melamine bearing perylenebisimides with cyanurate or barbiturates. [*Adapted from ref.31*]

Furthermore a large variety of functional materials have been fabricated using hydrogen bonding interactions owing to its directionality and moderate strength.[32-42] For example, recently Noro and Matsushita *et al.* described the use of hydrogen bonding as the secondary interaction to develop supramolecular polymer gels that are three dimensional networks of melt macromolecules and they

differed from the conventional supramolecular gels because they were comprised of polymers instead of low molecular weight compounds.[43] Weck and co-workers successfully fabricated novel multiresponsive reversible polymer networks based on both hydrogen-bonding and metal coordination.[44] They synthesized a multifunctionalized polymer scaffold containing cyanuric acid based hydrogen bonding motifs and palladated pincer complex based metal coordination motifs. Reversible crosslinking strategy was adopted using 2,4-diaminotriazine and bipyridine as the crosslinking agents via hydrogen bonding and metal coordination respectively and the resulting supramolecular polymer networks showed thermo-responsive as well as chemo-responsive behaviours.

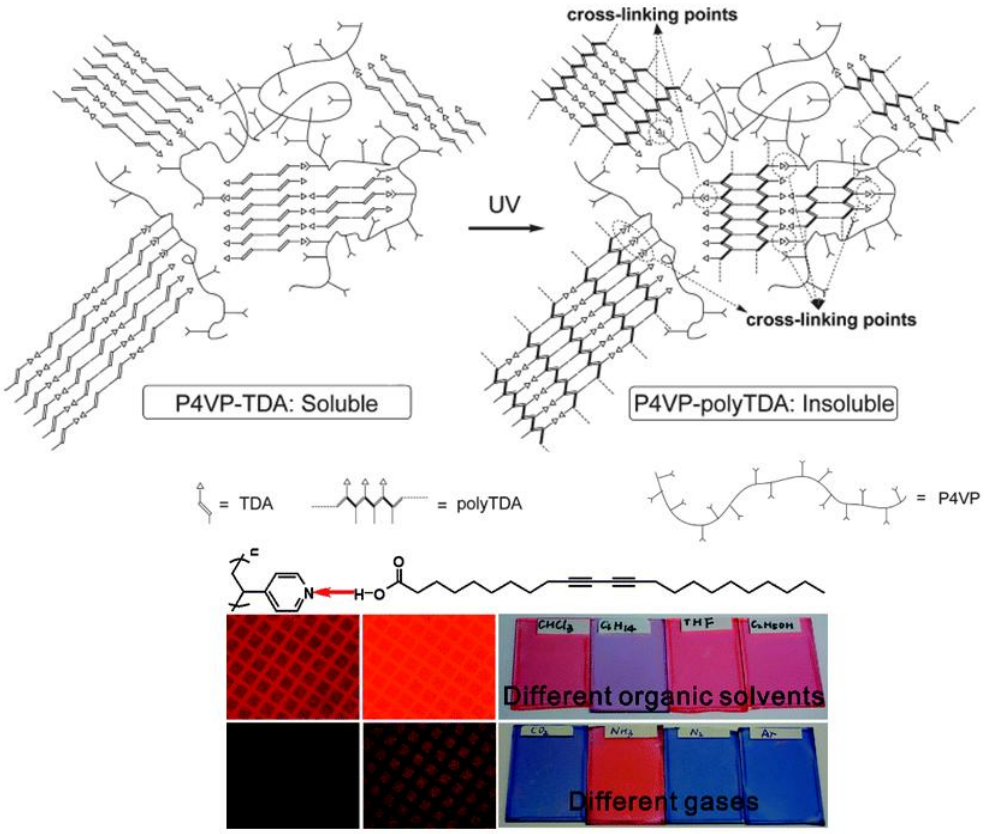

Figure-5.4. P4VP-PolyTDA photo-crosslinked hydrogen bonded network formation with corresponding photolithography pattern and sensing of organic solvents and gases. [*Adapted from ref.45*]

Bubeck *et al.* reported hydrogen bonded complexes of carboxylic group containing polydiacetylenes with poly(4-vinyl pyridine) for photolithography and sensing applications (figure-5.4).[45] They fabricated hydrogen bond stabilized thin films of diacetylenes, that were subsequently photopolymerized to yield the blue phase of the polydiacetylenes. The crosslinked network of the hydrogen bonded complex became insoluble in common solvents and thus could be used for photolithography. The sensor capabilities of the hydrogen bonded crosslinks for various solvents and gases were also demonstrated by means of blue to red color changes of polydiacetylenes.

Liquid-crystals are yet another exciting class of materials with a wide variety of potential applications in the fields ranging from display technology to organic electronics.[46] By combining supramolecular ordering with the fluid properties of the liquid-crystalline state, these materials offer the possibility to self-organise into addressable 2D and 3D arrangements exhibiting high processability and self-healing properties.[47] Frè chet and Kato [48,49] were the first to study the topic of hydrogen bonded liquid crystalline supramolecular materials and later also independently by Zimmermann *et al.*[50] In the early 1990s Frè chet and co-workers reported a series of publications demonstrating the use of hydrogen bonding to non-covalently attach liquid crystalline mesogens onto polymer backbones including poly(siloxane)s and poly(arcylate)s.[51-58] A variety of liquid crystalline mesophases including smectic and nematic ones were obtained through small variations of the mesogen and/or the polymeric backbone.

The same group of Kato and Frè chet *et al.* have reported a supramolecular liquid crystalline polymer network built by the self-assembly of a polyacrylate with benzoic acid side-chains and 4,4'-bipyridine held together by hydrogen bonding forces (figure-5.5) and these networks exhibited reversible phase transitions.[59] On heating this sample to isotropic state, some hydrogen bonds break to form the disordered state meanwhile on cooling H-bonds are formed again which resulted in smectic A (Sm A) phase.

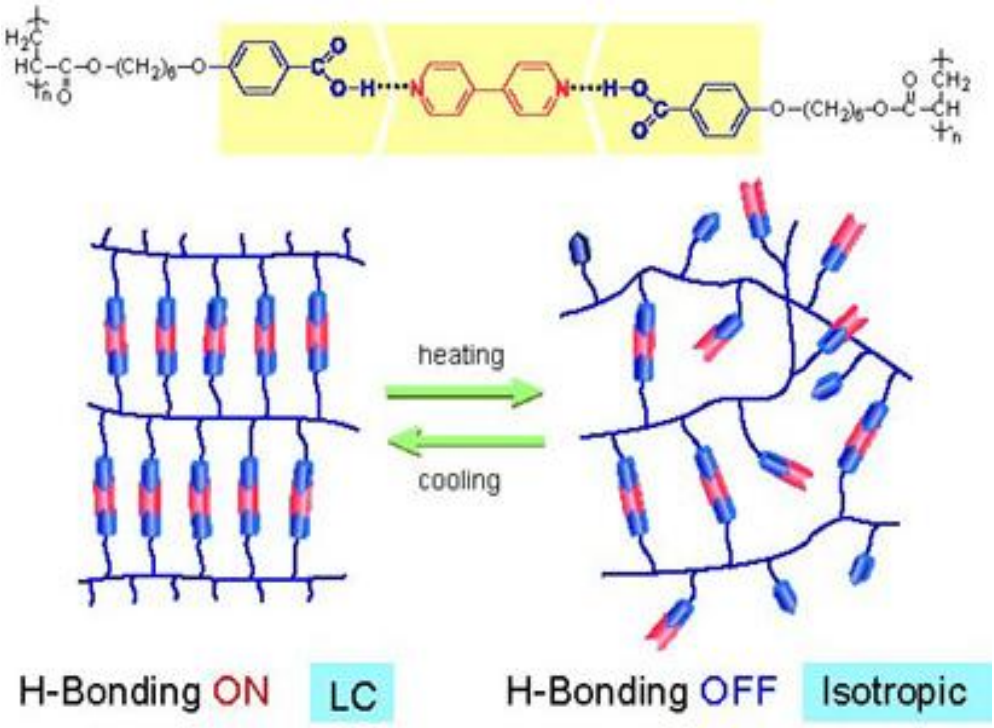

Figure-5.5. Liquid crystalline supramolecular polymer network formed by hydrogen bonding interactions between polyacrylate with benzoic acid side-chain and bipyridine crosslinker. [*Adapted from ref.59*]

Ros and co-workers demonstrated an interesting extension of the work by Frè chet and Kato where they utilized the self-assembly approach to synthesize hydrogen bonded bent-core side-chain liquid crystalline polymers.[60] Two distinct synthetic schemes were demonstrated in their report: (i) the non-covalent functionalization of polymer backbones via hydrogen bonding and (ii) the pre-polymerization assembly of the mesogen with the monomer followed by the photo-polymerization of the self-assembled mesogen/monomer complex (figure-5.6). Both synthetic routes were proved to be successful, yielding polymeric materials with similar liquid crystalline behavior, thus demonstrating the versatility of hydrogen bonding as a functionalization and templating tool.

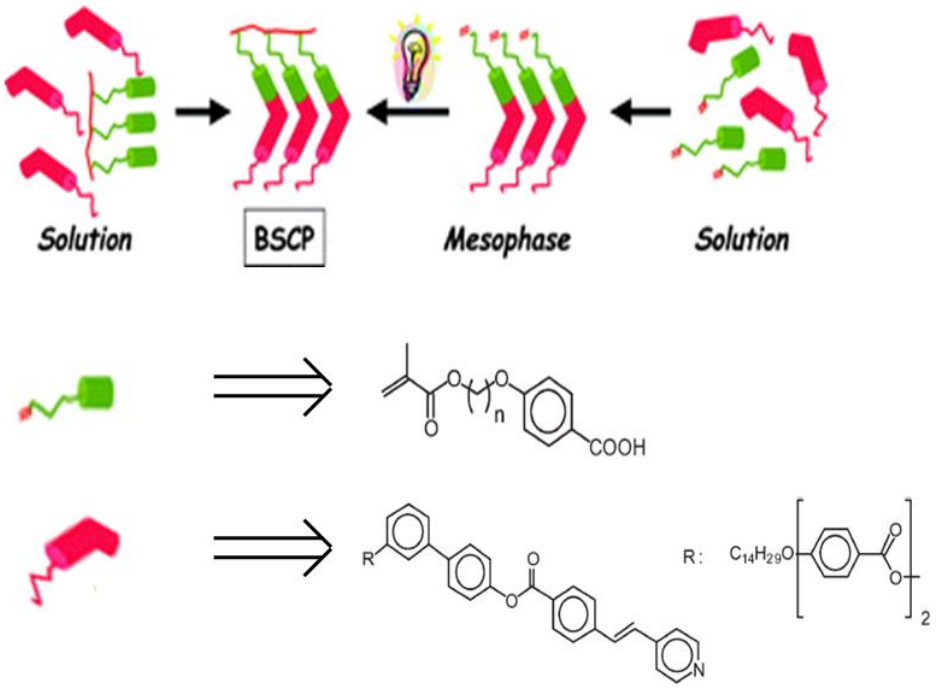

Figure-5.6. Alternative routes to prepare self-assembled bent-core liquid crystalline supramolecular polymers by hydrogen bonding between pyridine and benzoic acid. (structures of H-bond donors and acceptors given) [*Adapted from ref.60*]

Ikkala *et al.* in a recent report disclosed a liquid crystalline blend of a mesogenic molecule cholestryl hemi-succinate (CholHS) with P4VP via hydrogen bonding, where a series of complexes were prepared with different molecular weights of P4VP (figure-5.7).[61] It was found that the blends formed microphase separated smectic A (Sm A) structures where the periods correspond to a head-to-head arrangement of the mesogens as found from the investigation using small angle X-ray scattering (SAXS), polarised optical microscopy (POM) and differential scanning calorimetry (DSC). At low degrees of CholHS complexation liquid crystallinity was found to be most stable, meanwhile at high degrees of complexation competing effects due to CholHS crystallization dominated and also depended on the thermal history. Further hierarchical structure within structure

self-assembled morphologies were also constructed by combining block copolymer PS-*b*-P4VP and CholHS.

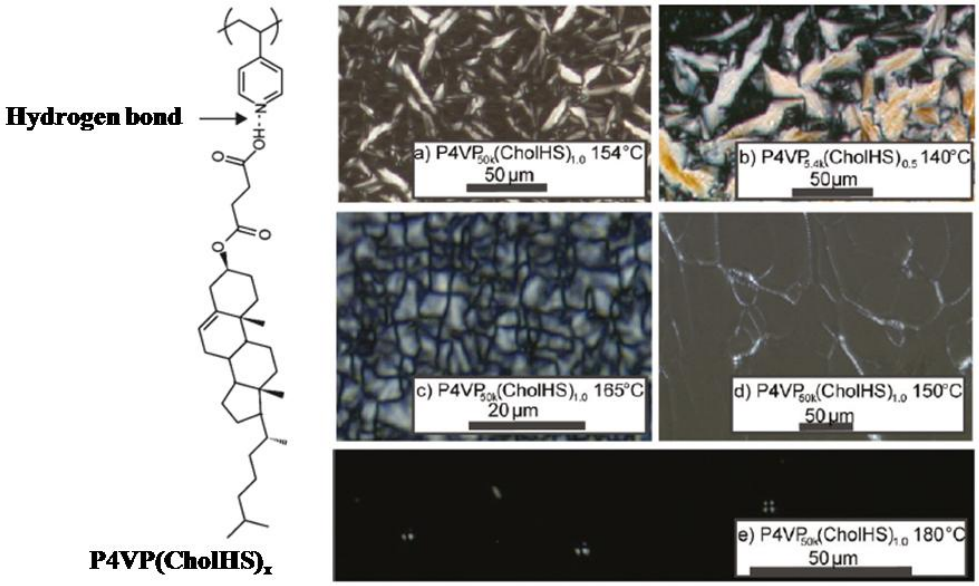

Figure-5.7. Hydrogen bonded complexation of a mesogenic amphiphile CholHS with P4VP and the liquid crystalline textures formed therein. [*Adapted from ref.61*]

In this chapter a mesogenic three dimensional polymer network of perylene and naphthalene bisimides have been designed and constructed utilizing the principles of supramolecular chemistry through non-covalent interactions. The secondary interaction chosen was hydrogen bonding due to its specificity and dynamic nature. Also the major reason for the increased interest in the rylenebisimides (perylene as well as naphthalene bisimides) stems not only from their attractive combination of electronic properties, but also due to the fantastic tunability of molecular electronic properties by well established organic chemistry strategies, through either variation of substituent on the imide nitrogen atoms or on the rylene skeleton.[62,63]

Ditopic hydrogen bonding donor modules of perylene and naphthalene bisimides were designed so as to act as supramolecular crosslinking agents to a multiple hydrogen bond acceptor polymer viz., P4VP as shown in scheme-5.1. The

schematic has been explained using naphthalene core as a representative example. Liquid crystalline self-organization in organic semiconductors has proved to be highly promising for efficient charge transport in organic electronic devices.[64-69] Both the ditopic rylenebisimides exhibited mesomorphic liquid crystalline nature that was made use of to understand the intrinsic packing ability of the mesogens. Detailed DSC, POM and XRD studies were undertaken for the investigation. Further the study unravels the effect of hydrogen bonded supramolecular crosslinking with P4VP on the final material properties of resulting polymer network of the electronically active cores.

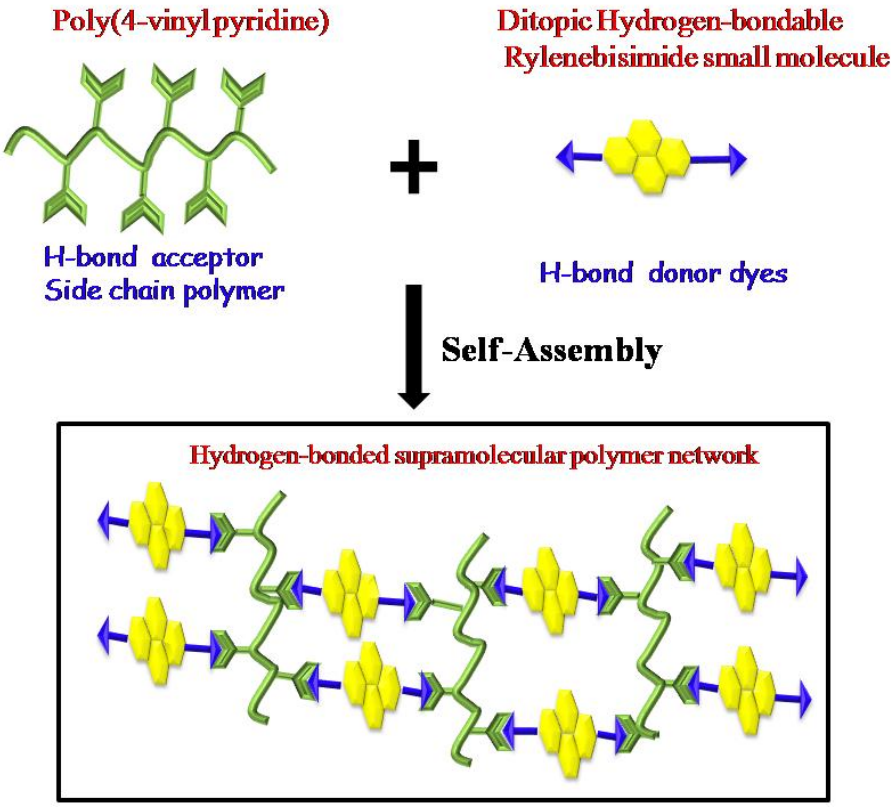

Scheme-5.1

The non-covalently crosslinked polymers were prepared by solution mixing of the hydrogen bond donor and acceptor components followed by solvent evaporation method. FT-IR studies were used to monitor the hydrogen bonding between the pyridine and phenol functional groups. The mesomorphic aspects of

the hydrogen bonded crosslinks were also thoroughly investigated by DSC and POM techniques. The self-assembling features were correlated to the packing nature of the mesogens using both low angle and wide angle XRD experiments and supported by molecular modelling studies. The bulk morphologies of the supramolecular networks were mapped using transmission electron microscopy (TEM). As a part of routine screening analysis of materials suitable for device applications, the charge transport behaviours of the rylenebisimides as well as their polymer network counterparts were subjected to space charge limited current (SCLC) measurements.

5.2. Experimental Section

5.2.1. Materials: Poly(4-vinylpyridine) (P4VP) (Mw =60,000) was purchased from Aldrich. It was dried in vacuum oven at 60 °C for 3 days prior to use. The other starting materials naphthalene tetracarboxylic acid dianhydride (NTCDA), perylene tetracarboxylic acid dianhydride (PTCDA), 3-pentadecylphenol (PDP) and other reagents were also purchased from Aldrich and used without any further purification. All solvents used were of analytical grade and carefully dried before use according to standard procedures.

5.2.2. Instrumentation Details: ^{1}H and ^{13}C-NMR spectra were recorded in $CDCl_3$ along with trace amounts of deuterated trifluoroacetic acid (TFA) using Bruker AVENS 200 MHz spectrophotometer. Chemical shifts (δ) are reported in ppm at 298 K, with trace amount of tetramethylsilane (TMS) as internal standard. MALDI-TOF analysis was carried out on a Voyager-De-STRMALDI-TOF (Applied Biosystems, Framingham, MA, USA) instrument equipped with 337 nm pulsed nitrogen laser used for desorption and ionization. The operation was in a reflector mode with an accelerating voltage of 25 kV. Micromolar solutions of the compounds in THF were mixed with Dithranol matrix and spotted on stainless steel MALDI plate and dried well. Size exclusion chromatography (SEC) in tetrahydrofuran (THF) was done using polystyrene standards for calibration. Waters 515 Pump connected through two series of Styragel HR columns (HR-3 and HR-4E) and Waters 2414 differential refractometer was used for analyzing the samples. The flow rate of the THF was maintained as 1 mL throughout the experiments, and 2-3 mg in 1mL of the samples were filtered and injected for recording the chromatograms at 30 °C. Infrared spectra were obtained using Bruker α-T spectrophotometer in the range of 4000-400 cm^{-1}. All the complexes were directly drop cast from DMF solutions onto KBr pellets and solvent evaporated off slowly at 60-70°C, followed by drying in vacuum oven overnight. Thermogravimetric analysis (TGA) was performed using a PerkinElmer STA 6000 thermogravimetric analyser. Samples were run from 40 to 800 °C with a heating

rate of 10 °C/min under nitrogen. DSC (differential scanning calorimetry) measurements were performed on TA Q10 differential scanning calorimeter. Typically, 3-4 mg of samples was placed in an aluminium pan, sealed properly and scanned at a heating rate of 10 °C/min under nitrogen atmosphere. The instrument was calibrated with indium standards before measurements. The first heating cycles were avoided to get rid of thermal history of the samples. Wide Angle X-ray Diffractogram (WXRD) were obtained using a Philips analytical diffractometer with CuKα emission. All the samples were recorded in the (2θ) range of 2–50 degrees using a PANalytical X'pert Pro dual goniometer diffractometer and analyzed using X'pert software. An X'celerator solid-state detector was employed in wide-angle experiments. The radiation used was CuKα (1.54 Å) with a Ni filter, and the data collection was carried out using a flat holder in Bragg–Brentano geometry. The optical microscope images were taken on a LEICA DM2500 polarized light microscope attached with a digital camera. Transmission Electron microscopy (TEM) was done using an FEI-Tecnai^{TM}-F20 electron microscope operating at 200 kV. Sandwich structures on ITO coated glass and Au substrates were fabricated for the SCLC studies. Thin films of the samples were drop-cast and spin coated on the substrates. The thickness was determined using Dektak surface profiler. The top Al electrode defining the area of the film (0.1 cm^2) was coated using thermal deposition method in high vacuum. All measurements were carried out under inert atmosphere.

5.2.3. Synthesis

(i) 4-amino-3-pentadecyl phenol: The synthesis procedure followed was the same as described in section 3.2.3.(i) in accordance with the literature procedure.[70] Yield : 80%. ^{1}H NMR (200 MHz, $CDCl_3$, δ ppm): 7.20 (d, 1H, Ar-H), 6.53-6.47 (m, 2H, Ar-H), 2.63 (t, 2H, Ar-C**H$_2$**-),1.60 (t, 2H, Ar-CH_2-C**H$_2$**), 1.36–1.23 (b, other aliphatic 24H), 0.86(t, 3H, Ar-$(CH_2)_{14}$-CH_3). ^{13}C NMR (50 MHz, $CDCl_3$,δ ppm): 146.8, 138.7, 126.2, 117.5, 113.4, 30.9, 29.5, 22.7, 14.3. FT-IR (KBr, cm^{-1}): 3432, 3350, 3296, 1647, 1585, 1416, 1334, 914,732, 675. MALDI-TOF MS

(Dihydroxybenzoic acid matrix): m/z calculated for $C_{21}H_{37}NO$: 319.29; found 320.31$[M+1]^+$.

Synthesis of Symmetrical Perylenebisimide (PDP-SPBI)

(ii) N, N'-Bis-(3-pentadecylphenyl)-perylene–3,4:9,10–tetracarboxylic bisimide : In a 500 mL round bottom flask (2.0 g, 5.1 mmol) perylene-3,4:9,10-tetracarboxylic acid dianhydride (PTCDA), (3.58 g, 11.22 mmol) 4-amino-3-pentadecylphenol and 0.5 g $Zn(OAc)_2$ in 30 g molten imidazole were stirred at 160 °C for 6 hours under nitrogen atmosphere. The reaction mixture was then cooled to room temperature and stirred with 400 mL 2N HCl overnight. The dark red precipitate was filtered and rinsed thoroughly with water and methanol. Finally dried at 120 °C and this crude product was purified several times by column chromatography method using $CHCl_3$/Methanol (95/5 v/v) solvent mixture. Yield : 63 %. ^{1}H NMR (200 MHz, $CDCl_3$ + d-TFA) δ ppm: 8.89 (m, 8H, perylene ring), 7.10-6.92 (3m, 6H, PDP-Ar**H**), 2.36 (t, 4H; PDP-Ar-C**H**$_2$), 1.53 (t, 4H; PDP-Ar-CH_2-C**H**$_2$), 0.86 (m, 6H, terminal C**H**$_3$ groups of C-15 alkyl chain), 1.26-1.12 (other aliphatic protons). ^{13}C NMR (50 MHz, $CDCl_3$, δ ppm) : 166.25, 163.31, 162.4, 159.2, 158.6, 155.84, 142.9, 139.8, 135.7, 135.2, 131.3, 129.7, 127.2, 125.1, 123.3, 122.8, 113.3, 106.2, 55.6, 32.7, 31.9, 29.9, 26.9, 22.8, 14.3.FT-IR (KBr, cm^{-1}): 3359, 2925, 2854, 1711, 1694, 1664, 1582, 1499, 1452, 1345, 1298, 1250,1198, 1180, 1094, 979, 876, 839, 813, 796, 768, 643. MALDI-TOF MS (Dithranol matrix): m/z calculated for $C_{66}H_{78}N_2O_6$: 995.36; found 996.55$[M+1]^+$. Elemental analysis calculated (%): C 79.64, H 7.90, N 2.81; found: C 78.86, H 7.60, N 3.05.

Synthesis of Symmetrical Naphthalenebisimide (PDP-SNBI)

(iii) N, N'-Bis-(3-pentadecylphenyl)-naphthalene-1,4:5,8-tetracarboxylic bisimide: Naphthalene-1,4:5,8-tetracarboxylic dianhydride (2.0 g, 7.45 mmol) was heated in 25g molten imidazole reagent followed by addition of 4-amino-3-pentadecylphenol (5.23 g, 16.41 mmol) under nitrogen atmosphere. It was stirred at 160 °C for 6 hours in presence of catalytic amount of $Zn(OAc)_2$. The reaction

mixture was then cooled to room temperature and stirred overnight with 250 mL 2N HCl. The precipitate was filtered, washed with water followed by methanol and dried at 120 °C. Purified yellow product was obtained by multiple column chromatography method using $CHCl_3$/Methanol (97/3 v/v) solvent mixture. Yield : 48 %. ^{1}H NMR (200 MHz, $CDCl_3$ + d-TFA) δ ppm: 8.87 (dd, 4H, naphthalene ring), 7.07-6.81(3t, 6H, PDP-Ar**H**), 2.39 (t, 4H; PDP-Ar-C**H**$_2$), 1.54(t, 4H; PDP-Ar-CH_2-C**H**$_2$), 0.87 (m, 6H, terminal C**H**$_3$ groups of C-15 alkyl chain), 1.24-1.13 (other aliphatic protons). ^{13}C NMR (50 MHz, $CDCl_3$, δ ppm) : 163.52, 162.4, 159.2, 158.6, 142.9, 139.8, 135.7, 135.2, 131.3, 129.7, 127.2, 125.1, 123.3, 122.8, 113.3, 106.2, 55.6, 32.7, 31.9, 29.9, 26.9, 22.8, 14.3.FT-IR (KBr, cm^{-1}): 3365, 2922, 2853, 1714, 1666, 1582, 1500, 1452, 1348, 1298, 1250, 1181, 1093, 980, 876, 840, 769,750, 640. MALDI-TOF MS (Dithranol matrix): m/z calculated for $C_{56}H_{74}N_2O_6$: 871.22 ; found 872.37$[M+1]^+$. Elemental analysis calculated (%): C 77.20, H 8.56, N 3.22; found: C 76.84, H 8.17, N 3.15.

Sample preparation: The ditopic symmetrical perylene and naphthalene bisimides namely **PDP-SPBI** and **PDP-SNBI** as well as poly(4-vinylpyridine) (P4VP) were dried in vacuum oven at 60 °C for 3 days. Stoichiometrically balanced **P4VP(PDP-SPBI)$_{1.0}$** and **P4VP(PDP-SNBI)$_{1.0}$** complexes were prepared from dry DMF (N, N'-dimethylformamide) solutions, where the subscript '1.0' denotes equal number of phenol functional groups from **PDP-SPBI**/**PDP-SNBI** per vinyl pyridine (VP) repeat unit in the P4VP polymer chain. In a typical procedure P4VP was first dissolved in DMF to which desired amount of **PDP-SPBI** or **PDP-SNBI** were added and the solutions were stirred for 24 hours under nitrogen atmosphere. Concentration of the solutions were kept as low as 1wt%. Subsequently the solvent was evaporated slowly on a hot plate at 50-60 °C and the complexes were further dried in vacuum oven at 55 °C for 3 days, slowly cooled to room temperature and stored in dessiccator thereafter.

5.3. Results and Discussion

5.3.1. Synthesis and Characterization of Ditopic Perylene and Naphthalene bisimides

The ditopic hydrogen bondable symmetrical perylene and naphthalene bisimides were designed by end capping the respective cores with 3-pentadecylphenol groups at both termini so that the resulting small molecules would act as hydrogen bond donor dyes using the phenolic-OH group. Scheme-5.2 depicts the typical synthetic procedure used for both the symmetrical bisimides along with the corresponding reagents and reaction conditions.

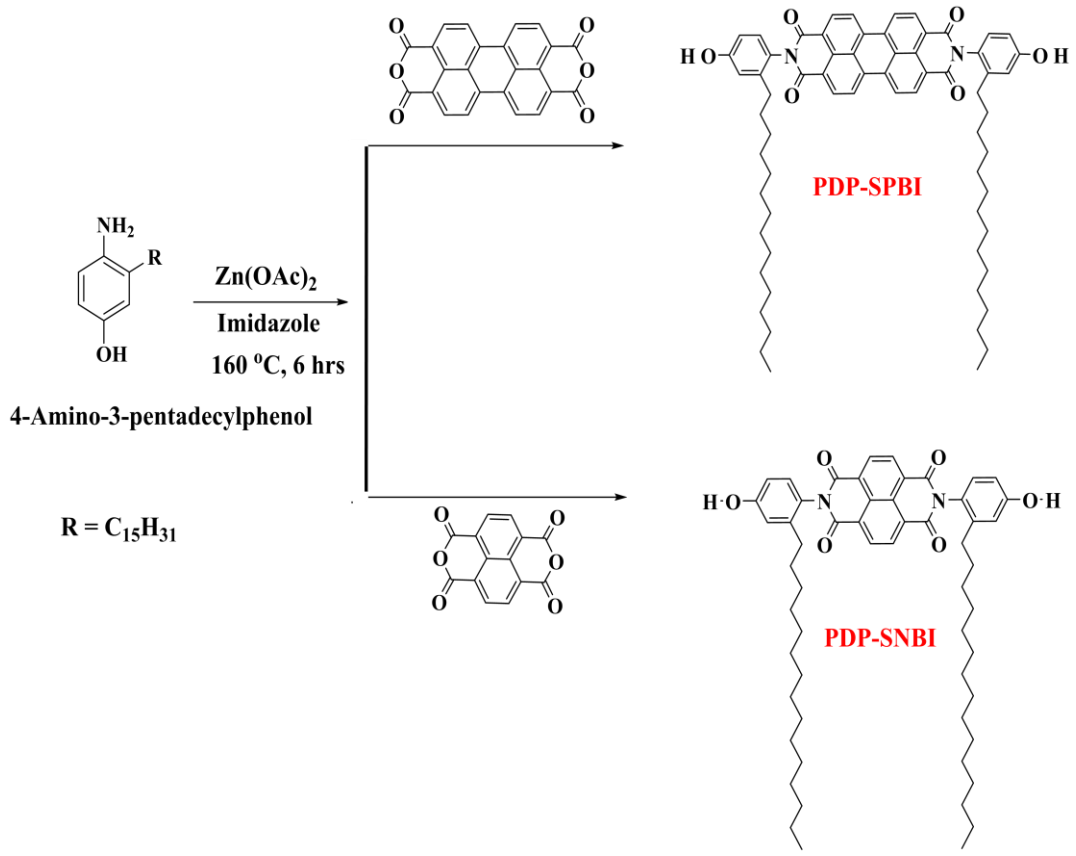

Scheme-5.2. Synthesis of ditopic hydrogen bondable symmetrical perylene and naphthalene bisimides.

Simple imidization of the perylene and naphthalene tetracarboxylic dianhydrides were carried out with 2.2 equivalents of the 4-amino-3-pentadecylphenol, which in turn was derived from a renewable resource based amphiphilic 3-pentadecylphenol (PDP). The resulting ditopic hydrogen bonding perylene and naphthalene bisimide modules were named as **PDP-SPBI** and **PDP-SNBI** and their chemical structures are also given in scheme-5.2. Molten imidazole was found essential for the reaction to proceed along with catalytic amount of zinc acetate. Most other high boiling solvents such as N,N'-dimethylformamide (DMF), N,N'-dimethylacetamide (DMAc) were found to be ineffective to give desired bisimides in good yields. Both the products were subjected to thorough purification by repeated column chromatography technique at least three times.

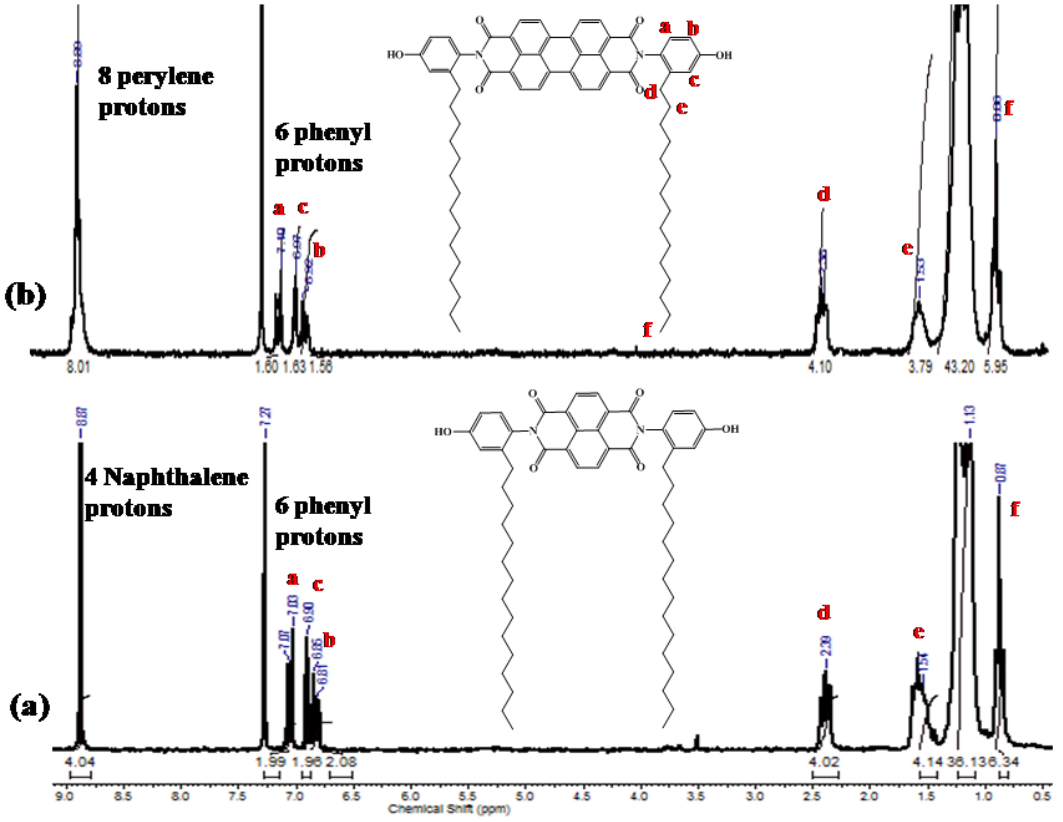

Figure-5.8. ^{1}H-NMR spectra of symmetrical (a) **PDP-SNBI** and (b) **PDP-SPBI** recorded at room temperature.

The structures of the functionalized perylene and naphthalene bisimides were characterized by ^{1}H-NMR, ^{13}C-NMR, FT-IR and MALDI-TOF spectroscopic methods. The stacked ^{1}H-NMR spectra of symmetrical **PDP-SPBI** and **PDP-SNBI** is given in figure-5.8. A mixture of $CDCl_3$ and deuterated trifluoroacetic acid was used as the NMR solvent because of the low solubility of the rigid symmetrical bisimides in $CDCl_3$ alone. Both the compounds had similar spectra with the only difference in the integration value and pattern of the perylene and naphthalene ring core protons. The different types of protons have been labelled using alphabets. The perylene and naphthalene core protons appeared as sharp multiplets corresponding to eight and four protons at 8.89 and 8.87 ppm respectively. The three aromatic protons of the PDP ring attached on either side of the rylene cores appeared in the region 6.81 - 7.10 ppm with their characteristic splitting patterns and were labelled as 'a', 'b' and 'c'. Their integration value of six matched very well with that of the perylene or naphthalene core protons, which confirmed the formation of the product. Further evidence for the attachment of PDP ring on both sides of the rylene core were obtained from the aliphatic protons corresponding to the immediate -CH_2- and end -CH_3 groups (labelled as 'd', 'e' and 'f') of the C_{15} alkyl chain at meta position of the phenol also perfectly matching in integration to the respective number of protons.

Both the samples **PDP-SPBI** and **PDP-SNBI** were subjected to MALDI-TOF analysis and the corresponding mass spectra is given in figure-5.9. The MALDI-TOF spectra was recorded using Dithranol as the matrix and the molecular ion peaks were obtained for $[M+1]^+$ species in the case of both **PDP-SPBI** and **PDP-SNBI.** The size exclusion chromatography (SEC) analysis for these two symmetrical rylenebisimides were done using two polystyrene beads column in series and tetrahydrofuran as the eluting solvent. The corresponding chromatograms exhibited single peaks which demonstrated the purity of the samples as given in figure-5.10. As expected, the compound **PDP-SPBI** with high molar mass was eluted at a lower retention time and the lower molar mass compound **PDP-SNBI** at relatively higher retention time.

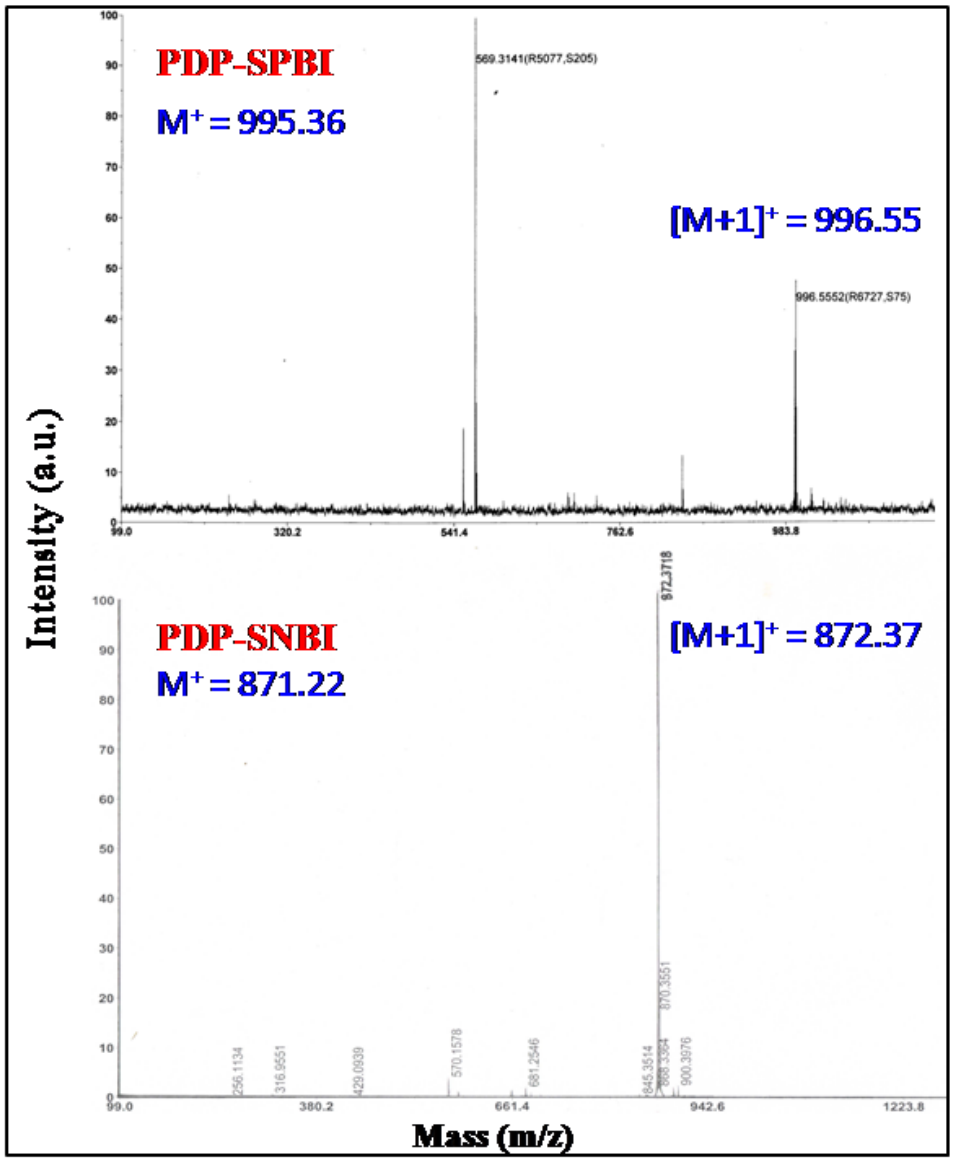

Figure-5.9. MALDI-TOF spectra of symmetrical (a) **PDP-SNBI** and (b) **PDP-SPBI.**

Their thermal stability was studied by thermogravimetric analysis (TGA) run under nitrogen atmosphere from 30 °C to 800 °C. The TGA plots for **PDP-SPBI** and **PDP-SNBI** are given in figure-5.11 and it could be seen that both the molecules exhibited high thermal stability with no signs of decomposition upto 400 °C. Thus these molecules are well suitable for fabrication of optoelectronic devices that may require high temperature processing.

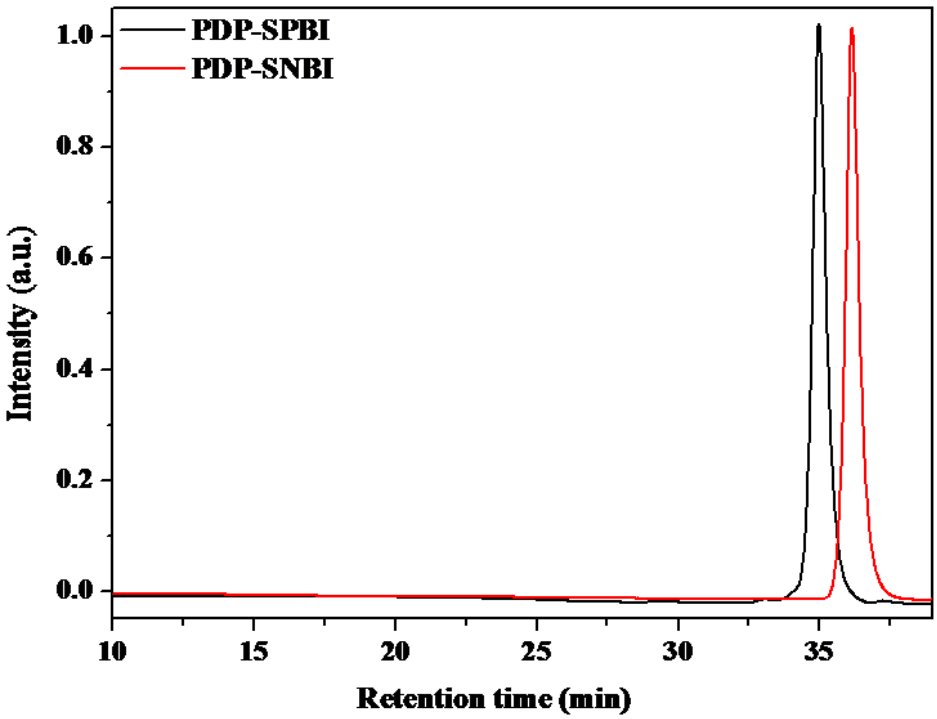

Figure-5.10. Size exclusion chromatography plots for **PDP-SNBI** and **PDP-SPBI.**

The phase behaviour of these two symmetrical rylenebisimide small molecules was investigated by differential scanning calorimetric (DSC) analysis. The **PDP-SPBI** molecule had very high melting point (> 400^{o}C) and because of the experimental limitations at such higher temperatures, it was not possible to heat the perylene derivative to the isotropization temperature. As a result the DSC thermogram of **PDP-SPBI** (figure-5.12) run from 30 to 300 °C did not show any thermal phase transitions in the heating as well as cooling cycle.

On the other hand, the lower analogue **PDP-SNBI** exhibited melting transition ~ 280 °C due to its lower extent of rigidity compared to **PDP-SPBI** molecule. Typically 2-3 mg of the powdered **PDP-SNBI** sample was subjected to DSC analysis at 10 °C /min heating and cooling rates in the temperature region 30 °C to 350 °C. The first heating cycle erases the prehistory of the sample and hence was discarded. The corresponding DSC thermogram of **PDP-SNBI** is depicted in figure-5.13 with the second heating and first cooling cycles.

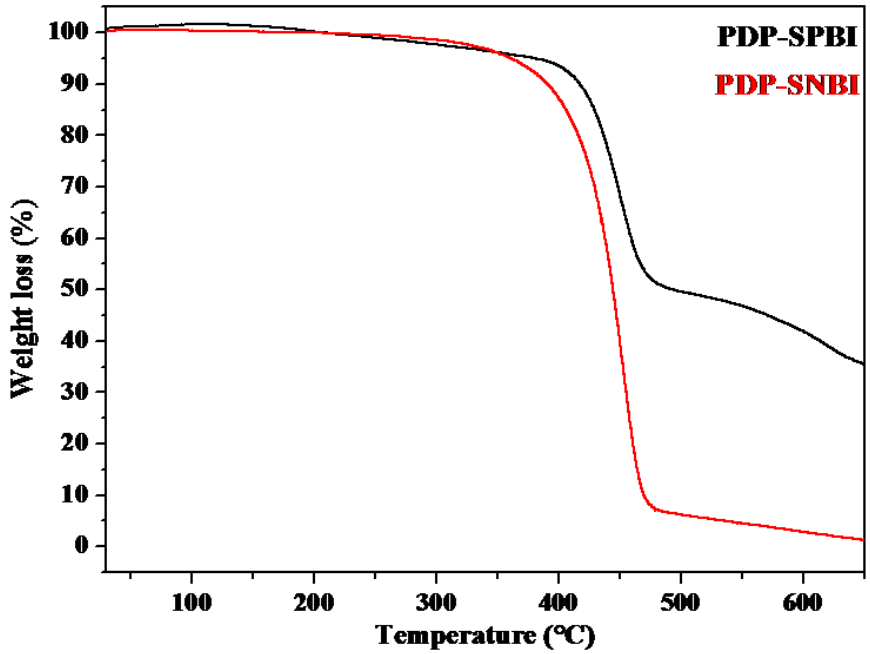

Figure-5.11. TGA thermogram for **PDP-SNBI** and **PDP-SPBI** molecules.

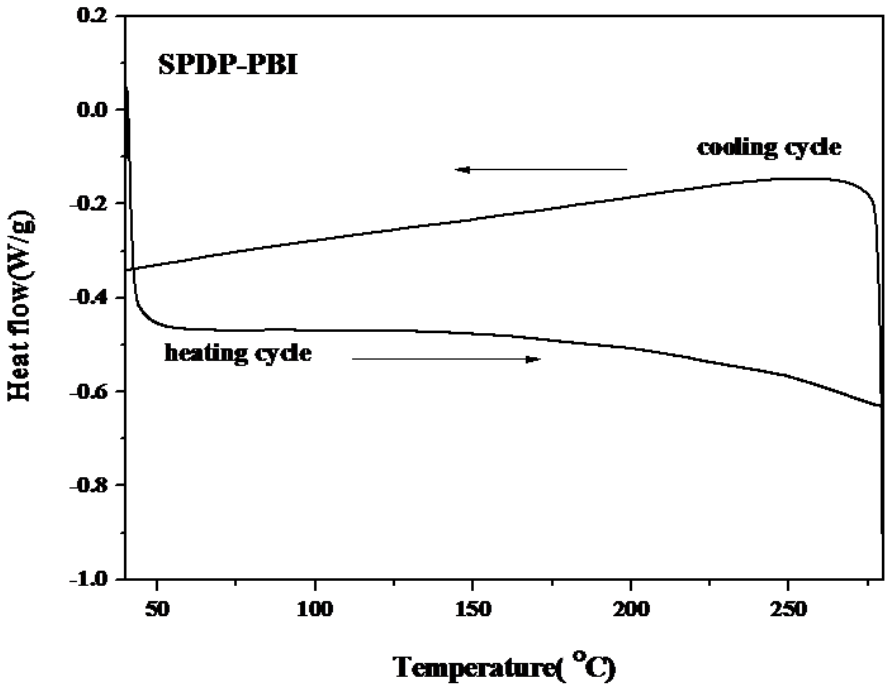

Figure-5.12. DSC thermogram for **PDP-SPBI** molecule run in the range 30 to 300°C.

The **PDP-SNBI** molecule showed multiple transitions in the heating as well as cooling scans which indicated its thermotropic liquid crystalline (LC) character. Upon heating, two transitions were observed; namely from crystal to liquid crystalline at 84 °C and from liquid crystalline to complete isotropic state around 280 °C. The transitions observed in the heating cycle were not exactly reversed in the cooling cycle; rather very close multiple transitions were found in the temperature region from 250 -230 °C along with a broad transition around 72 °C.

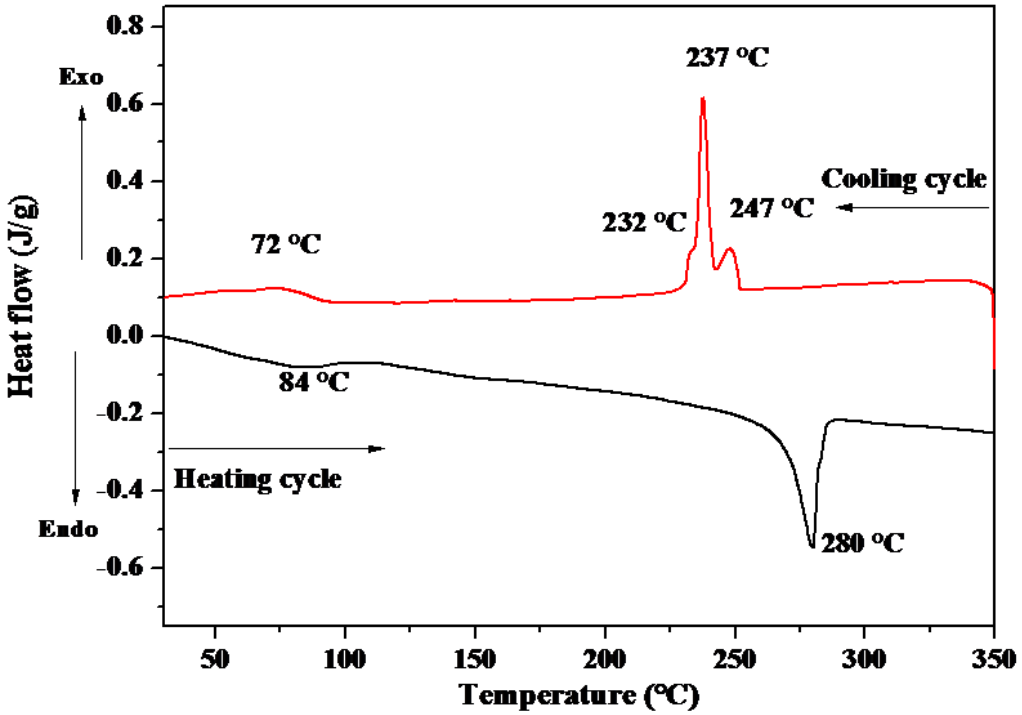

Figure-5.13. DSC thermogram for **PDP-SNBI** molecule run in the range 30 to 350°C.

The mesogenic behaviour and solid state organization of the rylenebisimides were further investigated by X-ray diffraction (XRD) and polarized light optical microscope (POM) imaging studies. The complete wide angle X-ray diffraction patterns of the bulk **PDP-SPBI** sample recorded at room temperature is shown in figure-5.14 with the relevant d-spacing values. This XRD pattern obtained for the solvent crystallized sample at room temperature itself showed the absence of a

typical crystalline solid and confirmed the presence of an LC state, specifically a columnar phase. In the columnar LC phases, the supramolecular columns are packed in a 2D lattice with long range positional order, but the individual molecules within the columns are disorderly packed reminiscent of a fluid.[71,72]

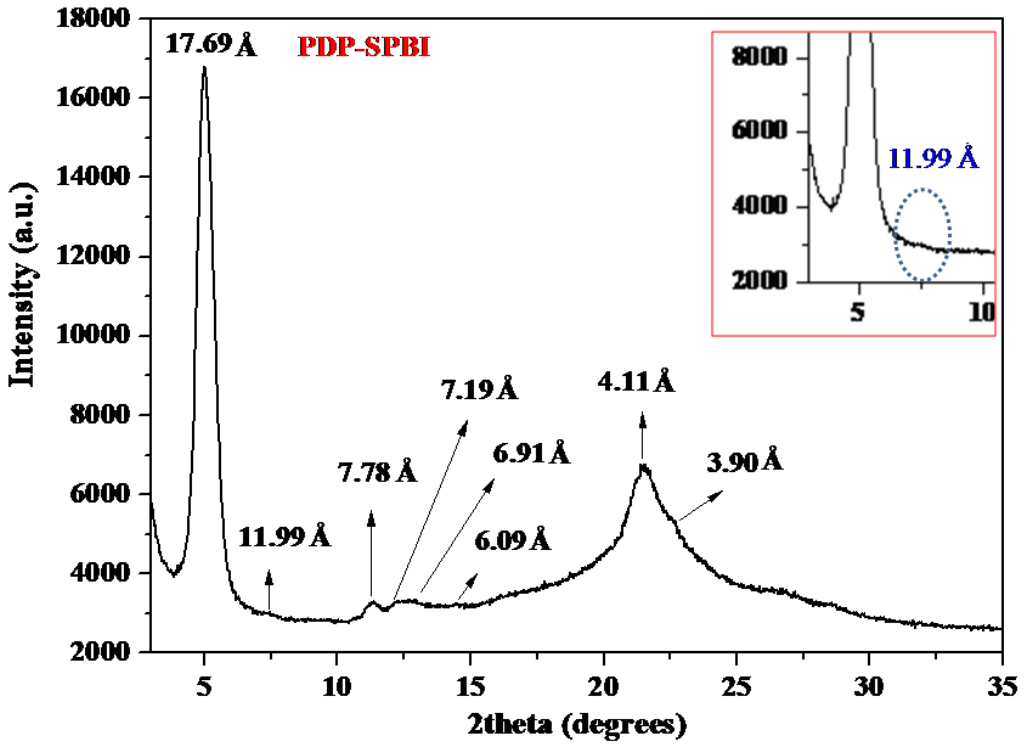

Figure-5.14. WXRD pattern for bulk **PDP-SPBI** molecule recorded at room temperature.

The XRD pattern of columnar phases are often characterized by a very sharp peak in the small angle region and diffused peaks in the wide angle region. The 2D lattice of the columnar structure is deduced from the d-spacing ratios of Bragg reflections in the small angle region. The XRD pattern of **PDP-SPBI** sample had five reflections in sequence corresponding to the d-spacing 17.69 Å, 11.99 Å, 7.78 Å, 7.19 Å, 6.91 Å in the low angle regime with the reciprocal spacing ratio 1 : 1.47 : 2.27 : 2.46 : 2.56. In close agreement with several literature reports, this Bragg reflection pattern strongly pointed towards a rectangular columnar (**Col_r**) arrangement of the mesogens with lattice parameters a = 35.38 Å and b = 12.74

Å.[73-78] The observed XRD pattern could not be assigned to a hexagonal columnar (**Col_h**) lattice due to the lack of reciprocal d-spacing ratio 1: √3 : √4 : √7 : √9 and **Col_h** phases are unequivocally characterized by only a single maximum at low angle ($0 < 2\theta < 5°$) with non-existence of multiple reflections in the higher angle region, except a broad diffused halo around $2\theta = 20°$.[73,79-81]

For the less symmetric rectangular columnar phases there is no fixed ratio between the spacings, but usually a very sharp fundamental small angle (200) reflection and a very close satellite kind of (110) reflections (very low intensity) are seen.[81] Also the wide angle region from 2θ = 15-25° of **PDP-SPBI** showed a sharp reflection around 21.48° instead of broad halo which indicated almost ordered alkyl components and a small shoulder hump around 22.61° corresponding to d-spacing value of 3.90 Å that could be attributed to the π-π stacking distance of the perylene aromatic cores within the columns.

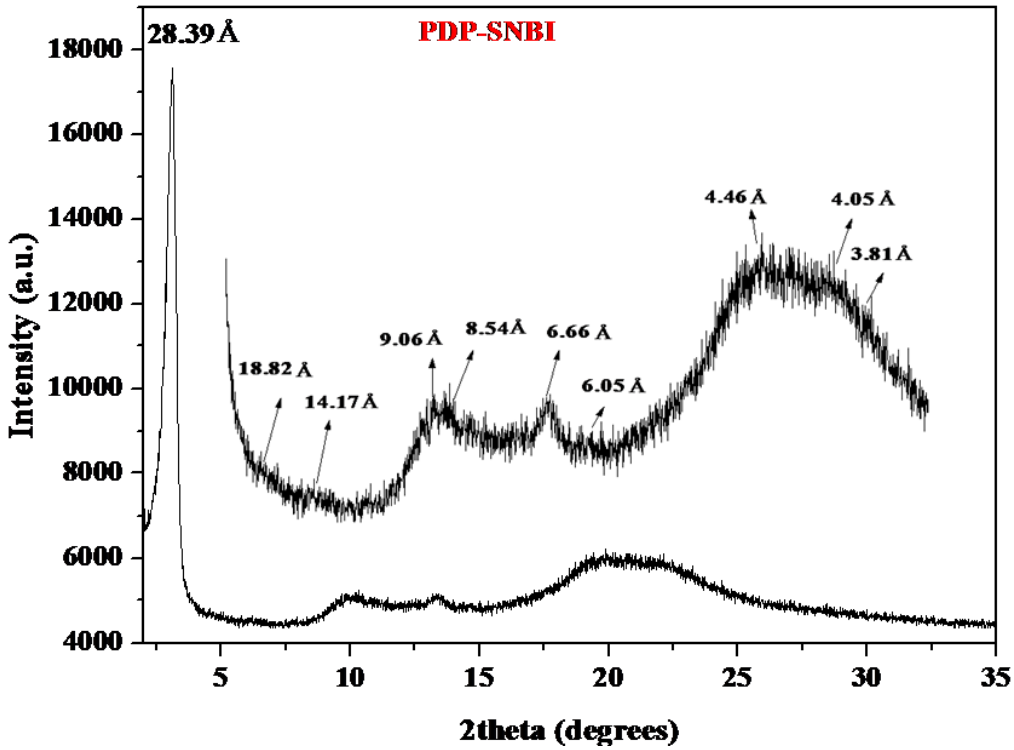

Figure-5.15. WXRD pattern for bulk **PDP-SNBI** molecule recorded at room temperature.

In a similar manner the XRD pattern of **PDP-SNBI** (figure-5.15) also suggested a rectangular columnar arrangement with the reciprocal ratio of five Bragg reflections at 28.39 Å, 18.82 Å, 14.17 Å, 9.06 Å, 8.54 Å calculated to be 1 : 1.51 : 2.00 : 3.13 : 3.32 respectively. Based on literature reports the first two peaks at 28.39 Å and 18.82 Å could be assigned to the (200) and (110) reflections of the rectangular columnar (**Col_r**) lattice with packing parameters a = 56.78 Å and b = 19.94 Å.[73-78] The lattice parameters as well as the fundamental sharp reflection (28.39 Å) of the **PDP-SNBI** was found to be much larger than that observed for **PDP-SPBI**, which indicated an elongation of the rectangular lattice preferably along the 'a' direction. Further the mid-wide angle XRD region of **PDP-SNBI** exhibited much broader halos indicating the higher extent of disordered or fluid like nature of the aliphatic chains.

The mesomorphic textures formed by thermotropic liquid crystalline (LC) phases of **PDP-SNBI** were then imaged using polarized light optical microscope (POM) which was attached to a programmable temperature controlled hot stage. The sample was kept on a glass substrate and heated at the rate of 10 °C /min to 300 °C where it melted completely and was then maintained at isothermal for 2-3 minutes. The isothermal phase appeared dark under the cross polarizer. Subsequently, the melt was cooled at the same rate of 10 °C/min and the birefringent liquid crystalline phases started appearing initially with flow properties and then slowly developed to form uniform mesomorphic textures. The images were captured using the attached high resolution camera. Very small grain sized, irregular broken focal-conic or spherulitic type textures typical for columnar phases were observed. Figure-5.16 (a) and (b) shows the broken focal-conic type textures exhibited by **PDP-SNBI** that was retained at room temperature upon cooling from the isotropic melt at the rate of 10 °C/min. Similar POM images has been recently reported for crescent shape-persistent aromatic oligoamides which was attributed to a rectangular columnar (**Col_r**) phase and other diverse mesogenic phases like

lamellar columnar (**L_{col}**), discotic nematic (**N_D**) were also obtained by manipulating the backbones and side chains.[74]

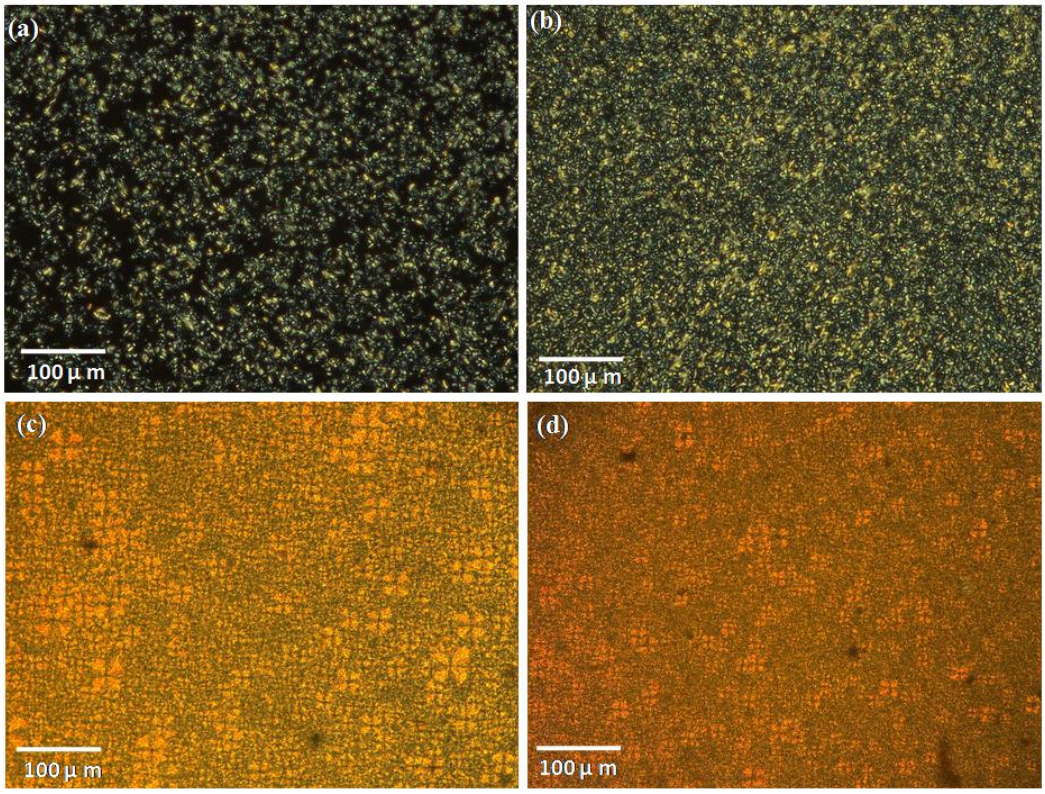

Figure-5.16. Optical microscope images of the thermotropic mesophases of **PDP-SNBI** observed through cross polarizers during cooling from isotropic at 244 °C.

The **PDP-SNBI** sample upon rapid cooling from the isotropic state to room temperature, typical fan-like spherulitic textures with very small domain growth were also seen as given in figure-5.16 (c) and (d). This type of textures are also reported for both **Col_h** and **Col_r** phases.[82-85] For example Laschat *et al.* observed similar spherulitic domains formed by potassium thiocyanate (KSCN) salts of triphenylene-substituted [18] crown-6-ethers which were assigned to rectangular columnar mesophases.[82] Due to the minor structural differences between the hexagonal and rectangular lattice (see figure-5.17), textures known for **Col_h** phases are also observed for **Col_r** phase. However broken-fan-shaped and mosaic textures are found to be more common for **Col_r** phase. [73,81]

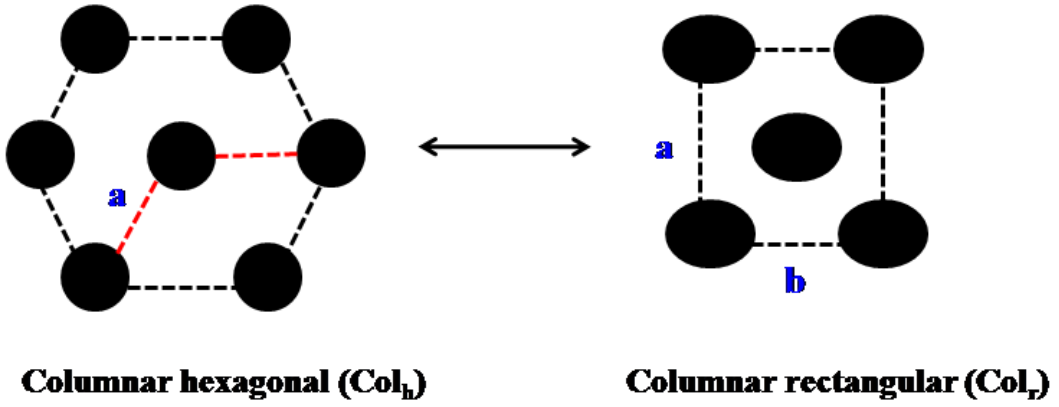

Figure-5.17. Illustration of columnar orientation relation between hexagonal (**Col$_h$**) and rectangular (**Col$_r$**) lattice.

Mesomorphic liquid crystalline phases can form in pure compounds or even mixture of components not only as a function of temperature (thermotropic) but also in mixtures in which one of the component is the solvent that provides the necessary freedom of movement for the mesogens to form concentration dependent mesomorphic phases (lyotropic).[86] Amongst the different types of mesogens, the amphiphilic molecules are best known to form lyotropic mesophases that relies on the self-assembly of chemically distinct molecular segments into separate micro-domains in order to reduce the unfavourable interactions.[87]

In the case of **PDP-SPBI** molecule the isotropization temperature was above 400 °C and as a result the mesomorphic textures could not be observed by thermal treatment. But the XRD pattern of **PDP-SPBI** molecule was very closely resembling that of **PDP-SNBI** molecule and since they were also structurally similar differing only in the extent of rigidity in terms of the rylene core, it was envisioned that the **PDP-SPBI** should also possess similar kind of liquid crystalline character. In such an attempt to find out whether this molecule also had the intrinsic ability to undergo a self-organization of the mesogens, lyotropic LC properties were examined in tetrahydrofuran (THF) solvent in which both the **PDP-**

SPBI and **PDP-SNBI** molecules were freely soluble. Indeed it was found that both the molecules were lyotropic liquid crystals, the POM images corresponding to that of 1 wt% THF solution of **PDP-SPBI** is given in figure-5.18.

The reasonably viscous solution of **PDP-SPBI** in THF was sandwiched between two cover slips and observation under POM showed pronounced birefringent images that confirmed the formation of lyotropic liquid crystalline phase arising from the anisotropic self-organization of the mesogens. Two types of lyotropic textures were observed : towards the middle of the cover slips very small grain sized broken fan like textures similar to that obtained for **PDP-SNBI** and towards the periphery pseudo-focal conics with strong birefringence were clearly visible. Such structures have been typically reported for rectangular columnar phases.[78,88,89] Most probable reason for the formation of two types of textures appears to be the concentration gradient existing between the middle and peripheral portions of the thin film formed within the cover slips.

The lyotropic textures obtained were found to be retained even after the solvent was evaporated off slowly and indicated the intrinsic tendency of rod-like **PDP-SPBI** molecule to form rectangular columnar phase as the thermodynamically stable structure. Similar flake-like lyotropic columnar textures were reported recently for rod-like π-conjugated anion responsive acyclic oligopyrroles and the texture was assigned to rectangular columnar.[78] In fact columnar phases are not the characteristics of discotic mesogen alone, several other types of mesogens such as surfactant molecules are also reported to aggregate into columnar architectures that form lyotropic columnar phases.[90,91]

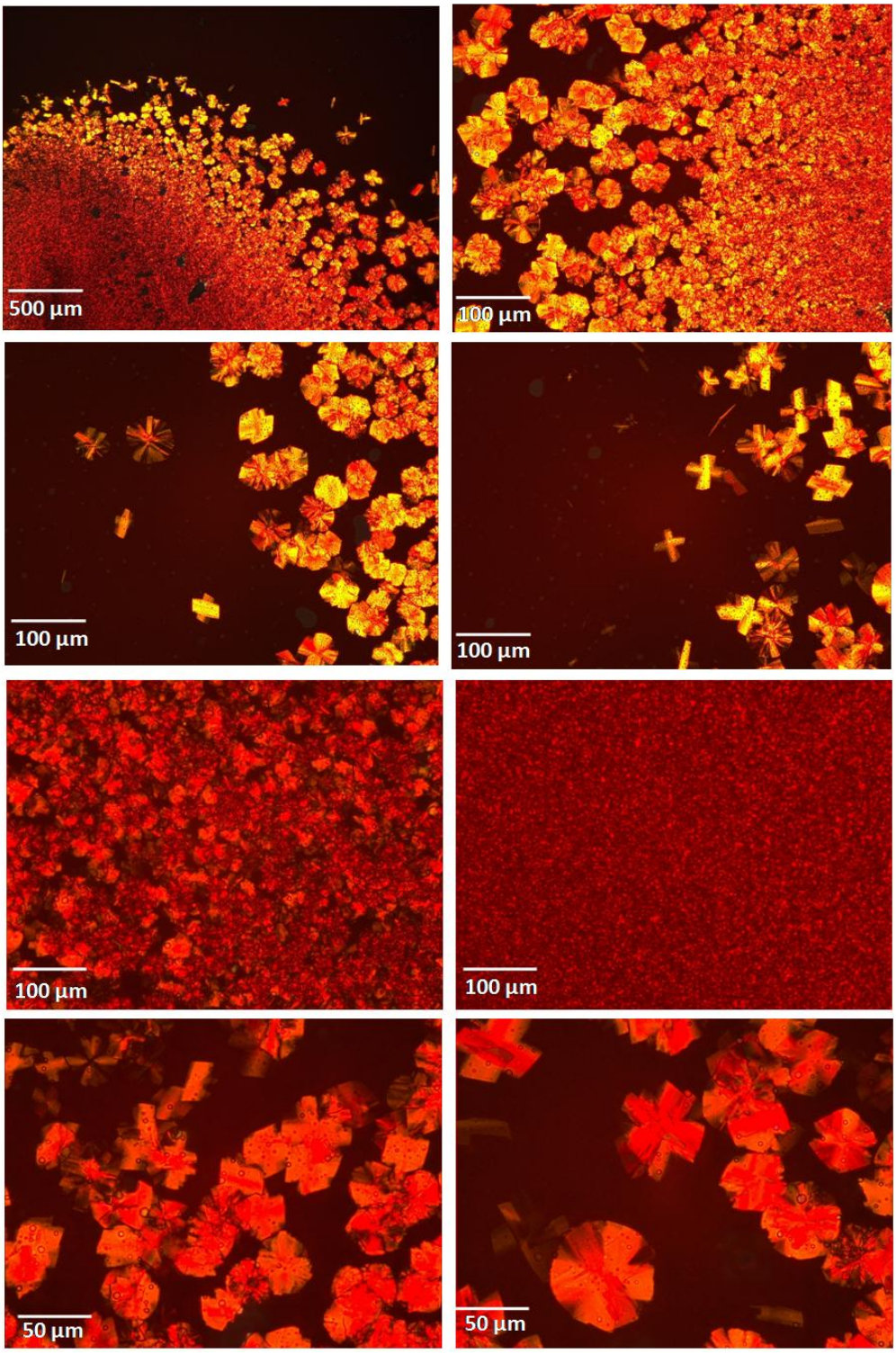

Figure-5.18. Polarised optical microscopy images of the lyotropic phases formed by **PDP-SPBI** molecule from 1wt% THF solution.

The **PDP-SNBI** molecule also exhibited lyotropic liquid crystalline phase in addition to thermotropic. The lyotropic rectangular columnar phases formed by 1 wt% THF solution of **PDP-SNBI** is also given in figure-5.19. The textures were not so well defined; nevertheless, it may be noted that similar texture was observed for **PDP-SNBI** from thermal treatment. Thus it could be concluded that both the rylenebisimide molecules possessed the inherent capability to form well organized columnar superstructures irrespective of the processing methods - either by solution processing or thermal treatment.

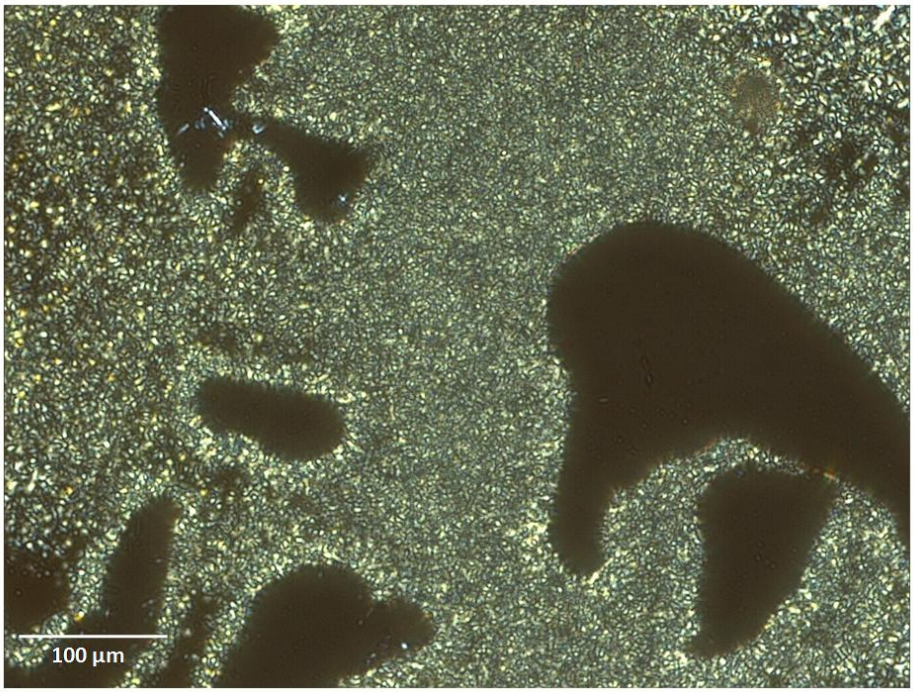

Figure-5.19. Polarised optical microscopy image of the lyotropic phases formed by **PDP-SNBI** molecule from 1wt% THF solution.

The columnar LC phases are classified based on the type of lattice in which the columns are arranged, the hexagonal columnar $\mathbf{Col_h}$ (figure-5.20 (a)) phase being most commonly adopted by discotic mesogens. [46,73,83] When the columns are arranged less symmetrically, rectangular columnar $\mathbf{Col_r}$ phases are formed with face centered lattices deviating only slightly from the hexagonal symmetry. Non-

circular shape of the mesogens or anisotropic distribution of volume occupied by the liquid-like alkyl chains are most often the reason for the formation of asymmetric columns. As a result the molecules are tilted with respect to the column axis in a rectangular columnar phase which makes the cross-sectional view appear elliptic.[92-94] Depending on the symmetries assigned to the 2D rectangular lattice, different types of $\mathbf{Col_r}$ phases have been identified like $P2_1/a$, P2/a and C2mm point group symmetries (figure-5.20 (b) & (c)).[73] Other lattice arrangements such as tetragonal and oblique are rare (figure-5.20(d)). Eventhough the rylenebisimides **PDP-SNBI** and **PDP-SPBI** used in the present study were confirmed to form a rectangular columnar type packing, the unambiguous determination of the symmetry point group is difficult.

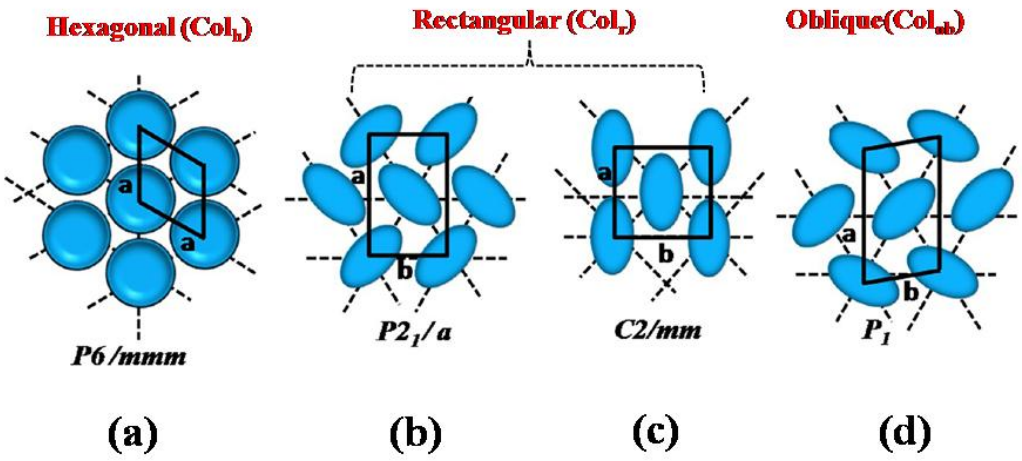

Figure-5.20. Schematic illustration of the cross-sectional view of 2D lattices for most common columnar LC phases. [*Adapted from ref.73*]

Molecular modelling studies using theoretical calculations based on density functional theory (DFT) were done to assess and correlate the observed packing picture with the individual molecular length of the structure directing ditopic rylenebisimide molecules. The energy minimized structures of the individual **PDP-SNBI** and **PDP-SPBI** molecules in the gas phase at absolute zero, obtained using the DFT are shown in the figure-5.21. In both the molecules the rylene core was flat with the two phenyl groups perpendicular to the middle core. The molecular

lengths of **PDP-SNBI** and **PDP-SPBI** along the rigid part of the molecules were found to be 18.27 Å and 22.61 Å respectively. The length of the fully extended C15 alkyl chain in all-trans conformation was around 19.47 Å and the two set of these chains on either side of the **PDP-SPBI** molecule were in a gauche conformation with respect to each other, whereas in **PDP-SNBI** they were almost staggered as shown in figures 5.21 (b) & (d) respectively.

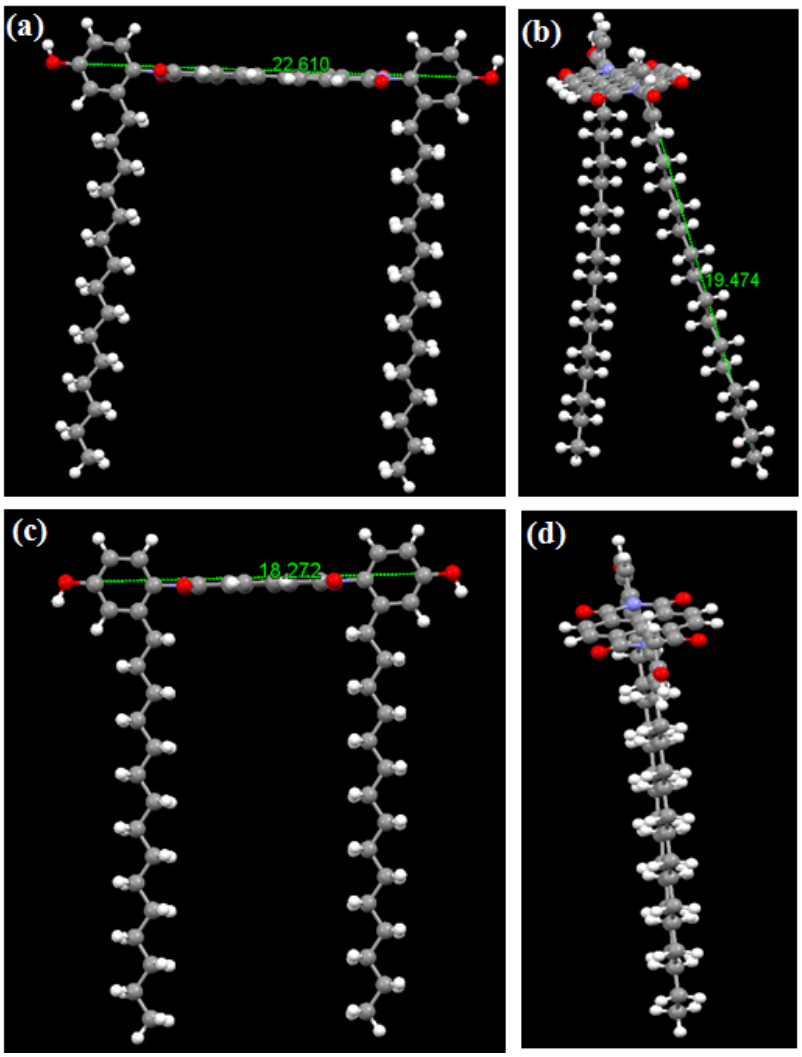

Figure-5.21. Energy minimized structures of **PDP-SPBI** (a) & (b) and **PDP-SNBI** (c) & (d).

Therefore the overall shape of the molecules were not circular, the rigid-rod aromatic cores could be envisioned as having an elliptical shape tapered on both ends due to the perpendicularity between PDP and rylene rings (figure-5.22(a)). The liquid like long C_{15} alkyl chains could be imagined projecting on either side towards the periphery (omitted in the schematic structures for clarity). In order to accommodate the steric demand from these peripheral aliphatic chains, the molecules must undergo tilting with respect to the column axis characteristic of **Col_r** type packing (figure-5.22(b)). Several similarly shaped columnar LC molecules have been reported to arrange in such a tilted fashion.[95-97]

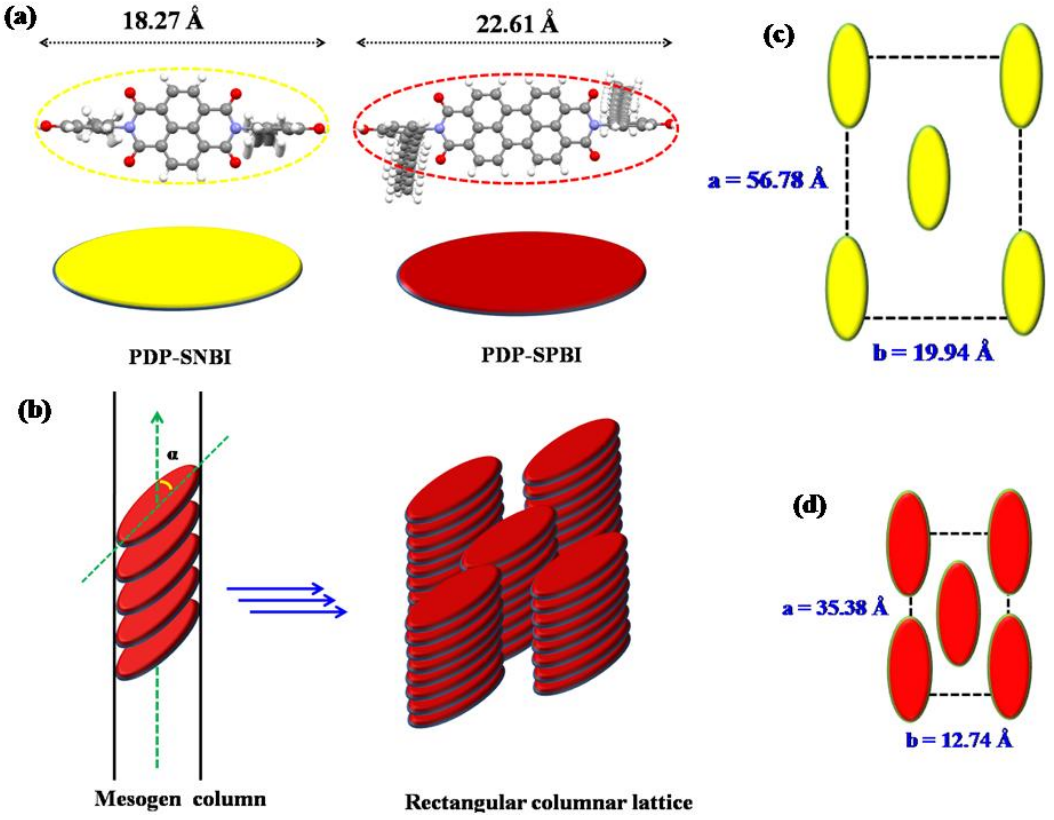

Figure-5.22. Schematic illustration of the columnar packing of **PDP-SPBI** and **PDP-SNBI.**

However, the intercolumnar distance in the case of **PDP-SNBI** (28.39 Å) was found to be significantly larger than the molecular core length along the rigid axis (18.27 Å); whereas for **PDP-SPBI** the intercolumnar distance (17.69 Å) was smaller compared to the rigid core length (22.61 Å). This difference could be expected to arise from the different extent of relative nanophase segregation of the polar aromatic cores and non-polar alkyl chains in **PDP-SNBI** and **PDP-SPBI**. The only other difference between the two rylenebisimides is the rigidity to flexibility balance; the rigid portion more dominating in **PDP-SPBI** in contrast to the flexible portion for **PDP-SNBI.** However the observed packing difference suggests that the mesogen columns are much closer or most probably interdigitated in **PDP-SPBI** that seems to result in small intercolumnar distance (figure-5.22(d)). On the other hand, **PDP-SNBI** columns are relatively farther apart in the rectangular lattice (figure-5.22(c)).

5.3.2. Hydrogen bonded Supramolecular Crosslinking of PDP-SPBI and PDP-SNBI with P4VP

The two ditopic rylenebisimide molecules namely **PDP-SPBI** and **PDP-SNBI** were independently subjected to supramolecular crosslinking with poly(4-vinyl pyridine) (P4VP) via hydrogen bonding between the pyridine and phenol groups. For the supramolecular crosslinking experiments, calculated amounts of P4VP was dissolved in minimum volume of DMF as solvent and the respective rylenebisimides were added in half the molar ratio to the number of pyridine units on the P4VP chain because each ditopic molecule contained two phenol functional groups with which they co-ordinate to the pyridine rings. The mixture of interacting components were stirred overnight at slightly elevated temperatures around 60^{o}C to ensure homogeneous complexation. The solutions were then slowly brought to room temperature and subsequently the solvent was completely evaporated off by gradual heating around 45-50 °C. Further the samples were also dried in vacuum oven for 2-3 days and stored under inert conditions thereafter. The

chemical structures of the two supramolecular crosslinked rylenebisimide based polymer networks as proposed are shown in figure-5.23.

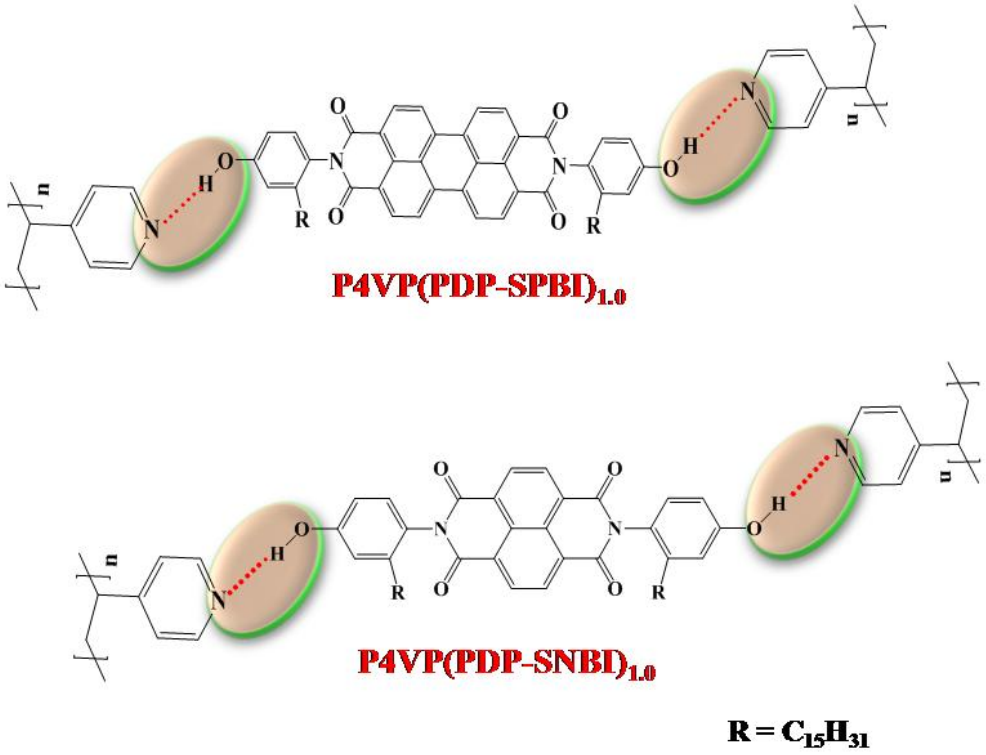

Figure-5.23. Chemical structures of the hydrogen bonded supramolecular crosslinks.

The two set of supramolecular polymer networks were abbreviated as **P4VP(PDP-SPBI)$_{1.0}$** and **P4VP(PDP-SNBI)$_{1.0}$**, where the subscript 1.0 indicated the stoichiometric hydrogen bonding between the pyridine and phenol groups in both the complexes. The hydrogen bonding sites are pointed out in highlighted circles. The linear topology of ditopic hydrogen bonding modules in the rylenebisimides gave rise to the crosslinking nature to the complexes.

5.3.3. Evidence for Hydrogen bonding

As explored in the previous chapters, FT-IR spectroscopy was used to monitor the hydrogen bonding between the pyridine and phenol groups in the supramolecular crosslinked polymer networks. The FT-IR spectra of thin films of neat components P4VP, **PDP-SPBI**, **PDP-SNBI** as well as their respective hydrogen bonded complexes viz., **P4VP(PDP-SPBI)$_{1.0}$** and **P4VP(PDP-SNBI)$_{1.0}$** were measured directly from drop cast samples onto potassium bromide pellets from DMF solution which were dried in vacuum at 60 °C for overnight in order to remove all traces of solvent. In order to analyze the hydrogen bonded crosslinking in **P4VP(PDP-SPBI)$_{1.0}$** and **P4VP(PDP-SNBI)$_{1.0}$** samples, the FT-IR spectroscopy studies on P4VP(PDP)$_x$ systems from literature was used for comparison where the most important stretching modes of P4VP traced were at 993 cm^{-1} and the 1413 cm^{-1}.[98]

Similar results were reproduced in this study and thus it was verified that significant extent of hydrogen bond was formed between the phenol groups of ditopic rylenebisimides and the pyridyl functional groups of P4VP in the supramolecular crosslinks. Figure-5.24 (a) & (b) shows the FT-IR results in the absorption region from 1020-970 cm^{-1} and 1430-1395 cm^{-1} respectively for the two supramolecular crosslinks. Both **PDP-SNBI** and **PDP-SPBI** had no peaks at 993 cm^{-1}, but exhibited prominent peaks near 983 cm^{-1} and 966 cm^{-1} in the case of former and latter respectively. Upon complexation with P4VP, these peaks remained intact, but new peaks around 1007 cm^{-1} characteristic of hydrogen bonded pyridine ring appeared in the case of both **P4VP(PDP-SPBI)$_{1.0}$** and **P4VP(PDP-SNBI)$_{1.0}$** with no trace of free pyridine band at 993 cm^{-1} visible in the supramolecular crosslinks. Similarly the free pyridine band around 1413 cm^{-1} was found at shifted wavenumbers in **P4VP(PDP-SPBI)$_{1.0}$** and **P4VP(PDP-SNBI)$_{1.0}$** at 1419 cm^{-1} and 1421 cm^{-1} respectively.

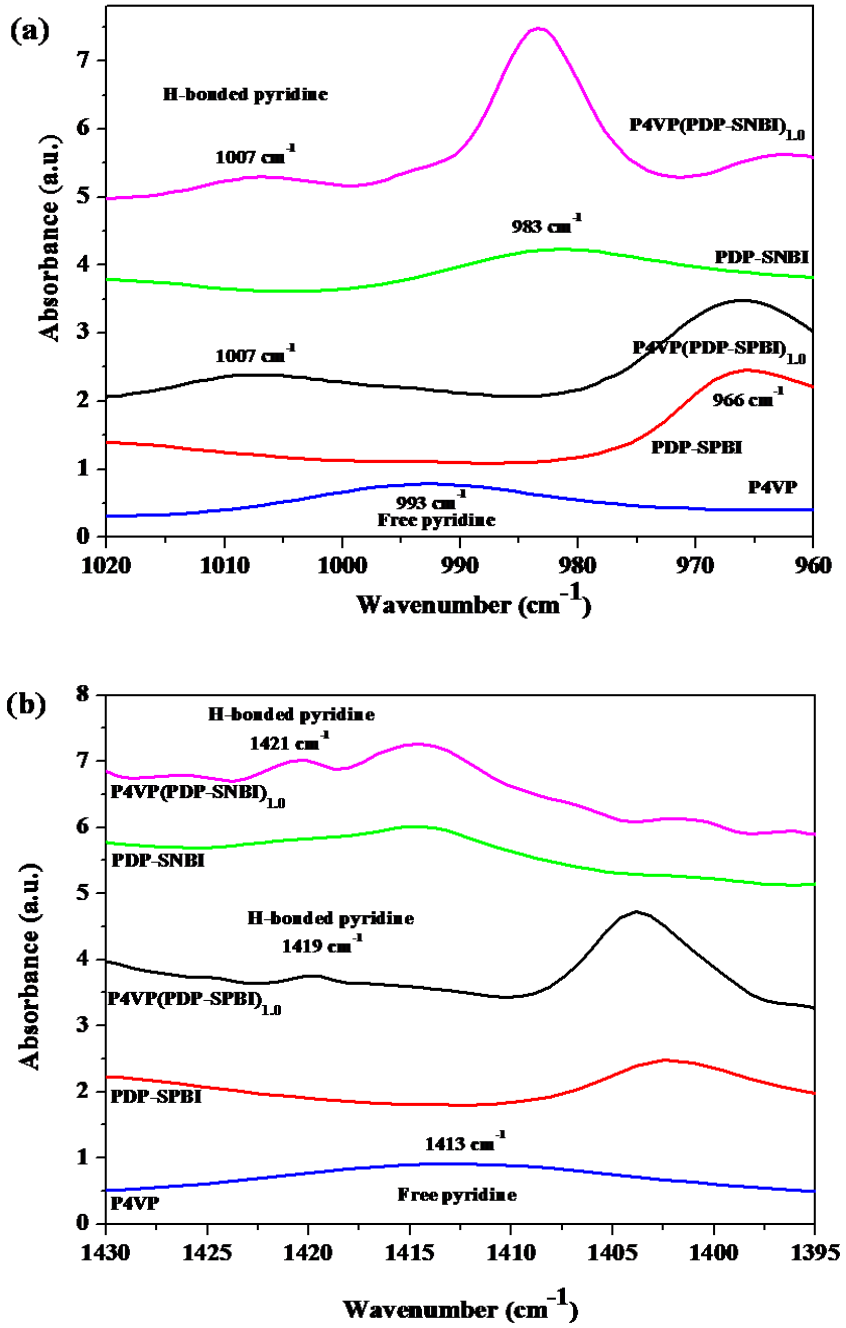

Figure-5.24. FT-IR spectra of P4VP, **PDP-SPBI**, **PDP-SNBI**, **P4VP(PDP-SPBI)$_{1.0}$** and **P4VP(PDP-SNBI)$_{1.0}$** in the region (a) 1020-970 cm^{-1} and (b) 1430-1395 cm^{-1}.

5.3.4. Characterization of the Mesomorphic Supramolecular Crosslinks

(a) Low angle and wide angle X-ray diffraction studies

In order to identify the ordered structures formed by the mesomorphic hydrogen bonded supramolecular polymer crosslinks, their packing behaviour were primarily investigated using X-ray diffraction studies. Figure-5.25 shows the low angle X-ray diffractogram of **P4VP(PDP-SNBI)$_{1.0}$** system recorded at room temperature from 2θ = 2 – 5°. The packing pattern is compared with that of the pure components P4VP and **PDP-SNBI**. The amorphous P4VP had complete absence of low angle reflections.

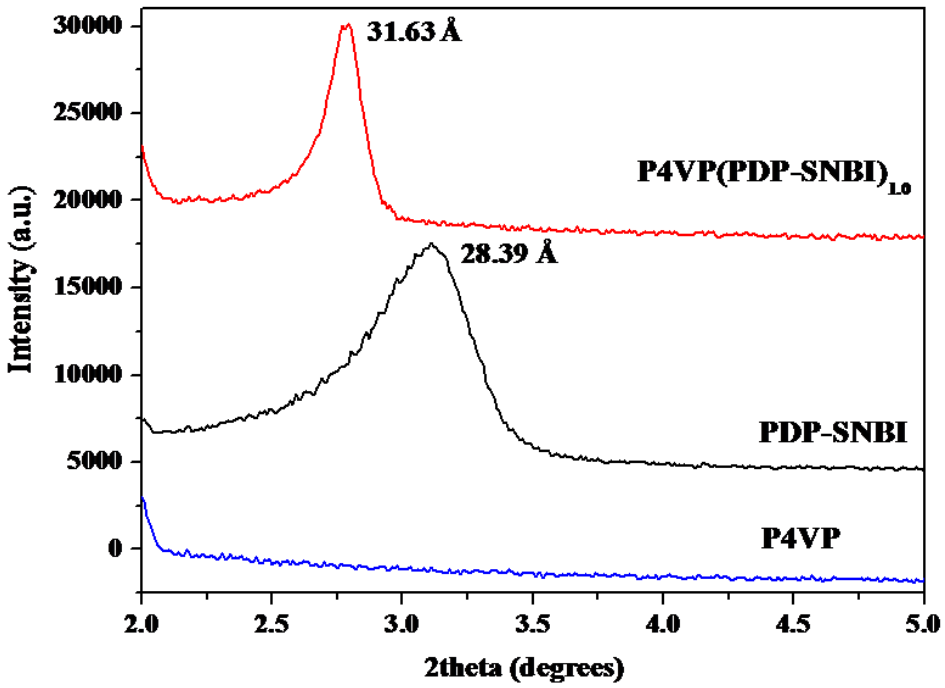

Figure-5.25. Low angle XRD trace of **P4VP(PDP-SNBI)$_{1.0}$** recorded at room temperature and compared with that of pristine P4VP and **PDP-SNBI.** (d-spacing values given nearby the peaks)

But the low angle region of pure **PDP-SNBI** had a diffraction maxima around 2θ = 3.10° corresponding to a d-spacing of 28.39 Å calculated by means of Bragg's law, whereas in the corresponding polymer complex **P4VP(PDP-SNBI)$_{1.0}$** the

fundamental reflection showed a comparatively longer period of approximately 31.63 Å observed at 2θ = 2.79°. This primary observation indicated that the major repeat distance in the supramolecular structures got increased (~3 Å shift) compared to the pristine **PDP-SNBI**.

Similarly, the low angle XRD trace of **P4VP(PDP-SPBI)$_{1.0}$** along with its precursor **PDP-SPBI** molecule is given in the figure-5.26. In this case hydrogen bonded crosslinking with P4VP caused ~2 Å increase in the periodicity on moving from pure **PDP-SPBI** to its polymer network **P4VP(PDP-SPBI)$_{1.0}$** with d-spacings around 17.69 Å and 19.57 Å respectively.

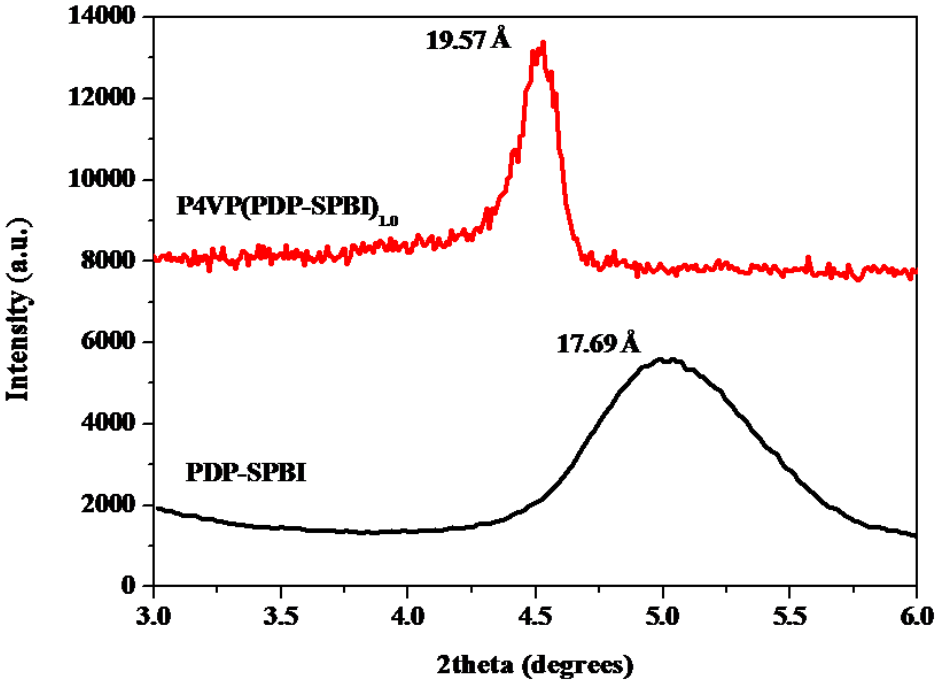

Figure-5.26. Low angle XRD trace of **P4VP(PDP-SPBI)$_{1.0}$** recorded at room temperature and compared with that of pristine P4VP and **PDP-SPBI.** (d-spacing values given nearby the peaks)

The observed increase in the fundamental periodicity of the supramolecular complexes of both **PDP-SNBI** and **PDP-SPBI** with P4VP confirmed that due to hydrogen bonding on both sides of the ditopic rylenebisimides, the newly formed

self-assembled structures would comprise of P4VP layers intercalated into the rylene domains. Further the small periodicity increment (~2-3 Å) also suggests the P4VP polymer chains to undergo significant unfolding to form very thin layers so as to accommodate stoichiometric hydrogen bonding with the ditopic rylenebisimides giving rise to a highly close packed 3D structure.

The wide angle XRD data of the P4VP, **PDP-SNBI** and **P4VP(PDP-SNBI)$_{1.0}$** system recorded at room temperature from 2θ = 5 – 40° is given in figure-5.27. Amorphous nature of pure P4VP was evident from the two broad halos in the wide angle region with no signs of crystallinity. Compared to the precursor **PDP-SNBI** molecule the **P4VP(PDP-SNBI)$_{1.0}$** showed multiple sharp reflections in the 2θ region 5 – 20°.

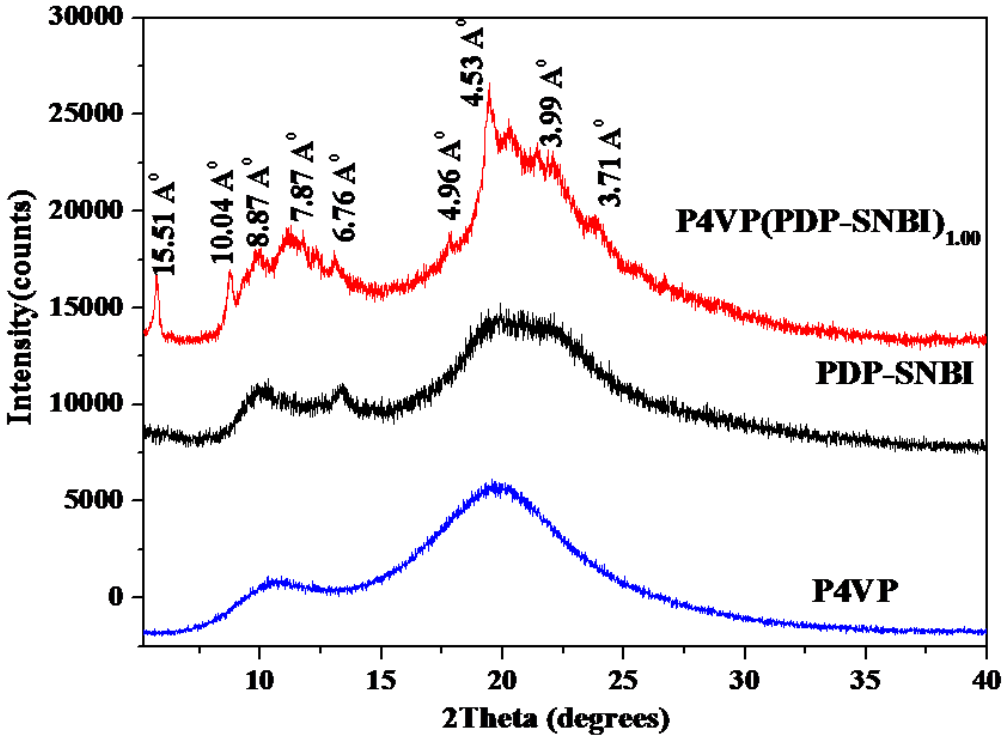

Figure-5.27. Wide angle X-ray diffractogram of **P4VP(PDP-SNBI)$_{1.0}$** recorded at room temperature and compared with the precursors.

The detailed comparison of the d-spacing values with corresponding 2θ are given in table-5.1. Combined small angle and wide angle XRD traces of **P4VP(PDP-**

SNBI)$_{1.0}$ showed the first five d-spacings of 31.63 Å, 15.51 Å, 10.04 Å, 8.87 Å and 7.87 Å. These values were in the ratio 1 : 1/2 : 1/3 : 1/3.5 : 1/4, which confirmed the formation of a lamellar ordering into the columnar arrangement (**L$_{col}$**) existing in the hydrogen bonded supramolecular crosslink.[74,99] Moreover the broad alkyl region from 17-22° in the pristine **PDP-SNBI** got transformed into several sharp reflections in the **P4VP(PDP-SNBI)$_{1.0}$** along with the clear peaks in the 22-23° region corresponding to core-core interactions. This indicated the higher extent of ordering in the alkyl components as well as stronger aromatic core interactions induced by the hydrogen bonded crosslinking compared to the relatively loosely packed fluid like columnar arrangement in the pristine **PDP-SNBI** molecule.

The wide angle XRD spectra of perylene based crosslinked system showed very similar trend as that of the naphthalene ones as given in figure-5.28.

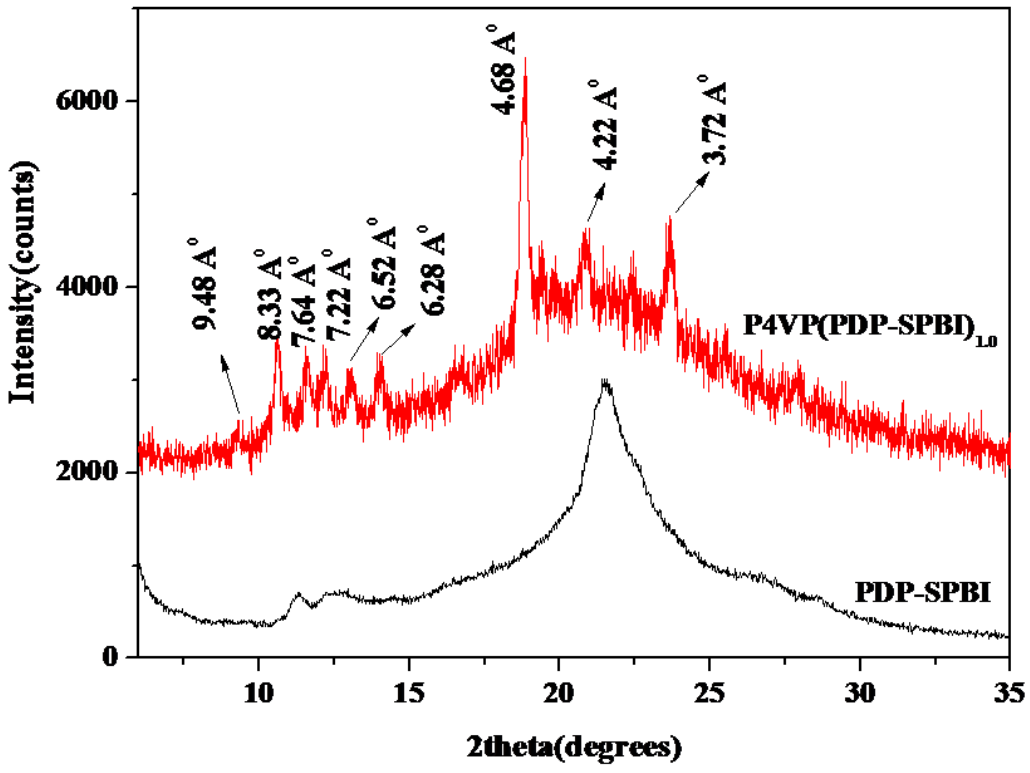

Figure-5.28. Wide angle X-ray diffractogram of **P4VP(PDP-SPBI)$_{1.0}$** recorded at room temperature and compared with the precursor **PDP-SPBI**.

Clear and sharp multiple higher order reflections appeared throughout the wide angle region of **P4VP(PDP-SPBI)$_{1.0}$** compared to the neat **PDP-SPBI**, which confirmed the increased level of ordering in the crosslinked structure. Furthermore, here also the disordered rectangular columnar phase **PDP-SPBI** seemed to have been transformed into ordered lamello-columnar (**L$_{col}$**) arrangement in **P4VP(PDP-SPBI)$_{1.0}$** supramolecular crosslink as evident from the observed d-spacing values around 19.57 Å, 9.48 Å, 8.33 Å, 7.64 Å, 7.22 Å, 6.52 Å and so on (see Table-5.1).

The presence of reflections at 9.48 Å, 6.52 Å and 4.68 Å corresponding to the second, third and fourth order multiples of the fundamental d-spacing confirmed the lamellar ordering.[74] However the other mixed reflections could not yet be assigned, but it was proposed to be arising from the concomitant columnar packing. The complete summary of the interplanar d-spacing and 2θ values of the supramolecular crosslinked structures of **P4VP(PDP-SPBI)$_{1.0}$** and **P4VP(PDP-SNBI)$_{1.0}$** complexes and their precursor rylenebisimide molecules from combined low and wide angle XRD data recorded at room temperature (25 °C) is given in table-5.1.

A schematic illustration of the structural change in the packing diagram of the ditopic rylenebisimides before and after hydrogen bonded crosslinking with P4VP is shown in figure-5.29. The ditopic rylenebisimides which adopted a thermodynamically stable columnar arrangement in a rectangular 2D lattice, upon hydrogen bonding with P4VP on both sides got frozen into fixed positions of a lamellar lattice. The top views of the initially present rectangular columnar lattice of the pristine rylenebisimides and the hydrogen bonded lamellar ordering are shown in figure-5.29(a) and the corresponding 3D lattices are given in figure-5.29(b). In effect this transformation from **Col$_r$** to **L$_{col}$** results in alternate layers of P4VP and the rylenebisimide lamellae where the rylenebisimide layers are still arranged in columnar fashion.

Table-5.1. Summary of XRD data

Sample	**2θ (degrees)**	**d-spacing (Å)**
PDP-SNBI	3.11	28.39
	4.69	18.82
	6.23	14.17
	9.74	9.06
	10.34	8.54
	13.36	6.66
	19.78	4.46
	21.79	4.05
	23.19	3.81
PDP-SPBI	4.99	17.69
	7.36	11.99
	11.34	7.78
	12.26	7.19
	12.77	6.91
	14.48	6.09
	21.48	4.11
	22.61	3.90
$P4VP(PDP\text{-}SNBI)_{1.0}$	2.79	31.63
	5.69	15.51
	8.79	10.04
	9.94	8.87
	11.21	7.87
	17.80	4.96
	19.47	4.53
	22.08	3.99
	23.82	3.71
$P4VP(PDP\text{-}SPBI)_{1.0}$	4.51	19.57
	9.30	9.48
	10.59	8.33
	11.54	7.64
	12.21	7.22
	13.04	6.52
	14.05	6.28
	16.61	5.33
	18.84	4.68
	20.91	4.22
	23.75	3.72

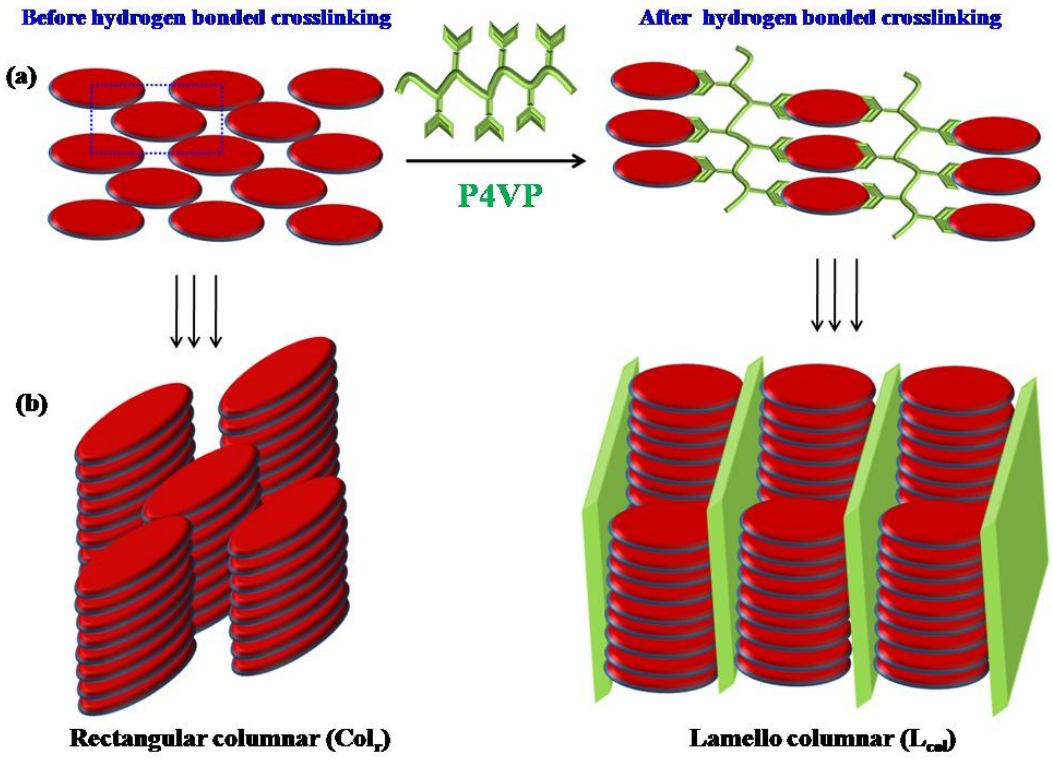

Figure-5.29. Schematic illustration of the packing diagram transformation from **Col$_r$** to **L$_{col}$**.

(b) Lyotropic liquid crystalline properties of the complexes

The 1wt% THF solutions of the supramolecular complexes **P4VP(PDP-SPBI)$_{1.0}$** and **P4VP(PDP-SNBI)$_{1.0}$** were examined by POM studies to confirm whether the lyotropic liquid crystalline nature of the ditopic rylenebisimide mesogens were retained in the complexes also. Under the microscope, it was found that the solutions of both the polymer crosslinks sandwiched between two cover slips exhibited liquid like flow along with strong birefringence. Figure-5.30 depicts the lyotropic LC textures formed by **P4VP(PDP-SPBI)$_{1.0}$** and **P4VP(PDP-SNBI)$_{1.0}$**. This study indicated that even after crosslinking with P4VP, the mesomorphic self-assembling tendency of the rylenebisimides were preserved in the complexes. Thus solution processable liquid crystalline rylenebisimide based polymeric crosslinks

were successfully developed that might prove to be potential candidates as n-type materials for optoelectronics applications.

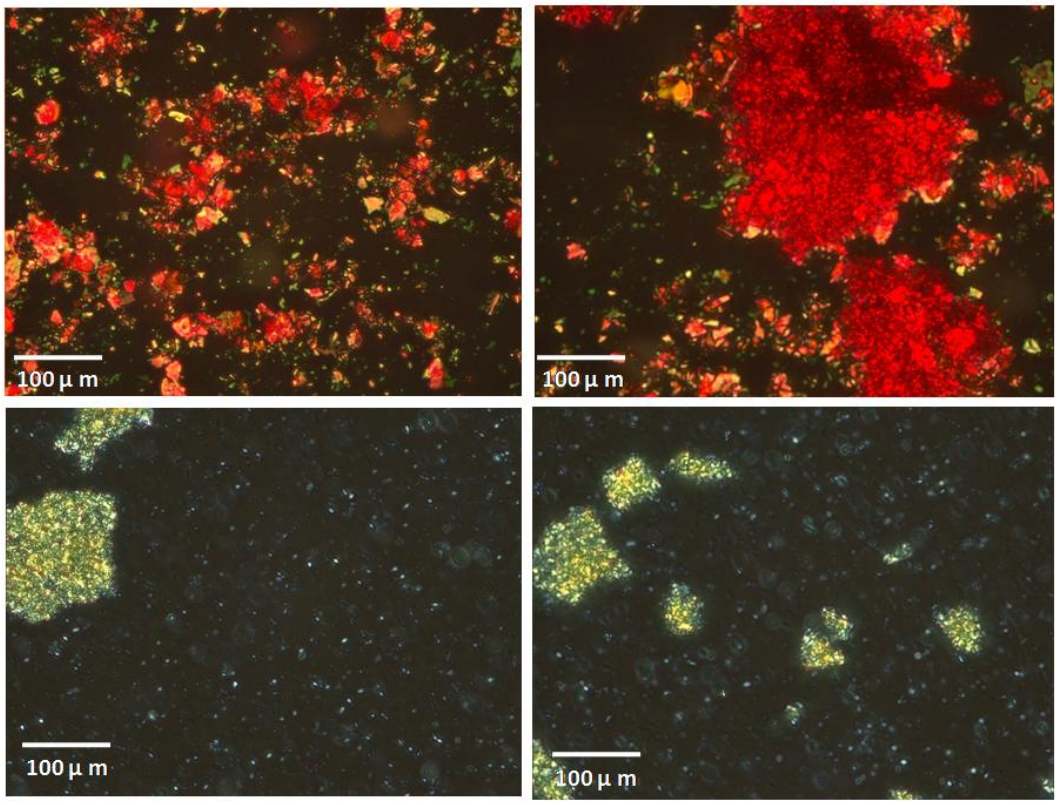

Figure-5.30. Polarised optical microscopy images of the lyotropic textures developed in 1wt% THF solution of **P4VP(PDP-SPBI)$_{1.0}$** (top) and **P4VP(PDP-SNBI)$_{1.0}$** (bottom).

(c) Nanoscale morphology analysis - TEM imaging studies

Thin film morphology of the supramolecular crosslinked polymer networks viz., **P4VP(PDP-SPBI)$_{1.0}$** and **P4VP(PDP-SNBI)$_{1.0}$** were examined by transmission electron microscopy (TEM) imaging. Drop-cast samples from 2mg/mL DMF solution were prepared directly onto copper grids for analysis. Images with improved contrast were obtained only after staining with iodine vapors, which is the commonly adopted procedure for P4VP based systems.[100-102]

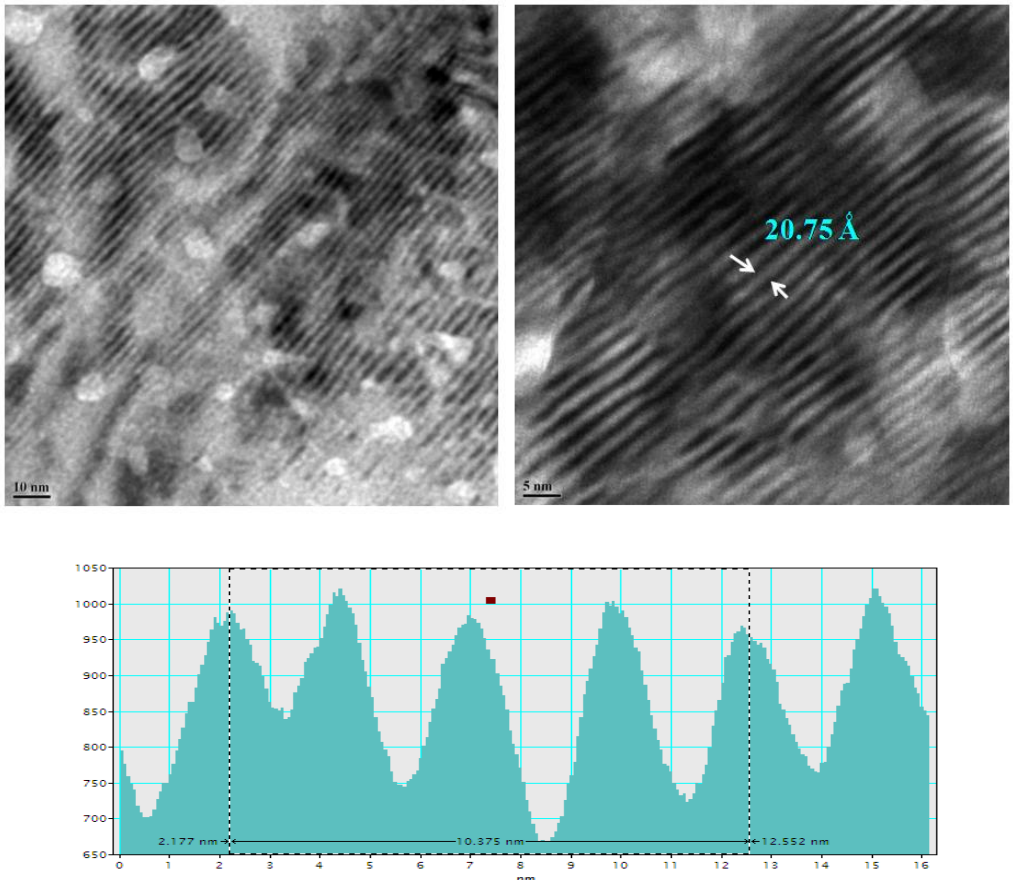

Figure-5.31. TEM images of the lamellar morphology formed by **P4VP(PDP-SPBI)$_{1.0}$** complex.

Similar to the literature reports for hydrogen bonded supramolecular assemblies of P4VP with different kinds of surfactant molecules,[100-103] here also clear striated lamellar self-assemblies were observed for both perylene and naphthalene based supramolecular complexes from the TEM imaging studies. Figure-5.31 shows the TEM images of the stained sample of **P4VP(PDP-SPBI)$_{1.0}$** polymer network at two different magnifications. The corresponding histogram profile is also given. As already discussed in previous chapters also, the P4VP domains of the lamellae appeared dark due to the selective staining by iodine whereas the bright lines correlate with the highly polar rylenebisimide regions.

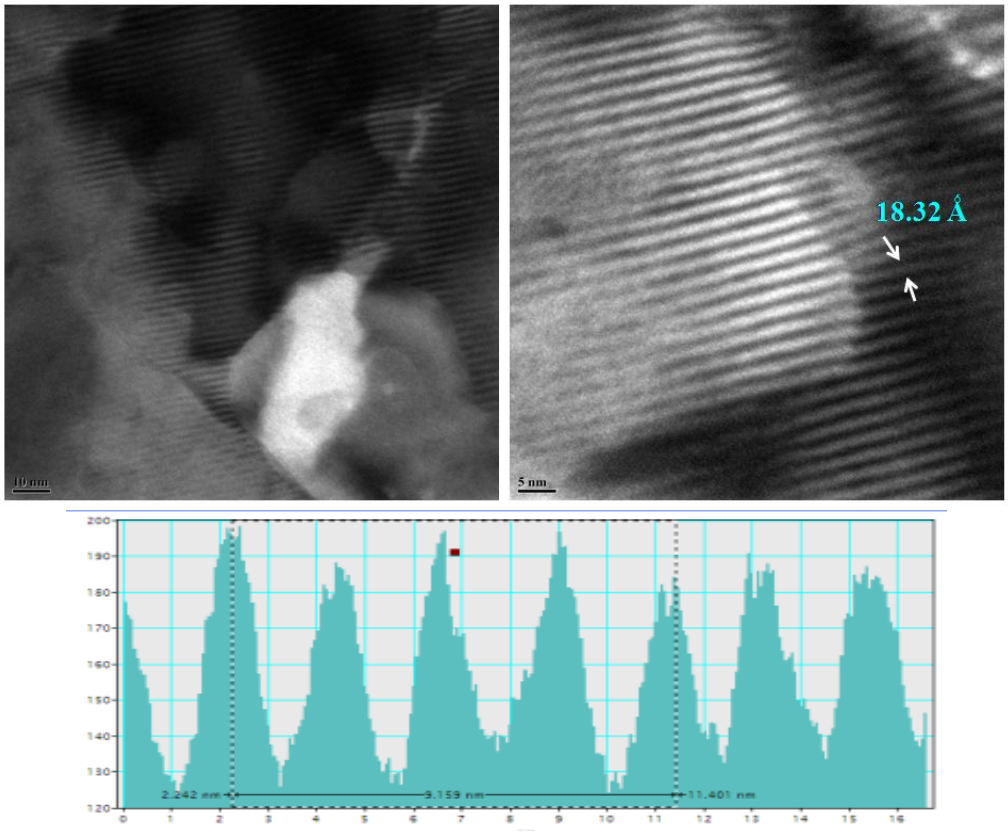

Figure-5.32. TEM images of the lamellar morphology formed by **P4VP(PDP-SNBI)$_{1.0}$** complex.

Similarly TEM images of the stained sample of **P4VP(PDP-SNBI)$_{1.0}$** polymer network is given in figure-5.32. Coincidently the domain spacing values corresponding to the rylenebisimides (both PDP-SNBI and PDP-SPBI) obtained from the average of five bright lines matched very well with their molecular length calculated from DFT studies.

The molecular length of **PDP-SPBI** along the rigid axis (without considering the C_{15} alkyl chain around 22.61 Å from molecular modelling was found very close to the width of the bright line 20.75 Å corresponding to the **PDP-SPBI** layer of the **P4VP(PDP-SPBI)$_{1.0}$** lamellar structure directly imaged by TEM. Meanwhile in the case of **P4VP(PDP-SNBI)$_{1.0}$** the lengths obtained from DFT and TEM were almost the same ~18 Å. Thus the nanolevel morphology analysis of the

supramolecular complexes using TEM were found to be in good agreement with their packing diagram shown schematically in figure-5.29. For example this analogy has been explained using the **P4VP(PDP-SPBI)$_{1.0}$** case as given in figure-5.33 and same applies to **P4VP(PDP-SNBI)$_{1.0}$** as well.

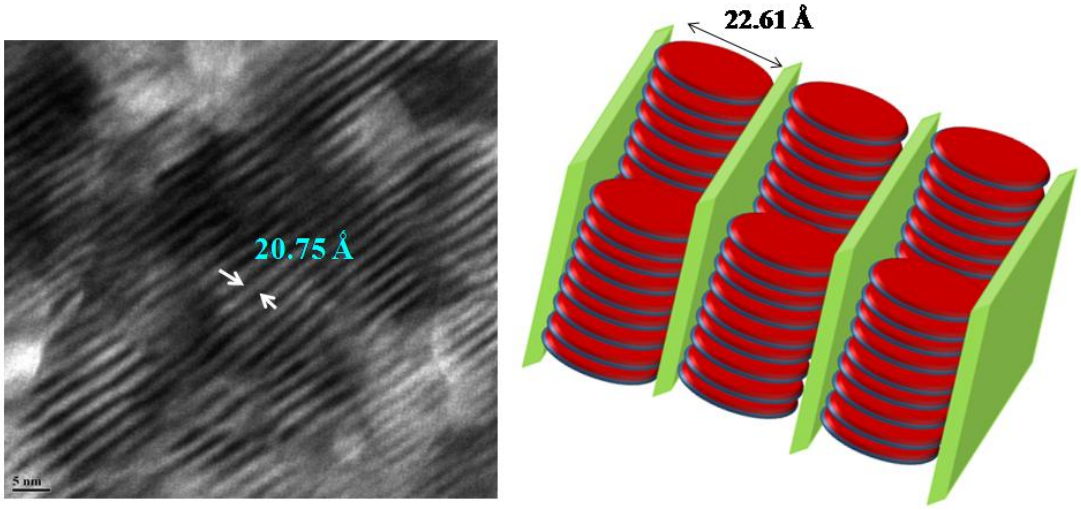

Figure-5.33. TEM images of the lamellar morphology correlated with the lamello-columnar arrangement formed by **P4VP(PDP-SPBI)$_{1.0}$** complex.

5.3.5. Charge carrier Mobility Measurements

Charge carrier mobility of the active material is one of the most critical parameter that determines the overall performance of organic electronic based devices. Optimal hole or electron mobility of organic materials are pre-requisites for achieving high efficacy in OFETs and high fill factors in OPVs.[104] Also organic materials with good mobility values are scarce and as a result it has now become a common practice to conduct carrier mobility measurements for screening of the new materials that could be future prospects for device applications. Therefore the mobility of carriers in the device type structures with the **P4VP(PDP-SPBI)$_{1.0}$** and **P4VP(PDP-SNBI)$_{1.0}$** crosslinked polymer networks as the electronically active material were measured using the technique based on space-charge-limited current (SCLC).[105,106] The principle involved is that, when the injected space charge exceeds the resident charge, the current is directly related to the mobility. The

experimental set up and procedures were similar to that adopted for the supramolecular side-chain polymer systems discussed in the previous chapters, the only difference was in the structural connectivity of the active polymeric material.

Using the Mott-Gurney square law[106] the electron mobilities were extracted by fitting the equation (1) onto I-V characteristics from the SCLC region of the curve :

$$I_{SCLC} = \left(\frac{9}{8}\right) \varepsilon\varepsilon_0 \mu \left(\frac{V^2}{L^3}\right) \qquad (1)$$

where I_{SCLC} is the current density in SCLC region, V is the applied voltage, ε and ε_0 are the relative dielectric constant of the organic layer and permittivity of the free space respectively, μ is the charge carrier mobility, and L is the thickness of the organic layer.

The pristine **PDP-SPBI** as shown in figure-5.34 exhibited the classical SCLC regime, with a very low bulk mobility estimate of $\approx 1.22 \times 10^{-6}$ $cm^2V^{-1}s^{-1}$.

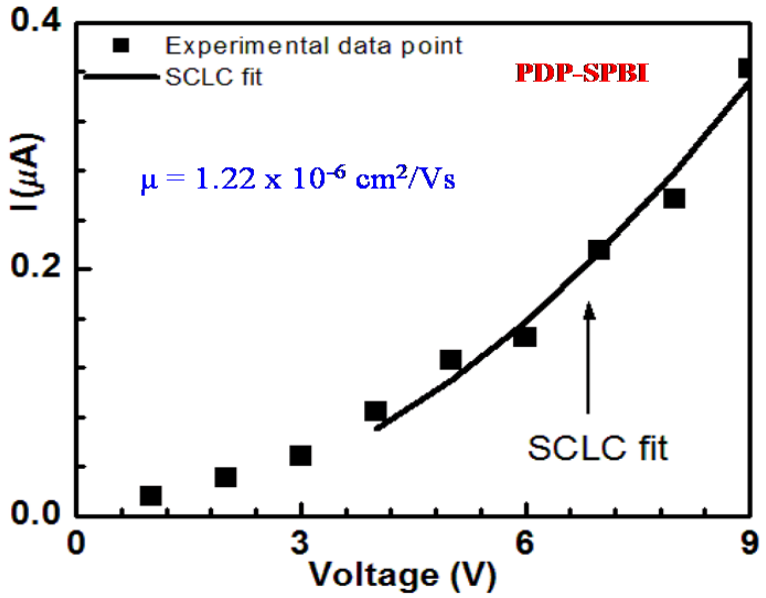

Figure-5.34. I(V) characteristics of **PDP-SPBI** with the dashed line indicating the SCLC fit and mobility estimates.

On the other hand the corresponding polymer network **P4VP(PDP-SPBI)$_{1.0}$** showed improved trend of conductance with very large charge density. The mobility estimate from the trap free regime of the I-V curve (figure-5.35) was found to be around 0.6 $cm^2V^{-1}s^{-1}$. In contrast to the perylene based system, the carrier mobility measurements for the naphthalene based system could not be conducted due to high porosity of the fabricated films.

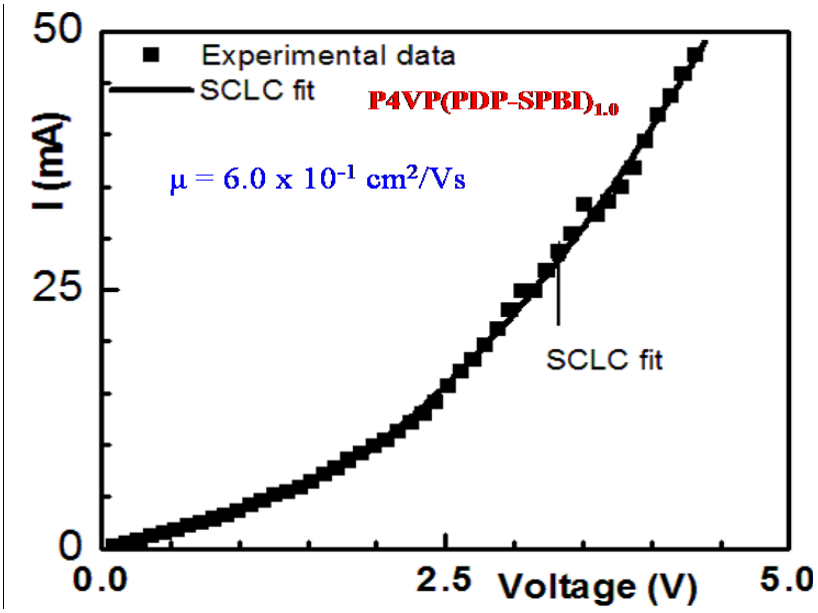

Figure-5.35. I(V) characteristics of **P4VP(PDP-SPBI)$_{1.0}$** with the dashed line indicating the SCLC fit and mobility estimates.

5.4. Conclusions

Taking aid of the structural fine tuning of the rylene bisimides, this chapter described the design and synthesis of ditopic hydrogen bondable small molecule monomers of both - perylene and naphthalene bisimides with pentadecyl phenol (PDP) units at both the imide positions. Complete synthesis and characterization of these two symmetric PDP - based rylene bisimides viz., **PDP-SPBI** and **PDP-SNBI** has been detailed. Both the rylenebisimides exhibited mesomorphic liquid crystalline properties that were probed using XRD, POM and molecular modelling studies. These combined studies revealed the inherent tendency of these molecules to self-assemble into a rectangular columnar lattice, irrespective of thermal or solvent treatment as evident from their thermotropic and lyotropic phases. By virtue of the molecular design, these two-point H-bond donor semiconductor molecules when complexed with H-bond acceptor side chain polymer P4VP, gave rise to an n-type semiconductor supramolecular crosslinked polymer network. The complexations were as usual confirmed by FT-IR studies. Bulk structure analysis using XRD as well as direct imaging using TEM revealed the nanostructured columnar lamellae formation in both **P4VP(PDP-SPBI)$_{1.0}$** and **P4VP(PDP-SNBI)$_{1.0}$**. However the charge transport properties could successfully be measured only for the perylene based systems which demonstrated better mobilities for the supramolecular crosslinked polymer network compared to the pristine molecule. Thus liquid crystalline rylenebisimides based solution processable supramolecular crosslinks with lamello-columnar arrangement of the active cores were successfully fabricated. The increased constraint by supramolecular cross linking on the alignment of the semiconductor rylenebisimide moieties to fixed channels facilitated smooth electron hopping. If the network structure had been constructed using covalent bonds, due to high crosslinking density dynamic behaviour and mesomorphic properties are not expected to retain after crosslinking.

5.5. References

[1] F. Garnier, A. Yassar, R. Hajlaoui, G. Horowitz, F. Deloffre, B. Servet, S. P. Ries, *J. Am. Chem. Soc.* **1993**, *115*, 8716.

[2] Z. Bao, *Adv. Mater.* **2000**, *12*, 227.

[3] X. L. Chen, A. J. Lovinger, Z. Bao, J. Sapjeta, *Chem. Mater.* **2001**, *13*, 1341.

[4] H. Sirringhaus, R. J. Wilson, R. H. Friend, M. Inbasekaran, W. Wu, E. P. Woo, M. Grell, D. D. C. Bradley, *Appl. Phys. Lett.* **2000**, *77*, 406.

[5] Q. Lu, K. Liu, H. Zhang, Z. Du, X. Wang, F. Wang, *ACS nano* **2009**, *3*, 3861.

[6] M. Pope, C. E. Swenberg, *Electronic processes in organic crystals*, Oxford University, New York, **1982**.

[7] Z. H. Wang, E. M. Scherr, A. G. MacDiarmid, A. J. Epstein, *Phy. Rev. B* **1992**, *45*, 4190.

[8] C.-H. Huang, N. D. Mc Clenaghan, A. Kuhn, J. W. Hofstraat, D. M. Bassani, *Org. Lett.* **2005**, *7*, 3409.

[9] Y. Wang, Y. Chen, R. Li, S. Wang, W. Su, P. Ma, M. R. Wasielewski, X. Li, J. Jiang, *Langmuir* **2007**, *23*, 5836.

[10] C. W. Struijk, A. B. Sieval, J. E. J. Dakhorst, M. van Dijk, P. Kimkes, R. B. M. Koehorst, H. Donker, T. J. Schaafsma, S. J. Picken, A. M. van de Craats, J. M. Warman, H. Zuilhof, E. J. R. Sudholter, *J. Am. Chem. Soc.* **2000**, *122*, 11057.

[11] K. Balakrishnan, A. Datar, T. Naddo, J. Huang, R. Oitker, M. Yen, J. Zhao, L. Zang, *J. Am. Chem. Soc.* **2006**, *128*, 7390.

[12] T. T. Steckler, X. Zhang, J. Hwang, R. Honeyager, S. Ohira, X.-H. Zhang, A. Grant, S.Ellinger, S. A. Odom, D. Sweat, D. B. Tanner, A. G. Rinzler, S. Barlow, J.-L. Brédas, B. Kippelen, S. R. Marder, J. R. Reynolds, *J. Am. Chem. Soc.* **2009**, *131*, 2824.

[13] H. Usta, A. Facchetti, T. J. Marks, *J. Am. Chem. Soc.* **2008**, *130*, 8580.

[14] J. Zaumseil, H. Sirringhaus, *Chem. Rev.* **2007**, *107*, 1296.

[15] Z. Zhu, D. Waller, R. Gaudiana, M. Morana, D. Mühlbacher, M. Scharber, C. Brabec, *Macromolecules* **2007**, *40*, 1981.

[16] M. X. Chen, E. Perzon, N. Robisson, S. K. M. Jonsson, M. R. Andersson, M. Fahlman, M. Berggren, *Synth. Met.* **2004**, *146*, 233.

[17] A. P. Kulkarni, X. Kong, S. A. Jenekhe, *Macromolecules* **2006**, *39*, 8699.

[18] N. Blouin, A. Michaud, D. Gendron, S. Wakim, E. Blair, R. Neagu-Plesu, M. Belletête, G. Durocher, Y. Tao, M. Leclerc, *J. Am. Chem. Soc.* **2008,** *130*, 732.

[19] M. M. Wienk, M. Turbiez, J. Gilot, R. A. J. Janssen, *Adv. Mater.* **2008**, *20*, 2556.

[20] F. H. Beijer, R. P. Sijbesma, J. A. J. M. Vekemans, E. W. Meijer, H. Kooijman, A. L. Spek, *J. Org. Chem.* **1996**, *61*, 6371.

[21] F. H. Beijer, R. P. Sijbesma, H. Kooijman, A. L. Spek, E. W. Meijer, *J. Amer. Chem. Soc.* **1998**, *120*, 6761.

[22] R. F. M. Lange, M. Van Gurp, E. W. Meijer, *J. Polym. Sci., Part A: Polym. Chem.* **1999**, *37*, 3657.

[23] F. H. Beijer, H. Kooijman, A. L. Spek, R. P. Sijbesma, E. W. Meijer, *Angew. Chem. Int.Ed.* **1998**, *37*, 75.

[24] T. F. A. de Greef, E. W. Meijer, *Nature* **2008**, *453*, 171.

[25] S. K. Chang, A. D. Hamilton, *J. Am. Chem. Soc.* **1988**, *110*, 1318.

[26] P. Tecilla, A. D. Hamilton, *J. Am. Chem. Soc.* **1990**, 1232.

[27] S. K. Chang, D. Van Engen, E. Fan, A. D. Hamilton, *J. Am. Chem. Soc.* **1991**, *113*, 7640.

[28] V. Berl, M. Schmutz, M. J. Krische, R. G. Khoury, J.-M. Lehn, *Chem. -Eur. J.* **2002**, *8*,1227.

[29] G. M. Whitesides, E. E. Simanek, J. P. Mathias, C. T. Seto, D. Chin, M. Mammen, D. M. Gordon, *Acc. Chem. Res.* **1995**, *28*, 37.

[30] T. Seki, T. Karatsu, A. Kitamura, S. Yagai, *Polym. J.* **2012**, *44*, 600.

[31] T. Seki, Y. Maruya, K.-i. Nakayama, T. Karatsu, A. Kitamura, S. Yagai, *Chem. Commun.* **2011**, *47*, 12447.

[32] T. Steiner, *Angew. Chem. Int. Ed.* **2002**, *41*, 48.

[33] L. J. Prins, D. N. Reinhoudt, P. Timmerman, *Angew. Chem. Int. Ed.* **2001**, *40*, 2382.

[34] F. J. M. Hoeben, P. Jonkheijm, E. W. Meijer, A. P. H. J. Schenning, *Chem. Rev.* **2005**, *105*, 1491.

[35] O. Levy, R. V. Chepulskii, G. L. W. Hart, S. Curtarolo, *J. Am. Chem. Soc.* **2010**, *132*, 833.

[36] S. Yagai, T. Kinoshita, Y. Kikkawa, T. Karatsu, A. Kitamura, Y. Honsho, S. Seki, *Chem. -Eur. J.* **2009**, *15*, 9320.

[37] S. Yagai, S. Kubota, H. Saito, K. Unoike, T. Karatsu, A. Kitamura, A. Ajayaghosh, M. Kanesato, Y. Kikkawa, *J. Am. Chem. Soc.* **2009**, *131*, 5408.

[38] J. Zhang, F. J. M. Hoeben, M. J. Pouderoijen, A. P. H. J. Schenning, E. W. Meijer, F. C. De Schryver, S. De Feyter, *Chem. -Eur. J.* **2006**, *12*, 9046.

[39] F. J. M. Hoeben, J. Zhang, C. C. Lee, M. J. Pouderoijen, M. Wolffs, F. Würthner, A. P. H. J. Schenning, E. W. Meijer, S. De Feyter, *Chem. -Eur. J.* **2008**, *14*, 8579.

[40] I. De Cat, C. Roger, C. C. Lee, F. J. M. Hoeben, M. J. Pouderoijen, A. P. H. J. Schenning, F. Wurthner, S. De Feyter, *Chem. Commun.* **2008**, 5496.

[41] P. Jonkheijm, A. Miura, M. Zdanowska, F. J. M. Hoeben, S. De Feyter, A. P. H. J. Schenning, F. C. De Schryver, E. W. Meijer, *Angew. Chem. Int. Ed.* **2004**, *43*, 74.

[42] P. G. A. Janssen, A. Ruiz-Carretero, D. González-Rodríguez, E. W. Meijer, A. P. H. J. Schenning, *Angew. Chem. Int. Ed.* **2009**, *48*, 8103.

[43] A. Noro, M. Hayashi, Y. Matsushita, *Soft Matter* **2012**, *8*, 6416.

[44] K. P. Nair, V. Breedveld, M. Weck, *Macromolecules* **2011**, *44*, 3346.

[45] S. Wu, F. Shi, Q. Zhang, C. Bubeck, *Macromolecules* **2009**, *42*, 4110.

[46] S. Laschat, A. Baro, N. Steinke, F. Giesselmann, C. Hägele, G. Scalia, R. Judele, E. Kapatsina, S. Sauer, A. Schreivogel, M. Tosoni, *Angew. Chem. Int. Ed.* **2007**, *46*, 4832.

[47] *Liquid Crystalline Semiconductors.* Bushby, Richard J.; Kelly, Stephen M.; O'Neill, Mary (Eds.); Springer Series in Material Science **2013**, Vol.169, IX, 272.

[48] T. Kato, J. M. J. Frè chet, *Macromolecules* **1989**, *22*, 3818.

[49] T. Kato, N. Mizoshita, K. Kanie, *Macromol. Rapid Commun.* **2001**, *22*, 797.

[50] M. Suárez, J.-M. Lehn, S. C. Zimmerman, A. Skoulios, B. Heinrich, *J. Am. Chem. Soc.* **1998**, *120*, 9526.

[51] T. Kato, H. Kihara, T. Uryu, A. Fujishima, J. M. J. Frè chet, *Macromolecules* **1992**, *25*, 6836.

[52] U. Kumar, T. Kato, J. M. J. Frè chet, *J. Am. Chem. Soc.* **1992**, *114*, 6630.

[53] T. Kato, H. Kihara, S. Ujiie, T. Uryu, J. M. J. Frè chet, *Macromolecules* **1996**, *29*, 8734.

[54] K. Araki, T. Kato, U. Kumar, J. M. J. Frè chet, *Macromol. Rapid Commun.* **1995**, *16*, 733.

[55] U. Kumar, J. M. J. Frè chet, T. Kato, S. Ujiie, K. Timura, *Angew. Chem. Int. Ed.* **1992**, *31*, 1531.

[56] T. Kato, M. Fukumasa, J. M. J. Frè chet, *Chem. Mater.* **1995**, *7*, 368.

[57] T. Kato, T. Uryu, F. Kaneuchi, C. Jin, J. M. Frè chet, *Liquid Crystals* **1993**, *14*, 1311.

[58] M. Fukumasa, T. Kato, T. Uryu, J. M. J. Frè chet, *Chem. Lett.* **1993,** 65.

[59] T. Kato, H. Kihara, U. Kumar, T. Uryu, J. M. J. Frè chet, *Angew. Chem. Int. Ed.* **1994**, *33*,1644.

[60] J. Barbera, N. Gimeno, I. Pintre, M. B. Ros, J. L. Serrano, *Chem. Commun.* **2006**, 1212.

[61] J. T. Korhonen, T. Verho, P. Rannou, O. Ikkala, *Macromolecules* **2010**, *43*, 1507.

[62] X. Zhan, A. Facchetti, S. Barlow, T. J. Marks, M. A. Ratner, M. R. Wasielewski, S. R. Marder, *Adv. Mater.* **2011**, *23*, 268.

[63] C. Li, H. Wonneberger, *Adv. Mater.* **2012**, *24*, 613.

[64] C. D. Simpson, J. Wu, M. D. Watson, K. Müllen, *J. Mater. Chem.* **2004**, *14*, 494.

[65] Z. An, J. Yu, S. C. Jones, S. Barlow, S. Yoo, B. Domercq, P. Prins, L. D. A. Siebbeles, B. Kippelen, S. R. Marder, *Adv. Mater.* **2005**, *17*, 2580.

[66] L. Schmidt-Mende, A. Fechtenkötter, K. Müllen, E. Moons, R. H. Friend, J. D. MacKenzie, *Science* **2001**, *293*, 1119.

[67] C. W. Struijk, A. B. Sieval, J. E. J. Dakhorst, M. van Dijk, P. Kimkes, R. B. M.Koehorst, H. Donker, T. J. Schaafsma, S. J. Picken, A. M. van de Craats, J. M. Warman, H. Zuilhof, E. J. R. Sudhölter, *J. Am. Chem. Soc.* **2000**, *122*, 11057.

[68] Z. Chen, M. G. Debije, T. Debaerdemaeker, P. Osswald, F. Würthner, *Chem. Phys. Chem.* **2004**, *5*, 137.

[69] F. Würthner, C. Thalacker, S. Diele, C. Tschierske, *Chem. -Eur. J.* **2001**, *7*, 2245.

[70] S. B. Mhaske, R. V. Bhingarkar, M. B. Sabne, R. Mercier, S. P. Vernekar, *J. Appl.Polym. Sci.* **2000**, *77*, 627.

[71] S. Laschat, A. Baro, N. Steinke, F. Giesselmann, C. Hägele, G. Scalia, R. Judele, E. Kapatsina, S. Sauer, A. Schreivogel, M. Tosoni, *Angew. Chem. Int. Ed.* **2007**, *46*, 4832.

[72] S. Chandrashekhar, "*Handbook of Liquid Crystals, Vol. 2B, Low Molecular Weight Liquid Crystals* II." D. Demus, J. W. Goodby, G. W. Gray, H. W. Spiess, V. Vill, Eds.; Wiley VCH: Weinheim, Germany, **1998**, p.750.

[73] A. S. Achalkumar, U. S. Hiremath, D. S. S. Rao, S. K. Prasad, C. V. Yelamaggad, *J. Org. Chem.* **2013**, *78*, 527.

[74] S. Zou, L. He, J. Zhang, Y. He, L. Yuan, L. Wu, J. Luo, Y. Wang, W. Feng, *Org. Lett.* **2012**, *14*, 3584.

[75] K. Kishikawa, S. Nakahara, Y. Nishikawa, S. Kohmoto, M. Yamamoto, *J. Am. Chem. Soc.* **2005**, *127*, 2565.

[76] J. Miao, L. Zhu, *Soft Matter* **2010**, *6*, 2072.

[77] C. V. Yelamaggad, A. S. Achalkumar, D. S. S. Rao, S. K. Prasad, *J. Mater. Chem.* **2007**, *17*, 4521.

[78] H. Maeda, Y. Terashima, Y. Haketa, A. Asano, Y. Honsho, S. Seki, M. Shimizu, H. Mukai, K. Ohta, *Chem. Commun.* **2010**, *46*, 4559.

[79] U. S. Hiremath, *Tetrahedron Lett.* **2013**, *54*, 3419.

[80] M. Lehmann, M. Jahra, J. Gutmann, *J. Mater. Chem.* **2008,** *18*, 2995.

[81] J. Seo, S. Kim, S. H. Gihm, C. R. Park, S. Y. Park, *J. Mater. Chem.* **2007**, *17*, 5052.

[82] M. Kaller, C. Deck, A. Meister, G. Hause, A. Baro, S. Laschat, *Chem. -Eur. J.* **2010**, *16*, 6326.

[83] N. Zharnikova, N. Usol'tseva, E. Kudrik, M. Thelakkat, *J. Mater. Chem.* **2009**, *19*, 3161.

[84] M. Kaller, S. Tussetschläger, P. Fischer, C. Deck, A. Baro, F. Giesselmann, S. Laschat, *Chem. -Eur. J.* **2009**, *15*, 9530.

[85] N. Steinke, M. Jahr, M. Lehmann, A. Baro, W. Frey, S. Tussetschlager, S. Sauer, S. Laschat, *J. Mater. Chem.* **2009**, *19*, 645.

[86] S. T. Hyde, "*Handbook of Applied Surface and Colloid Chemistry*." K. Holmberg, D. O. Shah, M. J. Schwuger, Eds.; Wiley: Weinheim, **2001**, p.299.

[87] I. C. Sage, "*Handbook of Liquid Crystals, Vol 1, Fundamentals*" D. Demus, J. Goodby, G. W. Gray, H. W. Spiess, V. Vill, Eds.; Wiley: Weinheim, Germany, **1998**, p.731.

[88] K. Kishikawa, S. Furusawa, T. Yamaki, S. Kohmoto, M. Yamamoto, K. Yamaguchi, *J. Am. Chem. Soc.* **2002**, *124*, 1597.

[89] A. Tracz, J. K. Jeszka, M. D. Watson, W. Pisula, K. Müllen, T. Pakula, *J. Am. Chem. Soc.* **2003**, *125*, 1682.

[90] P. Ekwall, "*Advances in Liquid Crystals*" Vol 1, Ed.: G. H. Brown, Academic Press, New York, **1975**.

[91] J. Malthete, A. M. Levelut, N. H. Tinh, *J. Phys. Lett.* **1985,** *46*, L875.

[92] F. Morale, R. W. Date, D. Guillon, D. W. Bruce, R. L. Finn, C. Wilson, A. J. Blake, M. Schröder, B. Donnio, *Chem. -Eur. J.* **2003**, *9*, 2484.

[93] S. N. Chvalun, J. Blackwell, J. D. Cho, I. V. Bykova, V. Percec, *Acta. Polym.* **1999**, *50*, 51.

[94] A. F. Thunemann, D. Ruppelt, C. Burger, K. Müllen, *J. Mater. Chem.* **2000**, *10*, 1325.

[95] F. Würthner, C. Thalacker, S. Diele, C. Tschierske, *Chem. -Eur. J.* **2001**, *7*, 2245.

[96] M. Shirakawa, N. Fujita, T. Tani, K. Kaneko, S. Shinkai, *Chem. Commun.* **2005**, 4149.

[97] T. Yasuda, K. Kishimoto, T. Kato, *Chem. Commun.* **2006**, 3399.

[98] J. Ruokolainen, G. ten Brinke, O. Ikkala, M. Torkkeli, R. Serimaa, *Macromolecules* **1996**, *29*, 3409.

[99] P. Kohn, L. Ghazaryan, G. Gupta, M. Sommer, A. Wicklein, M. Thelakkat, T. Thurn-Albrecht, *Macromolecules* **2012**, *45*, 5676.

[100] B. J. Rancatore, C. E. Mauldin, S.-H.Tung, C. Wang, A. Hexemer, J. Strzalka, J. M. J. Frè chet, T. Xu, *ACS Nano* **2010,** *4*, 2721.

[101] B. Nandan, M. K. Vyas, M. Böhme, M. Stamm, *Macromolecules* **2010,** *43*, 2463.

[102] C. -H. Lee,S.-H. Tung, *Soft Matter* **2011,** *7*, 5660.

[103] M. C. Luyten, G. O. R. A. Van Ekenstein, G. Ten Brinke, *Macromolecules* **1999,** *32*, 4404.

[104] A. Facchetti, *Chem. Mater.* **2011,** *23*, 733.

[105] M. -A. Muth, M. C. Orozco, M. Thelakkat, *Adv. Funct. Mater.* **2011**, *21*, 4510.

[106] A. M. Goodman, A. Rose, *J. Appl. Phys.* **1971,** *41*, 2823.

Chapter-6

Conclusions and Future Perspectives

Summary and Conclusions

Solution processable polymeric n-type semiconductor materials are scarce in literature. The device development using these n-type semiconductors till date is far from the performance achieved with p-type materials. Among the non-fullerene type acceptor materials, the rylenebisimides specifically perylene and naphthalene bisimides are the most promising n-type organic semiconductor materials explored for optoelectronics applications. But majority of the rylenebisimide based polymeric materials reported involves tedious synthetic procedures and often lead to rigid materials with low practical applicability. In this context the present thesis entitled ***"Development of Novel Methacrylic and Supramolecular Comb Polymers of Rylenebisimides for applications in Optoelectronics"*** described the design and development of new categories of rylenebisimide based polymeric materials that could find successful applications in the field of optoelectronics. The design strategies liberally utilized principles of covalent as well as non-covalent chemistry with equal ease. Each chapter progressed forward with a new contribution to the field.

Initial attempts were made to incorporate the n-type semiconductor perylenebisimide molecules into a urethane methacrylate comb polymer scaffold by covalent chemistry approach, as pendent groups. Accordingly the urethane methacrylate comb monomers of a soluble perylenebisimide as well as that of two other simple aromatic units namely cardanol and 3-pentadecylphenol were successfully synthesized by playing around with isocyanate-alcohol chemistry. But unfortunately in spite of several attempts with varied reaction conditions, the simple free-radical polymerization of the perylenebisimide methacrylate comb monomers failed miserably. On the other hand the cardanol and 3-pentadecylphenol based urethane methacrylate comb monomers under the same polymerization conditions successfully gave the corresponding comb polymers. The solvent induced self-assembly properties of these polymers were thoroughly studied using different microscopic techniques like scanning electron (SEM),

transmission electron (TEM) and atomic force (AFM) microscopy. The polymers exhibited three - dimensional honeycomb morphology in $CHCl_3$ whereas in THF they formed spheres. The cardanol derived polymer PCIH showed a tendency for multiple morphologies like spheres and tubes in THF. However the failure at producing a covalently incorporated side-chain perylenebisimide polymer led to the search for alternate methods of incorporation into processable polymer scaffolds.

So far no studies have been reported, involving non-covalent approach to incorporate perylenebisimides into side chain polymer templates. For the first time we demonstrated the fabrication of a hydrogen bonded supramolecular comb polymer of perylenebisimide, that possessed unique combination of high crystallinity and solution processability properties desirable for device applications. A novel amphiphilic unsymmetrical perylenebisimide (**PDP-UPBI**) suitably functionalized for hydrogen bonding interactions was designed and synthesized with 3-pentadecylphenol group on one imide nitrogen atom. Utilizing the hydrogen bonding interactions between phenolic-OH of **PDP-UPBI** and pyridine groups of a readymade polymer P4VP, the supramolecular comb polymer was successfully formed by simple solution mixing of the two components. Well defined nanostructured polymeric supramolecular assemblies with uniform lamellar structures in the domain range of 5 – 10 nm were revealed by TEM imaging and XRD studies. ^{1}H-NMR and photophysical studies proved that once hydrogen bonded, the supramolecular complex behaved as a single entity at both high and low concentrations. However the most attractive highlight of this approach remained the ability to retain the crystallinity of the perylene bisimide small molecule along with the processability afforded by the polymer. The concept of superior organization found in the hydrogen bonded supramolecular comb polymer of perylenebisimide with P4VP was further ascertained by the charge carrier mobility measurements conducted for both the pristine molecule and the complex. An electron mobility value of the supramolecular complex measured by SCLC was found to be several orders higher than that of the pristine **PDP-UPBI** small molecule. Thus a new class of perylenebisimide based polymeric material was

contributed, which could become a potential n-type semiconductor material with excellent ordering, processability and hence better performance.

Further, with the aim to develop n-type polymeric semiconductor materials with much better performance, the same concept of hydrogen bonded supramolecular comb polymers with P4VP was extended to the lower analogue rylenebisimide namely naphthalenebisimides (NBI). NBI are compact, electron deficient class of polycyclic aromatic compounds with better solubility in common organic solvents compared to the perylene counterpart and they also possess high crystallinity and enhanced field effect mobilities. Unsymmetrical naphthalenebisimide (**PDP-UNBI**) structurally similar to the **PDP-UPBI** was synthesized and stoichiometrically complexed with P4VP. X-ray diffraction (XRD) analyses and direct imaging by TEM confirmed the formation of uniform lamellar morphology of the naphthalene based supramolecular comb polymer with alternate P4VP and **PDP-UNBI** layers. The higher tendency of the naphthalenebisimide molecules to crystallize was made use of to get the single crystal structure of the **PDP-UNBI** small molecule alone. Thus the single crystal XRD studies on **PDP-UNBI** added further information to the probable packing behaviour of the unsymmetrical rylenebisimides within the P4VP polymer lattice. This is the first such report with single crystal studies on a small molecule that has been used to compare the packing picture before and after being incorporated into a polymer scaffold by supramolecular interactions. As anticipated, the supramolecular complex of **PDP-UNBI** with P4VP exhibited better electron mobilities than its perylene counterpart as proved from the SCLC measurements. Also, with the aim to combine high crystallinity and solution processability of naphthalenebisimides with the broader absorption spectra of perylenebisimides, yet another series of stoichiometrically balanced 1:1 random co-comb polymer complexes of P4VP with **PDP-UPBI** and **PDP-UNBI** varying only in the relative compositions of perylene and naphthalene cores were also prepared. All of these random co-comb polymer complexes were also found to exhibit clear lamellar structures but with varying periodicities. However among the series of random co-comb polymer complexes,

the sample with equimolar ratios (50/50) of **PDP-UNBI** and **PDP-UPBI** gave reliable electron transport characteristics.

Keeping the chemical functionalities and basic concept of hydrogen bonded supramolecular interaction the same, a structural fine tuning of the rylenebisimides (both perylene and naphthalene bisimide) was utilized to design and synthesize two ditopic hydrogen-bond donor dyes viz., **PDP-SNBI** and **PDP-SPBI** that could coordinate to P4VP from both termini. These ditopic hydrogen-bond donor rylenebisimide small molecules exhibited inherent columnar self-assembly characteristic of liquid crystalline materials as explored from the XRD, POM, molecular modelling studies etc. Simple solution mixing of these ditopic dyes with P4VP afforded hydrogen bonded supramolecular semiconductor crosslinked polymer network with preserved mesomorphic properties. Packing diagram and morphology evaluation using XRD and TEM experiments revealed a structure transformation from rectangular-columnar to lamello-columnar self-organization. Towards the end, the materials were screened for device applications using SCLC measurements which revealed that among the two systems compared, the perylenebisimide based supramolecular polymer network exhibited better charge transport characteristics.

To conclude, this thesis work dealt with specific focus to develop rylenebisimide based new n-type semiconductor polymeric materials especially via supramolecular chemistry routes. Structure-property relationships were addressed in depth utilizing several scientific techniques. Further, the newly developed materials were also examined to the level of device performance for future applications. To cut short, the thesis contributed a breakthrough concept for all-polymer n-type semiconductor materials with high ordering as well as processability along with better device performance which is practically still a dream!

Scope for Future Research

Based on the findings from the present thesis, the concept of supramolecular interactions has been successfully proved to fabricate better performing solution processable polymeric materials of otherwise rigid organic n-type semiconductor molecules. But there seems still scope for further studies to improve the desirable aspects for commercial device applications. There are several challenges in the field of n-type semiconductor materials; one of the main problem to be tackled is that, the transport in n-channel conductors is degraded easily by air, which acts as electron traps together with the dielectric surface trapping sites. Fluorinated side chains and electron withdrawing groups on bay positions are good solutions used to overcome this problem. Therefore if studies are performed using the same concept of supramolecular comb polymer explored in this thesis where the rylenebisimides would be liberally decorated with fluorinated alkyl chains on one side and hydrogen bondable moieties on other, well ordered n-type polymeric materials with high air stability, processability and hence best performance could be anticipated.

The same concept could also be extended to incorporate both n-type and p-type organic semiconductor materials into a single polymer matrix so as to form uniformly arranged donor-acceptor (D-A) arrays within 5-10 nm scale so that the dissociation of excited state electron-hole pair (exciton) can occur effectively before recombination occurs. Such materials could find potential applications in different optoelectronics applications - specifically the organic solar cells. Such supramolecular D-A polymeric arrays can be achieved as shown in the scheme-6.1. Donor and acceptor based polymerizable monomers suitably decorated with functionalities for supramolecular interactions such as hydrogen bonding, metal-ligand coordination etc could be synthesized. Pre-associated D-A monomer arrays can be achieved in the solution fabricated films by the interplay of the in-built self-assembling interactions such as π-π stacking, van der Waals forces etc. Once the molecules are custom arranged, instant polymerization techniques like photo polymerization by UV-curing can be applied to form uniform donor-acceptor films

highly organized in the 5-10 nm scale. Different types of donor segments like oligophenylenevinylenes, oligothiophenes, oligofluorenes can be attempted to screen the best ones in conjunction with different acceptor materials such as perylene and naphthalene bisimides. The strategy suggested here may prove to exhibit better final properties than would be obtained by blending of two independent donor and acceptor polymers which always leads to eventual macrophase separation.

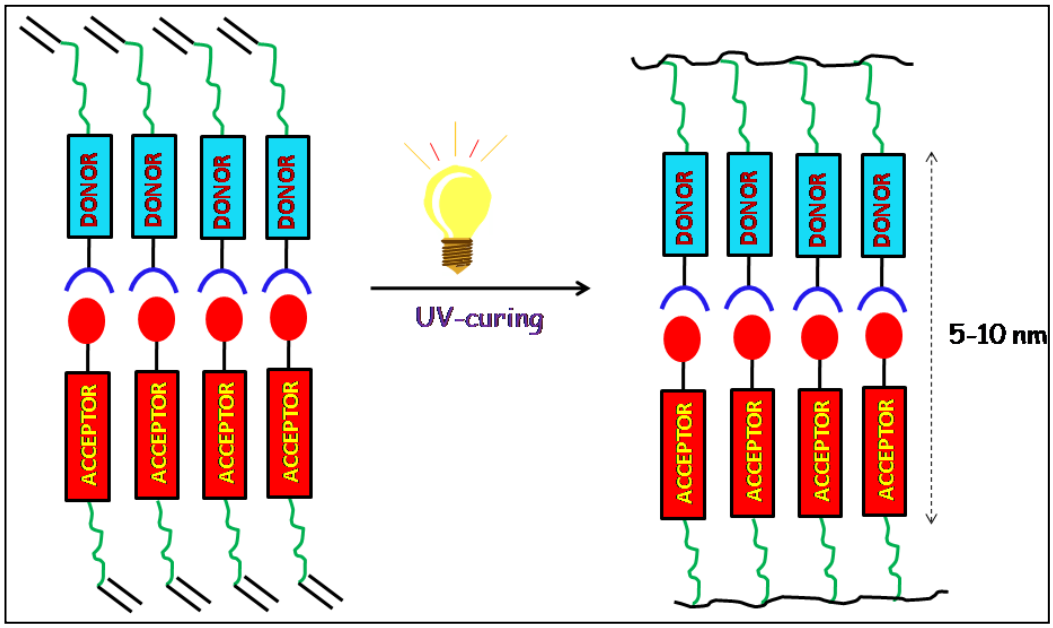

Scheme-6.1

Publications in International Journals:

1. N. Rekha, P. Kumar, K. S. Narayan, S. K. Asha, "Nanostructured Crystalline Comb Polymer of Perylenebisimide by Directed Self-Assembly: Poly(4-vinylpyridine)-Pentadecylphenol Perylenebisimide", Adv. Funct. Mater. **2013**, *23*, 2033.
2. N. Rekha, S. K. Asha, "Solvent-Induced Self-Assembly of Hydrogen bonded P4VP-Perylenebisimide Comb Polymer", J. Mater. Chem. C **2013,** DOI: 10.1039/C3TC31015A.
3. N. Rekha, S. K. Asha, "Solvent-Induced Self-Assembly in Cardanol-Based Urethane Methacrylate Comb Polymers", J. Polym. Sci., Part A: Polym. Chem. **2009,** *47*, 2996.
4. N. Rekha, S. K. Asha, "Synthesis and FTIR Spectroscopic Investigation of the UV Curing Kinetics of Telechelic Urethane Methacrylate Crosslinkers Based on the Renewable Resource-Cardanol", J. Appl. Polym. Sci. **2008,** *109*, 2781. [*This work is not included in the thesis*]
5. S. Patil, S. Datar, N. Rekha, S. K. Asha, C. V. Dharmadhikari, "Charge storage and electron transport properties of gold nanoparticles decorating a urethane-methacrylate comb polymer network", Nanoscale, **2013**, *5*, 4404. [*This work is not included in the thesis*]
6. N. Rekha, S. K. Asha, "Supramolecular P4VP - Pentadecylphenol Naphthalenebisimide Comb Copolymer: Synthesis, Mesoscopic organization and Charge transport properties" [***Manuscript under preparation***]
7. N. Rekha, S. K. Asha, "Supramolecular Random comb copolymers of Pentadecylphenol based Naphthalene and Perylene Bisimides via hydrogen bonded self assembly with poly(4-vinyl pyridine)" [***Manuscript under preparation***]
8. N. Rekha, S. K. Asha, "n-Type Semiconductor Supramolecular Crosslinked Polymer Network : Liquid crystalline assembly of Rylene bisimides with P4VP via hydrogen bonding" [***Manuscript under preparation***]

Workshop and Conferences Attended:

1. N. Rekha, S. K. Asha, "Highly Crystalline Nanostructured Comb Polymer of Perylenebisimide by Directed Self-Assembly", PolyTech-2012, International Conference on Advances in Polymeric Materials & Nanotechnology, Pune, India, December 15-17, **2012**. (*Oral Presentation*)
2. N. Rekha, S. K. Asha, "Self-assembly in Side-chain Perylenebisimide Polymers via covalent and non-covalent interactions", Humboldt Kolleg on Science Globalization and Human Development, Goa, India, November 11-13, **2011**. (*Oral Presentation*)
3. N. Rekha, S. K. Asha, "Self Assembly in Acrylic Rigid Comb Polymers", National Science Day Celebrations, NCL, Pune, India, February 25, **2009**. (Selected for Best poster award in the area of Polymer Sciences) (*Poster Presentation*)
4. N. Rekha, S. K. Asha, "Self-Assembly in Hydrogen bonded Methacrylic Comb Polymers ", 11th CRSI National Symposium in Chemistry, NCL, Pune, India, February 6-8, **2009**. (*Poster Presentation*)
5. N. Rekha, S. K. Asha, "Hydrogen Bonded Urethane Methacrylate Polymers from Renewable Natural Resource-Cardanol",ICAMC-2007, International Conference on Advanced Materials and Composites, Thiruvananthapuram, India, October 24-26, **2007**. (*Poster Presentation*)
6. N. Rekha, S. K. Asha, "Hydrogen Bonded Urethane Methacrylate Polymers from Renewable Natural Resource-Cardanol", IUMRS-ICAM 2007, The 10th International Conference on Advanced Materials, Bangalore, India, October 8-13, **2007**. (*Poster Presentation*)